

Productos naturales bioactivos de organismos marinos de la Península de Yucatán, México

Autor: Dawrin Jesus Pech Puch

Tesis Doctoral UDC / 2020

Directores:

Dr. Carlos Jiménez González

Dr. Jaime Rodríguez González

Programa de Doctorado en Química Ambiental y Fundamental



UNIVERSIDADE DA CORUÑA

Acta de Tesis

El tribunal, nombrado por el Excmo. Sr. Rector de la Universidade da Coruña para calificar la tesis doctoral titulada “**Productos naturales bioactivos de organismos marinos de la Península de Yucatán, México**” dirigida por los Drs. Carlos Jiménez González y Jaime Rodríguez González y, presentada por Don Dawrin Jesus Pech Puch y constituido en el día de la fecha por los miembros que subscriben la presente Acta, una vez efectuada la defensa por el doctorando y contestadas las objeciones y/o sugerencias que se le han formulado, ha otorgado porla calificación de:

En A Coruña, a..... de de 2020

PRESIDENTE

Dra. Rosario Hernández Galán
Catedrática
Universidad de Cádiz

SECRETARIO

Dr. Jesús Fernández Arteaga
Profesor Titular
Universidad de Huelva

VOCAL

Roberto Gomez de Souza Berlinck
Profesor Titular
Universidad de São Paulo

Firmado

Firmado

Firmado



Don Dawrin Jesus Pech Puch:

Presenta la memoria adjunta, titulada “**Productos naturales bioactivos de organismos marinos de la Península de Yucatán, México**” para optar al grado de Doctor en Química que ha sido realizado bajo la dirección de los Doctores Carlos Jiménez González y Jaime Rodríguez González en los laboratorios del Centro de Investigaciones Científicas Avanzadas (CICA) de la Universidade da Coruña.

A Coruña, a __ de febrero de 2020.

Fdo. Dawrin Jesus Pech Puch

Fdo. Carlos Jiménez González

Fdo. Jaime Rodríguez González



D. **Carlos Jiménez González** y D. **Jaime Rodríguez González** Catedráticos de Universidad, pertenecientes al Departamento de Química (Área de Química Orgánica) de la Facultad de Ciencias de la Universidade da Coruña,

Certifican:

Que la memoria adjunta, titulada “**Productos naturales bioactivos de organismos marinos de la Península de Yucatán, México**”, ha sido realizada bajo su dirección por el licenciado en Biología Marina Don **Dawrin Jesus Pech Puch**, en el Área de Química Orgánica dependiente del Departamento de Química.

Considerando que constituye trabajo de Tesis, autorizan su presentación en la Universidade da Coruña para optar al grado de Doctor en Química.

Y para que así conste, expiden el presente certificado en A Coruña, a ___ de febrero de 2020.

Fdo. Carlos Jiménez González

Fdo. Jaime Rodríguez González

Dedicatoria

Después de mas de tres años lejos del lugar al que llamamos hogar,
viviendo aventuras nuevas, aprendiendo cosas únicas y tratando
durante cada uno de estos días de adaptarnos lo mejor posible....

A mi vida y mi familia:

Mar y el pequeño Alastor

A todos los que siempre están con nosotros: Abuelas, Abuelos,
Madres, Padres, hermanas, hermanos, sobrinos, sobrinas, tíos, tías,
primos, primas, amigos, amigas y perrunos.



Navegando siempre contigo Dani!

Agradecimientos

Quiero empezar dándole las gracias a mis directores Dr. Carlos Jiménez González y Dr. Jaime Rodríguez González por permitirme formar parte de su equipo de investigación PRONAMAR integrado dentro del grupo QUIMOLMAT. Les agradezco mucho por su paciencia, tiempo, enseñanzas, confianza, pero sobretodo por hacerme sentir como uno mas dentro de este gran grupo de investigación.

A todo el personal (administrativo, docentes, técnicos e investigadores) de la Universidad de la Coruña que día a día nos permiten desarrollar nuestra investigación: Centro de Investigaciones Científicas Avanzadas (CICA-UDC), a la Facultad de Ciencias y Departamento de Química de la Universidad de la Coruña, al Servicio de Apoyo a la Investigación (SAI-UDC), a la Unidad de Apoyo a la Docencia e Investigación (UADI-UDC) y a la Escuela de Doctorado de la UDC. Así como a la Red de Infraestructuras de Apoyo a la Investigación y el Desarrollo Tecnológico (RIAIDT) de la Universidad de Santiago de Compostela (USC) y al Centro de Supercomputación de la Xunta de Galicia (CESGA) por todos los cálculos computacionales realizados.

Al Dr. Marcel Jaspars de la Universidad de Aberdeen en el Reino Unido, por abrirme las puertas del “Marine Biodiscovery Centre” (MBC), a todas las personas de dicho centro que me acogieron y me hicieron sentir como un integrante mas en su laboratorio.

Al departamento de Biología Marina de la Universidad Autónoma de Yucatán (UADY), en particular a los investigadores Dr. Carlos González Salas, Dr. Sergio Guillen Hernández y Dr. Harold Villegas Hernández, por todo su apoyo en la obtención de permisos de colecta, permisos de investigación en las áreas naturales protegidas, logística para el traslado y soporte en la recolección de los organismos.

A la Bióloga Patricia Gómez del Instituto de Ciencias del Mar y Limnología de la Universidad Nacional Autónoma de México (ICMyL-UNAM), por la identificación taxonómica de las esponjas marinas.

Al Dr. Alejandro Beceiro y su grupo de investigación del Instituto de Investigación Biomédica de A Coruña (INIBIC) por realizar los ensayos biológicos antibacterianos.

Al Dr. Javier Sánchez Céspedes y todo su grupo de investigación del Instituto de Biomedicina de Sevilla (IBiS) por realizar los ensayos biológicos antivirales.

Al Dr. Fernando Reyes y su grupo de investigación de la Fundación MEDINA en Granada por realizar los ensayos biológicos de actividad citotóxica y antiproliferativa.

A la empresa PHARMAMAR que nos dio soporte con los primeros ensayos de actividad y por permitirnos formar parte de la determinación estructural de la Nocardiomicina.

A las diversas fuentes de financiación que me fueron otorgadas:

A mi país México, que a través del Consejo Nacional de Ciencia y Tecnología (CONACYT), me fue otorgada la beca para poder cursar los primeros tres años de mis estudios de doctorado en el extranjero. Numero de CVU: 493462, Registro: 281800 y Solicitud: 440688.

A mi estado Yucatán, que por medio de la Secretaria de Investigación , Innovación y Educación Superior (SIIES), me fue financiado el transporte México-España, España-México.

Al programa “AXUDA PARA ESTADÍAS PREDOUTORAIS INDITEX-UDC 2019” por otorgarme el apoyo para poder realizar una estadía de investigación en la Reino Unido y permitirme optar por el doctorado con mención internacional.

Al proyecto “Axudas de Consolidacion de Grupos de Investigacion” , por el contrato con numero de referencia: ED431C 2018/39, que me permitió concluir en tiempo y forma mi formación como investigador.

Al programa INTERREG V A of Spain-Portugal (POCTEP) y Agrupación Estratégica CICA-INIBIC ED431E 2018/03 (Consellería de Educación, Universidades e Formación Profesional) de la Xunta de Galicia.

Al proyecto “Desarrollo de aplicaciones de los sideróforos y sus receptores de membrana para el diseño de nuevos métodos de control de infecciones bacterianas en acuicultura (SIDEROVAC)” financiado por el Ministerio de Economía y Competitividad, referencia AGL2015-63740-C2-2-R.

Al proyecto “Factores de virulencia bacterianos como dianas terapéuticas en peces: caracterización de sideróforos y desarrollo de nuevos tratamientos contra forunculosis y tenacibaculosis (SIDEROTREAT)” financiado por el Ministerio de Ciencia, Innovación y Universidades, referencia RTI2018-093634-B-C22.

A los proyectos “Ayudas para la consolidación y estructuración de unidades de investigación competitivas. Grupo de Química molecular y de materiales. QUIMOLMAT” financiados por la Xunta de Galicia, referencias GRC2014/042 y ED431C 2018/039.

Índice

Abreviaturas	1
Resumen	4
Introducción	8
Objetivos	16
CAPÍTULO 1. Precedentes de los Productos Naturales Marinos aislados de las costas de la Península de Yucatán	17
CAPÍTULO 2. Recolección, extracción y evaluación farmacológica de organismos marinos procedentes de la Península de Yucatán	48
2.1 Recolección y extracción de los organismos.....	49
2.2 Resultados de la actividad antibacteriana de los extractos.....	51
2.3 Resultados de la actividad antiviral y antiproliferativa de los extractos	76
CAPÍTULO 3. Aislamiento, elucidación estructural y evaluación farmacológica de los productos naturales marinos aislados	95
3.1 Aislamiento de productos naturales.....	96
3.2 Estudio químico de la esponja <i>Spongia tubulifera</i>	97
3.3 Estudio químico de la esponja <i>Ircinia felix</i>	127
3.4 Estudio químico de la esponja <i>Agelas dilatata</i>	174
3.5 Estudio químico de la gorgonia <i>Briareum asbestinum</i>	203
CAPÍTULO 4. Aplicación de nuevas metodologías de RMN en la determinación de la configuración relativa de productos naturales	251
4.1 Metodologías utilizadas para la determinación de la estructura tridimensional de un compuesto orgánico.....	252
4.1.1 Ejemplos de metodologías en la determinación de la configuración relativa.....	252
4.1.2 Ejemplos de metodologías en la determinación de la configuración absoluta.....	261
4.2 Determinación de la configuración relativa del briarano B-3 usando la ¹ H RCSA.....	268
4.3 Determinación de la configuración relativa de la nocardíomicina usando el análisis configuracional de RMN basado en <i>J</i> dependiente de la temperatura y en cambios de disolvente.....	274
General conclusions	297
Difusión de la investigación	300

Abreviaturas

AF	Ácido fórmico
COSY	CORrelation SpectroscopY
c	Cuadruplete
d	Doblete
Da	Dalton (unidad de masa atómica)
DCM	Diclorometano
dd	Doblete de dobletes
ddd	Doble doble doblete
DEPT	Distorsionless Enhancement by Polarization Transfer
DFT	Teoría de los funcionales de la densidad (<i>Density functional theory</i>)
DMSO	Dimetilsulfóxido
DW	Agua destilada (<i>Distilled water</i>)
ECD	Dicroísmo circular electrónico (<i>Electronic Circular Dichroism</i>)
EGDMA	Dimetacrilato de etilenglicol (<i>Ethylene glycol dimethacrylate</i>)
EMA	Agencia Europea de Medicamentos (<i>European Medicines Agency</i>)
ESI	Ionización por electroespray (<i>Electrospray ionization</i>)
FA	Acido fórmico (<i>Formic Acid</i>)
FAB	Fast Atom Bombardment
FD	Fracción de diclorometano
FDA	Administración de Alimentos y Medicamentos de Estados Unidos (<i>Food and Drug Administration</i>)
FH	Fracción de hexano
FM	Fracción de metanol/agua
FT-IR	Espectroscopia infrarroja con transformada de fourier
g	Gramo
GI₅₀	Inhibición del crecimiento del 50%
h	Hora
HMBC	Heteronuclear Multiple Bond Correlation
HPLC	Cromatografía líquida de alta eficacia (<i>High Performance Liquid Chromatography</i>)
HR	Alta resolución (<i>High Resolution</i>)
HSQC	Heteronuclear Single Quantum Correlation
HSQC-HECADE	HSQC-HECADE: Heteronuclear Couplings from ASSCI-domain Experiments with E.COSY
Hz	Hercio
IC₅₀	Concentración de inhibición del 50%
J	Constante de acoplamiento
J-HMBC	J-resolved Heteronuclear Multiple Bond Correlation
L	Litro
LC₅₀	Dosis letal del 50%
LR	Baja resolución (<i>Low Resolution</i>)
M	Concentración molar
m	Multiplete
mg	Miligramo
MHz	Megahercio
min	Minuto
mL	Mililitro
mmol	Milimol

MMA	Metacrilato de metilo (<i>Methyl Methacrylate</i>)
MMA-<i>d</i>₈	Metacrilato de metilo perdeuterado (<i>Deuterated Methyl Methacrylate</i>)
MS	Espectrometría de masas (<i>Mass Spectrometry</i>)
<i>m/z</i>	Relación masa/carga
M⁺	Ión molecular
NOESY	Nuclear Overhauser Enhancement Spectroscopy
NP	Fase Normal (<i>Normal Phase</i>)
PMMA	Polimetacrilato de metilo protonado (<i>Protonated poly methyl methacrylate</i>)
PMMA-<i>d</i>₈	Polimetacrilato de metilo perdeuterado (<i>Deuterated poly methyl methacrylate</i>)
PNM's	Productos Naturales Marinos
Poly-HEMA	Poly 2-hidroxietil metacrilato (también conocido como HEMA)
Q	Factor de calidad de Cornilescu
Q_{csa}	Factor de calidad de la anisotropía de desplazamiento químico
RDC	Acoplamiento dipolar residual (<i>Residual Dipolar Coupling</i>)
RMN	Resonancia Magnética Nuclear
RMN ¹H	RMN de protón
RMN ¹³C	RMN de carbono
ROE	Rotating-frame Overhauser Effect
ROESY	Rotating-frame Overhauser Enhancement Spectroscopy
RP	Fase reversa (<i>Reverse Phase</i>)
s	Singulete
SPE	Extracción en fase sólida (<i>Solid Phase Extraction</i>)
SVD	Single value decomposition
t	Triplete
T	Temperatura
TFA	Ácido trifluoroacético (<i>Trifluoroacetic acid</i>)
TGA	Administración de productos terapéuticos de Australia (<i>Therapeutic Goods Administration</i>)
TGI	Inhibición total del crecimiento (<i>Total Growth Inhibition</i>)
TOCSY	Total Correlation Spectroscopy
TOF	Tiempo de vuelo (<i>Time of Flight</i>)
UV	Ultravioleta
WB	Fracción butanólica
WW	Fracción acuosa
t_r	Tiempo de retención
XRD	Difracción de rayos X (<i>X-Ray diffraction</i>)
[α]^D	Rotación óptica específica
°C	Grado Celsius
1D	Monodimensional
2D	Bidimensional
δ	Desplazamiento químico en ppm (RMN)
λ	Longitud de onda
μL	Microlitro

Resumen

Esta tesis doctoral describe la primera investigación exhaustiva sobre los productos naturales marinos de organismos recolectados a lo largo de las costas de la Península de Yucatán, México. Se recolectaron un total de 65 organismos que corresponden a 55 especies diferentes de las cuales 41 son esponjas, 13 ascidias y 1 gorgonia. Se utilizó la estrategia de aislamiento bioguiado y técnicas de desreplicación, mediante las cuales pudimos obtener 31 moléculas, de las que 10 resultaron ser nuevos compuestos naturales, mostrando algunos de ellos interesantes actividades biológicas. Cabe destacar que para la determinación estructural de algunos de los nuevos compuestos se han empleado por primera vez la aplicación de dos nuevas metodologías para la determinación de la configuración relativa de productos naturales marinos: la anisotropía de desplazamiento químico de protón (^1H RCSA) y la utilización del análisis configuracional de RMN basado en J dependiente de la temperatura y en cambios de disolvente.

Capítulo 1. Se hace una recopilación de las publicaciones que recogen las investigaciones en el área de los productos naturales marinos de la península de Yucatán hasta mediados del año 2019. Esta revisión bibliográfica dio origen a una publicación en la revista *Marine Drugs* (*Mar. Drugs*. **2020**, *18*, 59).

Capítulo 2. Se describe la recolección de 65 organismos marinos en las costas de la Península de Yucatán, México y su posterior extracción para así obtener los correspondientes extractos orgánicos. A continuación, se presentan los resultados de las actividades antibacteriana, antivírica y antiproliferativa de todos los extractos obtenidos. El fraccionamiento biodirigido de uno de los extractos marinos permitió aislar e identificar los compuestos causantes de la actividad antibacteriana para la esponja *Amphimedon compressa*.

Capítulo 3. Se describe el aislamiento, la determinación estructural y la evaluación farmacológica de los compuestos puros obtenidos de las esponjas *Spongia tubulifera*, *Ircinia felix*, *Agelas dilatata* y la gorgonia *Briareum asbestinum*, organismos colectados en las costas de la Península de Yucatán, México. La elucidación estructural de las moléculas se realizó a partir de la utilización de técnicas espectroscópicas de RMN, UV e IR y espectrométricas (MS), mientras que la configuración absoluta se obtuvo a partir de cálculos computacionales (DFT), dicroísmo circular electrónico (ECD) y rayos X. Tres de los compuestos aislados de *S. tubulifera* mostraron una actividad citotóxica frente a líneas celulares de cáncer, otros dos aislados de *I. felix* presentaron una actividad antivírica muy potente frente a dos tipos de virus y finalmente dos de los metabolitos secundarios aislados de *A. dilatata* revelaron actividad frente a dos cepas bacterianas multiresistentes.

Capítulo 4. Se expone la aplicación de dos nuevas metodologías para la determinación de la configuración relativa de dos nuevos productos naturales marinos: a) el uso del RMN de protón anisotrópico (^1H RCSA) para obtener la configuración relativa del briarano B-3 a escala de microgramos de muestra y la aplicación del análisis configuracional de RMN basado en J dependiente de la temperatura y en cambios de disolvente, para determinar la configuración relativa de la nocardiomicina.

Resumo

Esta tese doutoral describe a primeira investigación exhaustiva sobre produtos naturais mariños procedentes de organismos recollidos ao longo das costas da Península de Yucatán, México. Recolléronse un total de 65 organismos, correspondentes a 55 especies diferentes, das cales 41 son esponxas, 13 ascites e 1 gorgonia. Utilizáronse a estratexia de illamento bioguideo e as técnicas de eliminación, a través das cales conseguimos obter 31 moléculas, das cales 10 atopáronse novos compostos naturais, mostrando algunhas interesantes actividades biolóxicas. Cómpre salientar que para a determinación estrutural dalgúns dos novos compostos, a aplicación de dúas novas metodoloxías para a determinación da configuración relativa dos produtos naturais mariños utilizouse por primeira vez: a anisotropía de desprazamento químico de protóns (^1H RCSA) e a uso da análise configuracional baseada en J de cambios dependentes de temperatura e solventes.

Capítulo 1. Faise unha recompilación das publicacións que recollen a investigación na área de produtos naturais mariños da Península de Yucatán ata mediados do ano 2019. Esta revisión bibliográfica deu lugar a unha publicación na revista *Marine Drugs* (*Mar. Drugs*. **2020**, *18*, 59).

Capítulo 2. Descríbese a colección de 65 organismos mariños nas costas da península de Yucatán, México e a súa posterior extracción para obter os correspondentes extractos orgánicos. A continuación móstranse os resultados das actividades antibacterianas, antivirais e antiproliferativas de todos os extractos obtidos. O fraccionamento biodireccionado dun dos extractos mariños permitiu illar e identificar os compostos que causan actividade antibacteriana para a esponxa *Amphimedon compressa*.

Capítulo 3. Descríbense o illamento, determinación estrutural e avaliación farmacolóxica dos compostos puros obtidos de esponxas *Spongia tubulifera*, *Ircinia felix*, *Agelas dilatata* e gorgonia *Briareum asbestinum*, organismos recollidos nas costas da península de Yucatán, México. A elucidación estrutural das moléculas fíxose a partir do uso de técnicas espectroscópicas RMN, UV e IR e espectrometría (MS), mentres que a configuración absoluta obtívose a partir de cálculos computacionais (DFT), dicroísmo electrónico electrónico (ECD) e raios X. Tres dos compostos illados de *S. tubulifera* mostraron unha actividade citotóxica contra as liñas celulares do cancro, outros dous illados de *I. felix* mostraron unha actividade antiviral moi potente contra dous tipos de virus e finalmente dous dos metabolitos secundarios. Os illados de *A. dilatata* revelaron actividade contra dúas cepas bacterianas multirresistentes.

Capítulo 4. Preséntase a aplicación de dúas novas metodoloxías para a determinación da configuración relativa de dous novos produtos naturais mariños: a) o uso de protóns anisotrópicos RMN (^1H RCSA) para obter a configuración relativa da escala de briarano B-3 de microgramos de mostra e a aplicación de análises configuracional de RMN baseada en J dependente da temperatura e cambios de disolventes para determinar a configuración relativa da nocardiomicina.

Abstract

This doctoral thesis describes the first exhaustive research on marine natural products from organisms collected along the coasts of the Yucatan Peninsula, Mexico. A total of 65 organisms were collected that correspond to 55 different species of which 41 are sponges, 13 ascidians and 1 gorgonian. The bioguided isolation strategy and dereplication techniques were used, through which we were able to obtain 31 molecules, of which 10 were found to be new natural compounds, showing some of them interesting biological activities. It should be noted that for the structural determination of some of the new compounds, the application of two new methodologies for the determination of the relative configuration of marine natural products has been used for the first time: the proton chemical shift anisotropy (^1H RCSA) and the use of variable temperature and solvent dependent NMR *J*-based configurational analysis.

Chapter 1. A compilation is made of the publications that collect the research in the area of marine natural products of the Yucatan Peninsula until the middle of the year 2019. This bibliographic review gave rise to a publication in the journal *Marine Drugs* (*Mar. Drugs*. **2020**, *18*, 59).

Chapter 2. The collection of 65 marine organisms on the coasts of the Yucatan Peninsula, Mexico and their subsequent extraction is described in order to obtain the corresponding organic extracts. The results of the antibacterial, antiviral and antiproliferative activities of all the extracts obtained are presented below. The biodirected fractionation of one of the marine extracts allowed to isolate and identify the compounds that cause antibacterial activity for the *Amphimedon compresssa* sponge.

Chapter 3. The isolation, structural determination and pharmacological evaluation of the pure compounds obtained from sponges *Spongia tubulifera*, *Ircinia felix*, *Agelas dilatata* and gorgonian *Briareum asbestinum*, organisms collected on the coasts of the Yucatan Peninsula, Mexico, are described. The structural elucidation of the molecules was made from the use of NMR, UV and IR and spectrometric (MS) spectroscopic techniques, while the absolute configuration was obtained from computational calculations (DFT), electronic circular dichroism (ECD) and X-rays. Three of the compounds isolated of *S. tubulifera* showed a cytotoxic activity against cancer cell lines, two other compounds isolated of *I. felix* showed a very potent antiviral activity against two types of viruses and finally two of the secondary metabolites isolated of *A. dilatata* revealed activity against two multiresistant bacterial strains.

Chapter 4. The application of two new methodologies for the determination of the relative configuration of two new marine natural products is presented: a) the use of anisotropic proton NMR (^1H RCSA) to obtain the relative configuration of the briarane B-3 in scale of micrograms of sample and the application of the variable temperature and solvent dependent NMR *J*-based configurational analysis to determine the relative configuration of nocardiomycin.

Introducción

Aunque un “Producto Natural” (PN) estrictamente hablando, es todo compuesto orgánico producido por cualquier organismo viviente, este término suele identificarse con el de metabolito secundario y con moléculas relativamente pequeñas cuyo peso molecular es menor a 1500 Da. Los metabolitos secundarios se caracterizan, a diferencia de los primarios, por el hecho de que: no parecen ser esenciales a los organismos en los que se encuentran; suelen ser específicos de una especie o grupo de organismos (ya sea género, familia, clase, etc.); se cree que realizan una función ecológica en el organismo del que se aísla, relacionada en muchas ocasiones con el mecanismo químico de defensa frente a otros organismos; su producción se realiza durante estados muy específicos de su crecimiento y está influenciada en gran medida por el medio y las condiciones que lo rodean (adaptación); y se producen generalmente en muy pequeña cantidad.^{i,ii}

Los registros mas tempranos sobre productos naturales se encontraron en tabletas de arcilla en escritura cuneiforme. Por ejemplo, en Mesopotamia (2600 AC) se documentaron los aceites de *Cupressus sempervirens* (Ciprés) y *Commiphora* (Mirra), que todavía se usan para tratar la tos, resfriados e inflamaciones. El papiro Ebers (2900 AC), es un registro farmacéutico egipcio que documenta más de 700 medicamentos a base de plantas, desde gárgaras, píldoras, infusiones hasta ungüentos. En relación con la medicina tradicional china (1100 AC), es de destacar las obras: Wu Shi Er Bing Fang (contiene 52 recetas), Shennong Herbal (aproximadamente 100 AC, 365 medicamentos) y Tang Herbal (659 DC, 850 medicamentos) que constituyen registros documentados importantes de los usos de productos naturales.ⁱⁱⁱ Entre las principales figuras destacadas en Europa se encuentran, el filósofo y científico natural, Teofrasto (aproximadamente 300 AC) el cual en su libro “Historia de las plantas”, se encargó de describir los usos medicinales de las plantas y señaló la capacidad de éstas para cambiar sus características a través del cultivo; mientras que el médico griego Dioscorides (100 DC) durante sus viajes con ejércitos romanos, llevo a cabo el registro de las colecciones, el almacenamiento y los usos de las hierbas medicinales. Toda esta larga tradición en el uso de productos naturales apenas se preservó durante la Edad Media, siendo los monasterios de Inglaterra, Irlanda, Francia y Alemania los encargados de conservar parte de estos conocimientos.ⁱⁱⁱ Pero fueron los árabes los que mejor conservaron y expandieron parte del conocimiento grecorromano sobre los usos de sus propios recursos, junto con las hierbas chinas e indias que no eran familiares para el mundo grecorromano en esos años. Así, los árabes fueron los primeros en poseer farmacias privadas en donde trabajaba un farmacéutico, medico, filosofo y poeta persa, conocido como Avicena, quien contribuyó de manera significativa al desarrollo de las ciencias de la farmacia y la medicina a través de obras como Canon Medicinæ.ⁱⁱⁱ

Aunque el uso de productos naturales como fármacos se ha descrito a lo largo de la historia en forma de medicamentos tradicionales, remedios, pociones y aceites, muchos de los productos naturales responsables de la actividad aún no habían sido identificados. La fuente dominante de conocimiento de los usos de los productos naturales de plantas medicinales es un resultado de la experimentación del hombre a través del ensayo y error durante cientos de años y mediante pruebas de palatabilidad ó muertes prematuras en busca de remedios disponibles para el tratamiento de enfermedades.^{iii,iv} Un ejemplo es el género de plantas *Salvia*, que crece en toda la región del suroeste de los Estados Unidos, así como el noroeste de México y que fue utilizado por las tribus indias del sur de California como ayuda en el parto. Los bebés recién nacidos eran depositados sobre las cenizas calientes de *Salvia*, ya que se creía que de esta forma se hacían inmunes a todas las enfermedades respiratorias de por vida.ⁱⁱⁱ

Las prácticas medicinales tradicionales constituyeron la base de la mayoría de los primeros fármacos mucho antes de los estudios clínicos, farmacológicos y químicos actuales.^{iv} Probablemente, el ejemplo más famoso y conocido hasta la fecha el desarrollo del analgésico, el ácido acetilsalicílico (aspirina) derivado del producto natural salicina que se obtiene de la corteza del árbol de sauce *Salix alba*.^v El estudio de *Papaver somniferum* (amapola de opio) trajo consigo el aislamiento del primer producto natural puro, la morfina, reportada por primera vez en 1803 y que es uno de los mejores analgésicos que se conocen. Cuando en la década de 1870 la morfina bruta derivada de la planta *P. somniferum* se hirvió en anhídrido acético para producir diacetilmorfina (heroína) se encontró que era fácil convertirla en codeína (analgésico). Historicamente, hay registros de que los sumerios y los griegos en la antigüedad utilizaban extractos de amapola con fines medicinales, mientras que los árabes ya describían el opio como adictivo.^v

Las plantas fueron la primera fuente importante de productos naturales y todavía sigue siendo una de las más utilizadas. En la actualidad, los PN obtenidos de plantas son los que presentan un mayor rango de aplicaciones farmacológicas. Teniendo en cuenta que hay aproximadamente unas 250 000 especies de angiospermas (plantas con flores) y 700 de gimnospermas, y que aún quedan el 90% de las angiospermas por estudiar, nos da idea de la enorme tarea que queda por hacer en este campo. Uno de los ejemplos más espectaculares y recientes de los últimos años es la comercialización de Taxol®, aislado del árbol *Taxus brevifolia*, que se utiliza como compuesto anticanceroso para el tratamiento del cáncer de ovario.^{v,vi}

Por otro lado los microorganismos, como los hongos, han sido utilizados por los humanos durante miles de años. Fueron empleados en la preparación de bebidas alcohólicas (levaduras), medicamentos en medicina tradicional e incluso con fines culturales. Actualmente con los avances en microbiología, sus usos se han extendido en el control biológico, en la obtención de enzimas, de antibióticos y de otros productos farmacológicamente activos.^{iv}

Sin duda, uno de los descubrimientos de productos naturales más espectaculares derivados de un hongo (*Penicilium notatum*) es el de la penicilina, que fue descubierta accidentalmente por Fleming en 1929.^{vii} Este descubrimiento dio lugar al aislamiento, estudios clínicos y comercialización de penicilinas sintéticas, que finalmente revolucionaron la investigación en el descubrimiento de fármacos.^{viii} Después de la publicación de los primeros datos clínicos sobre la Penicilina G entre 1942 y 1944, hubo un esfuerzo mundial para descubrir nuevos antibióticos y productos naturales bioactivos a partir de microorganismos.^{ix} En 1953, Edmundo Kornfeld aisló por primera vez la vancomicina, un antibiótico glicopeptídico producido en cultivos de *Amycolatopsis orientalis*, que es activo contra una amplia gama de organismos grampositivos como estafilococos y estreptococos, así como contra bacterias gramnegativas, micobacterias y hongos, siendo aprobado como fármaco por la FDA en 1958.^{vii}

Por todo lo anterior, no es sorprendente que aproximadamente el 80 % de la población mundial siga dependiendo principalmente de medicamentos tradicionales todavía.^x Los datos de auditoría nacional con receta en 1976 ya mostraban que aproximadamente el 40 % de las prescripciones de Estados Unidos contenían productos naturales derivados de plantas y microorganismos.^x

Si tenemos en cuenta las últimas décadas, la naturaleza sigue siendo una fuente directa o de inspiración para el desarrollo de numerosos fármacos, como lo demuestra el hecho de que más del 60% de los nuevas entidades químicas aprobadas por las autoridades sanitarias en el período comprendido entre 1981-2010 tienen alguna relación estructural con la de un producto natural.^{xi,xii}

Si bien las plantas y microorganismos terrestres han demostrado ser una fuente novedosa de productos bioactivos, el ambiente marino constituye una fuente alentadora al ofrecer también nuevas entidades estructurales. El reconocido químico de Productos Naturales Marinos (PNMs) William Fenical afirmó: “No somos organismos marinos, así que hasta alrededor de 1970 nadie pensó en el océano y fue dejado como un profundo secreto. Me parecía ridículo que el océano, con un hábitat tan vasto, hubiera escapado a la atención de alguien, pero hay buenas razones, la gente teme al océano, ya que lo ha sido considerado un lugar hostil e inhóspito”.^{xiii} Dado el hecho de que más del 70 % de la superficie de la Tierra está cubierta por océanos y teniendo en cuenta además la rica biodiversidad del mar (varios filos del reino animal, como el Porífera y Bryozoa son exclusivamente acuáticos) estas esperanzas parecen realmente justificadas.^{xiv,xv}

Productos naturales marinos

Las primeras investigaciones en el campo de la química de los PNM_s se mostraron en un pequeño congreso organizado en 1967 en Rhode Island, EEUU, bajo el título “Drogas procedentes del mar”. El título, un tanto ambicioso y escéptico, es un eslogan que ha perdurado a lo largo de las décadas como una metáfora para el desarrollo de medicamentos a partir de productos naturales marinos.^{xvi} Actualmente, el desarrollo de fármacos cuya fuente son productos naturales de origen marino se ha ido convirtiendo en realidad, tal como lo demuestra el auge que tuvo este campo en los últimos 50 años. Esta exploración se ha justificado por el gran número de compuestos marinos encontrados, como el ácido okadaico, un compuesto producido por dinoflagelados que actúa como inhibidor de las proteínas fosfatasa 1 y 2A y la xestospongina C, un metabolito de una esponja marina con actividad bloqueante intercelular.

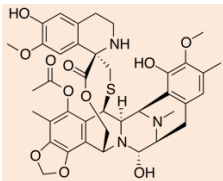

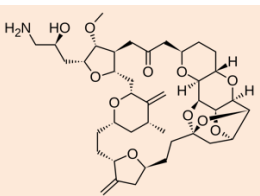

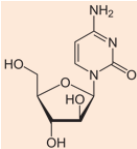

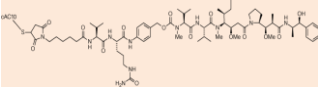

Sin embargo, la exploración del medio marino y los organismos (algas, esponjas, tunicados y briozoos) fue posible gracias a las técnicas de buceo libre moderno, la introducción del sistema de buceo autónomo (SCUBA en 1970), el uso de sumergibles tripulados (1980) y más recientemente el uso de vehículos operados remotamente (ROV) (1990), mientras que por la parte de química fue posibilitado por, el avance en las técnicas cromatográficas y de elucidación estructural principalmente la RMN. A finales de los años 50, la búsqueda de fármacos de procedencia marina ya había atraído algún interés con la publicación de tres artículos por Werner Bergmann, sobre tres arabino- y ribopentosilnucleósidos inusuales aislados de unas esponjas recolectadas en Florida. Estos compuestos fueron la base del desarrollo de los fármacos Ara-A (vidarabina) y Ara-C (citarabina), dos nucleósidos con actividad anticancerosa y antiviral respectivamente, que han sido usados clínicamente durante décadas.^{xvi}

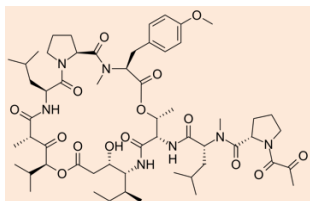
El papel de los productos naturales en la búsqueda de compuestos con aplicaciones farmacológicas ha sufrido muchos cambios en los pasados 50 años. Aunque desde mediados de los años 90 se produjo un declive en el interés de las compañías farmacéuticas por los PN, sin embargo continuaron existiendo grupos de investigación académicos emprendedores en este campo, la mayoría asociados con la industria. Además, en los últimos diez años en el campo de los PN se puede apreciar un cierto renacimiento, gracias al desarrollo de nuevas metodologías analíticas, espectroscópicas, espectrométricas y de los denominados ensayos de alta producción (high-throughput screening)^{xvii,xviii} que junto con la decadencia de algunas estrategias que se pensaban prometedoras, como fue la química combinatoria, han logrado impulsar de nuevo a esta disciplina.

El primer compuesto de origen marino comercializado tal como se aisló de su fuente natural y que se utiliza con fines farmacológicos fue ω -conotoxina MVIIA

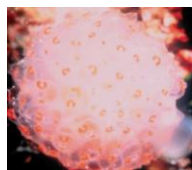
(ziconotide/Prialt®), un péptido aislado de un caracol marino de aguas tropicales que fue aprobado en 2004 para el tratamiento de dolor crónico en los EE.UU. El segundo compuesto fue el antitumoral desarrollado por la empresa española PharmaMar, ecteinascidina-743, (ET-743/Yondelis®/Trabectedina). Aislado de un tunicado tropical fue aprobado por la Agencia Europea del Medicamento (EMA) en octubre de 2007 para el tratamiento de cáncer de tejido blando. Además de los dos compuestos anteriores, otros seis han sido aprobados por diferentes agencias de medicamentos, mostrando actividades antivirales, cardiovasculares y anticancerosas (Tabla 1).^{xix}

Tabla 1. Productos naturales marinos aprobados como fármacos en el mundo.

Nombre genérico y estructura química	Organismo donde fue aislado	Nombre comercial	Aprobado por	Área terapéutica
 <p>Trabectedina (ET-743)</p>	 <p>Tunicado <i>Ecteinascidia turbinata</i></p>	Yondelis®	EMA-2007 FDA-2015	Cáncer
 <p>Mesilato de eribulina (E7389)</p>	 <p>Esponja <i>Halichondria okadai</i></p>	Havalen®	FDA-2010	Cáncer
 <p>Citarabina (Ara-C)</p>	 <p>Esponja <i>Tethya cripta</i></p>	Cytosar-U®	FDA-1969	Cáncer
 <p>Brentuximab vedotin (SNG-35)</p>	 <p>Liebre marina <i>Dolabella auricularia</i></p>	Adcetris®	FDA-2011	Cáncer



Plitidepsina

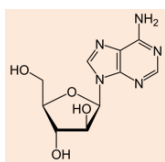


Tunicado
Applidium albicans

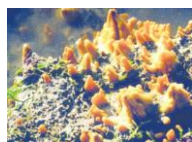
Aplidin®

TGA-2018

Cáncer



Vidarabina
(Ara-A)

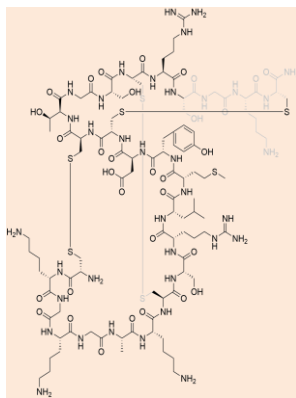


Esponja
Tethya crypta

Vira-A®

FDA-1976

Antiviral



Ziconotide

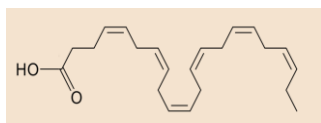
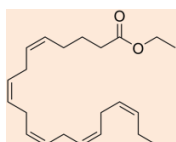


Conido
Conus magus

Prialt®

FDA-2004

Analgésico



Omega-3-acidoetil ésteres



Peces

Lovaza®

FDA-2004

Cardiovascular

Los productos naturales marinos abarcan una gama de estructuras desde muy simples hasta muy complejas. Afortunadamente con el avance tecnológico en la capacidad de análisis estructural de moléculas orgánicas, ha sido posible determinar la estructura completa de compuestos naturales tan complejos como la palitoxina, que cuenta con 64 centros estereogénicos. Sin embargo, la presencia de varios centros estereogénicos, no solo en la palitoxina, sino en la mayoría de los productos naturales marinos ha dificultado su síntesis para realizar tanto estudios preclínicos como su comercialización.^{xx}

La mayor dificultad que encuentra el desarrollo de compuestos naturales de origen marino como fármacos radica en el problema de suministro, es decir, en la obtención de la suficiente cantidad de producto que permita realizar los ensayos farmacológicos y su posterior comercialización. Por ejemplo, las esponjas marinas, que son la fuente de muchos compuestos bioactivos tales como discodidermólido y hemiasterlina, son metazoos muy primitivos que viven exclusivamente en hábitats marinos y que la obtención de los compuestos de interés a partir de su cultivo en cautividad se ve dificultada debido a la necesidad de la presencia de una fauna microbiana asociada para que los produzcan. Por esta razón, los compuestos de interés deben de ser extraídos y purificados de los especímenes en su medio natural, que en el caso de que sean recolectados mediante buceo en aguas muy profundas, requieren la ayuda de sumergibles provistos de un brazo robótico que encarece todavía más dichas recolecciones. Por ello, el desarrollo de los sistemas de acuicultura de ciertos invertebrados marinos sería crucial como uno de los métodos para intentar de solventar los problemas de suministro.^{xx}

Aproximadamente 29 000 PNMs han sido aislados hasta la fecha^{xxi}, los cuales poseen estructuras inusuales y completamente diferentes a los productos naturales aislados de organismos terrestres. Esta gran variedad estructural en los PNMs se puede atribuir a la necesidad de producir metabolitos secundarios como herramientas de defensa para poder sobrevivir en los ambientes extremos de temperatura, salinidad, presión y competencia.^{xxii}

Los principales grupos y filos de organismos marinos que han sido estudiados para la búsqueda de PNMs hasta ahora se pueden agrupar en: macroorganismos, incluyendo a Porifera (esponjas) Cnidaria (corales, anémonas y medusas), Mollusca (principalmente nudibranchios y conidos), Bryozoa (briozoarios), Chordata (tunicados y ascidias), Echinodermata (principalmente pepinos de mar) Dinophyta (dinoflagelados), Chlorophyta (algas verdes), Ochrophyta (algas pardas), Rhodophyta (algas rojas), Tracheophyta (pastos marinos y mangles) y microorganismos Proteobacteria, Actinobacteria, Cyanobacteria y Ascomycota (hongos).^{xxiii}

Hasta el año 2017, más del 60 % de los PNMs habían sido aislados de tan solo tres filos, Porifera, Cnidaria and Ascomycota. En el periodo comprendido de 1971 a 2015 más del 30 % de los PNMs se habían aislado de las esponjas. Sin embargo, en los últimos años (2012-2017) tuvo lugar un incremento en el número de nuevos compuestos aislados de microorganismos. Por otra parte el 79.7 % de los productos naturales marinos han sido descubiertos en el hemisferio norte, mientras que el restante 20.3 % de los compuestos fueron encontrados en el hemisferio sur.^{xxiii} En relación a los estudios farmacológicos, la mayoría de las evaluaciones estuvieron enfocadas hasta el año 2004 en las actividades: antitumoral (41 %), antibiótica (20 %), uso en agricultura (6 %), antiviral (5 %), antiinflamatoria (3 %) e inmunomoduladora (1 %).^{xxiii}

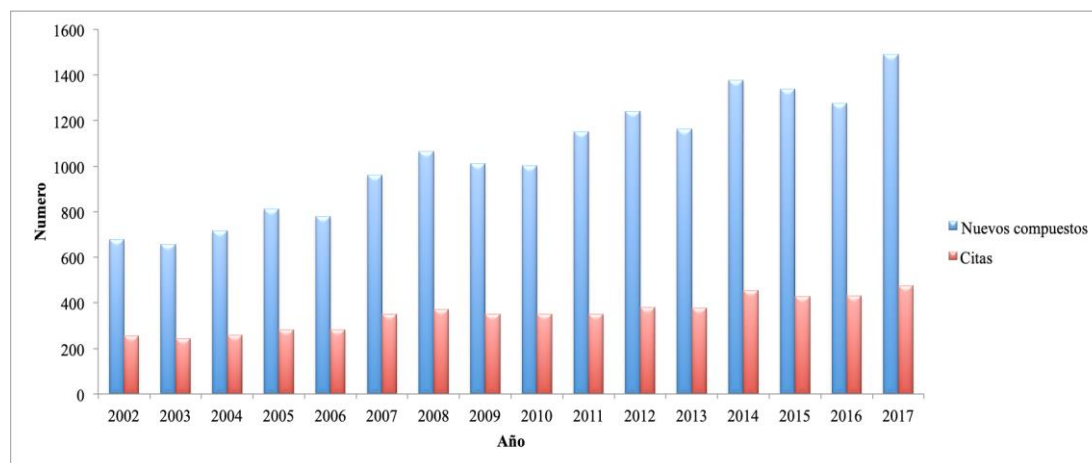


Figura 1. Número de productos naturales marinos aislados durante el periodo 2002-2017.

Entre el periodo comprendido entre el año 2002 y 2017 se aprecia un incremento considerable en el numero de nuevas entidades aisladas, pasando de 677 a 1490 nuevos PNM, y de 257 a 477 documentos publicados (citas) respectivamente (Figura 1).^{xxiii} En los últimos años, se han descrito un número significativo de nuevos metabolitos con potentes propiedades farmacológicas a partir de los organismos marinos. Aunque todavía son muy pocos los fármacos comercializados derivados de compuestos aislados de organismos marinos, en la actualidad existen al menos 22 productos naturales marinos que se encuentran en alguna de las fases de análisis clínico (III, II ó I).^{xxiv}

Referencias

- i. a) Jiménez C. *An. Quim.* **2013**, *109*, 134-141. b) Rodríguez, J. *An. Quím* **2003**, *1*, 5-13.
- ii. Colegate S.M.; Molyneux R.J. in *Bioactive Natural Products: Detection, Isolation and Structure Determination* (ed. CRC Press) 421, Boca Raton, FL, USA, **2008**.
- iii. Cragg G.M.; Newman D.J. *Pure Appl. Chem.* **2005**, *77*, 7-24.
- iv. Kinghorn A.D.; Pan L.; Fletcher J.N.; Chai H. *J. Nat. Prod.* **2011**, *74*, 1539-1555.
- v. Dias D.A.; Urban S.; Roessner U. *Metabolites* **2012**, *2*, 303-336.
- vi. Cseke L.J.; Kirakosyan A.; Kaufmann P.B.; Warber S.L.; Duke J.A.; Briemann H.L. in *Natural Products from Plants* (2nd ed. CRC, Taylor and Francis) 640 Boca Raton, FL, USA, **2006**.
- vii. Alder A.L., in *The History of Penicillin Production* (ed. American Institute of Chemical Engineers) 100 New York, NY, USA, **1970**.
- viii. Mann J. in *The Elusive Magic Bullet: The Search for the Perfect Drug* (ed. Oxford University Press) 209 New York, NY, USA, **1999**.
- ix. Fabbretti A.; Gualerzi C.O.; Brandi L. *FEBS Lett.* **2011**, *585*, 1673-1681.
- x. Cragg G.M.; Newman D.J.; Snader K.M. *J. Nat. Prod.* **1997**, *67*, 52-60.
- xi. Li J.W.H.; Vederas J. C. *Science* **2009**, *325*, 161.
- xii. Newman D. J.; Cragg G. M. *J. Nat. Prod.* **2012**, *75*, 311.
- xiii. Marris E., *Nature* **2006**, *443*, 904-905.
- xiv. Capon J.R. *Eur. J. Org. Chem.* **2001**, *4*, 633.
- xv. Haefner B. *Drug Discov. Today* **2003**, *8*, 536-544.
- xvi. Molinski T.F.; Saludes J.P., *Nat. Rev. Drug. Discov.* **2009**, *8*, 69-85.
- xvii. Koehn F.E.; Carter G.T. *Nature Rev. Drug Discovery* **2004**, *4*, 206.
- xviii. Jarvis L. M. *Chem. Engin. News* **2007**, *85*, 22.

- xix. Jiménez C. *ACS Med. Chem. Lett.* **2018**, *9*, 959–961.
- xx. Mendola D. In *Drugs from the Sea* (ed. Fusetani) 133, Karger, Basilea, **2000**.
- xxi. Moghadamtousi S.Z.; Nikzad S.; Kadir H.A.; Abubakar S.; Zandi K. *Mar. Drugs* **2015**, *13*, 4520-4538.
- xxii. Romano G.; Costantini M.; Sansone C.; Lauritano C.; Ruocco N.; Ianora A. *Mar. Environ. Res.* **2017**, *128*, 58–69.
- xxiii. Carroll A.R.; Copp B.R.; Davis R.A.; Keyzers R.A.; Prinsep M.R. *Nat. Prod. Rep.* **2019**, *36*, 122 y artículos de la serie.
- xxiv. Pereira F. *Expert. Opin. Drug Discov.* **2019**, *14*, 717-722.

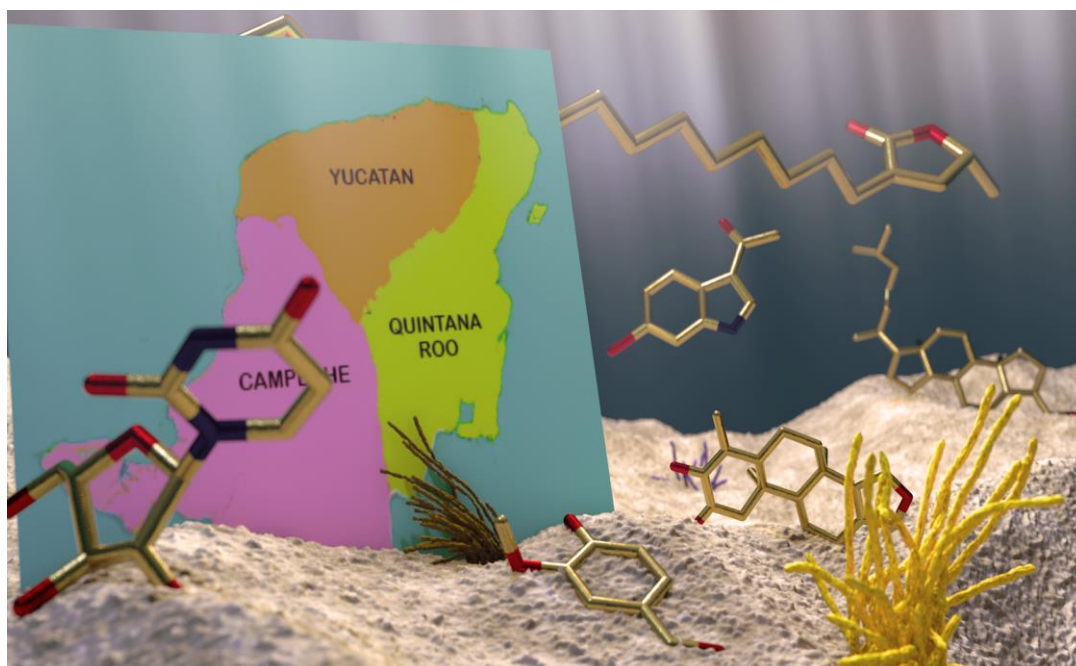
Objetivos

El objetivo general de esta tesis es el descubrimiento de nuevos productos naturales bioactivos procedentes de invertebrados recolectados en las costas de la Península de Yucatán, México. Para alcanzar este objetivo general se proponen cuatro objetivos específicos:

- a) Recolección de los organismos de estudio (esponjas, ascidias o gorgonias), identificación taxonómica de las especies colectadas y generación de los extractos crudos y fracciones.
- b) Selección de los organismos a estudiar en base a los criterios de actividad biológica y desreplicación de sus extractos y fracciones.
- c) Aislamiento, elucidación y determinación de la estructura química tridimensional de los compuestos mediante técnicas espectroscópicas, espectrométricas y cálculos computacionales.
- d) Evaluación de la actividad antibacteriana, antivírica y antiproliferativa de los productos naturales aislados.

CAPÍTULO 1

**Precedentes de los
Productos Naturales
Marinos aislados de las
costas de la Península de
Yucatán**



En este primer capítulo se presentan los precedentes bibliográficos sobre las investigaciones relacionadas con los productos naturales de origen marino aislados de las costas de la Península de Yucatán, México, hasta mediados del año 2019. Para enmarcar estos precedentes se realizaron búsquedas en las bases de datos y plataformas científicas: SciFinder, Google académico, Web of Science, Scopus, así como las páginas de los principales centros de investigación, instituciones e investigadores que desarrollan líneas afines a los PNM en Yucatán, México (Universidad Nacional Autónoma de México (UNAM), Centro de Investigaciones Científicas Avanzadas (CINVESTAV), Universidad Autónoma de Yucatán (UADY), etc.).

Esta recopilación representa la primera revisión sobre los PNM de la Península de Yucatán, México. Se analizaron 95 documentos científicos, los cuales permitieron conocer que se han estudiado 145 especies de organismos marinos pertenecientes a 12 filos con fines de bioprospección o aislamiento de PNM, destacándose que hasta el 2019 se han aislado tan sólo 66 metabolitos secundarios de 18 especies diferentes de organismos marinos.

Los PNM encontrados se han clasificado en 4 grupos y 10 subgrupos siguiendo los criterios de origen biogénico, de acuerdo a las siguientes categorías: policétidos (policétidos alifáticos, glicolípidos y ácidos aromáticos), terpenoides (diterpenos, sesterpenos, esteroides y saponinas triterpénicas), compuestos nitrogenados (derivados de indoles, nucleósidos, bases nitrogenadas y conotoxinas) y biopolímeros. Para cada uno de los PNM se presenta una descripción sobre la información que existe del mismo: determinación de su estructura tridimensional, ensayos de actividad biológica, organismos de donde se aislaron y lugar de recolección.

Esta revisión bibliográfica se ha publicado en la revista *Marine Drugs* (*Mar. Drugs* **2020**, *18*, 59).

Marine Natural Products from the Yucatan Peninsula

Dawrin Pech-Puch, Mar Pérez-Povedano, Oscar A. Lenis-Rojas,¹ Jaime Rodríguez,* and Carlos Jiménez*

Centro de Investigacións Científicas Avanzadas (CICA) e Departamento de Química, Facultade de Ciencias, Universidade da Coruña, 15071 A Coruña, Spain

* Correspondence: Centro de Investigacións Científicas Avanzadas (CICA) e Departamento de Química, Facultad de Ciencias, Universidade da Coruña, 15071 A Coruña, Spain. Tel: +34 981 167000. Fax: +34 981 167065. *E-mail address*: jaime.rodriguez@udc.es (Jaime Rodríguez); carlos.jimenez@udc.es, (Carlos Jiménez).

Abstract: Mexico is one of the three areas of the world with the greatest terrestrial and cultural biological diversity. The diversity of Mexican medicinal flora has been studied for a long time and several bioactive compounds have been isolated. Even though the Yucatan Peninsula occupies 17.4% of the total of the Mexican coast, with a great biological diversity in its coasts and the ocean, the investigation of marine resources and particularly the potential of Mexican marine resources has not been intensively investigated. There are very few studies on the chemistry of natural products from marine organisms collected along the coasts of the Yucatan Peninsula and most of them are limited to the evaluation of the biological activity of their organic extracts. The investigations carried out on marine species from the Yucatan Peninsula resulted in the identification of a wide structural variety of natural products that include polyketides, terpenoids, nitrogen compounds and biopolymers with cytotoxic, antibacterial, antifouling and neurotoxic activities. This review describes the literature of bioprospecting and the exploration of the natural product diversity of marine organisms from the coasts of the Yucatan Peninsula up to the mid 2019.

Keywords: Natural Products; Yucatan Peninsula; Marine Biodiversity

¹Present address: Instituto de Tecnologia Química e Biolóxica António Xavier, ITQB, Av. da República, EAN, 2780-157 Oeiras, Portugal

1. Introduction

Due to the extremely rich biodiversity of the marine environment, the potential of marine natural products in drug discovery is invaluable. The marine environment contains a large number of species which are the source of a wide range of structurally diverse bioactive secondary metabolites. Approximately 29,000 marine natural products are known, from which eight compounds have become commercialized drugs. During the last decade, more than 1000 new marine natural products have been annually isolated, but the set of new and unique structures is far from being exhausted [1][2]. The interest in marine organisms has been increasing, since they are capable of producing a great diversity of novel metabolites such as unusual nucleosides, bioactive terpenes, sterols, cyclic peptides, alkaloids, fatty acids, peroxides and amino acid derivatives, many of them with high potential for pharmacological applications [3].

The Yucatan Peninsula in Mexico, which comprises the Mexican states of Campeche, Quintana Roo and Yucatan, is known as a biotic province [4]. Although marine organisms constitute a recognized source of a wide range of structurally diverse natural products, research focused on marine natural products from the Yucatan Peninsula is still in infancy, mainly when compared to the numerous studies of those isolated from terrestrial organisms, especially from plants [5].

On the other hand, a priority task for the conservation and management of coastal areas, such as the Yucatan Peninsula, and for the discovery of new sources of novel natural products, is the study of their biodiversity. The first effort aimed at determining the state of health of the coast of the Yucatan Peninsula was reported in 2010. Pech-Pool and Ardisson Herrera described the identification of more than 400 thousand organisms from marine and coastal environments and lagoons, belonging to 529 species which were distributed in 13 phyla, 26 classes, 28 orders, 113 families, and 358 genera. Of the registered species, 45% (237) corresponded to the Arthropod (Crustacea); 22% (118) to Mollusca; 14% (72) to the Nematoda and 13% (68) to the Annelida phyla. The remaining 6% (33) belonged to the Echinodermata, Nemertea, Platyhelminthes, Sipuncula, Porifera, Chaetognatha, Chordata and Cnidaria phyla [6]. More specifically, taxonomic identification of coral and sponges was also described. Thus, from a total of 31 registered coral species, 15 corresponded to order Scleractinia, being Poritidae and Faviidae the most important families which were represented by four species each; other 15 species were octocorals, 7 of them belonged to Plexauridae family, and finally, the remaining species was a hydrocoral [7]. On the other hand, most of the registered sponges belonged to three classes: Calcarea, Hexactinellidae and Demospongiae, the last being the most predominant and with the greatest diversity. The 50 species registered were distributed in 10 orders, 2 subclasses, 25 families and 35 genera [8]. The results of studies focused on marine biodiversity in specific benthic communities were also reported. For example, the biodiversity analysis of the Alacranes Reef, one of the largest platform-type reefs in Mexico, covering an approximate area of 333.7 km², showed that this benthic community consists mainly of macroalgae (50.1%), seagrass (16.2%), algal mat (13.6%), scleractin corals (11.1%), octocorals (7.6%), sponges (0.6%) and other vagile and sessile organisms (0.5%) and hydrocorals (0.3%) [9]. A very recent report published in 2019 describes 31 ascidian species from the Yucatan Peninsula which were grouped into 13 families and 19 genera, being two species, *Clavelina* sp. and *Pyura* sp., described for the first time [10].

With the present review, we will cover the current knowledge of bioprospecting and the exploration of the natural product diversity of marine organisms collected along the coasts of Yucatan Peninsula up to the mid 2019.

2. Marine Natural Products from the Yucatan Peninsula

Although the number of secondary metabolites isolated from marine organisms collected along the coasts of the Yucatan Peninsula is not very high, they display a great diversity of structures and biological activities. Based upon the putative biogenetic origins, they can be grouped into the following categories as polyketides (aliphatic polyketides, glycolipids, and aromatic acids), terpenoids (diterpenes and sesterterpenes, steroids, and triterpenoids saponins), nitrogen compounds (indole derivatives, nucleosides, nitrogenous bases, and conotoxins), and biopolymers.

The following sections show a detailed list of the isolated natural products from the reported species along with their biological activities, as well as the taxonomic identification of marine organisms from which they were obtained.

2.1. Polyketides

2.1.1. Aliphatic polyketides

The interest in the study of fatty acid derivatives from marine organisms, specifically ω -3 polyunsaturated fatty acids, was sparked from the approval of Lovaza® by the FDA as a mixture of ethyl esters of eicosapentanoic acid and docosahexaenoic acid as a therapeutic agent for reducing serum triglycerides [1]. The Italian researcher group led by Cimino from Naples published in 1999 the isolation and structure elucidation of three new fatty acid derivatives, the butenolic lipids **1-3** from the gorgonian *Pterogorgia anceps*, collected at Puerto Morelos, Quintana Roo state. The new fatty acid derivatives were identified as (*R*)-3-hexadecyl-5-methylfuran-2(5*H*)-one (**1**), (*R*)-3-(14-((3*S*,4*R*,5*R*)-4-hydroxy-5-methyl-2-oxotetrahydrofuran-3-yl)tetradecyl)-5-methylfuran-2(5*H*)-one (**2**), and (*R*)-4-hydroxy-5-methyl-3-(14-((*R*)-5-methyl-2-oxo-2,5-dihydrofuran-3-yl)tetradecyl)furan-2(5*H*)-one (**3**). The proposed stereochemistry was confirmed by acetylation of **2** and **3** to give the acetate derivatives **4** and **5**, respectively [11]. Palmitic acid (**6**) was also isolated from the sponge *Haliclona tubifera* (now *H. (Reniera) tubifera*) collected on the coasts of the Yucatan state [12] (Figure 1).

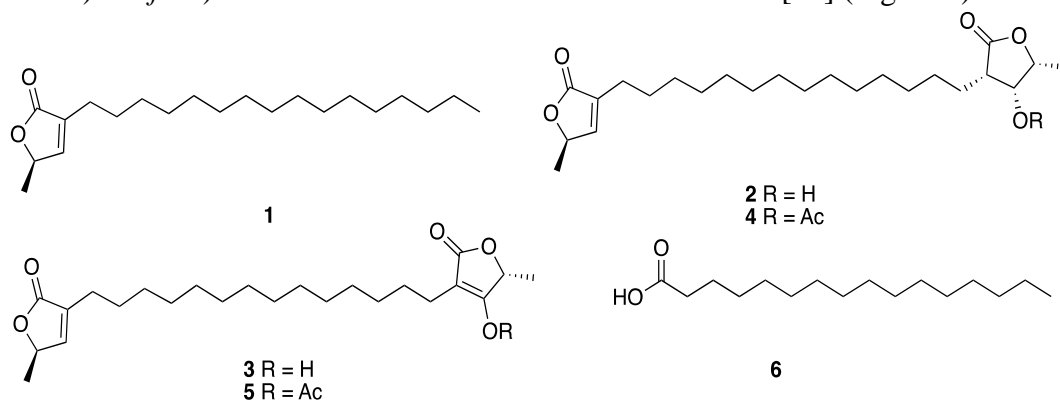


Figure 1. Structures of the aliphatic polyketides **1-3**, along with their synthetic acetate derivatives **4** and **5**, isolated from the gorgonian *Pterogorgia anceps* and palmitic acid (**6**) isolated from the sponge *Haliclona tubifera* (now *H. (Reniera) tubifera*).

2.1.2. Glycolipids

Marine glycolipids are amphiphilic compounds which are divided into two main groups: glycoacylglycerolipids (GALs) and glycosphingolipids (GSLs). Glycoacylglycerolipids are composed by a glycerol unit glycosylated at one primary alcoholic function. Sulfoquinovosyldiacylglycerols constitute one of the most common types of glycoacylglycerolipids (GALs) found in marine organisms and some of them are present in large amounts in photosynthetic membranes of cyanobacteria, algae and higher plants. Antiviral activity against HIV-1 was reported for some sulfoquinovosyldiacylglycerols isolated from cyanobacteria [13]. Freile-Pelegrin and collaborators reported in 2010, from the brown algae *Lobophora variegata*, collected at Puerto Morelos in Quintana Roo state, the isolation and structure elucidation of a new glycoacylglycerolipid, 1-*O*-palmitoyl-2-*O*-oleoyl-3-*O*-(6''''-sulfo- α -D-quinovopyranosyl)-glycerol (**7**) along with two known glycolipids: 1-*O*-palmitoyl-2-*O*-myristoyl-3-*O*-(6''''-sulfo- α -D-quinovopyranosyl)-glycerol (**8**), and 1,2-di-*O*-palmitoyl-3-*O*-(6''''-sulfo- α -D-quinovopyranosyl)-glycerol (**9**). The mixture of the three sulfoquinovosyldiacylglycerols **7-9** showed high *in vitro* antiprotozoal activity against *Entamoeba histolytica* (IC₅₀ value of 3.9 μ g/mL) and moderate activity against *Trichomonas vaginalis* trophozoites (IC₅₀ value 8.0 μ g/mL), with good selective index (SI > 10). However, they were less effective than metronidazole used as control (IC₅₀ = 0.13 and 0.04 μ g/mL, respectively) [14]. The relative configuration of the glycerol unit in **7-9** was not specified (Figure 2).

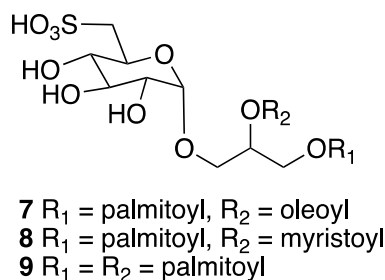


Figure 2. Structures of marine glycolipids isolated from the brown algae *Lobophora variegata*.

2.1.3. Aromatic acids

Several aromatic acids such as *p*-hydroxybenzaldehyde (**10**), vanillin (**11**), benzoic acid (**12**), *p*-hydroxybenzoic acid (**13**), and phenylacetic acid (**14**) were isolated from the sponge *Haliclona tubifera* (now *H. (Reniera) tubifera*) [12] (Figure 3).

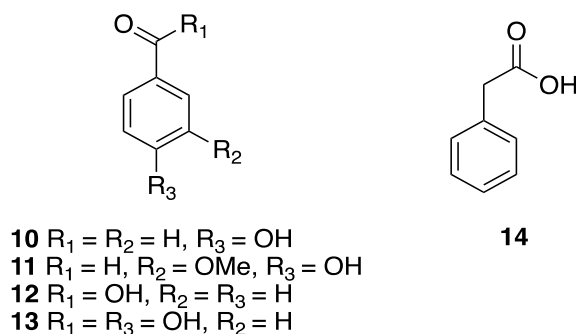


Figure 3. Structures of aromatic acids isolated from the sponge *Haliclona tubifera* (now *H. (Reniera) tubifera*).

2.2. Terpenoids

2.2.1. Diterpenes and sesterterpenes

Terpenoid biogenesis is one of the dominant pathway of most marine natural products, mainly those isolated from cnidarians followed by sponges. The wide variety of biological activities found in marine terpenes together with their ecological role in the marine environment, makes them a very interesting target of study apart from being potential drugs [15]. Pech-Puch *et al.* reported in 2019 the isolation and structural characterization of seven terpenoids from the sponge *Spongia tubulifera* (now *S. (Spongia) tubulifera*) collected at Rio Indio, Quintana Roo state. Two of them resulted to be new natural products, 3 β -hydroxyspongia-13(16),14-dien-2-one (**15**) and 19-dehydroxy-spongian diterpene 17 (**16**) while the remaining five corresponded to previous reported terpenes, three spongia furanoditerpenes: 9-nor-3-hydroxyspongia-3,13(16)14-trien-2-one (**17**), 3 β , 19 dihydroxyspongia-13(16),14-dien-2-one (epispongiadiol) (**18**) and spongian diterpene 17 (**19**); the furanoditerpene ambliol C (**20**) and the sesterterpene scalarin (**21**). The pharmacological analysis of the isolated compounds displayed a very mild cytotoxic activity for **15**, **18** and **20** while they showed no antimicrobial (*Acinetobacter baumannii*, *Pseudomonas aeruginosa*, *Klebsiella pneumoniae* and *Staphylococcus aureus*) or antiviral (HAdV5 and HAdV5-GFP) activities [16] (Figure 4).

From the *organic extracts of the brown seaweed Dictyota ciliolata*, collected at the Caribbean coast of Quintana Roo state, Caamal-Fuentes *et al.* isolated the diterpenes pachydictyol A (**22**) and dictyol B acetate (**23**) in 2014. Cytotoxic and antiproliferative activities of the isolated compounds were evaluated on a panel of cancer cell lines (oral carcinoma (KB), epithelial carcinoma of the larynx (Hep-2), breast adenocarcinoma (MCF-7), and cervix adenocarcinoma (SiHa)) and a human cell embryonic kidney cell line HEK-293 as the control). Compound **22** exhibited inhibitory activity against all cancer cell lines tested, whereas diterpene **23** showed cytotoxic activity against epithelial carcinoma of the larynx-HEP-2 (CC₅₀=19.6 μ g/ml) and antiproliferative activity against breast-MCF-7 (IC₅₀=38.3 μ g/ml) and cervix-SiHa (IC₅₀=34.4 μ g/ml) [17] (Figure 4).

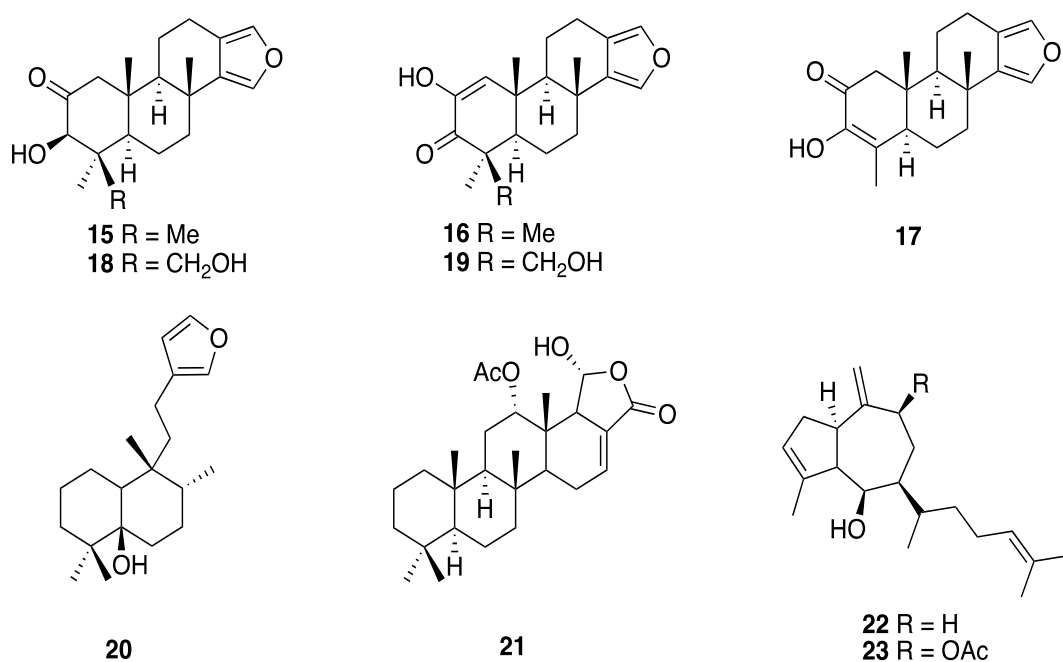


Figure 4. Structures of diterpenes **15-20** and sesterterpene **21** isolated from the sponge *Spongia tubulifera* (now *S. (Spongia) tubulifera*) and diterpenes **22** and **23** isolated from the algae *Dictyota ciliolata*.

2.2.2. Steroids

High diversity unusual structures of steroid derivatives with multiple potent biological properties have been isolated from marine organisms. Bohlin *et al.* reported in 1981 several marine steroids as acetates from the sponge *Teichaxinella morchella* (now *Axinella corrugata*) collected at a depth of 15 m at Puerto Morelos in Quintana Roo state. Two new sterols, (22*E*,24*S*)-3*E*-acetoxymethyl-24-methyl-27-nor-A-nor-5 α -cholest-22-ene (A-nor-patinosterol) (**24**) and (22*E*,24*R*)-3*E*-acetoxymethyl-23, 24-dimethyl-A-nor-5 α -cholest-22-ene (A-nor-dinosterol) (**25**), along with six known sterols, (22*E*)-3*E*-acetoxymethyl-A-nor-5 α -cholest-22-ene (**26**), 3*E*-acetoxymethyl-A-nor-5 α -cholestane (**27**), (22*E*,24*S*)-3*E*-acetoxymethyl-24-ethyl-A-nor-5 α -cholest-22-ene (**28**), (22*E*,24*R*)-3*E*-acetoxymethyl-24-ethyl-A-nor-5 α -cholest-22-ene (**29**), (22*E*,24*S*)-3*E*-acetoxymethyl-24-methyl-A-nor-5 α -cholest-22-ene (**30**), and (22*E*,24*R*)-3*E*-acetoxymethyl-24-methyl-A-nor-5 α -cholest-22-ene (**31**) were isolated. Furthermore, four known steroids were also detected, (24*S*)-3*E*-acetoxymethyl-24-methyl-A-nor-5 α -cholestane (**32**), (24*R*)-3*E*-acetoxymethyl-24-methyl-A-nor-5 α -cholestane (**33**), (24*R*)-3*E*-acetoxymethyl-24-ethyl-A-nor-5 α -cholestane (**34**), and (24*S*)-3*E*-acetoxymethyl-24-ethyl-A-nor-5 α -cholestane (**35**) [18]. The relative configuration at C-3 and C-20 of **24-35** was not specified (Figure 5) and no biological data were reported for these compounds.

From two brown algae, *Padina sanctae-crucis* and *Turbinaria tricostata*, collected at the Caribbean coast of Quintana Roo state, were reported in 2014 the isolation of fucosterol (**36**) and 24*E*-hydroperoxy-24-vinylcholesterol (**37**). Cytotoxic (CC₅₀) and antiproliferative (IC₅₀) activity assays on a panel of human cancer cell lines (KB, Hep-2, MCF-7 and SiHa) and a human cell embryonic kidney cell line HEK-293 as the control, showed that **36** is cytotoxic against Hep-2 and SiHa cell lines (CC₅₀ of 14.8 and 18.6 μ g/mL, respectively), with a high selectivity index towards Hep-2 (SI=10) and antiproliferative activity against MCF-7 and SiHa (IC₅₀ of 43.3 and 34.0 μ g/mL, respectively). Fucosterol (**36**) was also isolated from the brown algae *Dictyota ciliolata*. Steroid **37** displayed not only the highest cytotoxic activity (CC₅₀ of 3.1 μ g/mL) but also

a high selectivity index (SI=16.2) on KB cell lines. Additionally, **37** exhibited a moderate cytotoxic activity towards Hep-2, MCF-7 and SiHa cell lines (CC₅₀ of 10.5, 12.1 and 18.9 µg/mL, respectively) with lower selectivity index (SI of 4.7, 4.1 and 12.6, respectively) [17] (Figure 5).

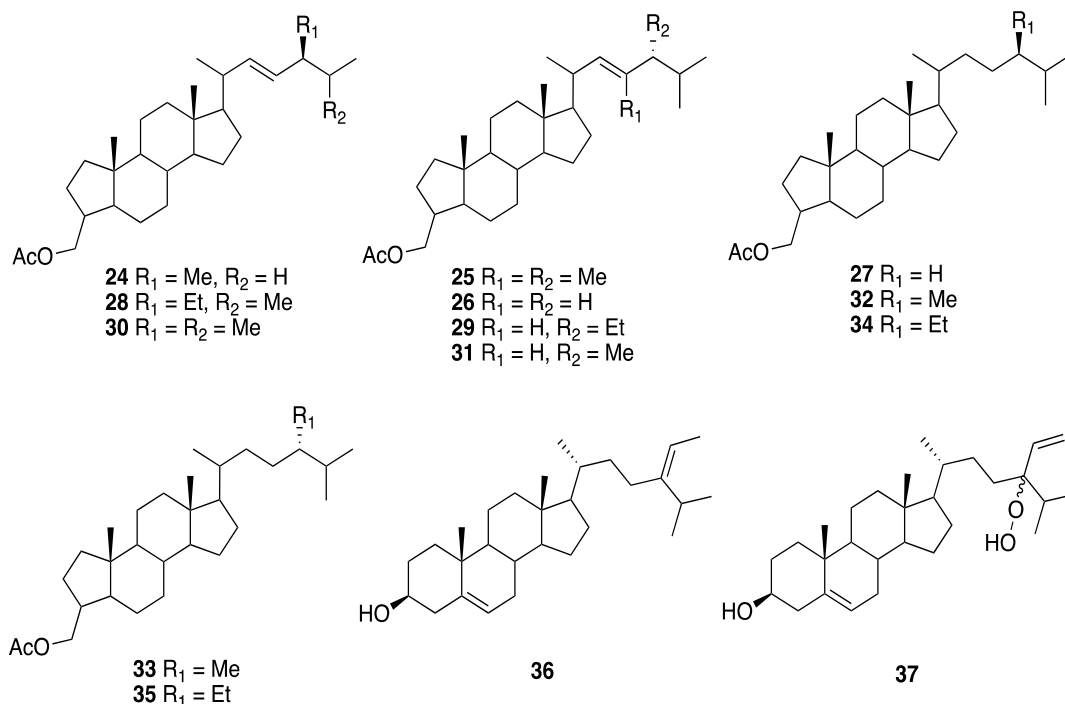


Figure 5. Steroid structures of the A-nor-5 α -cholestane **24-35** isolated from the sponge *Teichaxinella morchella* (now *Axinella corrugata*) and the cholesterol derivatives **36** and **37** isolated from the brown algae *Padina sanctae-crucis* and *Turbinaria tricostata*.

2.2.3. Triterpenoid saponins

Sea cucumbers constitute a rich source of triterpenoid saponins, some of them exerting pharmacological effects [19]. From the sea cucumber *Astichopus multifidus*, collected on the Yucatan Peninsula coasts, Mena-Rejón and collaborators reported in 2016 the isolation and the structural elucidation of three oligoglycoside triterpenes. Two of them, stichloroside B₂ (**38**) and astichoposide C (**39**), were known, while the third one, named as astichoposide D (**40**), turned out to be a new natural product. Antiproliferative activity assays against two cancer lines, MCF-7 (ATCC HTB-22) and a highly invasive triple-negative breast cancer MDA-MB-231 (ATCC HTB-26), displayed that **38** had the highest antiproliferative activity against MCF-7 cells (6.45 µM) while **39** had the highest antiproliferative activity against MDA-MB-231 cells (3.80 µM) [20]. The research group of Mena-Rejón also reported in 2013 the isolation of the known triterpenoid saponin holothurin B₂ (**41**) from the sea cucumber *Holothuria floridana* (now *H. (Halodeima) floridana*) [21] (Figure 6).

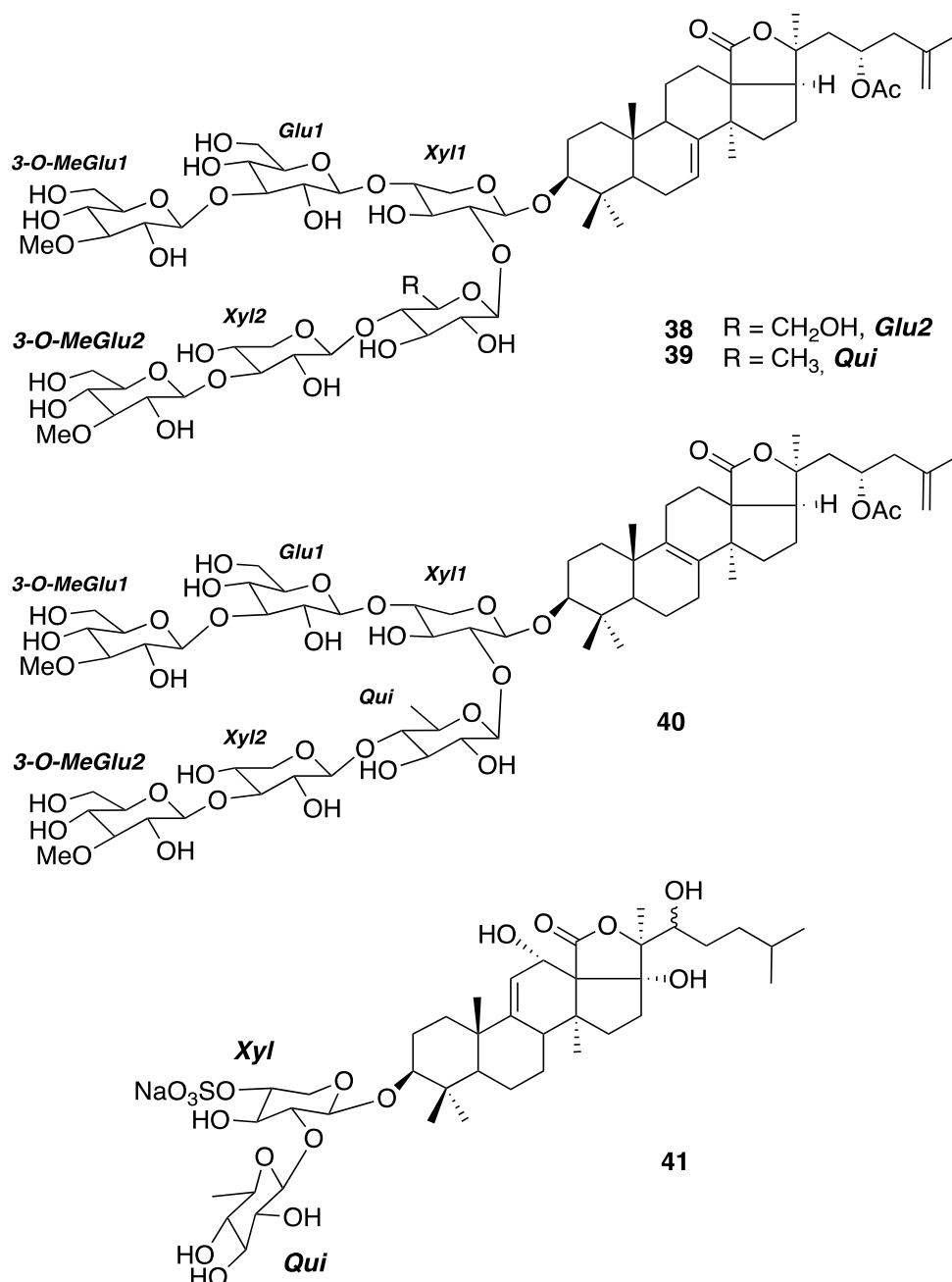


Figure 6. Structures of the triterpenoid saponins isolated from the sea cucumbers: the hexaglycosides **38–40** from *Astichopus multifidus* and the diglycoside **41** from *Holothuria floridana* (now *H. (Halodeima) floridana*).

2.3. Nitrogen compounds

2.3.1. Indole derivatives

Two indole, indole-3-carbaldehyde (**42**) and its brominated derivate, 6-bromoindole-3-carbaldehyde (**43**), were isolated by Olguin-Urbe *et al.* in 1997 from two different sources, the tunicate *Stomozoa murrayi* (currently known as *Stomozoa roseola*) and the bacterium *Acinetobacter* sp. associated to its surface [22] The tunicate was collected at a depth of 3-5 m in Puerto Morelos, Quintana Roo state, very close to the Institute of Marine Sciences and Limnology research station of the National Autonomous University of Mexico (UNAM). These compounds were evaluated in several biological assays. The brominated indole **43** displays antimicrobial activity by inhibiting the growth

of four marine bacterial strains SM-S2, SM-Z, *Bacillus marinus*, and *Vibrio campbellii*, while its debrominated analog **42** shows no inhibitory activity. On the other hand, both compounds exhibit antifouling activity by completely inhibiting the settlement of *Balanus amphitrite* (now *Amphibalanus amphitrite*) at the highest concentration tested at 100 µg/mL and even, the most active compound **43** is able to inhibit larval settlement by 80% at 10 µg/mL. Finally, these compounds showed no antipredatory (deterrent) activity against the *Serranus cabrilla* fish, collected in Mediterranean Sea, nor significant antifungal activity against the diatom *Nitzschia acicularis* (Figure 7).

The isolation of another indole, serotonin (**44**), from the salivary glands of *Octopus maya* collected in Sisal, Yucatan state was reported by Pech-Puch *et al.* in 2016 [23]. The neurotoxic activity previously found in its extract was attributed to that compound (Figure 7).

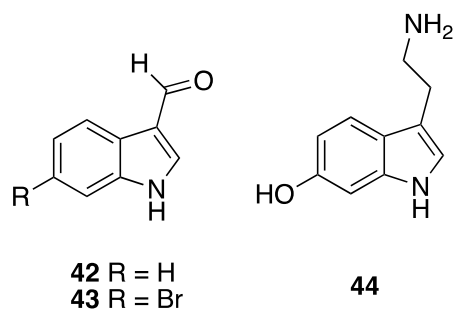


Figure 7. Structures of indole derivatives **42** and **43** from the tunicate *Stomozoa murrayi* (now *Stomozoa roseola*) and the bacterium *Acinetobacter* sp. and **44** from the mollusk *Octopus maya*.

2.3.2. Nucleosides and nitrogenous bases

The importance of the study of nucleosides comes from the fact that the arabino-nucleosides spongthymidine and spongouridine, isolated from a marine sponge, were the first marine natural products that showed their potential as drugs because they constituted the basis of the development of the first synthetic nucleosides approved as therapeutic drugs: the anticancer cytarabine (*ara-C*) and the antiviral vidarabine (*ara-A*) [1].

Three nucleosides, thymidine (**45**), 2'-desoxyuridine (**46**), and uridine (**47**), were isolated from the sponge *Halichondria magniconulosa* (now *H. (Halichondria) magniconulosa*) collected at 0.5-1 m of depth in Chabihau, Yucatan state, and reported in 2018 by the research group of Mena-Rejón [24]. The same year, Medina-Gómez *et al.* reported the isolation of cytosine (**48**) from the sponge *Haliclona tubifera* (now *H. (Reniera) tubifera*) [12] (Figure 8). No biological data were reported for **45-48**.

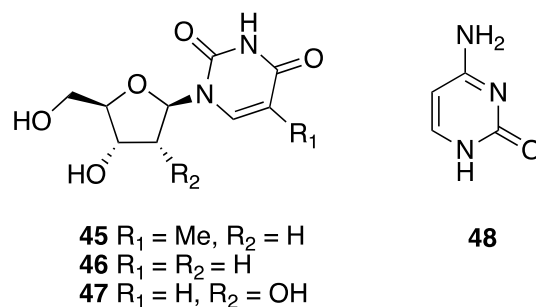


Figure 8. Structures of nucleosides **45-47** and nitrogenous base **48** isolated from the sponges *Halichondria magniconulosa* (now *H. (Halichondria) magniconulosa*) and *Haliclona tubifera* (now *H. (Reniera) tubifera*), respectively.

2.3.3. Conotoxins

The venomous fish-hunting cone snails belonging to the *Conus* genus is composed of a collection of toxin peptides that serve to immobilize prey by targeting different physiological mechanisms in their neuromuscular system. In this way, ω -conotoxin MVIIA, isolated from *Conus magus*, is commercialized as the synthetic Prialt[®] (ziconatide) which constituted the first FDA-approved drug that was directly derived from a marine natural product as a pain control drug [1]. On the basis of this background, the research group led by Aguilar from the Institute of Neurobiology-UNAM at Queretaro in Mexico, reported the isolation of new conotoxins from three different snails, mainly belonging to the *Conus* genus, collected along the coasts of the Mexican Caribbean.

Thus, the study of the extract of the venomous duct of *Conus delessertii* (now *Conasprella delessertii*), mollusk collected in Quintana Roo state, allowed Aguilar and collaborators to report four new peptides: conotoxin de13a (**49**) and conotoxin de7a (**50**) reported in 2005, conotoxin de7b (**51**) reported in 2009 and conotoxin de13b (**52**) reported in 2013. Conotoxin de13a (**49**) contains 32 amino acids (3486.76 Da) and was defined as a new class of conotoxins. This peptide is characterized by the presence of a high content of posttranslationally modified amino acids, such as 5-hydroxylysine, and residues of cysteine arranged in a pattern (C-C-C-CC-C-C-C) which were not previously described in conotoxins [25]. On the other hand, conotoxin de7a (**50**) contains 28 amino acids (3170.0 Da), some of them modified post-transductionally, and a residue (- γ CCS-) previously found only in two other conotoxins [26]. Conotoxin de7b (**51**), bearing 28 amino acids including six cysteine residues, is characterized by existing in different post-transductionally modified isomorphs (with molecular masses varying from 3078.6 to 3154.6 Da), some of them containing γ -carboxy-glutamate and/or 4-hydroxyproline at positions 4, 7 and/or 14 [27]. Finally, conotoxin de13b (**52**) has the same arrangement of cysteine residues as conotoxin de13a (**49**) [28] (Figure 9).

From the extract of venom duct of a second mollusk, *Conus spurius*, Aguilar and collaborators reported the isolation of twelve new conotoxin derivatives **53-64**, from two different places: Quintana Roo and Campeche states. Conotoxin sr5a (**53**), reported in 2006, is a hydrophobic peptide belonging to the T-1 conotoxin family with a molecular mass of 1616.60 Da and a pair of disulfide bridges. In a biological test in mice, this conotoxin caused a depressed behavioral activity [29]. One year later, two new α -conotoxins of 18 amino acids, SrIA (**54**) and SrIB (**55**), with molecular mass of 2202.9 and 2158.8 Da, respectively, were reported. With the aim of looking for new therapeutic alternatives against brain diseases (schizophrenia, nocturnal frontal lobe epilepsy and Alzheimer's disease), conotoxins **54** and **55** were evaluated as antagonists to nicotinic

acetylcholine receptors. The results suggested not only that these conotoxins can operate as nicotinic acetylcholine receptor inhibitors but also, that they bind to nicotinic acetylcholine receptors with a very high affinity, increasing their intrinsic cholinergic response and making them excellent model tools for studying toxin-receptor interaction [30]. The fourth new peptide, conotoxin sr11a (**56**), with a molecular weight of 3650.77 Da, was reported in 2007, being the first I-conotoxin isolated from the Western Atlantic. This peptide produces stiffening of body, limbs and tail when injected intracranially into mice [31]. Conotoxin sr7a (**57**), containing 32 amino acids (3330.74 Da) and reported in 2007, displays several *in vivo* effects, such as hyperactivity in mice and paralysis in freshwater snails (*Pomacea paludosa*), while it was inactive in intramuscular trials with the limpet *Patella opea* and the freshwater fish *Lebistes reticulatus* [32]. In contrast, conorfamide-Sr2 (CNF-Sr2, **58**) reported in 2008, with a molecular mass of 1468.70 Da and without cysteine residues, exhibits paralytic activity in the limpet *Patella opea* and produces hyperactivity in the freshwater snail *Pomacea paludosa* and in mouse [33]. From specimens of *Conus spurius*, collected in Isla Arena, Campeche state, were isolated and identified by reverse transcription polymerase chain reaction, seven conotoxins. Four of them belong to the T-1 conotoxin family, [18V] sr5a (**59**), [18T] sr5a (**60**), “extended” (**61**), and “hydrophilic” (**62**) which were reported in 2009 [34] and they are very similar to the conotoxin sr5a (**53**). The other three, reported in 2010, were the known conotoxin sr11a (**56**) already reported in 2007 [31] and the new conotoxins, sr11b (**63**) and sr11c (**64**) [35] (Figure 9).

Finally, Aguilar and collaborators reported in 2009 the isolation of a new peptide, pal9a (**65**) (3678.84 Da) with 34 amino acids including 6 cysteine residues, from a third mollusk, *Polystira albida*, collected in Campeche state. This is the first P-conotoxin-like turritoxin isolated from a member of family Turridae from the Western Atlantic [36] (Figure 9).

49. DCOTSCOTT CANGWECCKGYOCVNKACSGCTH*

O = 4-hydroxyproline
W = 6-bromotryptophan
K = 5-hydroxylysine
* = amidated C-terminus

50. ACKOKNNLCAITγMAγCCSGFCLYRCS*

O = hydroxyproline
Y = γ-carboxyglutamate
* = amidated C-terminus

51. DCI(P/O)GG(E/γ)NCDVFR(O/P)YRCCSGYCILLCA

O = 4 hydroxyproline
Y = γ-carboxyglutamate
3 disulfide bridges between C-C-CC-C-C

52. DCPTSCPTT CANGWECCKGYPCVRQHCSCGNH*

W = 6-bromotryptophan
K = 5-hydroxylysine
* = amidated C-terminus

53. IINWCCLIFYQCC

54. RTCCSROTCRMγYPγLCG*

O = hydroxyproline
Y = γ-carboxyglutamate
2 disulfide bridges between CC-C-C
* = amidated C-terminus

55. RTCCSROTCRMEYPγLCG*

O = hydroxyproline
Y = γ-carboxyglutamate
2 disulfide bridges between CC-C-C
* = amidated C-terminus

56. CRTEGM SC γ γNQCCWRSCCRGECEAPCRFGP*

Y = γ-carboxyglutamate
4 disulfide bridges between C-C-CC-CC-C-C
* = amidated C-terminus

57. CLQFGSTCFLGDDDI CCSGECFYSGGTFGICS*

3 disulfide bridges between C-C-CC-C-C
* = amidated C-terminus

59. IINWCCLVIFYQCC

60. IINWCCLTFYQCC

63. CDS DGT S C T S N M E C C G Y G C C S G T C Q T P C R F G P *

4 disulfide bridges between C-C-CC-CC-C-C
* = amidated C-terminus

64. CSDEGASCEK K S D C C F L S C C W S V C D R P C R L V P *

4 disulfide bridges between C-C-CC-CC-C-C
* = amidated C-terminus

65. NVCDGDACPDGVCRSGCTCDFNVAQRKDTCFYPQ*

3 disulfide bridges between C-C-C-C-C-C
* = amidated C-terminus

58. GPMγDPLγIIRI*

Y = γ-carboxyglutamate
* = amidated C-terminus

61. INWCCLIFYQCCL

62. I M A G C C P R F Y Q C C Y P *

* = amidated C-terminus

Figure 9. Structures of conotoxins **49-65** isolated from cone snails belonging to the *Conus* genus and *Polystira albida*.

2.4. Biopolymers

Freile-Pelegrín and collaborators reported in 2018 the characterization of L-carrageenan (**66**), obtained from the direct extraction of the red algae *Solieria filiformis* collected at Telchac in the Yucatan state. This polysaccharide shows a high antiviral activity against Herpes simplex virus with EC₅₀ value of 6.3 µg/mL [37] (Figure 10).

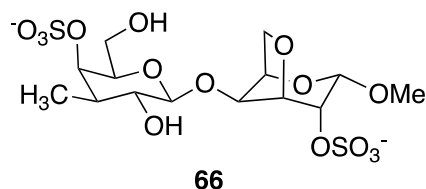


Figure 10. Structure of L-carrageenan isolated from the red algae *Solieria filiformis*.

3. Bioprospecting overview

A total of 95 scientific documents were recorded and analyzed in this review, including 82 articles, 4 postgraduate dissertation theses and 9 meeting abstract communications. They describe the reports related to research on pharmacological surveys of extracts, chemical composition and isolation of marine natural products. A total of 145 species of marine organisms are enclosed, belonging to 12 phyla (Table 1 and 2), being the most representative Rhodophyta (27%), Chlorophyta (22%), Phaeophyta (17%) and Cnidaria (14%) (Figure 11).

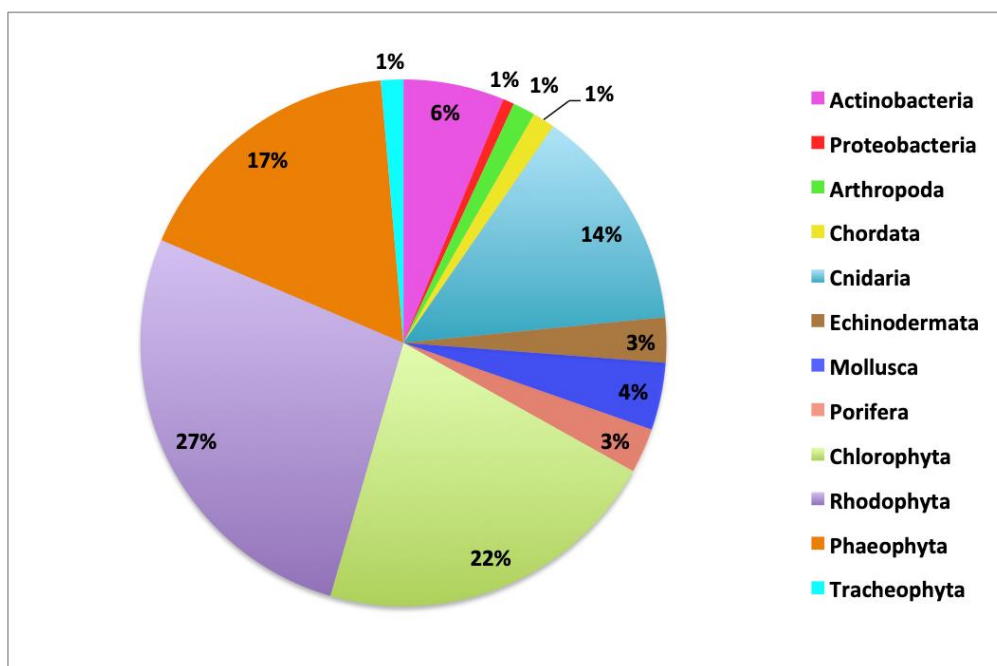


Figure 11. Distribution of the reported marine organisms by phylum.

Table 1. Reported marine species of the Yucatan Peninsula in which natural products were isolated.

Phylum	Species	Compounds isolated and biogenetic origin	Ref.
Proteobacteria	<i>Acinetobacter</i> sp.	42, 43 (Nitrogen compounds)	[22]
Chordata (Ascidian)	<i>Stomozoa murrayi</i> (now <i>Stomozoa roseola</i>)	42, 43 (Nitrogen compounds)	[22]
Cnidaria (Coral)	<i>Pterogorgia anceps</i>	1-3 (Polyketides)	[11]
Echinodermata (Sea cucumbers)	<i>Astichopus multifidus</i>	38-40 (Terpenoids)	[20]
	<i>Holothuria floridana</i> (now <i>H. (Halodeima) floridana</i>)	41 (Terpenoid)	[21]
Mollusca (Mollusks)	<i>Conus delessertii</i> (now <i>Conasprella delessertii</i>)	49-52 (Nitrogen compounds)	[25-28]
	<i>Conus spurius</i>	53-64 (Nitrogen compounds)	[29-35]
	<i>Octopus maya</i>	44 (Nitrogen compound)	[23]
	<i>Polystira albida</i>	65 (Nitrogen compound)	[36]
Porifera (Sponges)	<i>Halichondria magniconulosa</i> (now <i>H. (Halichondria) magniconulosa</i>)	45-47 (Nitrogen compounds)	[24]
	<i>Haliclona tubifera</i> (now <i>H. (Reniera) tubifera</i>)	6, 10-14 (Polyketides) and 48 (Nitrogen compound)	[12]
	<i>Spongia tubulifera</i> (now <i>S. (Spongia) tubulifera</i>)	15-21 (Terpenoids)	[16]
	<i>Teichaxinella morchella</i> (now <i>Axinella corrugata</i>)	24-35 (Terpenoids)	[18]
Phaeophyta (Brown algae)	<i>Dictyota ciliolata</i>	22, 23, 36 (Terpenoids)	[17]
	<i>Lobophora variegata</i>	7-9 (Polyketides)	[14]
	<i>Padina sanctae-crucis</i>	36, 37 (Terpenoids)	[17]
	<i>Turbinaria tricostata</i>	36, 37 (Terpenoids)	[17]
Rhodophyta (Red algae)	<i>Solieria filiformis</i>	66 (Biopolymer)	[37]

Table 2. Reported marine species from Yucatan Peninsula related to bioprospecting without determining the chemical composition.

Domain: Bacteria

Kingdom: Bacteria

Phylum	Genus or Species	References
Actinobacteria	<i>Streptomyces</i>	[39]
	<i>Saccharomonospora</i>	
	<i>Dietzia</i>	
	<i>Nocardiopsis</i>	
	<i>Pseudonocardia</i>	
	<i>Verrucosispora</i>	
	<i>Brachybacterium</i>	
	<i>Jiangella</i>	
<i>Salinispora</i>		

Domain: Eukarya

Kingdom: Animalia

Arthropoda (Crustaceans)	<i>Bathynomus giganteus</i>	[40]
	<i>Limulus Polyphemus</i>	[41]
Chordata (Ascidians)	<i>Trididemnum solidum</i>	[42]
Cnidaria (Anemones)	<i>Actiinidae</i> Gen. sp. nov.*	[43]
	<i>Anthopleura texaensis</i>	
	<i>Bartholomea annulata</i>	[44-47]
	<i>Bunodeopsis antilliensis</i>	[38]
	<i>Bunodeopsis globulifera</i> (now <i>Viatrix globulifera</i>)	[48,49]
	<i>Condylactis gigantea</i>	[50]
	<i>Lebrunia danae</i> (now <i>L. neglecta</i>)	[47,51]
	<i>Stichodactyla helianthus</i>	[47,52]
	<i>Telmatactis bernoni</i> *	[43]
Cnidaria (Corals)	<i>Millepora alcicornis</i>	[53-57]
	<i>Millepora complanata</i>	[53,55,58-62]
	<i>Porites astreoides</i>	[63]
	<i>Pseudodiploria strigosa</i>	[63]
	<i>Siderastrea siderea</i>	[63]
Cnidaria (Jellyfish)	<i>Aurelia aurita</i>	[64,65]
	<i>Carybdea marsupialis</i>	[47,66,67]
	<i>Cassiopea xamachana</i> (now <i>Cassiopea andromeda</i>)	[47,68,69]
	<i>Linuche unguiculata</i>	[47]
	<i>Pelagia noctiluca</i>	[70]
Echinodermata	<i>Holothuria mexicana</i>	[71]

(Sea cucumbers)	(now <i>H. (Halodeima) mexicana</i>)	
	<i>Isostichopus badionotus</i>	[72-74]
Mollusca (Mollusks)	<i>Conus austini</i> (now <i>C. cancellatus</i>)	[75]
	<i>Conus spurius</i>	[75,76]
	<i>Gemmula periscelida</i>	[77]
	<i>Octopus maya</i>	[78]
	<i>Polystira albida</i>	[75,77]

Domain: Eukarya

Kingdom: Plantae

Chlorophyta (Green algae)	<i>Acetabularia schenckii</i> (now <i>A. subg. Acicularia schenckii</i>)	[79]
	<i>Avrainvillea cf digitata</i> sp.	[80-83]
	<i>Avrainvillea longicaulis</i>	[79]
	<i>Avrainvillea nigricans</i>	[84]
	<i>Caulerpa ashmeadii</i>	[79,85]
	<i>Caulerpa cupressoides</i>	[79,85,86]
	<i>Caulerpa mexicana</i>	[85]
	<i>Caulerpa paspaloides</i>	[79,85]
	<i>Caulerpa prolifera</i>	[79,85,87]
	<i>Caulerpa racemosa</i>	[85]
	<i>Caulerpa racemosa</i> var. <i>racemosa</i>	[88]
	<i>Caulerpa sertularioides</i>	[79,87]
	<i>Caulerpa taxifolia</i>	[79]
	<i>Cladophora prolifera</i>	[79]
	<i>Cladophora vagabunda</i>	[79]
	<i>Codium decorticatum</i>	[79,83]
	<i>Codium isthmocladum</i>	[85,88,89]
	<i>Enteromorpha intestinalis</i> (now <i>Ulva intestinalis</i>)	[79]
	<i>Halimeda incrassata</i>	[80-83,85]
	<i>Halimeda monile</i>	[79]
	<i>Halimeda opuntia</i>	[86]
	<i>Halimeda tuna</i>	[79-83,86]
	<i>Penicillus capitatus</i>	[85,86]
	<i>Penicillus dumetosus</i>	[79-83,90]
	<i>Penicillus lamourouxii</i>	[80-83]
	<i>Penicillus pyriformis</i>	[79]
<i>Rhizocephalus phoenix</i>	[81,82]	
<i>Rhizocephalus phoenix</i> f. <i>brevifolius</i>	[80,83]	
<i>Udotea conglutinata</i>	[79-83]	
<i>Udotea flabellum</i>	[80-83,86,91]	

	<i>Udotea occidentalis</i>	[85]
Phaeophyta (Brown algae)	<i>Dictyopteris jamaicensis</i>	[83]
	<i>Dictyota bartayresiana</i>	[86]
	<i>Dictyota caribaea</i>	[80-83,92]
	<i>Dictyota cervicornis</i> (now <i>Canistrocarpus cervicornis</i>)	[79,86]
	<i>Dictyota ciliolata</i>	[79,93,94]
	<i>Dictyota crenulata</i>	[79]
	<i>Dictyota dichotoma</i>	[89]
	<i>Dictyota menstrualis</i>	[85]
	<i>Lobophora variegata</i>	[79-83]
	<i>Padina boergesenii</i>	[86]
	<i>Padina durvillaei*</i>	[86]
	<i>Padina gymnospora</i>	[79,86,88]
	<i>Padina pavonica</i>	[83]
	<i>Padina perindusiata</i>	[80-83,92]
	<i>Padina sanctae-crucis</i>	[93,94]
	<i>Sargassum cymosun</i>	[86]
	<i>Sargassum filipendula</i>	[84-86,88,92]
	<i>Sargassum fluitans</i>	[80-83,86,93-96]
	<i>Sargassum hystrix</i>	[84, 86]
	<i>Sargassum polyceratium</i>	[86]
<i>Sargassum pteropleuron</i>	[79,86]	
<i>Sargassum ramifolium</i>	[79]	
<i>Sargassum vulgare</i>	[86]	
<i>Turbinaria tricostata</i>	[79,86,93,97]	
<i>Turbinaria turbinata</i>	[80-83,86,92]	
Rhodophyta (Red algae)	<i>Acanthophora spicifera</i>	[79]
	<i>Agardhiella</i> sp.	[80-83]
	<i>Agardhiella subulata</i>	[89]
	<i>Bryothamnion triquetrum</i> (now <i>Alsidium triquetrum</i>)	[79-83,85,86,89]
	<i>Ceramium nitens</i>	[79-83,85]
	<i>Champia salicornioides</i>	[79,80,82,83]
	<i>Chondria atropurpurea</i>	[79]
	<i>Chondria baileyana</i>	[79]
	<i>Chondrophycus papillosus</i> (now <i>Palisada perforata</i>)	[79]
	<i>Chondrophycus poiteaui</i> (now <i>Yuzurua poiteaui</i>)	[79]
	<i>Digenea simplex</i>	[79,85,86]
	<i>Eucheuma isiforme</i> (now <i>Eucheumatopsis isiformis</i>)	[79-83,85,88,98]
	<i>Gracilaria blodgettii</i>	[99]

	<i>Gracilaria bursa-pastoris</i>	[79]
	<i>Gracilaria caudata</i> (now <i>Crassiphycus caudatus</i>)	[79-83,85]
	<i>Gracilaria cervicornis</i>	[80-83,99]
	<i>Gracilaria cornea</i> (now <i>Crassiphycus corneus</i>)	[79,85,88,100]
	<i>Gracilaria crassissima</i> (now <i>Crassiphycus crassissimus</i>)	[99,100]
	<i>Gracilaria cylindrica</i>	[79]
	<i>Gracilaria damaecornis</i> *	[80-83]
	<i>Gracilaria</i> sp.	[80-83]
	<i>Gracilaria tikvahiae</i>	[79]
	<i>Gracilariopsis tenuifrons</i>	[79,101]
	<i>Halymenia floresia</i> (now <i>H. floresii</i>)	[84,79,80,82,83,85, 89,102,103]
	<i>Heterosiphonia gibbesii</i>	[79-83]
	<i>Hydropuntia cornea</i> (now <i>Crassiphycus corneus</i>)	[80-83,95]
	<i>Hypnea musciformis</i>	[104]
	<i>Hypnea spinella</i>	[79]
	<i>Jania capillacea</i>	[80-83]
	<i>Laurencia intricata</i>	[79,86,87]
	<i>Laurencia microcladia</i>	[80-83]
	<i>Laurencia obtusa</i>	[79,84-86]
	<i>Laurencia papillosa</i> (now <i>Palisada perforata</i>)	[86]
	<i>Laurencia poiteaui</i> (now <i>Palisada poiteaui</i>)	[85,86]
	<i>Liagora ceranoides</i>	[79]
	<i>Nemalion helmintoides</i> *	[79]
	<i>Rhodymenia pseudopalmata</i>	[95,105,106]
	<i>Solieria filiformis</i>	[95,107,108]
	<i>Spyridia filamentosa</i>	[87]
Tracheophyta (Seagrasses)	<i>Syringodium filiforme</i>	[87]
	<i>Thalassia testudinum</i>	[87]

* Organisms not found in World Register of Marine Species (WORMS database) [109]

The mollusk *Conus spurius* and two algae, *Halymenia floresia* (now *H. floresii*) and *Sargassum fluitans*, with 9 reports each, were the most reported species. The coral *Millepora complanata* and eight algae, *Halimeda tuna*, *Penicillus dumetosus*, *Udotea flabellum*, *Bryothamnion triquetrum* (now *Alsidium triquetrum*), *Ceramium nitens*, *Eucheuma isiforme* (now *Eucheumatopsis isiformis*), *Gracilaria caudata* (now *Crassiphycus caudatus*), *Lobophora variegata* and *Turbinaria turbinata*, with 6-8 reports each, follow the list as it is shown in Figure 12.

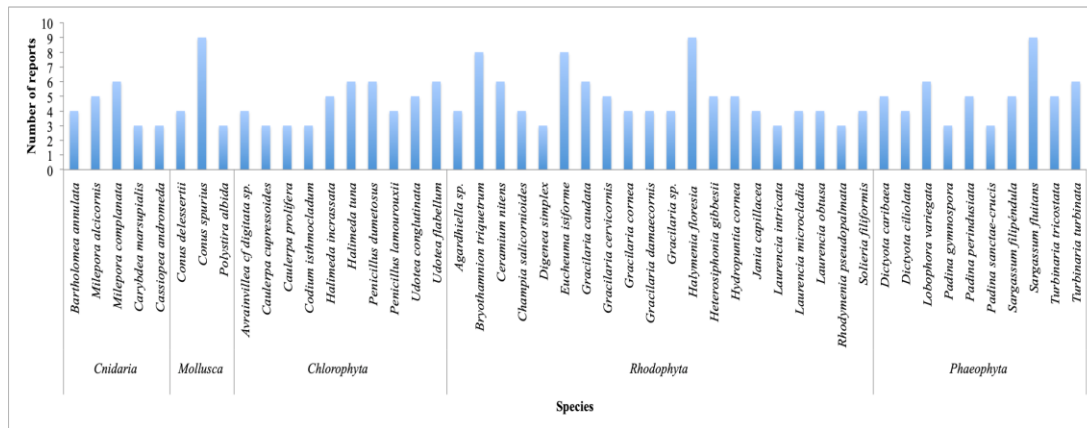


Figure 12. Number of publications of reported marine species organized by phylum. Only those species that have three or more reports are displayed.

From the territorial distribution point of view, the highest number of reports corresponds to marine organisms collected at the coast of Yucatan state (38%), followed by the coasts of Quintana Roo state (36%) and finally, the coasts of Campeche state (4%). However, 22% of the reports did not specify the state where the marine organisms were collected (Figure 13).

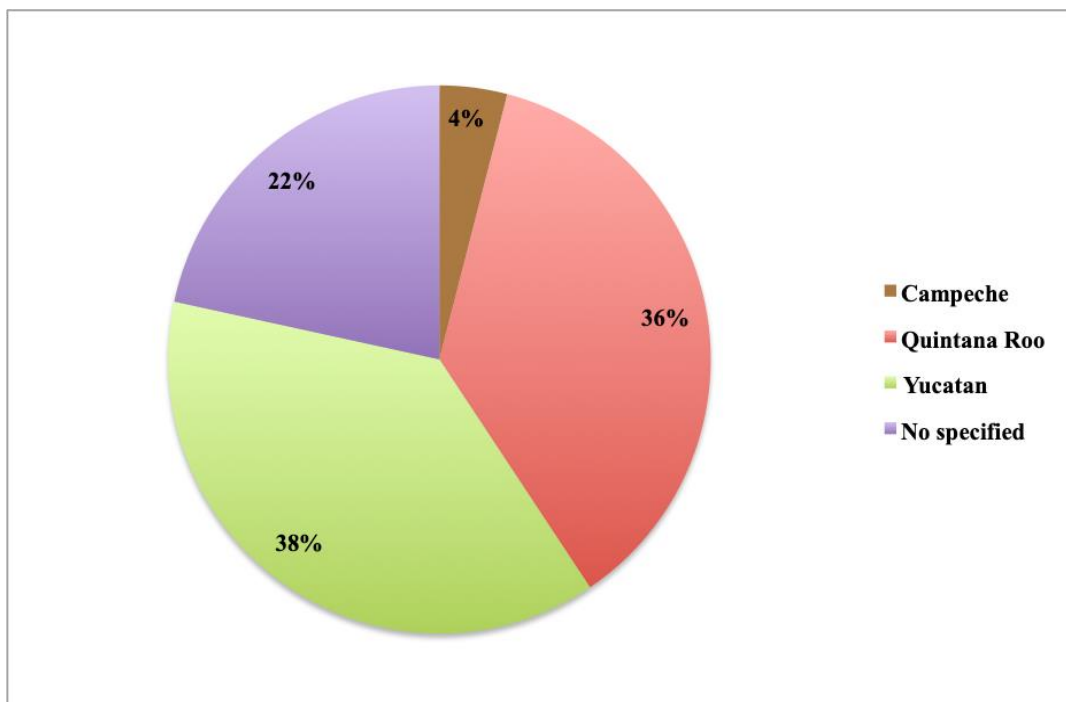


Figure 13. Geographic distribution of collections sources in percentage by state.

Figure 14 displays the number of reports per year. As far as we know, the first report was published in 1981 and since then, the number of publications related to the search for natural marine products of the Yucatan Peninsula has been increasing. However, this increase was not constant, being the years 2007, 2013, 2014 and 2016 with 7 publications each, when more reports were published.

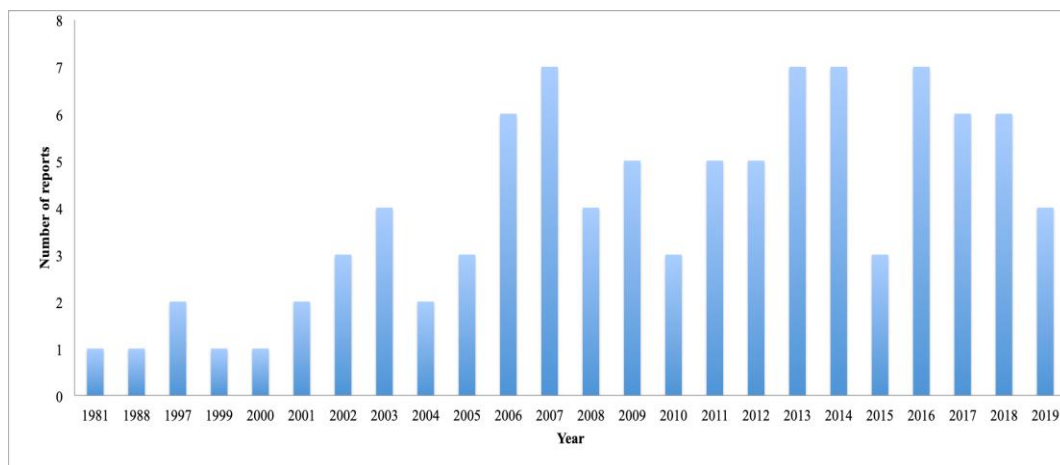


Figure 14. Number of publications per year.

4. Conclusions

The present review represents the first comprehensive report of natural products that have been isolated from marine organisms collected along the coasts of The Yucatan Peninsula, covering literature up to mid 2019. As result of 38 years of investigations of marine organisms collected in the Yucatan Peninsula, 66 marine natural products were isolated from 18 species belonging to 8 different phyla (**Proteobacteria** (*Acinetobacter* sp.), **Chordata** (ascidian: *Stomozoa murrayi* (now *Stomozoa roseola*), **Cnidaria** (*Pterogorgia anceps*), **Echinodermata** (*Astichopus multifidus* and *Holothuria floridana* (now *H. (Halodeima) floridana*)), **Mollusca** (*Conus delessertii* (now *Conasprella delessertii*), *Conus spurius*, *Octopus maya* and *Polystira albida*), **Porifera** (*Halichondria magniconulosa* (now *H. (Halichondria) magniconulosa*), *Haliclona tubifera* (now *H. (Reniera) tubifera*), *Spongia tubulifera* (now *S. (Spongia) tubulifera*) and *Teichaxinella morcella* (now *Axinella corrugata*)), **Rhodophyta** (*Solieria filiformis*) and **Phaeophyta** (*Dictyota ciliolata*, *Lobophora variegata*, *Padina sanctae-crucis* and *Turbinaria tricostata*) (Table 1). Out off the 66 marine natural products identified, 26 correspond to structures not previously reported. These 26 new chemical entities correspond to 3 aliphatic polyketides (**1-3**), 1 glycolipid (**7**), 2 diterpenes (**15, 16**), 2 steroids (**24, 25**), 1 triterpenoid saponin (**40**) and 17 conotoxins (**49-65**).

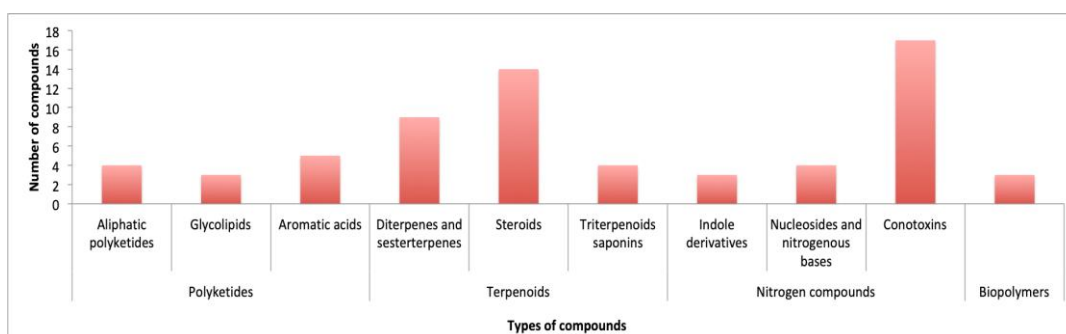


Figure 15. Biosynthetic classes of the reported marine natural products.

The overall biogenetic distribution of the reported compounds is displayed in Figure 15. The terpenoid biogenesis is again the most prominent pathway (40.9%) enclosing the diterpenes-sesterterpenes (9 compounds), steroids (14 compounds) and triterpenoids saponins (4 compounds). On the other hand, conotoxins, with 17 compounds (25.8%) constitute the largest group of the reported natural products.

The biological studies of the isolated compounds are focused on cytotoxic or antiproliferative activities (diterpenes **15**, **18**, **20**, **22** and **23**; steroids **36** and **37**, and triterpenoids saponins **38** and **39**), the antimicrobial, antifouling, antipredatory (deterrent) and anti-algal activity (indole derivative **42** and **43**), the antiprotozoal activity (glycolipids **7-9**), neurotoxic activity (indole derivative **44**), behavioral activity in animal models (conotoxins **53**, **56-58**), and finally in the interesting pharmacological activities against brain diseases of the new conotoxins **54** and **55**, and the high antiviral activity of the known biopolymer L-carrageenan (**66**).

As a concluding remark, this review shows the potential of the Yucatan Peninsula as an interesting source of new marine natural products, not only because of its unique and rich diversity of marine organisms, but also due to the small number of works published so far, which indicates that this area of research has been poorly investigated. For these reasons, the marine biodiversity of the Yucatan Peninsula can be considered as a poor exploited source of new bioactive marine natural products which could be the base of the development of new drugs.

Author Contributions: Conceptualization, Carlos Jiménez, Dawrin Pech-Puch and Jaime Rodríguez; Funding acquisition and Resources, Jaime Rodríguez and Carlos Jiménez ;Writing – original draft, Dawrin Pech-Puch; Mar Pérez-Povedano, Oscar A. Lenis-Rojas Writing – review & editing, Dawrin Pech-Puch; Jaime Rodríguez and Carlos Jiménez.

Funding: This work was supported by grants RTI2018-093634-B-C22 (AEI/FEDER, EU) from the State Agency for Research (AEI) of Spain, co-funded by the FEDER Programme from the European Union, and GRC2018/039 and ED431E 2018/03 of CICA-INIBIC strategic group from Xunta de Galicia. D.P.P. received a fellowship from the program National Council of Science and Technology (CONACYT) of Mexico and the Secretariat of Research, Innovation and Higher Education (SIIES) of Yucatan (Mexico). O.A.L.R. received a financial support from MostMicro unit. Project LISBOA-01-0145-FEDER-007660 of Portugal.

References

1. Jiménez, C. Marine Natural Products in Medicinal Chemistry. *ACS Med. Chem. Lett.* **2018**, *9*, 959–961.
2. Altmann, K. H. Drugs from the Oceans: Marine Natural Products as Leads for Drug Discovery. *Chimia.* **2017**, *71*, 646–652.
3. Mayer, A. M. S.; Rodríguez, A. D.; Tagliatela-Scafati, O.; Fusetani, N. Marine Pharmacology in 2012-2013: Marine Compounds with Antibacterial, Antidiabetic, Antifungal, Anti-Inflammatory, Antiprotozoal, Antituberculosis, and Antiviral Activities; Affecting the Immune and Nervous Systems, and Other Miscellaneous Mechanisms of Action. *Mar. Drugs* **2017**, *15*, 273.
4. Barrera, A. La Península de Yucatán Como Provincia Biótica. *Rev. Soc. Mex. Hist. Nat.* **1962**, *23*, 71–105.
5. Hernández-Bolio, G. I.; Ruiz-Vargas, J. A.; Peña-Rodríguez, L. M. Natural Products from the Yucatecan Flora: Structural Diversity and Biological Activity. *J. Nat. Prod.* **2019**, *82*, 647–656.
6. Pech Pool, D.; Ardisson Herrera, P. L. Diversidad en el Bentos Marino-Costero. In *Biodiversidad y Desarrollo Humano en Yucatán*; Duran, R., Méndez, M, Eds.;

- CICY, PPD-FMAM, CONABIO, SEDUMA: Yucatán, México, 2010; pp 144–146. ISBN: 978-607-7823-08-7.
7. Garza Pérez, J. R.; Simões, N.; Chiappa Carrara, X.; Cucio, C.; Mascaró Miquelajáuregui, M.; Oseguera Cruz, M.; Lozano Aburto, M.; Acosta González, G. Comunidades Coralinas de las Bajas de Sisal. In *Biodiversidad y Desarrollo Humano en Yucatán*; Duran, R., Méndez, M., Eds.; CICY, PPD-FMAM, CONABIO, SEDUMA: Yucatán, México, 2010; pp 148-149. ISBN: 978-607-7823-08-7.
 8. Torruco Gómez, D.; González Solís, A. Las Esponjas y Su Importancia. In *Biodiversidad y Desarrollo Humano en Yucatán*; Duran, R., Méndez, M., Eds.; CICY, PPD-FMAM, CONABIO, SEDUMA: Yucatán, México, 2010; pp 202-203. ISBN: 978-607-7823-08-7.
 9. Acosta González, G.; Arias González, J. E. Comunidades Bentónicas Del Arrecife Alacranes. In *Biodiversidad y Desarrollo Humano en Yucatán*; Duran, R., Méndez, M., Eds.; CICY, PPD-FMAM, CONABIO, SEDUMA: Yucatán, México, 2010; p 147. ISBN: 978-607-7823-08-7.
 10. Palomino-Alvarez, L. A.; Moreira Rocha, R.; Simões, N. Checklist of Ascidians (Chordata, Tunicata) from the Southern Gulf of Mexico. *Zookeys* **2019**, 832, 1–33.
 11. Guo, Y. W.; Gavagnin, M.; Mollo, E.; Trivellone, E.; Cimino, G. Three New Butenolide Lipids from the Caribbean Gorgonian *Pterogorgia anceps*. *J. Nat. Prod.* **1999**, 62, 1194–1196.
 12. Medina-Gómez, S.; Mirón-López, G.; Quijano-Quiñones, R. Caracterización Estructural de Compuestos Obtenidos a Partir de Esponja de Mar Empleando Resonancia Magnética Nuclear y Cálculos Teóricos. In 11° Foro en Ciencias Químicas y Bioquímicas. Posgrado Inst. en Ciencias Químicas y Bioquímicas. Mérida, Yucatán, México, 12-13 april 2018; pp 23–24.
 13. Fattorusso, E.; Mangoni, A. In Progress in the Chemistry of Organic Natural Products, Herz, W.; Kirby, G.W.; Moore, R.E.; Steglich, W.; Tamm, C., Eds.; Springer-Verlag: Berlin, 1997; pp. 215-301. ISBN: 978-3-7091-7456-2.
 14. Cantillo-Ciau, Z.; Moo-Puc, R.; Quijano, L.; Freile-Pelegrín, Y. The Tropical Brown Alga *Lobophora variegata*: A Source of Antiprotozoal Compounds. *Mar. Drugs* **2010**, 8, 1292–1304.
 15. Carroll, A. R.; Copp, B. R.; Davis, R. A.; Keyzers, R. A.; Prinsep, M. R. Marine Natural Products. *Nat. Prod. Rep.* **2019**, 36, 122–173.
 16. Pech-Puch, D.; Rodríguez, J.; Cautain, B.; Sandoval-Castro, C. A.; Jiménez, C. Cytotoxic Furanoditerpenes from the Sponge *Spongia tubulifera* Collected in the Mexican Caribbean. *Mar. Drugs* **2019**, 17, 416.
 17. Caamal-Fuentes, E.; Moo-Puc, R.; Freile-Pelegrín, Y.; Robledo, D. Cytotoxic and Antiproliferative Constituents from *Dictyota Ciliolata*, *Padina Sanctae-Crucis* and *Turbinaria Tricostata*. *Pharm. Biol.* **2014**, 52, 1244–1248.
 18. Bohlin, L.; Sjöstrand, U.; Djerassi, C.; Sullivan, B. Minor and Trace Sterols in Marine Invertebrates. Part 20. 3E-Hydroxy-methyl-A-nor-Patinosterol and 3E-Hydroxymethyl-A-nor-dinosterol. Two New Sterols with Modified Nucleus and Side-Chain from the Sponge *Teichaxinella morchella*. *J.C.S. Perkin Trans.1* **1981**, 1023–1028.
 19. Khotimchenko, Y. Pharmacological Potential of Sea Cucumbers. *Int. J. Mol. Sci.* **2018**, 19, 1342.
 20. Graniel-Sabido, M. J.; Mirón-López, G.; León-Deniz, L. V.; Moo-Puc, R. E.; Quintal-Novelo, C. J.; Quijano, L.; Mena-Rejón, G. J. Total NMR Assignment of

- a New Antiproliferative Triterpene Oligoglycoside from the Sea Cucumber *Astichopus multifidus*. *Tetrahedron Lett.* **2016**, *57*, 4375–4378.
21. Salazar-Mendoza, J.; Padilla-Montaño, N.; León-Deniz, L. V.; Mena-Rejón, G. J.; Quijano, L. Actividad Antifúngica de Metabolitos Aislados de la Pared Corporal de *Holoturia Floridana*. In *Foro en Ciencias Químicas y Bioquímicas. Posgrado Institucional en Ciencias Químicas y Bioquímicas*. Mérida, Yucatán, México, 17 may 2013. pp 19–20.
 22. Olguin-Uribe, G.; Abou-Mansour, E.; Boulander, A.; Débard, H.; Francisco, C.; Combaut, G. 6-Bromoindole-3-Carbaldehyde, from an *Acinetobacter* sp. Bacterium Associated with the Ascidian *Stomozoa murrayi*. *J. Chem. Ecol.* **1997**, *23*, 2507–2521.
 23. Pech-Puch, D.; Cruz-López, H.; Canche-Ek, C.; Campos-Espinosa, G.; García, E.; Mascaro, M.; Rosas, C.; Chávez-Velasco, D.; Rodríguez-Morales, S. Chemical Tools of *Octopus maya* During Crab Predation Are Also Active on Conspecifics. *PLoS One* **2016**, *11*, 1–22.
 24. Salazar Mendoza, J.; Mirón López, G.; Mena Rejón, G. J. Estudio Químico de *Halichondria Magniconulosa* (Porifera: Demospongiae) del Litoral del Estado de Yucatán. In *11° Foro en Ciencias Químicas y Bioquímicas. Posgrado Institucional en Ciencias Químicas y Bioquímicas*. Mérida, Yucatán, México, 12-13 april 2018. pp 5–6.
 25. Aguilar, M. B.; López-Vera, E.; Ortiz, E.; Becerril, B.; Possani, L. D.; Olivera, B. M.; Heimer de la Cotera, E. P. A Novel Conotoxin from *Conus delessertii* with Posttranslationally Modified Lysine Residues. *Biochemistry* **2005**, *44*, 11130–11136.
 26. Aguilar, M. B.; López-Vera, E.; Imperial, J. S.; Falcón, A.; Olivera, B. M.; Heimer de la Cotera, E. P. Putative γ -Conotoxins in Vermivorous Cone Snails: The Case of *Conus delessertii*. *Peptides* **2005**, *26*, 23–27.
 27. Aguilar, M. B.; Flores-Torres, A.; Batista, C. V. F.; Falcón, A.; López-Vera, E.; Heimer de la Cotera, E. P. Structural Characterization of Five Post-translationally Modified Isomorphs of a Novel Putative δ -Conotoxin from the Vermivorous Snail *Conus delessertii* from the Mexican Caribbean Sea. *Peptides* **2009**, *30*, 458–466.
 28. Aguilar, M. B.; Ortiz, E.; Kaas, Q.; López-Vera, E.; Becerril, B.; Possani, L. D.; Heimer de la Cotera, E. P. Precursor De13.1 from *Conus delessertii* Defines the Novel G Gene Superfamily. *Peptides* **2013**, *41*, 17–20.
 29. Aguilar, M. B.; Lezama-Monfil, L.; Maillo, M.; Pedraza-Lara, H.; López-Vera, E.; Heimer de la Cotera, E. P. A biologically active hydrophobic T-1-Conotoxin from the Venom of *Conus spurius*. *Peptides* **2006**, *27*, 500–505.
 30. López-Vera, E.; Aguilar, M. B.; Schiavon, E.; Marinzi, C.; Ortiz, E.; Restano Cassulini, R.; Batista, C. V. F.; Possani, L. D.; Heimer de la Cotera, E. P.; Peri, F.; Becerril, B.; Wanke, E. Novel α -Conotoxins from *Conus spurius* and the α -Conotoxin EI Share High-Affinity Potentiation and Low-Affinity Inhibition of Nicotinic Acetylcholine Receptors. *FEBS J.* **2007**, *274*, 3972–3985.
 31. Aguilar, M. B.; López-Vera, E.; Heimer de la Cotera, E. P.; Falcón, A.; Olivera, B. M.; Maillo, M. I-Conotoxins in Vermivorous Species of the West Atlantic: Peptide Sr11a from *Conus spurius*. *Peptides* **2007**, *28*, 18–23.
 32. Luna-Ramírez, K. S.; Aguilar, M. B.; Falcón, A.; Heimer de la Cotera, E. P.; Olivera, B. M.; Maillo, M. An O-Conotoxin from the Vermivorous *Conus spurius* Active on Mice and Mollusks. *Peptides* **2007**, *28*, 24–30.
 33. Aguilar, M. B.; Luna-Ramírez, K. S.; Echeverría, D.; Falcón, A.; Olivera, B. M.; Heimer de la Cotera, E. P.; Maillo, M. Conorfamide-Sr2, a gamma-

- carboxyglutamate-containing FMRFamide-related Peptide from the Venom of *Conus spurius* with Activity in Mice and Mollusks. *Peptides* **2008**, *29*, 186–195.
34. Zamora-Bustillos, R.; Aguilar, M. B.; Falcón, A.; Heimer de la Cotera, E. P. Identification, by RT-PCR, of Four Novel T-1-Superfamily Conotoxins from the Vermivorous Snail *Conus spurius* from the Gulf of Mexico. *Peptides* **2009**, *30*, 1396–1404.
 35. Zamora-Bustillos, R.; Aguilar, M. B.; Falcón, A. Identification, by Molecular Cloning, of a Novel Type of I₂-Superfamily Conotoxin Precursor and Two Novel I₂-Conotoxins from the Worm-Hunter Snail *Conus spurius* from the Gulf of México. *Peptides* **2010**, *31*, 384–393.
 36. Aguilar, M. B.; Chan de la Rosa, R. A.; Falcón, A.; Olivera, B. M.; Heimer de la Cotera, E. P. Peptide pal9a from the Venom of the Turrid Snail *Polystira Albida* from the Gulf of Mexico: Purification, Characterization, and Comparison with P-Conotoxin-like (framework IX) Conoidean Peptides. *Peptides* **2009**, *30*, 467–476.
 37. Peñuela, A.; Robledo, D.; Bourgougnon, N.; Bedoux, G.; Hernández-Núñez, E.; Freile-Pelegrín, Y. Environmentally Friendly Valorization of *Solieria filiformis* (Gigartinales, Rhodophyta) from IMTA Using a Biorefinery Concept. *Mar. Drugs* **2018**, *16*, 487.
 38. Fenton-Navarro, B.; Arreguín-L, B.; García-Hernández, E.; Heimer, E.; Aguilar, M. B.; Rodríguez-A, C.; Arreguín-Espinosa, R. Purification and Structural Characterization of Lectins from the Cnidarian *Bunodeopsis Antillienis*. *Toxicon* **2003**, *42*, 525–532.
 39. Parera-Valadez, Y.; Yam-Puc, A.; López-Aguilar, L. K.; Borges-Argáez, R.; Figueroa-Saldivar, M. A.; Cáceres-Farfán, M.; Márquez-Velázquez, N. A.; Prieto-Davó, A. Ecological Strategies Behind the Selection of Cultivable Actinomycete Strains from the Yucatan Peninsula for the Discovery of Secondary Metabolites with Antibiotic Activity. *Microb. Ecol.* **2019**, *77*, 839–851.
 40. Pless, D. D.; Aguilar, M. B.; Falcón, A.; Lozano-Alvarez, E.; Heimer de la Cotera, E. P. Latent Phenoloxidase Activity and N-Terminal Amino Acid Sequence of Hemocyanin from *Bathynomus giganteus*, a Primitive Crustacean. *Arch. Biochem. Biophys.* **2003**, *409*, 402–410.
 41. Méndez Alpuche, A. A. Caracterización fisicoquímica de biopolímeros obtenidos del exoesqueleto de la Cacerolita de mar, *Limulus polyphemus*. M.S. Thesis, Centro de Investigacion Científica de Yucatán A. C., Yucatán, México, 2017. pp 1-68.
 42. Rinehart, K. L.; Kishore, V.; Bible, K. C.; Sakai, R.; Sullins, D. W.; Li, K. Didemnins and Tunichlorin: Novel Natural Products from the Marine Tunicate *Trididemnum solidum*. *J. Nat. Prod.* **1988**, *51*, 1–21.
 43. Cruz-Hernández, E.; Rodríguez-Morales, S. Sea Anemones from Yucatan Peninsula as Source of Bioactive Compounds. *Toxicol. Lett.* **2016**, *259*, S198.
 44. Sánchez-Rodríguez, J.; Zugasti-Cruz, A.; Burnnet, J. W. Cutaneous Stings from *Bartholomea annulata*. *Contact Dermatitis* **2001**, *44*, 314–315.
 45. Santamaría, A.; Sánchez-Rodríguez, J.; Zugasti, A.; Martínez, A.; Galván-Arzate, S.; Segura-Puertas, L. A Venom Extract from the Sea Anemone *Bartholomea annulata* Produces Haemolysis and Lipid Peroxidation in Mouse Erythrocytes. *Toxicology* **2002**, *173*, 221–228.
 46. Sánchez-Rodríguez, J.; Zugasti, A.; Santamaría, A.; Galván-Arzate, S.; Segura-Puertas, L. Isolation, Partial Purification and Characterization of Active Polypeptide from the Sea Anemone *Bartholomea annulata*. *Basic Clin. Pharmacol. Toxicol.* **2006**, *99*, 116–121.

47. Morales-Landa, J. L.; Zapata-Pérez, O.; Cedillo-Rivera, R.; Segura-Puertas, L.; Simá-Alvarez, R.; Sánchez-Rodríguez, J. Antimicrobial, Antiprotozoal, and Toxic Activities of Cnidarian Extracts from the Mexican Caribbean Sea. *Pharm. Biol.* **2007**, *45*, 37–43.
48. Monroy-Estrada, H. I.; Chirino, Y. I.; Soria-Mercado, I. E.; Sánchez-Rodríguez, J. Toxins from the Caribbean Sea Anemone *Bunodeopsis globulifera* Increase Cisplatin-Induced Cytotoxicity of Lung Adenocarcinoma Cells. *J. Venom. Anim. Toxins Incl. Trop. Dis.* **2013**, *19*, 12.
49. Flores-Pérez, A. J.; Sánchez-Rodríguez, J. Isolation and Purification of Neurotoxins from the Caribbean Sea Anemone *Bunodeopsis globulifera*. *Toxicol. Lett.* **2016**, *259*, S198.
50. Santos, Y.; Martínez, M.; Sandoval, A.; Rodríguez, A. A.; Falcón, A.; Heimer de la Cotera, E. P.; Aguilar, M. B.; Flores, P.; Felix, R.; Arreguín, R. Arrhythmogenic Effect of a Crude Extract from Sea Anemone *Condylactis gigantea*: Possible Involvement of rErg1 Channels. *Toxicon* **2013**, *67*, 47–54.
51. Sánchez-Rodríguez, J.; Cruz-Vazquez, K. Isolation and Biological Characterization of Neurotoxic Compounds from the Sea Anemone *Lebrunia danae* (Duchassaing and Michelotti, 1860). *Arch. Toxicol.* **2006**, *80*, 436–441.
52. Monroy-Estrada, H. I.; Segura-Puertas, L.; Galván-Arzate, S.; Santamaría, A.; Sánchez-Rodríguez, J. The Crude Venom from the Sea Anemone *Stichodactyla helianthus* Induces Haemolysis and Slight Peroxidative Damage in Rat and Human Erythrocytes. *Toxicol In Vitro* **2007**, *21*, 398–402.
53. García-Arredondo, A.; Rojas-Molina, A.; Ibarra-Alvarado, C.; Iglesias-Prieto, R. Effects of Bleaching on the Pharmacological and Toxicological Activities Elicited by the Aqueous Extracts Prepared from Two “Fire Corals” Collected in the Mexican Caribbean. *J. Exp. Mar. Bio. Ecol.* **2011**, *396*, 171–176.
54. Hernández-Matehuala, R.; Vuelvas-Solórzano, A. A.; Zepeda-Rodríguez, A.; Palma, L.; Rojas, A. Acute Toxicity and Brine Shrimp Cytotoxicity Induced by the Venom of the Fire Coral *M. alcicornis* Collected in the Mexican Caribbean. *Toxicon* **2012**, *60*, 156–157.
55. García-Arredondo, A.; Rojas, A.; Ibarra-Alvarado, C.; Iglesias-Prieto, R. A Comparison of the Structural Characteristics of the Nematocysts of the “Fire Corals” *Millepora alcicornis* and *M. complanata*, and Their Hemolytic and Vasoconstrictor Effects. *Toxicon* **2012**, *60*, 150.
56. Hernández-Matehuala, R.; Rojas-Molina, A.; Vuelvas-Solórzano, A. A.; Garcia-Arredondo, A.; Ibarra Alvarado, C.; Olguín-López, N.; Aguilar, M. Cytolytic and Systemic Toxic Effects Induced by the Aqueous Extract of the Fire Coral *Millepora alcicornis* Collected in the Mexican Caribbean and Detection of Two Types of Cytolisin. *J. Venom. Anim. Toxins Incl. Trop. Dis.* **2015**, *21*, 36.
57. Olguín-López, N.; Hernández-Elizárraga, V. H.; Hernández-Matehuala, R.; Cruz-Hernández, A.; Guevara-González, R.; Caballero-Pérez, J.; Ibarra-Alvarado, C.; Rojas-Molina, A. Impact of El Niño-Southern Oscillation 2015-2016 on the Soluble Proteomic Profile and Cytolytic Activity of *Millepora alcicornis* (“Fire Coral”) from the Mexican Caribbean. *PeerJ* **2019**, *7*, 1–26.
58. Rojas, A.; Torres, M.; Rojas, J. I.; Feregrino, A.; Heimer-de la Cotera, E. P. Calcium-Dependent Smooth Muscle Excitatory Effect Elicited by the Venom of the Hydrocoral *Millepora complanata*. *Toxicon* **2002**, *40*, 777–785.
59. Ibarra-Alvarado, C.; García, J. A.; Aguilar, M. B.; Rojas, A.; Falcón, A.; Heimer de la Cotera, E. P. Biochemical and Pharmacological Characterization of Toxins Obtained from the Fire Coral *Millepora complanata*. *Comp. Biochem. Phys. C.*

- 2007, 146, 511–518.
60. García-Arredondo, A.; Rojas, A.; Ibarra-Alvarado, C.; Bah, M. Systemic Toxicity of the “Fire Coral” *Millepora complanata*: Isolation of a Non-Protein Vasoconstrictor Fraction with Lethal Activity in Mice. *Toxicon* **2012**, 60, 153–154.
 61. García-Arredondo, A.; Rojas-Molina, A.; Bah, M.; Ibarra-Alvarado, C.; Gallegos-Corona, M. A.; García-Servín, M. Systemic Toxic Effects Induced by the Aqueous Extract of the Fire Coral *Millepora complanata* and Partial Purification of Thermostable Neurotoxins with Lethal Effects in Mice. *Comp. Biochem. Phys. C* **2015**, 169, 55–64.
 62. Hernández-Elizárraga, V. H.; Olguín-López, N.; Hernández-Matehuala, R.; Ocharán-Mercado, A.; Cruz-Hernández, A.; Guevara-González, R. G.; Caballero-Pérez, J.; Ibarra-Alvarado, C.; Sánchez-Rodríguez, J.; Rojas-Molina, A. Comparative Analysis of the Soluble Proteome and the Cytolytic Activity of Unbleached and Bleached *Millepora complanata* (“Fire Coral”) from the Mexican Caribbean. *Mar. Drugs* **2019**, 17, 393.
 63. García-Arredondo, A.; Rojas-Molina, A.; Ibarra-Alvarado, C.; Lazcano-Pérez, F.; Arreguín-Espinosa, R.; Sánchez-Rodríguez, J. Composition and Biological Activities of the Aqueous Extracts of Three Scleractinian Corals from the Mexican Caribbean: *Pseudodiploria strigosa*, *Porites astreoides* and *Siderastrea siderea*. *J. Venom. Anim. Toxins Incl. Trop. Dis.* **2016**, 22, 32.
 64. Segura-Puertas, L.; Avila-Soria, G.; Sánchez-Rodríguez, J.; Ramos-Aguilar, M. E.; Burnett, J. W. Some Toxicological Aspects of *Aurelia aurita* (Linné) from the Mexican Caribbean. *J. Venom. Anim. Toxins* **2002**, 8, 269–282.
 65. Ponce, D.; López-Vera, E.; Aguilar, M. B.; Sánchez-Rodríguez, J. Preliminary Results of the in Vivo and in Vitro Characterization of a Tentacle Venom Fraction from the Jellyfish *Aurelia aurita*. *Toxins* **2013**, 5, 2420–2433.
 66. Sánchez-Rodríguez, J.; Torrens, E.; Segura-Puertas, L. Partial Purification and Characterization of a Novel Neurotoxin and Three Cytolysins from Box Jellyfish (*Carybdea marsupialis*) Nematocyst Venom. *Arch. Toxicol.* **2006**, 80, 163–168.
 67. Lazcano-Pérez, F.; Arellano, R. O.; Garay, E.; Arreguín-Espinosa, R.; Sánchez-Rodríguez, J. Electrophysiological Activity of a Neurotoxic Fraction from the Venom of Box Jellyfish *Carybdea marsupialis*. *Comp. Biochem. Phys. C* **2017**, 191, 177–182.
 68. Torres, M.; Aguilar, M. B.; Falcón, A.; Sánchez, L.; Radwan, F. F. Y.; Burnett, J. W.; Heimer-de la Cotera, E. P.; Arellano, R. O. Electrophysiological and Hemolytic Activity Elicited by the Venom of the Jellyfish *Cassiopea xamachana*. *Toxicon* **2001**, 39, 1297–1307.
 69. Orduña-Novoa, K.; Segura-Puertas, L.; Sánchez-Rodríguez, J.; Meléndez, A.; Nava-Ruíz, C.; Rembao, D.; Santamaria, A.; Galván-Arzate, S. Possible Antitumoral Effect of the Crude Venom of *Cassiopea xamachana* (Cnidaria: Scyphozoa) on Tumors of the Central Nervous System Induced by N-Ethyl-N-Nitrosourea (ENU) in Rats. *Proc. West. Pharmacol. Soc.* **2003**, 46, 85–87.
 70. Sánchez-Rodríguez, J.; Lucio-Martínez, N. L. Isolation and Prepurification of Active Compounds in Venom from *Pelagia noctiluca* (Scyphozoa: Pelagiidae) from the Caribbean Sea. *Cien. Mar.* **2011**, 37, 369–377.
 71. González Vásquez, J. M.; Mena Rejón, G. J.; Quijano, L. Obtención de Saponinas Triterpénicas Potencialmente Citotóxicas a Partir de la Pared Corporal de *Holothuria Mexicana*. In Foro en Ciencias Químicas y Bioquímicas. Posgrado Institucional en Ciencias Químicas y Bioquímicas. Mérida, Yucatán, México, 17

- may 2013. pp 65–66.
72. Pérez-Vega, J. A.; Olivera-Castillo, L.; Gómez-Ruiz, J. A.; Hernández-Ledesma, B. Release of Multifunctional Peptides by Gastrointestinal Digestion of Sea Cucumber (*Isostichopus badionotus*). *J. Funct. Foods* **2013**, *5*, 869–877.
 73. Pérez Espadas, A. R. Evaluación de la actividad citotóxica y componentes del pepino de mar *Isostichopus Badionotus* (Selenka, 1867) del litoral de la Península de Yucatán, México. PhD Thesis; Universidad Autónoma de Nuevo León, Nuevo Leon, Mexico, 2014. pp 1-107.
 74. Pérez-Espadas, A. R.; Verde-Star, M. J.; Rivas-Morales, C.; Oranday-Cárdenas, A.; Morales-Rubio, M. E.; León-Deniz, L. V.; Canul-Canché, J.; Quijano, L. In Vitro Cytotoxic Activity of *Isostichopus badionotus*, A Sea Cucumber from Yucatan Peninsula Coast. *J. Pharm. Nutr. Sci.* **2014**, *4*, 183–186.
 75. Rojas, A.; Feregrino, A.; Ibarra-Alvarado, C.; Aguilar, M. B.; Falcon, A.; Heimer de la Cotera, E. P. Pharmacological Characterization of Venoms Obtained from Mexican Toxoglossate Gastropods on Isolated Guinea Pig Ileum. *J. Venom. Anim. Toxins incl. Trop. Dis.* **2008**, *14*, 497–513.
 76. Aguilar, M. B.; Pérez-Reyes, L. I.; López, Z.; Heimer de la Cotera, E. P.; Falcón, A.; Ayala, C.; Galván, M.; Salvador, C.; Escobar, L. I. Peptide sr11a from *Conus spurius* Is a Novel Peptide Blocker for Kv1 Potassium Channels. *Peptides* **2010**, *31*, 1287–1291.
 77. López-Vera, E.; Heimer De La Cotera, E. P.; Maillo, M.; Riesgo-Escovar, J. R.; Olivera, B. M.; Aguilar, M. B. A Novel Structural Class of Toxins: The Methionine-Rich Peptides from the Venoms of Turrid Marine Snails (Mollusca, Conoidea). *Toxicon* **2004**, *43*, 365–374.
 78. Tello Cetina, J.; Chan Pat, A.; Rivera Muñoz, G.; Tamayo Cortes, J.; Jimenez Suaste, N.; Loria Sunsa, H. Uso de la Melanina del Pulpo (*Octopus maya*) de Yucatán como Agente Antibacteriano. *Rev. Cuba. Investig. Pesq.* **2018**, *35*, 13–17.
 79. Zubia, M.; Robledo, D.; Freile-Pelegrin, Y. Antioxidant Activities in Tropical Marine Macroalgae from the Yucatan Peninsula, Mexico. *J. Appl. Phycol.* **2007**, *19*, 449–458.
 80. Freile-Pelegrin, Y.; Robledo, D.; Chan-Bacab, M. J.; Ortega-Morales, B. O. Antileishmanial Properties of Tropical Marine Algae Extracts. *Fitoterapia* **2008**, *79*, 374–377.
 81. Moo-Puc, R.; Robledo, D.; Freile-Pelegrin, Y. Evaluation of Selected Tropical Seaweeds for in Vitro Anti-Trichomonas Activity. *J. Ethnopharmacol.* **2008**, *120*, 92–97.
 82. Moo-Puc, R.; Robledo, D.; Freile-Pelegrín, Y. Actividad Citotóxica y Antiproliferativa in Vitro de Macroalgas Marinas de Yucatán, México. *Cien. Mar.* **2009**, *35*, 345–358.
 83. León-Deniz, L. V.; Dumonteil, E.; Moo-Puc, R.; Freile-Pelegrin, Y. A. Antitrypanosomal in Vitro Activity of Tropical Marine Algae Extracts. *Pharm. Biol.* **2009**, *47*, 864–871.
 84. Morales, J. L.; Cantillo-Ciau, Z. O.; Sánchez-Molina, I.; Mena-Rejón, G. J. Screening of Antibacterial and Antifungal Activities of Six Marine Macroalgae from Coasts of Yucatán Peninsula. *Pharm. Biol.* **2006**, *44*, 632–635.
 85. Freile-Pelegrin, Y.; Morales, J. L. Antibacterial Activity in Marine Algae from the Coast of Yucatan, Mexico. *Bot. Mar.* **2004**, *47*, 140–146.
 86. De Lara-Isassi, G.; Álvarez-Hernández, S.; Collado-Vides, L. Ichthyotoxic Activity of Extracts from Mexican Marine Macroalgae. *J. Appl. Phycol.* **2000**, *12*,

45–52.

87. García Granados, R. U. Efecto Hipoglucémico, Hipolipidémico y Citotóxico de Macroalgas y Pastos Marinos Del Golfo de México. M.S. Thesis, Universidad Autónoma Metropolitana Unidad Iztapalapa, Mexico, D.F., 2015. pp 1-96.
88. Robledo, D.; Freile Pelegrín, Y. Chemical and Mineral Composition of Six Potentially Edible Seaweed Species of Yucatan. *Bot. Mar.* **1997**, *40*, 301–306.
89. Gomez Hernandez, M. Actividad Antifúngica de Extractos de Macroalgas Marinas de La Costa de Yucatán. M.S. Thesis, Centro de Investigación Científica de Yucatán, A.C., Yucatán, México, 2018. pp 1-110.
90. Moo-Puc, R.; Robledo, D.; Freile-Pelegrin, Y. Improved Antitumoral Activity of Extracts Derived from Cultured *Penicillium dumetosus*. *Trop. J. Pharm. Res.* **2011**, *10*, 177–185.
91. Moo-Puc, R.; Robledo, D.; Freile-Pelegrin, Y. Enhanced Antitumoral Activity of Extracts Derived from Cultured *Udotea flabellum* (Chlorophyta). *Evid. Based Complement. Alternat. Med.* **2011**, *2011*, 1–7.
92. García-Ríos, V.; Ríos-Leal, E.; Robledo, D.; Freile-Pelegrin, Y. Polysaccharides Composition from Tropical Brown Seaweeds. *Phycol. Res.* **2012**, *60*, 305–315.
93. Caamal-Fuentes, E.; Chale-Dzul, J.; Moo-Puc, R.; Freile-Pelegrin, Y.; Robledo, D. Bioprospecting of Brown Seaweed (Ochrophyta) from the Yucatan Peninsula: Cytotoxic, Antiproliferative, and Antiprotozoal Activities. *J. Appl. Phycol.* **2014**, *26*, 1009–1017.
94. Chale-Dzul, J.; Freile-Pelegrín, Y.; Robledo, D.; Moo-Puc, R. Protective Effect of Fucoidans from Tropical Seaweeds against Oxidative Stress in HepG2 Cells. *J. Appl. Phycol.* **2017**, *29*, 2229–2238.
95. Bedoux, G.; Caamal-Fuentes, E.; Boulho, R.; Marty, C.; Bourgougnon, N.; Freile-Pelegrín, Y.; Robledo, D. Antiviral and Cytotoxic Activities of Polysaccharides Extracted from Four Tropical Seaweed Species. *Nat. Prod. Commun.* **2017**, *12*, 807–811.
96. Quintal-Novelo, C.; Rangel-Méndez, J.; Ortiz-Tello, Á.; Graniel-Sabido, M.; Pérez-Cabeza de Vaca, R.; Moo-Puc, R. A *Sargassum Fluitans* Borgesen Ethanol Extract Exhibits a Hepatoprotective Effect in Vivo in Acute and Chronic Liver Damage Models. *Biomed Res. Int.* **2018**, *2018*, 1–9.
97. Chale-Dzul, J.; Moo-Puc, R.; Robledo, D.; Freile-Pelegrín, Y. Hepatoprotective Effect of the Fucoidan from the Brown Seaweed *Turbinaria tricostata*. *J. Appl. Phycol.* **2014**, *27*, 2123–2135.
98. Freile-Pelegrín, Y.; Robledo, D.; Azamar, J. A. Carrageenan of *Euclidean isiforme* (Solieriaceae, Rhodophyta) from Yucatán, Mexico. I. Effect of Extraction Conditions. *Bot. Mar.* **2006**, *49*, 65–71.
99. Freile-Pelegrín, Y.; Murano, E. Agars from Three Species of *Gracilaria* (Rhodophyta) from Yucatán Peninsula. *Bioresour. Technol.* **2005**, *96*, 295–302.
100. Espinoza-Avalos, J.; Hernández-Garibay, E.; Zertuche-González, J. A.; Meave del Castillo, M. E. Agar de Dos Especies Coexistentes de *Gracilaria* (Gracilariaceae) del Caribe Mexicano. *Cien. Mar.* **2003**, *29*, 211–228.
101. Zubia, M.; Freile-Pelegrín, Y.; Robledo, D. Photosynthesis, Pigment Composition and Antioxidant Defences in the Red Alga *Gracilariopsis tenuifrons* (Gracilariales, Rhodophyta) under Environmental Stress. *J. Appl. Phycol.* **2014**, *26*, 2001–2010.
102. Freile-Pelegrín, Y.; Azamar, J. A.; Robledo, D. Preliminary Characterization of Carrageenan from the Red Seaweed *Halymenia floresii*. *J. Aquat. Food Prod. Technol.* **2011**, *20*, 73–83.

103. Godínez Ortega, J. L.; Robledo Ramírez, D. ; Freile Pelegrín, Y.; Ríos Castillo, T. Seasonal Fatty Acid Composition of *Halymenia floresii* (Rhodophyta) in Yucatan, Mexico. *Rev. Latinoam. Quim.* **2012**, *40*, 99–105.
104. Vázquez-Delfín, E.; Robledo, D.; Freile-Pelegrín, Y. Microwave-assisted Extraction of the Carrageenan from *Hypnea musciformis* (Cystocloniaceae, Rhodophyta). *J. Appl. Phycol.* **2014**, *26*, 901–907.
105. Peralta-García, E.; Caamal-Fuentes, E.; Robledo, D.; Hernández-Núñez, E.; Freile- Pelegrín, Y. Lipid Characterization of Red Alga *Rhodymenia pseudopalmata* (Rhodymeniales, Rhodophyta). *Phycol. Res.* **2016**, *65*, 58–68.
106. Pliego-Cortés, H.; Caamal-Fuentes, E.; Montero-Muñoz, J.; Freile-Pelegrín, Y.; Robledo, D. Growth, Biochemical and Antioxidant Content of *Rhodymenia pseudopalmata* (Rhodymeniales, Rhodophyta) Cultivated under Salinity and Irradiance Treatments. *J. Appl. Phycol.* **2017**, *29*, 2595–2603.
107. Morán-Santibañez, K.; Cruz-Suárez, L. E.; Ricque-Marie, D.; Robledo, D.; Freile- Pelegrín, Y.; Peña-Hernández, M. A.; Rodríguez-Padilla, C.; Trejo-Avila, L. M. Synergistic Effects of Sulfated Polysaccharides from Mexican Seaweeds against Measles Virus. *Biomed Res. Int.* **2016**, *2016*, 1–11.
108. Caamal-Fuentes, E.; Robledo, D.; Freile-Pelegrín, Y. Physicochemical Characterization and Biological Activities of Sulfated Polysaccharides from Cultivated *Solieria filiformis* Rhodophyta. *Nat. Prod. Commun.* **2017**, *12*, 803–8
109. WoRMS Editorial Board (2019). World Register of Marine Species. Available from <http://www.marinespecies.org> at VLIZ. Accessed 2019-12-03. doi:10.14284/170.

CAPÍTULO 2

**Recolección, extracción y
evaluación farmacológica
de organismos procedentes
de la Península de Yucatán**

2.1 Recolección y extracción de los organismos

Con el objetivo de explicar la metodología llevada a cabo para la recolecta y extracción que se utilizó en esta investigación, se detallan a continuación los pasos llevados a cabo con todas las muestras recogidas.

Ante la falta de información sobre la riqueza de especies marinas existente en la Península de Yucatán, particularmente de los tres grupos de invertebrados marinos (esponjas, ascidias y gorgonias) más interesantes para desarrollar nuestra investigación. Se procedió a realizar un primera búsqueda de todas las especies reportadas hasta la fecha de esponjas, ascidias y gorgonias en costas de la Península de Yucatán, dando como resultado la presencia de 67 especies de esponjas, 56 de ascidias y 35 de gorgonias en aguas yucatecas. Seguidamente procedimos a realizar una búsqueda en la base de datos SciFinder sobre el número de estudios químicos que existían para cada una de las 158 especies reportadas, tomándose las fotografías correspondientes a cada especie usando bases de datos como WORMS, poriferadatabase, etc. Con toda la información anterior procedimos a la generación de catalogos de cada uno de los tres grupos de organismos de interés, los cuales nos facilitaron la selección de las especies a coleccionar en el campo, concentrando nuestros esfuerzos en el estudio de especies muy poco estudiadas o que presentaran un historial rico en la producción de moléculas estructuralmente novedosas ó actividades biológicas significativas.

Las muestras fueron colectadas a mano usando técnicas de buceo libre y autónomo (SCUBA) durante tres periodos diferentes: septiembre-diciembre 2016, enero-marzo 2017 y septiembre 2018, en seis diferentes sitios de muestreo pertenecientes a dos diferentes regiones de la Península de Yucatán: Caribe Mexicano (Isla de Cozumel, Rio Indio, Mahahual y Bermejo en el estado de Quintana Roo) y el Banco de Campeche (Arrecife Alacranes y Progreso en el estado de Yucatán). Se priorizaron los buceos en zonas con una alta riqueza biológica como: arrecifes coralinos, islas y manglares.

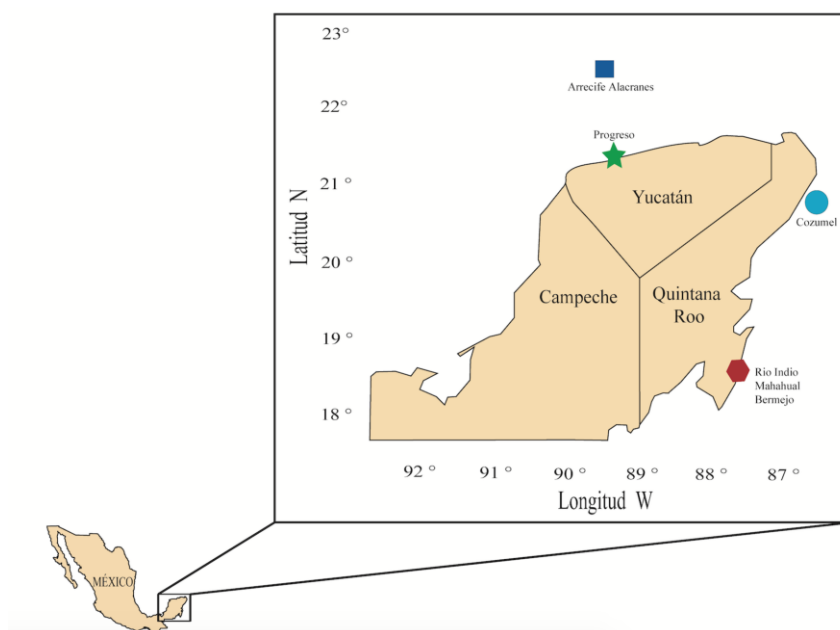


Figura 2.1 Mapa de la Península de Yucatán y los seis lugares de muestreo.

Las muestras fueron colectadas en bolsas de plástico, etiquetadas usando un código de acuerdo a las zonas de colecta, y finalizada la colecta estas fueron puestas inmediatamente en neveras con hielo para su transporte al laboratorio. Cuando el traslado al laboratorio implicaba más de dos tres días de viaje, las muestras fueron introducidas en botes Nalgene® color ambar y fijadas usando una mezcla de agua:etanol 1:1. Siempre se trató de fotografiar a todos los especímenes antes y después de cada colecta. Una parte de cada organismo fue depositado en la colección correspondiente. Las esponjas en la colección nacional del phylum porifera Gerardo Green del Instituto de Ciencias del Mar y Limnología de la Universidad Nacional Autónoma de México (ICMyL-UNAM), mientras que las ascidias y la gorgonia fueron depositadas en la colección de biología marina de la Universidad Autónoma de Yucatán, México (UADY).

La identificación taxonómica de las esponjas fue realizada por la bióloga Patricia Gomez (ICMyL-UNAM, México), mientras que las ascidias y la gorgonia fueron identificadas por la bióloga María Elsa Vázquez Otero (Universidad de Vigo, España), el biólogo Harold Villegas-Hernández (UADY, México) y el biólogo marino Dawrin Pech Puch (CICA, UDC).

Una vez identificadas, cada una de las especies se trocearon y se sometieron a una extracción con una mezcla de diclorometano-metanol (1:1), repitiéndose este proceso tres veces cada 24 horas con un volumen de 500 mL (1.5 L de volumen total) a 25 °C. Después de la filtración, el disolvente fue eliminado a vacío usando el rotavapor a 40 °C y el extracto fue conservado a -20°C en viales de vidrio cerrados herméticamente.

Los extractos obtenidos fueron sometidos a ensayos de actividad antibacteriana, antiviral y antiproliferativa, a través de una serie de colaboraciones con el Instituto de Investigación Biomédica de A Coruña (INIBIC), el Instituto de Biomedicina de Sevilla (IBiS) y la Fundación MEDINA en Granada. Los resultados de estas evaluaciones se presentan a continuación.

2.2 Resultados de la actividad antibacteriana de los extractos

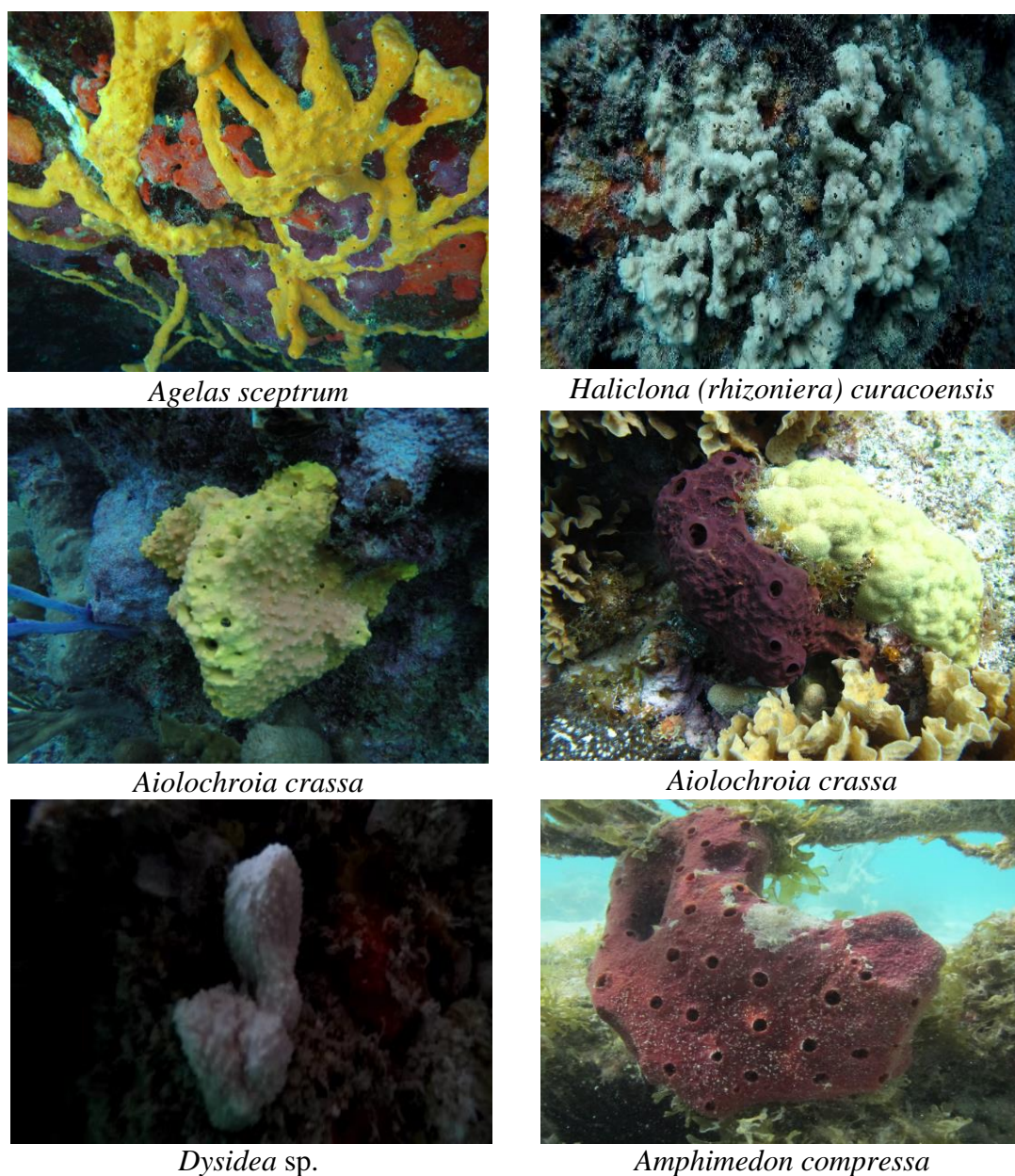


Figura 2.2. Fotografías de los organismos recolectados en las costas de la Península de Yucatán, cuyos extractos presentaron actividad antibacteriana.

En este apartado se describen los resultados de la evaluación biológica de 64 extractos de organismos marinos frente a cuatro especies de patógenos bacterianos altamente resistentes: tres bacterias Gram-negativas: *Acinetobacter baumannii*, *Klebsiella pneumoniae* and *Pseudomonas aeruginosa* y una Gram-positiva *Staphylococcus aureus*, utilizando la técnica de microdilución (MIC). Poco más del 12 % de los extractos evaluados mostraron actividades antibacterianas frente a uno o mas de las patógenos utilizados durante los ensayos. El aislamiento bioguiado del extracto de la esponja *Amphimedon compressa* permitió identificar a los compuestos responsables de su actividad antibacteriana.

Estos resultados dieron origen al trabajo que se presenta a continuación y que será sometido a publicación.

Marine organisms from the Yucatan Peninsula (Mexico) as a potential natural source of new antibacterial compounds

Dawrin Pech-Puch¹, Mar Perez-Povedano¹, Marta Martínez-Guitián², Cristina Lasarte-Monterrubio², Juan Carlos Vázquez-Ucha², Lourdes Novoa-Olmedo², Germán Bou², Jaime Rodríguez¹, Alejandro Beceiro² and Carlos Jiménez¹

¹Centro de Investigaciones Científicas Avanzadas (CICA) e Departamento de Química, Facultade de Ciencias, Universidade da Coruña, 15071 A Coruña, Spain

²Servicio de Microbiología. Instituto de Investigación Biomédica (INIBIC), Agrupación Estratégica CICA-INIBIC. Complejo Hospitalario Universitario A Coruña, 15006, A Coruña, Spain

* Correspondence: Centro de Investigaciones Científicas Avanzadas (CICA) e Departamento de Química, Facultad de Ciencias, Universidade da Coruña, 15071 A Coruña, Spain. Tel: +34 981 167000. Fax: +34 981 167065. *E-mail address*: jaime.rodriguez@udc.es (Jaime Rodríguez); carlos.jimenez@udc.es, (Carlos Jiménez).

Abstract: The in vitro antibacterial activity of organic extracts of 51 sponges (Porifera) and 13 ascidians (Chordata) collected on the coast of the Yucatan Peninsula (Mexico) was tested by screening the extracts against four multidrug-resistant (MDR) bacterial pathogens: the Gram-negative *Acinetobacter baumannii*, *Klebsiella pneumoniae* and *Pseudomonas aeruginosa* and the Gram-positive *Staphylococcus aureus*. The minimum inhibitory concentrations (MICs) of the organic extracts of each marine organism were determined by broth microdilution assay. Extracts of 8 of the species, in particular *Agelas citrina* and *Haliclona (Rhizoniera) curacaoensis*, displayed activity against some of the pathogens tested. This study is the first to carry out antimicrobial screening of extracts of marine sponges and ascidians collected from the Yucatan Peninsula.

Keywords: Antimicrobial; Multidrug Resistance; Yucatan Peninsula

1. Introduction

The Yucatan Peninsula in Mexico is the area where the great Mayan culture became established and developed. The Maya people had extensive knowledge about the natural resources available and they maintained a long tradition of using the flora and fauna from the region to meet their basic needs in relation to food, health and housing. In a recent large ethnobiological study of contemporary Mayan culture (Durán-García et al., 2016), is reported that some 145 of the estimated 2300 vascular plants known to grow in the region are used as food sources while another 680 are used for medicinal purposes. The same study refers to different applications of various wildlife species: 81 terrestrial vertebrates, mainly reptiles, birds and mammals, are used as food sources and at least 40 wild vertebrates are used for medicinal purposes. More specifically, in relation to marine resources, 62 teleostean, 3 elasmobranch, 4 molluscan and 4 crustacean species are commercially harvested (Durán-García et al., 2016).

The discovery of remains of toxic marine animals such as stingrays, puffer fishes, cone snails, sponges and corals in caches in archaeological sites of the ancient Mayan

civilization indicated that the venom or toxins of these organisms may have been used for specific purposes, e.g. to induce pain or in ritual contexts (Maxwell, 2000). Sponges were used in ancient Greek civilization for medical and pharmacological purposes because of their absorbent, compressive and sterile properties (Voultsiadou, 2010). However, direct uses for marine organisms in Mayan culture are not known in many cases.

Antimicrobial resistance (AMR) has become a global health emergency and is placing the great historical achievements made with the discovery of antibiotics in the 20th century at risk. The use and development of antibiotics did not take into account the rapid evolution of the bacteria being targeted, and antimicrobial resistance has emerged hand in hand with the routine clinical use of antibiotics. It has been estimated that AMR is responsible for more than 25,000 deaths a year in the European Union, and it has been predicted that this number could rise to more than 10 million deaths worldwide by 2050, overcoming pathologies such as cancer and heart disease (O'Neill, 2016). In addition, AMR has been estimated to cause economic losses of 1.5 billion euros a year in European health systems. International organisations such as the Food and Agriculture Organization (FAO), the World Organisation for Animal Health (OIE) and the World Health Organization (WHO) have established AMR as one of the main research objectives within the field of health in the next decade. This scenario indicates the need for extraordinary efforts to be made both from scientific and academic communities and from society in general, in the search for solutions to this global health problem.

The WHO has published a list of priority pathogens for R&D of new antibiotics. The list includes various species identified as of critical priority, such as *Acinetobacter baumannii*, carbapenem-resistant *Enterobacteriaceae* and *Pseudomonas aeruginosa*, and several species identified as of high priority, such as *Staphylococcus aureus* resistant to methicillin and vancomycin (WHO, 2017). Hospital outbreaks caused by these pathogens have increased significantly in recent decades, causing serious health problems (Maragakis and Perl, 2008). Carbapenems are last-line antibiotics used to treat multi-resistant strains of these Gram-negative pathogens. However, resistance to these antimicrobials increased substantially in the first decade of this century (Meletis, 2016). Colistin is one of the few remaining antimicrobials that is effective against these Gram-negative pathogens, with resistance rates below 10%. Unfortunately, there are important drawbacks associated with the use of colistin, including high nephrotoxicity, poor distribution in cerebrospinal fluid and lung and rapidly increasing resistance rates (Gales et al., 2011) Under these circumstances, the need for new therapeutic options for the treatment of multi-resistant pathogen infections is indisputable. Most recently developed antimicrobials are derived from already known antibiotics. The discovery of new antimicrobials is closely followed by the development of resistance to these, and drugs with new mechanisms of action that overcome the current mechanisms of resistance are urgently required (Isler et al., 2019).

Oceans have become an important natural source of bioactive molecules, mainly because they cover a great proportion of Earth's surface (more than 70%) and are highly diverse ecosystems. The distinctive physical and chemical conditions of the marine environment facilitate the production of molecules with unique structural, chemical and biological characteristics that are not found in natural products isolated from terrestrial sources (Kong et al., 2010). Most of the biological activities associated with natural marine products are cytotoxic and anticancer properties (Hu et al., 2015). Natural products and their derivatives that can be related to molecules isolated from marine organisms and which have been approved as therapeutic agents belong to six structural types (Jiménez, 2018). The alkaloid Yondelis® (trabectedin, ecteinascidin 743), a marine

natural product isolated from the tunicate *Ecteinascidia turbinata* (Cuevas et al., 2009) and the antibody-drug conjugate (ADC) Adcetris® (brentuximab vedotin), a derivative of dolastatin 10, originally isolated from extracts of the sea hare *Dolabella auricularia*, (Katz et al., 2011) represent two examples of anticancer agents approved by the FDA. Moreover, a large number of marine-derived drug candidates are currently under evaluation in clinical trials. Porifera (sponges) and Cnidaria (soft coral and gorgonians) along with marine microorganisms are currently the most productive sources of new natural products (Altmann et al., 2017).

In tropical waters, species and their predators compete strongly for space, and marine organisms produce secondary metabolites as chemical defence mechanisms (Carroll et al., 2019). Mexico has been considered one of the three areas in the world with the highest terrestrial and marine biological diversity (Bye et al., 1995), and although the chemical diversity of the Mexican medicinal flora has long been investigated, yielding a wide variety of bioactive compounds (Peña et al., 2019), the chemical potential of the marine resources has not been widely explored (Pech-Puch et al., 2020). The Mexican territory covers an area of 2,946,825 km² and has 11,122 km of coastline, which extends from the Pacific Ocean to the Caribbean Sea and the Gulf of Mexico, including the Baja California peninsula (northwest) and the Yucatan peninsula (southeast), which hosts a rich marine flora and fauna (Morales et al., 2006). More specifically, the Gulf of Mexico and the Caribbean Sea, which meet in the Yucatan channel, constitute two outstanding marine ecosystems. This particular geographical location promotes the existence of a high diversity and abundance of different marine species, which represent a potential source of bioactive compounds and food (Morales et al., 2006). The Yucatan Peninsula occupies 17.4% of the coastline of Mexico and it has a great biological diversity on the shore and in the ocean. Moreover, it has a considerable extension of shores and other biological zones, such as mangrove forests, tropical reefs and protected natural areas (Celestún, Ría Lagartos, Dzilam de Bravo and Reef Alacranes, among others), where the chemical properties of natural products remain untapped (Aguilar et al., 2008; INEGI, 2017). The few studies of marine organisms collected from the Yucatan peninsula have focused almost exclusively on describing the biological activities of the organic extracts, mainly antibacterial (Freile-Pelegrín et al., 2004), antifungal (Morales et al., 2006), antioxidant (Zubia et al., 2007), antiparasitic (Morales-Landa et al., 2007; Moo-Puc et al., 2008), ichthyotoxic (De Lara-Issasi et al., 2000) and cytotoxic (Moo-Puc et al., 2009) extracts. Most of the marine organisms that have been studied are algae, with fewer studies of cnidarians and holothuroids, and very few of sponges and tunicates (Morales-Landa et al., 2007; García-Arredondo et al., 2016).

In light of this background, we have begun a research project focusing on the chemistry and biological activity of sponges and ascidians from the Yucatan Peninsula (Pech-Puch et al., 2019). In this article, we report the evaluation of the antibacterial activity of 64 organic extracts from marine invertebrate species collected along the coasts of the Yucatan Peninsula, selected on the basis of chemotaxonomic criteria. We prioritized those species of marine organisms belonging to genera or families from which compounds with unusual structures have been extracted or that have previously shown remarkable biological activity. One of the active sponge extracts was further fractionated and the compounds responsible for the antimicrobial activity were isolated.

2. Materials and methods

2.1. Animal collection and identification

Samples of animals were collected by snorkelling and SCUBA diving in different coastal zones of the Yucatan Peninsula, Mexico, during three different periods: September-December 2016, January-March 2017 and September 2018. The selected species were collected from two different regions: Mexican Caribbean (Cozumel Island, Rio Indio, Mahahual and Bermejo, Quintana Roo) and Campeche Bank (Alacranes Reef and Progreso, Yucatan) in areas with high biological diversity such as coral reefs, islands and mangrove forests (Figure 1).

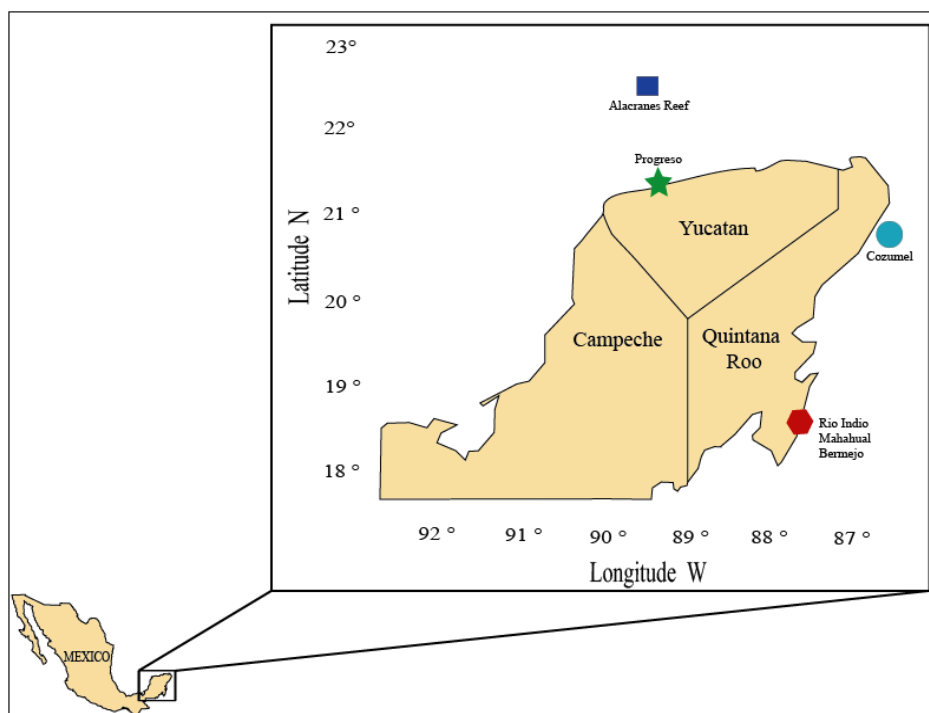


Figure 1. Sites of collection of marine organisms in the Yucatan Peninsula, Mexico.

The samples were labelled with a code according to the collection site, stored in plastic bags and chilled on ice during transport to the laboratory. Voucher specimens of sponges were deposited in the Phylum Porifera Gerardo Green National Collection of the Institute of Marine Sciences and Limnology (ICMyL) at the National Autonomous University of Mexico (UNAM), Mexico City, while voucher specimens of ascidians were deposited in the Marine Biology Collection at the Autonomous University of Yucatan (UADY) in Yucatan, Mexico.

The sponges were identified at the ICMyL-UNAM (Mexico) while the ascidians were identified at the University of Vigo (Spain) and the Autonomous University of Yucatan (Mexico). Taxonomic information, voucher labels, collection sites, previous antimicrobial activity records of the species or genus studied and yield of extracts (% from wet weight) of the 64 selected marine organisms are shown in Table 1.

Table 1. Taxonomic information, voucher numbers, site of collection, yield of the organic extract and previously reported antibacterial activity for the species under study.

Phylum: Chordata

Order: Aplousobranchia

Family	Organism	Code	Site	Yield (gr)	Antibacterial activity reported	References
Clavelinidae	<i>Clavelina</i> sp.	T18-M1	Progreso, Yucatan (Mangrove)	5.0	Example of species of this genus: <i>C. pictus</i> . Stereoisomers of piclavins A2 to A4 present a low activity against Gram positive bacteria (<i>S.aureus</i> , <i>B. cereus</i> and <i>C. michiganensis</i>).	Raub et al., 1992
	<i>Didemnum perlucidum</i>	E8-2	Rio Indio, Quintana Roo	1.8	Low activity against <i>S. aureus</i> , and not active against <i>E. coli</i> and <i>P. aeruginosa</i> .	Bianco et al., 2015
	<i>Didemnum</i> sp.	T18-M4	Progreso, Yucatan (Mangrove)	3.5	Example of species of this genus: Antimicrobial activity of <i>Didemnum</i> sp. against <i>E. faecalis</i> , <i>S. aureus</i> , <i>S. typhimurium</i> , <i>S. marcescens</i> and <i>P. aeruginosa</i> .	Arumugam et al., 2019
Didemnidae	<i>Didemnum</i> sp.	E01	Bermejo, Quinta Roo	3.7	Bactericidal effect except in <i>S. aureus</i> , wherein it presented bacteriostatic effect.	Lima et al., 2014
	<i>Trididemnum solidum</i>	E7-2	Rio Indio, Quintana Roo	3.4	No previous reports for this species.	
	<i>Polysyncraton</i> sp.	EY18-8	Progreso, Yucatan	3.6	No previous reports for this genus.	
Polycitoridae	<i>Eudistoma amanitum</i>	RIO18-T1	Río Indio, Quintana Roo	3.6	No previous reports for this genus.	
	<i>Eudistoma</i> sp.	TY18-2	Progreso, Yucatan	2.9	No previous reports for this genus.	
Polyclinidae	<i>Polyclinum</i> sp.	T18-M5	Progreso, Yucatan (Mangrove)	1.8	The extract of a <i>Polyclinum</i> sp. yielded MIC of >1000 mg/L for <i>S. aureus</i> , <i>E. coli</i> and <i>P. aeruginosa</i> .	Bianco et al., 2015
Order: Phlebobranchia						
Asciidiidae	<i>Phallusia nigra</i>	TY18-1	Progreso, Yucatan	5.5	Low antimicrobial activity against <i>B. subtilis</i> , <i>S. aureus</i> , <i>E. aerogenes</i> , <i>E. coli</i> , <i>K. pneumoniae</i> , <i>P. aeruginosa</i> , <i>S. paratyphii</i> , <i>S. typhii</i> and <i>V. cholerae</i> .	Jaffaralii et al., 2008
Perophoridae	<i>Ecteinascidia</i> sp.	T18-M2	Progreso, Yucatan (Mangrove)	9.0	No previous reports for this genus.	
Order: Stolidobranchia						

Molgulidae	<i>Molgula</i> sp.	T18-M6	Progreso, Yucatan (Mangrove)	3.9	No previous reports for this genus.	
Styelidae	<i>Polycarpa</i> sp.	E41	Alacranes Reef, Yucatan	2.4	No previous reports for this genus.	
Phylum: Porifera						
Order: Agelasida						
	<i>Agelas citrina</i>	CZE56	Cozumel, Quintana Roo	1.9	Antimicrobial activity against <i>E. coli</i> and inhibition of its quorum sensing. No antimicrobial activity against <i>C. violaceum</i> and inhibition of its quorum sensing with high concentrations.	Quintana et al., 2015
Agelasidae	<i>Agelas clathrodes</i>	E27-2	Cozumel, Quintana Roo	11.2	Clathrocin did not display antimicrobial activity against <i>E. faecalis</i> , <i>S. aureus</i> and <i>E. coli</i> , but displayed low antifungal activity against <i>C. albicans</i> .	Zidar et al., 2014
	<i>Agelas clathrodes</i>	MA18-10	Mahahual, Quintana Roo	7.2		
	<i>Agelas dilatata</i>	E25-1	Cozumel, Quintana Roo	21.3	No previous reports for this species.	
	<i>Agelas sceptrum</i>	E26-2	Cozumel, Quintana Roo	4.6	Sceptrin displayed antimicrobial activity against <i>S. aureus</i> , <i>B. subtilis</i> and <i>P. aeruginosa</i> .	Walker et al., 1998
Order: Axinellida						
Heteroxyidae	<i>Myrmekioderma gyroderma</i>	CZE18	Cozumel, Quintana Roo	7.5	No previous reports for this species.	
	<i>Ectyoplasia ferox</i>	MA18-9	Mahahual, Quintana Roo	5.9	No previous reports for this species.	
Raspailiidae	<i>Ectyoplasia</i> sp.	MA18-13	Mahahual, Quintana Roo	2.2	No previous reports for this genus.	
Order: Chondrillida						
Chondrillidae	<i>Chondrilla caribensis f. hermatypica</i>	MA18-6	Mahahual, Quintana Roo	2.1	No growth inhibition of <i>S. aureus</i> , <i>S. epidermidis</i> and <i>E. coli</i> .	Marques et al., 2018
	<i>Chondrilla</i> sp.	RIO18-1	Río Indio, Quintana Roo	4.6	No previous reports for this genus.	
Order: Clathrinida						
Clathrinidae	<i>Clathrina</i> sp.	EY18-10	Progreso, Yucatan	1.4	No previous reports for this genus.	
Leucettidae	<i>Leucetta floridana</i>	E2-2	Bermejo, Quinta Roo	1.3	No previous reports for this species.	
Order: Clionaida						
Clionaidae	<i>Cliona delitrix</i>	EY18-1	Progreso, Yucatan	5.2	<i>Quorum sensing</i> inhibition in <i>E. coli</i> .	Quintana et al., 2015

	<i>Cliona varians</i>	EY18-3	Progreso, Yucatan	1.8	No observed antibacterial activity against <i>E. coli</i> or <i>C. violaceum</i> .	Quintana et al., 2015
Order: Dictyoceratida						
Dysideidae	<i>Dysidea</i> sp.	EY18-12	Progreso, Yucatan	3.3		
	<i>Ircinia felix</i>	E9-2	Rio Indio, Quintana Roo	43.5	<i>Quorum sensing</i> inhibition in <i>C. violaceum</i> . No effects on bacterial growth observed for this species.	Quintana et al., 2015 Sepčić et al., 2010
Irciniidae	<i>Ircinia felix</i>	MA18-11	Mahahual, Quintana Roo	1.7	Antibacterial activity against <i>B. subtilis</i> .	
	<i>Ircinia strobilina</i>	E24-2	Cozumel, Quintana Roo	14.1	Antibacterial activity against <i>B. subtilis</i> . No growth inhibition of <i>E. coli</i> .	Sepčić et al., 2010.
	<i>Ircinia strobilina</i>	E52	Bermejo, Quinta Roo	4.9		
Spongiidae	<i>Spongia tubulifera</i>	E11-2	Rio Indio, Quintana Roo	29.8	No previous reports for this species.	
Order: Haplosclerida						
	<i>Callyspongia longissima</i>	E28	Alacranes Reef, Yucatan	1.8	No previous reports for this species.	
Callyspongiidae	<i>Callyspongia plicifera</i>	E31	Alacranes Reef, Yucatan	1.2	Antibacterial activity against <i>E. coli</i> .	Sepčić et al., 2010
	<i>Callyspongia vaginalis</i>	E16	Cozumel, Quintana Roo	0.9	Antibacterial activity against <i>B. subtilis</i> .	Sepčić et al., 2010
Chalinidae	<i>Haliclona (Rhizoniera) curacaoensis</i>	EY18-4	Progreso, Yucatan	7.9	No previous reports for this species.	
	<i>Amphimedon compressa</i>	E29	Alacranes Reef, Yucatan	12.9	Antibacterial activity against <i>E. coli</i> , <i>P. aeruginosa</i> and MRSA S. aureus.	Xu et al., 2007
	<i>Niphates digitalis</i>	E15	Cozumel, Quintana Roo	2.5	No previous reports for this species.	
Niphatidae	<i>Niphates erecta</i>	E49	Alacranes Reef, Yucatan	1.6		
	<i>Niphates erecta</i>	MA18-7	Mahahual, Quintana Roo	2.8	No previous reports for this species.	
	<i>Niphates erecta</i>	MA18-12	Mahahual, Quintana Roo	2.5		
Petrosiidae	<i>Xestospongia muta</i>	EP	Alacranes Reef, Yucatan	5.9	No growth or <i>quorum sensing</i> inhibition of <i>E. coli</i> or <i>C. violaceum</i> .	Quintana et al., 2015
Order: Homosclerophorida						

Plakinidae	<i>Plakinastrella onkodes</i>	E3	Bermejo, Quinta Roo	1.5	No previous reports for this species.	
Order: Poecilosclerida						
Crambeidae	<i>Monanchora arbuscula</i>	E35	Alacranes Reef, Yucatan	9.6	No previous reports for this species.	
Microcionidae	<i>Clathria gomezae</i>	EY18-11	Progreso, Yucatan	3.6	No previous reports for this species.	
	<i>Clathria virgultosa</i>	E7-E34	Alacranes Reef, Yucatan	33.1	No previous reports for this species.	
Mycalidae	<i>Mycale laevis</i>	MA18-1	Mahahual, Quintana Roo	2.3	No previous reports for this species.	
	<i>Mycale laevis</i>	MA18-5	Mahahual, Quintana Roo	2.9		
Order: Scopalinida						
	<i>Scopalina ruetzleri</i>	DNY	Rio Indio, Quintana Roo	9.2		
Scopalinidae	<i>Scopalina ruetzleri</i>	E53	Cozumel, Quintana Roo	2.2	No previous reports for this species.	
	<i>Scopalina ruetzleri</i>	EY18-7	Progreso, Yucatan	20.0		
Order: Suberitida						
Halichondriidae	<i>Halichondria melanadocia</i>	E18-M1	Progreso, Yucatan (Mangrove)	3.6	No previous reports for this species.	
Suberitidae	<i>Aptos</i> sp.	E38	Alacranes Reef, Yucatan	4.0	No previous reports for this species.	
Order: Tethyida						
Tethyidae	<i>Tethya</i> sp.	E20	Cozumel, Quintana Roo	6.6	No previous reports for this species.	
Order: Tetractinellida						
Geodiidae	<i>Meloplus hajdii</i>	E4	Bermejo, Quinta Roo	4.4	Antibacterial activity against <i>Mycobacterium</i> sp.	Arai et al., 2016
Tetillidae	<i>Cinachyrella kuekenthali</i>	MA18-2	Mahahual, Quintana Roo	2.1	Antibacterial activity of aqueous and ethanolic extracts against different species of the genus <i>Staphylococcus</i> sp.	Laport et al., 2012
Order: Verongiida						
	<i>Aiolochoiria crassa</i>	E50	Alacranes Reef, Yucatan	5.2	No previous reports for this species.	
Aplysinidae	<i>Aiolochoiria crassa</i>	MA18-4	Mahahual, Quintana Roo	8.7		
	<i>Aplysina cauliformis</i>	E36	Alacranes Reef, Yucatan	6.3	Antibacterial activity against <i>M. tuberculosis</i> H37Rv.	De Oliveira et al., 2006

<i>Aplysina fistularis</i>	E46	Alacranes Reef, Yucatan	2.7	No previous reports for this species.
<i>Aplysina fulva</i>	E42	Alacranes Reef, Yucatan	1.8	No previous reports for this species.
<i>Aplysina fulva</i>	EY18-5	Progreso, Yucatan	2.9	
<i>Aplysina muricyanna</i>	E47	Alacranes Reef, Yucatan	4.4	No previous reports for this species.

2.2. Preparation of the organic extracts

Tissue slices from each species were exhaustively extracted with a mixture of dichloromethane-methanol (1:1), i.e. three times each with 500 mL of solvent (1.5 L total volume) at 25 °C for 24 h. The solvent was filtered and then removed under vacuum at 40 °C with a rotatory evaporator. The extracts were stored at -20 °C in tightly sealed glass vials.

2.3. Bioguided isolation of the *Amphimedon compressa* crude extract

Whole bodies of *A. compressa* (wet weight, 509.2 g; dry weight, 64.0 g) were sliced and exhaustively extracted, as previously described, to yield 8.3 g of a crude residue. Fractionation of 8.2 g of the residue by Solid Phase Extraction (SPE), using a stepped gradient from H₂O to CH₃OH and then CH₂Cl₂ (H₂O (100%), H₂O/CH₃OH (2:1, 1:1, and 1:2), CH₃OH (100%), CH₃OH/ CH₂Cl₂ (1:1) and CH₂Cl₂ 100%), yielded seven fractions (R1-R7). The fractions were concentrated under reduced pressure producing the following weights: R1: 6.7 g, R2: 213.3 mg; R3: 71.6 mg; R4: 74.7 mg; R5: 931.4 mg; R6: 192.3 g; R7: 11.1 mg. In the evaluation of the fractions in the both microdilution assay (see below), fractions R3 and R4 displayed antibacterial activity. Part of the most active fraction R4 (50 mg) was further fractionated by HPLC, in an Agilent 1100 liquid chromatography system equipped with a solvent degasser, quaternary pump and diode array detector (Agilent Technologies, Waldbronn, Germany) using a semipreparative Luna C18 reverse phase column (5 μ, 100 Å, 250 × 10 mm). The mobile phase consisted of (A) H₂O with 0.04% of trifluoroacetic acid (B) CH₃OH with 0.04% of trifluoroacetic acid at a flow rate of 2.0 mL/min. A combination of gradient and isocratic elution was used, starting with 90% A and 10% B, changing to 67% of B in 10 min, followed by 5 min isocratic at 67% of B, 2 min gradient from 67% to 75% of B, 23 min of isocratic at 75% of B, and finally changing to 100% of B in 5 min. A major peak, subfraction R4H2, eluted with a retention time of 16.8 min, was collected and concentrated under reduced pressure to produce 8.0 mg of yellow solid which was identified by NMR analysis as a mixture of cyclic alkylpyridine oligomers halitoxins and amphitoxins. The structure was analyzed by nuclear magnetic resonance (NMR). The ¹H and ¹³C NMR spectra were recorded on a Bruker Avance 500 spectrometer at 500 and 125 MHz, respectively. Bioguided fractionation was performed using an antibacterial activity assay against the four bacterial pathogens, as detailed in below.

2.4. Antibacterial activity assays

2.4.1. Culture preparation

The bacterial strains used to study the antibacterial activity of the crude extracts as well as their main characteristics are shown in Table 2. The bacteria studied were the Gram-negative pathogens *A. baumannii* (strain ATCC 17978), *P. aeruginosa* (strain ATCC 27853) and *K. pneumoniae* (strain ATCC 700603) and the Gram-positive pathogen *S. aureus* (strains ATCC 29213). For bioguided fractionation of *A. compressa*, the following bacterial strains were also used: *A. baumannii* ABRIM, *K. pneumoniae* Kp3380, *P. aeruginosa* PA01 and *S. aureus* USA 300 LAC. Strain PA01 is a reference strain, commonly used in research and the other three strains are clinical isolates collected from samples from the Complejo Hospitalario Universitario A Coruña (CHUAC) hospital in Spain.

Gram-negative and Gram-positive strains were routinely grown or maintained in Luria-Bertani (LB), and in Trypticase soya broth (TSB) media, respectively, supplemented with 2% agar or the antibiotic ampicillin (30 mg/L), when needed. All strains were grown at 37 °C and stored in 10 % glycerol at -80 °C.

Table 2. Description of bacterial type strains used.

Bacterial sp.	Strains	Description
<i>A. baumannii</i>	ATCC ^a 17978 ABRIM (clinical isolate)	Gram-negative rod-shaped bacterium, can produce pneumonia, blood infections, wound and surgical site infections and urinary tract infections. (Antunes et al., 2014)
<i>K. pneumoniae</i>	ATCC 700603 Kp3380 (clinical isolate)	Gram-negative rod-shaped capsulate bacterium, produces pneumonia, urinary tract infections, sepsis, meningitis, diarrhea, and soft tissue infections. (Podschun and Ullman, 1998)
<i>P. aeruginosa</i>	ATCC 27853 PA01 (reference strain)	Gram-negative, encapsulated, rod-shaped bacterium. It infects the airway, urinary tract, burns, and wounds, and also causes other blood infections. (Basetti et al., 2018)
<i>S. aureus</i>	ATCC 29213 USA LAC 300 (clinical isolate)	Gram-positive, round-shaped bacterium, one of the most common causes of bacteremia and infective endocarditis, it can also cause various skin and soft-tissue infections. (Tong et al., 2015)

^a American Type Culture Collection

2.4.2. Microdilution method: Minimum inhibitory concentration

The minimum inhibitory concentrations (MICs) were determined by the broth microdilution method (CLSI, 2012). Briefly, the bacterial strains were cultured overnight at 37 °C in Mueller Hinton II agar plates (Becton Dickinson) and the turbidity of the bacterial suspensions was standardized at 0.5 on the McFarland scale to establish the inocula. The crude extracts of the test samples were dissolved in dimethylsulfoxide (DMSO). Two-fold serial dilutions of the extracts in Mueller Hinton II broth medium (Sigma) were carried out in 96-wells microplates, to produce a range of extract concentrations of 0.5-256 mg/L. DMSO was present at a maximum concentration of 2.5%

v/v in the well containing the highest concentration of extract (256 mg/L). One well in each row contained growth media and bacterial suspension and was used as a positive growth control. Another well containing medium only was used as a negative control. Solvent controls of DMSO and growth medium were included to determine whether the concentrations used interfered with bacterial growth. The MIC was evaluated after incubation 20-24 h to 37 °C and was established as the lowest concentration of the compound at which the bacterial strains did not grow. All extracts were tested in triplicate.

3. Results and discussion

A total of 64 marine organisms (51 sponges and 13 ascidians) were collected from two different, species-rich ecosystems in the Yucatan Peninsula in Mexico: a coral reef and a mangrove forest. For the collection, specimens belonging to genera or families from which structurally novel compounds had previously been extracted and/or that displayed interesting biological activities were prioritized (selected from the SciFinder and Antimarin databases by applying chemotaxonomic criteria). Each organism was exhaustively extracted (three times) with a mixture of dichloromethane-methanol (1:1) to produce the corresponding organic extract. Aliquots of each extract were evaluated in antibacterial activity tests using the gold standard broth microdilution method.

The bacterial pathogens *A. baumannii*, *P. aeruginosa*, *K. pneumoniae* and *S. aureus* were included in this study because they form part of the ESKAPE group (an acronym that gather the names of six bacterial pathogens commonly associated with antimicrobial resistance), recognised as some of the clinically most relevant nosocomial pathogens. There is an urgent and growing need for new classes of antibiotics to use in realistic therapies that can ensure the level of infection control required in medical procedures (Mulani et al., 2019).

In clinical microbiology, microbial susceptibility is defined by breakpoints, which are the lowest antibiotic concentrations that inhibit bacterial growth of any species in strains lacking resistance mechanisms (Isler et al., 2019). According to the main clinical microbiology societies such as the European Committee on Antimicrobial Susceptibility Testing (EUCAST) or Clinical and Laboratory Standards Institute (CLSI), recommendations regarding breakpoints should always include three types of data: i) microbiological, ii) pharmacokinetic and pharmacodynamic and iii) clinical (http://www.eucast.org/clinical_breakpoints). Three broad categories of microorganisms are generally considered: susceptible, intermediate and resistant. The breakpoints vary significantly, mainly depending on the bacterial species and the type of antibiotic used. Thus, the MICs are very valuable as a standardized measure of the antibiotic activity against bacteria.

Marine extracts are very complex mixtures rather than pure compounds, and we therefore decided to use arbitrary breakpoints to quantify the antimicrobial activity of the extracts. We established three categories of antibacterial activity to classify the extracts: high activity (MIC \leq 8 mg/L); intermediate activity (MIC 16-64 mg/); and low or no activity (MIC \geq 128 mg/L).

Of the 64 extracts, 9 displayed in vitro antimicrobial activity against one or more bacterial pathogens according to the aforementioned classification. The inactive extracts were derived from tunicates, and the active extracts were derived from 8 sponges: *Agelas citrina*, *Agelas dilatata*, *Agelas sceptrum*, *Aiolochoira crassa* (collected from two different locations: Mahahual in Quintana Roo state and Alacranes Reef in Yucatan state), *Amphimedon compressa*, *Dysidea* sp., *Monanchora arbuscula* and *Haliclona*

(*Rhizoniera*) *curacaoensis* (Table 3). Three of the sponges showed antimicrobial activity against the four bacteria tested. *Agelas citrina* showed the highest activity (MIC of 8 mg/L for the three Gram-negative species and a MIC of 0.5 mg/L for the Gram-positive *S. aureus*), followed by *Amphimedon compressa* with a MIC of 32 mg/L for the four bacterial species and finally *H. (Rhizoniera) curacaoensis*, with a MIC of 4-32 mg/L for the three Gram-negative and a MIC of 4 mg/L for *S. aureus*. The remaining five extracts displayed antimicrobial activity with MIC values ranging from 16 to 128 mg/L. Thus, the *M. arbuscula* extract showed good activity against *S. aureus*, with a MIC of 16 mg/L, but was inactive against the three Gram-negative bacteria. The *Dysidea* sp. extract also displayed antibacterial activity, with MIC values of 16 and 32 mg/L for *A. baumannii* and *S. aureus*, respectively. The *Agelas dilatata* extract yielded MIC values of 32-128 mg/L for two of the Gram-negative bacteria and a MIC of 64 mg/L for *S. aureus*. For the extracts of *Aiolochoiria crassa* collected from two different sites, the MIC values ranged from 32-64 mg/L for *A. baumannii* and *S. aureus*. Finally, the *Agelas sceptrum* extract yielded a MIC value of 64 mg/L for *P. aeruginosa* (Table 3).

Table 3. Minimum inhibitory concentration (MIC) of organic extracts of marine organisms from the Yucatan Peninsula.

Code	Spp	MIC (mg/L)			
		<i>A. baumannii</i> ATCC 17978	<i>K. pneumoniae</i> ATCC 700603	<i>P. aeruginosa</i> ATCC 27823	<i>S. aureus</i> ATCC 29213
T18-M1	<i>Clavelina</i> sp.	≥512	≥512	≥512	≥512
E8-2	<i>Didemnum perlucidum</i>	≥512	≥512	≥512	>512
T18-M4	<i>Didemnum</i> sp.	≥512	≥512	≥512	≥512
E01	<i>Didemnum</i> sp.	≥512	≥512	≥512	≥512
E7-2	<i>Trididemnum solidum</i>	≥512	≥512	>512	>512
EY18-8	<i>Polysyncraton</i> sp.	≥512	≥512	≥512	≥512
RIO18-T1	<i>Eudistoma amanitum</i>	≥512	≥512	≥512	≥512
TY18-2	<i>Eudistoma</i> sp.	≥512	≥512	≥512	≥512
T18-M5	<i>Polyclinum</i> sp.	≥512	≥512	≥512	≥512
TY18-1	<i>Phallusia nigra</i>	≥512	≥512	≥512	≥512
T18-M2	<i>Ecteinascidia</i> sp.	≥512	≥512	≥512	≥512
T18-M6	<i>Molgula</i> sp.	≥512	≥512	≥512	≥512
E41	<i>Polycarpa</i> sp.	≥512	≥512	≥512	≥512
CZE56	<i>Agelas citrina</i>	8	8	8	0.5
E27-2	<i>Agelas clathrodes</i>	≥512	≥512	≥512	>512
MA18-10	<i>Agelas clathrodes</i>	≥512	≥512	≥512	≥512
E25-1	<i>Agelas dilatata</i>	128	64	32	64
E26-2	<i>Agelas sceptrum</i>	≥512	256	64	>512
CZE18	<i>Myrmekioderma gyroderma</i>	≥512	≥512	≥512	≥512
MA18-9	<i>Ectyoplasia ferox</i>	≥512	≥512	≥512	≥512
MA18-13	<i>Ectyoplasia</i> sp.	≥512	≥512	≥512	≥512

MA18-6	<i>Chondrilla caribensis</i> <i>f. hermatypica</i>	≥512	≥512	≥512	≥512
RIO18-1	<i>Chondrilla</i> sp.	≥512	≥512	≥512	≥512
EY18-10	<i>Clathrina</i> sp.	≥512	≥512	≥512	≥512
E2-2	<i>Leucetta floridana</i>	128	256	≥512	128
EY18-1	<i>Cliona delitrix</i>	≥512	≥512	≥512	≥512
EY18-3	<i>Cliona varians</i>	≥512	≥512	≥512	≥512
EY18-12	<i>Dysidea</i> sp.	16	≥512	≥512	32
E9-2	<i>Ircinia felix</i>	≥512	≥512	≥512	≥512
MA18-11	<i>Ircinia felix</i>	≥512	≥512	≥512	≥512
E24-2	<i>Ircinia strobilina</i>	≥512	≥512	≥512	≥512
E52	<i>Ircinia strobilina</i>	≥512	≥512	≥512	≥512
E11-2	<i>Spongia tubulifera</i>	≥512	≥512	≥512	≥512
E28	<i>Callyspongia</i> <i>longissima</i>	≥512	≥512	≥512	≥512
E31	<i>Callyspongia plicifera</i>	≥512	≥512	≥512	≥512
E16	<i>Callyspongia vaginalis</i>	≥512	≥512	≥512	≥512
EY18-4	<i>Haliclona (Rhizoniera)</i> <i>curacoensis</i>	4	16	32	4
E29	<i>Amphimedon</i> <i>compressa</i>	32	32	32	32
E15	<i>Niphates digitalis</i>	≥512	≥512	≥512	≥512
E49	<i>Niphates erecta</i>	≥512	≥512	≥512	≥512
MA18-7	<i>Niphates erecta</i>	≥512	≥512	≥512	≥512
MA18-12	<i>Niphates erecta</i>	≥512	≥512	≥512	≥512
EP	<i>Xestospongia muta</i>	≥512	≥512	≥512	≥512
E3	<i>Plakinastrella onkodes</i>	≥512	≥512	≥512	≥512
E35	<i>Monanchora</i> <i>arbuscula</i>	≥512	≥512	≥512	16
EY18-11	<i>Clathria gomezae</i>	≥512	≥512	≥512	≥512
E7-E34	<i>Clathria virgultosa</i>	≥512	≥512	≥512	≥512
MA18-1	<i>Mycale laevis</i>	≥512	≥512	≥512	≥512
MA18-5	<i>Mycale laevis</i>	≥512	≥512	≥512	≥512
DNY	<i>Scopalina ruetzleri</i>	≥512	≥512	≥512	≥512
E53	<i>Scopalina ruetzleri</i>	≥512	≥512	≥512	≥512
EY18-7	<i>Scopalina ruetzleri</i>	≥512	≥512	≥512	≥512
E18-M1	<i>Halichondria</i> <i>melanadocia</i>	≥512	≥512	≥512	≥512
E38	<i>Aaptos</i> sp.	≥512	≥512	≥512	≥512
E20	<i>Tethya</i> sp.	≥512	≥512	≥512	≥512
E4	<i>Melophlus hajdui</i>	≥512	≥512	≥512	≥512
MA18-2	<i>Cinachyrella</i> <i>kuekenthali</i>	≥512	≥512	≥512	≥512
E50	<i>Aiolochoxia crassa</i>	64	128	>128	32

MA18-4	<i>Aiolochoiria crassa</i>	32	128	128	64
E36	<i>Aplysina cauliformis</i>	≥512	≥512	≥512	≥512
E46	<i>Aplysina fistularis</i>	≥512	≥512	≥512	≥512
E42	<i>Aplysina fulva</i>	≥512	≥512	≥512	≥512
EY18-5	<i>Aplysina fulva</i>	≥512	≥512	≥512	≥512
E47	<i>Aplysina muricyanna</i>	≥512	≥512	≥512	≥512
	Imipenem positive control	0.5	0.25	2	nt
	Vancomycin positive control	nt	nt	nt	1

*nt: not tested

Comparison of the MICs with those of known antibiotics revealed the high activity of some extracts. For example, penicillins (piperacillin and ticarcillin) and even carbapenems (meropenem) belonging to the β -lactam antibiotic group, for which MIC values less than respectively 16 mg/L and less than 8 mg/L for the causative strain, are used successfully to treat infections caused by Gram-negative pathogens. Aminoglycosides (e.g. amikacin), for which MICs less than 16 mg/L have been determined, are generally clinically effective against Gram-negative species. For example, teicoplanin and linezolid are widely used to treat infections caused by *S. aureus* and are effective against strains with which MICs less than 4 mg/L have been determined. Antibiotics such as fosfomycin, with low toxicity or adequate PK/PD parameters, reach high concentrations in serum and can be used to treat strains for which MICs < 32 mg/L have been determined (EUCAST, 2000).

The extract of *Agelas citrina* exhibited in vitro antibacterial activity similar to that of most antibiotics used in routine clinical practice, against both Gram-negative (MIC 8 mg/L) and Gram-positive (MIC 0.5 mg/L) pathogens. The extract of *H. (Rhizoniera) curacaoensis* also displayed high activity against *A. baumannii* (MIC of 4 mg/L), a pathogen considered one of the opportunistic pathogens most threatening to global health and for which limited therapeutic options are available. The high genetic plasticity of this organism allows it to adapt quickly to unfavourable contexts and readily develop antibiotic resistance. This pathogen has been cited by some authors as a paradigm of multidrug-resistance (Beceiro, 2018). Very few antimicrobials display higher in vitro activity against *A. baumannii* than this extract, e.g. imipenem and colistin, which are used as last-line antibiotics to treat severe infections (susceptibility breakpoint ≤ 2 mg/L). The in vitro activity of *H. (Rhizoniera) curacaoensis* against *S. aureus* (MIC 4 mg/L), was similar to the susceptibility breakpoints reported for antimicrobials used to treat this pathogen, such as vancomycin and linezolid (susceptibility breakpoints of ≤ 2 and ≤ 4 mg/L, respectively).

In addition to three of the extracts being active against all pathogenic species tested (*Agelas citrina*, *Amphimedon compressa* and *H. (Rhizoniera) curacaoensis*), the narrow-spectrum antibacterial activity displayed by another three extracts (*M. arbuscula*, *Dysidea* sp. and *Agelas sceptrum* against a maximum of two of the four bacteria tested) is also worth highlighting (Table 3). Most antibiotics used to treat bacterial infections are active against multiple species showing relevant benefits for use in clinical settings. However, the use of broad-spectrum antibiotics has two main drawbacks: i) selection for resistant, pathogenic and non-pathogenic bacteria leads to selection for resistance genes that decrease the usefulness of that antibiotic; and ii) the use of broad-spectrum antibiotics has a deleterious effect on the host microbiome (Melander et al., 2018). These are the main reasons why the US Food and Drug Administration (FDA) has approved fewer broad-

spectrum antibiotics for use in the last two decades. Narrow-spectrum antimicrobials that do not select for cross-resistance and that decrease the possible damage to the host microbiome are urgently needed in the fight against infections caused by multidrug-resistant pathogens (Maxson and Mitchell, 2016)

Furthermore, the antibacterial activity of the selected extracts is expected to be enhanced by isolation of the active compounds from these complex mixtures of compounds. Moreover, synergistic or antagonistic interactions between the different components of the extracts are also possible. All of these factors must be taken into consideration in order to initiate the processes of isolation and identification of the corresponding antibacterial agent(s).

As far as we are aware, there are no previous studies of the antibacterial activity of *H. (Rhizoniera) curacaoensis*, *Aiolochoiria crassa* or *Agelas dilatata*. However, antibacterial activities of the remaining five sponges have been reported. Thus, agelasidines with antifungal activity against *Candida albicans* have been extracted from *Agelas citrina*, one of the most promising crude extracts in the present study, and (-)-agelasidine C (MIC 0.5 mg/L) was found to be the most active (Stout et al., 2012). More recently, new pyrrole–imidazole alkaloids (denominated citrinamines) were isolated from the same species and were found to be able to inhibit the growth of the Gram-positive bacteria *Micrococcus luteus* and *Mycobacterium phlei* (Cychon et al., 2015). Inhibition of the growth of *E. coli* and *Pseudomonas putida* by extracts of this sponge has also been reported (Quintana et al., 2015). Furthermore, the presence of antibacterial activity in its extracts has also been reported in a study of the inhibition of growth of some non-pathogenic marine bacteria (Mora-Cristancho et al., 2011). In the present study, we detected high activity of the extract from *Agelas citrina* (MIC \leq 8 mg/L) against the four pathogens tested.

Previous studies on *Amphimedon compressa* reported the isolation and identification of new alkyl pyridine alkaloids, which displayed potent antibacterial activities against *E. coli*, *P. aeruginosa*, *Cryptococcus neoformans* and methicillin-resistant *S. aureus* and also antifungal activity against *C. albicans* and *Aspergillus fumigatus* (Xu et al., 2007). Although antifungal activity of batzelladine L (previously isolated from the sponge *M. arbuscular*) against *Aspergillus flavus* has been described, antibacterial activity was not reported for neither this compound or the extract of this sponge (Arevabini et al., 2014).

The antimicrobial agent sceptrin has been isolated from *Agelas sceptrum*, yielding MICs of 15 mg/L for pathogenic species such as *S. aureus*, *P. aeruginosa* and *C. albicans* (Bernan et al., 1993, Walker et al. 1981). The antibacterial activity displayed by the extract of *A. sceptrum* against *K. pneumoniae* and *P. aeruginosa* (MICs of 256 and 64 mg/L, respectively) in the present study is consistent with the aforementioned findings. Finally, the antibacterial activity of extracts of species belonging to the genus *Dysidea* has previously been reported; e.g. new sesquiterpenes isolated from the sponge *Dysidea* sp. displayed antibacterial activity against *E. coli* and *S. aureus* (Zhang et al., 2016). In the present study, *Dysidea* sp. extracts displayed antibacterial activity against *A. baumannii* and *S. aureus* (with MICs of 16 and 32 mg/L, respectively).

3.1 Antibacterial activity and bioguided isolation of *Amphimedon compressa* crude extract

The crude extract of *A. compressa* was submitted to a bioguided fractionation because of the promising antibacterial activity detected (MIC of 16 mg/L for the four bacterial species tested in the microdilution assay). A combination of Solid Phase Extraction (SPE) with RP-18 cartridge (Merck KGaA) and reverse phase High Performance Liquid Chromatography (RP-HPLC) was used to fractionate the organic extract and purify the active compounds. The bioguided fractionation of the organic extract of *A. compressa* allowed us to separate fractions R3 and R4 which were eluted by SPE with respectively 1:1 and 1:2 mixtures of H₂O and CH₃OH. Both fractions yielded the highest (and identical) MIC values (2-16 mg/L, Tables 4 and 5) for all pathogens tested. Taking into account that the ¹H NMR spectra of both fractions were very similar, suggesting that they contained similar compounds, and the fact that fraction R4 appeared to be purer than the R3 fraction, the former was chosen for further fractionation by RP-HPLC. The RP-HPLC chromatogram displayed a major peak (subfraction R4H2) with a retention time of 16.8 min (Figure 2).

Table 4. Minimum inhibitory concentration (MIC recorded in mg/L) of the SPE fractions separated from the crude extract of *Amphimedon compressa*.

Fraction	MIC (mg/L)			
	<i>A. baumannii</i> ATCC 17978	<i>K. pneumoniae</i> ATCC 700603	<i>P. aeruginosa</i> ATCC 27823	<i>S. aureus</i> ATCC 29213
R1	128	256	64	nt
R2	128	256	256	nt
R3	8	16	16	2
R4	8	16	16	2
R5	>512	>512	>512	nt
R6	>512	>512	>512	nt
R7	>512	>512	>512	nt

*nt: not tested

Table 5. Minimum inhibitory concentration (MIC recorded in mg/L) of the most active SPE fractions and HPLC subfraction R4H2 from *Amphimedon compressa*.

Bacterial strain		Fraction		
		R3	R4	R4H2
<i>A. baumannii</i>	ATCC 17978	8	8	4
	ABRIM	8	8	4
<i>K. pneumoniae</i>	ATCC 700603	16	16	4
	ST15	8	8	2
<i>P. aeruginosa</i>	ATCC 27853	16	16	2
	PA01	16	16	4
	ATCC 29213	2	2	2
<i>S. aureus</i>	USA 300	1	1	1

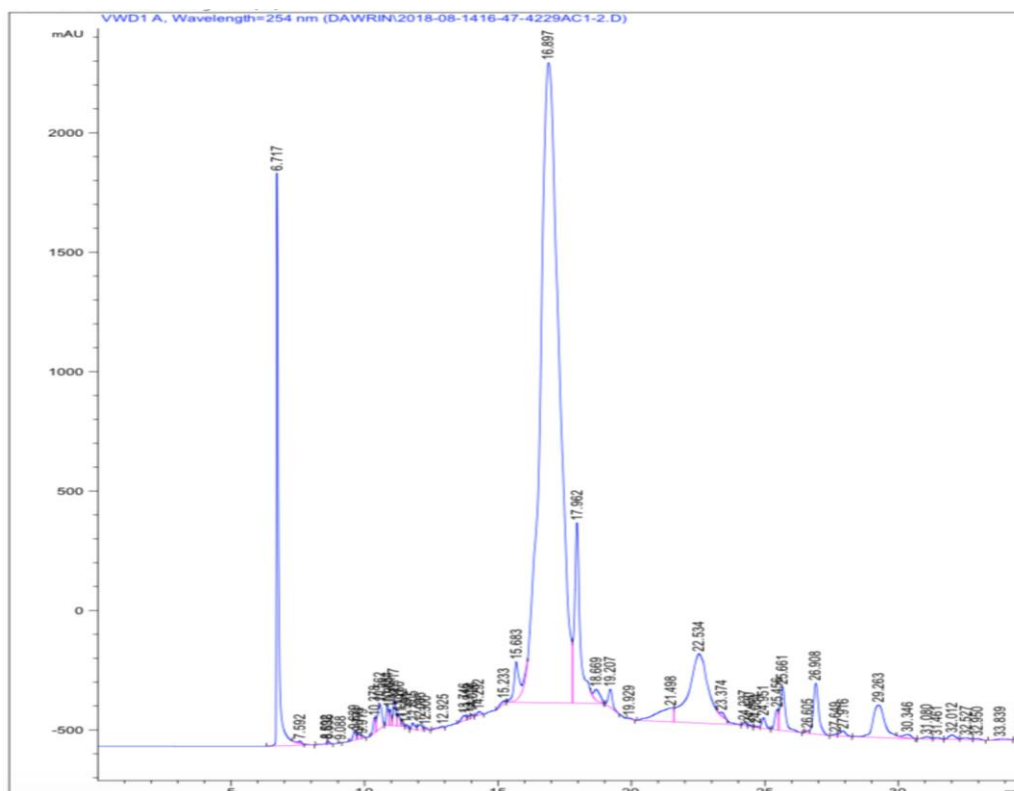


Figure 2. RP-HPLC chromatogram of the SPE fraction R4 of the sponge *Amphimedon compressa*.

The ^1H -NMR spectrum of subfraction R4H2 shows proton aromatic signals at δ_{H} 8.88 (s), 8.85 (d), 8.41 (d) and 8.02 (dd), suggesting the presence of pyridine rings, proton olefinic signals at δ_{H} 5.73 (m), 5.58 (m) and 4.60 (t), indicating the presence of double bonds, and proton signals at δ_{H} 3.68 (d), 2.20 (m), 2.02 (m) and 1.39 (m) ppm, characteristic of carbon aliphatic chains (Figure 3). The presence of a pyridine moiety and olefinic carbons was confirmed by the carbon resonances in the ^{13}C -NMR spectrum, at δ_{C} 146.5, 145.2, 144.5, 143.5, 135.3, 129.0, 125.3, which also displayed the presence of carbon aliphatic chains with carbon resonances at δ_{C} 63.0, 32.6, 31.1, 30.6, 30.6, 30.4, 30.2, 28.4 and 27.3 ppm (Figure 4). Comparison of the 1D NMR data with previously reported data allowed us to identify a mixture of amphitoxins and halitoxins in subfraction R4H2 (Figure 5) (Albrizio et.al., 1995, Berlinck et al., 1996, Schmitz et.al., 1978). The structure of amphitoxin differs from that of halitoxin in that it has an additional carbon-carbon double bond in the alkyl chain that joins the pyridinium rings. Subfraction R4H2 displayed higher antibacterial activity than fraction R4, yielding an MIC value of 2-4 mg/L for different strains of *A. baumannii*, *K. pneumoniae* and *P. aeruginosa* and a MIC value of 1 mg/L for both strains of *S. aureus* (Tables 4 and 5).

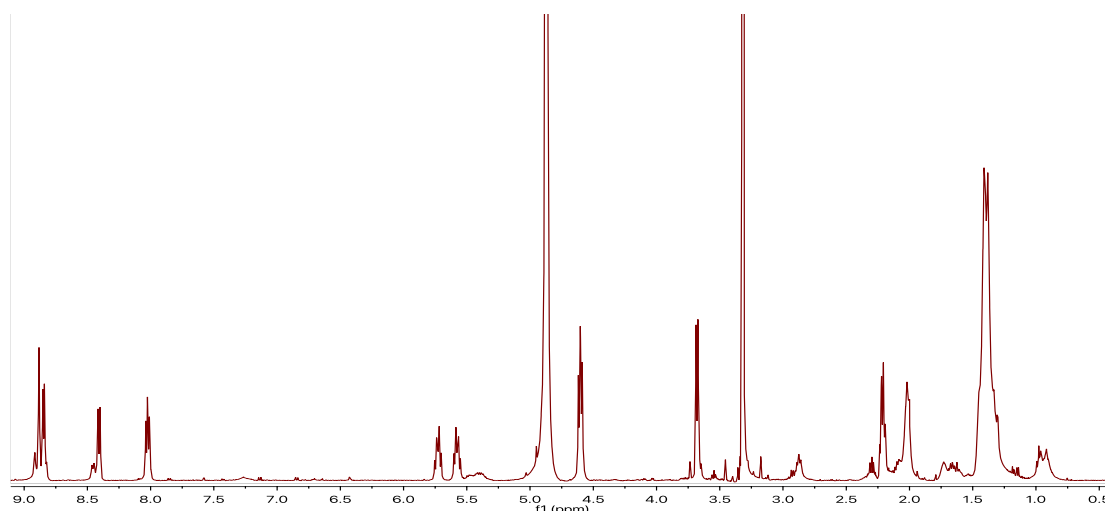


Figure 3. ^1H NMR spectrum of the R4H2 subfraction (500 MHz, CD_3OD).

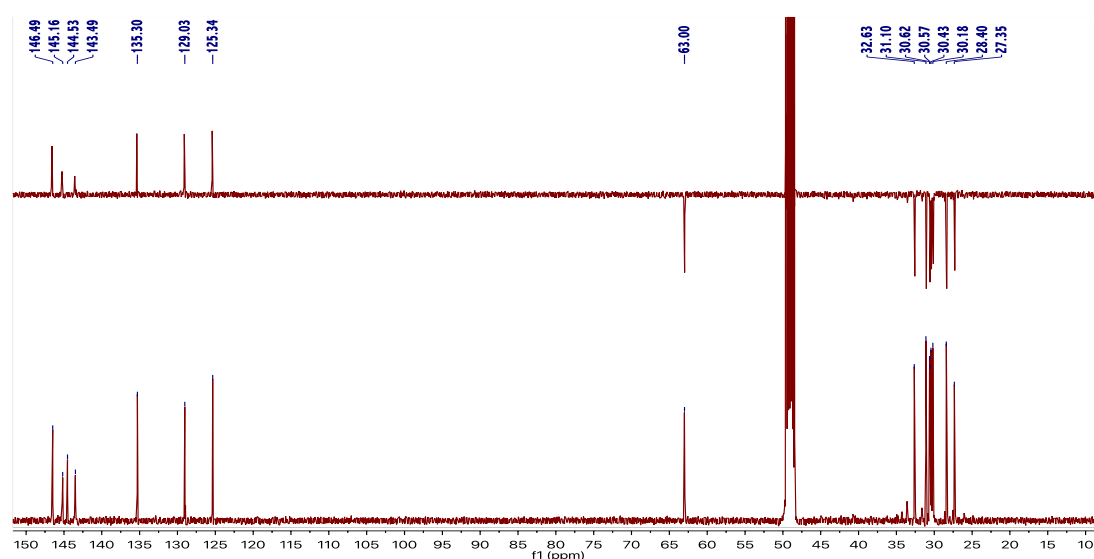


Figure 4. ^{13}C NMR and DEPT-135 spectra of the R4H2 subfraction (125 MHz, CD_3OD).

Sponges of the order Haplosclerida, to which *Amphimedon compressa* belongs, constitute well-known sources of bioactive natural products, in particular of alkylpyridine and alkylpiperidine alkaloids (Arevabinia et al., 2014). Halitoxins and amphitoxins are cyclic alkylpyridine oligomers of challenging separation and structural characterization due to their polycharged structures and high molecular weights (Albrizio et al., 1995, Berlinck et al., 1996, Schmitz et al., 1978). Halitoxins and amphitoxins exert a multitude of biological actions. Regarding antibacterial activity, these compounds are able to inhibit bacterial attachment of *Vibrio harveyi*, a motile marine bacterium, but have not been reported to inhibit growth of the species (Kelly et al., 2003). Furthermore, these compounds have also been reported to show antibacterial activity against marine environmental isolates (MICs 4-256 mg/L) (Kelman et al., 2001) as well as antifungal activity (Arevabinia et al., 2014). However, the antibacterial activity of halitoxins and amphitoxins detected in this study against the main multidrug-resistant human pathogens had not yet previously been observed.

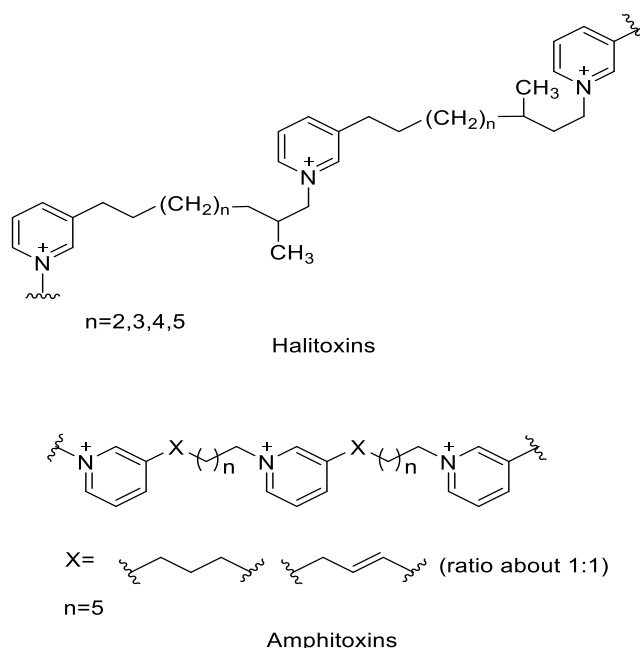


Figure 5. Substructure of halitoxins and amphitoxins present in the R4H2 subfraction from *Amphimedon compressa*.

4. Conclusions

There is an urgent need for successful treatments for patients with infections caused by multidrug-resistant bacteria. Developing new antibiotics that contribute to fighting against antibacterial resistance is one of the main current objectives in public health.

Sixty-four marine organisms, 51 sponges (Porifera) and 13 ascidians (Chordata), selected on the basis of chemotaxonomic criteria, were collected on the coast of the Yucatan Peninsula in Mexico and organic extracts were obtained from each. One aliquot of each extract was submitted to in vitro antibacterial screening against four species of multidrug-resistant (MDR) bacterial pathogens: the Gram-negative *Acinetobacter baumannii*, *Klebsiella pneumoniae* and *Pseudomonas aeruginosa* and the Gram-positive *Staphylococcus aureus*. Minimum inhibitory concentrations (MICs) (determined by microdilution assay) indicated antibacterial activity of nine extracts from 8 sponges *Agelas citrina*, *Agelas dilatata*, *Agelas sceptrum*, *Aiolochoia crassa* (collected from two

different locations, Mahahual, Quintana Roo and Alacranes Reef), *Amphimedon compressa*, *Dysidea* sp., *Monanchora arbuscula* and *Haliclona (Rhizoniera) curacaoensis*. Some of the extracts showed similar MIC values to known antibiotics such as penicillins and aminoglycosides. Isolation of pure compounds from the complex mixtures constituting the extracts is expected to yield greater antibacterial activity. Indeed, the bioguided fractionation of one of the active extracts, from the sponge *Amphimedon compressa*, produced a mixture of halitoxins and amphitoxins which displayed notable antibacterial in vitro activity against four pathogenic bacteria. This is the first report of the antimicrobial activity of halitoxins and amphitoxins against major multidrug-resistant human pathogens.

These organisms will be subjected to further detailed analysis to isolate biologically active molecules in the search for new compounds. Furthermore, the promising antibacterial activities detected in this study indicate the coast of Yucatan Peninsula as a potential source of a great variety of marine organisms worthy of further research. This type of study can serve as a basis for the development of new antibacterial agents effective against the principal multidrug-resistant bacterial pathogens for which the therapeutic options are increasingly scarce. This study constitutes the first report of antibacterial activity for a wide collection of sponges and ascidians collected on the coast of the Yucatan Peninsula.

Acknowledgements: This work was supported by grant RTI2018-093634-B-C22 (AEI/FEDER, EU) from the State Agency for Research (AEI) of Spain, co-funded by the FEDER Programme from the European Union, by projects PI15/00860 and PI18/00501 to GB and PI14/00059 and PI17/01482 to AB (Instituto de Salud Carlos III) and BLUEBIOLAB (0474_BLUEBIOLAB_1_E), Programme INTERREG V A of Spain-Portugal (POCTEP). The study was also funded by projects IN607A 2016/22 (GAIN-Agencia Gallega de Innovación-Consellería de Economía, Emprego e Industria) and GRC2018/039 and Agrupación Estratégica CICA-INIBIC ED431E 2018/03 (Consellería de Educación, Universidades e Formación Profesional) from Xunta de Galicia (autonomous government of the region).

Support was also provided by Planes Nacionales de I+D+i 2013-2016 and ISCIII, Subdirección General de Redes y Centros de Investigación Cooperativa, Ministerio de Economía y Competitividad, Spanish Network for Research in Infectious Diseases (REIPI RD16/0016/006) co-financed by European Development Regional Fund "A way to achieve Europe" and the operative program Intelligent Growth 2014-2020. J.C.V.U. was financially supported by the pFIS Programme (FI18/00315), M.M.G. was financially supported by a Clara Roy grant (SEIMC) and C.L.M. by IN606A-2019/029. D.P.P. received a fellowship from the program National Council of Science and Technology (CONACYT) of Mexico and the Secretariat of Research, Innovation and Higher Education (SIIES) of Yucatan (Mexico).

References

- Aguilar, V., Kolb, M., Hernández, D., Urquiza, T., Koleff, P., 2008. Prioridades de Conservación de la Biodiversidad Marina en México. CONABIO. Biodiversitas 79, 1-15.
- Albrizio S., Ciminiello P., Fattorusso E., Magno S., Pawlik J.R., 1995. Amphitoxin, a new high molecular weight antifeedant pyridinium salt from the Caribbean sponge *Amphimedon compressa*. Journal of Natural Products 58, 647-652.
- Altmann, K.-H., 2017. Drugs from the Oceans: Marine Natural Products as Leads for Drug Discovery. Chimia 71, 646–652.
- Antunes, L.C.S., Visca, P., Towner, K.J., 2014. *Acinetobacter baumannii*: evolution of a global pathogen. Pathogens and Disease 71, 292-301.
- Arai, M., Yamano, Y., Kamiya, K., Setiawan, A., Kobayashi, M., 2016. Anti-dormant mycobacterial activity and target molecule of melophlins, tetramic acid derivatives isolated from a marine sponge of *Melophlus* sp. Journal of Natural Medicines 70, 467-475.
- Arumugam, V., Venkatesan, M., Ramachandran, K., Ramachandran, S., Palanisamy S.K., Sundaresan, U. 2019. Purification, Characterization and Antibacterial Properties of Peptide from Marine Ascidian *Didemnum* sp. International Journal of Peptide Research and Therapeutics. 1–8.
- Bassetti, M., Vena, A., Croxatto, A., Righi, E., Guery, B., 2018. How to manage *Pseudomonas aeruginosa* infections. Drugs in Context 7, 1–18. <https://doi.org/10.7573/dic.212527>.
- Berlinck R.G., Ogawa C.A., Almeida A.M., Sanchez M.A., Malpezzi E.L., Costa L.V., Hajdu E., de Freitas J.C., 1996. Chemical and pharmacological characterization of halitoxin from *Amphimedon viridis* (Porifera) from the southeastern Brazilian coast. Comparative Biochemistry and Physiology. Pharmacology, Toxicology & Endocrinology 115, 155-63.
- Bernan, V.S., Roll, D.M., Ireland, C.M., Greenstein, M., Maiese, W.M., Steinberg, D. A., 1993. A study on the mechanism of action of sceptrin, an antimicrobial agent isolated from the South Pacific sponge *Agelas mauritiana*. Journal of Antimicrobial Chemotherapy 32, 539–550.
- Bianco, É.M., Krug, J.L., Zimath, P.L., Kroger, A., Paganelli, C.J., Boeder, A.M., Dos Santos, L., Tenfen, A., Ribeiro, S.M., Kuroshima, K.N., Alberton, M.D., Mendes de Cordova, C.M., Rebelo, R.A., 2015. Antimicrobial (including antimollicutes), antioxidant and anticholinesterase activities of Brazilian and Spanish marine organisms – evaluation of extracts and pure compounds. Revista Brasileira de Farmacognosia 25, 668–676.
- Bye, R., Linares, E., Estrada, E., 1995. Biological diversity of medicinal plants in Mexico. In: Arnason, J.T., Mata, R., Romeo, J.T. (Eds.), Phytochemistry of Medicinal Plants: Recent Advances in Phytochemistry vol 29. Plenum Press, New York, p. 65.
- Carroll, A. R., Copp, B. R., Davis, R. A., Keyzers, R. A., Prinsep, M. R., 2019. Marine Natural Products. Natural Product Reports, 36, 122–173.
- Clinical and Laboratory Standards Institute, 2012. Performance standards for antimicrobial susceptibility testing: 17th informational supplement M07-A9. CLSI, Wayne, PA, USA.
- Cuevas C., Francesch A., 2009. Development of Yondelis® (trabectedin, ET-743). A semisynthetic process solves the supply problem. Natural Products Reports 26, 322-337.

- Cychon, C., Lichte, E., Köck, M., 2015. The marine sponge *Agelas citrina* as a source of the new pyrrole–imidazole alkaloids citrinamines A–D and N-methylagelongine. *Beilstein Journal of Organic Chemistry* 11, 2029–2037.
- De Lara-Issasi, G., Álvarez-Hernández, S., Collado-Vides, L., 2000. Ichthyotoxic activity of extracts from Mexican marine macroalgae. *Journal of Applied Phycology* 12, 45-52.
- De Oliveira, M.F., De Oliveira, J.H., Galetti, F.C., De Souza, A.O., Silva, C.L., Hajdu, E., Peixinho, S., Berlinck, R.G., 2006. Antimycobacterial Brominated Metabolites from Two Species of Marine Sponges. *Planta Medica* 72, 437–441.
- Durán-García R., Méndez-González M., Larqué-Saavedra A., 2016. The Biodiversity of the Yucatan Peninsula: A Natural Laboratory. *Progress in Botany* 78, 237-258.
- European Committee on Antimicrobial Susceptibility Testing (EUCAST), 2000. Terminology relating to methods for the determination of susceptibility of bacteria to antimicrobial agents. *Clinical Microbiology and Infection* 6, 503–508.
- European Committee on Antimicrobial Susceptibility Testing (EUCAST), 2019. Clinical breakpoints and dosing of antibiotics. http://www.eucast.org/clinical_breakpoints/ (accessed on December 2019).
- Freile-Pelegrín, Y., Morales, J.L., 2004. Antibacterial activity in marine algae from the coast of Yucatan, Mexico. *Botanica Marina* 47, 140-146.
- Gales, A.C., Jones, R.N., Sader, H.S., 2011. Contemporary activity of colistin and polymyxin B against a worldwide collection of Gram-negative pathogens: results from the SENTRY Antimicrobial Surveillance Program (2006-09). *Journal of Antimicrobial Chemotherapy* 66, 2070–2074.
- García-Arredondo, A., Rojas-Molina, A., Ibara-Alvarado, C., Lazcano-Pérez, F., Arreguín-Espinosa, R., Sánchez-Rodríguez, J., 2016. Composition and biological activities of the aqueous extracts of three scleractinian corals from the Mexican Caribbean: *Pseudodiploria stigosa*, *Porites astreoides* and *Siderastrea siderea*. *Journal of Venomous Animals and Toxins Including Tropical Diseases* 22, 2-14.
- Hu, Y., Chen, J., Hu, G., Yu, J., Zhu, X., Lin, Y., Chen, S., Yuan, J. 2015. Statistical Research on the Bioactivity of New Marine Natural Products Discovered during the 28 Years from 1985 to 2012. *Marine Drugs* 13, 202- 221.
- Instituto Nacional de Estadística y Geografía (INEGI), 2017. Anuario Estadístico y Geográfico por Entidad Federativa. Instituto Nacional de Estadística y Geografía, México, p 638.
- Isler, B., Doi, Y., Bonomo, R.A., Paterson, D.L., 2019. New Treatment Options Against Carbapenem-Resistant *Acinetobacter baumannii* Infections. *Antimicrobial Agents Chemotherapy* 63, 1-18.
- Jaffarali, H.A., Tamilselvi, M., Sivakumar, V., 2008. Antibacterial activity of the marine ascidians *Phallusia nigra* and *Herdmania pallida* from the Tuticorin coast, India. *Journal of Biological Research (Thessalon)* 10, 171-179.
- Jiménez, C., 2008. Marine natural products in medicinal chemistry. *ACS Medicinal Chemistry Letters* 9, 959–961.
- Katz J., Janik J.E., Younes A., 2011. Brentuximab Vedotin (SGN-35). *Clinical Cancer Research* 17, 6428-6436.
- Kelly S.R., Jensen P.R., Henkel T.P., Fenical W., Pawlik J.R., 2003. Effects of Caribbean sponge extracts on bacterial attachment. *Aquatic Microbial Ecology* 31, 175-182.
- Kelman D., Kashman Y., Rosenberg E., Ilan M., Ifrach I., Loya Y., 2001. Antimicrobial activity of the reef sponge *Amphimedon viridis* from the Red Sea: evidence for selective toxicity. *Aquatic Microbial Ecology* 24, 9-16.
- Kong, D. X., Jiang, Y. Y., Zhang, H. Y., 2010. Marine natural products as sources of

- novel scaffolds: achievement and concern. *Drug Discovery Today* 15, 884–886.
- Laport, M.S., Marinho, P.R., Santos, O.C. da S., De Almeida, P., Romanos, M.T.V., Muricy, G., Brito, M.A.V.P., Giambiagi-deMarval, M., 2012. Antimicrobial activity of marine sponges against coagulase-negative *staphylococci* isolated from bovine mastitis. *Veterinary Microbiology* 155, 362–368.
- Lima B. de A. 2014. *Revista Brasileira de Farmacognosia*, 24, 651–659.
- Maragakis, L.L., Perl, T.M., 2008. *Acinetobacter baumannii*: Epidemiology, Antimicrobial Resistance, and Treatment Options. *Clinical Infectious Diseases* 46, 1254–1263.
- Marques, D.N., De Almeida, A.S., Sousa, A.R. de O., Pereira, R., Andrade, A.L., Chaves, R.P., Carneiro, R.F., De Vasconcelos, M.A., Do Nascimento-Neto, L.G., Pinheiro, U., Videira, P.A., Teixeira, E.H., Nagano, C.S., Sampaio, A.H., 2018. Antibacterial activity of a new lectin isolated from the marine sponge *Chondrilla caribensis*. *International Journal of Biological Macromolecules* 109, 1292–1301.
- Maxson, T., Mitchell, D.A., 2016. Targeted treatment for bacterial infections: prospects for pathogen-specific antibiotics coupled with rapid diagnostics. *Tetrahedron* 72, 3609–3624.
- Maxwell, D., 2000. Beyond Maritime Symbolism: toxic marine objects from ritual contexts at Tikal. *Ancient Mesoamerica* 11, 91–98.
- Melander, R.J., Zurawski, D.V., Melander, C., 2018. Narrow-spectrum antibacterial agents. *Medicinal Chemistry Communications* 9, 12–21.
- Meletis, G., 2015. Carbapenem resistance: overview of the problem and future perspectives. *Therapeutic Advances in Infectious Disease* 3(1), 15–21.
- Mora-Cristancho, J.A., Arévalo-Ferro, C., Ramos, F.A., Tello, E., Duque, C., Lhullier, C., Falkenberg, M., Schenkel, E.P., 2011. Antifouling Activities against Colonizer Marine Bacteria of Extracts from Marine Invertebrates Collected in the Colombian Caribbean Sea and on the Brazilian Coast (Santa Catarina). *Z. Naturforsch., C, Journal of Biosciences* 66, 515–526.
- Morales, J.L., Cantillo-Ciau, Z., Sánchez-Molina, I., Mena-Rejón, G., 2006. Screening of Antibacterial and Antifungal Activities of Six Marine Macroalgae from Coast of Yucatan Peninsula. *Pharmaceutical Biology* 4, 632–635.
- Morales-Landa, J.L., Zapata-Pérez, O., Cedillo-Rivera, R., Segura-Puertas, L., Simá-Álvarez, R., Sánchez-Rodríguez, J., 2007. Antimicrobial, Antiprotozoal, and Toxic Activities of Cnidarian Extracts from the Mexican Caribbean Sea. *Pharmaceutical Biology* 45, 37–43.
- Moo-Puc, R., Robledo, D., Freile-Pelegri, Y., 2008. Evaluation of selected tropical seaweeds for *in vitro* anti-trichomonal activity. *Journal of Ethnopharmacology* 120, 92–97.
- Moo-Puc, R., Robledo, D., Freile-Pelegri, Y., 2009. *In vitro* cytotoxic and antiproliferative activities of marine macroalgae from Yucatan, Mexico. *Ciencias Marinas* 35, 35–358.
- Mulani, M.S., Kamble, E.E., Kumkar, S.N., Tawre, M.S., Pardesi, K.R., 2019. Emerging Strategies to Combat ESKAPE Pathogens in the Era of Antimicrobial Resistance: A Review. *Frontiers Microbiology* 10, 539.
- O'Neill, J., 2016. Review on Antimicrobial Resistance. Tackling drug-resistant infections globally. World Health Organization (WHO).
- Podschun, R., Ullmann, U., 1998. *Klebsiella* spp. as Nosocomial Pathogens: Epidemiology, Taxonomy, Typing Methods, and Pathogenicity Factors. *Clinical Microbiology Reviews* 11, 589–603.
- Quintana, J., Brango-Vanegas, J., Costa, G.M., Castellanos, L., Arévalo, C., Duque, C., 2015. Marine organisms as source of extracts to disrupt bacterial communication:

- bioguided isolation and identification of quorum sensing inhibitors from *Ircinia felix*. *Revista Brasileira de Farmacognosia* 25, 199–207.
- Raub, M.F., Cardellina II, J.H., Spande, T.F., 1992. The piclavines, antimicrobial indolizidines from the tunicate *Clavelina picta*. *Tetrahedron Letters*, 33, 2257–2260.
- Sepčić, K., Kauferstein, S., Mebs, D., Turk, T., 2010. Biological Activities of Aqueous and Organic Extracts from Tropical Marine Sponges. *Marine Drugs* 8, 1550–1566.
- Schmitz, F.J., Hollenbeak, K.H., Campbell, D.C., 1978. Marine natural products: halitoxin, toxic complex of several marine sponges of the genus ^[L]_[SEP]Haliclona. *The Journal of Organic Chemistry* 43, 3916–3922.
- Stout, E.P., Yu, L.C., Molinski, T.F., 2012. Antifungal Diterpene Alkaloids from the Caribbean Sponge *Agelas citrina*: Unified Configurational Assignments of Agelasidines and Agelasines. *European Journal of Organic Chemistry* 2012, 5131–5135.
- Tong, S.Y.C., Davis, J.S., Eichenberger, E., Holland, T.L., Fowler, V.G., 2015. *Staphylococcus aureus* Infections: Epidemiology, Pathophysiology, Clinical Manifestations, and Management. *Clinical Microbiology Reviews* 28, 603–661.
- Voultsiadou, E., 2010. Therapeutic properties and uses of marine invertebrates in the ancient Greek world and early Byzantium. *Journal of Ethnopharmacology* 130, 237–247.
- Walker, R.P., Faulkner, D.J., Van Engen, D., Clardy, J., 1981. Scepterin, an antimicrobial agent from the sponge *Agelas sceptrum*. *Journal of the American Chemical Society* 103, 6772–6773.
- World Health Organization (WHO), 2017. WHO priority pathogens list for R&D of new antibiotics. https://www.who.int/medicines/publications/WHO-PPL-Short_Summary_25Feb-ET_NM_WHO.pdf (accessed October 2019).
- Xu, N.J., Sun, X., Yan, X.J., 2007. A new cyclostelletamine from sponge *Amphimedon compressa*. *Chinese Chemical Letters* 18, 947–950.
- Zhang, X., Xu, H.-Y., Huang, A.M., Wang, L., Wang, Q., Cao, P.Y., Yang, P.M., 2016. Antibacterial Meroterpenoids from the South China Sea Sponge *Dysidea* sp. *Chemical and Pharmaceutical Bulletin* 64, 1036–1042.
- Zidar, N., Montalvão, S., Hodnik, Ž., Nawrot, D., Žula, A., Ilaš, J., Kikelj, D., Tammela, P., Mašič, L.P., 2014. Antimicrobial Activity of the Marine Alkaloids, Clathrocin and Oroidin, and Their Synthetic Analogues. *Marine Drugs* 12, 940–963.
- Zubia, M., Robledo, D., Freile-Pelegri, Y., 2007. Antioxidant activities in tropical marine macroalgae from the Yucatan Peninsula, Mexico. *Journal of Applied Phycology* 19, 49–458.

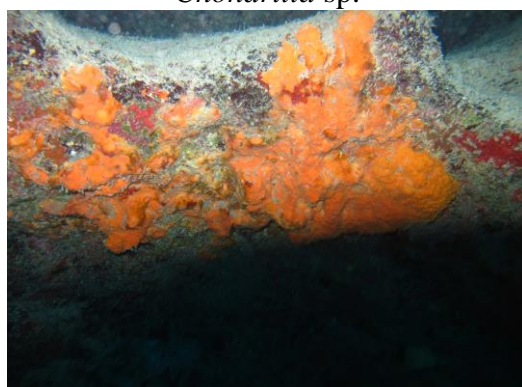
2.3 Resultados de la actividad antiviral y antiproliferativa de los extractos



Chondrilla sp.



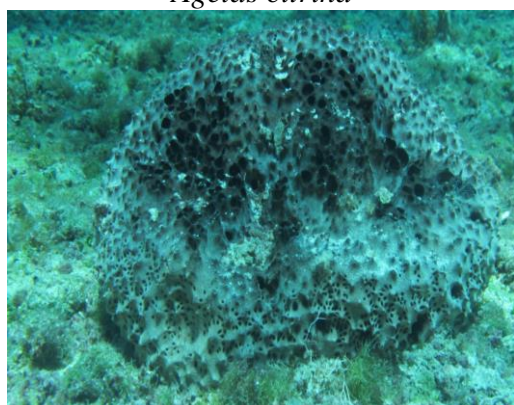
Niphates digitalis



Agelas citrina



Agelas clathrodes



Ircinia strobilina



Eudistoma amanitum

Figura 2.3. Fotografías de los organismos recolectados en las costas de la Península de Yucatán, cuyos extractos fueron sometidos a ensayos de actividad biológica.

En esta sección se describen los resultados de la evaluación biológica de 65 extractos de organismos marinos frente a dos variedades de adenovirus humanos: HAdV5 y HAdV5-GFP, y cinco líneas celulares de cáncer: carcinoma de pulmón humano (A549), melanoma de piel humana (A2058), carcinoma de hepatocitos (HepG2), adenocarcinoma de mama (MCF7) y carcinoma de páncreas (MiaPaca-2). Alrededor del 14 % de los extractos evaluados mostraron actividades antivirales frente a los virus ensayados mientras que el 37% resultaron activos frente al menos una línea celular de cáncer.

Parte de los extractos aun continúan en fases de evaluación biológica y cuando finalicen estos ensayos, los resultados daran origen a un trabajo que será sometido a publicación.

Antiviral and antiproliferative potential of marine organisms from the Yucatan Peninsula, Mexico

Dawrin Pech-Puch¹, Mar Perez-Povedano¹, Harold Villegas-Hernandez², Fernando Reyes⁴, Javier Sánchez-Céspedes⁵, Patricia Gómez³, Jaime Rodríguez^{1*} and Carlos Jiménez^{1*}

¹ Centro de Investigaciones Científicas Avanzadas (CICA) e Departamento de Química, Facultade de Ciencias, AE CICA-INIBIC, Universidade da Coruña, 15071 A Coruña, Spain

² Departamento de Biología Marina. Campus de Ciencias Biológicas y Agropecuarias. Universidad Autónoma de Yucatán. Carretera Mérida-Xmatkuil Km. 15.5, C.P. 97315, Mérida, Yucatán, México

³ Unidad Académica de Ecología y Biodiversidad Acuática, Instituto de Ciencias del Mar y Limnología, Universidad Nacional Autónoma de México. CDMX, México

⁴ Fundación MEDINA, Centro de Excelencia en Investigación de Medicamentos Innovadores en Andalucía, Avda. del Conocimiento 34, 18016 Granada, Spain

⁵ Unit of Infectious Diseases, Microbiology and Preventive Medicine, Institute of Biomedicine of Seville (IBiS), University Hospital Virgen del Rocío/CSIC/University of Seville, E41013 Seville, Spain

* Correspondence: Centro de Investigaciones Científicas Avanzadas (CICA) e Departamento de Química, Facultad de Ciencias, AE CICA-INIBIC, Universidade da Coruña, 15071 A Coruña, Spain. Tel: +34 981 167000. Fax: +34 981 167065. *E-mail address*: jaime.rodriguez@udc.es (Jaime Rodríguez); carlos.jimenez@udc.es, (Carlos Jiménez).

Abstract. Viral infections are one of the main human health problems in recent decades and the cancer remains one of the most lethal diseases worldwide. There is no specific antiviral drug approved to treat the human adenovirus (HAdV) so far and the off-label treatments currently available show great variability in their effectiveness. In relation to cancer, most of the available drugs are designed to act on specific targets by altering the activity of involved transporters and genes. Taking into account the high antiviral and antiproliferative activity against tumour cell lines displayed by some marine natural products reported in the literature, we evaluated sixty five marine organisms: 51 sponges (Porifera), 13 ascidians (Chordata) and 1 gorgonian (Cnidaria), collected from Yucatan Peninsula, Mexico, to antiviral assays against two human adenovirus, HAdV5 and HAdV5-GFP, and to anticancer test against five human tumour cell lines, human lung carcinoma (A549), human skin melanoma (A2058), hepatocyte carcinoma (HepG2), breast adenocarcinoma (MCF7) and pancreas carcinoma (MiaPaca-2). Nine extracts displayed inhibition activity against human adenovirus being the organic extracts of *Dysidea* sp., *Agelas citrina* and *Chondrilla* sp. the three most active ones. On the other hand, twenty four showed antiproliferative activity against at least one tumour cell line, being the extracts of the ascidian *Eudistoma amanitum* and the sponge *Haliclona (rhizoniera) curacoensis* the most active ones. This work constitutes the first wide antiviral and antiproliferative screening report of the marine sponges, ascidians, and a gorgonian collected from the Yucatan Peninsula, Mexico.

Keywords: Antiviral; Antiproliferative; Yucatan Peninsula

1. Introduction

Human adenoviruses (HAdV) are nonenveloped viruses with an icosahedral capsid containing a linear double-stranded DNA whose size ranging 34 to 37 kb in size (Lion, 2014). Currently, more than 64 serotypes have been identify and grouped into 7 HAdV species (HAdV-A to -G) in *Mastadenovirus* genus (Qiu et al., 2018). HAdV infections are common in the human population, as indicated by the high seroprevalence of anti-adenovirus antibodies (ranging from 80 to 90% in sub-Saharan Africa, and from 30 to 70% in Europe and North America), but in otherwise healthy adults, these infections are generally mild and self-limited (Grosso et al., 2017; Inturi et al., 2018). On the other hand, with the advances in molecular techniques of diagnosis, HAdV have been found to be increasingly involved in occasional cases and outbreaks of community-acquired pneumonia (CAP) in healthy population (Kajon and Ison, 2014; Yu et al., 2015; Tan et al., 2016; Jonnalagadda et al., 2017; Yoon et al., 2017). In immunocompromised patients, HAdV infections present with a wide clinical symptomatology including pneumonia, colitis, hepatitis, hemorrhagic cystitis, tubule-interstitial nephritis or encephalitis, which can result in disseminated disease with high morbidity and mortality in this population especially in the pediatric units (Lion, 2014; Sulejmani et al., 2018).

Despite HAdV significant clinical impact, currently there is not an approved drug to treat these infections and the off-label antiviral drugs available, ribavirin, ganciclovir and cidofovir, although they have demonstrated *in vitro* efficacy against HAdV, their clinical efficacy is very variable and their use is also limited by their poor bioavailability and side effects (nephrotoxicity or bone marrow suppression). Brincidofovir (CMX001), a lipidic conjugate of cidofovir, that finished a phase III clinical trial in 2016 with no reported results so far (ClinicalTrials.gov Identifier: NCT02087306) and is now being evaluated for the treatment of serious HAdV infection or disease (ClinicalTrials.gov Identifier: NCT02596997) represents the only potential alternative to be used for the treatment of HAdV infections (Toth et al., 2008; Paolino et al., 2011). Based on this scenario, the research on additional drugs with increased anti-HAdV efficacy is thus necessary.

On the other hand, cancer remains one of the most life-threatening diseases and an economic burden worldwide (Torre et al., 2015). Cancer is an abnormal growth of cells and tissues, mainly influenced by the environmental and genetic factors of each person. More than 277 types of cancer have been identified and diagnosed among which prostate, breast, lung, colon, rectum, bronchus and urinary bladder cancers are the predominant ones (Wogan et al., 2004; Kumar and Adki, 2018; Khalifa et al., 2019).

In 2018, approximately 18 million new cases of cancer reported globally, resulting in approximately 10 million deaths (Bray et al., 2018; Vogelstein and Kinzler, 2004). Currently three cancer treatments are available, surgery, radiotherapy and chemotherapy (Bray et al., 2018). Unlike surgery and radiotherapy, which are methods mainly indicated for solid tumours, chemotherapy is a treatment that interferes with the process of growth and cell division in tumour cells (Ma and Wang, 2009).

New drug therapies have extended human life span and improved the quality of life, and nowadays several drugs for cancer chemotherapy exist and the therapeutic success is considerably high for various treatments, however tumour recurrence and metastasis are also usual in some cases (Widmer et al., 2014; Kuczynski et al., 2013). In this regard, society has become more and more reliant upon the availability of safe and efficacious pharmaceutical products with fewer side effects.

Considering that the marine world provides approximately half of the total biodiversity on earth (Vo and Kim, 2010; Aneiros and Garateix, 2004), and of course the

vast expanse of the ocean, this underwater environment would represent an exceptional opportunity for the search of new chemical compounds (Bhadury et al., 2006) for the anticancer and antiviral therapies. Today, around 29,000 new compounds were reported from marine species, such as sponges, ascidians, corals, and bacteria, and they represent a huge structural diversity of secondary metabolites with very promising candidates to be developed as a drug (Blunt et al., 2017; Pye et al., 2017).

Up to date, agencies such as U.S. Food and Drug Administration (FDA), European Medicines Agency (EMA), Japanese Ministry of Health and Australia's Therapeutic Goods Administration have approved only 8 marine pharmaceutical clinical compounds as therapeutic drugs, and 22 drug candidates in phase III, II, or I of drug development (Pereira, 2019). Five of the approved drugs are used for the cancer treatment, Cytarabine (*ara-C*), Trabectedin, Eribulin mesylate, Brentuximab vedotin and plitidepsin (dehydrodidemnin B), while just one was used as antiviral compound, the Vidarabine (*ara-A*) (Jiménez, 2008).

The coasts of Mexico extend up to 11,122 km of maritime littorals from the Pacific Ocean to the Caribbean Sea and the Gulf of Mexico, where a rich marine flora and fauna can be found (Morales et al., 2006). Even so, the underwater Mexican ecosystems remains very little explored.

Particularly, the Yucatan Peninsula (YP), with 1500 km of coastline, includes the Mexican States of Campeche, Yucatan and Quintana Roo (Herrera-Silveira et al., 2004) and occupies approximately 14% of total Mexican coast and it has a great biological diversity in the shore and the ocean (Bye et al. 1995). All along the western and northern coasts of the YP extends a region known as the Campeche Bank (CB) with abundant coral reef ecosystems either well offshore (>100 km, such as Alacranes reef, Cayo Arenas, Cayo Arcas, among others) or closer to the shore of the Yucatan state (such as Sisal, Madagascar and Serpiente); both have been recognized as important biodiversity hotspots (Jordán-Dahlgren, 2003; Tunnell, 2007; Zarco-Perelló et al. 2013; Ortiz-Lozano et al. 2013). Additionally, the eastern coast of YP is part of the Mesoamerican Reef, which contains the largest barrier reef in the Western Hemisphere, stretching nearly 700 miles from the northern tip of the YP down through the Honduran Bay Islands (Almada-Villela et al. 2013).

The potential of Mexican marine resources along the coasts of the YP has not been intensively investigated. Most of the few reports are limited to the evaluation of the biological activity of their organic extracts and there are very few studies on the chemistry of natural products (Pech-Puch et al., 2020).

As far as we know, the only study of the antiviral activity in extracts of marine organisms of the YP was the report about the high activity of the L-carrageenan polysaccharide obtained from the red algae *Solieria filiformis* (Peñuela et al., 2018). In relation to antiproliferative activity of the marine extracts of YP, there only two reports corresponding to the evaluation of 30 extracts exclusively from seaweeds (Caamal-Fuentes et al., 2014) (Moo-Puc et al., 2009), and for all the studies of marine natural products from YP just four compounds with antiproliferative activity have been isolated; the diterpene dictyol B acetate, the steroid fucosterol (Caamal-Fuentes et al., 2014) and the triterpenoid saponins, stichloroside B₂ and astichoposide C (Graniel-Sabido et al., 2016).

In our continuing search for new biological compounds, we decide to explore the marine biodiversity of YP waters. In this work, we want to report the antiviral and antiproliferative screening studies, of 65 organic extracts from marine invertebrate species collected along the coasts of the YP.

2. Materials and methods

2.1. Animal collection and identification

Marine organisms were collected by snorkelling and SCUBA diving during three different periods of time: September-December 2016, January-March 2017 and September 2018. The selected species were collected from two different regions of the Yucatan Peninsula: Mexican Caribbean (Cozumel Island, Rio Indio, Mahahual and Bermejo, Quintana Roo) and Campeche Bank (Alacranes Reef and Progreso, Yucatan) in areas that were chosen for their biological diversity such as coral reefs, islands and mangroves (Figure 1).

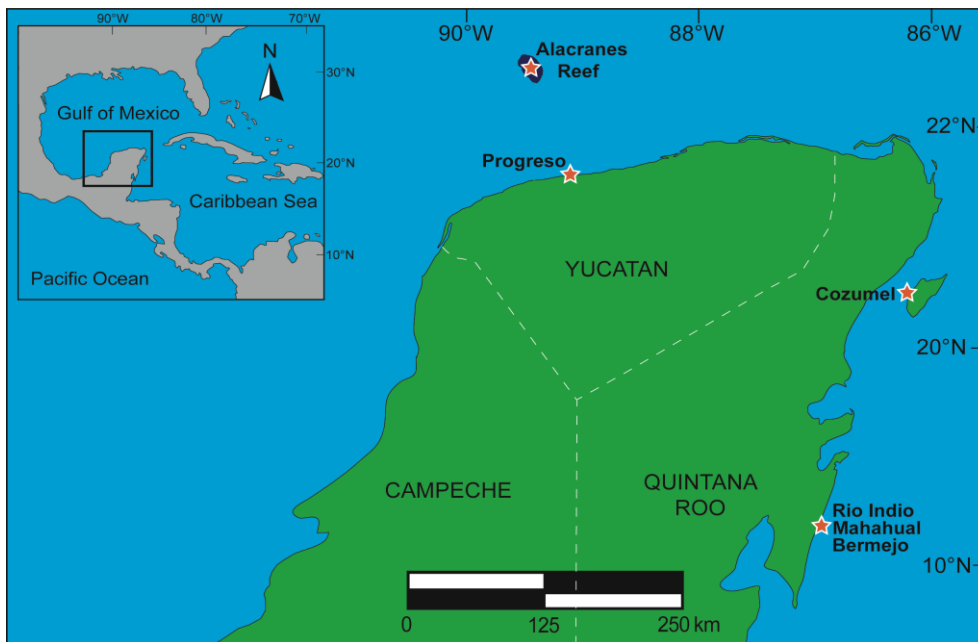


Figure 1. Sites of collection of marine organisms in the Yucatan Peninsula, Mexico.

After collection, the samples were labelled using a code according to the collection sites, were stored in plastic bags and chilled on ice during transport to the laboratory. Voucher specimens for all species were deposited in two different collection sites: sponges in the Phylum Porifera Gerardo Green National Collection of the Instituto de Ciencias del Mar y Limnología (ICMyL) at the National Autonomous University of Mexico (UNAM) in Ciudad de Mexico while ascidians and gorgonian in the Marine Biology Collection at Autonomous University of Yucatan (UADY) in Yucatan, Mexico.

The taxonomic identification of sponges was performed by biologist Patricia Gómez (ICMyL-UNAM, Mexico), ascidians by the biologists María Elsa Vázquez Otero (Universidad de Vigo, Spain), and Harold Villegas-Hernandez (Universidad Autónoma de Yucatan, Mexico), and the gorgonian by marine biologist Dawrin Pech-Puch (CICA-Universidade da Coruña, Spain). Taxonomic information, voucher labels, collection sites and yield of extracts (% from wet weight) of the 65 selected marine organisms are shown in Table 1.

Table 1. Taxonomic information, voucher numbers, site of collection, yield of the organic extract for the species studied.

Phylum: Chordata

Order: Aplousobranchia

Family	Organism	Code	Site	Yield (gr)
Clavelinidae	<i>Clavelina</i> sp.	T18-M1	Progreso, Yucatan (Mangrove)	5.0
	<i>Didemnum perlucidum</i>	E8-2	Rio Indio, Quintana Roo	1.8
	<i>Didemnum</i> sp.	T18-M4	Progreso, Yucatan (Mangrove)	3.5
Didemnidae	<i>Didemnum</i> sp.	E01	Bermejo, Quinta Roo	3.7
	<i>Trididemnum solidum</i>	E7-2	Rio Indio, Quintana Roo	3.4
	<i>Polysyncraton</i> sp.	EY18-8	Progreso, Yucatan	3.6
Polycitoridae	<i>Eudistoma amanitum</i>	RIO18-T1	Rio Indio, Quintana Roo	3.6
	<i>Eudistoma</i> sp.	TY18-2	Progreso, Yucatan	2.9
Polyclinidae	<i>Polyclinum</i> sp.	T18-M5	Progreso, Yucatan (Mangrove)	1.8
Asciidiidae	<i>Phallusia nigra</i>	TY18-1	Progreso, Yucatan	5.5
Perophoridae	<i>Ecteinascidia</i> sp.	T18-M2	Progreso, Yucatan (Mangrove)	9.0
Molgulidae	<i>Molgula</i> sp.	T18-M6	Progreso, Yucatan (Mangrove)	3.9
Styelidae	<i>Polycarpa</i> sp.	E41	Alacranes Reef, Yucatan	2.4
Briareidae	<i>Briareum asbestinum</i>	BA-3	Rio Indio, Quintana Roo	3.9
	<i>Agelas citrina</i>	CZE56	Cozumel, Quintana Roo	1.9
	<i>Agelas clathrodes</i>	E27-2	Cozumel, Quintana Roo	11.2
Agelasidae	<i>Agelas clathrodes</i>	MA18-10	Mahahual, Quintana Roo	7.2
	<i>Agelas dilatata</i>	E25-1	Cozumel, Quintana Roo	21.3
	<i>Agelas sceptrum</i>	E26-2	Cozumel, Quintana Roo	4.6
Heteroxyidae	<i>Myrmekioderma gyroderma</i>	CZE18	Cozumel, Quintana Roo	7.5
Raspailiidae	<i>Ectyoplasia ferox</i>	MA18-9	Mahahual, Quintana Roo	5.9
	<i>Ectyoplasia</i> sp.	MA18-13	Mahahual, Quintana Roo	2.2
Chondrillidae	<i>Chondrilla caribensis</i> f. <i>hermatypica</i>	MA18-6	Mahahual, Quintana Roo	2.1
	<i>Chondrilla</i> sp.	RIO18-1	Rio Indio, Quintana Roo	4.6
Clathrinidae	<i>Clathrina</i> sp.	EY18-10	Progreso, Yucatan	1.4
Leucettidae	<i>Leucetta floridana</i>	E2-2	Bermejo, Quinta Roo	1.3
Clionaidae	<i>Cliona delitrix</i>	EY18-1	Progreso, Yucatan	5.2
	<i>Cliona varians</i>	EY18-3	Progreso, Yucatan	1.8
Dysideidae	<i>Dysidea</i> sp.	EY18-12	Progreso, Yucatan	3.3
	<i>Ircinia felix</i>	E9-2	Rio Indio, Quintana Roo	43.5
Irciniidae	<i>Ircinia felix</i>	MA18-11	Mahahual, Quintana Roo	1.7
	<i>Ircinia strobilina</i>	E24-2	Cozumel, Quintana Roo	14.1
	<i>Ircinia strobilina</i>	E52	Bermejo, Quinta Roo	4.9
Spongiidae	<i>Spongia tubulifera</i>	E11-2	Rio Indio, Quintana Roo	29.8
Callyspongiidae	<i>Callyspongia longissima</i>	E28	Alacranes Reef, Yucatan	1.8

	<i>Callyspongia plicifera</i>	E31	Alacranes Reef, Yucatan	1.2
	<i>Callyspongia vaginalis</i>	E16	Cozumel, Quintana Roo	0.9
Chalinidae	<i>Haliclona (rhizoniera) curacaoensis</i>	EY18-4	Progreso, Yucatan	7.9
	<i>Amphimedon compressa</i>	E29	Alacranes Reef, Yucatan	12.9
	<i>Niphates digitalis</i>	E15	Cozumel, Quintana Roo	2.5
Niphatidae	<i>Niphates erecta</i>	E49	Alacranes Reef, Yucatan	1.6
	<i>Niphates erecta</i>	MA18-7	Mahahual, Quintana Roo	2.8
	<i>Niphates erecta</i>	MA18-12	Mahahual, Quintana Roo	2.5
Petrosiidae	<i>Xestospongia muta</i>	EP	Alacranes Reef, Yucatan	5.9
Plakinidae	<i>Plakinastrella onkodes</i>	E3	Bermejo, Quintana Roo	1.5
Crambeidae	<i>Monanchora arbuscula</i>	E35	Alacranes Reef, Yucatan	9.6
Microcionidae	<i>Clathria gomezae</i>	EY18-11	Progreso, Yucatan	3.6
	<i>Clathria virgultosa</i>	E7-E34	Alacranes Reef, Yucatan	33.1
	<i>Mycale laevis</i>	MA18-1	Mahahual, Quintana Roo	2.3
Mycalidae	<i>Mycale laevis</i>	MA18-5	Mahahual, Quintana Roo	2.9
	<i>Scopalina ruetzleri</i>	DNY	Rio Indio, Quintana Roo	9.2
Scopalinae	<i>Scopalina ruetzleri</i>	E53	Cozumel, Quintana Roo	2.2
	<i>Scopalina ruetzleri</i>	EY18-7	Progreso, Yucatan	20.0
Halichondriidae	<i>Halichondria melanadocia</i>	E18-M1	Progreso, Yucatan (Mangrove)	3.6
Suberitidae	<i>Aaptos</i> sp.	E38	Alacranes Reef, Yucatan	4.0
Tethyidae	<i>Tethya</i> sp.	E20	Cozumel, Quintana Roo	6.6
Geodiidae	<i>Melophlus hajdui</i>	E4	Bermejo, Quintana Roo	4.4
Tetillidae	<i>Cinachyrella kuekenthali</i>	MA18-2	Mahahual, Quintana Roo	2.1
	<i>Aiolochoira crassa</i>	E50	Alacranes Reef, Yucatan	5.2
	<i>Aiolochoira crassa</i>	MA18-4	Mahahual, Quintana Roo	8.7
	<i>Aplysina cauliformis</i>	E36	Alacranes Reef, Yucatan	6.3
Aplysinidae	<i>Aplysina fistularis</i>	E46	Alacranes Reef, Yucatan	2.7
	<i>Aplysina fulva</i>	E42	Alacranes Reef, Yucatan	1.8
	<i>Aplysina fulva</i>	EY18-5	Progreso, Yucatan	2.9
	<i>Aplysina muricyanna</i>	E47	Alacranes Reef, Yucatan	4.4

2.2. Preparation of the organic extracts

Sliced bodies of each species were exhaustively extracted with the mixture of dichloromethane-methanol (1:1), three times with 500 mL (1.5L total volume) at 25 °C for 24 h each extraction. After filtration, the solvent was then removed by rotatory evaporator at 40 °C and stored at -20 °C for further in tightly sealed glass vials.

2.3 Antiviral assays

2.3.1 Viruses and cells

Human A549 (human lung carcinoma) and 293 (human embryonic kidney) cell lines were from the American Type Culture Collection (ATCC, Manassas, VA). The 293 β 5 stable cell line overexpressing the human β 5 integrin subunit was kindly provided by Dr. Glen Nemerow (Nguyen et al. 2010). Both cell lines were propagated in Dulbecco's modified Eagle medium (DMEM, Life Technologies/Thermo Fisher) supplemented with 10% fetal bovine serum (FBS) (Omega Scientific, Tarzana, CA), 10 mM HEPES, 4 mM L-glutamine, 100 U/ml penicillin, 100 μ g/ml streptomycin, and 0.1 mM non-essential amino acids (complete DMEM). Wild-type HAdV5 was obtained from ATCC. The HAdV5-GFP showed in this work is a replication-defective virus with a CMV promoter-driven enhanced green fluorescent protein (eGFP) reporter gene cassette in place of the E1/E3 region (Nepomuceno et al. 2007) HAdV were propagated in 293 β 5 cells and isolated from the cellular lysate by cesium chloride (CsCl) density gradient combined with ultracentrifugation. Virus concentration was calculated as previously reported.

2.3.2 Plaque assay

Natural compounds were tested using low MOI infections (0.06 vp/cell) and at concentrations of 10 μ M in a plaque assay. Compounds with a HAdV inhibition greater than 90% were tested in a dose-response assay ranging from 10 to 0.625 μ M in another plaque assay. For organic extracts, the followed procedure was the same but starting concentration was 10 μ g/ml. Selected extracts were tested in a dose-response assay ranging from 10 to 0.625 μ g/ml in another plaque assay. Briefly, 293 β 5 cells were seeded in 6-well plates at a density of 4×10^5 cells per well in duplicate for each condition. When cells reached 80–90% confluency, they were infected with HAdV5-GFP (0.06 vp/cell) and rocked for 2 h at 37°C. After the incubation the inoculum was removed, and the cells were washed once with PBS. The cells were then carefully overlaid with 4 mL/well of equal parts of 1.6% (water/vol) Difco Agar Noble (Becton, Dickinson & Co., Sparks, MD) and 2 \times EMEM (Minimum Essential Medium Eagle, BioWhittaker) supplemented with 2 \times penicillin/streptomycin, 2 \times L-glutamine, and 10% FBS. The mixture also contained the drugs in concentrations ranging from 10 to 0.625 μ M. Following incubation for 7 days at 37°C, plates were scanned with a Typhoon 9410 imager (GE Healthcare Life Sciences) and plaques were quantified with ImageJ (Schneider et al. 2012) This assay was performed in duplicate.

2.3.3 Cytotoxicity assay

The cytotoxicity of the compounds was analyzed by commercial kit AlamarBlue® (Invitrogen, Ref. DAL1025). A549 cells at a density of 5×10^3 cells/well in 96-well plates were seeded. Decreasing concentrations of each compound (200 μ M, 150 μ M, 100 μ M, 80 μ M, 60 μ M, 40 μ M, 30 μ M, 20 μ M, 10 μ M, 5 μ M, 2.5 μ M, 0 μ M) or extract (100 μ g/ml, 80 μ g/ml, 60 μ g/ml, 40 μ g/ml, 30 μ g/ml, 20 μ g/ml, 10 μ g/ml, 5 μ g/ml, 2.5 μ g/ml,

1.25 µg/ml, 0 µg/ml) were diluted in 100 µL of Dulbecco's Modified Eagle Medium (DMEM). Cells were then incubated at 37°C for 48 hours following the manufacturer's indications. The cytotoxic concentration 50 (CC₅₀) value was calculated using the statistical package GraphPad Prism. This assay was performed in duplicate.

2.3.4 Entry assay

The anti-HAdV activity was initially measured in an entry assay using human A549 epithelial cells (3×10^5 cells/well in corning black wall, clear bottom 96-well plates) infected with HAdV5-GFP (2000 vp/cell) in the presence 50 µM of the candidates and in a dose–response assay. A standard infection curve was generated in parallel by infecting cells in the absence of extracts using serial 2-fold dilutions of virus. All reactions were done in triplicate. Cells, viruses, and drugs were incubated for 48 h at 37 °C and 5% CO₂. Infection, as measured by HAdV5-mediated GFP expression, was analyzed using a Typhoon 9410 imager (GE Healthcare Life Sciences) and quantified with ImageQuantTL (GE Healthcare Life Sciences).

2.3.5 Statistical analyses

Statistical analyses were performed with the GraphPad Prism 5 suite. Data are presented as the mean of duplicate samples ± standard deviation (SD).

2.4 Antiproliferative assays

Colorimetric MTT ((3-(4,5-Dimethylthiazol-2-yl)-2,5-diphenyltetrazolium bromide)) assays were carried out to assess the cell viability of the samples against a panel of five different tumour cell lines (i.e., human lung carcinoma A549 ATCC[®] CCL-185TM, human skin melanoma A2058 ATCC[®] CRL-11147TM, hepatocyte carcinoma HepG2 ATCC[®] HB-8065TM, breast adenocarcinoma MCF7 ATCC[®] HTB-22TM and pancreas carcinoma MiaPaca-2 ATCC[®] CRL-1420TM). All cells were obtained from the American Type Culture Collection (ATCC, Manassas, VA, USA). A549 cells were grown in Ham's F12K medium with 2 mM Glutamine, 10% Fetal Bovine Serum (FBS), 100 U/mL penicillin and 100 µg/mL streptomycin. A2058 and HepG2 were grown in ATCC formulated Eagle's M essential medium (MEM) with 10% FBS, 2 mM l-glutamine, 1 mM sodium pyruvate and 100 µM MEM non-essential amino acids. MCF-7 cells were grown in the previous medium supplemented with 0.01 mg/mL of bovine insulin. MiaPaca-2 cells were grown in Dulbecco's Modified Eagle's Medium (DMEM) with 10% FBS, 100U/mL penicillin and 100 µg/mL streptomycin (Audoin et al. 2013) The antiproliferative activity was assessed after 48 h of treatment of the compound at the concentrations of 30, 15 and 7.5 µg/mL.

3. Results and discussion

The organic extracts of 65 marine organisms, corresponding to 50 sponges, 13 ascidians and 1 gorgonian, collected from two different ecosystems in the Yucatan Peninsula, coral reef and mangroves were evaluated in antiviral and antiproliferative activity tests. Around 14 % of the extracts showed antiviral activity against the viruses tested and 37 % of them displayed antitumor activity against one or more tumour cell lines.

3.1 Antiviral screening

Nine extracts displayed significant *in vitro* antiviral activity against human adenovirus (HAdV) in particular, extracts from the ascidian *Clavelina* sp. and eight sponges, *Agelas citrina*, *Myrmekioderma gyroderma*, *Ectyoplasia* sp., *Chondrilla* sp., *Dysidea* sp., *Monanchora arbuscula*, *Aaptos* sp., and *Cinachyrella kuekenthali* as reflected in Table 2.

Table 2. IC₅₀, CC₅₀, SI, % inhibition HAdV5 infection and % Inhibition HAdV5-GFP entry assay of organic extracts of marine organisms from the Yucatan Peninsula.

Code	Organism	IC ₅₀ Plaque assay	% of inhibition HAdV5 infection (10 µg/ml)	IC ₅₀ Entry assay	% Inhibition HAdV5-GFP entry assay (12.5 µg/ml)	CC ₅₀	Selectivity index
T18-M1	<i>Clavelina</i> sp.	3.65 ± 1.56	80.95 ± 1.04	nt	38.82 ± 2.37	39.69 ± 1.30	10.87
E8-2	<i>Didemnum perlucidum</i>	nt	nt	nt	nt	nt	nt
T18-M4	<i>Didemnum</i> sp.	nt	47.32 ± 1.38	nt	nt	nt	nt
E01	<i>Didemnum</i> sp.	nt	16.67 ± 0.00	nt	nt	nt	nt
E7-2	<i>Trididemnum solidum</i>	nt	nt	nt	nt	nt	nt
EY18-8	<i>Polysyncraton</i> sp.	nt	0.00 ± 0.00	nt	nt	nt	nt
RIO18-T1	<i>Eudistoma amanitum</i>	nt	0.00 ± 0.00	nt	nt	nt	nt
TY18-2	<i>Eudistoma</i> sp.	nt	27.47 ± 3.11	nt	nt	nt	nt
T18-M5	<i>Polyclinum</i> sp.	nt	38.54 ± 1.38	nt	nt	nt	nt
TY18-1	<i>Phallusia nigra</i>	nt	4.64 ± 10.18	nt	nt	nt	nt
T18-M2	<i>Ecteinascidia</i> sp.	nt	37.56 ± 4.14	nt	nt	nt	nt
T18-M6	<i>Molgula</i> sp.	nt	42.72 ± 17.85	nt	nt	nt	nt
E41	<i>Polycarpa</i> sp.	nt	23.07 ± 10.87	nt	nt	nt	nt
BA-3	<i>Briareum asbestinum</i>	nt	nt	nt	nt	nt	nt
CZE56	<i>Agelas citrina</i>	1.06 ± 0.41	97.24 ± 0.02	4.74 ± 0.53	100.00 ± 0.00	5.35 ± 2.45	5.05
E27-2	<i>Agelas clathrodes</i>	nt	nt	nt	nt	nt	nt
MA18-10	<i>Agelas clathrodes</i>	nt	6.25 ± 16.51	nt	nt	nt	nt
E25-1	<i>Agelas dilatata</i>	nt	nt	nt	nt	nt	nt
E26-2	<i>Agelas sceptrum</i>	nt	nt	nt	nt	nt	nt
CZE18	<i>Myrmekioderma gyroderma</i>	7.48 ± 1.69	71.03 ± 5.85	nt	0.00 ± 0.00	22.26 ± 2.23	2.98
MA18-9	<i>Ectyoplasia ferox</i>	nt	35.00 ± 11.21	nt	nt	nt	nt

MA18-13	<i>Ectyoplasia sp.</i>	10.00± 0.00	85.68 ± 7.35	nt	0.00±0.00	39.77± 7.88	3.97
MA18-6	<i>Chondrilla caribensis f. hermatypica</i>	nt	0.00 ± 0.00	nt	nt	nt	nt
RIO18-1	<i>Chondrilla sp.</i>	1.31 ± 0.10	97.24 ± 3.90	1.09 ± 0.79	99.72 ± 0.29	2.45 ± 0.48	1.87
EY18-10	<i>Clathrina sp.</i>	nt	0.00 ± 0.00	nt	nt	nt	nt
E2-2	<i>Leucetta floridana</i>	nt	nt	nt	nt	nt	nt
EY18-1	<i>Cliona delitrix</i>	nt	0.00 ± 0.00	nt	nt	nt	nt
EY18-3	<i>Cliona varians</i>	nt	0.00 ± 0.00	nt	nt	nt	nt
EY18-12	<i>Dysidea sp.</i>	1.12 ± 0.02	98.17 ± 0.52	5.24 ± 0.50	98.24 ± 0.72	19.46 ± 0.30	17.38
E9-2	<i>Ircinia felix</i>	nt	nt	nt	nt	nt	nt
MA18-11	<i>Ircinia felix</i>	nt	51.05 ± 10.25	nt	nt	nt	nt
E24-2	<i>Ircinia strobilina</i>	nt	nt	nt	nt	nt	nt
E52	<i>Ircinia strobilina</i>	nt	0.00 ± 0.00	nt	nt	nt	nt
E11-2	<i>Spongia tubulifera</i>	nt	nt	nt	nt	nt	nt
E28	<i>Callyspongia longissima</i>	nt	0.00 ± 0.00	nt	nt	nt	nt
E31	<i>Callyspongia plicifera</i>	nt	54.13 ± 6.43	nt	nt	nt	nt
E16	<i>Callyspongia vaginalis</i>	nt	47.00 ± 5.45	nt	nt	nt	nt
EY18-4	<i>Haliclona (rhizoniera) curacoensis</i>	nt	51.65 ± 14.50	nt	nt	nt	nt
E29	<i>Amphimedon compressa</i>	nt	nt	nt	nt	nt	nt
E15	<i>Niphates digitalis</i>	nt	46.66 ± 9.99	nt	nt	nt	nt
E49	<i>Niphates erecta</i>	>10.00	41.00 ± 8.64	nt	0.00±0.00	nt	nt
MA18-7	<i>Niphates erecta</i>	nt	27.50 ± 12.68	nt	nt	nt	nt
MA18-12	<i>Niphates erecta</i>	nt	48.96 ± 1.47	nt	nt	nt	nt
EP	<i>Xestospongia muta</i>	nt	18.58 ± 8.77	nt	nt	nt	nt
E3	<i>Plakinastrella onkodes</i>	nt	17.29 ± 0.00	nt	nt	nt	nt
E35	<i>Monanchora arbuscula</i>	nt	98.97 ± 1.46	nt	nt	6.45± 2.41	nt
EY18-11	<i>Clathria gomezae</i>	nt	0.00 ± 0.00	nt	nt	nt	nt
E7-E34	<i>Clathria virgultosa</i>	nt	nt	nt	nt	nt	nt
MA18-1	<i>Mycale laevis</i>	nt	0.00 ± 0.00	nt	nt	nt	nt
MA18-5	<i>Mycale laevis</i>	nt	0.00 ± 0.00	nt	nt	nt	nt
DNY	<i>Scopalina ruetzleri</i>	nt	nt	nt	nt	nt	nt
E53	<i>Scopalina ruetzleri</i>	nt	37.17 ± 7.51	nt	nt	nt	nt

EY18-7	<i>Scopalina ruetzleri</i>	nt	0.00 ± 0.00	nt	nt	nt	nt
E18-M1	<i>Halichondria melanadocia</i>	nt	25.86 ± 2.44	nt	nt	nt	nt
E38	<i>Aaptos sp.</i>	10.00±0.00	72.00 ± 10.97	nt	0.00±0.00	22.72±2.89	2.27
E20	<i>Tethya sp.</i>	nt	52.89 ± 5.18	nt	nt	nt	nt
E4	<i>Melophlus hajdui</i>	nt	48.71 ± 2.32	nt	nt	nt	nt
MA18-2	<i>Cinachyrella kuekenthali</i>	10.00±0.00	73.08 ± 3.26	nt	0.00±0.00	30.06 ± 9.95	3.00
E50	<i>Aiolochoira crassa</i>	>10.00	35.29 ± 10.70	nt	0.00±0.00	nt	nt
MA18-4	<i>Aiolochoira crassa</i>	nt	0.00 ± 0.00	nt	nt	nt	nt
E36	<i>Aplysina cauliformis</i>	nt	0.00 ± 0.00	nt	nt	nt	nt
E46	<i>Aplysina fistularis</i>	nt	18.00 ± 2.82	nt	nt	nt	nt
E42	<i>Aplysina fulva</i>	nt	10.00 ± 3.26	nt	nt	nt	nt
EY18-5	<i>Aplysina fulva</i>	nt	0.00 ± 0.52	nt	nt	nt	nt
E47	<i>Aplysina muricyanna</i>	nt	16.00 ± 12.62	nt	nt	nt	nt
Cidofovir positive control		24.06 ± 5.90	nt	nt	nt	50.06 ± 9.80	7.50

*nt: not tested

The extracts of the sponges *Dysidea sp.*, *Agelas citrina* and *Chondrilla sp.* showed the higher activity with more than 97 % of inhibition against HAdV5 at 10 µg/ml concentration and IC₅₀ values between 1.0-1.3 µM in the plaque assays. The same sponges species showed more than 98 % inhibition in the entry assay at 12.5 µg/ml and IC₅₀ values of 5.24 µM for *Dysidea sp.*, 4.74 µM for *Agelas citrina* and 1.09 µM for *Chondrilla sp.* The CC₅₀ values were 19.46 µM for *Dysidea sp.*, 5.35 µM for *Agelas citrina* and 1.09 µM for *Chondrilla sp.* The sponge *Dysidea sp.* displayed the best selectivity index (SI=17.38), followed by *Agelas citrina* (SI=5.05) and finally *Chondrilla sp.* (SI=1.87).

The sponge *Monanchora arbuscula* showed a high activity with more than 97 % of inhibition against HAdV5 infection at 10 µg/ml.

The ascidian *Clavelina sp.* displayed more than 80% inhibition of HAdV5 infection at 10 µg/ml, and a IC₅₀ of 3.6 µM in the plaque assay. In the entry assay, it showed 39 % of inhibition at 12,5 µg/ml and in addition, it presented the best CC₅₀ value of all the organisms, with 39.69 µM and the second best selectivity index (10.87).

The sponges *Myrmekioderma gyroderma*, *Ectyoplasia sp.*, *Cinachyrella kuekenthali* and *Aaptos sp.* showed of 71-85 % of inhibition against HAdV5 infection with 10 µg/ml, and IC₅₀ values between 7.4-10 µM. The CC₅₀ values were 22.26 µM for *Myrmekioderma gyroderma*, 39.77 µM for *Ectyoplasia sp.*, 30.06 µM for *Cinachyrella kuekenthali* and 22.72 µM for *Chondrilla sp.* and the selectivity index for the four sponges showed values between 2.27-3.97.

3.2 Antiproliferative screening

Twenty four extracts were able to induce growth inhibition in one or more tumour cell lines, in particular those from four ascidians (*Clavelina sp.*, *Trididemnum solidum*, *Polysyncraton sp.* and *Eudistoma amanitum*) and from twenty sponges (*Agelas citrina*,

Myrmekioderma gyroderma, *Chondrilla caribensis f. hermatypica*, *Leucetta floridana*, *Cliona varians*, *Dysidea* sp., *Spongia tubulifera*, *Haliclona (rhizoniera) curacoensis*, *Amphimedon compressa*, *Plakinastrella onkodes*, *Monanchora arbuscula*, *Clathria gomezae*, *Mycale laevis*, *Scopalina ruetzleri* (collected in Progreso, Yucatan and Rio Indio, Quintana Roo), *Aptos* sp., *Tethya* sp., *Cinachyrella kuekenthali* and *Aiolochoira crassa* (collected in Alacranes Reef, Yucatan and Mahahual, Quintana Roo). The extracts of two organisms, the ascidian *Eudistoma amanitum* and the sponge *Haliclona (rhizoniera) curacoensis*, showed the best antiproliferative activities with a 97% growth inhibition in all the cell lines at all concentrations tested (Table 3).

Table 3. Antiproliferative activity of organic extracts of marine organisms from Yucatan Peninsula.

	Organism	Human lung carcinoma (A549)			Human skin melanoma (A2058)			Hepatocyte carcinoma (HepG2)			Breast adenocarcinoma (MCF7)			Pancreas carcinoma (MiaPaca2)		
		30 µg/ml	15 µg/ml	7.5 µg/ml	30 µg/ml	15 µg/ml	7.5 µg/ml	30 µg/ml	15 µg/ml	7.5 µg/ml	30 µg/ml	15 µg/ml	7.5 µg/ml	30 µg/ml	15 µg/ml	7.5 µg/ml
T18-M1	<i>Clavelina</i> sp.	93	93	84	98	95	92	98	96	93	91	79	50	94	90	85
E8-2	<i>Didemnum perlucidum</i>	17	17	13	19	10	11	67	51	45	0	10	3	2	2	3
T18-M4	<i>Didemnum</i> sp.	2	9	0	4	1	3	35	8	8	4	12	7	4	4	0
E01	<i>Didemnum</i> sp.	2	9	3	8	0	3	8	4	2	8	11	12	8	7	3
E7-2	<i>Trididemnum solidum</i>	73	51	25	87	69	29	92	71	52	52	31	9	65	4	3
EY18-8	<i>Polysyncrator</i> sp.	15	18	9	50	23	13	80	60	53	34	23	4	8	2	3
RIO18-T1	<i>Eudistoma amanitum</i>	99	99	99	99	100	100	100	99	99	100	100	100	100	97	99
TY18-2	<i>Eudistoma</i> sp.	2	2	5	8	1	0	35	24	21	10	5	4	6	3	3
T18-M5	<i>Polycinum</i> sp.	3	10	3	5	1	3	47	27	17	3	5	3	2	1	1
TY18-1	<i>Phallusia nigra</i>	13	10	1	2	3	4	25	7	4	8	3	1	4	0	1
T18-M2	<i>Ecteinascidia</i> sp.	4	4	7	5	1	3	33	9	8	2	4	7	6	4	4
T18-M6	<i>Molgula</i> sp.	6	11	4	16	10	1	48	29	18	1	5	3	2	0	2
E41	<i>Polycarpa</i> sp.	1	10	0	24	7	1	67	47	32	14	20	14	1	3	4
BA-3	<i>Briareum asbestinum</i>	nt	nt	nt	nt	nt	nt	nt	nt	nt	nt	nt	nt	nt	nt	nt
CZE56	<i>Agelas citrina</i>	49	26	6	100	100	100	100	69	21	100	100	46	100	1	3
E27-2	<i>Agelas clathrodes</i>	21	17	8	20	9	6	53	26	21	0	8	3	4	2	3
MA18-10	<i>Agelas clathrodes</i>	8	8	1	19	1	3	29	6	6	18	5	12	4	1	2
E25-1	<i>Agelas dilatata</i>	22	24	16	25	18	11	63	42	39	7	2	5	6	3	4
E26-2	<i>Agelas sceptrum</i>	22	16	4	39	27	20	66	55	48	6	17	12	3	2	3
CZE18	<i>Myrmekioderma gyroderma</i>	29	12	3	74	13	1	100	100	40	73	11	1	80	0	3
MA18-9	<i>Ectyoplasia ferox</i>	16	18	3	6	3	4	82	1	0	4	9	3	3	6	5
MA18-13	<i>Ectyoplasia</i> sp.	43	20	10	37	18	5	86	47	22	41	20	5	26	4	2
MA18-6	<i>Chondrilla caribensis f. hermatypica</i>	60	56	27	69	2	2	99	81	26	96	25	4	3	8	9
RIO18-1	<i>Chondrilla</i> sp.	1	9	1	4	2	3	24	8	1	15	9	1	3	2	3
EY18-10	<i>Clathrina</i> sp.	7	15	3	9	0	2	33	10	7	14	6	5	5	1	2
E-2	<i>Leucetta floridana</i>	100	66	6	100	98	16	100	99	36	100	51	7	100	23	2
EY18-1	<i>Cliona delitrix</i>	7	13	4	16	2	2	43	23	9	13	3	7	7	8	5
EY18-3	<i>Cliona varians</i>	69	32	15	22	9	2	80	66	47	2	2	0	29	5	1

EY18-12	<i>Dysidea sp.</i>	52	12	2	64	15	1	96	65	18	86	41	4	27	3	4
E9-2	<i>Ircinia felix</i>	9	17	9	30	16	11	61	41	39	4	10	1	21	4	3
MA18-11	<i>Ircinia felix</i>	5	7	4	7	6	0	35	20	17	3	10	1	14	6	1
E24-2	<i>Ircinia strobilina</i>	20	22	24	39	37	38	66	47	44	10	13	3	3	1	17
E52	<i>Ircinia strobilina</i>	7	10	1	3	2	2	10	3	1	5	4	1	1	0	1
E11-2	<i>Spongia tubulifera</i>	13	12	0	35	9	0	84	55	24	31	20	1	51	16	4
E28	<i>Calyspongia longissima</i>	21	17	4	24	6	0	60	35	29	2	4	5	2	1	1
E31	<i>Calyspongia plicifera</i>	36	33	21	25	11	5	65	47	31	3	10	1	20	7	5
E16	<i>Calyspongia vaginalis</i>	3	8	1	6	1	2	12	5	0	14	8	9	3	2	3
EY18-4	<i>Haliclona (rhizoniera) curacoensis</i>	100	100	99	100	100	100	100	100	100	100	100	100	100	100	100
E29	<i>Amphimedon compressa</i>	100	100	86	99	36	26	100	69	47	68	36	11	27	4	4
E15	<i>Niphates digitalis</i>	1	11	3	12	3	1	23	5	1	7	10	1	2	0	2
E49	<i>Niphates erecta</i>	7	12	2	13	3	1	35	15	4	24	6	12	2	0	0
MA18-7	<i>Niphates erecta</i>	11	15	5	9	0	2	47	26	17	31	5	4	4	0	0
MA18-12	<i>Niphates erecta</i>	25	16	4	51	7	1	77	49	31	2	17	5	2	4	1
EP	<i>Xestospongia muta</i>	2	7	0	1	3	3	44	18	12	16	2	1	1	1	1
E3	<i>Plakinastrella onkodes</i>	100	100	84	100	98	6	100	100	90	100	56	11	100	63	3
E35	<i>Monanchora arbuscula</i>	67	56	48	100	100	94	99	98	93	100	99	87	100	89	90
EY18-11	<i>Clathria gomezae</i>	39	21	1	84	8	4	76	37	10	22	9	2	3	3	2
E7-E34	<i>Clathria virgultosa</i>	22	10	9	21	10	4	55	34	27	4	3	0	2	1	2
MA18-1	<i>Mycale laevis</i>	9	17	9	29	18	9	68	50	36	3	10	8	26	11	4
MA18-5	<i>Mycale laevis</i>	8	13	1	10	2	1	29	2	5	5	8	9	2	2	1
DNY	<i>Scopalina ruetzleri</i>	66	36	21	97	34	5	94	76	46	42	1	3	4	0	2
E53	<i>Scopalina ruetzleri</i>	8	11	1	9	1	2	53	26	14	5	2	5	6	2	1
EY18-7	<i>Scopalina ruetzleri</i>	13	24	16	31	22	13	71	51	42	3	5	2	1	3	4
E18-M1	<i>Halichondria melanadocia</i>	10	9	8	15	5	0	37	23	11	4	10	6	30	1	2
E38	<i>Aaptos sp.</i>	75	71	63	99	99	98	93	89	86	67	69	56	95	91	77
E20	<i>Tethya sp.</i>	81	72	58	99	91	96	90	87	83	75	72	50	97	86	8
E4	<i>Melophylus hajdii</i>	8	2	9	16	0	2	53	16	7	14	1	11	6	3	3
MA18-2	<i>Cinachyrella kukenthalii</i>	78	71	59	98	98	97	91	88	84	57	64	46	93	89	68
E50	<i>Aiolochoira crassa</i>	7	6	2	16	4	1	92	73	48	11	3	1	3	2	3
MA18-4	<i>Aiolochoira crassa</i>	11	10	4	31	13	4	95	62	36	27	6	14	2	1	1
E36	<i>Aplysina cauliformis</i>	20	14	3	18	11	7	52	39	28	22	7	10	3	3	4
E46	<i>Aplysina fistularis</i>	15	12	1	15	7	3	45	34	26	23	6	10	6	2	3
E42	<i>Aplysina fulva</i>	7	9	2	13	4	1	23	1	2	11	1	6	6	2	2
EY18-5	<i>Aplysina fulva</i>	32	24	14	23	10	4	60	46	35	1	4	3	9	1	4
E47	<i>Aplysina muricyama</i>	4	4	4	8	2	0	21	8	6	19	8	15	5	3	3
DMSO		0			0			0			0			0		
Doxorubicin 50µM		90			100			99			100			100		
MMS 4µM		100			100			100			100			100		

*nt: not tested

The extracts of six organisms (the ascidian *Clavelina* sp. and the sponges *Plakinastrella onkodes*, *Monanchora arbuscula*, *Aaptos* sp., *Tethya* sp. and *Cinachyrella kuekenthali*) displayed also a very good activity in all the cell lines, but with changes in the percentage of inhibition according to the concentration tested. For example, two organisms, *Clavelina* sp. and *Plakinastrella onkodes*, showed more than 84 % growth inhibition of the human lung carcinoma cell line (A549) at all concentrations while the six organisms displayed more than 91 % growth inhibition of the human skin melanoma cell line (A2058) at all concentrations, except the sponge *Plakinastrella onkodes* that not show antiproliferative activity to 7.5 µg/mL. In the particular case of the hepatocyte carcinoma cell line (HepG2), the six species showed more than 83 % growth inhibition at all concentrations. In the case of the breast adenocarcinoma (MCF7), only the sponge *Monanchora arbuscula* displayed more than 87 % growth inhibition at all concentrations tested, while the species *Clavelina* sp. and *P. onkodes* showed more than 91 % growth inhibition at 30 µg/mL. Finally, the six organisms displayed antiproliferative activity of the pancreas carcinoma cell line (MiaPaca-2) with a percentage of inhibition between 63-100 % at all concentrations, except for the sponges *Plakinastrella onkodes* and *Tethya* sp. that did not show any activity at 7.5 µg/mL.

The extracts of five sponges were active against four cell lines, being more effective in some types of cancer. The three extracts most active were the sponge *Agelas citrina* that displayed 100 % of growth inhibition of the human skin melanoma cell line (A2058) at all concentrations tested, of HepG2 at 30 µg/mL, of MCF7 at 30 and 15 µg/mL, and MiaPaca-2b at 30 µg/mL of concentration; followed by the sponge *Myrmekeioderma gyroderma* extract that showed 100 % of growth inhibition of the hepatocyte carcinoma cell line (HepG2) to 30 and 15 µg/mL, and more than 73 % of growth inhibition against A2058, MCF7 and MiaPaca-2 to 30 µg/mL. Finally, the extract of the sponge *Amphimedon compressa* showed more than 86 % of growth inhibition of the human lung carcinoma cell line (A549) at all concentrations tested, also it showed more than 99 % of growth inhibition of A2058 and HepG2 cell lines at 30 µg/mL and more than 68 % of HepG2 and MCF7 cell lines at 15 µg/mL.

The other two sponges, *Chondrilla caribensis f. hermatypica* displayed more than 56 % of growth inhibition of A549 (30 and 15 µg/mL), A2058 (30 µg/mL), HepG2 (30 and 15 µg/mL) and MiaPaca-2 (30 µg/mL) and the sponge *Dysidea* sp. showed more than 52 % of growth inhibition against A2058, HepG2, MCF7 and MiaPaca-2 cell lines to 30 µg/mL.

The sponge *Scopalina ruetzleri* was the only that showed more than 66 % of growth inhibition of A549, A2058 and HepG2 cell lines at 30 µg/mL. The extract of the sponge *Leucetta floridana* showed 100 % of growth inhibition of all cell lines and more than 98 % growth inhibition of A2058 and HepG2 cell lines at 15 µg/mL. On the other hand, the extract of sponge *Clathria gomezae* displayed more than 76 % of growth inhibition of A2058 and HepG2 cell lines at 30 µg/mL.

It is worth mentioning that more than 50 % of the extracts tested showed antiproliferative activity against the hepatocyte carcinoma cell line (HepG2), forty one extracts exhibited at least more than 50 % of growth inhibition at 30 µg/mL concentration, and the organisms, *Polysyncraton* sp., *Cliona varians*, *Spongia tubulifera*, *Mycale laevis*, *Scopalina ruetzleri* (collected in Progreso, Yucatan) and *Aiolochoia crassa* (collected in Alacranes Reef, Yucatan and Mahahual, Quintana Roo), only displayed activity against the cell line HepG2.

4. Conclusions

Sixty-five organic extracts from marine organisms, corresponding to fifty-one sponges (Porifera), thirteen ascidians (Chordata) and one gorgonian (Cnidaria), were collected along the coast of Yucatan Peninsula in Mexico which were selected on the basis of chemotaxonomical criteria. An aliquot of each extract was submitted to an *in vitro* antiviral and antiproliferative screening against two types of virus and five tumour cell lines. Evaluation through microdilution assays displayed an important antiviral activity of nine extracts corresponding to eight sponges (*Agelas citrina*, *Myrmekioderma gyroderma*, *Ectyoplasia* sp., *Chondrilla* sp., *Dysidea* sp., *Monanchora arbuscula*, *Aaptos* sp., and *Cinachyrella kuekenthali*) and one ascidian (*Clavelina* sp.) The extracts of the sponges *Dysidea* sp., *Agelas citrina* and *Chondrilla* sp. showed the best antiviral activity. The observed IC₅₀ values of these extracts were significantly lower than those shown by cidofovir (IC₅₀ = 24.06 ± 5.9 µM; CC₅₀ = 50.06 ± 9.8 µM; SI = 7.5), the drug of choice to treat HAdV infections. The high inhibition value registered for the extracts of these three sponges suggests that the antiviral action mechanism could be related with early steps in the HAdV replicative cycle.

In contrast, the sponges *Myrmekioderma gyroderma*, *Ectyoplasia* sp., *Cinachyrella kuekenthali* and *Aaptos* sp. these did not show antiviral activity in the inhibition entry assays, suggesting that the mechanism of action of the compounds present in each extract could be related with later steps in the HAdV replicative cycle.

Twenty-four extracts showed antiproliferative activity and corresponding to twenty sponges (*Agelas citrina*, *Myrmekioderma gyroderma*, *Chondrilla caribensis* f. *hermatypica*, *Leucetta floridana*, *Cliona varians*, *Dysidea* sp., *Spongia tubulifera*, *Haliclona (rhizoniera) curacoensis*, *Amphimedon compressa*, *Plakinastrella onkodes*, *Monanchora arbuscula*, *Clathria gomezae*, *Mycale laevis*, *Scopalina ruetzleri* (collected in Progreso, Yucatan and Rio Indio, Quintana Roo), *Aaptos* sp., *Tethya* sp., *Cinachyrella kuekenthali* and *Aiolochoxia crassa* (collected in Alacranes Reef, Yucatan and Mahahual, Quintana Roo) and four ascidians (*Clavelina* sp., *Trididemnum solidum*, *Polysyncraton* sp. and *Eudistoma amanitum*). Two organisms, the ascidian *Eudistoma amanitum* and the sponge *Haliclona (rhizoniera) curacoensis*, displayed the best antiproliferative activity. Additionally, more than 50 % of the extracts showed antiproliferative activity against the hepatocyte carcinoma cell line (HepG2).

Acknowledgments: This work was supported by Grants AGL2015-63740-C2-2-R and RTC-2016-4611-1 (AEI/FEDER, EU) from the State Agency for Research (AEI) of Spain, both co-funded by the FEDER Programme from the European Union. DPP received a fellowship from the program National Council of Science and Technology (CONACYT) of Mexico and the Secretariat of Research, Innovation and Higher Education (SIIES) of Yucatan (Mexico).

References

- Almada-Villela, P.C., Sale P., Gold-Bouchot G., Kjerfve B., 2003. Mesoamerican barrier reef systems project: manual of methods for the MBRS synoptic monitoring program. Selected Methods for Monitoring Physical and Biological Parameters for Use in the Mesoamerican Region. MBRS Technical Document No. 4. pp. 156.
- Aneiros, A., Garateix, A., 2004. Bioactive peptides from marine sources: Pharmacological properties and isolation procedures. Journal of

- Chromatography B 803, 41–53.
- Audoin, C., Bonhomme, D., Ivanisevic, J., De La Cruz, M., Cautain, B., Monteiro, M.C., Reyes, F., Rios, L., Perez, T., Thomas, O.P. 2013. Balibalosides, an original family of glucosylated sesterterpenes produced by the Mediterranean sponge *Oscarella balibaloi*. *Marine Drugs* 11, 1477–1489.
- Bhadury, P., Mohammad, B.T., Wright, P.C., 2006. The current status of natural products from marine fungi and their potential as anti-infective agents. *Journal of Industrial Microbiology and Biotechnology* 33, 325–337.
- Blunt, J.W., Copp, B.R., Keyzers, R.A., Munro, M.H.G., Prinsep, M.R., 2017. Marine natural products. *Natural Product Reports* 34(3), 235-294.
- Bray, F., Ferlay, J., Soerjomataram, I., Siegel, R.L., Torre, L.A., Jemal, A., 2018. Global cancer statistics 2018: GLOBOCAN estimates of incidence and mortality worldwide for 36 cancers in 185 countries. *CA A Cancer Journal for Clinicians* 68, 394–424.
- Bye, R., Linares, E., Estrada, E., 1995. Biological diversity of medicinal plants in México. In: Arnason, J.T., Mata, R., Romeo, J.T. (Eds.), *Phytochemistry of Medicinal Plants: Recent Advances in Phytochemistry*, vol 29. Plenum Press, New York, p. 65.
- Caamal-Fuentes, E., Chale-Dzul, J., Moo-Puc, R., Freile-Pelegrin, Y., Robledo, D., 2014. Bioprospecting of Brown Seaweed (Ochrophyta) from the Yucatan Peninsula: Cytotoxic, Antiproliferative, and Antiprotozoal Activities. *Journal of Applied Phycology* 26, 1009–1017.
- Caamal-Fuentes, E., Moo-Puc, R., Freile-Pelegrín, Y., Robledo, D., 2014. Cytotoxic and Antiproliferative Constituents from *Dictyota Ciliolata*, *Padina Sanctae-Crucis* and *Turbinaria Tricostata*. *Pharmaceutical Biology* 52, 1244–1248.
- Grael-Sabido, M. J., Mirón-López, G., León-Deniz, L. V., Moo-Puc, R. E., Quintal-Novelo, C. J., Quijano, L., Mena-Rejón, G. J., 2016. Total NMR Assignment of a New Antiproliferative Triterpene Oligoglycoside from the Sea Cucumber *Astichopus multifidus*. *Tetrahedron Letters* 57, 4375–4378.
- Grosso, F.; Stoilov, P.; Lingwood, C.; Brown, M.; Cochrane, A., 2017. Suppression of Adenovirus Replication by Cardiogenic Steroids. *Journal of virology*, 91 (3): e01623-16.
- Hernández-Bolio, G. I.; Ruiz-Vargas, J. A.; Peña-Rodríguez, L. M. Natural Products from the Yucatecan Flora: Structural Diversity and Biological Activity. *J. Nat. Prod.* **2019**, 82, 647–656.
- Herrera-Silveira, J.A., Comin, F.A., Aranda-Cirerol, N., Troccoli, L., Capurro, L., 2004. Coastal water quality assessment in the Yucatan Peninsula: management implications. *Ocean & Coastal Management* 47, 625-639.
- Inturi, R., Mun, K., Singethan, K., Schreiner, S., Punga, T., 2018. Human Adenovirus Infection Causes Cellular E3 Ubiquitin Ligase MKRN1 Degradation Involving the Viral Core Protein pVII. *Journal of virology*, 92(3), e01154-17.
- Jiménez, C., 2008. Marine natural products in medicinal chemistry. *ACS Medicinal Chemistry Letters* 9, 959–961.
- Jonnalagadda, S., Rodríguez, O., Estrella, B., Sabin, L.L., Sempértegui, F., Hamer, D.H., 2017. Etiology of severe pneumonia in Ecuadorian children. *PLoS One* 12(2), e0171687.
- Jordán-Dahlgren., 2003. Gorgonian distribution patterns in coral reef environments of the Gulf of Mexico: evidence of sporadic ecological connectivity?. *Coral Reefs* 21, 205-215.
- Kajon, A.E., Ison, M.G., 2014. Severe Infections with Human Adenovirus 7d in 2

- Adults in Family, Illinois, USA. *Emerging infectious diseases*, 22 (4), 730-3.
- Khalifa, S.A.M., Elias, N., Farag, M.A., Chen, L., Saeed, A., Hegazy, M.E.F., Moustafa, M.S., Abd El-Wahed, A., Al-Mousawi, S.M., Musharraf, S.G., Chang, F.-R., Iwasaki, A., Suenaga, K., Alajlani, M., Göransson, U., El-Seedi, H.R., 2019. Marine Natural Products: A Source of Novel Anticancer Drugs. *Marine Drugs* 17, 491.
- Kuczynski, E.A., Sargent, D.J., Grothey, A., Kerbel, R.S., 2013. Drug rechallenge and treatment beyond progression—implications for drug resistance. *Nature Reviews Clinical Oncology* 10(10), 571-87.
- Kumar M.S., Adki K.M., 2018. Marine natural products for multi-targeted cancer treatment: A future insight. *Biomedicine & Pharmacotherapy* 105, 233-245.
- Lion, T., 2014. Adenovirus infections in immunocompetent and immunocompromised patients. *Clinical microbiology reviews* 27, 441–462.
- Ma, X., Wang, Z., 2009. Anticancer drug discovery in the future: an evolutionary perspective. *Drug Discovery Today* 14(23-24), 1136-42.
- Moo-Puc, R., Robledo, D., Freile-Pelegrián, Y., 2009. Actividad Citotóxica y Antiproliferativa in Vitro de Macroalgas Marinas de Yucatán, México. *Ciencias Marinas* 35, 345–358.
- Morales, J.L., Cantillo-Ciau, Z., Sánchez-Molina, I., Mena-Rejón, G., 2006. Screening of Antibacterial and Antifungal Activities of Six Marine Macroalgae from Coast of Yucatán Peninsula. *Pharmaceutical Biology* 4, 632-635.
- Nepomuceno, R. R., Pache, L., Nemerow, G. R., 2007. Enhancement of gene transfer to human myeloid cells by adenovirus-fiber complexes. *Molecular Therapy* 15, 571–578.
- Nguyen, E. K., Nemerow, G. R., Smith, J. G., 2010. Direct evidence from single-cell analysis that human α -defensins block adenovirus uncoating to neutralize infection. *Journal of Virology* 84, 4041–4049.
- Ortiz-Lozano, L., Pérez-España H., Granados-Barba A., González-Gándara C., Gutiérrez-Velázquez A., Martos J., 2013. The Reef Corridor of the Southwest Gulf of Mexico: Challenges for its management and conservation. *Ocean & Coastal Management* 86, 22-32.
- Paolino, K., Sande, J., Perez, E., Loechelt, B., Jantausch, B., Painter, W., Anderson, M., Tippin, T., Lanier, E.R., Fry, T., DeBiasi, R.L., 2011. Eradication of disseminated adenovirus infection in a pediatric hematopoietic stem cell transplantation recipient using the novel antiviral agent CMX001. *Journal of clinical virology* 50(2), 167-70.
- Pech-Puch, D., Rodríguez, J., Cautain, B., Sandoval-Castro, C. A., Jiménez, C., 2019. Cytotoxic Furanoditerpenes from the Sponge *Spongia tubulifera* Collected in the Mexican Caribbean. *Marine Drugs* 17, 416.
- Pech-Puch, D., Pérez-Povedano, M., Lenis-Rojas, O.A., Rodríguez, J., Jiménez, C. 2020. Marine Natural Products from the Yucatan Peninsula. *Marine Drugs* 18, 59.
- Peñuela, A., Robledo, D., Bourgougnon, N., Bedoux, G., Hernández-Núñez, E., Freile-Pelegrián, Y., 2018. Environmentally Friendly Valorization of *Solieria filiformis* (Gigartinales, Rhodophyta) from IMTA Using a Biorefinery Concept. *Marine Drugs* 16, 487.
- Pereira, F., 2019. Have marine natural product drug discovery efforts been productive and how can we improve their efficiency?. *Expert Opinion on Drug Discovery* 14 (8), 717-722.
- Pye, C.R., Bertin, M.J., Lokey, R.S., Gerwick, W.H., Linington, R.G., 2017.

- Retrospective analysis of natural products provides insights for future discovery trends. *Proceedings of the National Academy of Sciences of United States of America* 114(22), 5601-5606.
- Qiu, F. Z., Shen, X. X., Zhao, M. C., Zhao, L., Duan, S. X., Chen, C., Qi, J. J., Li, G. X., Wang, L., Feng, Z. S., Ma, X. J., 2018. A triplex quantitative real-time PCR assay for differential detection of human adenovirus serotypes 2, 3 and 7. *Virology Journal* 15 (1), 81.
- Schneider, C. A., Rasband, W. S., Eliceiri, K. W., 2012. NIH Image to ImageJ: 25 years of image analysis. *Nature Methods* 9, 671–675.
- Sulejmani, N., Nagai, S., Safwan, M., Rizzari, M.D., Raoufi, M., Abouljoud, M.S., Ramesh, M., 2018. Brincidofovir as Salvage Therapy for Adenovirus Disease in Intestinal Transplant Recipients. *Pharmacotherapy* 38, 470–475.
- Tan, D., Fu, Y., Xu, J., Wang, Z., Cao, J., Walline, J., Zhu, H., Yu, X., 2016. Severe adenovirus community-acquired pneumonia in immunocompetent adults: chest radiographic and CT findings. *Journal of thoracic disease*, 8 (5), 848-54.
- Tan, D., Zhu, H., Fu, Y., Tong, F., Yao, D., Walline, J., Xu, J., Yu, X., 2016. Severe Community-Acquired Pneumonia Caused by Human Adenovirus in Immunocompetent Adults: A Multicenter Case Series. *PLoS One* 11 (3), e0151199.
- Torre, L.A., Bray, F., Siegel, R.L., Ferlay, J., Lortet-Tieulent, J., Jemal, A., 2015. Global cancer statistics, 2012. *CA A Cancer Journal for Clinicians* 65(2), 87-108.
- Toth, K., Spencer, J.F., Dhar, D., Sagartz, J.E., Buller, R.M., Painter, G.R., Wold, W.S., 2008. Hexadecyloxypropyl-cidofovir, CMX001, prevents adenovirus-induced mortality in a permissive, immunosuppressed animal model. *Proceedings of the National Academy of Sciences of the United States of America* 105(20), 7293-7.
- Tunnell, Jr. J.W., 2007. Reef distribution. In: Tunnell, Jr. J.W., Chávez E.A., Withers K. (Eds.), *Coral Reefs of the Southern Gulf of Mexico*, Texas A&M University Press, Texas, pp. 17-29.
- Vo, T.S., Kim, S.K., 2010. Potential anti-HIV agents from marine resources: An overview. *Marine Drugs* 8, 2871–2892.
- Vogelstein, B., Kinzler, K. W., 2004. Cancer genes and the pathways they control. *Nature Medicine* 10, 789–799.
- Widmer, N., Bardin, C., Chatelut, E., Paci, A., Beijnen, J., Levêque, D, Veal, G., Astier, A., 2014. Review of therapeutic drug monitoring of anticancer drugs part two- targeted therapies. *European Journal of Cancer* 50 (12), 2020-36.
- Wogan, G.N., Hecht, S.S., Felton, J.S., Conney, A.H., Loeb, L.A., 2004. Environmental and chemical carcinogenesis. *Seminars in Cancer Biology* 14(6), 473–486.
- Yoon, B.W., Song, Y.G., Lee, S.H., 2017. Severe community-acquired adenovirus pneumonia treated with oral ribavirin: a case report. *BMC research notes* 10(1), 47.
- Yu, H.X., Zhao, M.M., Pu, Z.H., Wang, Y.Q., Liu, Y., 2015. Clinical data analysis of 19 cases of community-acquired adenovirus pneumonia in immunocompetent adults. *International Journal of Clinical and Experimental Medicine* 8, 19051–19057.
- Zarco-Perelló, S., Mascaró M., Garza-Pérez, R., Simoes N., 2013. Topography and coral community of the Sisal Reefs, Campeche Bank, Yucatán, México. *Hidrobiológica* 23(1), 28-41.

CAPÍTULO 3

Aislamiento, elucidación
estructural y evaluación
farmacológica de los
productos naturales marinos

3.1 Aislamiento de los productos naturales

La obtención de los metabolitos secundarios a partir de los extractos marinos se realizó siguiendo dos estrategias complementarias. Por una parte, se utilizaron los resultados de los ensayos de actividad de los extractos para realizar un fraccionamiento bioguiado, mientras que por otro lado, se utilizaron estudios de desreplicación con el objetivo de tener información sobre la presencia y tipo de compuestos que se encontraban en cada extracto en cuestión (Figura 3.1).

Ambos criterios nos permitieron hacer una selección de los extractos marinos más interesantes por su actividad o por la presencia de nuevos compuestos, los cuales de acuerdo al peso del extracto obtenido se sometieron a dos diferentes tipos de fraccionamiento (Figura 3.1):

- Aquellos extractos de peso mayor o igual a 10 g se fraccionaron mediante una extracción líquido-líquido siguiendo la metodología de Kupchan. Las fracciones resultantes se sometieron a un nuevo fraccionamiento en función de su polaridad, utilizando técnicas como la cromatografía en columna de gel de sílice ó extracción en fase sólida (SPE).
- Los extractos de peso inferior a los 10 g se sometieron directamente a un fraccionamiento por extracción en fase sólida, usando cartuchos de fase reversa.

Las fracciones de interés (biológicamente activas o con presencia de nuevos compuestos) se purificaron utilizando HPLC en fase normal ó fase reversa, dependiendo de la naturaleza química de las fracciones o tipos de compuestos presentes en las mismas.

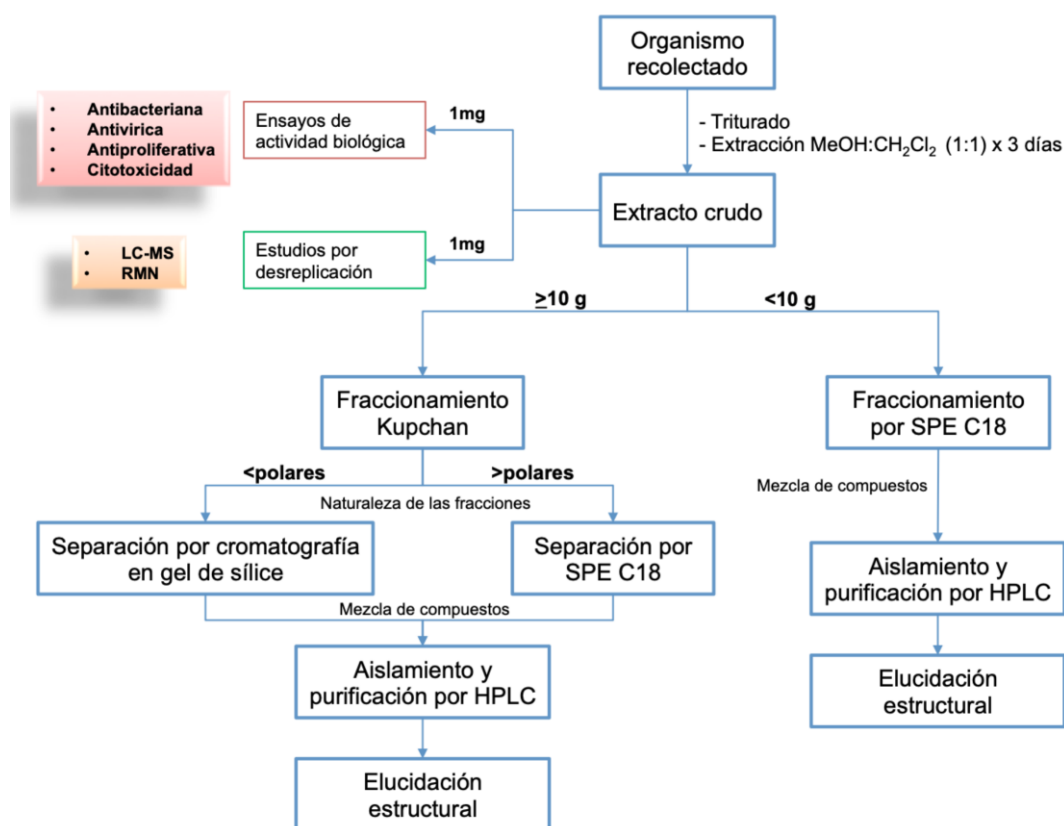


Figura 3.1. Esquema de fraccionamiento empleado en el aislamiento de los productos naturales puros.

3.2 Estudio químico de la esponja *Spongia tubulifera*

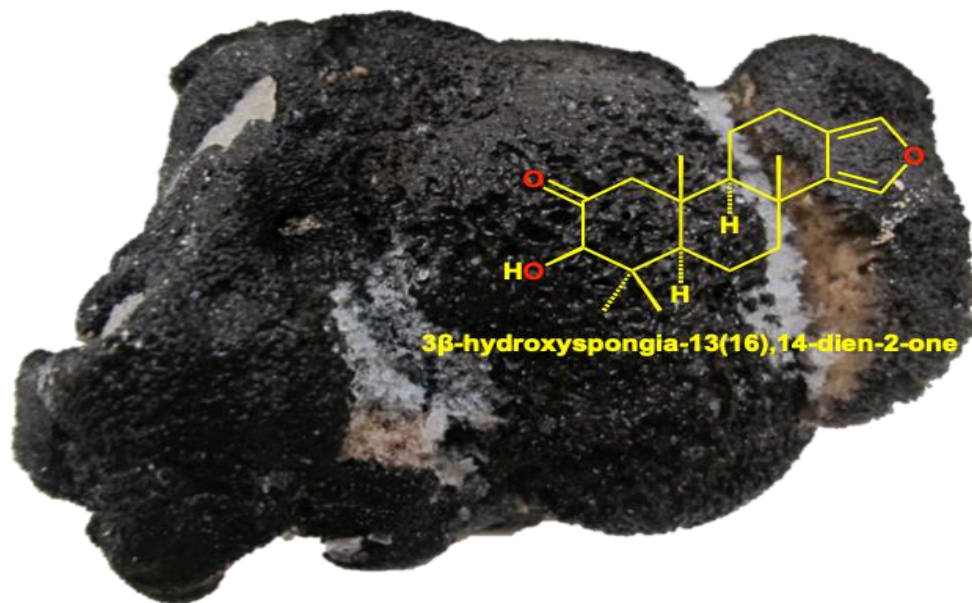


Figura 3.2. Fotografía de la esponja *Spongia tubulifera* (después de su recolección) y estructura del compuesto tipo furanoditerpeno.

En este apartado se describe el aislamiento y elucidación estructural de siete compuestos de naturaleza terpenoide obtenidos a partir de la esponja *Spongia tubulifera* recolectada en la costa de Rio Indio, Caribe Mexicano. La determinación estructural de los compuestos se realizó utilizando las técnicas de RMN 1D y 2D, HRESIMS e IR. Dos diterpenos resultaron ser nuevos compuestos y su configuración absoluta se obtuvo mediante el uso de ECD y cálculos computacionales DFT. Tres de los compuestos aislados presentaron actividades citotóxicas frente a líneas celulares de cáncer.

Estos resultados fueron publicados en la revista *Marine Drugs* (*Mar. Drugs*, **2019**, *17*, 416.)

Cytotoxic Furanoditerpenes from the Sponge *Spongia tubulifera* Collected in the Mexican Caribbean

Dawrin Pech-Puch ¹, Jaime Rodríguez ^{1,*}, Bastien Cautain ³, Carlos A. Sandoval-Castro ² and Carlos Jiménez ^{1,*}

¹ Centro de Investigaciones Científicas Avanzadas (CICA) e Departamento de Química, Facultade de Ciencias, Universidade da Coruña, 15071 A Coruña, Spain

² Universidad Autónoma de Yucatán, Campus de Ciencias Biológicas y Agropecuarias, Facultad de Medicina Veterinaria y Zootecnia, Km. 15.5 Carretera Mérida-Xmatkuil, Apdo. Postal 4-116, Itzimmá Mérida, Yucatán, México

³ Fundación MEDINA, Centro de Excelencia en Investigación de Medicamentos Innovadores en Andalucía, Avda. del Conocimiento 34, 18016 Granada, Spain

* Correspondence: Centro de Investigaciones Científicas Avanzadas (CICA) e Departamento de Química, Facultade de Ciencias, Universidade da Coruña, 15071 A Coruña, Spain. Tel: +34 981 167000. Fax: +34 981 167065. *E-mail address*: jaime.rodriguez@udc.es (Jaime Rodríguez); carlos.jimenez@udc.es, (Carlos Jiménez).

Abstract: Two new spongian furanoditerpenes, 3 β -hydroxyspongia-13(16),14-dien-2-one (**1**) and 19-dehydroxy-spongian diterpene **17** (**2**), along with five known terpenes, the spongian furanoditerpenes 9-nor-3-hydroxyspongia-3,13(16),14-trien-2-one (**3**), 3 β ,19 dihydroxyspongia-13(16),14-dien-2-one (epispongiadiol) (**4**) and spongian diterpene **17** (**5**), the furanoditerpene ambliol C (**6**) and the sesterterpene scalarin (**7**), were isolated from the methanolic extract of the sponge *Spongia tubulifera*, collected in the Mexican Caribbean. The planar structures of the new compounds were elucidated by 1D/2D NMR and IR spectroscopic analysis, HRESIMS and comparison of their spectral data with those reported in the literature. Absolute configurations were determined by comparison of the experimental electronic circular dichroism (ECD) spectrum with those calculated by time-dependent density functional (TD-DFT). Compounds **1**, **4** and **6** displayed weak cytotoxic activity against different human tumour cell lines.

Keywords: Spongian Furanoditerpenes; Marine Sponge; *Spongia tubulifera*; ECD-TDDFT; Cytotoxicity

1. Introduction

Specimens belonging to the genus *Spongia* have been subjected to numerous chemical investigations yielding a wide variety of C21 and other linear furanoterpenes, spongian diterpenes, scalarane sesterterpenoids, sesquiterpene quinones, sterols (including secosterols) and macrolides [1], many of which have shown biological activities including antibacterial [2,3], antiviral [4], antitumoral [5,6] and anti-inflammatory [7].

In our continuing investigations of diterpenes from marine organisms [8,9] and in particular from marine sponges [10], we have focused our attention on the sponge *S. tubulifera*, collected in the Mexican Caribbean due to the cytotoxic activity found in its

methanolic extract. To the best of our knowledge, the only previous reports of *S. tubulifera* were a comparative study of the fatty acids composition of specimens of this sponge collected at Ahogado Reef near La Parguera, Puerto Rico [11] and the assays of the antimicrobial activity against *Staphylococcus aureus* and *Candida albicans* of the organic extracts of specimens collected at Uraba' Gulf reefs in the Colombian Caribbean [12].

In this paper, we report the structure elucidation of two new spongian furanoditerpenes, 3 β -hydroxyspongia-13(16),14-dien-2-one (**1**) and 19-dehydroxyspongian diterpene 17 (**2**), along with five known terpenes, **3–7**, and their cytotoxic activity evaluation against a panel of five human tumour cell lines.

2. Results and Discussion

Specimens of the sponge *S. tubulifera*, collected by hand and SCUBA diving off the coast of the Mexican Caribbean, were extracted several times with CH₃OH//CH₂Cl₂ to give an extract which showed cytotoxic activity. The organic extract was subsequently partitioned between H₂O/CH₂Cl₂ and the CH₂Cl₂ portion was further fractionated into hexane, CH₂Cl₂ and aqueous methanolic fractions. The hexane fraction was submitted to silica gel flash chromatography using a gradient mixture of hexane and EtOAc to yield enriched terpene fractions that were then submitted repeatedly to reversed-phase HPLC separation (H₂O/CH₃OH mixtures) to yield **1–3** and **6**. The CH₂Cl₂ fraction was fractionated by Solid Phase Extraction (SPE) with a RP-18 column using a stepped gradient from H₂O, CH₃OH and CH₂Cl₂ to yield enriched terpene fractions that were separated by RP-HPLC using H₂O/CH₃OH mixtures to afford **4**, **5** and **7** (Figure 1).

Compound **1** was obtained as a colorless white powder. The molecular formula of **1** was determined on the basis of the M⁺ peak at *m/z* 316.2014, observed in its HREIM spectrum (calculated for C₂₀H₂₈O₃, 316.2038, 7 degrees of unsaturation) and from its ¹³C NMR spectrum. Its IR spectrum displays signals at 3500 and 1745 cm⁻¹, suggesting the presence of a hydroxyl group and a ketone carbonyl functionality, respectively.

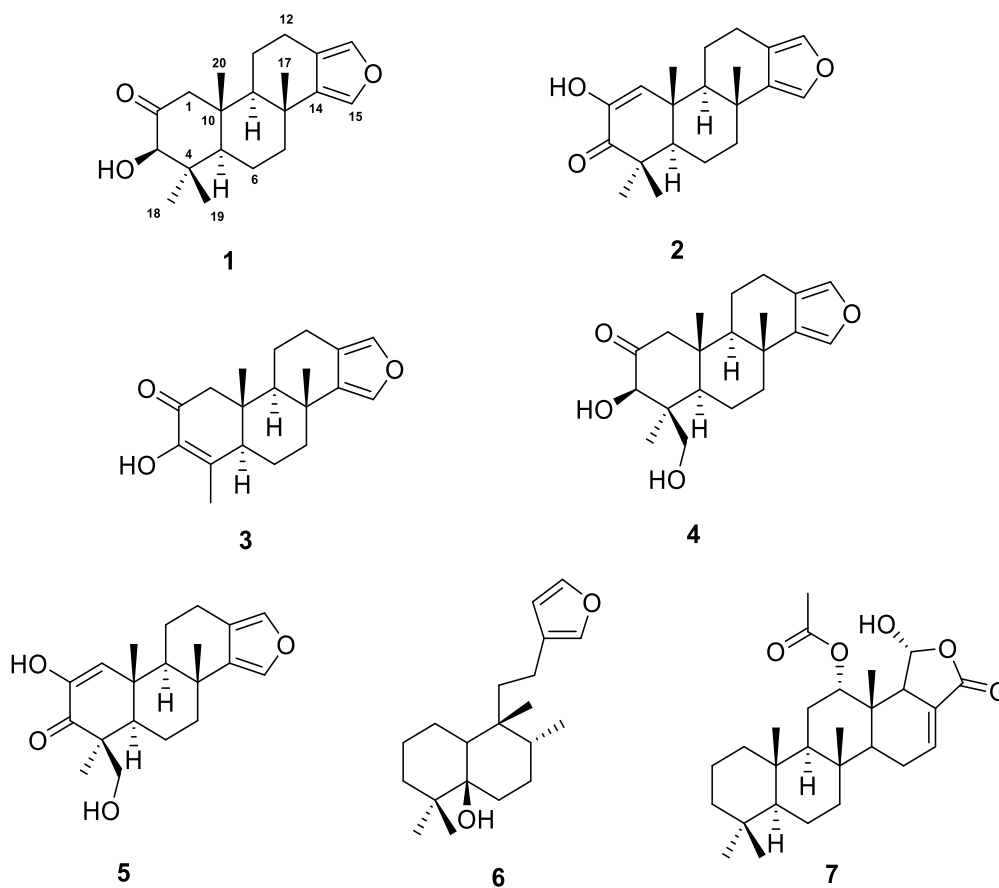


Figure 1. Structures of **1–7** isolated from *S. tubulifera*.

The ^{13}C NMR spectrum of **1** shows 20 signals (Table 1, Supplementary Material, Table S1) that in combination with the ^1H NMR and HSQC spectra indicated the presence of a spongian furanoditerpene bearing four tertiary methyl groups ($\delta_{\text{H}}/\delta_{\text{C}}$ 1.23, s/26.0, 1.21, s/29.4, 0.73, s/16.5, 0.88, s/17.3), a 3,4-disubstituted furan ring ($\delta_{\text{H}}/\delta_{\text{C}}$ 7.12, s/135.3, 7.07, s/137.1, 119.4, 136.8), one ketone carbonyl group (δ_{C} 211.1), a hydroxyl group at δ_{H} 3.48 and an oxymethine sp^3 carbon ($\delta_{\text{H}}/\delta_{\text{C}}$ 3.90, d/ 83.1). Comparison of the NMR data of **1** with those of reported for other spongian furanoditerpenes, along with the HMBC correlations shown in Figure 2, indicated that **1** has a similar structure to 3 α -hydroxyspongia-13(16),14-dien-2-one isolated from an unidentified *Spongia* collected in Australia [13]. The differences of the proton and carbon chemical shifts at C-3, e.g. $\delta_{\text{H}}/\delta_{\text{C}}$ 3.90 (d, $J = 1.5$ Hz)/ 83.1 in **1** instead of $\delta_{\text{H}}/\delta_{\text{C}}$ 4.36 (d, $J = 1.5$ Hz)/ 80.1 in 3 α -hydroxyspongia-13(16),14-dien-2-one, suggested that they differ only in the stereochemistry at C-3 and thus **1** must be its 3 β isomer. The NOESY correlations from H-3 at δ_{H} 3.90 to H-5 at δ_{H} 1.62 and H-18 at δ_{H} 1.21 indicated that these protons are in the same face of the molecule, confirming the β -orientation of the hydroxyl group at C-3. The relative configuration of the remaining stereogenic centers in **1** was also confirmed by its NOESY correlations (Figure 2). These data indicated that **1** is a new spongian furanoditerpene derivative with a 3 β -hydroxyspongia-13(16),14-dien-2-one structure.

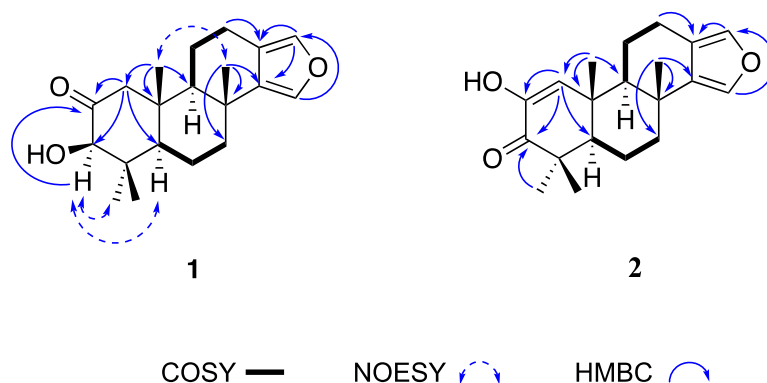


Figure 2. Key COSY, NOESY and HMBC correlations of **1** and **2**.

The absolute configurations of the stereogenic carbons of **1** were determined by comparison of the experimental and simulated electronic circular dichroism (ECD) spectra generated by time-dependent density functional theory calculations (TDDFT). Overall, the two possible enantiomers for **1**, (3*R*,5*R*,8*R*,9*R*,10*R*)-**1** and (3*S*,5*S*,8*S*,9*S*,10*S*)-**1**, were initially submitted to a conformational search with the Maestro Suite (Schrödinger). Four conformers were found within a 10.0 kcal/mol energy threshold from global minimum. All these conformers were geometrically optimized by density functional theory (DFT) method at the HSEH1PBE/cc-pVDZ functional (see computational details in the experimental section). The resulting ECD spectra were combined by Boltzmann weighting to give a composite spectrum for each enantiomer. Comparison of the experimental and calculated ECD spectra for **1** showed excellent agreement with the (3*R*,5*R*,8*R*,9*R*,10*R*)-**1** enantiomer (Figure 3). Thus, the absolute configurations of C-3, C-5, C-8, C-9 and C-10 were determined as 3*R*,5*R*,8*R*,9*R*,10*R*.

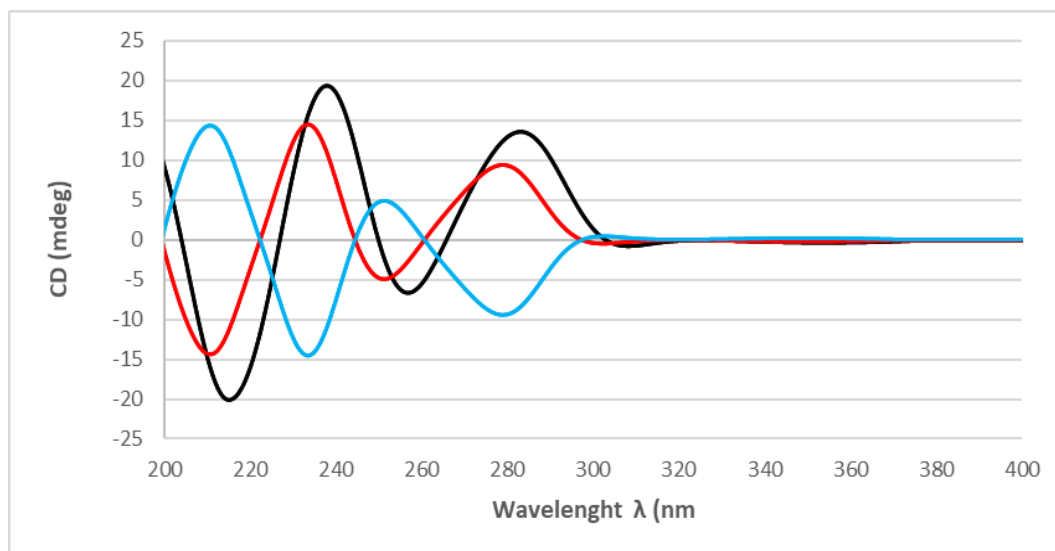


Figure 3. Experimental ECD spectrum (black line) of **1** and calculated ECD spectrum (red line) for (3*R*,5*R*,8*R*,9*R*,10*R*)-**1** and (blue line) for (3*S*,5*S*,8*S*,9*S*,10*S*)-**1**.

Table 1. ^{13}C (125 MHz) and ^1H (500 MHz) NMR Data in CDCl_3 of **1** and **2**.

Position	1		2	
	δ_{C} , type	δ_{H} , mult (<i>J</i> in Hz)	δ_{C} mult.	δ_{H} , mult (<i>J</i> in Hz)
1	53.3, CH	2.67, d (12.1) 2.13, d (12.1)	128.3, CH	6.54, s
2	211.1, C		144.3, C	
3	83.1, CH	3.90, d (1.5)	201.2, C	
4	45.7, C		44.3, C	
5	55.0, C	1.62, m	54.5, C	1.80, m
6	18.6, CH_2	1.66, m 1.80, m	19.1, CH_2	1.67, m
7	40.7, CH_2	1.68, m 2.20, m	40.4, CH_2	1.66, m 2.18, m
8	34.7, C		34.9, C	
9	56.1, CH	1.50, m	51.7, CH	1.48, dd (11.8, 1.7)
10	43.8, C		38.8, C	
11	18.9, CH_2	1.67, m	18.8, CH_2	1.91, dt (7.0, 1.7)
12	20.7, CH_2	2.49, m 2.82, m	20.7, CH_2	2.51, dddd (16.2, 12.2, 7.0, 1.7) 2.83, ddt (16.2, 6.3, 1.5)
13	119.4, C		119.5, C	
14	136.8, C		137.3, C	
15	135.3, CH	7.12, s	135.0, CH	7.09, s
16	137.1, CH	7.07, s	137.2, CH	7.06, s
17	26.0, CH_3	1.23, s	26.7, CH_3	1.28, s
18	29.4, CH_3	1.21, s	20.6, CH_3	1.16, s
19	16.5, CH_3	0.73, s	27.3, CH_3	1.23, s
20	17.3, CH_3	0.88, s	21.7, CH_3	1.22, s
OH		3.48, d (1.5)		5.93, s

The molecular formula of **2**, isolated as a colorless white powder, was established as $\text{C}_{20}\text{H}_{26}\text{O}_3$ based on the $[\text{M} + \text{Na}]^+$ at m/z 337.1803 in its (+)-HRESIM spectrum (calculated for $\text{C}_{20}\text{H}_{26}\text{O}_3\text{Na}$, 337.1780, 8 degrees of unsaturation) and on NMR data (Table 1, Supplementary Material, Table S2)). The IR spectrum of **2** shows absorptions due to hydroxyl (3505 cm^{-1}) and a conjugated ketone carbonyl (1650 cm^{-1}) groups.

The 20 carbon signals observed in the ^{13}C NMR spectrum of **2** along with the presence of two α -furan proton signals (δ_{H} 7.09 and 7.06) and four tertiary methyl groups (δ_{H} 1.28, 1.23, 1.22 and 1.16) in its ^1H NMR spectrum were indicative of a spongian furanoditerpene structure. The planar structure of **2** was established by a combination of 1D and 2D NMR spectroscopy. Comparison of the NMR data of **2** with those of **1** (see

Table 1) revealed that they share the same framework at the B, C and D rings but differ in the A-ring. Signals in the ^{13}C NMR spectrum of **2** for the conjugated ketone carbonyl group at δ_{C} 201.2 (C-3) and two sp^2 carbons, the non-protonated carbon at δ_{C} 144.3 (C-2) and the methine carbon at δ_{C} 128.3 (C-1), were consistent with the presence of a conjugated α,β -unsaturated ketone moiety.

The key ^1H - ^{13}C long range correlations between the olefinic proton at δ_{H} 6.54 (H-1) and the olefinic carbon at δ_{C} 144.3 (C-2), the ketone carbonyl carbon at δ_{C} 201.2 (C-3) and the carbon at δ_{C} 54.5 (C-5) along with the HMBC correlation from the methyl singlet at δ_{H} 1.22 (H-20) to the olefinic carbon at δ_{C} 128.3 (C-1) placed the α,β -unsaturated ketone in the A-ring (Figure 2). The exchangeable proton signal at δ_{H} 5.93 was indicative of an enolized α -diketone moiety in the A ring. The NMR data for this part of the molecule (see Table 1) are in agreement with those observed for other diterpenes containing the same A-ring in the tetracyclic framework such as spongian diterpene **17** (**5**), previously reported from the nudibranch *Doriprismatica* (=Glossodoris) *atomarginata* [14]. The diagnostic HMBC correlations displayed by the α -furan proton signals and the methyl groups Me-17 and Me-18 displayed in Figure 2 confirm **2** as a new spongian furanoditerpene that was named 19-dehydroxy-spongian diterpene **17**.

As in **1**, the absolute configurations of the stereogenic carbons of **2** were determined by comparison of the experimental to those generated by TDDFT on the two possible enantiomers. The two possible enantiomers for **2**, (5*R*, 8*R*, 9*R*, 10*R*)-**2** and (5*S*, 8*S*, 9*S*, 10*S*)-**2**, were initially submitted to a conformation search with the Maestro Suite (Schrödinger). Thus, 4 conformers were found within a 10.0 Kcal/mol energy threshold from a global minimum. All these conformers were geometrically optimized by density functional theory method at the HSEH1PBE/cc-pVDZ functional (see computational details in experimental section). As shown in Figure 4, the calculated ECD spectra for the (5*R*,8*R*,9*R*,10*R*)-**2** and its experimental data were almost identical. Thus, the absolute configurations of C-5, C-8, C-9 and C-10 of **2** were determined as 5*R*,8*R*,9*R*,10*R*.

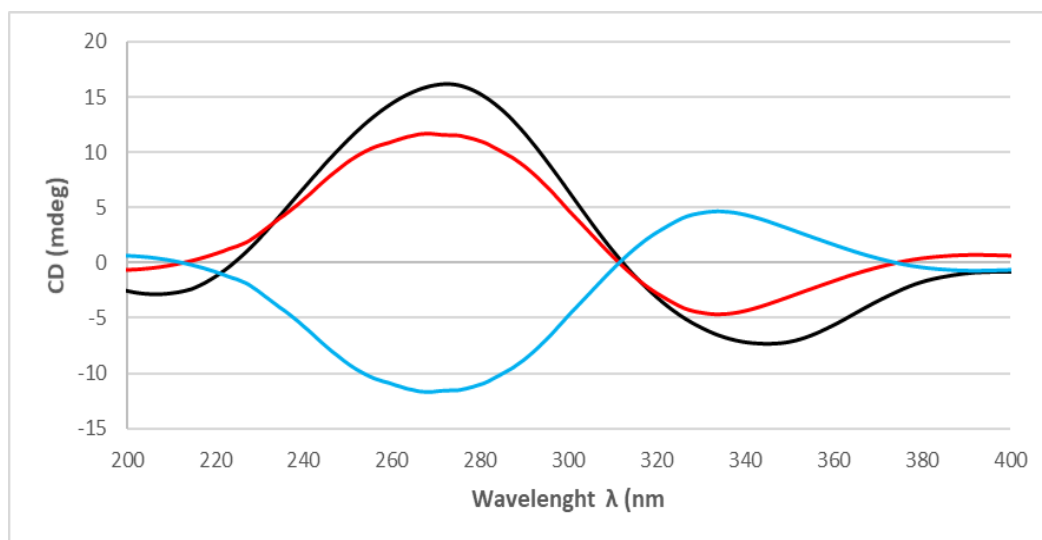


Figure 4. Experimental ECD spectrum (black line) of **2** and calculated ECD spectrum (red line) for (5*R*,8*R*,9*R*,10*R*)-**2** and (blue line) for (5*S*,8*S*,9*S*,10*S*)-**2**.

Spectral data (^1H and ^{13}C NMR, MS, $[\alpha]^{25}_{\text{D}}$) of **3** and **4** were identical with those reported for 19-*nor*-3-hydroxyspongia-3,13(16),14-trien-2-one (episongiadiol) [15] and 3 β -19-dihydroxyspongia-13(16),14-dien-2-one [16], respectively, isolated from an

unidentified *Spongia*; while the NMR/spectroscopic data for **5** matched with those reported for spongian diterpene 17, isolated from the nudibranch *Doriprismatica* (= *Glossodoris*) *atromarginata* [14]; the NMR/spectroscopic data for **6** were identical with those reported for ambliol C, isolated from the sponge *Dysidea amblia* [17], and the NMR/spectroscopic data for **7** matched with those reported for scalarin from the sponge *Cacospongia scalaris* by Fattorusso *et al.* [18] and later on from *Spongia nitens* by Cimino *et al.* [19].

The isolated compounds were submitted to biological activity assays. MTT assays were performed on human lung carcinoma A549 ATCC[®] CCL-185TM, human skin melanoma A2058 ATCC[®] CRL-11147TM, hepatocyte carcinoma HepG2 ATCC[®] HB-8065TM, breast adenocarcinoma MCF7 ATCC[®] HTB-22TM and pancreas carcinoma MiaPaca-2 ATCC[®] CRL-1420TM with doxorubicin as positive control [20]. Compounds **1** and **4** show a weak cytotoxic activity while **6** exhibits the highest cytotoxic activity with IC₅₀ values from 28.3 to 11.7 μM (Table 2). Previous biological studies of **4** indicated cytotoxic activity against the human tumor cell lines A549 (human lung carcinoma cells), HT-29 (human colorectal carcinoma cells) and P388 (leukemia cells lines) [21] and antiviral activity against VSV (vesicular stomatitis virus) and HSV-1 (herpes simplex virus type 1) [4]. On the other hand, it was reported that **6** induced *Artemia* sp. to death in a test of settlement and metamorphosis inhibition of larvae or juveniles [22]. Additionally, **1–7** did not show any significant antibacterial activity against *Acinetobacter baumannii*, *Pseudomonas aeruginosa*, *Klebsiella pneumoniae*, *Staphylococcus aureus* or antiviral activity against Human adenoviruses (HAdV5 y HAdV5-GFP).

Table 2. Cytotoxic Activity Data (IC₅₀ in μM) of **1**, **4** and **6**.^a

Tumour cell lines	Compound			
	1	4	6	Doxorubicin
A549 (lung)	88.1 ± 7.9	73.7 ± 6.3	28.3 ± 2.1	0.4 ± 0.2
A2058 (skin)	71.4 ± 2.5	53.9 ± 0.6	22.9 ± 0.7	0.1 ± 0.1
HepG2 (hepatocyte)	91.3 ± 15.8	60.1 ± 5.0	24.3 ± 0.2	0.1 ± 0.1
MCF-7 (breast)	nd	nd	19.9 ± 3.3	5.1 ± 0.5
MiaPaca-2 (pancreas)	90.0 ± 44.8	nd	11.7 ± 0.9	6.6 ± 0.5

^a IC₅₀, compound concentration that produces 50% inhibition on cell growth as compared to control cells. nd: not detected

3. Material and Methods

3.1. General Experimental Procedures

Optical rotations were measured on a JASCO DIP-1000 polarimeter, with a Na (589 nm) lamp and filter. IR spectra were measured on a FTIR Bruker Vector 22 spectrometer. ^1H , ^{13}C , and 2D NMR spectra were recorded on a Bruker Avance 500 spectrometer at 500 and 125 MHz, respectively, using CDCl_3 . LRESIMS and HRESIMS experiments were performed on the Applied Biosystems QSTAR Elite system. LREIMS and HREIMS Mass Spectrometer Thermo MAT95XP. HPLC separations were performed on the Agilent 1100 liquid chromatography system equipped with a solvent degasser, quaternary pump, and diode array detector (Agilent Technologies, Waldbronn, Germany) using a semipreparative reversed phase column Luna C18, 5 μ , 100 Å, 250 x 10 mm. Precoated silica gel plates (Merck, Kieselgel 60 F254, 0.25 mm) were used for TLC analysis and the spots were visualized under a UV light (254 nm) or by heating the plate pretreated with $\text{H}_2\text{SO}_4/\text{H}_2\text{O}/\text{AcOH}$ (1:4:20).

3.2. Animal Material

The sponge *Spongia tubulifera* was collected by hand and traditional SCUBA-diving in the coast of Mexican Caribbean (18°48'22.17"N / 87°39'32.61"W) at depths ranging from 10 to 15 meters in March 2017 and frozen immediately after collection. A voucher specimen 17YUE11ST was deposited in the Phylum Porifera Gerardo Green National Collection of the Instituto de Ciencias del Mar y Limnología (ICMyL) at the National Autonomous University of Mexico (UNAM).

3.3. Extraction and Isolation

Sliced bodies of *S. tubulifera* (wet weight, 157.7 g; dry weight, 40.2 g) were exhaustively extracted with $\text{CH}_3\text{OH}-\text{CH}_2\text{Cl}_2$ (1:1, 3 x 1.5 L) at 25 °C for 24 h each extraction. The combined extracts were concentrated under reduced pressure to give 12.0 g of a crude residue that was first partitioned between $\text{CH}_2\text{Cl}_2/\text{H}_2\text{O}$ (1:1 v/v). The resulting aqueous portion was extracted with *n*-butanol (200 mL) to yield the *n*-butanol fraction (1.44 g). The organic phase was concentrated under reduced pressure and partitioned between 10% aqueous CH_3OH (400 mL) and hexane (2 x 400mL) to give, after removing the solvent under reduced pressure, 526 mg of the hexane fraction. The H_2O content (% v/v) of the methanolic fraction was adjusted to 50% aqueous CH_3OH , and the mixture was extracted with CH_2Cl_2 (100 mL) to afford, after removing the solvent under reduced pressure, 1.51 g of the CH_2Cl_2 fraction and 2.38 g of the remaining aqueous methanolic fraction. The hexane fraction (526 mg) was subjected to a flash chromatography column on silica gel using a stepped gradient from hexane to EtOAc to give 14 fractions (FHC1-C14). Separation of the fraction FHC2, eluted with hexane/EtOAc (9:1, 93.9 mg), by RP-HPLC with a mobile phase consisting of an isocratic at 100% CH_3OH at a flow rate of 2.0 mL/min afforded **6** (13.5 mg; t_R = 8.4 min). Separation of the fraction FHC3, eluted with hexane/EtOAc (9:1, 20.0 mg), by RP-HPLC (isocratic 100% CH_3OH , flow rate 2.0 mL/min) gave **2** (2.6 mg; t_R = 9.7 min) and **6** (2.6 mg; t_R = 8.9 min). Separation of the fraction FHC4, eluted with hexane/EtOAc (8:2, 9.0 mg), by RP-HPLC with a mobile phase consisting of 5 min gradient from 90% to 95% of CH_3OH in H_2O , followed by a 10 min isocratic at 95% of CH_3OH in H_2O and, finally, a 5 min gradient from 95% to 100% of CH_3OH in H_2O at a flow rate of 2.0 mL/min yielded **2** (2.0 mg; t_R = 12.6 min). Separation of the fraction FHC5, eluted with hexane/EtOAc (8:2, 21.0 mg), by RP-HPLC with a mobile phase consisting of 5 min gradient from 90% to

95% of CH₃OH in H₂O, followed by a 15 min isocratic at 95% of CH₃OH in H₂O and, finally, a 10 min gradient from 95% to 100% of CH₃OH in H₂O at a flow rate of 2.0 mL/min afforded **2** (1.7 mg; *t_R* = 13.0 min) and **3** (1.5 mg; *t_R* = 12.0 min). Separation of the fraction FHC7, eluted with hexane/EtOAc (8:2, 27.2 mg), by RP-HPLC (isocratic 100% CH₃OH, flow rate 2.0 mL/min) yielded **1** (3.0 mg; *t_R* = 16.8 min). Separation of the fraction FHC8, eluted with hexane/EtOAc (8:2, 20.9 mg), by RP-HPLC with a mobile phase consisting of 5 min gradient from 90% to 95% of CH₃OH in H₂O followed by a 15 min isocratic at 95% of CH₃OH in H₂O and, finally, a 1 min gradient from 95% to 100% of CH₃OH in H₂O at a flow rate of 2.0 mL/min afforded **1** (1.8 mg; *t_R* = 11.0 min). The dichloromethane fraction (1.51 g) was subjected to Solid Phase Extraction (SPE) with RP-18 column (Merck KGaA) using a stepped gradient from H₂O to CH₃OH and then CH₂Cl₂, to give 6 fractions: H₂O (100%), H₂O/CH₃OH (2:1, 1:1 and 1:2), CH₃OH (100%) and CH₂Cl₂ 100%. Fraction eluted with H₂O/CH₃OH (1:2) was submitted to RP-HPLC separation using a mobile phase consisting of 20 min gradient from 50% to 100% of CH₃OH in H₂O followed by a 10 min isocratic at 100% of CH₃OH at a flow rate of 2.0 mL/min to afford **4** (9.2 mg; *t_R* = 10.0 min). Separation of the fraction eluted with CH₃OH (100%) by RP-HPLC using a mobile phase consisting of 30 min gradient from 80% to 100% of CH₃OH in H₂O at a flow rate of 2.0 mL/min afforded **7** (5.0 mg; *t_R* = 26.7 min) and **5** (3.1 mg; *t_R* = 29.7 min).

3.4. Computational calculations

Conformational searches were performed by using the corresponding module implemented in the Maestro Quantum mechanical software. OPLS 2005 force field with chloroform as solvent were used, and torsional enhanced sampling with 1000 or 10000 steps were fixed using an energy window of 10 kcal/mol. Molecular geometry optimizations were performed at the DFT theoretical level using the Gaussian 09W package firstly with a B3LYP/6-31G(d) combination and then with HSEH1PBE/cc-pVDZ auto for energy and frequencies calculations. After removing redundant conformers, theoretical Boltzmann energy population-weighted ECD was calculated by using two combinations: PBEPBE/6-311++(3d,2p) or CAM-B3LYP/6-311++(3d,2p) both with 24 states. Graphical theoretical ECD curves were obtained using the open software SpecDis V.1.71[23].

3.5. Metabolite characterization

(3R, 5R, 8R, 9R, 10R) 3β-hydroxyspongia-13(16),14-dien-2-one (1): Colorless white powder; $[\alpha]_D^{25} - 10.5$ (c 0.1, CHCl₃); IR (ATR neat) ν_{\max} 3500, 2920, 2810, 1745, 1430, 1371, 1229, 1120, 1050, 1038, 955, 882 cm⁻¹; ¹H NMR (500 MHz) and ¹³C NMR (125 MHz) see Table 1; HREIMS *m/z* 316.2014 [M]⁺ (calcd. for C₂₀H₂₈O₃, 316.2038).

(5R, 8R, 9R, 10R) 19-dehydroxy-spongian diterpene 17 (2): Colorless white powder; $[\alpha]_D^{25} + 18.7$ (c 0.1, CHCl₃); IR (ATR neat) ν_{\max} 3505, 2950, 2855, 2325, 1650, 1430, 1370, 1230, 1120, 1050, 1038, 955, 880, cm⁻¹; ¹H NMR (500 MHz) and ¹³C NMR (125 MHz) see Table 1; (+)-HRESIMS *m/z* 337.1803 [M + Na]⁺ (calcd. for C₂₀H₂₆O₃Na, 337.1780).

19-nor-3-hydroxyspongia-3,13(16),14-trien-2-one (3): Colorless white powder; $[\alpha]_D^{25} + 2.7$ (c 0.1, CHCl₃); (+)-HREIMS *m/z* 300.1719 [M]⁺ (calcd. for C₁₉H₂₄O₃, 300.1725).

3β, 19-dihydroxyspongia-13(16),14-dien-2-one (epispongiadiol) (4): Yellow powder; $[\alpha]_D^{25} + 18.2$ (c 0.1, CHCl₃); (+)-HRESIMS *m/z* 355.1890 [M+Na]⁺ (calcd. for C₂₀H₂₈O₄Na, 355.1885).

Spongian diterpene 17 (5): Yellow powder; $[\alpha]_D^{25}$ - 20.4 (c 0.1, CHCl₃); (+)-HRESIMS m/z 353.1723 [M+Na]⁺ (calcd. for C₂₀H₂₆O₄Na, 353.1723).

Ambliol C (6) Yellow powder; $[\alpha]_D^{25}$ - 33.3 (c 0.1, CHCl₃); (+)-HREIMS m/z 304.2379 [M]⁺ (calcd. for C₂₀H₃₂O₂, 304.2397).

Scalarin (7): Yellow powder; $[\alpha]_D^{25}$ + 41.2 (c 0.1, CHCl₃); (+)-HRESIMS m/z 467.2767 [M+Na]⁺ (calcd. for C₂₇H₄₀O₅Na, 467.2773).

3.6 Cytotoxic Assays

Colorimetric MTT ((3-(4,5-Dimethylthiazol-2-yl)-2,5-diphenyltetrazolium bromide)) assays were carried out to assess the cell viability of the samples against a panel of five different cancer cell lines (i.e., human lung carcinoma A549 ATCC[®] CCL-185TM, human skin melanoma A2058 ATCC[®] CRL-11147TM, hepatocyte carcinoma HepG2 ATCC[®] HB-8065TM, breast adenocarcinoma MCF7 ATCC[®] HTB-22TM and pancreas carcinoma MiaPaca-2 ATCC[®] CRL-1420TM). All cells were obtained from the American Type Culture Collection (ATCC, Manassas, VA, USA). A549 cells were grown in Ham's F12K medium with 2 mM Glutamine, 10% Fetal Bovine Serum (FBS), 100 U/mL penicillin and 100 µg/mL streptomycin. A2058 and HepG2 were grown in ATCC formulated Eagle's M essential medium (MEM) with 10% FBS, 2 mM l-glutamine, 1 mM sodium pyruvate and 100 µM MEM non-essential amino acids. MCF-7 cells were grown in the previous medium supplemented with 0.01 mg/mL of bovine insulin. MiaPaca-2 cells were grown in Dulbecco's Modified Eagle's Medium (DMEM) with 10% FBS, 100U/mL penicillin and 100 µg/mL streptomycin. The bioassays were performed as reported by Audoin et al. [20]. The cytotoxic activity was assessed after 72 h of treatment of the compound at the concentrations 0.098, 0.195, 0.391, 0.781, 1.563, 3.125, 6.250, 12.5, 25, 50 and 100 µM.

4. Conclusions

In summary, two new spongian furanoditerpenes, **1** and **2**, together with five known terpenes, four furanoditerpenes **3–6** and one sesterterpene **7**, were isolated from sponge *Spongia tubulifera* collected in the Mexican Caribbean as its metabolic components. The absolute configurations of the new compounds **1** and **2** were determined by comparison of experimental and calculated ECD spectra. Compounds **1**, **4** and **6** display weak cytotoxic activity against a panel of five human tumor cell lines. This work represents the first chemical study of the secondary metabolites from *S. tubulifera*.

Supplementary Materials: Table S1: NMR data of **1** in CDCl₃, Figures S1-S6: NMR spectra of **1** in CDCl₃; Figure S7: HREIMS of **1**; Table S2: NMR data of **2** in CDCl₃; Figures S7-S12: NMR spectra of **2** in CDCl₃; Figure S14: (+)-HRESIMS of **2**; Figures S15-S29: NMR spectra and MS of **3–7**.

Author Contributions: Conceptualization, Carlos Jiménez and Jaime Rodríguez; Extraction process: Dawrin Pech-Puch and Carlos A. Sandoval-Castro; Formal analysis, Dawrin Pech-Puch, Jaime Rodríguez and Carlos Jiménez; Computational calculations, Jaime Rodríguez, Carlos Jiménez and Dawrin Pech-Puch; Cytotoxic assays: Bastien Cautain; Investigation, Dawrin Pech-Puch, Funding acquisition and Resources, Jaime Rodríguez and Carlos Jiménez, Writing – original draft, Dawrin Pech-Puch; Writing – review & editing, Jaime Rodríguez and Carlos Jiménez.

Funding: This work was supported by Grants AGL2015-63740-C2-2-R and RTC-2016-4611-1 (AEI/FEDER, EU) from the State Agency for Research (AEI) of Spain, both co-

funded by the FEDER Programme from the European Union. DPP received a fellowship from the program National Council of Science and Technology (CONACYT) of Mexico and the Secretariat of Research, Innovation and Higher Education (SIIES) of Yucatan (Mexico).

Acknowledgments: We gratefully acknowledge the help of colleagues, Daniel Catzim Pech, Carlos González-Salas, Gabriel González Mapen, Jorge Peniche Pérez, Melissa Llanes López and Rodrigo Garcia Uribe for collecting the marine samples. We thank to Patricia Gomez for the taxonomic identification of the sponge. We would like to express our gratitude to Dr. Javier. Sanchez-Cespedes for the antiviral assays and to Dr. Alejandro Beceiro for the antimicrobial evaluation.

References

1. Máximo, P.; Ferreira, L.M.; Branco, P.; Lima, P.; Lourenço, A.; Benkendorff, K. The role of *Spongia* sp. In the discovery of marine lead compounds. *Mar. Drugs* **2016**, *14*, 0–71.
2. Gonzalez, A.G.; Estrada, D.M.; Martin, J.D.; Martin, V.S.; Perez, C.; Perez, R. New antimicrobial diterpenes from the sponge *Spongia officinalis*. *Tetrahedron* **1984**, *40*, 4109–4113.
3. Manzo, E.; Ciavatta, M.L.; Villani, G.; Varcamonti, M.; Sayem, S.M.A.; Van Soest, R.; Gavagnin, M. Bioactive terpenes from *Spongia officinalis*. *J. Nat. Prod.* **2011**, *74*, 1241–1247.
4. Kohmoto, S.; Mcconnell, O.J.; Wright, A.; Cross, S. Isospongiadiol, a Cytotoxic and Antiviral Diterpene from a Caribbean Depp Water Marine Sponge, *Spongia* sp. *Chem. Lett.* **1987**, 1687–1690.
5. Mori, D.; Kimura, Y.; Kitamura, S.; Sakagami, Y.; Yoshioka, Y.; Shintani, T.; Okamoto, T.; Ojika, M. Spongolactams, farnesyl transferase inhibitors from a marine sponge: Isolation through an LC/MS-guided assay, structures, and semisyntheses. *J. Org. Chem.* **2007**, *72*, 7190–7198.
6. Phan, C.S.; Kamada, T.; Hamada, T.; Vairappan, C.S. Cytotoxic sesterterpenoids from bornean sponge *Spongia* sp. *Rec. Nat. Prod.* **2018**, *12*, 643–647.
7. Marino, S. De; Iorizzi, M.; Zollo, F.; Debitus, C.; Menou, J.L.; Ospina, L.F.; Alcaraz, M.J.; Payá, M. New pyridinium alkaloids from a marine sponge of the genus *Spongia* with a human phospholipase A2 inhibitor profile. *J. Nat. Prod.* **2000**, *63*, 322–326.
8. Anta, C.; González, N.; Santafé, G.; Rodríguez, J.; Jiménez, C. New xenia diterpenoids from the Indonesian soft coral *Xenia* sp. *J. Nat. Prod.* **2002**, *65*, 766–768.
9. Urda, C.; Fernández, R.; Pérez, M.; Rodríguez, J.; Jiménez, C.; Cuevas, C. Protoxenincins A and B, Cytotoxic Long-Chain Acylated Xenicanes from the Soft Coral *Protodendron repens*. *J. Nat. Prod.* **2017**, *80*, 713–719.
10. Tarazona, G.; Bénédict, G.; Fernández, R.; Pérez, M.; Rodríguez, J.; Jiménez, C.; Cuevas, C. Can Stereoclusters Separated by Two Methylene Groups Be Related by DFT Studies? the Case of the Cytotoxic Meroditerpenes Halioxepines. *J. Nat. Prod.* **2018**, *81*, 343–348.
11. Carballeira, N.M.; Shalabi, F.; Cruz, C.; Rodríguez, J.; Rodríguez, E. Comparative study of the fatty acid composition of sponges of the genus *Ircinia*. Identification of the new 23-methyl-5,9-tetracosadienoic acid. *Comp. Biochem. Physiol.* **1991**, *100*, 489–492.

12. Galeano, E.; Martínez, A. Antimicrobial activity of marine sponges from Urabá Gulf, Colombian Caribbean region. *J. Mycol. Med.* **2007**, *17*, 21–24.
13. Searle, P.A.; Molinski, T.F. Scalemic 12-hydroxyambliofuran and 12-acetoxyambliofuran, five tetracyclic furanoditerpenes and a furanosesterterpene from *Spongia* sp. *Tetrahedron* **1994**, *50*, 9893–9908.
14. Yong, K.W.L.; Mudianta, I.W.; Cheney, K.L.; Mollo, E.; Blanchfield, J.T.; Garson, M.J. Isolation of norsesterterpenes and spongian diterpenes from *Dorisprismatica* (= *Glossodoris*) *atromarginata*. *J. Nat. Prod.* **2015**, *78*, 421–430.
15. Gunasekera, S.P.; Schmitz, F.J. New Spongian Diterpenoids from a Great Barrier Reef Sponge, *Spongia* sp. *J. Org. Chem.* **1991**, *56*, 1250–1253.
16. Kazlauskas, R.; Murphy, P.T.; Wells, R.J.; Noack, K.; Oberhänsli, W.E.; Schönholzer, P. A New Series of Diterpenes from Australian *Spongia* Species. *Aust. J. Chem.* **1979**, *32*, 867–880.
17. Walker, R.P.; Rosser, R.M.; Faulkner, J. Two New Metabolites of the Sponge *Dysidea ambliia* and Revision of the Structure of Ambliol C. *J. Org. Chem.* **1984**, *49*, 5160–5163.
18. Fattorusso, E.; Magno, S.; Santacroce, C.; Sica, D. Sclarin , a New Pentacyclic C-25 Terpenoid from the Sponge *Cacospongia scalaris*. *Tetrahedron* **1972**, *28*, 5993–5997.
19. Cimino, B.G.; Stefano, S. De; Minale, L.; Trivellone, E. 12-epi-Sclarin and 12-epi-Deoxosclarin, Sesterterpenes from the Sponge *Spongia Nitens*. *J. Chem. Soc. Perkin I.* **1977**, *1*, 1587–1593.
20. Audoin, C.; Bonhomme, D.; Ivanisevic, J.; De La Cruz, M.; Cautain, B.; Monteiro, M.C.; Reyes, F.; Rios, L.; Perez, T.; Thomas, O.P. Balibalosides, an original family of glucosylated sesterterpenes produced by the Mediterranean sponge *Oscarella balibaloi*. *Mar. Drugs* **2013**, *11*, 1477–1489.
21. Longley, R.E.; McConnell, O.J.; Essich, E.; Harmody, D. Evaluation of marine sponge metabolites for cytotoxicity and signal transduction activity. *J. Nat. Prod.* **1993**, *56*, 915–920.
22. Thompson, J.E.; Walker, R.P.; Faulkner, D.J. Screening and bioassays for biologically-active substances from forty marine sponge species from San Diego, California, USA. *Mar. Biol.* **1985**, *88*, 11–21.
23. Bruhn, T.; Schaumlöffel, A.; Hemberger, Y.; Bringmann, G. SpecDis: Quantifying the Comparison of Calculated and Experimental Electronic Circular Dichroism Spectra. *Chirality* **2013**, *25*, 243–249.

Supplementary Materials

Table S1. NMR data of **1** in CDCl₃ (125 MHz for ¹³C and 500 MHz for ¹H).

no.	δ _C type	δ _H , mult. (J in Hz)	COSY	HMBC	NOESY
1	53.3, CH	2.67, d (12.1)- 2.13, d (12.1)		2, 3, 5, 10, 20	3, 9, 11, 20
2	211.1, C				
3	83.1, CH	3.90, d (1.5)	OH	2, 4, 18, 19	1, 5, 18
4	45.7, C				
5	55.0, C	1.62, m	6	1, 18, 19	3
6	18.6, CH ₂	1.66, m-1.80, m	5, 7		18
7	40.7, CH ₂	1.68, m-2.20, m	6		17
8	34.7, C				
9	56.1, CH	1.50, m	11		1
10	43.8, C				
11	18.9, CH ₂	1.67, m	9, 12		1
12	20.7, CH ₂	2.49, m-2.82, m	11	13	
13	119.4, C				
14	136.8, C				
15	135.3, CH	7.12, s		13, 16	
16	137.1, CH	7.07, s		13, 14	
17	26.0, CH ₃	1.23, s		7, 8, 14	7, 20
18	29.4, CH ₃	1.21, s		3, 4, 5, 19	6, 19
19	16.5, CH ₃	0.73, s		3, 4, 5, 18	18
20	17.3, CH ₃	0.88, s		1, 9, 10	1, 17
OH		3.48, d (1.5)	3		

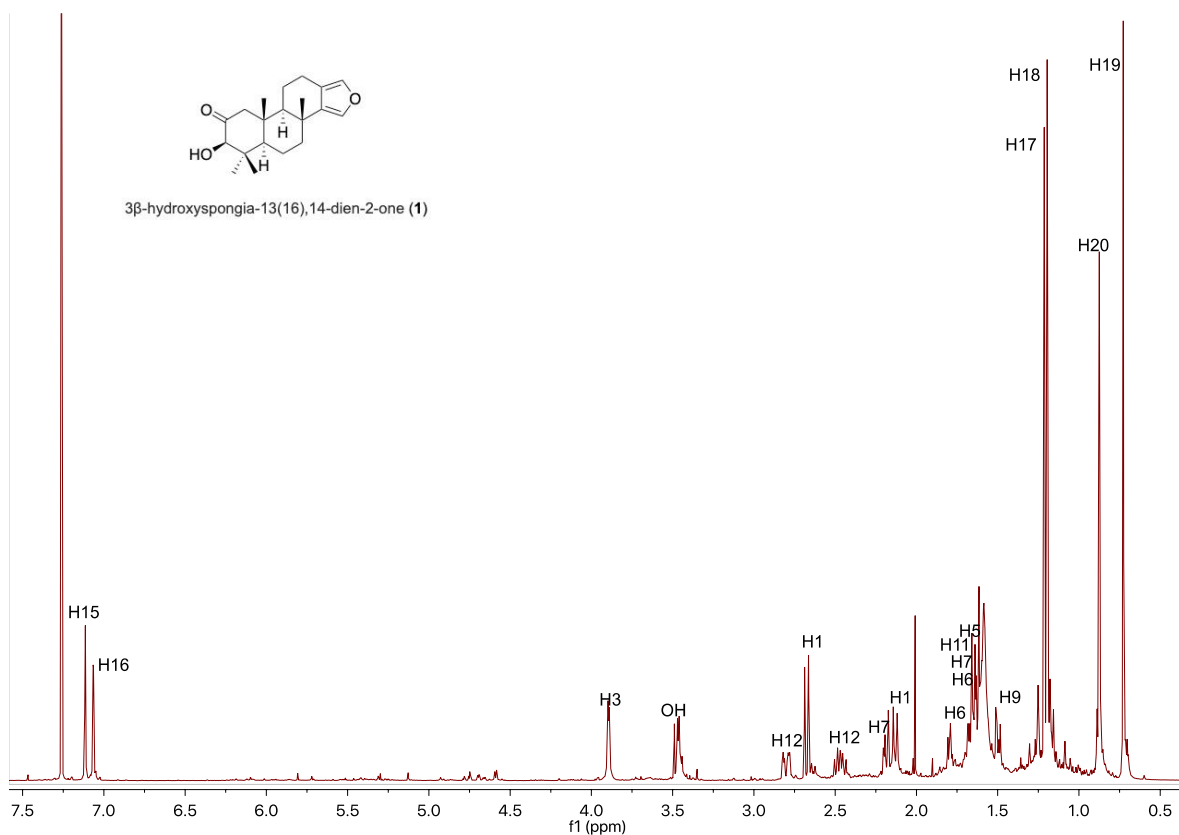


Figure S1. ^1H NMR spectrum of **1** (500 MHz, CDCl_3).

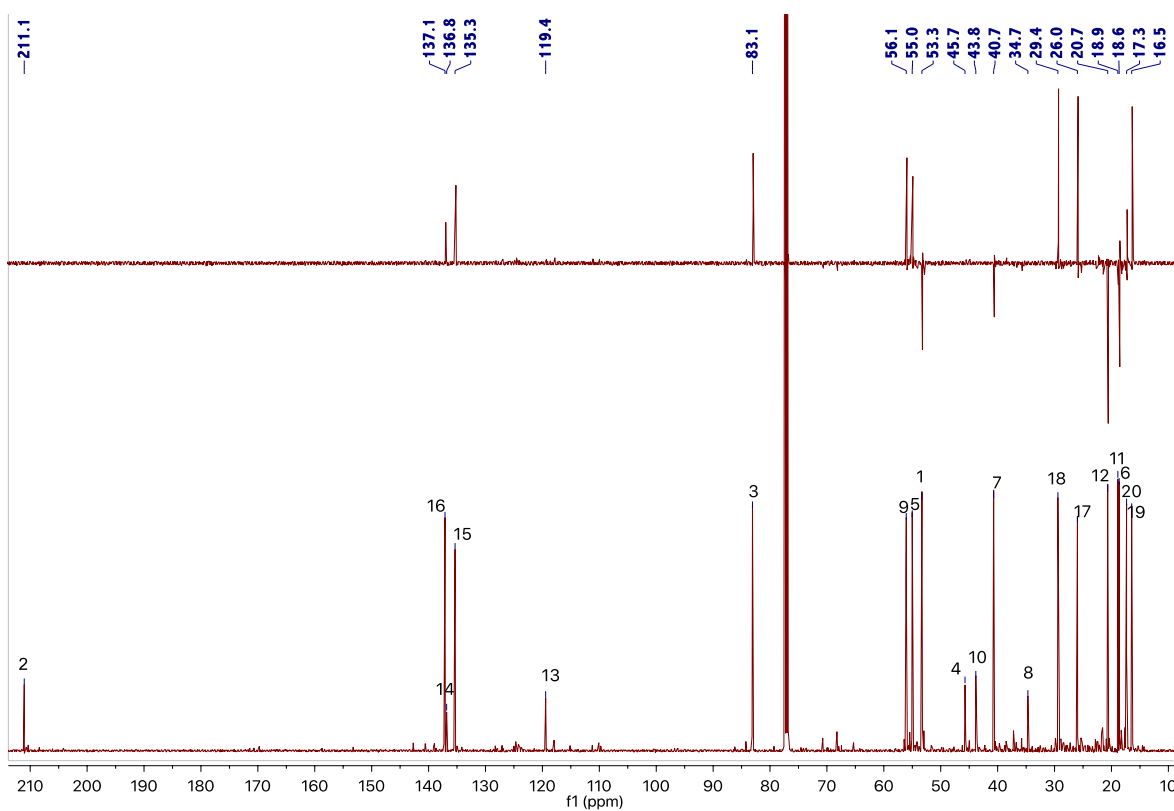


Figure S2. ^{13}C NMR and DEPT-135 spectra of **1** (125 MHz, CDCl_3).

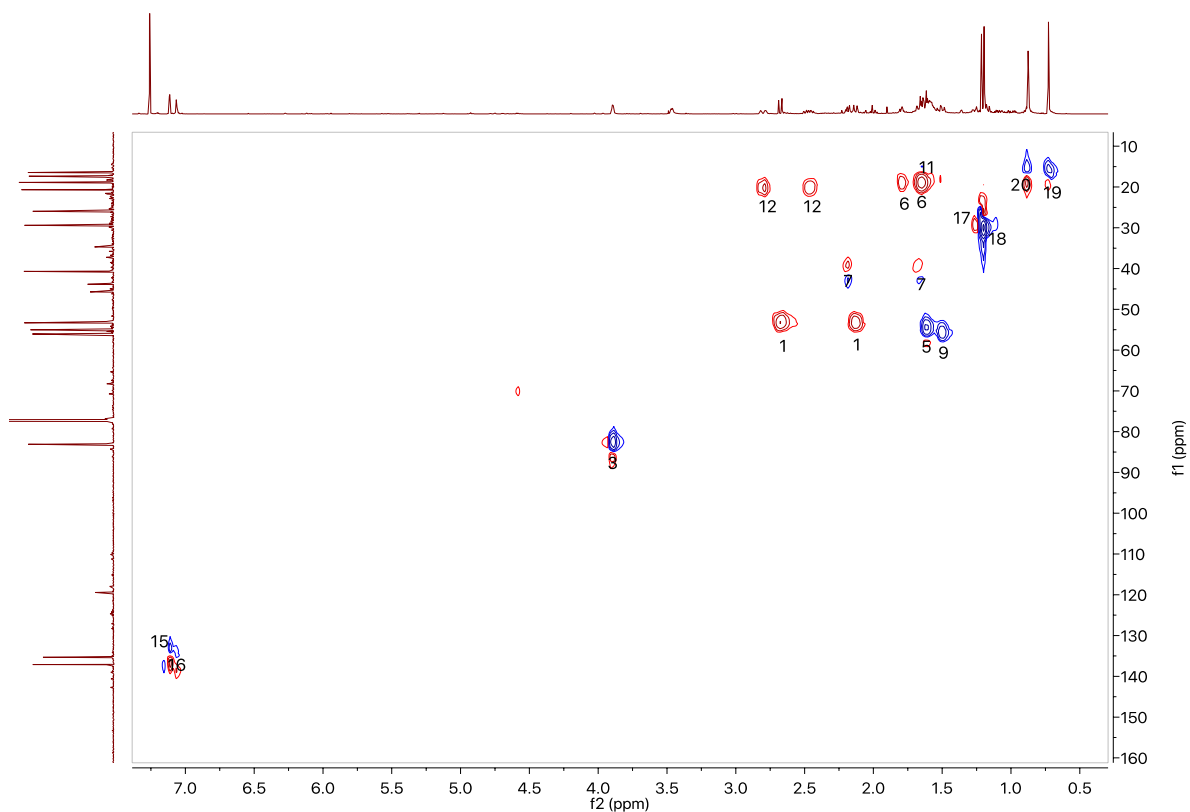


Figure S3. HSQC spectrum of **1** (500 MHz, CDCl_3). CH_2 : blue cross-peaks and CH or CH_3 : red cross-peaks.

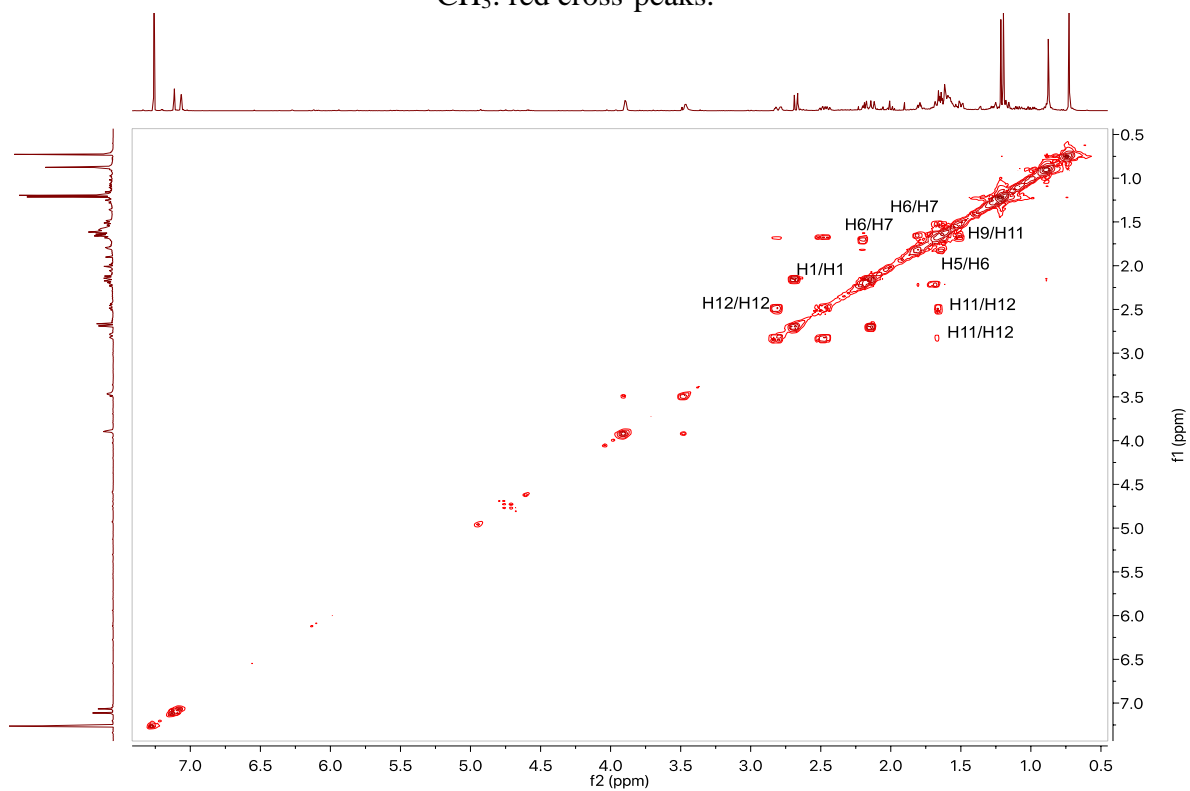


Figure S4. COSY spectrum of **1** (500 MHz, CDCl_3).

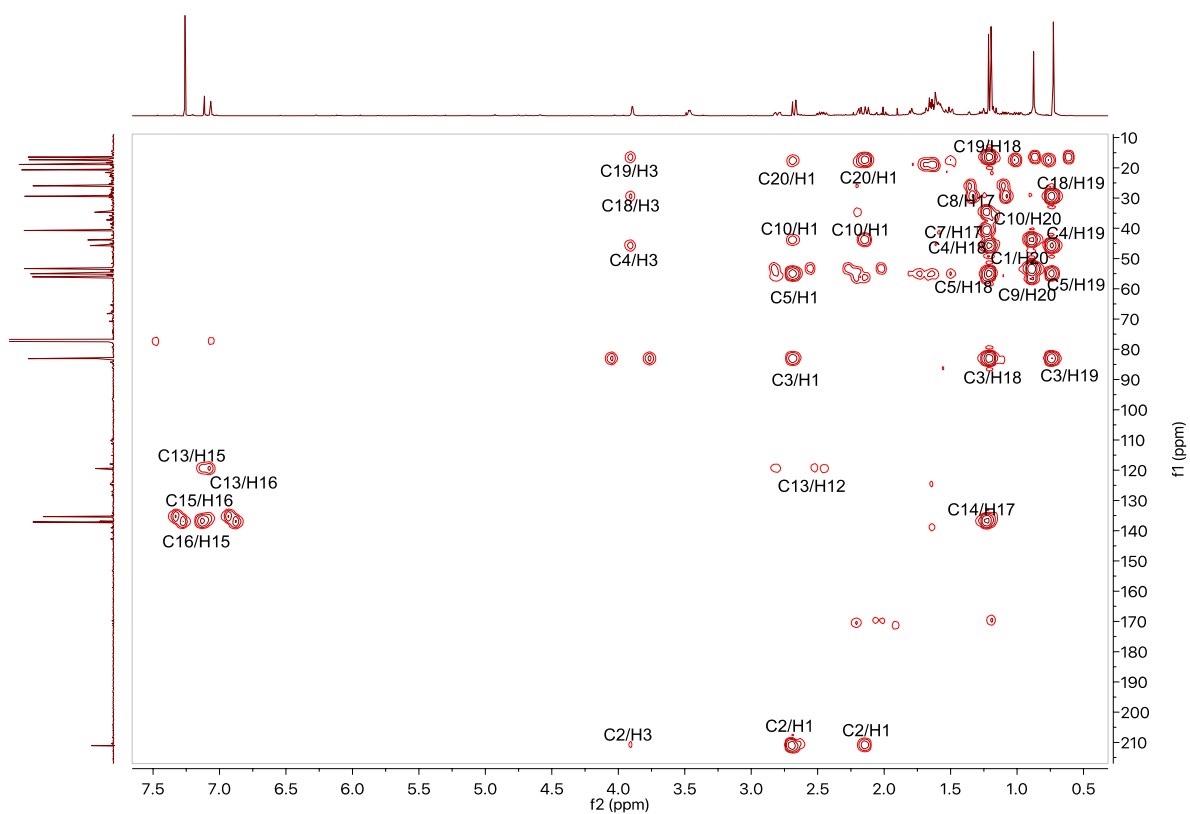


Figure S5. HMBC spectrum of **1** (500 MHz, CDCl₃).

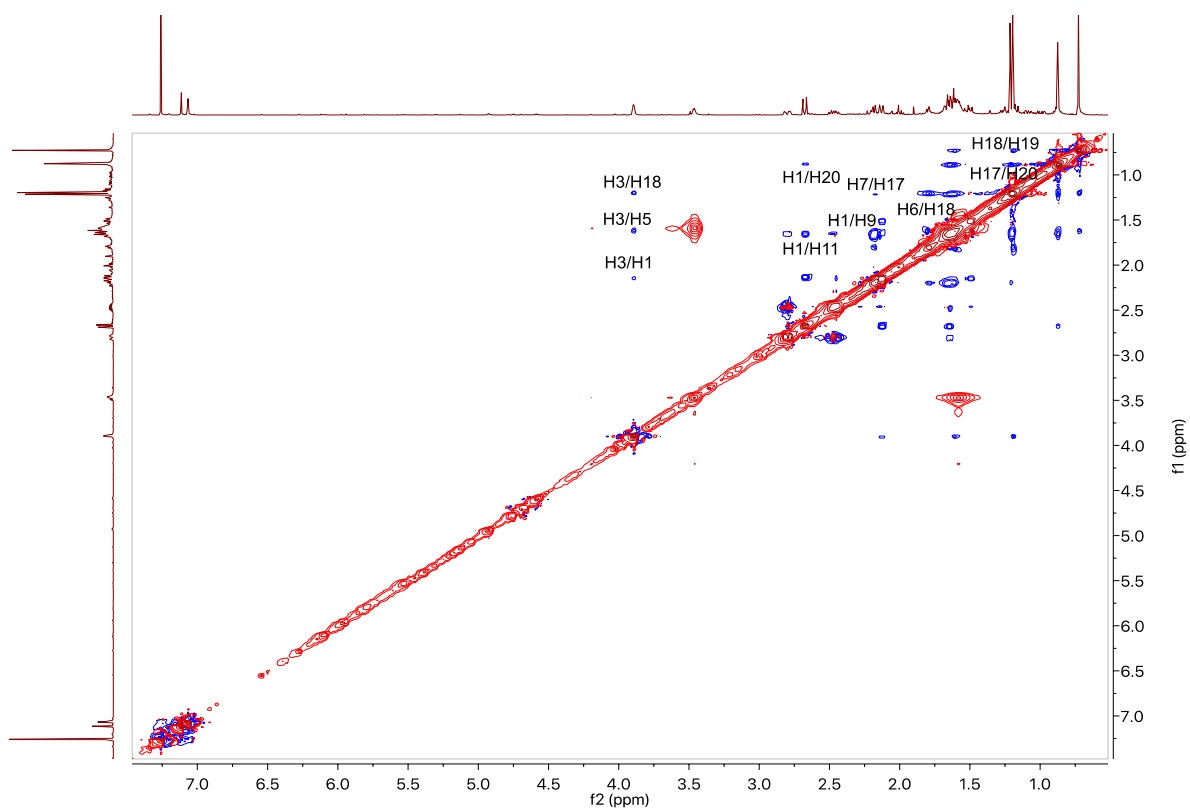


Figure S6. NOESY spectrum of **1** (500 MHz, CDCl₃).

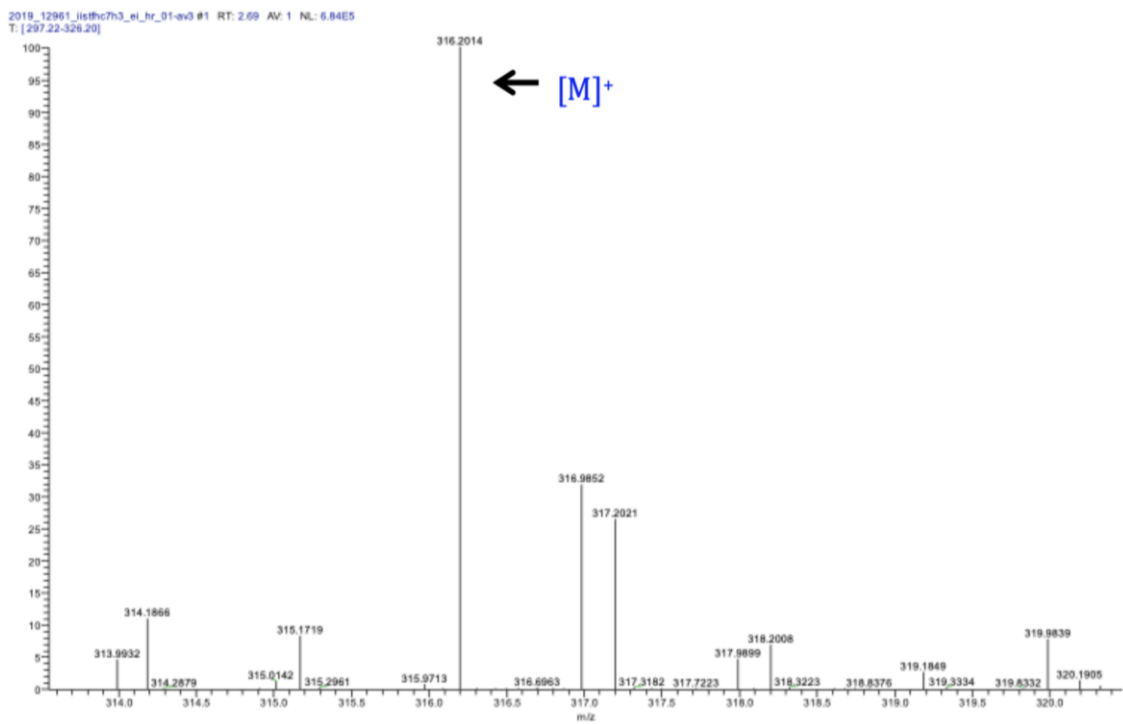


Figure S7. (+)-HREIMS of 1.

Table S2. NMR data of **2** in CDCl₃ (125 MHz for ¹³C and 500 MHz for ¹H).

no.	δ _c type	δ _H , mult. (<i>J</i> in Hz)	COSY	HMBC	NOESY
1	128.3, CH	6.54, s		2, 3, 5, 9	9, 11, 20
2	144.3, C				
3	201.2, C				
4	44.3, C				
5	54.5, C	1.80, m	6		
6	19.1, CH ₂	1.67, m	5, 7		
7	40.4, CH ₂	1.66, m-2.18, m	6		15
8	34.9, C				
9	51.7, CH	1.48, dd (11.8, 1.7)	11	5, 9	1
10	38.8, C				
11	18.8, CH ₂	1.91, dt (7.0, 1.7)	9, 12	13	1
12	20.7, CH ₂	2.51, dddd(16.2, 12.2, 7.0, 1.7) 2.83, ddt (16.2, 6.3, 1.5)	11	9, 13	16
13	119.5, C				
14	137.3, C				
15	135.0, CH	7.09, s		13, 16	7, 17
16	137.2, CH	7.06, s		13, 15	12
17	26.7, CH ₃	1.28, s		7, 8, 9, 14	15
18	20.6, CH ₃	1.16, s		3, 4, 5, 19	
19	27.3, CH ₃	1.23, s		3, 4, 5, 18	
20	21.7, CH ₃	1.22, s		1, 9, 10	1
OH		5.93, s		1, 2	

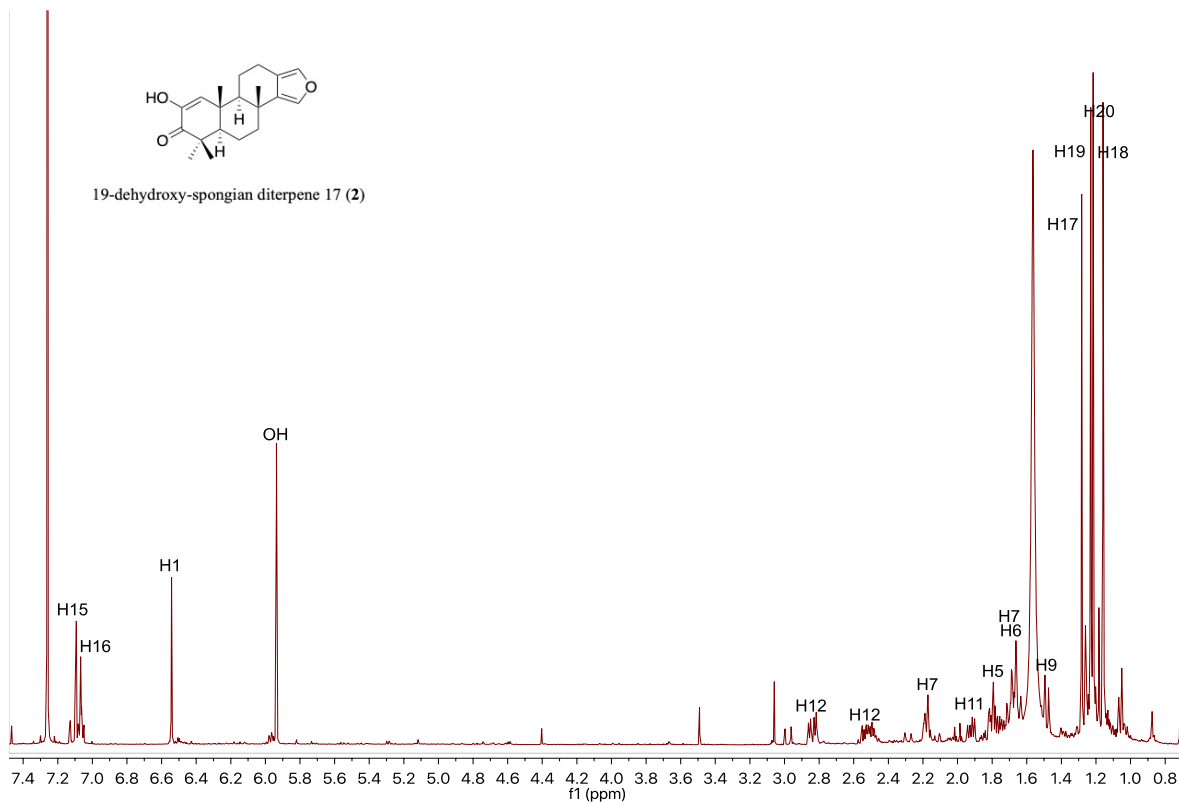


Figure S8. ^1H NMR spectrum of **2** (500 MHz, CDCl_3).

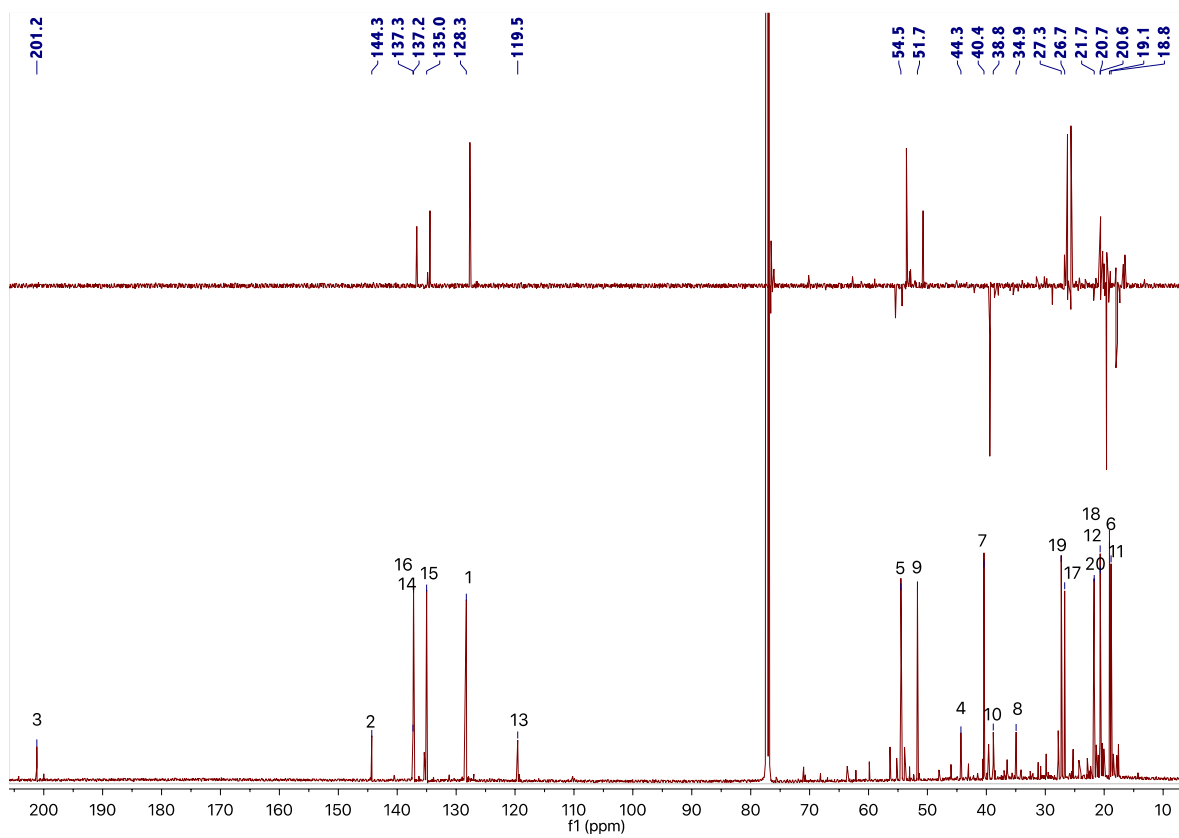


Figure S9. ^{13}C NMR and DEPT-135 spectra of **2** (125 MHz, CDCl_3).

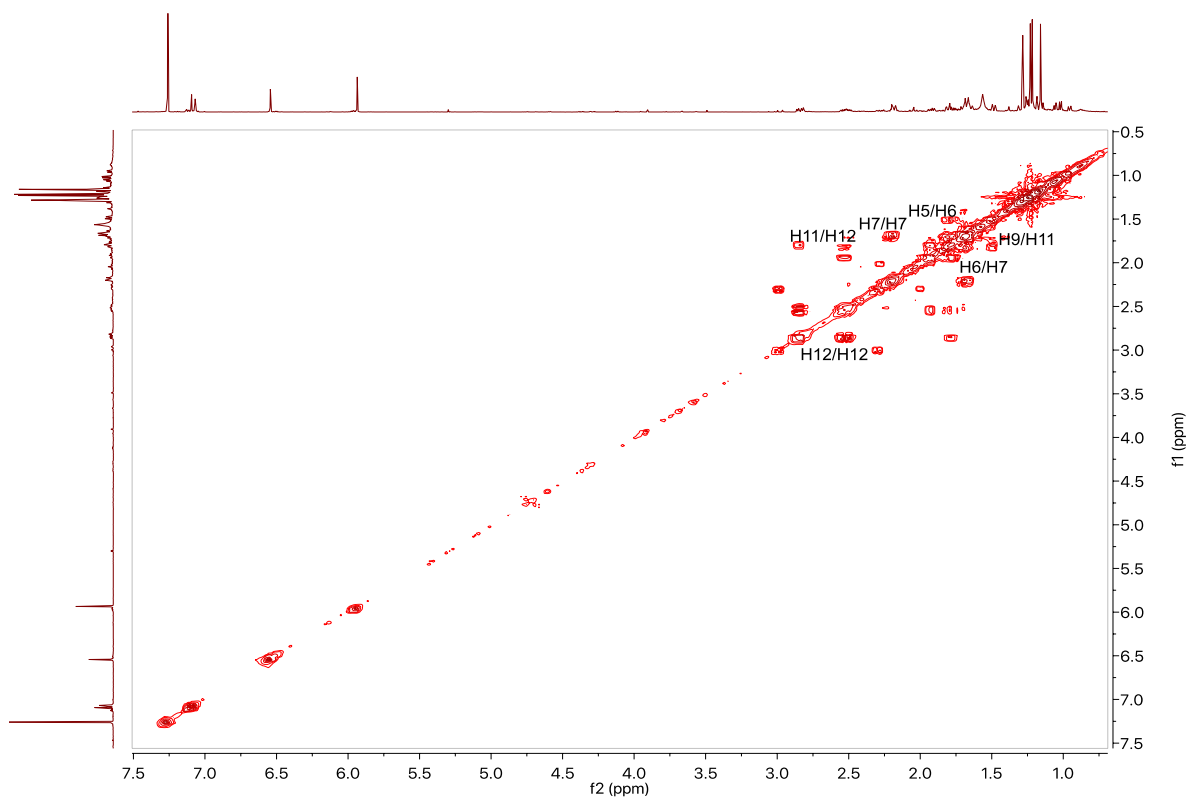


Figure S10. COSY spectrum of **2** (500 MHz, CDCl₃).

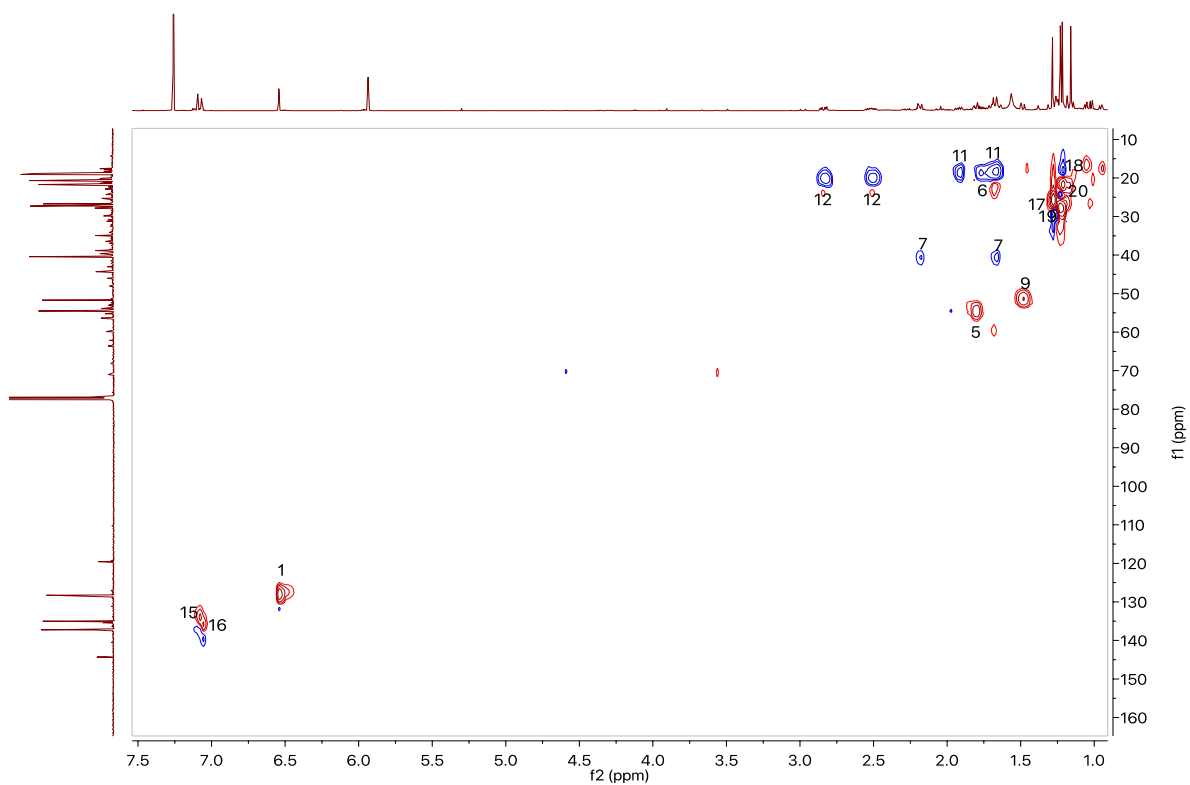


Figure S11. HSQC spectrum of **2** (500 MHz, CDCl₃). CH₂: blue cross-peaks and CH or CH₃: red cross-peaks.

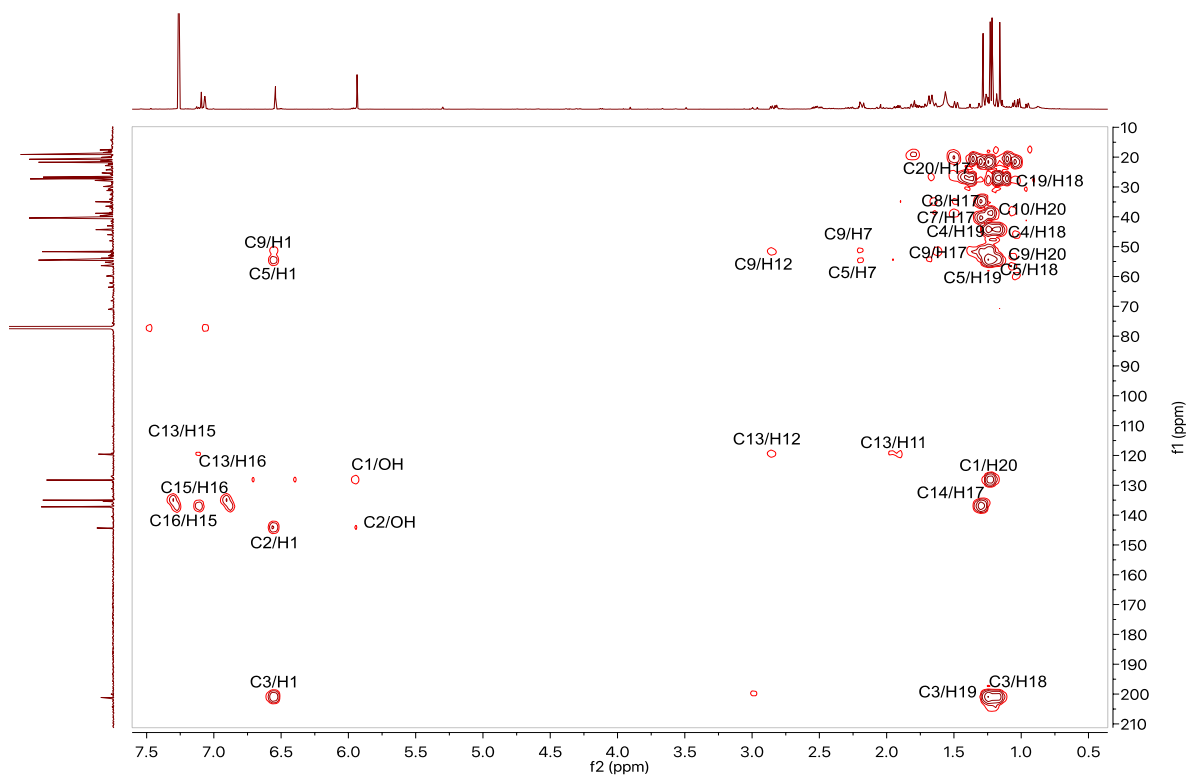


Figure S12. HMBC spectrum of **2** (500 MHz, CDCl₃).

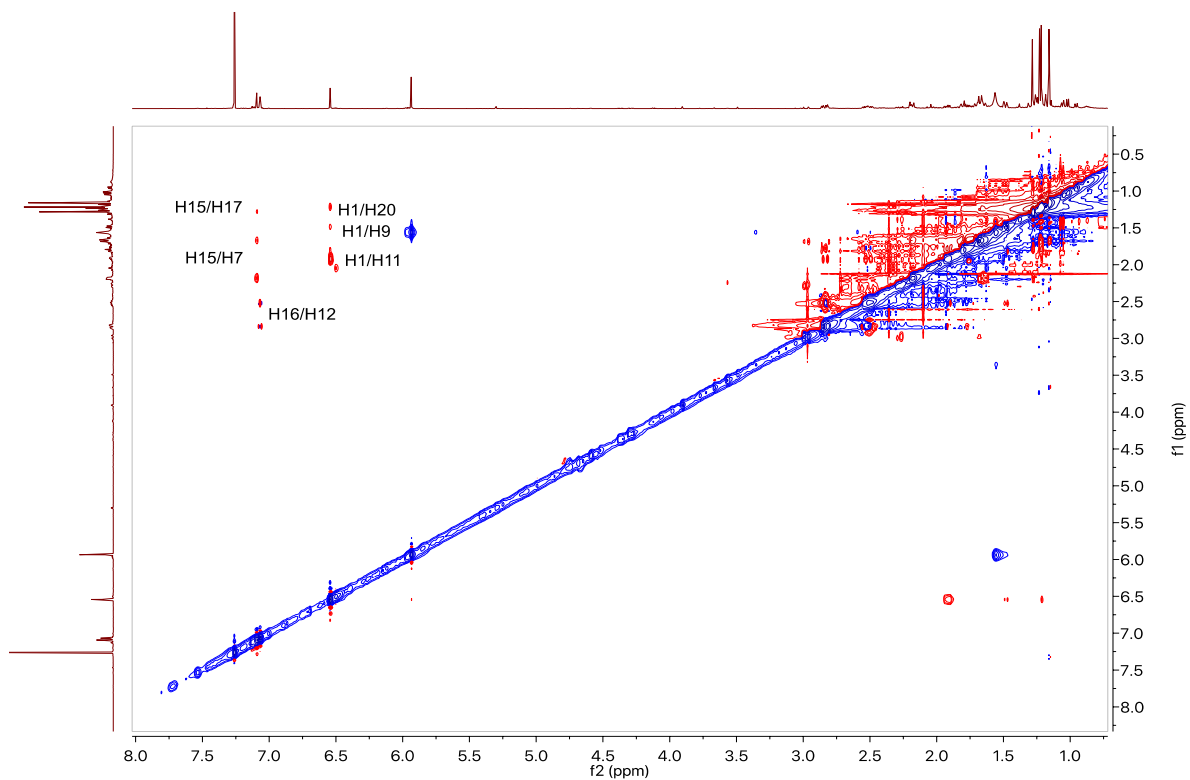


Figure S13. NOESY spectrum of **2** (500 MHz, CDCl₃).

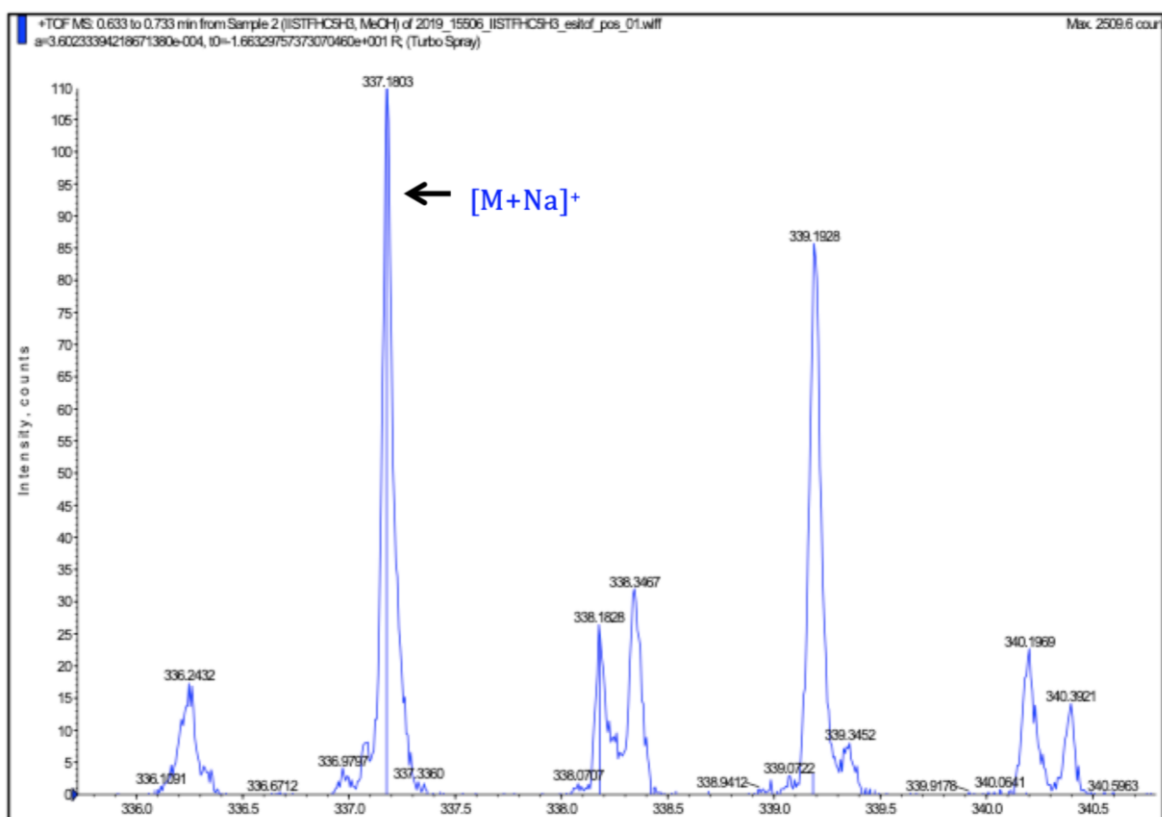


Figure S14. (+)-HRESIMS of **2**.

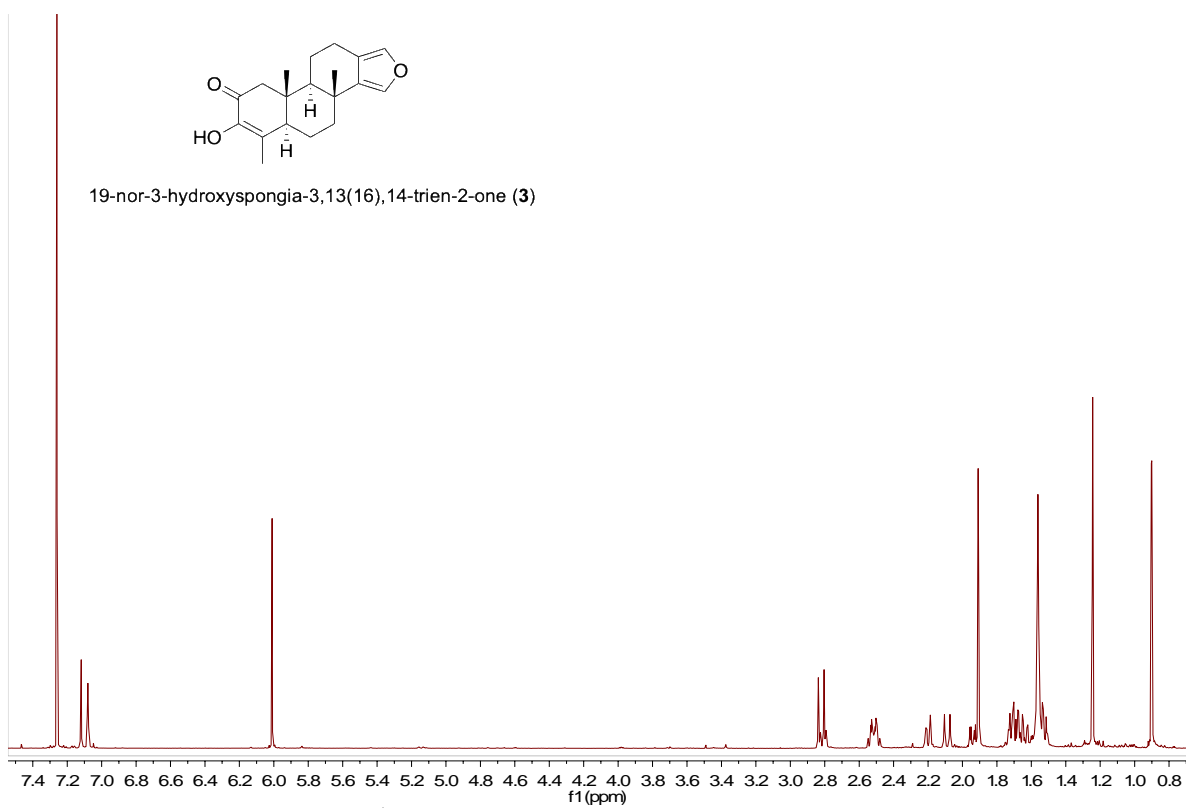


Figure S15. ¹H NMR spectrum of **3** (500 MHz, CDCl₃).

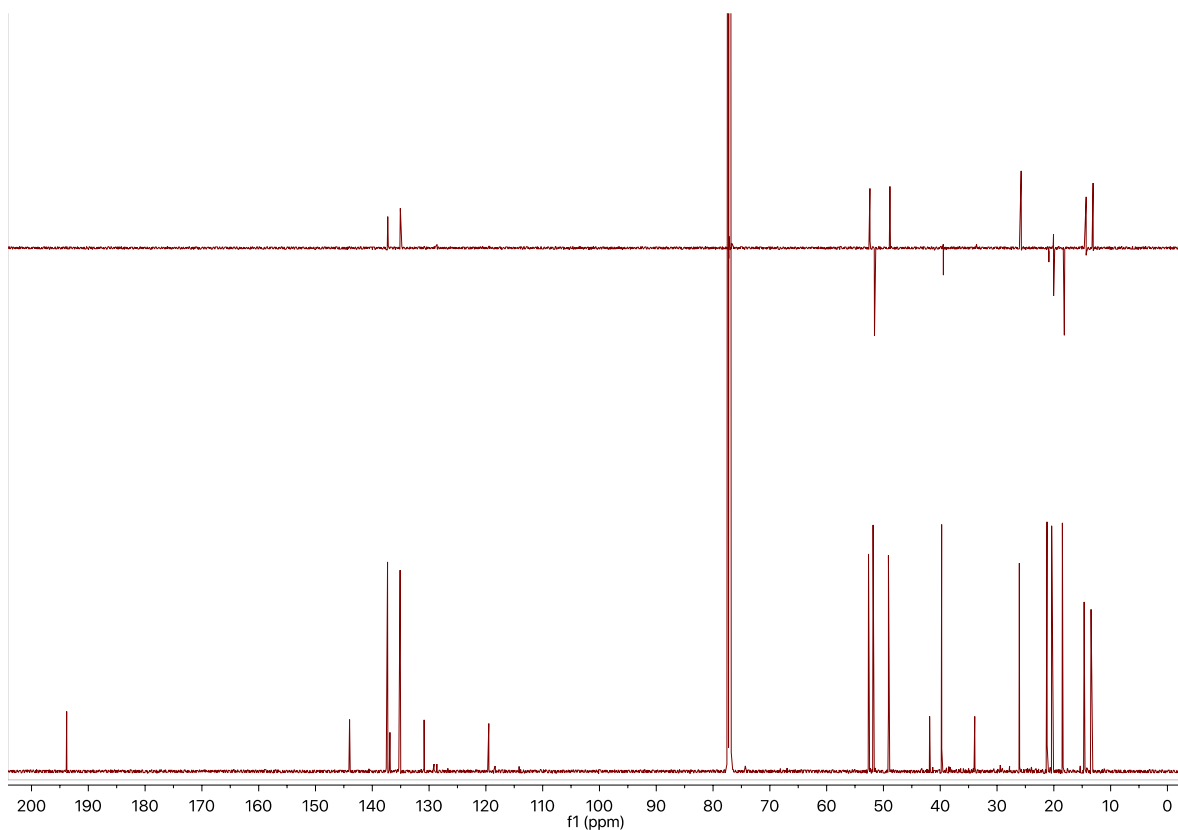


Figure S16. ^{13}C NMR and DEPT-135 spectra of **3** (125 MHz, CDCl_3).

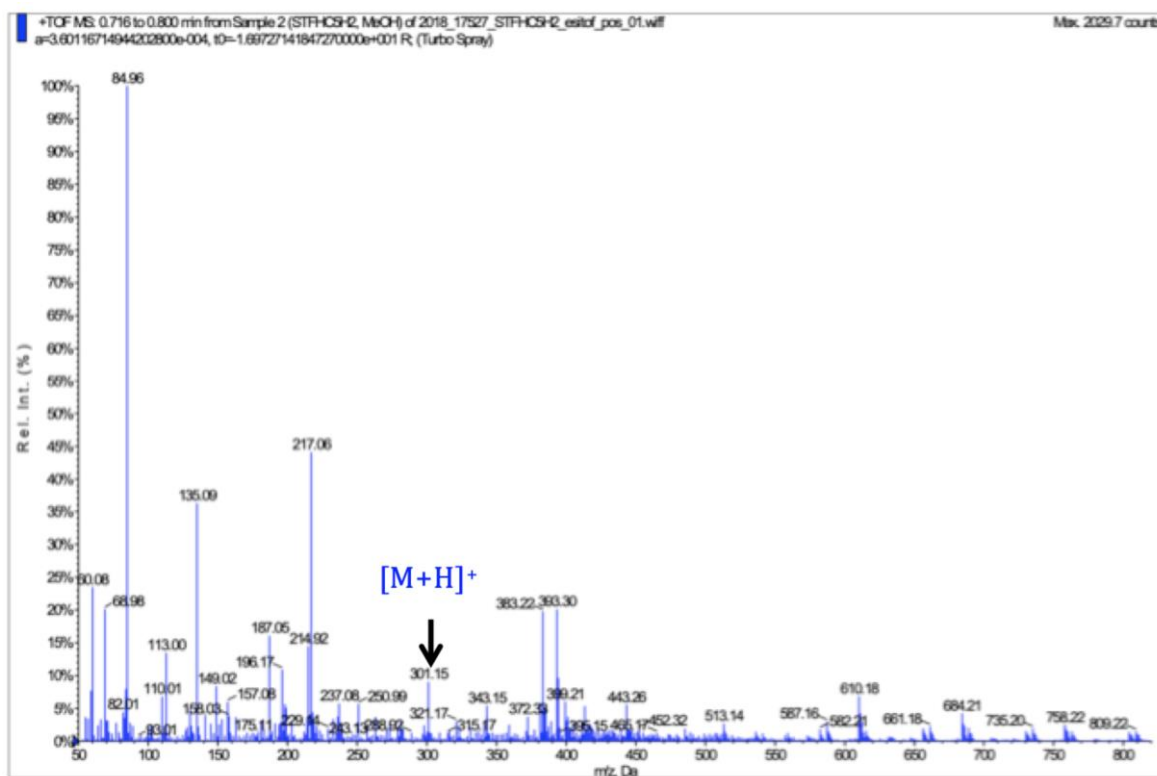


Figure S17. (+)-LRESIMS of **3**.

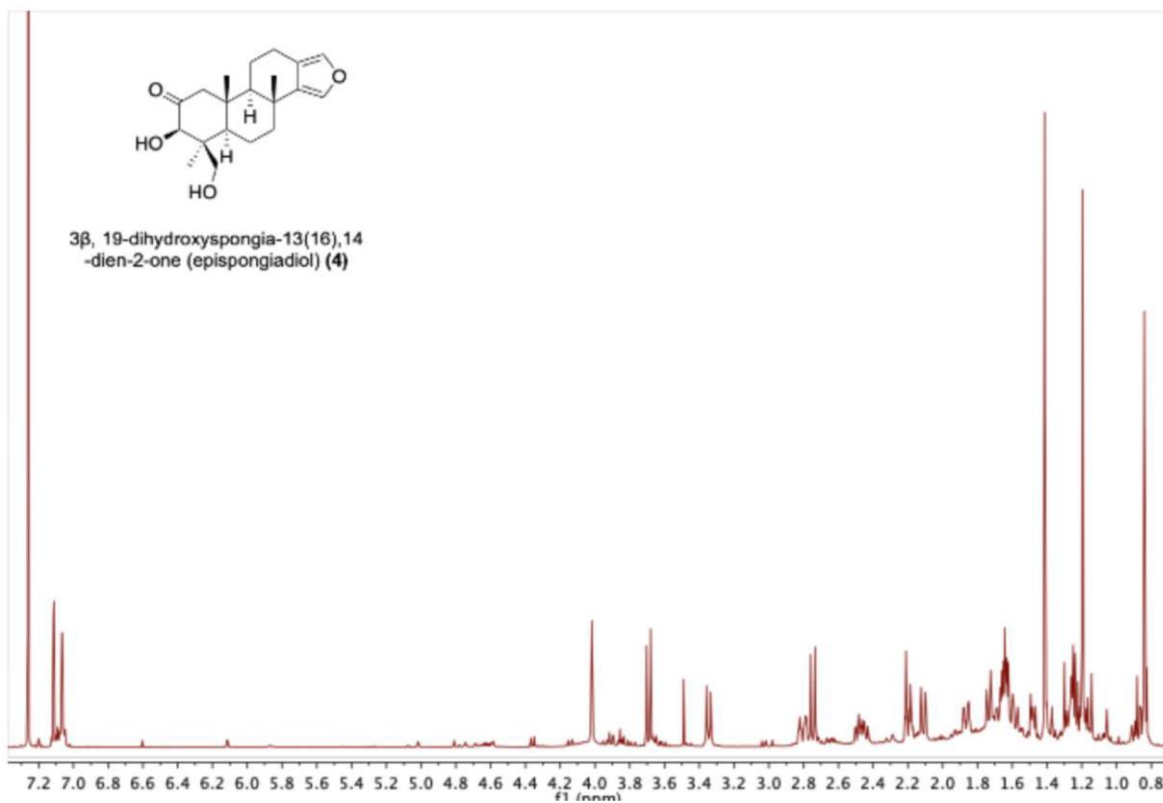


Figure S18. ¹H NMR spectrum of **4** (500 MHz, CDCl₃).

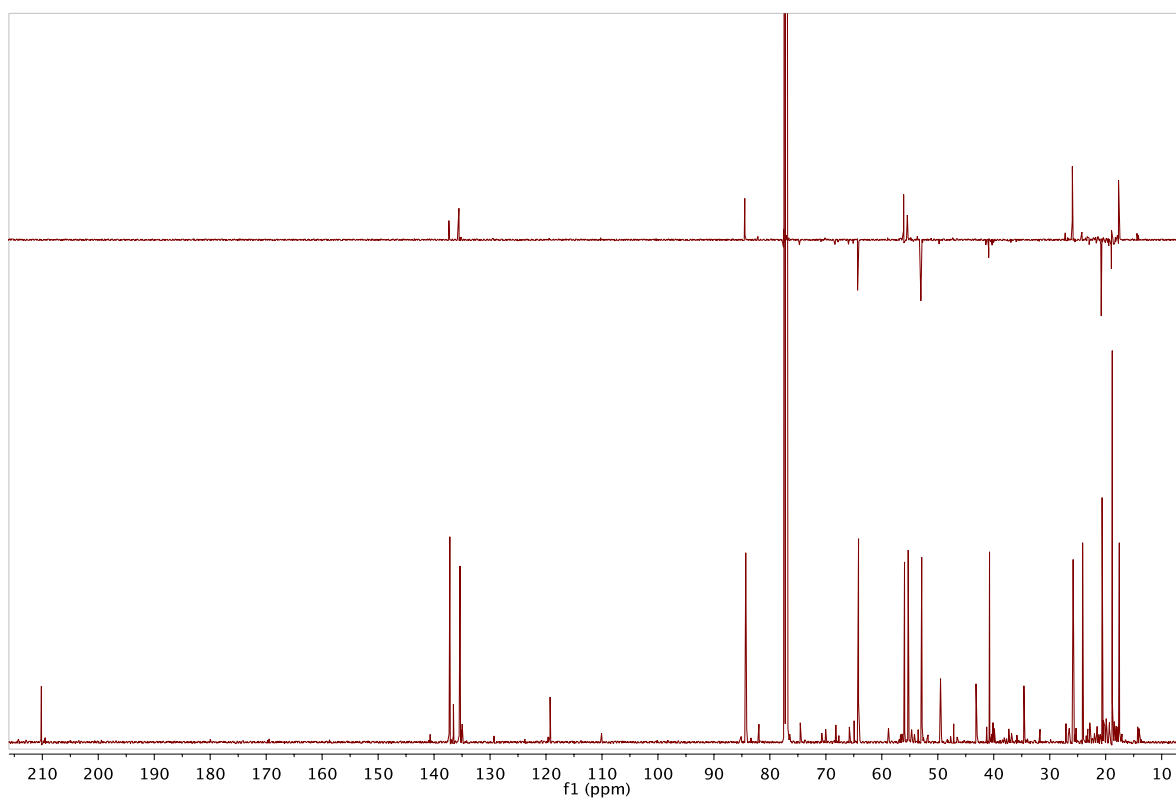


Figure S19. ¹³C NMR and DEPT-135 spectra of **4** (125 MHz, CDCl₃).

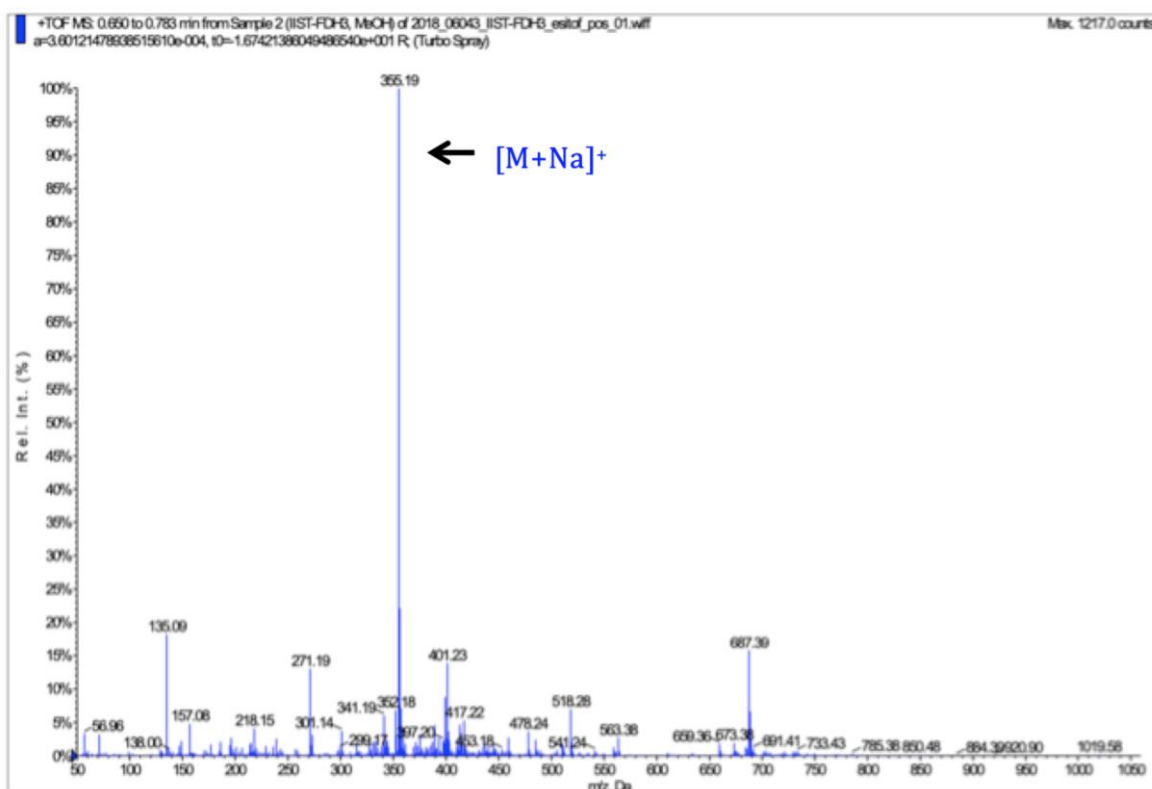
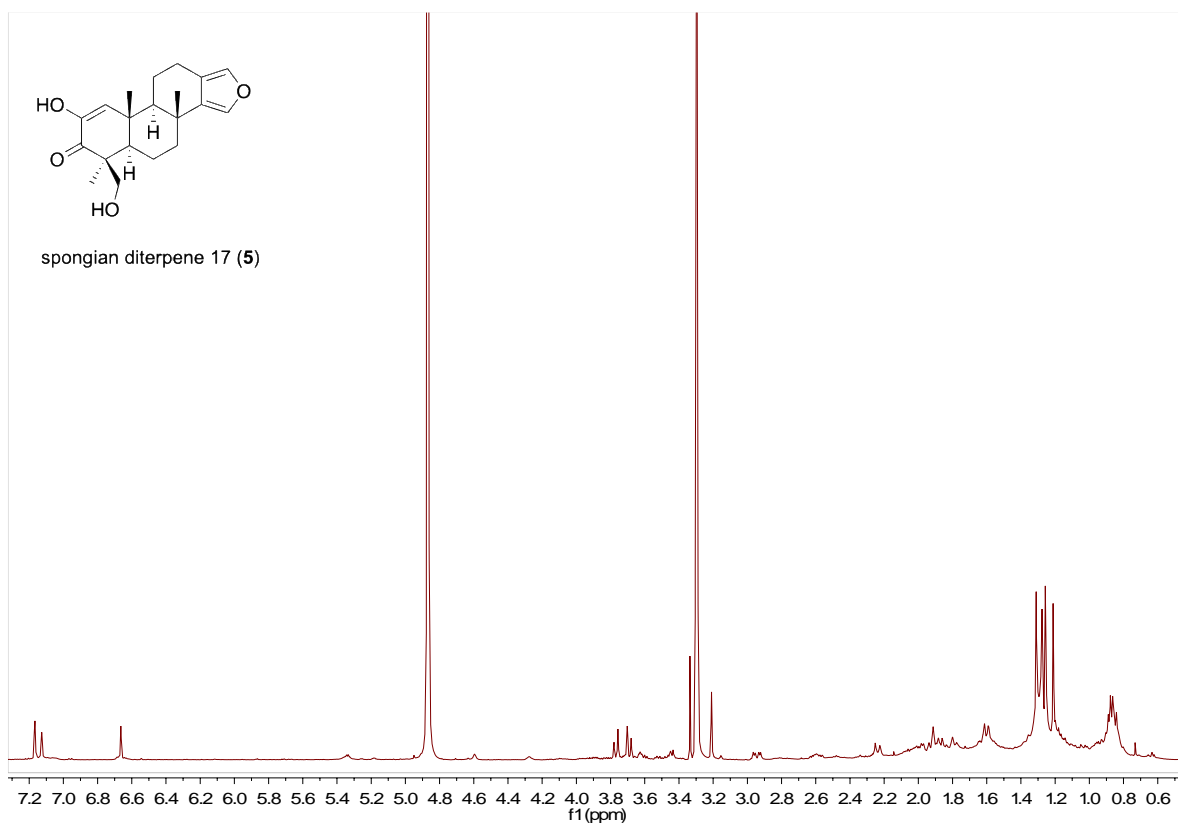


Figure S20. (+)-LRESIMS of 4.



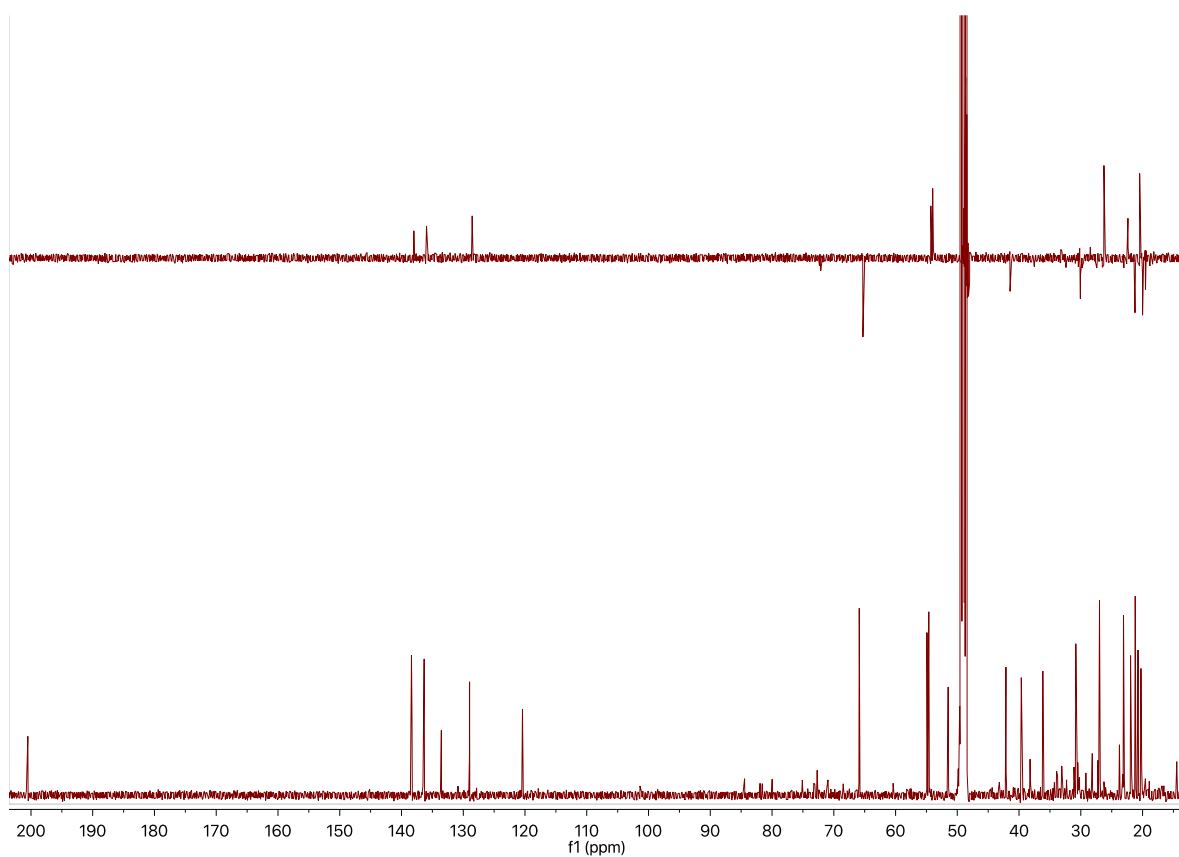


Figure S22. ^{13}C NMR and DEPT-135 spectra of **5** (125 MHz, CH_3OH).

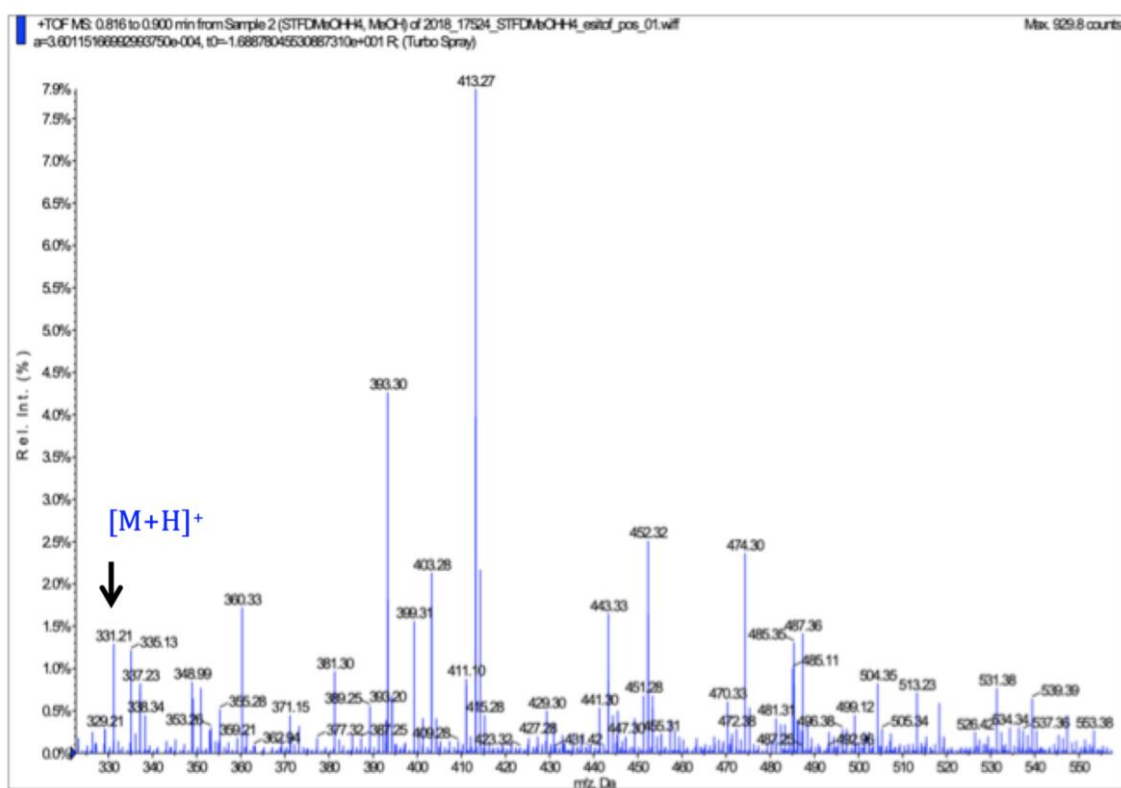


Figure S23. (+)-LRESIMS of **5**.

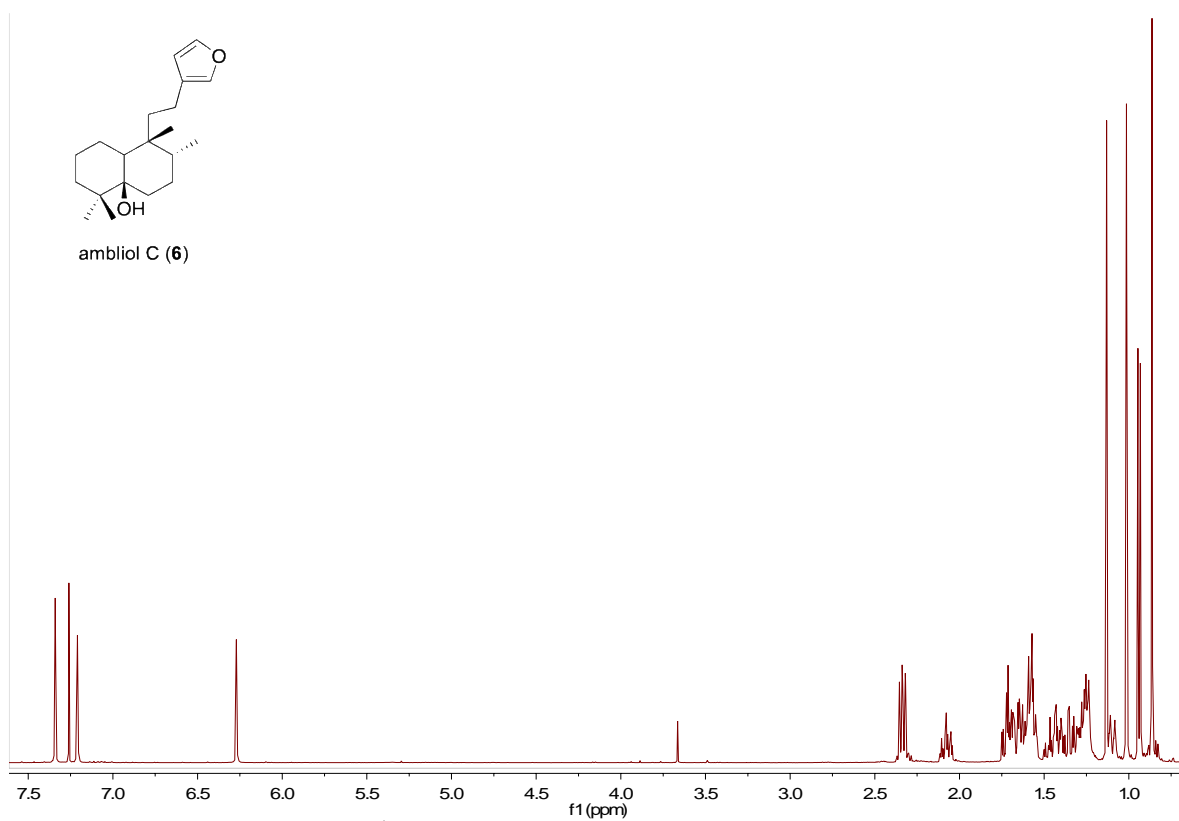


Figure S24. ¹H NMR spectrum of **6** (500 MHz, CDCl₃).

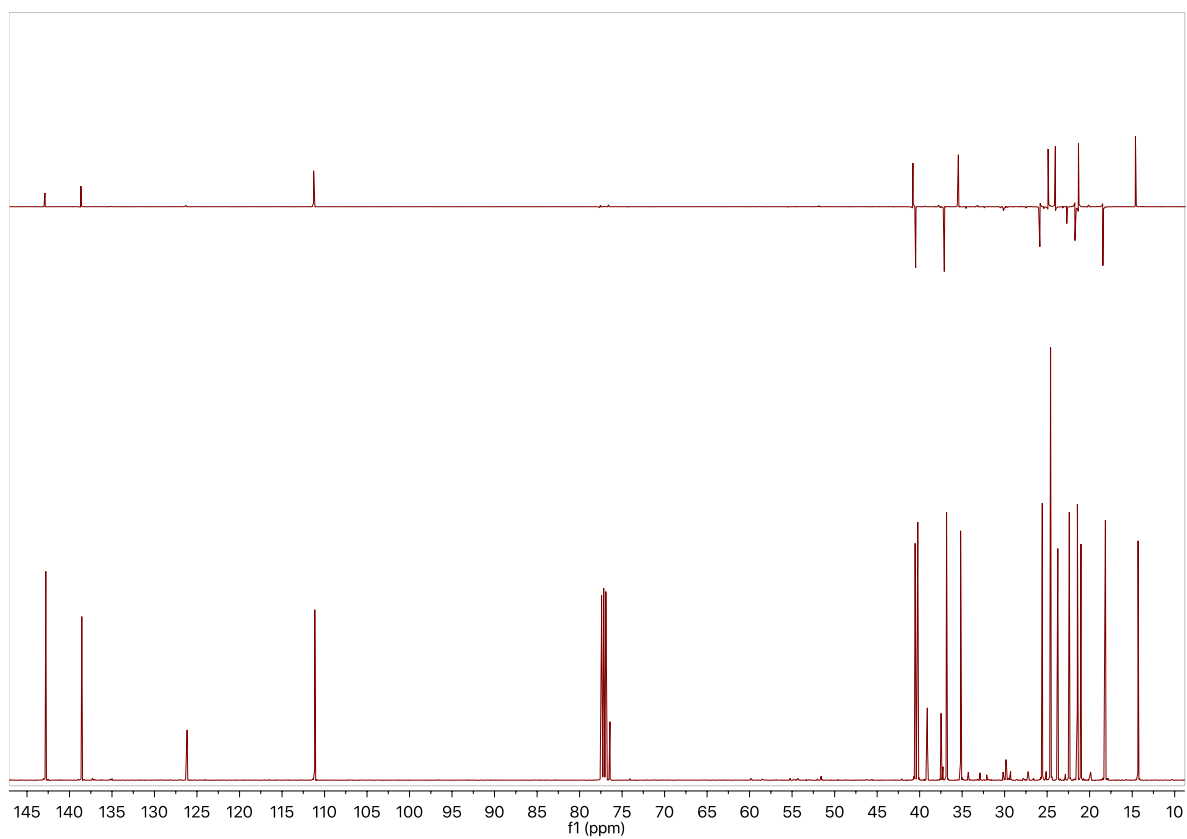


Figure S25. ¹³C NMR and DEPT-135 spectra of **6** (125 MHz, CDCl₃).

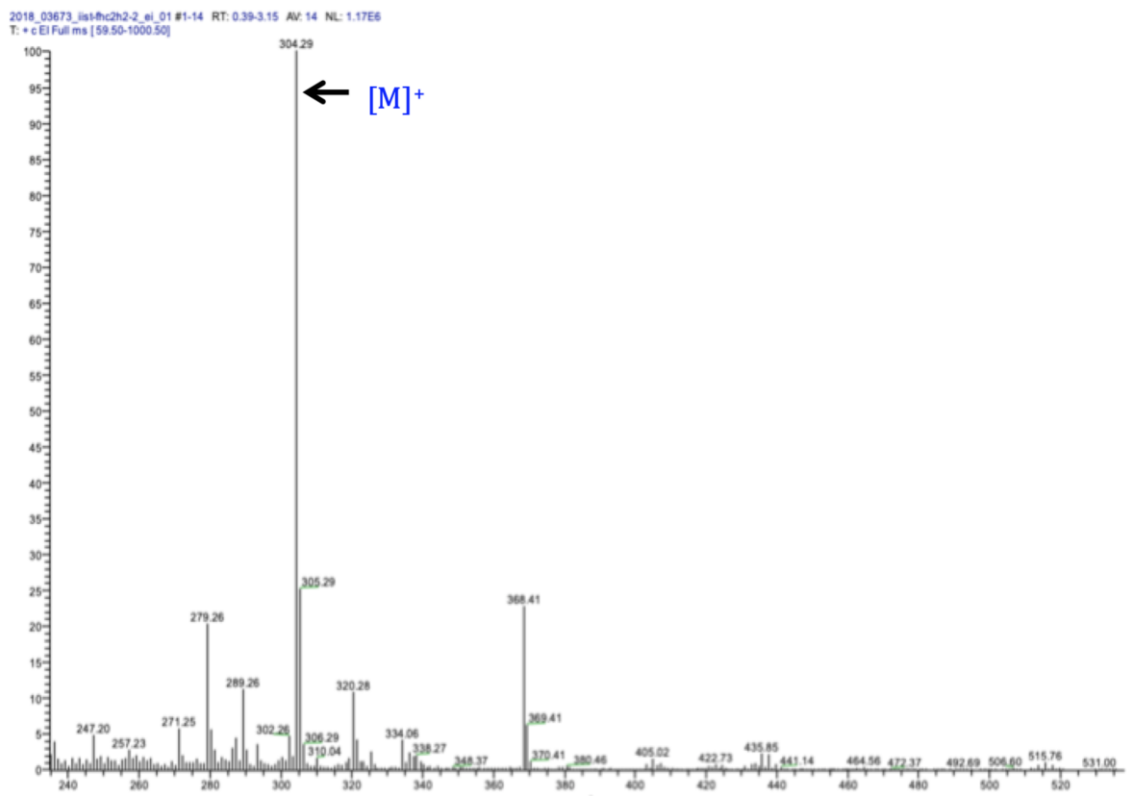


Figure S26. (+)-LREIMS of 6.

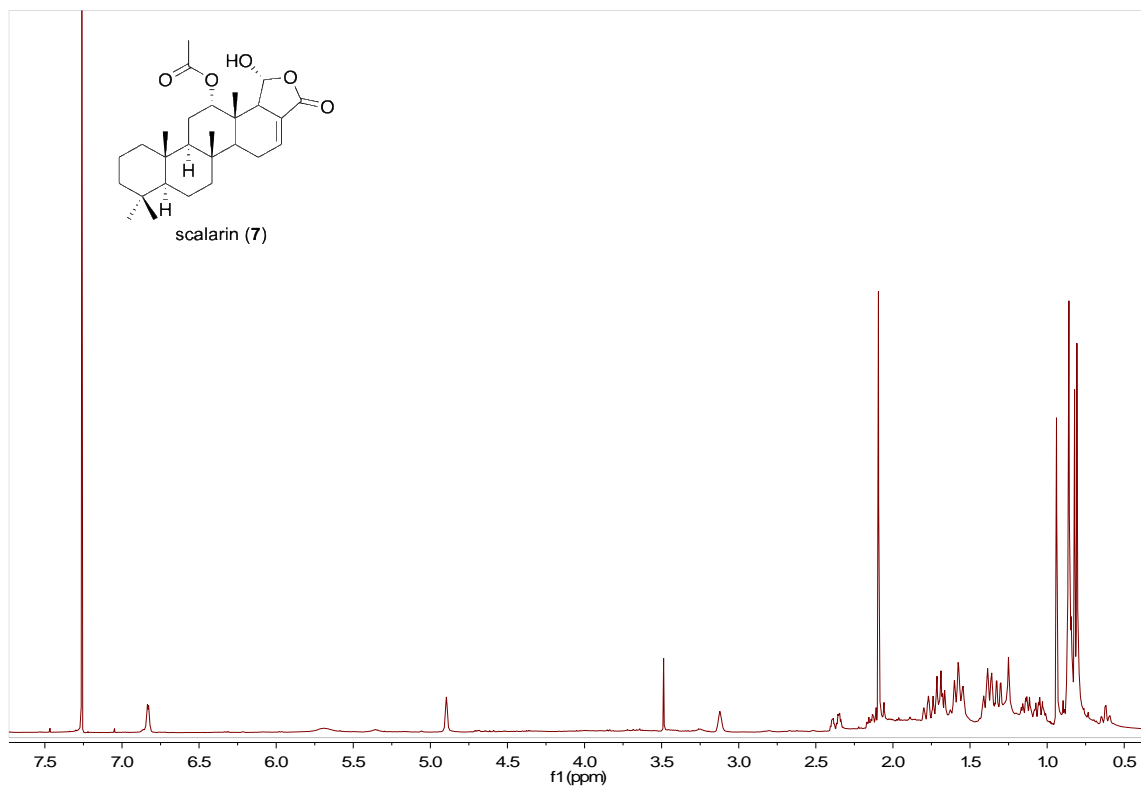


Figure S27. ^1H NMR spectrum of 7 (500 MHz, CDCl_3).

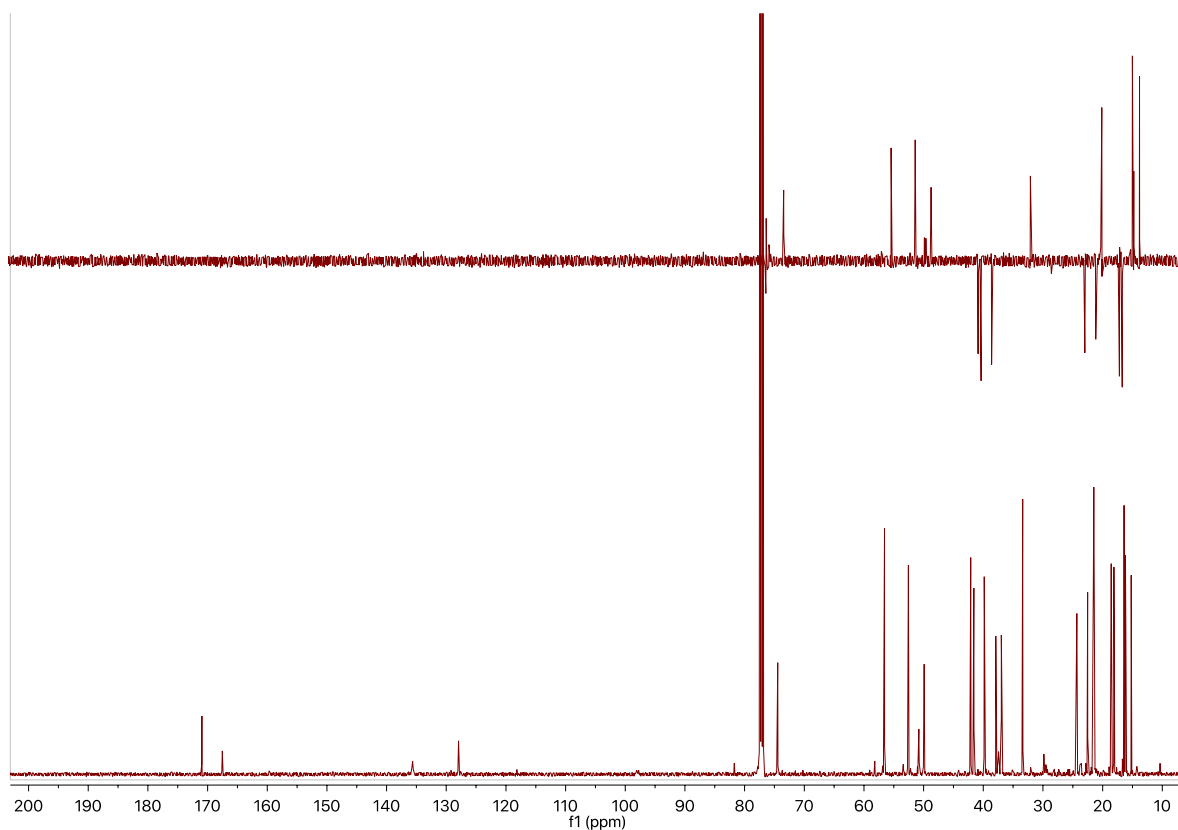


Figure S28. ^{13}C NMR and DEPT-135 spectra of **7** (125 MHz, CDCl_3).

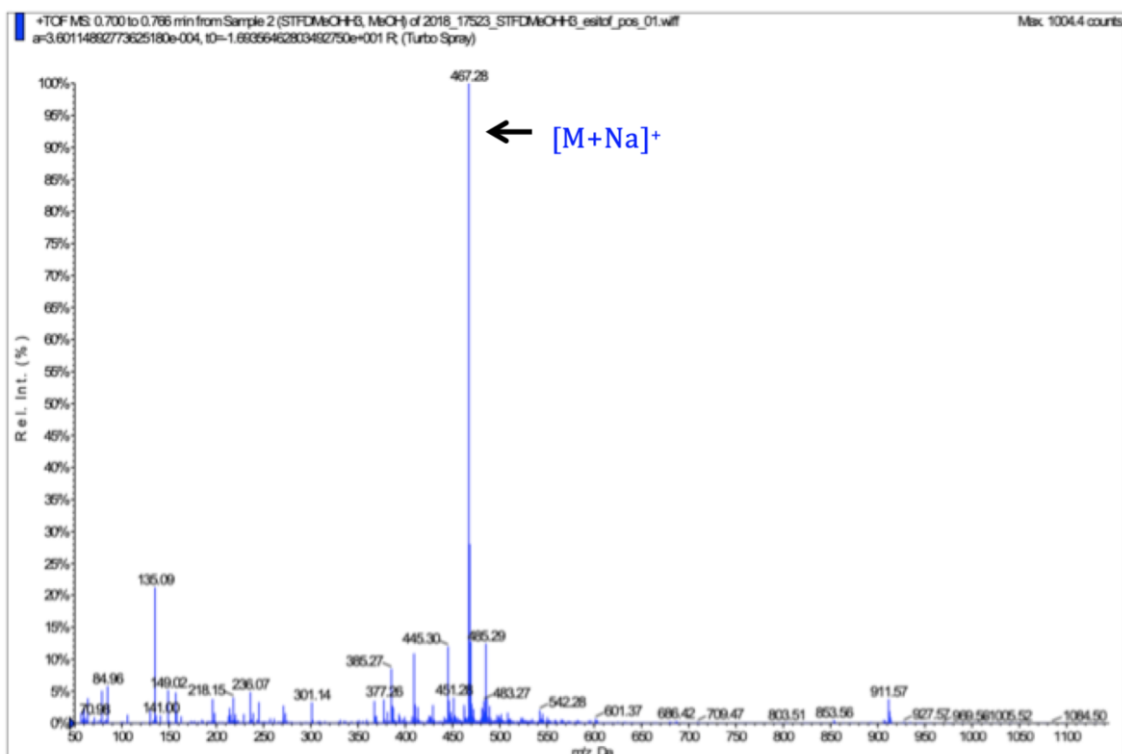


Figure S29. (+)-LRESIMS of **7**.

3.3 Estudio químico de la esponja *Ircinia felix*

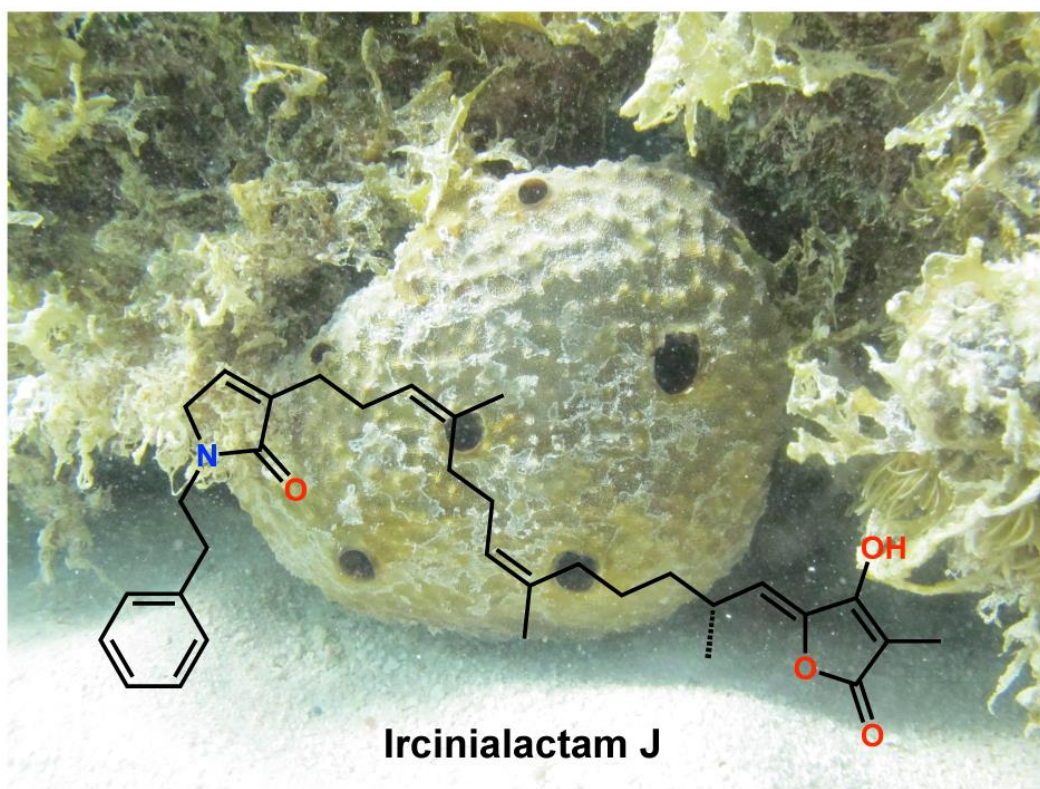


Figura 3.3. Fotografía de la esponja *Ircinia felix* (Rio Indio-México) y la estructura de la ircinialactama J.

En este apartado se describe el aislamiento y la elucidación estructural de seis compuestos de estructura tipo sesterpenoide obtenidos a partir de la esponja *Ircinia felix* colectada en la costa de Rio Indio, Caribe Mexicano. Su estructura plana se determinó mediante las técnicas de RMN 1D y 2D, HRESIMS e IR. Tres sesterpenoides resultaron ser nuevos compuestos y su configuración absoluta se obtuvo mediante el uso de ECD y cálculos computacionales (DFT). Dos de los productos naturales aislados mostraron una actividad muy potente frente a adenovirus humanos (hasta cerca de cinco veces más activas que el fármaco usado como control positivo) y no mostrando además una actividad citotoxicidad significativa.

Estos resultados forman parte de una patente internacional solicitada en agosto del año 2019. Los resultados obtenidos serán enviados próximamente a publicar.

Two antiviral Sesterterpenoids from the Marine Sponge *Ircinia felix*, Collected in Yucatan (Mexico)

Dawrin Pech-Puch¹, Judith Berastegui-Cabrera², Ana Serna-Gallego², Patricia Gómez³, Jerónimo Pachón^{2,4}, Jaime Rodríguez^{1*}, Carlos Jiménez^{2*} and Javier Sánchez-Céspedes^{2,4*}

¹ Center for Advanced Scientific Research (CICA) and Department of Chemistry, Faculty of Sciences, University of A Coruña, 15071 A Coruña, Spain

² Unit of Infectious Diseases, Microbiology and Preventive Medicine, Institute of Biomedicine of Seville (IBiS), University Hospital Virgen del Rocío/CSIC/University of Seville, E41013 Seville, Spain

³ Unidad Académica de Ecología y Biodiversidad Acuática, Instituto de Ciencias del Mar y Limnología, Universidad Nacional Autónoma de México. CDMX, México

⁴ Department of Medicine, University of Seville, 41009, Seville, Spain

* Correspondence: Centro de Investigaciones Científicas Avanzadas (CICA) e Departamento de Química, Facultad de Ciencias, Universidad da Coruña, 15071 A Coruña, Spain. Tel: +34 981 167000. Fax: +34 981 167065. *E-mail address*: carlos.jimenez@udc.es, (Carlos Jiménez) jaime.rodriguez@udc.es (Jaime Rodríguez); Unit of Infectious Diseases, Microbiology and Preventive Medicine, Institute of Biomedicine of Seville (IBiS), University Hospital Virgen del Rocío/CSIC/University of Seville, E41013 Seville, Spain. Tel: +34 955 923100. *E-mail address*: jsanchez-ibis@us.es (J. Sanchez-Céspedes).

Abstract: Three new sesterterpene lactams, named ircinialactams J-L (**4-6**), along with three known sesterterpene furans (**1-3**), were isolated from the sponge *Ircinia felix* collected off the coast of Yucatan (Mexico). Their molecular structures were determined by 1D and 2D NMR spectroscopy and high-resolution mass spectrometry. Electronic circular dichroism (ECD) spectroscopy in combination with time-dependent density functional theory calculations (TD-DFT) were used in the establishment of the 18*R* absolute configuration in **1** and **4-6**. (7*Z*,12*Z*,18*R*,20*Z*)-variabilin (**1**) and ircinialactam J (**4**) display significant antiviral activity against Human adenoviruses (HAdV) at low micromolar concentrations with no significant cytotoxicity. Furthermore, mechanistic assays suggest that **1** and **4** are targeting an early step of the HAdV replicative cycle before HAdV genomes reached the nucleus of the host cell. This article describes for the first time the presence of antiviral activity in sesterterpene lactams.

Keywords: Sesterterpene lactams; Antiviral; Adenovirus; *Ircinia felix*

1. Introduction

Human adenoviruses (HAdV) are non-enveloped viruses with an icosahedral capsid containing a linear double-stranded DNA [1]. Currently, the Human Adenovirus Working Group (HAdV) reports the existence of 90 human adenovirus (HAdV) types grouped into 7 HAdV species (HAdVA-G) [2, 3]. In otherwise healthy individuals, HAdV infections are generally mild and self-limited [4]. However, with the advances in the molecular techniques of diagnosis, HAdV have been found to be increasingly involved in occasional cases and outbreaks of community-acquired pneumonia (CAP) [5]. In immunocompromised patients, HAdV infections show a wide clinical symptomatology, including pneumonia, colitis, hepatitis, hemorrhagic cystitis, tubule-interstitial nephritis or encephalitis, which can result in disseminated disease with high morbidity and mortality in this population, especially in the pediatric units [6].

Despite HAdV's significant clinical impact, currently there is not an approved drug to treat these infections. Although the available broad spectrum of antiviral drugs such as ribavirin, ganciclovir and cidofovir have demonstrated *in vitro* efficacy against HAdV, treatment with these antivirals has revealed a very variable efficacy and their use has been limited by their poor bioavailability and severe side effects (nephrotoxicity or bone marrow suppression). Brincidofovir (CMX001), a lipidic conjugate of cidofovir, is the only potential alternative to be used for the treatment of HAdV infections [7]. A phase III clinical trial was completed in 2016, but results concerning its efficacy for the treatment of HAdV infections have not been reported yet (ClinicalTrials.gov Identifier: NCT02087306). This antiviral was administered to a small number of patients to treat Ebola virus disease during the 2014 outbreak, and now it is being evaluated for the treatment of serious HAdV infection or disease (ClinicalTrials.gov Identifier: NCT02596997). Based on this scenario, the research on additional drugs with increased anti-HAdV efficacy is still necessary.

Marine organisms represent a very prolific source of bioactive molecules to identify new antiviral candidate molecules [8]. As an example, the two natural arabino-nucleosides, spongothymidine and spongouridine, isolated from the Caribbean marine sponge *Cryptotethia crypta* were the basis for the development of the synthetic antiviral vidarabine (ara-A) used for the treatment of herpes simplex virus type 1 and 2 infections for many years as the first FDA-approved marine-derived antiviral product. Furthermore, they are also being considered the basis for the development of other antiviral nucleosides such as azidothymidine (AZT) and acyclovir [9].

The sponge *Ircinia felix* is an important source of marine sesterterpenoids that constitute a small group of terpenoids [10]. Some examples of reported compounds from that sponge are the furanosesterterpene tetric acids [11], the linear C₂₁ furanoterpenes [12] and the scalarane-type sesterterpenoids [13]. They display a wide range of biological activities including antibacterial, antiviral, cytotoxic, antinociceptive, antitumoral and anti-inflammatory [14].

As part of our ongoing efforts to find novel compounds from marine organisms [15, 16] and more specifically from sponges [17, 18], specimens of *Ircinia felix*, collected by hand in the Mexican Caribbean, were investigated because preliminary data from the organic extracts showed antiviral activity against HAdV. This paper reports the isolation, structure elucidation and biological evaluation of three new sesterterpene lactams, along with three known sesterterpene furans, characterized by the presence of a tetric acid moiety at one end, while a furan or a γ -lactam ring is located at the other end.

2. Results and Discussion

2.1. Animal material extraction and isolation

Specimens of the sponge *Ircinia felix* were extracted several times using MeOH to give a crude extract. This organic extract was then partitioned between water and solvents of increasing polarity to give an enriched sesterterpenes *n*-butanol fraction. The *n*-BuOH fraction was submitted to a solid phase extraction (SPE)-C18 (H₂O/MeOH/CH₂Cl₂ gradient system) and the resulting fractions were separated by reversed-phase HPLC to afford compounds **1–6** (Figure 1).

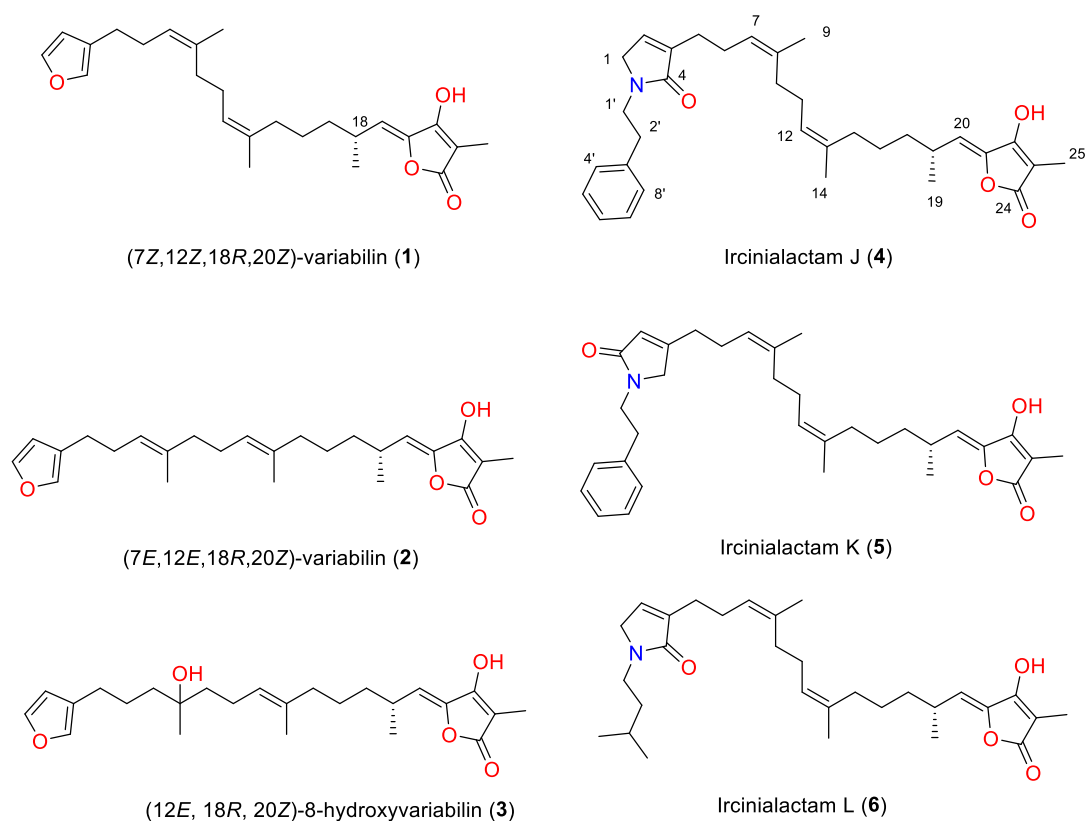


Figure 1. Sesterterpenes **1–6** isolated compounds from *Ircinia felix*.

The planar structures of compounds **1–3** were elucidated as (7Z,12Z,20Z)-variabilin [19], (7E,12E,20Z)-variabilin [20] and (12E,20Z)-8-hydroxyvariabilin [21], respectively, by comparison of their NMR data with those reported in the literature. The *R* configuration at C18 in compounds **2** and **3** was deduced by comparison of their optical rotation data with the corresponding reported values, including their enantiomers [22]. The structure of compound **1**, isolated from *Ircinia dendroides*, was reported without stereochemistry at C18 and its optical rotation [19]. The positive specific optical rotation value for **1** of $[\alpha]^{25}_D + 39.9$ suggested a 18*R* configuration. The absolute configuration of **1** was confirmed by comparison of the experimental and simulated electronic circular dichroism (ECD) spectrum generated by time-dependent density functional theory calculations (TDDFT) on the two possible enantiomers 18*R*-**1**- and 18*S*-**1** (Figure 2). Overall, the two enantiomers 18*R*-**1**- and 18*S*-**1** were initially submitted to a conformation search with the Maestro Suite (Schrödinger). Thus, 25 conformers were found within a 3.0 Kcal/mol energy threshold from global minimum. All these conformers were geometrically optimized by density functional theory method at the B3LYP functional

and 6-31G(d) basis set level (see computational details in section 3.4). As shown in Figure 2, the calculated ECD spectrum of 18*R*-**1** matched very well with the experimental one, supporting the 18*R* absolute configuration of **1**. Therefore, the NMR data (see full 1D and 2D NMR spectral data in the Supplementary Materials), ECD/TD-DFT calculations and the positive optical rotation value allowed us to identify **1** as (+)-(7*Z*,12*Z*,18*R*,20*Z*)-variabilin.

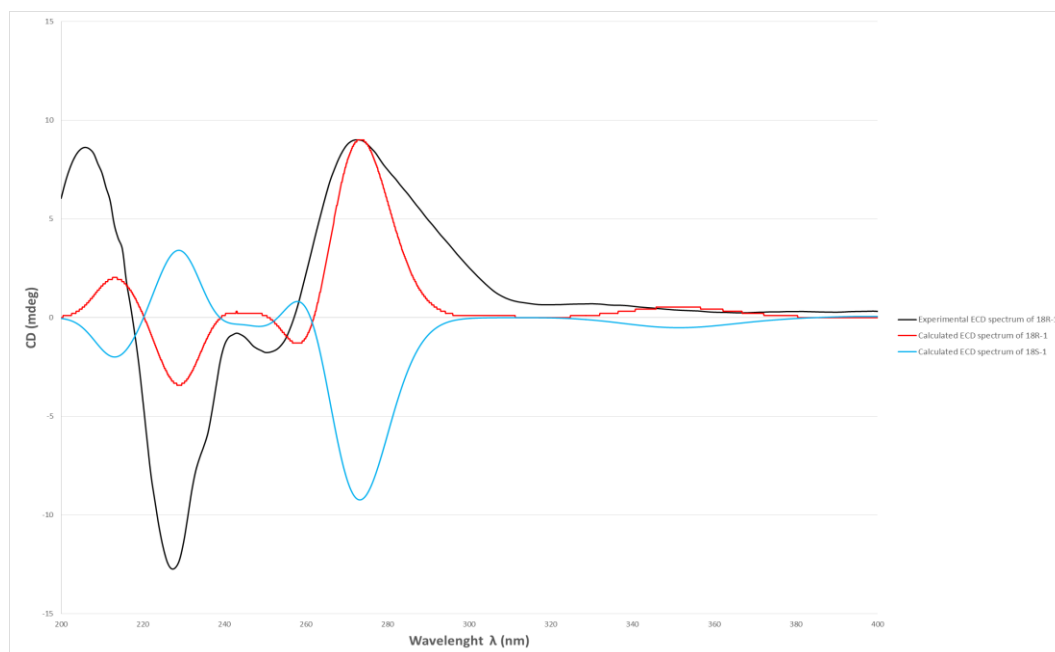


Figure 2. Experimental ECD spectrum of **1** and calculated ECD spectra of 18*R*-**1** and 18*S*-**1**.

The molecular formula of the white powder compound **4** was determined as $C_{33}H_{43}NO_4$ (13 degrees of unsaturation) with the aid of its (+)-HRESIM spectrum and ^{13}C NMR data. The ^{13}C NMR spectrum shows 33 signals (see Table 1) owing to nine sp^2 non-protonated carbons, including an amide (δ_C 172.7) and a lactone (δ_C 171.8), nine sp^2 methine, ten sp^3 methylene, one sp^3 methine carbons and four methyl groups.

The NMR data of **4** were very similar to those of compound **1**. The tetronic acid moiety was unambiguously located at one end, in addition to a linear polyprenyl chain bearing three double bonds at positions Δ^7 , Δ^{12} and Δ^{20} as in (7*Z*,12*Z*,18*R*,20*Z*)-variabilin (**1**). Thus, the *Z* geometry for the three double bonds in **4** was confirmed by the characteristic carbon chemical shifts of C-9, C-14 and C-20 at δ_C 23.8, 23.7 and 115.0, respectively [22]. Furthermore, NOESY correlations between the olefinic proton H-7 at δ_H 5.07/C-9 Me protons at δ_H 1.68 and the olefinic proton H-12 at δ_H 5.11/C-14 Me protons at δ_H 1.64, confirmed the *Z* geometry at Δ^7 and Δ^{12} .

Analysis of the 1H - 1H COSY and DEPT-135 edited HSQC spectra revealed the presence of a phenyl ring displaying the characteristic carbon signals at the δ_C 127–140 region and the corresponding proton signals around δ_H 7.20. Furthermore, the presence of an α,β -unsaturated- γ -lactam was deduced by the diagnostic resonances for carbons at δ_C 52.3, 136.5, 139.3 and 172.7 and for protons at δ_H 3.73 m and 6.65 (t, $J = 1.4$ Hz) as well as its connection to the phenyl ring through the nitrogen to two methylene groups by combined 2D-NMR experiments. Thus, long-range HMBC correlations from H-1 at δ_H 3.73 to C-2 and C-3, from H-2 at δ_H 6.65 to C-4, and from H-1' at δ_H 3.72 to C-1, C-4 and C-2' confirmed the presence of a phenethylamine lactam moiety in **4** instead of a furan ring in **1**. The connection between the polyprenyl portion and the phenethylamine lactam

group was secured by the HMBC correlation between H-6 at δ_{H} 2.23–2.17 and C-3 at δ_{C} 139.3 (Figure 3). The γ -lactam regiochemistry in **4** was deduced by the diagnostic proton chemical shift of the olefinic H-2 at δ_{H} 6.65 and by a key HMBC correlation between H-5 at δ_{H} 2.24 and C-4 at δ_{C} 172.7.

The 18*R* configuration in **4**, suggested from its positive specific optical rotation value of $[\alpha]_{\text{D}}^{25} + 3.4$, was confirmed in this case by comparison of the experimental and calculated ECD spectrum generated by TDDFT on model 1 (Figure S32) [23]. The initial systematic conformation search with the Maestro program for model **4** gave 11 conformers within a 3.0 Kcal/mol window, which were geometrically optimized at DFT level using the combination HSEH1PBE/cc-pVDZ. 9 conformers of each enantiomer were subjected to theoretical calculation of ECD using TD-DFT at TD-SCF-PBEPBE functional and 6-311G++(3d,2p) basis set in chloroform as solvent. The ECD spectrum of model **4** was simulated. The theoretical curve of model **4** matched to that of the experimental one, confirming the 18*R* absolute configuration in **4**. With all these spectroscopic data on hand, the chemical structure for compound **4** was assigned as depicted in Figure 1. This new member of the ircinialactam family was named (+)-ircinialactam J. Its structure is similar to ircinialactam I but differs in the configuration of Δ^7 and Δ^{12} double bonds and the Me group at C-18 [24].

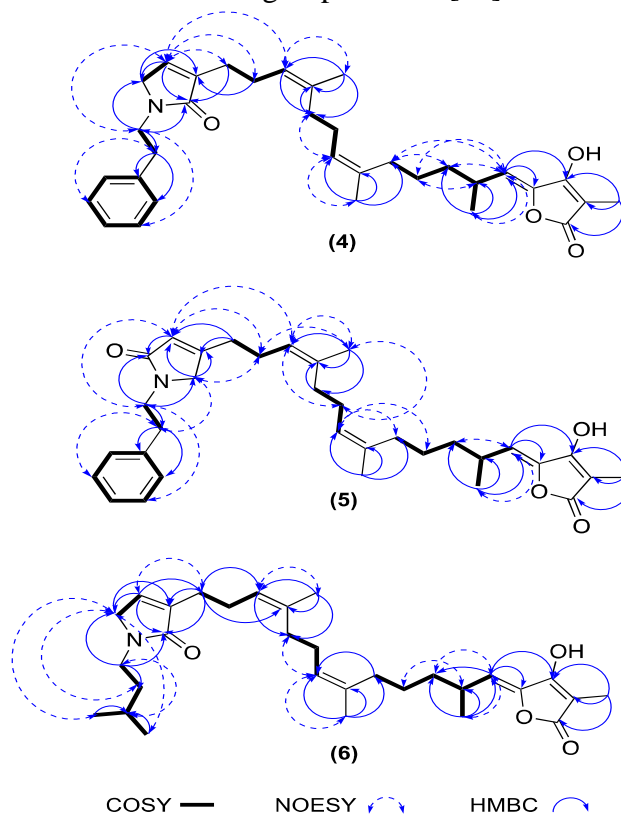


Figure 3. Selected 2D NMR correlations for ircinialactams J-L(**4–6**).

Another sesterterpene lactam, named ircinialactam K (**5**), showed the same molecular formula $\text{C}_{33}\text{H}_{43}\text{NO}_4$ as compound **4**, based on its HRESIM spectrum. The NMR data of **5** (Tables 1 and 2) are very similar to those of **4**, except those chemical shifts corresponding to the γ -lactam moiety. The different γ -lactam regiochemistry of **5** in relation to **4** was deduced by the diagnostic proton chemical shift of the olefinic H-2 in **5** at δ_{H} 5.79 instead of that in **4** at δ_{H} 6.65 and by the key NOESY correlation between H-4 at δ_{H} 3.73 and H-6 at δ_{H} 2.25 found in **5** (Figure 2). The γ -lactam regiochemistry was confirmed by the characteristic carbon resonances at δ_{C} 173.4 (C-1), 120.5 (C-2), 161.5

(C-3) and 56.3 (C-4), which are similar to those reported for ircinialactam B and G obtained from *Sarcotragus* sp. and *Psammocinia* sp., respectively [24] (both belonging to the same family as *Ircinia*), and 8-hydroxyircinialactam B isolated from an *Ircinia* sp. [22]. After interpretation of the NMR spectra, compound **5** was established as a γ -lactam regioisomer of compound **4**. The absolute configuration of **5** at C-18 was deduced as *R* on the basis of its positive optical rotation value of $[\alpha]_D^{25} +6.45$ and comparison of the ECD spectrum of **5** with that of **4** (Figure S32).

Table 1. ^{13}C NMR data of **4–6** in CDCl_3 (125 MHz, δ in ppm).

Position	4	5	6
1	52.3, CH	173.4, qC	51.4, CH
2	136.5, CH	120.5, CH	136.2, CH
3	139.3, C	161.5, qC	139.3, qC
4	172.7, C	56.3, CH ₂	172.5, qC
5	26.3, CH ₂	29.7, CH ₂	26.8, CH ₂
6	25.6, CH ₂	25.9, CH ₂	25.6, CH ₂
7	123.5, CH	123.1, CH	123.4, CH
8	137.0, qC	137.5, qC	137.0, qC
9	23.8, CH ₃	23.6, CH ₃	23.8, CH ₃
10	32.8, CH ₂	32.1, CH ₂	32.7, CH ₂
11	26.8, CH ₂	26.4, CH ₂	26.3, CH ₂
12	125.0, CH	124.6, CH	125.0, CH
13	135.9, qC	136.2, qC	135.9, qC
14	23.7, CH ₃	23.6, CH ₃	23.7, CH ₃
15	32.0, CH ₂	32.9, CH ₂	32.0, CH ₂
16	26.4, CH ₂	26.3, CH ₂	26.4, CH ₂
17	37.5, CH ₂	37.7, CH ₂	37.5, CH ₂
18	31.1, CH	31.2, CH	31.1, CH
19	21.2, CH ₃	21.1, CH ₃	21.2, CH ₃
20	115.0, CH	114.4, CH	115.0, CH
21	143.7, qC	143.9, qC	143.6, qC
22	162.8, qC	162.8, qC	162.8, qC
23	99.6, qC	99.4, qC	99.4, qC
24	171.8, qC	171.8, qC	171.8, qC
25	6.4, CH ₃	6.4, CH ₃	6.4, CH ₃
1'	44.8, CH ₂	44.1, CH ₂	41.3, CH ₂
2'	35.1, CH ₂	35.1, CH ₂	37.5, CH ₂
3'	138.4, qC	138.4, qC	26.0, CH
4'	128.9, CH	128.9, CH	22.5, CH ₃
5'	128.8, CH	128.7, CH	22.6, CH ₃
6'	126.9, CH	126.9, CH	
7'	128.8, CH	128.7, CH	
8'	128.9, CH	128.9, CH	

Finally, the (+)-HRESIM spectrum of **6** showed the $[\text{M}+\text{Na}]^+$ ion peak at m/z 506.3248, suggesting a molecular formula of $\text{C}_{30}\text{H}_{45}\text{NO}_4$. The ^1H and ^{13}C NMR spectral data of **6** resemble to those of **4** (see Table 1 and 2). More specifically, the tetronic acid,

the polyprenyl chain and the γ -lactam ring of **4** are the same as those of **6**, as deduced by COSY, HSQC and HMBC correlations. However, the *N*-phenethyl substituent on the γ -lactam ring in **4** was replaced by the *N*-isopentenyl group in **6** as evidenced by the ^1H and ^{13}C NMR spectra, which exhibited two methyl groups at δ_{H} 0.94 (d, $J = 6.5$ Hz)/ δ_{C} 22.5 & 22.6, linked to a methine group at δ_{H} 1.57 m/ δ_{C} 26.0 and this in turn to an ethyl group at δ_{H} 1.48 m/ δ_{C} 37.5 and δ_{H} 3.51 m/ δ_{C} 41.3. Besides, HMBC correlations from H-1' at δ_{H} 3.51 to C-1 at δ_{C} 51.4, C-4 at δ_{C} 172.5 and C-2' at δ_{C} 37.5 confirmed the presence of *N*-isopentenyl γ -lactam moiety (Figure 3). The γ -lactam regiochemistry in **6** was also deduced by the diagnostic proton chemical shift of the olefinic H-2 at δ_{H} 6.74 and by the key HMBC correlation from H-5 at δ_{H} 2.30 to C-4 at δ_{C} 172.5. Again, the same absolute configuration 18*R* was deduced for **6** from its positive optical rotation value of $[\alpha]_{\text{D}}^{25} +3.4$ and by comparison of the ECD spectrum of **6** with those of **4** and **5** (Figure S32). Compound **6** which bears an isopentenyl chain linked to a γ -lactam ring, as in sarcotrine A and its epimer, isolated from a marine sponge *Sarcotragus* sp [25], was therefore named (+)-ircianialactam L.

Table 2. ^1H NMR data of **4–6** in CDCl_3 (500 MHz; δ in ppm, J in Hz).

Position	4	5	6
1	3.73, m		3.92, m
2	6.65, t (1.4)	5.79, m	6.74, m
4		3.73, m	
5	2.24, m	2.31, m	2.30, m
6	2.23, m	2.25, m	2.15, m
	2.17, m		
7	5.07, m	5.03, m	5.08, m
9	1.68, d (1.3)	1.69, m	1.68, d (1.4)
10	1.97, m	1.98, m	1.95, m
11	2.03, m	2.01, m	2.09, m
12	5.11, m	5.11, m	5.11, m
14	1.64, d (1.2)	1.66, m	1.64, d (1.6)
15	2.00, m	1.97, m	1.95, m
16	1.44, m	2.01, m	1.26, m
	1.28, m		1.43, m
17	1.30, m	1.30, m	1.26, m
	1.43, m	1.43, m	1.43, m
18	2.83, m	2.81, m	2.82, m
19	1.05, d (6.7)	1.04, m	1.05, d (6.7)
20	5.49, d (10.1)	5.31, m	5.48, d (10.2)
25	1.83, s	1.80, s	1.82, s
1'	3.72, m	3.71, m	3.51, m
2'	2.91, t (7.3)	2.91, t (7.3)	1.48, m
3'			1.57, m
4'	7.29, m	7.31, m	0.94, d (6.5)
5'	7.19, m	7.21, m	0.94, d (6.5)
6'	7.21, m	7.25, m	
7'	7.19, m	7.19, m	
8'	7.29, m	7.29, m	

Putative biosynthetic pathway for the lactam functionality derived from the furan moiety as precursor has been speculated. Accordingly, the oxidation of the furan ring affords a mono-epoxide intermediate that after several transformations yields a lactone, which can further react with the suitable free amino acids producing the corresponding γ -lactams [24].

2.2 Antiviral activity

Antiviral assays against HAdV at low multiplicity of infection (MOI) (0.06 vp/cell) showed that both (7Z,12Z,18R,20Z)-variabilin (**1**) and ircinialactam J (**4**) exhibit significant inhibition of HAdV5 (species C) infection in a dose-dependent manner in human embryonic kidney *293 β 5 cells* (Figure 4A, 4B), with IC₅₀ values of 6.30 μ M and 5.23 μ M, respectively (Table 3). These IC₅₀ values were significantly lower than those shown by cidofovir, the drug of choice to treat HAdV infections (Table 3). As for the cellular cytotoxicity, **1** and **4** did not significantly alter cell viability as determined by the Alamar Blue Cell Viability Assay at concentrations < 50 μ M (Table 3). The cytotoxic concentration 50% (CC₅₀) for **1** and **4** are >200 and 139.45 μ M, respectively, significantly higher than the concentrations for their antiviral activity and in the same range to the CC₅₀ obtained for cidofovir, whose CC₅₀ value is 181.24 μ M (Table 3).

Table 3. CC₅₀, IC₅₀ and selective index (SI) values for **1**, **4** and cidofovir.

Compound	IC ₅₀ Plaque assay	Selective Index (SI)	CC ₅₀
1	6.30 \pm 0.70	>31.7	> 200
4	5.23 \pm 3.77	26.6	139.45 \pm 36.46
Cidofovir	24.36 \pm 6.09	7.4	181.24 \pm 35.10

Compounds **1** and **4** also reproducibly inhibited HAdV infection in a dose-dependent manner at high MOI (2,000 vp/cell) in a single round infection assay, showing IC₅₀ values of 35.50 and 11.49, respectively (Fig. 4C, 4D). Although not conclusive, the results obtained with this entry assay suggest that their mechanism of action could be related with early steps in the HAdV replicative cycle. After binding and internalization, the viral particles induce the lysis of the endosome by the exposure of the protein VI, a lytic protein, and then the partially uncoated HAdV capsid escapes to the cytoplasm. Once in the cytosol, HAdV is transported to the nuclear membrane where the viral genome is delivered into the nucleus to be processed for the generation of a new viral progeny. Our entry assay indicates that the treatment with **1** and **4** was inhibiting expression of the HAdV5-GFP transgene, suggesting inhibition of an early event before transcription and replication of HAdV genes since the vector used is a non-replicative virus, with the GFP reported gene replacing regions E1 and E3 of the HAdV genome.

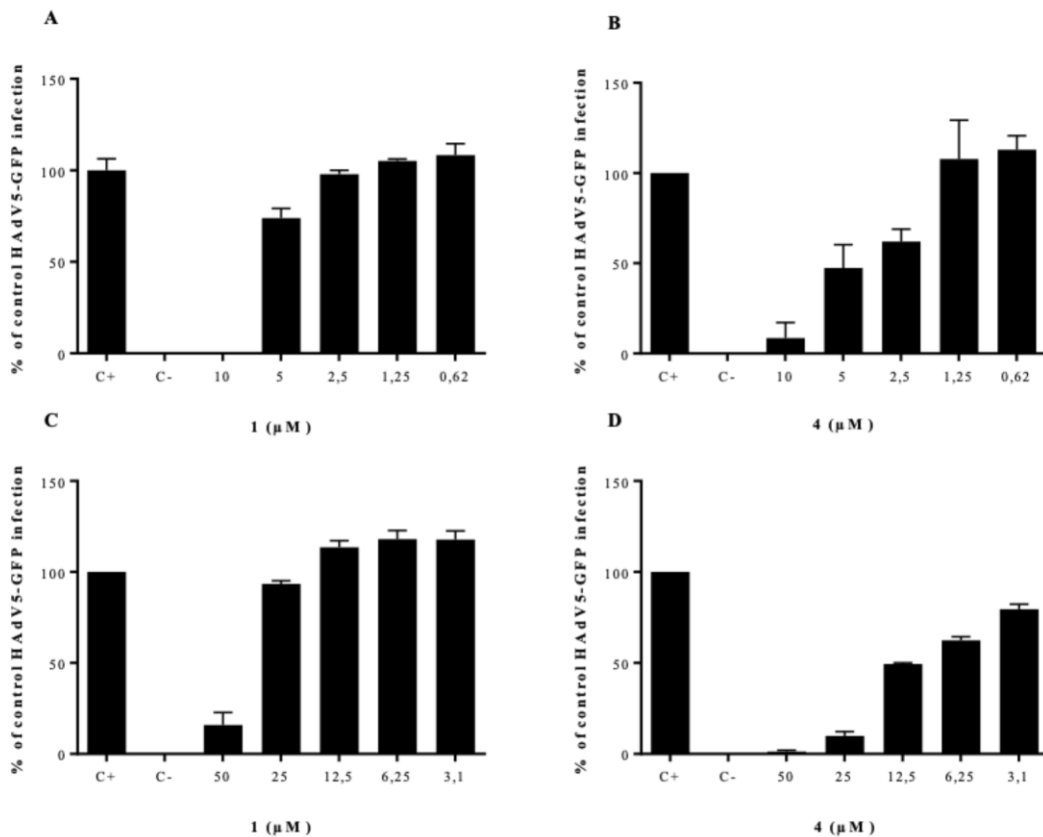


Figure 4. Inhibitory activity of **1** and **4**. The dose-dependent activity of **1** (A) and **4** (B) at low MOI on HAdV5-GFP in a plaque assay using the 293β5 cell line. Antiviral effects of **1** (C) and **4** (D) at high MOI in a single round infection assay using HAdV5-GFP on A549 cell line. For all panels, the negative control (-) is non-infected cells, while the positive control (+) is cells infected at the same MOI but in the absence of the compound. Data are presented as the mean ± SD from triplicate assays.

To gain a mechanistic insight of inhibition and establish if their activity was targeting early or late steps in the HAdV replicative cycle, **1** and **4** were further evaluated for their effect on the *de novo* HAdV DNA synthesis. A quantitative real-time PCR (qPCR) to measure the HAdV5 DNA replication was performed to measure HAdV DNA replication in the presence of **1** and **4** in a 24 h assay to avoid the impact of newly generated viral articles from subsequent rounds of infection. The presence of **1** and **4** at 50 μM concentration significantly inhibited ($p < 0.05$) HAdV5 replication by 91.26% and 99.79%, respectively (Figure 5A).

The inhibition in the HAdV DNA replication at the nucleus 24 hpi in the presence of these compounds suggested two possibilities. First, **1** and **4** could block the accessibility of HAdV genomes to the nucleus after endosomal escape. Second, they may be involved in the inhibition of HAdV replication by blocking a specific protein involved in this process, such as the DNA polymerase, or alternatively they could block transcription of the early genes, a prerequisite for DNA replication. To identify the exact moment in the HAdV replicative cycle at which **1** and **4** were acting, we decided to evaluate if the presence of these compounds affected nuclear delivery of HAdV genomes. At 45 min pi, there was a significant ($p < 0.05$) difference in the amount of HAdV5 DNA isolated from the nucleus of cells treated with **1** and **4** versus those treated with DMSO (Figure 5B). Altogether, the mechanistic assays performed suggested that both **1** and **4**

were targeting an early step of the HAdV replicative cycle before HAdV genomes reached the nucleus of the host cell.

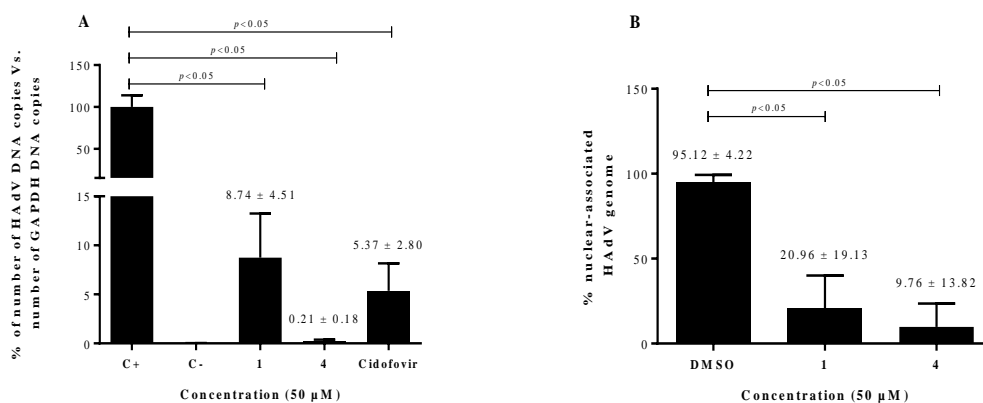


Figure 5. Inhibition of an early step of the HAdV replicative cycle. Compounds **1** and **4** significantly reduced de novo production of HAdV5 DNA copies compared to a positive control 24 h post-infection in a quantitative PCR assay (A). The presence of **1** and **4** significantly reduced the access of HAdV5 genomes to the nucleus (B). For all panels, the negative control (-) is non-infected cells, while the positive control (+) is cells infected at the same MOI but in the absence of the compound. Data are presented as the mean ± SD from triplicate assays.

In summary, three new sesterterpene lactams (**4–6**), together with three known sesterterpene furans (**1–3**), were isolated from the organic extract of the marine sponge *Ircinia felix*. Biological evaluation of these compounds displayed that **1** and **4** exhibited significant anti-HAdV activity that could lead to the optimization and clinical development of new molecules with anti-HAdV activity. The mechanism by which **1** and **4** block HAdV infections seems to be related with the entrance of the virus into the cell, but further studies will be necessary to verify their mechanisms of action. These two molecules may be used as prototypes for the optimization of a new set of antiviral molecules that could lead to the clinical development of a new anti-HAdV drug with high efficacy and low toxicity to be used for treatment of infections by this pathogen. Moreover, these results support the importance of further research of marine organisms for the discovery of new bioactive molecules with antiviral properties among others.

3. Material and Methods

3.1. General Experimental Procedures

Optical rotations were measured on a JASCO DIP-1000 polarimeter, with a Na (589 nm) lamp and filter. UV spectra were measured on a JASCO V-650 spectrophotometer. IR spectra were measured on a FTIR Bruker Vector 22 spectrometer. ^1H , ^{13}C , and 2D NMR spectra were recorded on a Bruker Avance 500 spectrometer at 500.13 and 125.0 MHz, respectively, using CDCl_3 . LRESIMS and HRESIMS experiments were performed on the Applied Biosystems QSTAR Elite system. HPLC separations were performed on the Agilent 1100 liquid chromatography system equipped with a solvent degasser, quaternary pump, and diode array detector (Agilent Technologies, Waldbronn, Germany). Precoated silica gel plates (Merck, Kieselgel 60 F254, 0.25 mm) were used for TLC analysis and the spots were visualized under a UV light (254 nm) or by heating the plate pretreated with $\text{H}_2\text{SO}_4/\text{H}_2\text{O}/\text{AcOH}$ (1:4:20).

3.2 Animal Material

The marine sponge *Ircinia felix* was collected by hand and traditional scuba-diving in the coast of Mexican Caribbean (18°48'13.49"N / 87°39'22.32"W) at depths ranging from 10 to 15 meters in March 2017 and frozen immediately after collection. A voucher specimen was deposited in the Phylum Porifera Gerardo Green National Collection of the Instituto de Ciencias del Mar y Limnología (ICMyL) at the National Autonomous University of Mexico (UNAM).

3.3 Extraction and Isolation

Sliced bodies of *Ircinia felix* (wet weight, 422.2 g; dry weight, 115.5 g) were exhaustively extracted with CH₃OH-CH₂Cl₂ (1:1, 3 x 1.5 L) at room temperature. The combined extracts were concentrated under reduced pressure to give 50.2 g of a dark green crude residue that was first partitioned between CH₂Cl₂/H₂O (1:1 v/v). The resulting aqueous portion was extracted with *n*-butanol (200 mL) to yield the *n*-butanol fraction (12.6 g). The organic phase was concentrated under reduced pressure and partitioned between 10% aqueous CH₃OH (400 mL) and hexane (2 x 400 mL). The H₂O content (% v/v) of the methanolic fraction was adjusted to 50% aqueous CH₃OH, and this mixture was extracted with CH₂Cl₂ (100 mL).

The *n*-butanol fraction was subjected to Solid Phase Extraction (SPE) with RP-18 (Merck KGaA) using a stepped gradient from H₂O (100%) to CH₃OH (100%) and then CH₂Cl₂. The fractions eluted with H₂O/CH₃OH (1:1 and 1:2 v/v) were concentrated under reduced pressure and submitted to HPLC separation using a semipreparative reversed-phase Luna C18 (250 mm x 10 mm, 5 μm) column with a mobile phase consisting of an isocratic at 80% CH₃CN in H₂O (v/v, each containing 0.04% formic acid) over 25 min, followed by a 5 min gradient from 80% to 70% of CH₃CN in H₂O and, finally, a 15 min isocratic at 70 % of CH₃CN, at a flow rate of 2.0 mL/min.

Separation of the fraction eluted with H₂O/CH₃OH (1:1, 140 mg) by HPLC under the above-described conditions yielded **3** (12.4 mg; *t_R* = 14.0 min), **4** (4.3 mg; *t_R* = 19.7 min), and **5** (8.5 mg; *t_R* = 23.2 min). Fraction eluted with H₂O/CH₃OH (1:2, 303.2 mg) was purified by HPLC under the same conditions to yield **1** (21.0 mg; *t_R* = 34.0 min), **2** (20.5 mg; *t_R* = 42.6 min) and **6** (17.5 mg; *t_R* = 39.6 min).

3.4 Computational calculations

Conformational searches were performed by using the corresponding module implemented in the Maestro Quantum mechanical software. OPLS 2005 force field with chloroform as solvent were used, and torsional enhanced sampling with 1000 or 10000 steps were fixed using an energy window of 3 kcal/mol. Molecular geometry optimizations were performed at the DFT theoretical level using the Gaussian 09W package firstly with a B3LYP/6-31G(d) combination and then with HSEH1PBE/cc-pVDZ auto for energy and frequencies calculations. After removing redundant conformers, theoretical Boltzmann energy population-weighted ECD was calculated by using two combinations: PBEPBE/6-311++(3d,2p) or CAM-B3LYP/6-311++(3d,2p) both with 24 states. Graphical theoretical ECD curves were obtained using the open software SpecDis V.1.71 [26].

3.5 Metabolite characterization

(+)-(7Z,12Z,18R,20Z)-variabilin (**1**): yellow oil; [α]_D²⁵ + 39.9 (c 0.1, MeOH); ¹H NMR (500 MHz) and ¹³C NMR (125 MHz) see Table S1; (+)-HRESIMS *m/z* 421.2366 [M + Na]⁺ (calcd. for C₂₅H₃₄O₄Na, 421.2349).

(7E,12E,18R,20Z)-variabilin (2): yellow oil; $[\alpha]_D^{25} + 24.8$ (c 0.1, MeOH); (+)-HRESIMS m/z 421.2376 $[M + Na]^+$ (calcd. for $C_{25}H_{34}O_4Na$, 421.2349).

(12E,18R,20Z)-8-hydroxyvariabilin (3): yellow solid; $[\alpha]_D^{25} + 37.4$ (c 0.15, MeOH); (+)-HRESIMS m/z 439.2475 $[M + Na]^+$ (calcd. for $C_{25}H_{36}O_5Na$, 439.2455).

(+)-Ircinialactam J (4): yellow solid; $[\alpha]_D^{25} + 3.4$ (c 0.25, MeOH); UV (MeOH) λ_{max} 220 nm; IR(ATR) ν_{max} 3505, 2950, 2910, 2856, 1755, 1730, 1670, 1430, 1371, 1229, 1120, 1050, 1038, 955, 936, 916, 882, 850, 811, 743 cm^{-1} ; 1H NMR (500 MHz) see Table 2 and ^{13}C NMR (125 MHz) see Table 1; (+)-HRESIMS m/z 540.3119 $[M + Na]^+$ (calcd. for $C_{33}H_{43}NO_4Na$, 540.3090).

(+)-Ircinialactam K (5): yellow solid; $[\alpha]_D^{25} + 6.4$ (c 0.2, MeOH); UV (MeOH) λ_{max} 220 nm; IR(ATR) ν_{max} 3505, 2950, 2910, 2856, 1775, 1730, 1670, 1440, 1391, 1229, 1120, 1050, 1038, 955, 929, 916, 882, 850, 811, 743 cm^{-1} ; 1H NMR (500 MHz) see Table 2 and ^{13}C NMR (500 MHz) see Table 1; (+)-HRESIMS m/z 540.3090 $[M + Na]^+$ (calcd. for $C_{33}H_{43}NO_4Na$, 540.3090).

(+)-Ircinialactam L (6): yellow solid; $[\alpha]_D^{25} + 3.4$ (c 0.15, MeOH); UV (MeOH) λ_{max} 220 nm; IR(ATR) ν_{max} 3505, 2950, 2910, 2858, 1775, 1733, 1670, 1440, 1391, 1229, 1120, 1050, 1038, 955, 929, 916, 882, 850, 815, 743 cm^{-1} ; 1H NMR (500 MHz) see Table 2 and ^{13}C NMR (125 MHz) see Table 1; (+)-HRESIMS m/z 506.3248 $[M + Na]^+$ (calcd. for $C_{30}H_{45}O_4Na$, 506.3246).

3.6 Viruses and cells

Human A549 (human lung carcinoma) and 293 (human embryonic kidney) cell lines were from the American Type Culture Collection (ATCC, Manassas, VA). The 293 β 5 stable cell line overexpressing the human β 5 integrin subunit was kindly provided by Dr. Glen Nemerow [27]. Both cell lines were propagated in Dulbecco's modified Eagle medium (DMEM, Life Technologies/Thermo Fisher) supplemented with 10% fetal bovine serum (FBS) (Omega Scientific, Tarzana, CA), 10 mM HEPES, 4 mM L-glutamine, 100 U/ml penicillin, 100 μ g/ml streptomycin, and 0.1 mM non-essential amino acids (complete DMEM). Wild-type HAdV5 was obtained from ATCC. The HAdV5-GFP showed in this work is a replication-defective virus with a CMV promoter-driven enhanced green fluorescent protein (eGFP) reporter gene cassette in place of the E1/E3 region [28]. HAdV were propagated in 293 β 5 cells and isolated from the cellular lysate by cesium chloride (CsCl) density gradient combined with ultracentrifugation. Virus concentration was calculated as previously reported.

3.7 Plaque assay

All natural extracts and purified compounds were dissolved in dimethyl sulfoxide (DMSO) at a stock concentration of 5 mM and stored at -20 °C. Compounds were tested using low MOI infections (0.06 vp/cell) and at concentrations of 10 μ M and in a dose-response assay ranging from 10 to 0.1 μ M in a plaque assay. Briefly, 293 β 5 cells were seeded in 6-well plates at a density of 4×10^5 cells per well in duplicate for each condition. When cells reached 80–90% confluency, they were infected with HAdV5-GFP (0.06 vp/cell) and rocked for 2 h at 37°C. After the incubation the inoculum was removed, and the cells were washed once with PBS. The cells were then carefully overlaid with 4 mL/well of equal parts of 1.6% (water/vol) Difco Agar Noble (Becton, Dickinson & Co., Sparks, MD) and 2 \times EMEM (Minimum Essential Medium Eagle, BioWhittaker) supplemented with 2 \times penicillin/streptomycin, 2 \times L-glutamine, and 10% FBS. The mixture also contained the drugs in concentrations ranging from 10 to 0.625 μ M following incubation for 7 days at 37°C; plates were scanned with a Typhoon 9410 imager

(GE Healthcare Life Sciences), and plaques were quantified with ImageJ [29]. This assay was performed in duplicate.

3.8 Cytotoxicity assay

The cytotoxicity of the compounds was analyzed by the commercial kit AlamarBlue® (Invitrogen, Ref. DAL1025). A549 cells at a density of 5×10^3 cells per well in 96-well plates were seeded. Decreasing concentrations of each derivative (200 μ M, 150 μ M, 100 μ M, 80 μ M, 60 μ M, 40 μ M, 30 μ M, 20 μ M, 10 μ M, 5 μ M, 2.5 μ M, 0 μ M) were diluted in 100 μ L of Dulbecco's Modified Eagle Medium (DMEM). Cells were then incubated at 37°C for 48 hours following the kit protocol. The cytotoxic concentration 50 (CC₅₀) value was obtained using the statistical package GraphPad Prism. This assay was performed in duplicate.

3.9 Entry assay

The anti-HAdV activity was initially measured in an entry assay using human A549 epithelial cells (3×10^5 cells/well in corning black wall, clear bottom 96-well plates) infected with HAdV5-GFP (2000 vp/cell) in the presence 50 μ M of the candidates and in a dose-response assay. A standard infection curve was generated in parallel by infecting cells in the absence of compounds using serial 2-fold dilutions of virus. All reactions were done in triplicate. Cells, viruses, and drugs were incubated for 48 h at 37 °C and 5% CO₂. Infection, as measured by HAdV5-mediated GFP expression, was analyzed using a Typhoon 9410 imager (GE Healthcare Life Sciences) and quantified with ImageQuantTL (GE Healthcare Life Sciences).

3.10 DNA Quantification by Real-Time PCR

A549 cells (1.5×10^5 cells/well in a 24-well plate) were incubated for 24 h in 500 μ L of complete DMEM, and they were infected with wild-type HAdV5 (HAdV5-wt) (100 vp/cell) when more than 90% of confluency were observed. Infected cells were incubated for 24 h at 37°C in 500 μ L of complete DMEM containing 50 μ M of compounds or the same volume of DMSO (positive control). Negative control was treated neither by HAdV nor by compounds. All samples were done in duplicate. After 24 h of incubation at 37°C, DNA was purified from the cell lysate with the QIAamp DNA Mini Kit (QIAGEN, Valencia, CA) following the manufacturer's instructions. TaqMan primers and probes for a common region of the HAdV5 were designed with the GenScript Real-Time PCR (TaqMan) Primer Design software (GenScript). Oligonucleotides sequences were: AQ1: 5'-GCC ACG GTG GGG TTT CTA AAC TT -3'; AQ2: 5'-GCC CCA GTG GTC TTA CAT GCA CAT -3' and Probe: 6-FAM-5'-TGC ACC AGA CCC GGG CTC AGG TAC TCC GA-3'-TAMRA. Real-time PCR mixtures consisted of 9,5 μ L of the purified DNA, AQ1 and AQ2 at a concentration of 200 nM each and Probe at a concentration of 50 nM in a total volume of 25 μ L. The PCR cycling protocol was 95°C for 3 min followed by 40 cycles of 95°C for 10 s and 60°C for 30 s. Human glyceraldehyde-3-phosphate dehydrogenase (GAPDH) gene was used as internal control. Oligonucleotide sequences for GAPDH and conditions were those previously reported by Rivera *et al.* [30].

For quantification, gene fragments from hexon and GAPDH were cloned into the pGEM-T Easy vector (Promega), and known concentrations of template were used to generate a standard curve in parallel for each experiment. All assays were performed in thermal cycler LightCycler® 96 System (Roche).

3.11 Nuclear-associated HAdV genomes

The nuclear delivery of HAdV genomes was assessed by real-time PCR following nuclear isolation from infected cells as previously reported [31]. Briefly, 1×10^6 A549 cells in 6-well plates were infected with wild-type HAdV5 (HAdV5-wt) at MOI 2,000 vp/cell in the presence of 50 μ M of the compounds or the same volume of DMSO for positive control. Forty-five minutes after infection, A549 cells were trypsinized and collected and then washed twice with PBS. Then, cytoplasmic and nuclear fractions were separated using a hypotonic buffer solution and NP-40 detergent. The cell pellet was resuspended in 500 μ L of 1 \times hypotonic buffer (20 mM Tris-HCl pH 7.4, 10 mM NaCl, 3 mM MgCl₂) and incubated for 15min at 4°C. Then, 25 μ L of NP-40 was added and the samples were vortexed. The homogenates were centrifuged for 10 min at 835g at 4°C. Following the removal of the cytoplasmic fraction (supernatant), HAdV DNA was isolated from the nuclear fraction (pellet) and the cytoplasmic fraction using the QIAamp DNA Mini Kit (QIAGEN, Valencia, CA).

3.12 Statistical analyses

Statistical analyses were performed with the GraphPad Prism 5 suite. Data are presented as the mean of duplicate samples \pm standard deviation (SD). $P < 0.05$ was considered statistically significant.

Supplementary Materials: Table S1: NMR data of compound 1 in CDCl₃, Figure S1-S5: NMR spectra of compound 1 in CDCl₃, Figure S6-S7: (+)-ESIMS of compound 1, Table S2: NMR data of ircinialactam J (4) in CDCl₃, Figure S8-S13: NMR spectra of ircinialactam J (4) in CDCl₃, Figure S14-S15: (+)-ESIMS of ircinialactam J (4), Table S3: NMR data of ircinialactam K (5) in CDCl₃, Figure S16-S21: NMR spectra of ircinialactam K (5) in CDCl₃, Figure S22-S23: (+)-ESIMS of ircinialactam K (5), Table S4: NMR data of ircinialactam L (6) in CDCl₃, Figure S24-S28: NMR spectra of ircinialactam L (6) in CDCl₃, Figure S29: NOESY spectrum of ircinialactam L (6) in C₆D₆, Figure S30-S31: (+)-ESIMS of ircinialactam L (6), Figure S32: Comparison of ECD spectra of compounds 4, 5 and 6 in CHCl₃, Figure S33-S38: NMR spectra and (+)-ESIMS of compound 2 and 3.

Author Contributions: Conceptualization, Carlos Jiménez and Javier Sánchez-Céspedes; Data curation, Dawrin Pech-Puch and Judith Berastegui-Cabrera; Formal analysis, Dawrin Pech-Puch, Judith Berastegui-Cabrera, Jaime Rodríguez, Carlos Jiménez and Javier Sánchez-Céspedes; Computational calculations, Jaime Rodríguez, Carlos Jiménez, Dawrin Pech-Puch; Funding acquisition, Jerónimo Pachón, Jaime Rodríguez, Carlos Jiménez and Javier Sánchez-Céspedes; Investigation, Dawrin Pech-Puch, Judith Berastegui-Cabrera, Ana Serna-Gallego and Patricia Gómez; Methodology, Jaime Rodríguez, Carlos Jiménez and Javier Sánchez-Céspedes; Project administration, Jaime Rodríguez, Carlos Jiménez and Javier Sánchez-Céspedes; Resources, Jerónimo Pachón, Jaime Rodríguez, Carlos Jiménez and Javier Sánchez-Céspedes; Supervision, Jaime Rodríguez, Carlos Jiménez and Javier Sánchez-Céspedes; Validation, Javier Sánchez-Céspedes; Visualization, Dawrin Pech-Puch, Judith Berastegui-Cabrera and Javier Sánchez-Céspedes; Writing – original draft, Dawrin Pech-Puch and Judith Berastegui-Cabrera; Writing – review & editing, Jaime Rodríguez, Carlos Jiménez and Javier Sánchez-Céspedes.

Funding: This work was supported by Grants AGL2015-63740-C2-2-R and RTC-2016-4611-1 from the Ministry of Science, Innovation and Universities of Spain, both co-funded by the FEDER Programme from the European Union and by Plan Nacional de I+D+i 2013-2016 and Instituto de Salud Carlos III, Ministerio de Economía, Industria y Competitividad, Spanish Network for Research in Infectious Diseases (REIPI RD16/0016/0009) – co-financed by “A way to achieve Europe” ERDF, the Instituto de Salud Carlos III, Proyectos de Investigación en Salud (PI15/00489, PI17/01055), and Proyectos de Desarrollo Tecnológico en Salud (DTS17/00130), and the Spanish Adenovirus Network (AdenoNet, BIO2015/68990-REDT). J.S.C. is supported by the “Contract to Access to the Spanish System of Research and Innovation of the Program of R+D+i of the University of Seville” (USE-13901-D) grant. DPP received a fellowship from the program National Council of Science and Technology (CONACYT) of Mexico and the Secretariat of Research, Innovation and Higher Education (SIIES) of Yucatan.

Acknowledgments: We gratefully acknowledge the help of colleagues, Daniel Catzim Pech, Carlos González-Salas, Gabriel González Mapen, Jorge Peniche Pérez, Melissa Ilanes López and Rodrigo Garcia Uribe for collecting the marine samples.

References

1. Lion, T., Adenovirus infections in immunocompetent and immunocompromised patients. *Clinical microbiology reviews* **2014**, *27*, 441–462.
2. HAdV_Working_Group <http://hadvbwg.gmu.edu/>.
3. Qiu, F. Z.; Shen, X. X.; Zhao, M. C.; Zhao, L.; Duan, S. X.; Chen, C.; Qi, J. J.; Li, G. X.; Wang, L.; Feng, Z. S.; Ma, X. J., A triplex quantitative real-time PCR assay for differential detection of human adenovirus serotypes 2, 3 and 7. *Viol. J.* **2018**, *15*, 81–86.
4. Grosso, F.; Stoilov, P.; Lingwood, C.; Brown, M.; Cochrane, A., Suppression of Adenovirus Replication by Cardiotonic Steroids. *J. Virol.* **2017**, *91*, e01623-1.
5. Yu, H. X.; Zhao, M. M.; Pu, Z. H.; Wang, Y. Q.; Liu, Y., Clinical data analysis of 19 cases of community-acquired adenovirus pneumonia in immunocompetent adults. *Int. J. Clin. Exp. Med.* **2015**, *8*, 19051–19057.
6. Sulejmani, N.; Nagai, S.; Safwan, M.; Rizzari, M. D.; Raoufi, M.; Abouljoud, M. S.; Ramesh, M., Brincidofovir as Salvage Therapy for Adenovirus Disease in Intestinal Transplant Recipients. *Pharmacotherapy* **2018**, *38*, 470–475.
7. Paolino, K.; Sande, J.; Perez, E.; Loechelt, B.; Jantausch, B.; Painter, W.; Anderson, M.; Tippin, T.; Lanier, E. R.; Fry, T.; DeBiasi, R. L., Eradication of disseminated adenovirus infection in a pediatric hematopoietic stem cell transplantation recipient using the novel antiviral agent CMX001. *J. Clin. Virol.* **2011**, *50*, 167–170.
8. Gogineni, V.; Schinazi, R. F.; Hamann, M. T., Role of Marine Natural Products in the Genesis of Antiviral Agents. *Chem. Rev.* **2015**, *115*, 9655–9706.
9. Jiménez, C., Marine Natural Products in Medicinal Chemistry. *ACS Med. Chem. Lett.* **2018**, *9*, 959–961.
10. Crews, P.; Jiménez, C.; O'Neil-Johnson, M., Using spectroscopic and database strategies to unravel structures of polycyclic bioactive marine sponge sesterterpenes. *Tetrahedron* **1991**, *47*, 3585–3600.
11. Martínez, A.; Duque, C.; Sato, N.; Fujimoto, Y., (8Z,13Z,20Z)-Strobilin and (7Z,13Z,20Z)-felinin: New furanosesterterpene tetronic acids from marine sponges of the genus *Ircinia*. *Chem. Pharm. Bull.* **1997**, *45*, 181–184.

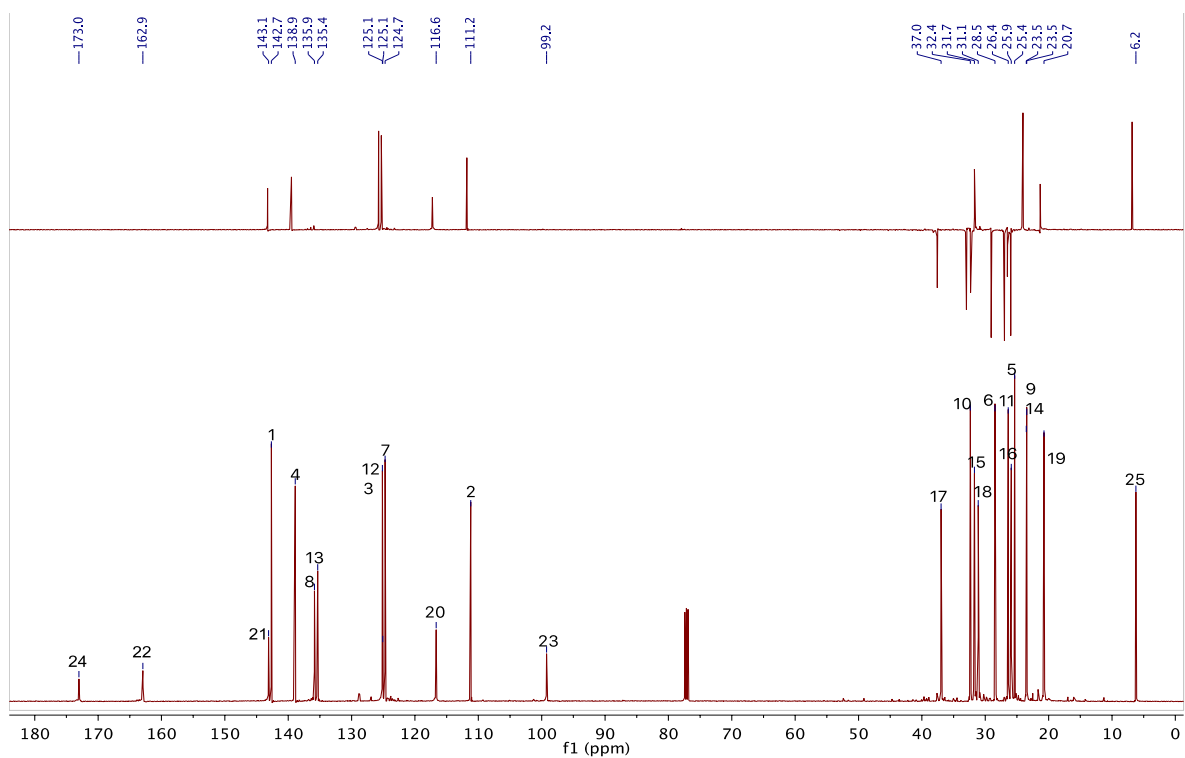
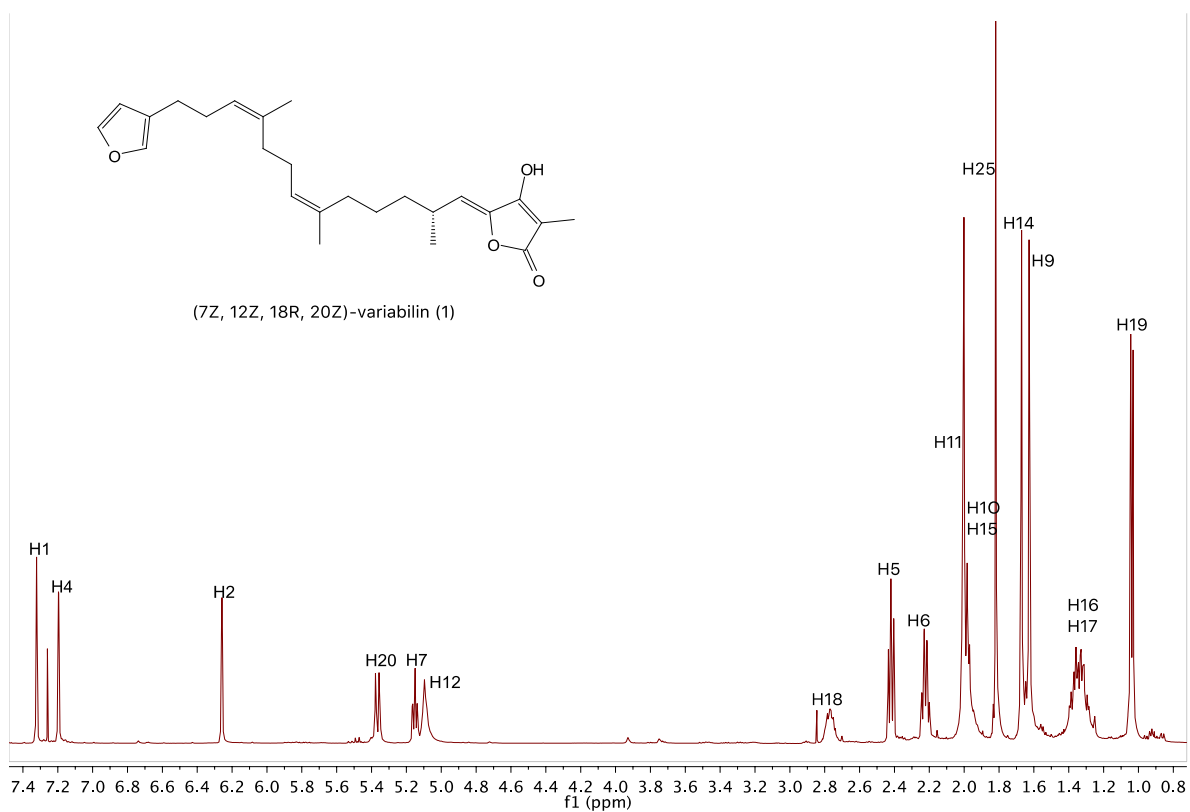
12. Barrow, C. J.; Blunt, J. W.; Munro, M. H. G.; Perry, N. B., Oxygenated furanosesterterpene tetronic acids from a sponge of the genus *Ircinia*. *J. Nat. Prod.* **1988**, *51*, 1294-1298.
13. Lai, Y. Y.; Lu, M. C.; Wang, L. H.; Chen, J. J.; Fang, L. S.; Wu, Y. C.; Sung, P. J., New Scalarane Sesterterpenoids from the Formosan Sponge *Ircinia felix*. *Mar. Drugs* **2015**, *13*, 4296–309.
14. Liu, Y.; Zhang, S.; Jung, J. H.; Xu, T., Bioactive Furanosesterterpenoids from Marine Sponges. *Top. Heterocycl. Chem.* **2007**, *11*, 231-238.
15. Anta, C.; Gonzalez, N.; Rodriguez, J.; Jimenez, C., A new secosterol from the Indonesian octocoral *Pachyclavularia violacea*. *J. Nat. Prod.* **2002**, *65*, 1357–1359.
16. Anta, C.; Gonzalez, N.; Santafe, G.; Rodriguez, J.; Jiménez, C., New Xenia diterpenoids from the Indonesian soft coral *Xenia* sp. *J. Nat. Prod.* **2002**, *65*, 766–768.
17. Rodríguez, J.; Jiménez, C.; Blanco, M.; Tarazona, G.; Fernández, R.; Cuevas, C., Lanosoic Acid: A Cytotoxic Zwitterion from *Theonella* sp. *Org Lett* **2016**, *18*, 5832–5835.
18. Tarazona, G.; Benedit, G.; Fernández, R.; Pérez, M.; Rodríguez, J.; Jiménez, C.; Cuevas, C., Can Stereoclusters Separated by Two Methylene Groups Be Related by DFT Studies? The Case of the Cytotoxic Meroditerpenes Halioxepines. *J. Nat. Prod.* **2018**, *81*, 343-348.
19. González González, A.; López Rodríguez, M.; San Martín Barrientos, A., On the Stereochemistry and Biogenesis of C21 Linear Furanoterpenes in *Ircinia* sp. *J. Nat. Prod.* **1983**, *46*, 256–261.
20. Martinez, A.; Duque, C.; Sato, N.; Tanaka, R.; Fujimoto, Y., (18*R*)-Variabilin from the Sponge *Ircinia felix*. *Nat. Prod. Lett.* **1995**, *6*, 1–6.
21. Barrow, C. J.; Blunt, J. W.; Munro, M. H. G.; Perry, N. B., Variabilin and Related Compounds from a Sponge of the Genus *Sarcotragus*. *J. Nat. Prod.* **1988**, *51*, 275–281.
22. Balansa, W.; Islam, R.; Fontaine, F.; Piggott, A. M.; Zhang, H.; Webb, T. I.; Gilbert, D. F.; Lynch, J. W.; Capon, R. J., Ircinialactams: subunit-selective glycine receptor modulators from Australian sponges of the family Irciniidae. *Bioorg. Med. Chem.* **2010**, *18*, 2912–2919.
23. Chianese, G.; Silber, J.; Luciano, P.; Merten, C.; Erpenbeck, D.; Topaloglu, B.; Kaiser M.; Tasdemir, D. Antiprotozoal linear furanosesterterpenoids from the marine sponge *Ircinia oros*. *Journal of natural products*, **2017** *80*, 2566-2571.
24. Prasad, P.; Zhang, A.; Salim, A. A.; Capon, R. J., Pursuing sesterterpene lactams in Australian Irciniidae sponges. *Fitoterapia* **2018**, *126*, 83–89.
25. Liu, Y.; Hong, J.; Lee, C. O.; Im, K. S.; Kim, N. D.; Choi, J. S.; Jung, J. H., Cytotoxic pyrrolo- and furanoterpenoids from the sponge *Sarcotragus* species. *J. Nat. Prod.* **2002**, *65*, 1307–1314.
26. Noguez, C.; SpecDis: Quantifying the Comparison of Calculated and Experimental Electronic Circular Dichroism Spectra. *Chirality* **2014**, *26*, 553–562.
27. Nguyen, E. K.; Nemerow, G. R.; Smith, J. G., Direct evidence from single-cell analysis that human {alpha}-defensins block adenovirus uncoating to neutralize infection. *J. Virol.* **2010**, *84*, 4041–4049.
28. Nepomuceno, R. R.; Pache, L.; Nemerow, G. R., Enhancement of gene transfer to human myeloid cells by adenovirus-fiber complexes. *Mol. Ther. J. Am. Soc. Gene Therapy* **2007**, *15*, 571–578.

29. Schneider, C. A.; Rasband, W. S.; Eliceiri, K. W., NIH Image to ImageJ: 25 years of image analysis. *Nat. Methods* **2012**, *9*, 671–675.
30. Rivera, A. A.; Wang, M.; Suzuki, K.; Uil, T. G.; Krasnykh, V.; Curiel, D. T.; Nettelbeck, D. M., Mode of transgene expression after fusion to early or late viral genes of a conditionally replicating adenovirus via an optimized internal ribosome entry site in vitro and in vivo. *Virology* **2004**, *320*, 121–34.
31. Schreiner, S.; Martinez, R.; Groitl, P.; Rayne, F.; Vaillant, R.; Wimmer, P.; Bossis, G.; Sternsdorf, T.; Marcinowski, L.; Ruzsics, Z.; Dobner, T.; Wodrich, H., Transcriptional activation of the adenoviral genome is mediated by capsid protein VI. *PLoS Pathog* **2012**, *8*, e1002549.

Supplementary Materials

Table S1. NMR data of compound **1** in CDCl₃ (500 MHz).

no.	δ_C type	δ_H , mult. (<i>J</i> in Hz)	COSY	HMBC
1	142.7, CH	7.32, t (1.7)	2	2
2	111.2, CH	6.26, q (1.7)	1	
3	125.1, qC			
4	138.9, qC	7.20, s (1)		2
5	25.4, CH ₂	2.42, t (7.5)	6	2, 3, 4, 6
6	28.5, CH ₂	2.23, q (7.3)	5, 7	5, 7, 8
7	124.7, CH	5.15, tq(7.1, 1.5)	6	9, 10
8	135.9, qC			
9	23.5, CH ₃	1.63, d(1.3)		7, 8
10	32.4, CH ₂	1.98, m	11	
11	26.4, CH ₂	2.00, m	10, 12	9, 10, 12
12	125.0, CH	5.10, m	11	11
13	135.4, qC			
14	23.4, CH ₃	1.67, q(1.7)		12, 13, 15
15	31.7, CH ₂	1.99, m	16	13, 17
16	25.9, CH ₂	1.34, m	15, 17	17
17	37.0, CH ₂	1.35, m	16, 18	
18	31.1, CH	2.80, bm	17, 19, 20	
19	20.7, CH ₃	1.04, d(6.7)	18	17, 18
20	116.6, CH	5.37, d(10)	18	17, 19, 21, 22
21	143.1, qC			
22	162.9, qC			
23	99.2, qC			
24	173.0, qC			
25	6.2, CH ₃	1.82, s		22, 23, 24



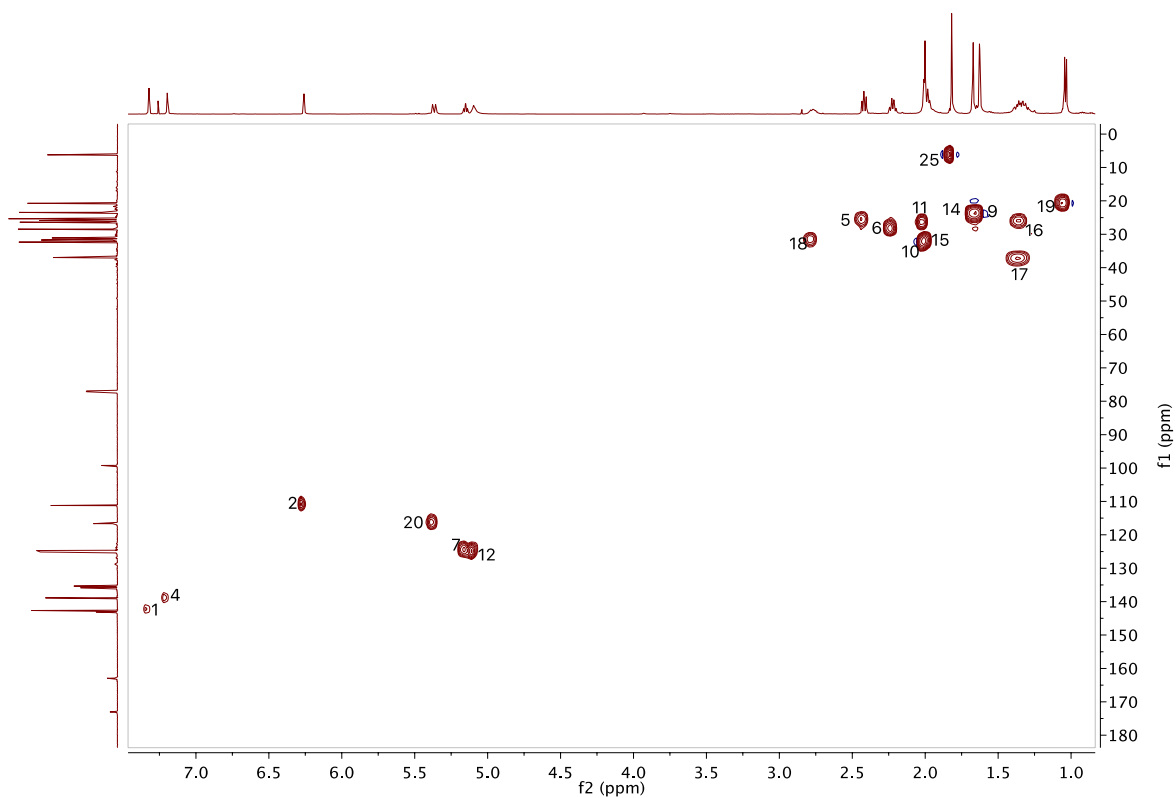


Figure S3. HSQC spectrum of compound **1** (500 MHz, CDCl₃).

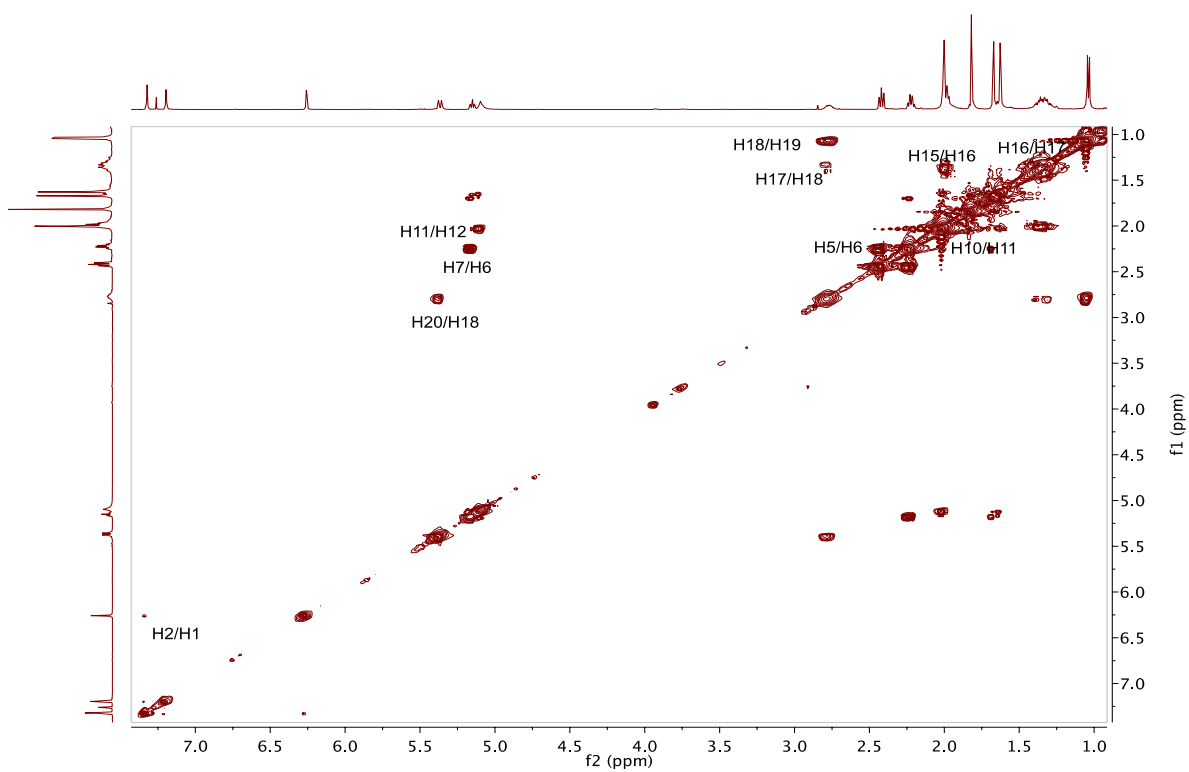


Figure S4. COSY spectrum of compound **1** (500 MHz, CDCl₃).

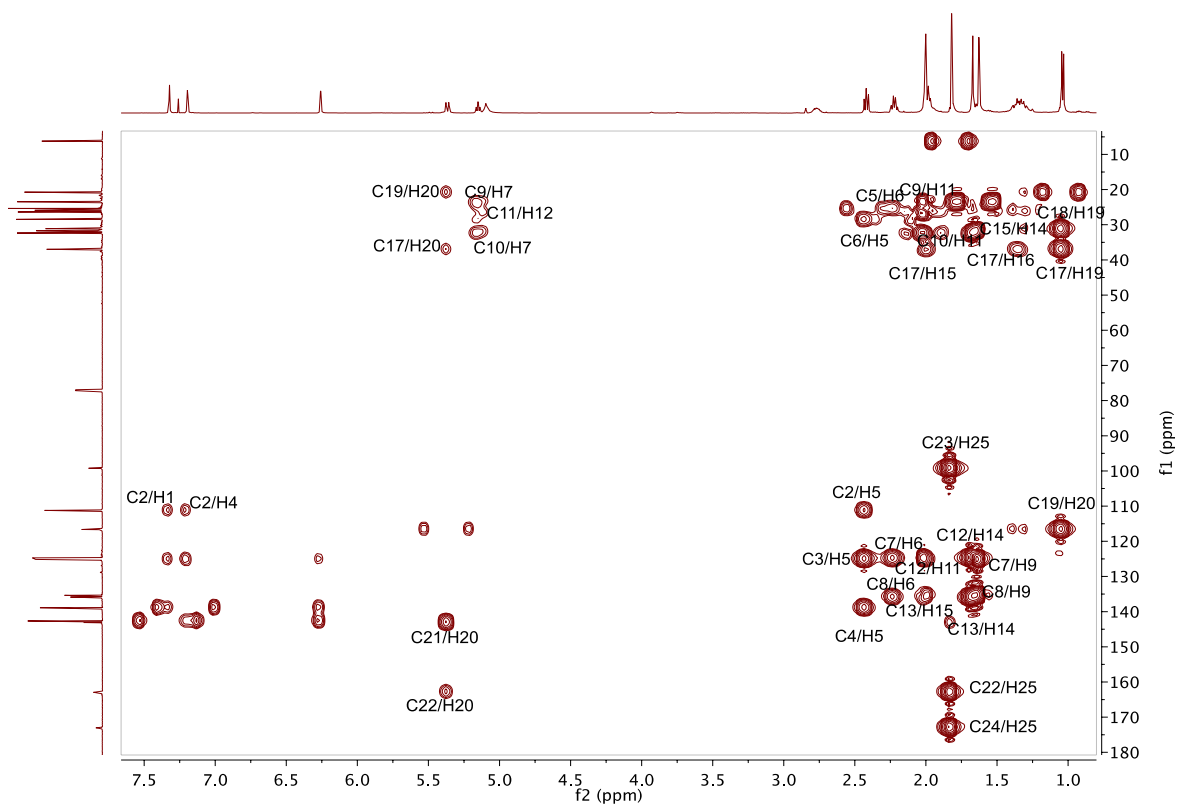


Figure S5. HMBC spectrum of compound **1** (500 MHz, CDCl_3).

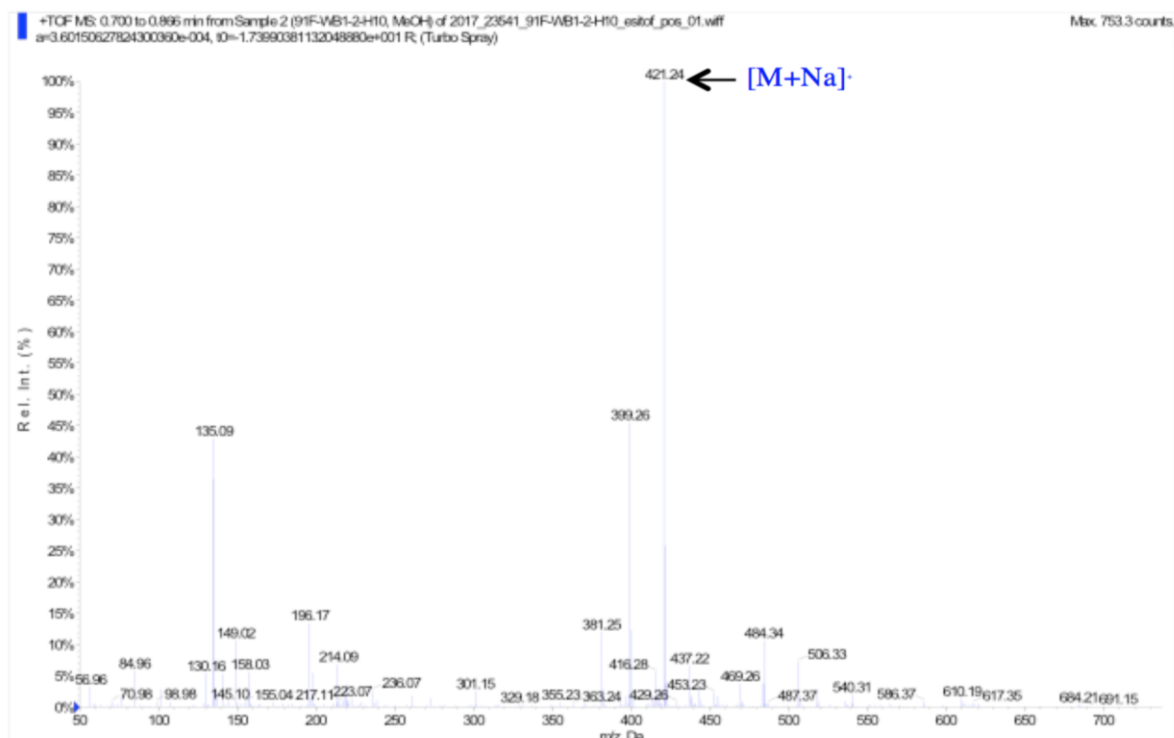


Figure S6. (+)-LRESIMS of compound **1**.

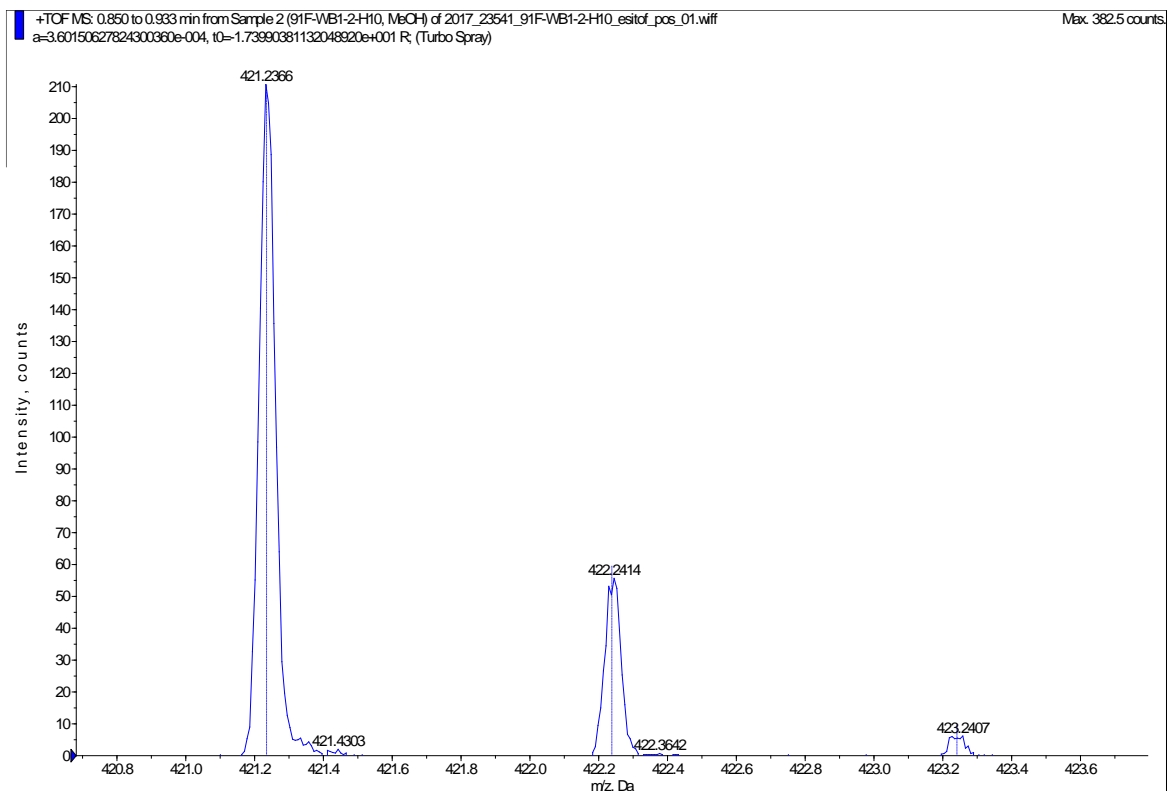


Figure S7. (+)-HRESIMS of compound **1**.

Table S2. NMR data of ircinialactam J (**4**) in CDCl₃ (500 MHz).

no.	δ_C	type	δ_H , mult. (<i>J</i> in Hz)	COSY	HMBC	NOESY
1	52.3	CH	3.73 m	2	2, 3	
2	136.5	CH	6.65 t (1.4)	1	1, 4	1', 5, 6, 7
3	139.3	qC				
4	172.7	qC				
5	26.3	CH ₂	2.24 m	6	4	2, 7
6	25.6	CH ₂	2.23 m 2.17 m	5, 7	3, 7	2, 7
7	123.5	CH	5.07 m	6	10	2, 5, 6, 9
8	137.0	qC				
9	23.8	CH ₃	1.68 d (1.3)		7, 8, 10	7
10	32.8	CH ₂	1.97 m	11	8	12
11	26.8	CH ₂	2.03 m	10, 12	12	12
12	125.0	CH	5.11 m	11	9	10, 11, 14
13	135.9	qC				
14	23.7	CH ₃	1.64 d (1.2)		12, 13, 15	12
15	32.0	CH ₂	2.00 m	16		16, 17, 20
16	26.4	CH ₂	1.44 m 1.28m	15, 17	17	15, 18, 20
17	37.5	CH ₂	1.30m 1.43m	16, 18		15, 18, 20
18	31.1	CH	2.83m	17, 19, 20		16, 17, 20
19	21.2	CH ₃	1.05 d (6.7)	18	17, 18, 20	20
20	115.0	CH	5.49 d (10.1)	18	17, 19, 21, 22	15, 16, 17, 18, 19
21	143.7	qC				
22	162.8	qC				
23	99.6	qC				
24	171.8	qC				
25	6.4	CH ₃	1.83 s		21, 22, 23, 24	
1'	44.8	CH ₂	3.72 m	2'	2', 1, 4	2', 7', 2
2'	35.1	CH ₂	2.91 t (7.3)	1'	1', 3', 8'	1', 5'
3'	138.4	qC				
4'	128.9	CH	7.29 m	5'		
5'	128.8	CH	7.19 m	4', 6'		2'
6'	126.9	CH	7.21 m	5', 7'		
7'	128.8	CH	7.19 m	6', 8'	2', 6'	1'
8'	128.9	CH	7.29 m	7'	3', 7'	

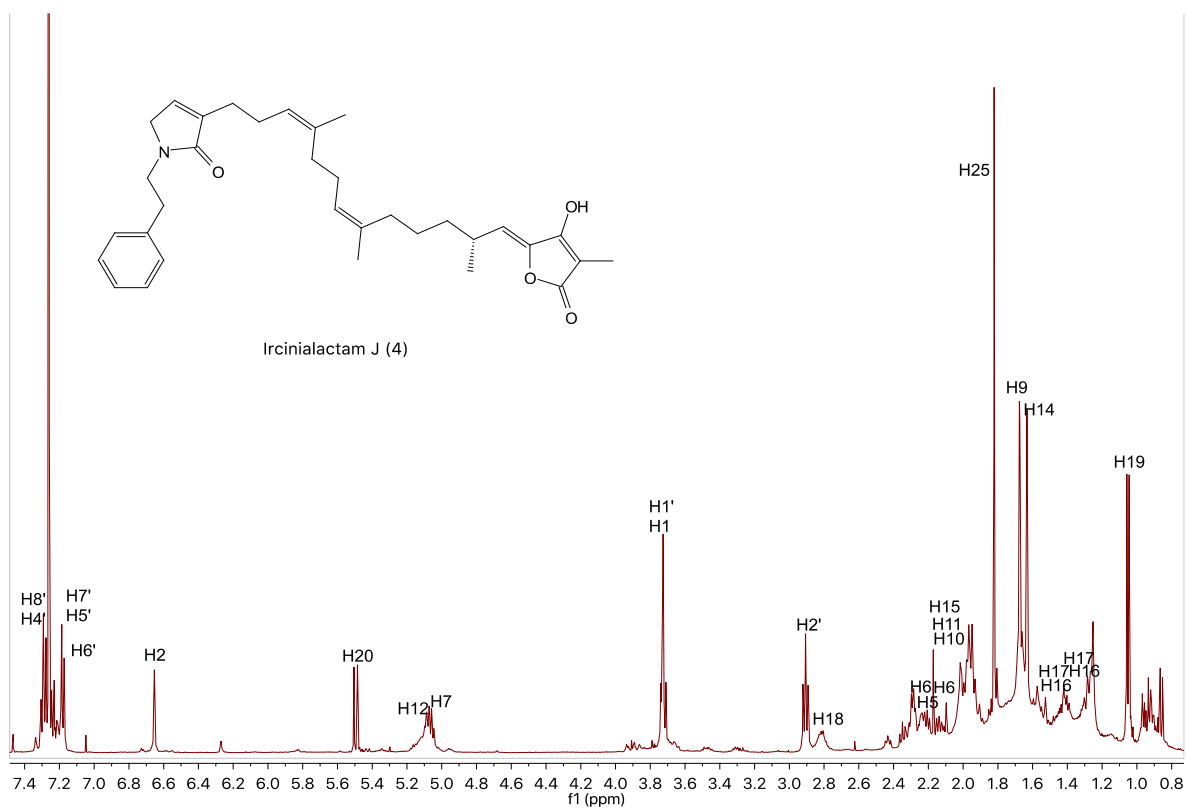


Figure S8. ¹H NMR spectrum of ircinialactam J (4) (500 MHz, CDCl₃).

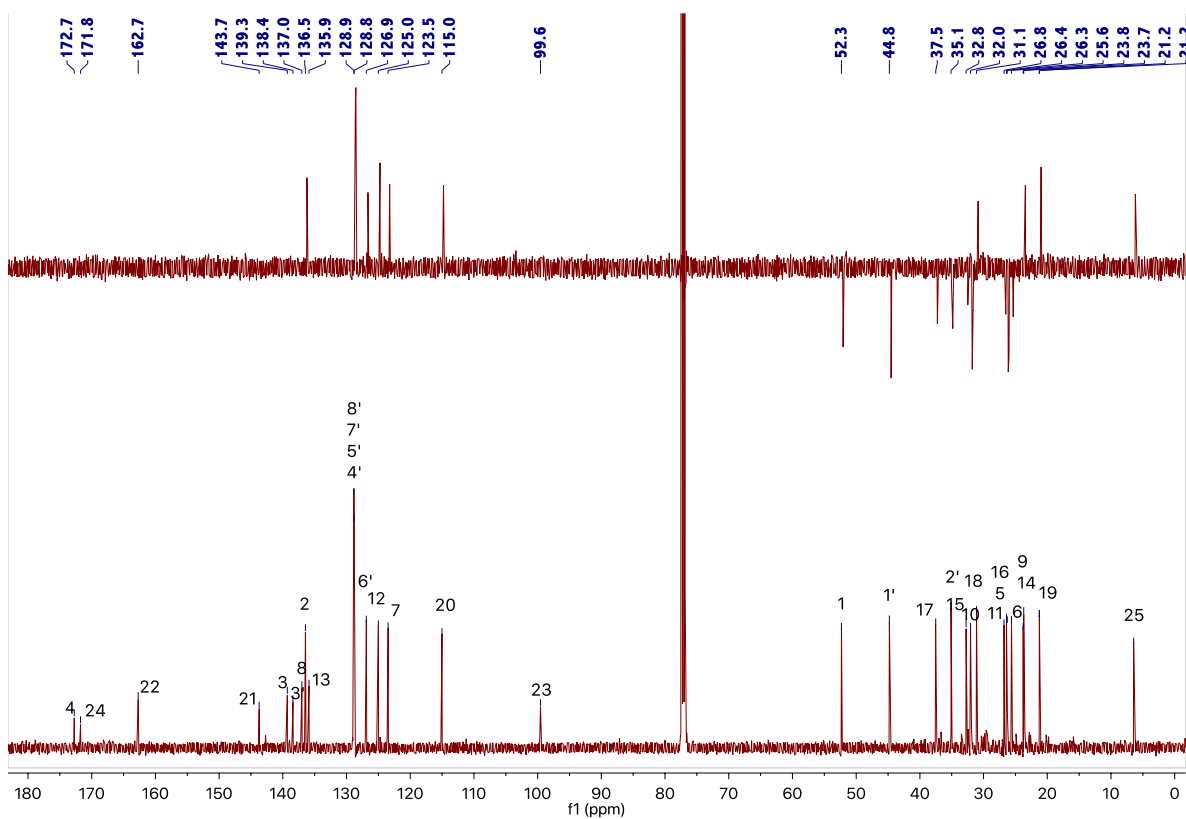


Figure S9. ¹³C NMR and DEPT-135 spectra of ircinialactam J (4) (500 MHz, CDCl₃).

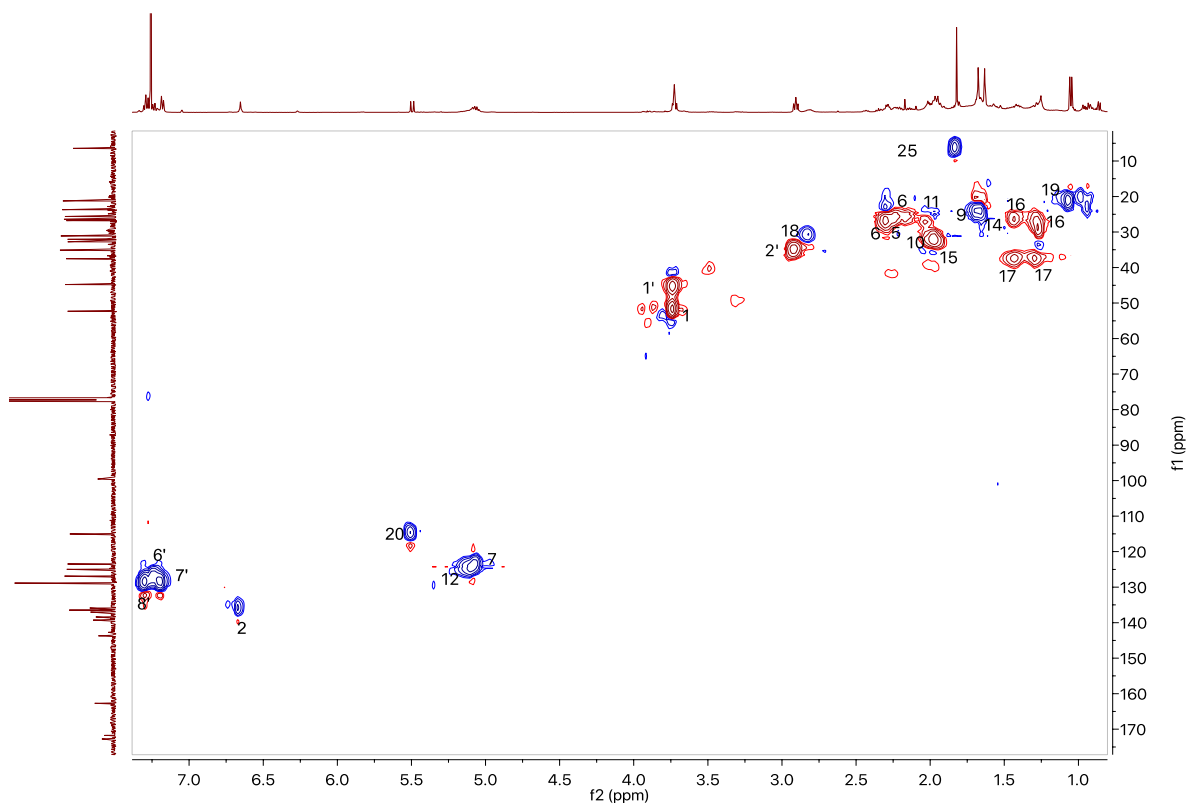


Figure S10. HSQC spectrum of ircinialactam J (**4**) (500 MHz, CDCl₃).

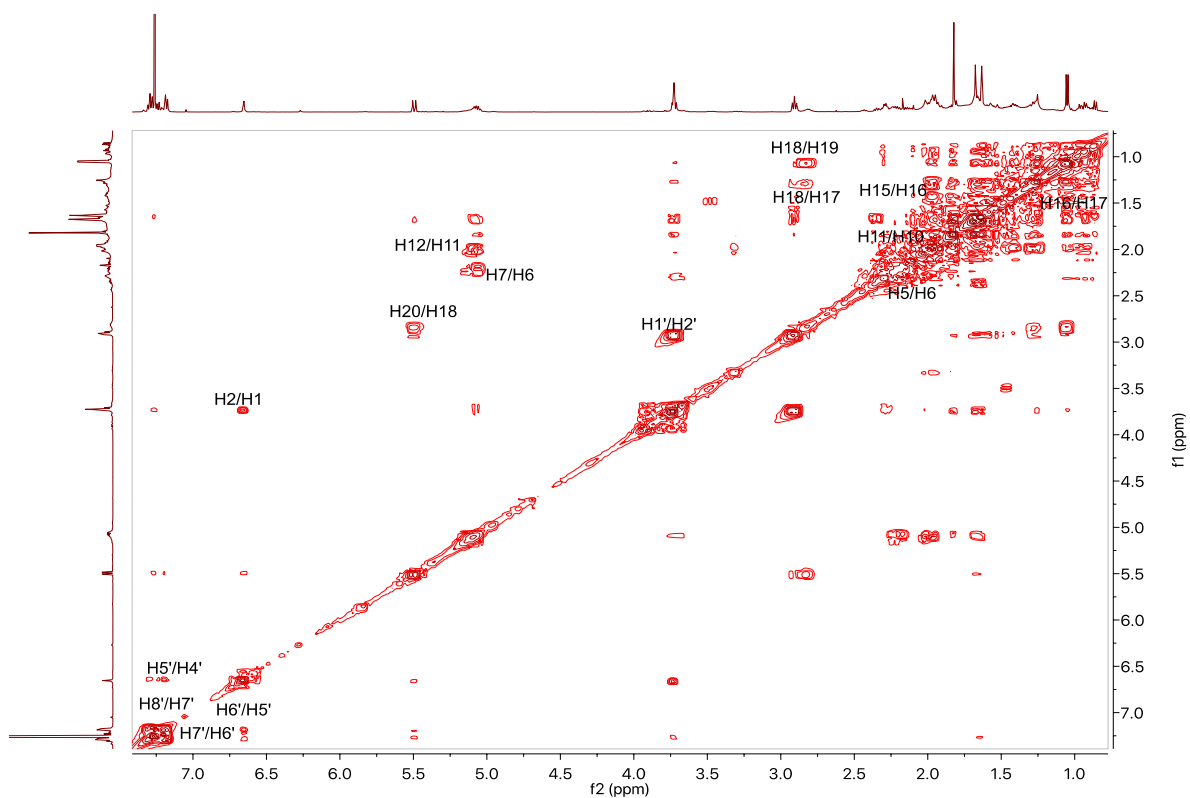


Figure S11. COSY spectrum of ircinialactam J (**4**) (500 MHz, CDCl₃).

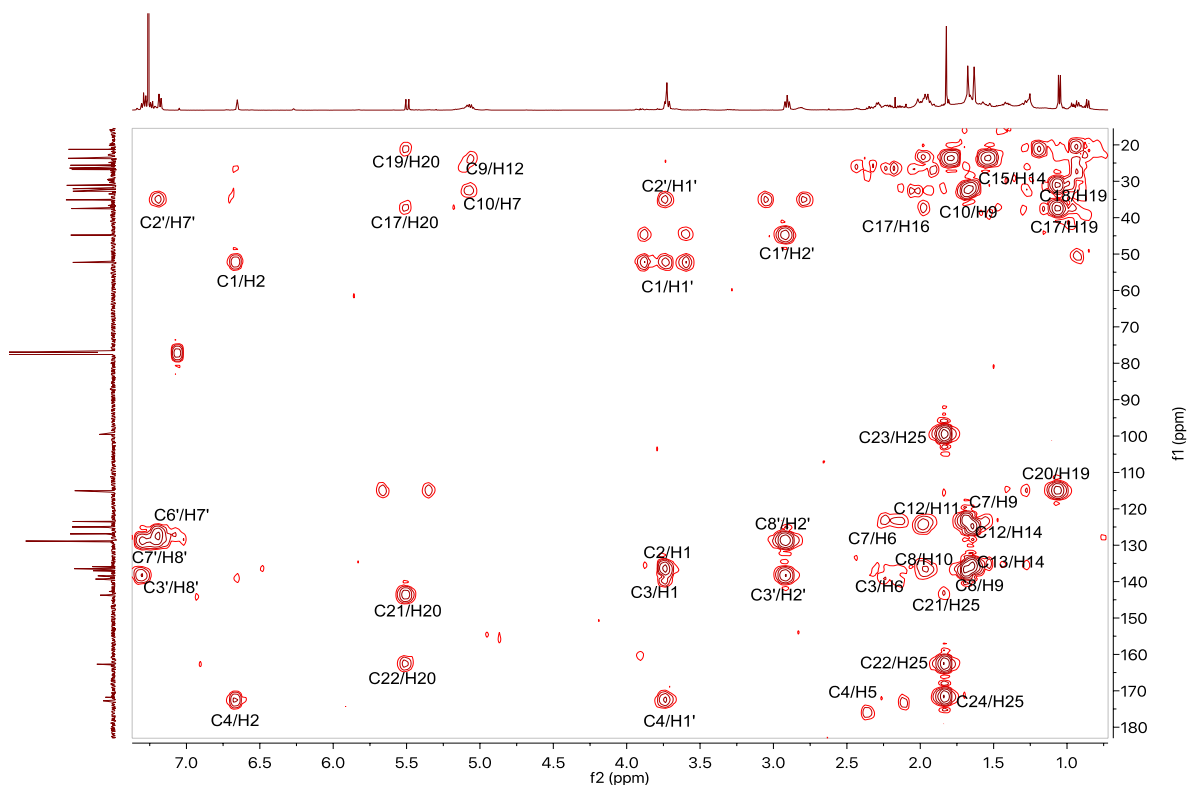


Figure S12. HMBC spectrum of ircinialactam J (**4**) (500 MHz, CDCl₃).

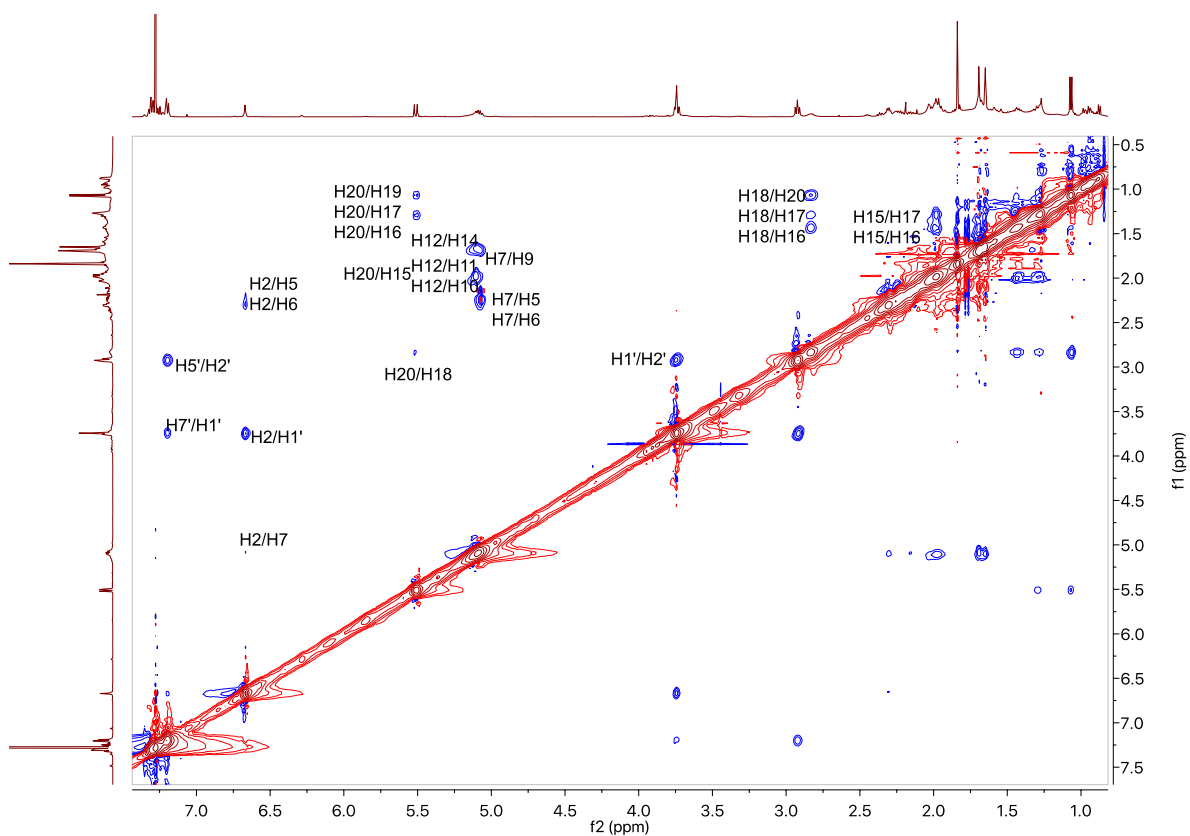


Figure S13. NOESY spectrum of ircinialactam J (**4**) (500 MHz, CDCl₃).

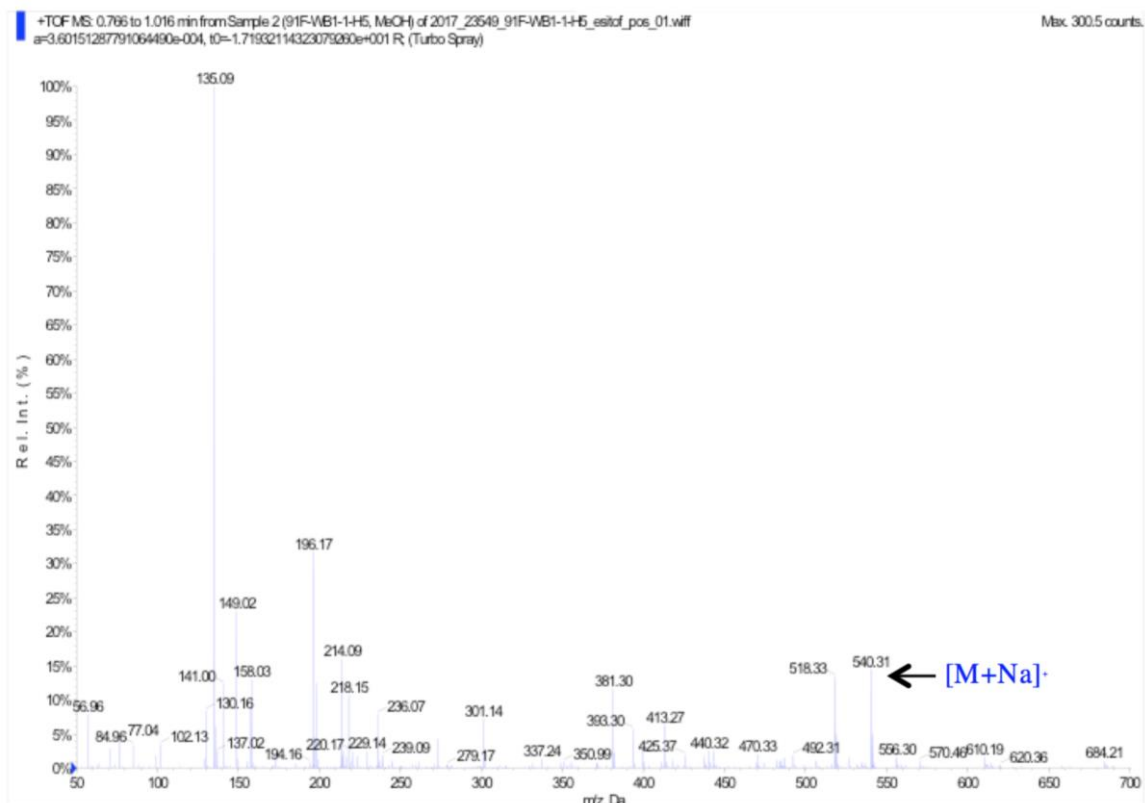


Figure S14. (+)-LRESIMS of ircinialactam J (4).

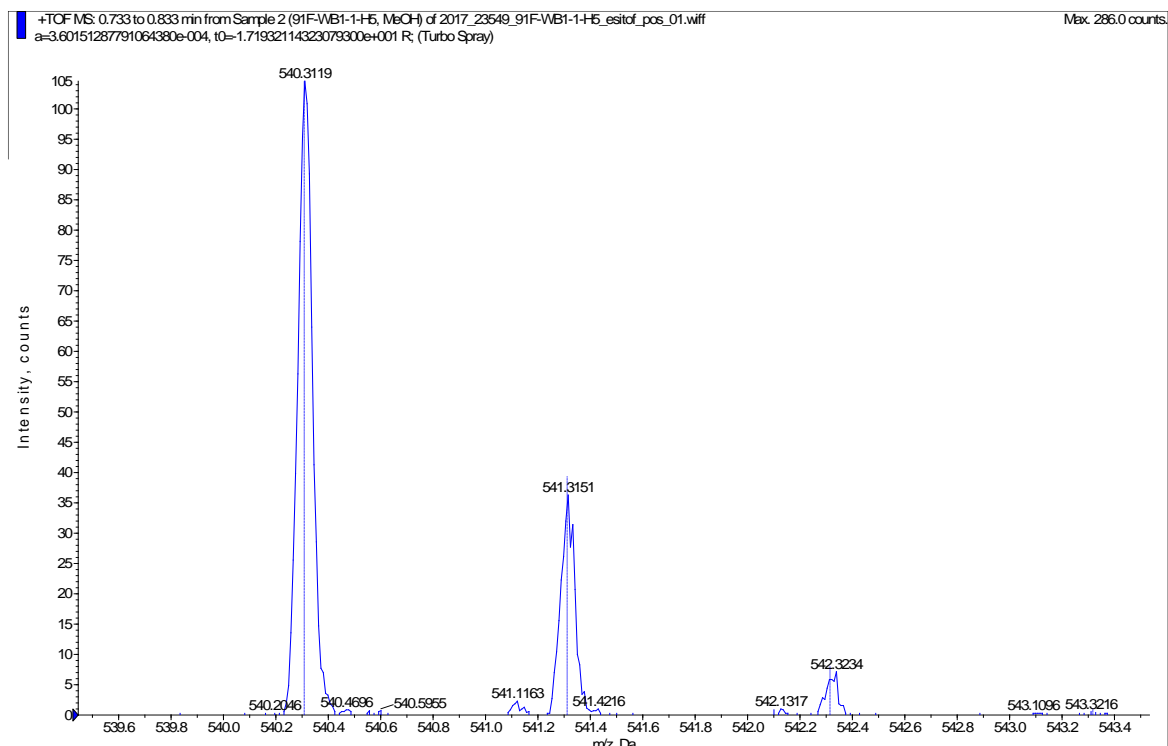


Figure S15. (+)-HRESIMS of ircinialactam J (4).

Table S3. NMR data of ircinialactam K (**5**) in CDCl₃ (500 MHz).

no.	δ_C type	δ_H , mult. (<i>J</i> in Hz)	COSY	HMBC	NOESY
1	173.4 qC				
2	120.5 CH	5.79 m		1	1', 6, 7, 11, 20
3	161.5 qC				
4	56.3 CH ₂	3.73 m		2, 3	2', 6
5	29.7 CH ₂	2.31 m	6	2, 3	
6	25.9 CH ₂	2.25 m	5, 7		2, 4, 7, 9
7	123.1 CH	5.03 m	6		2, 6, 9, 11
8	137.5 qC				
9	23.6 CH ₃	1.69 m		7, 8, 10	6, 7, 10, 11, 12
10	32.1 CH ₂	1.98 m	11	8	9
11	26.4 CH ₂	2.01 m	10, 12	12	2, 7, 9
12	124.6 CH	5.11 m	11		9, 15, 16
13	136.2 qC				
14	23.6 CH ₃	1.66 m		12, 13, 15	
15	32.9 CH ₂	1.97 m	16		12
16	26.3 CH ₂	2.01 m	15, 17		12
17	37.7 CH ₂	1.30 m 1.43 m	16, 18		18, 20
18	31.2 CH	2.81 m	17, 19, 20		17, 19, 20
19	21.1 CH ₃	1.04 m	18	17, 18, 20	18, 20
20	114.4 CH	5.31 m	18	17, 19, 21, 22	2, 17, 18, 19
21	143.9 qC				
22	162.8 qC				
23	99.4 qC				
24	171.8 qC				
25	6.4 CH ₃	1.80 s		22, 23, 24	
1'	44.1 CH ₂	3.71 m	2'	2', 3', 1, 4	2', 7', 2
2'	35.1 CH ₂	2.91 t (7.3)	1'	1', 3', 8'	1', 5', 4
3'	138.4 qC				
4'	128.9 CH	7.31 m	5'		
5'	128.7 CH	7.21 m	4', 6'		2'
6'	126.9 CH	7.25 m	5', 7'		
7'	128.7 CH	7.19 m	6', 8'	2', 6'	1'
8'	128.9 CH	7.29 m	7'	3', 7'	

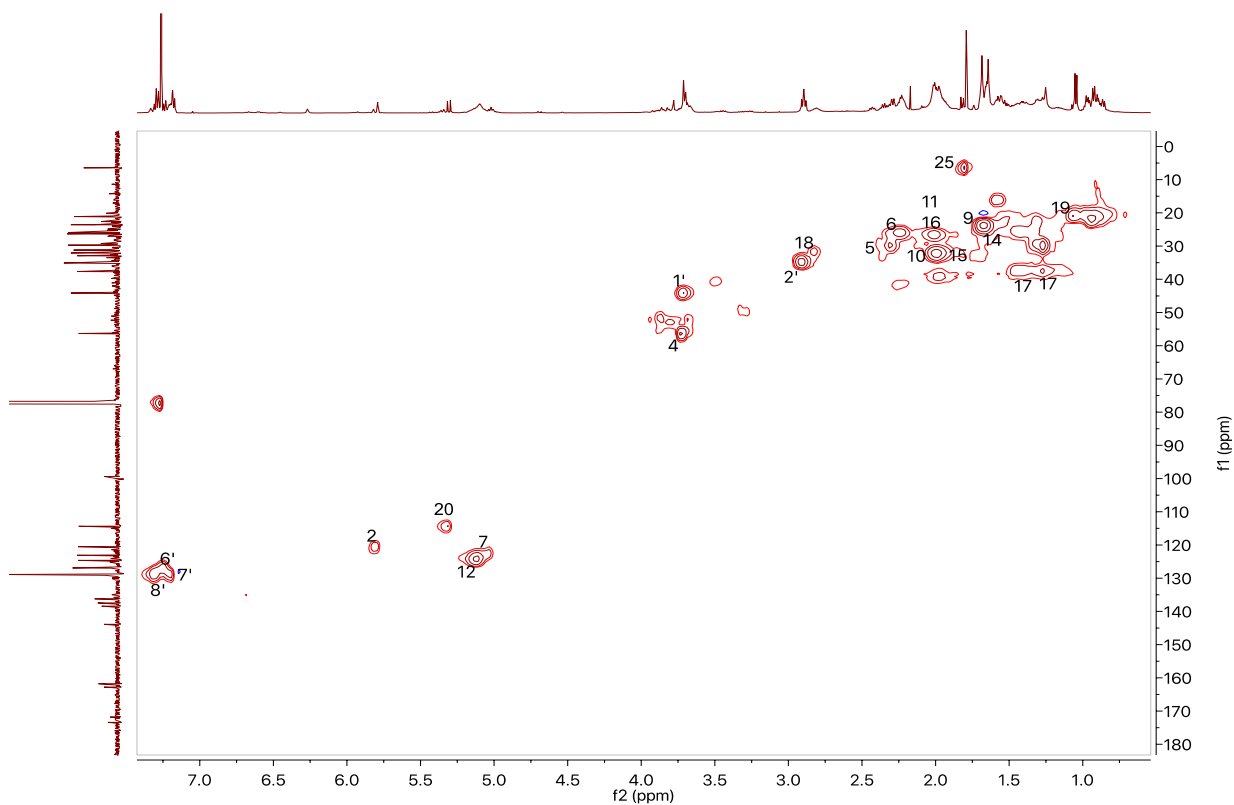


Figure S18. HSQC spectrum of ircinialactam K (**5**) (500 MHz, CDCl_3).

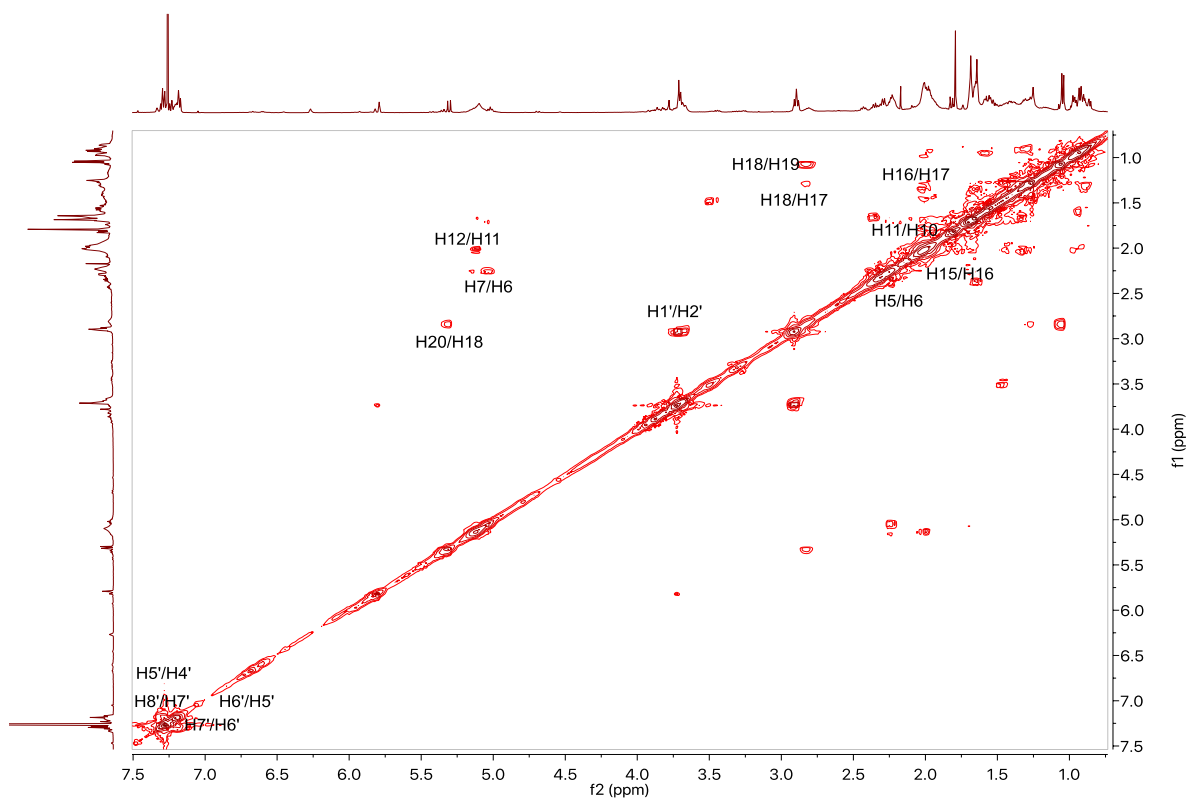


Figure S19. COSY spectrum of ircinialactam K (**5**) (500 MHz, CDCl_3).

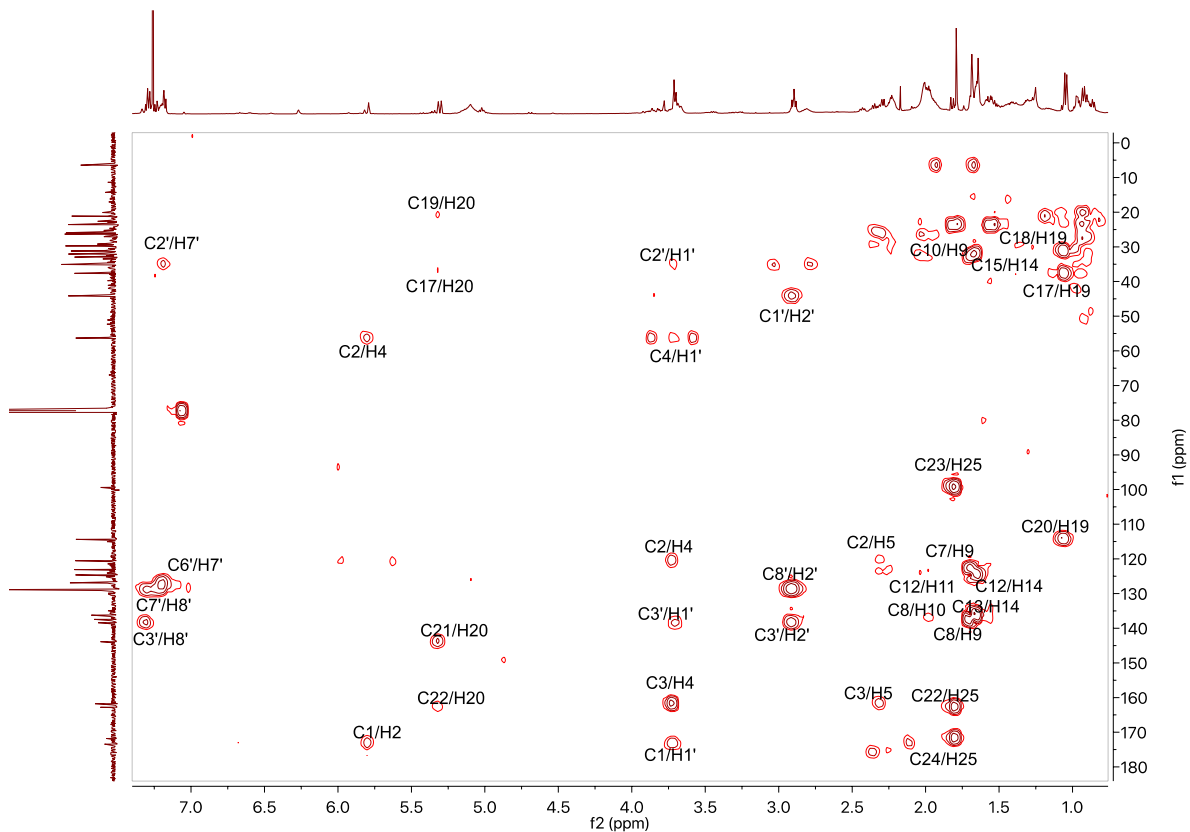


Figure S20. HMBC spectrum of ircinialactam K (**5**) (500 MHz, CDCl₃).

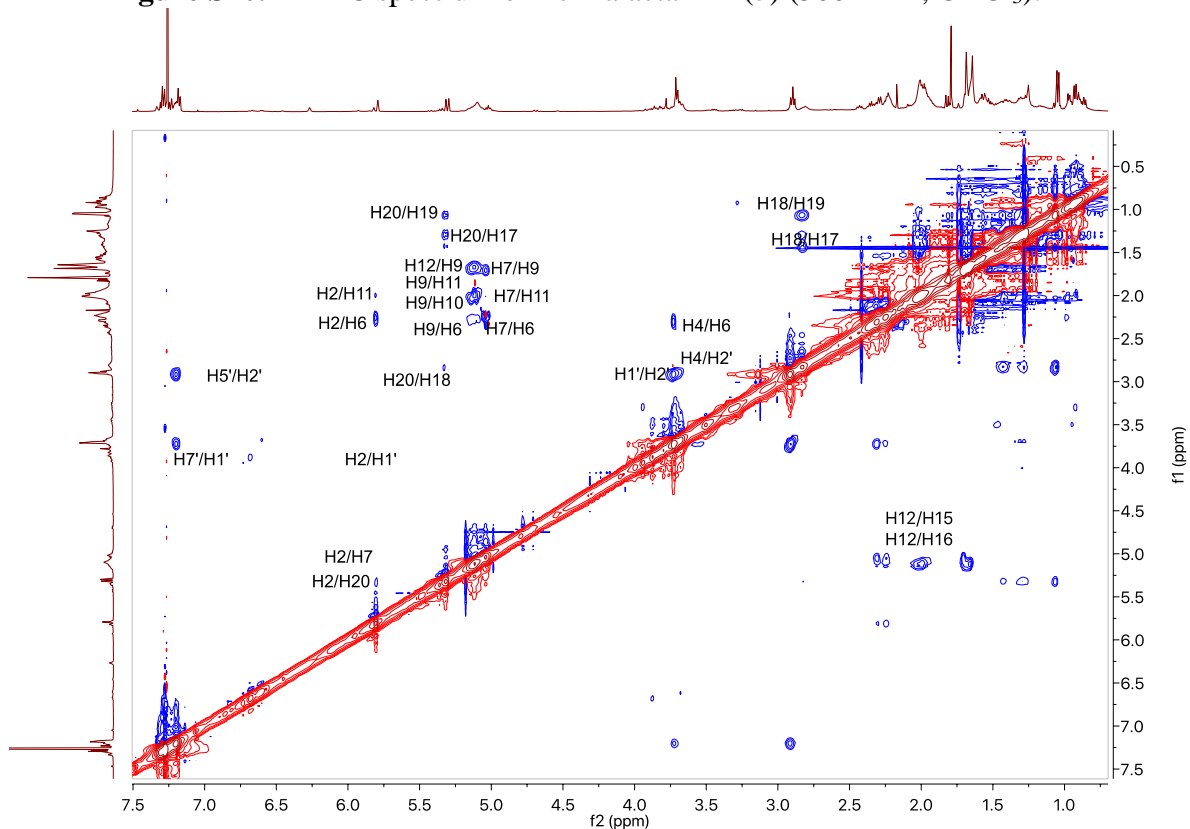


Figure S21. NOESY spectrum of ircinialactam K (**5**) (500 MHz, CDCl₃).

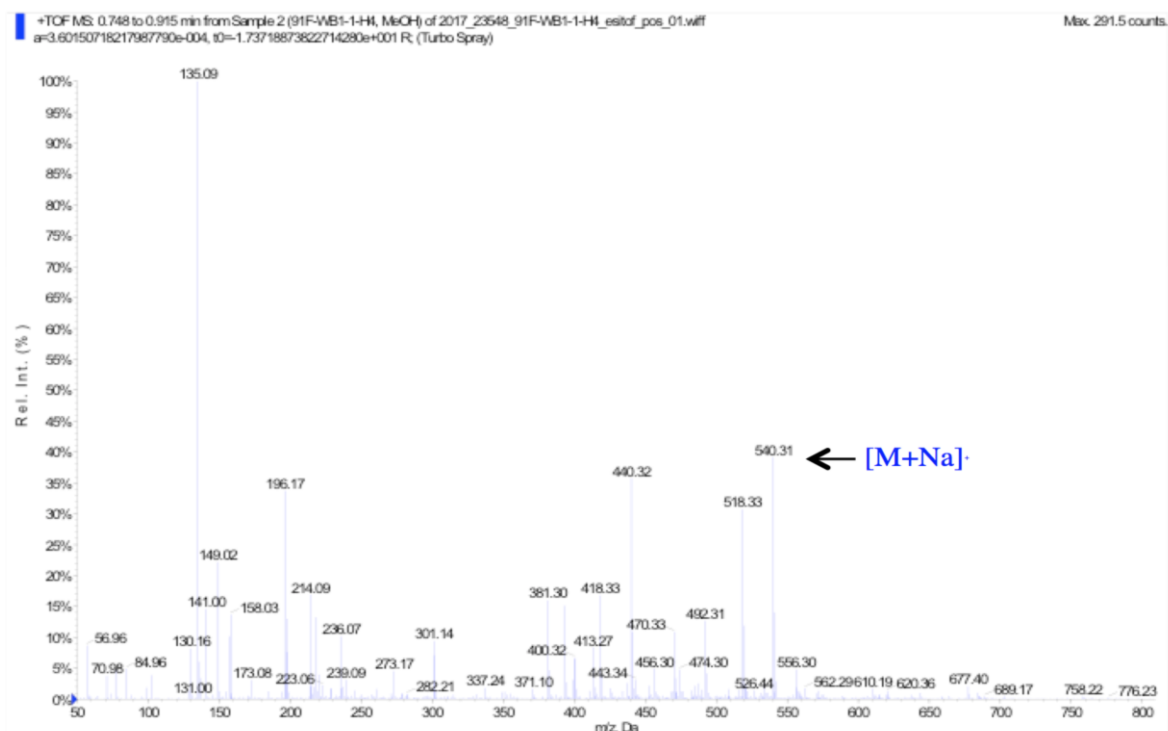


Figure S22. (+)-LRESIMS of ircinialactam K (5).

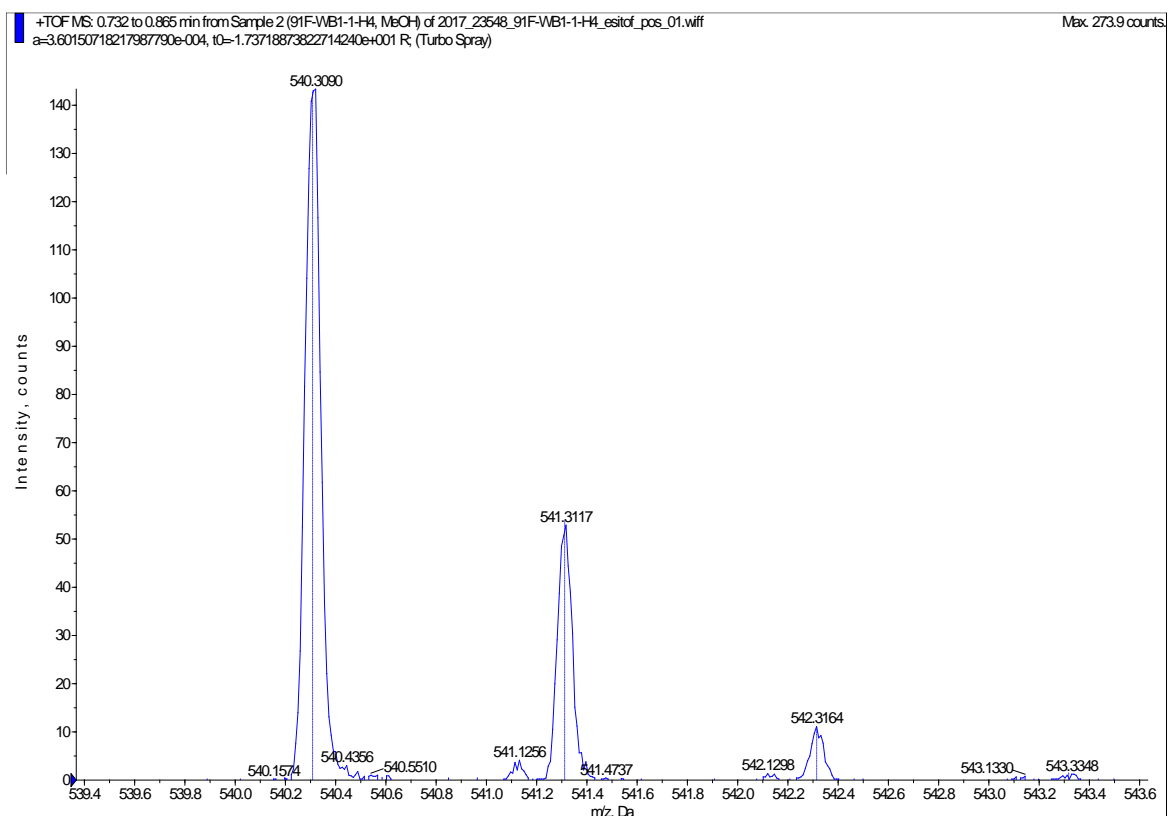


Figure S23. (+)-HRESIMS of ircinialactam K (5).

Table S4. NMR data of ircinialactam L (**6**) in CDCl₃ (500 MHz).

no.	δ_C	type	δ_H , mult. (<i>J</i> in Hz)	COSY	HMBC	NOESY
1	51.4	CH	3.92 m	2	2, 3, 4	2', 4', 5', 2
2	136.2	CH	6.74 m	1	1, 4, 5	1, 5
3	139.3	qC				
4	172.5	qC				
5	26.8	CH ₂	2.30 m	6	3, 4, 7, 8	
6	25.6	CH ₂	2.15 m	5, 7	7	
7	123.4	CH	5.08 m	6	10	5, 9
8	137.0	qC				
9	23.8	CH ₃	1.68 d (1.4)		7, 8, 10	7, 10
10	32.7	CH ₂	1.95 m	11		9, 12
11	26.3	CH ₂	2.09 m	10, 12		12
12	125.0	CH	5.11 m	11	9	10, 11, 14
13	135.9	qC				
14	23.7	CH ₃	1.64 d (1.6)		12, 13, 15	12
15	32.0	CH ₂	1.95 m	16	12, 13	
16	26.4	CH ₂	1.26 m 1.43 m	15, 17		17, 18
17	37.5	CH ₂	1.26 m 1.43 m	16, 18		16, 18, 20
18	31.1	CH	2.82 m	17, 19, 20		16, 17, 19, 20
19	21.2	CH ₃	1.05 d (6.7)	18	17, 18, 20	18, 20
20	115.0	CH	5.48 d (10.2)	18	17, 19, 21, 22	17, 18, 19
21	143.6	qC				
22	162.8	qC				
23	99.4	qC				
24	171.8	qC				
25	6.4	CH ₃	1.82 s		22, 23, 24	
1'	41.3	CH ₂	3.51m	2'	2', 1, 4	2', 3', 4', 5'
2'	37.5	CH ₂	1.48 m	1', 3'		1', 1
3'	26.0	CH	1.57 m	2', 4', 5'		1', 4', 5'
4'	22.5	CH ₃	0.94 d (6.5)	3'	3'	1', 3', 1
5'	22.6	CH ₃	0.94 d (6.5)	3'	3'	1', 3', 1

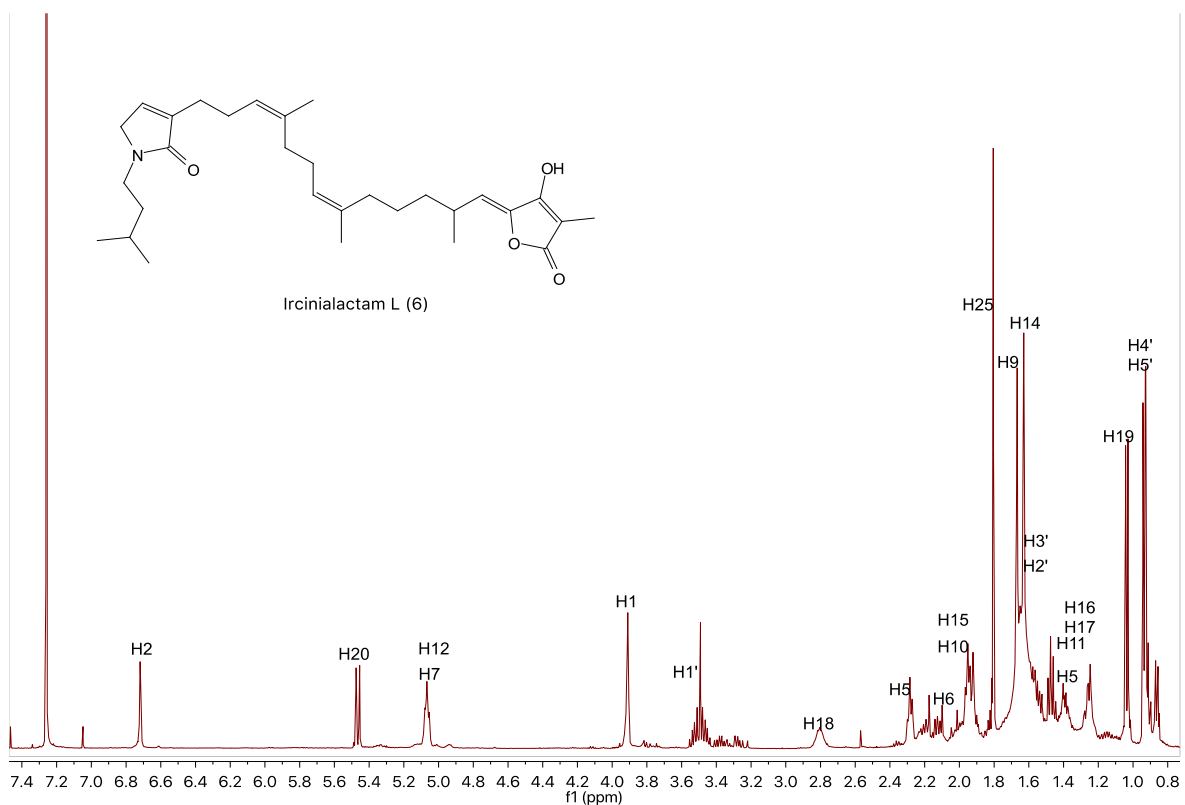


Figure S24. ¹H NMR spectrum of ircinialactam L (6) (500 MHz, CDCl₃).

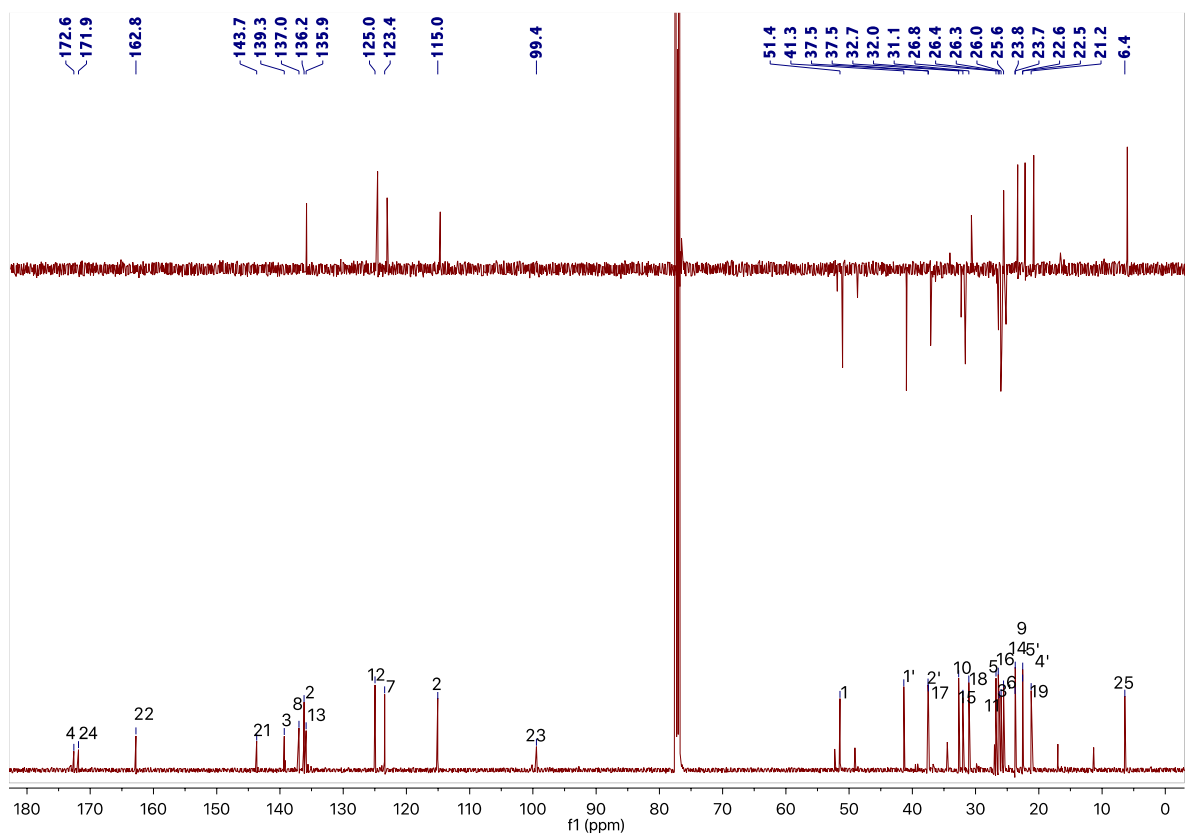


Figure S25. ¹³C NMR and DEPT-135 spectra of ircinialactam L (6) (500 MHz, CDCl₃).

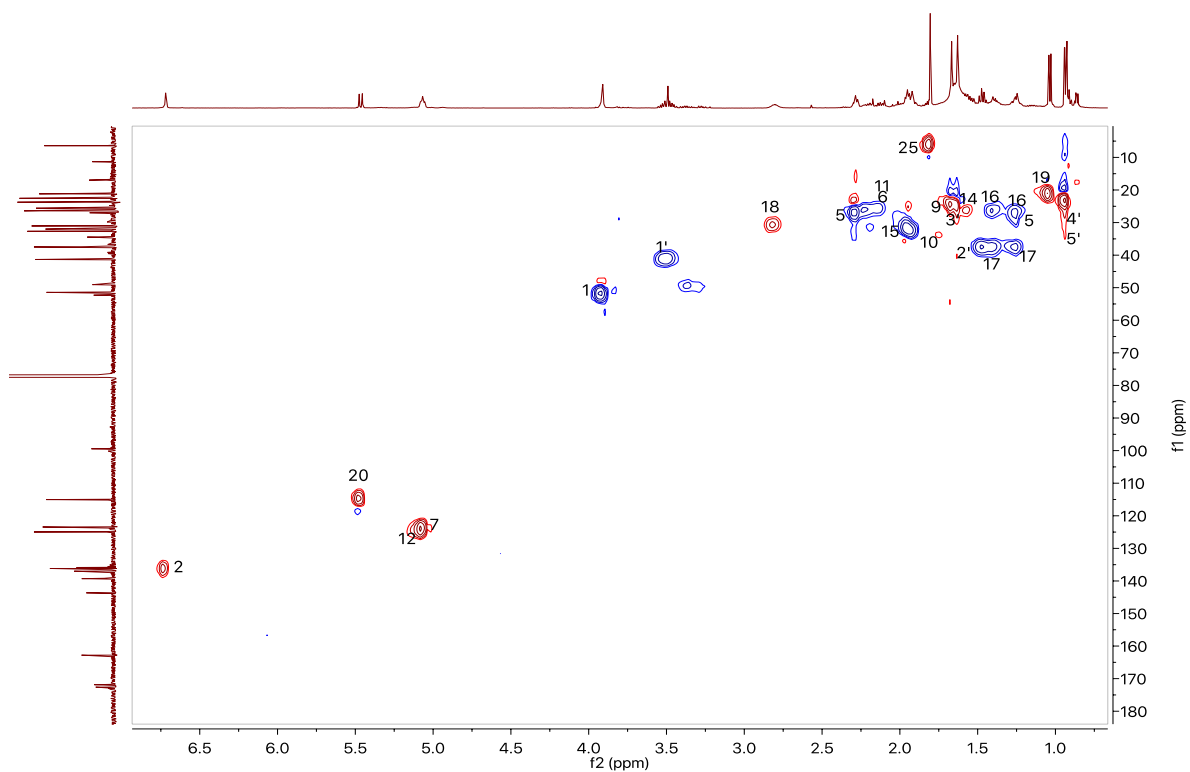


Figure S26. HSQC spectrum of ircinialactam L (**6**) (500 MHz, CDCl₃).

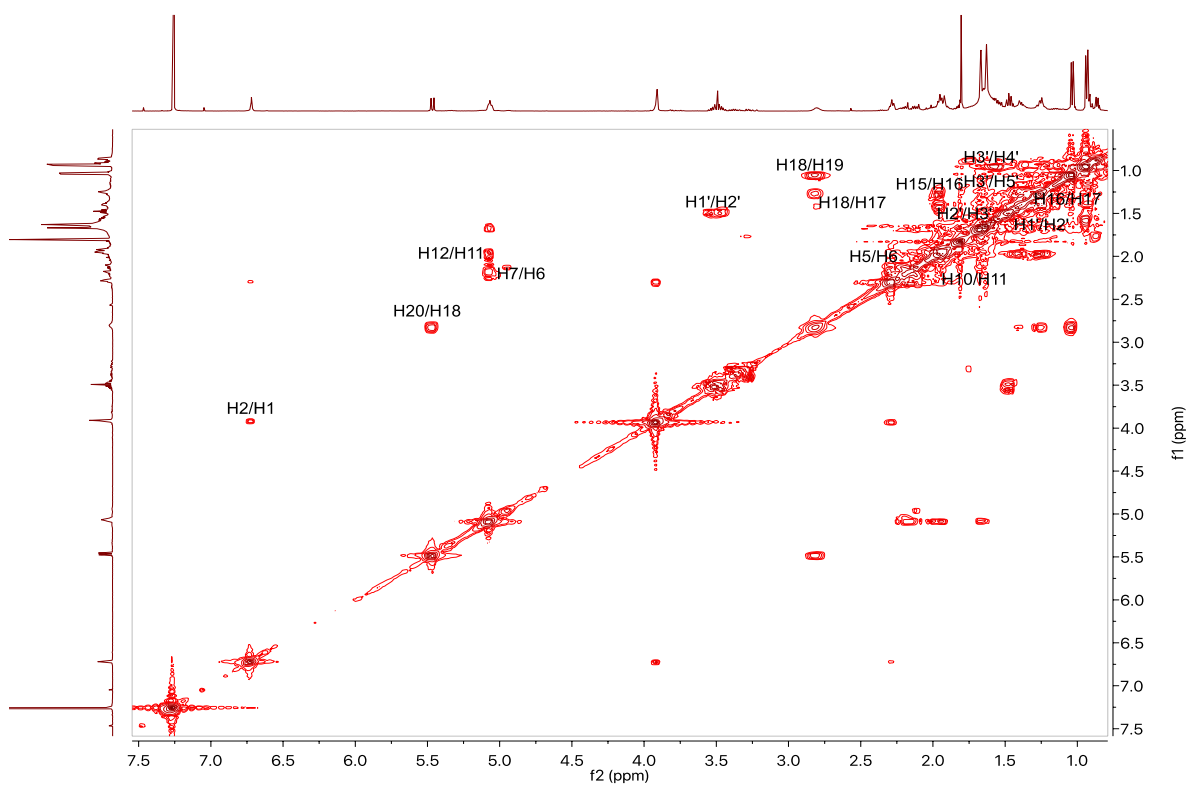


Figure S27. COSY spectrum of ircinialactam L (**6**) (500 MHz, CDCl₃).

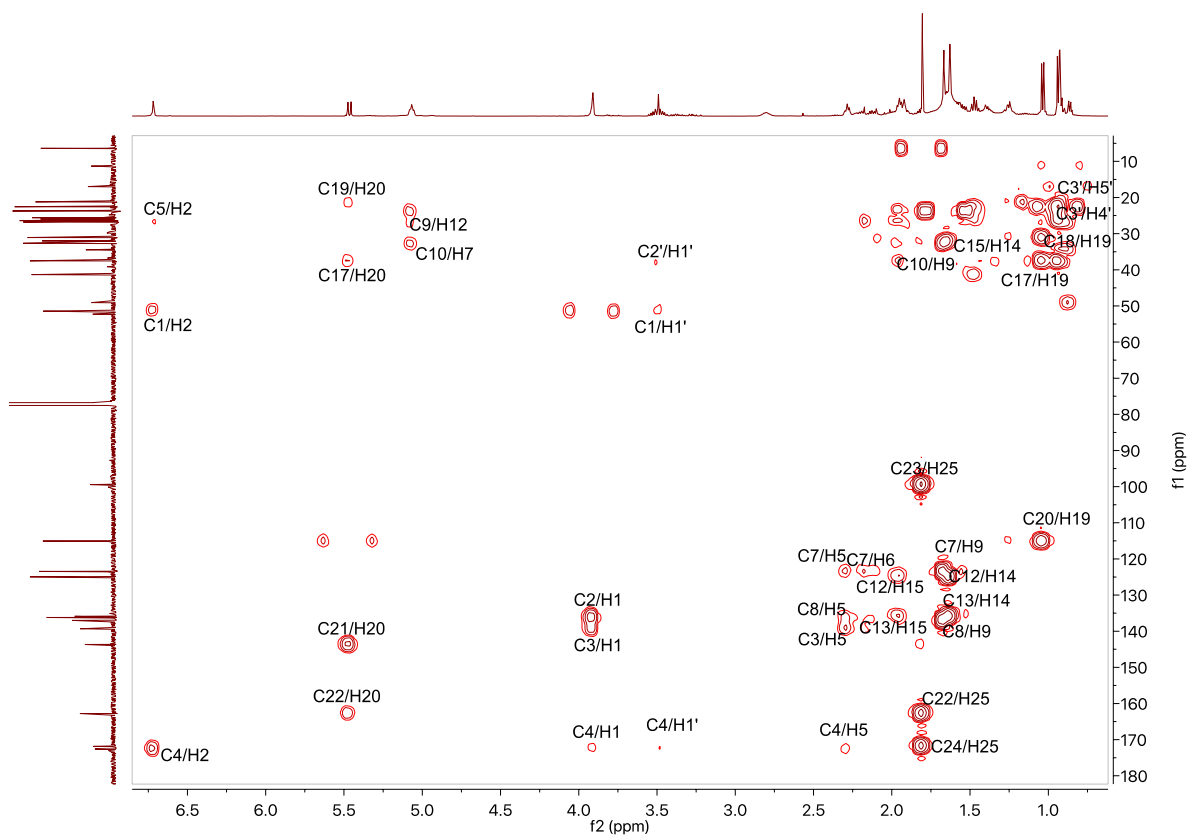


Figure S28. HMBC spectrum of ircinialactam L (6) (500 MHz, CDCl₃).

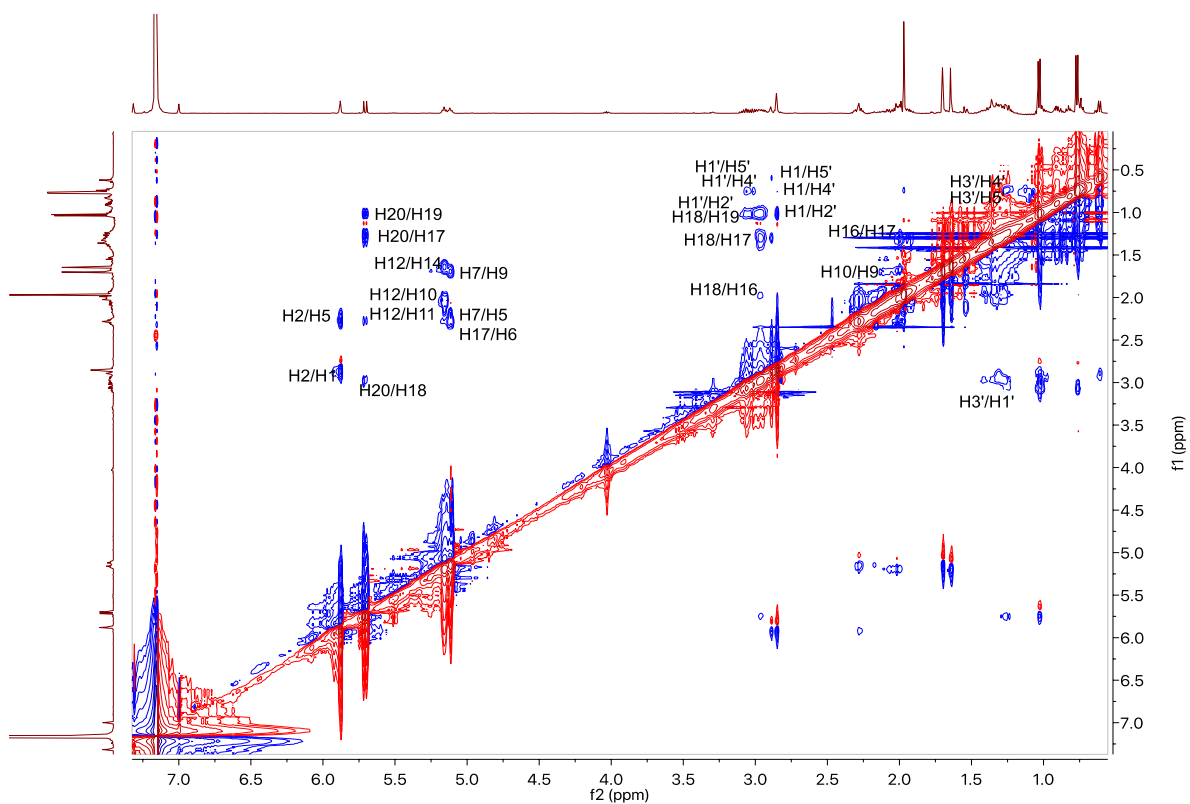


Figure S29. NOESY spectrum of ircinialactam L (6) (500 MHz, C₆D₆).

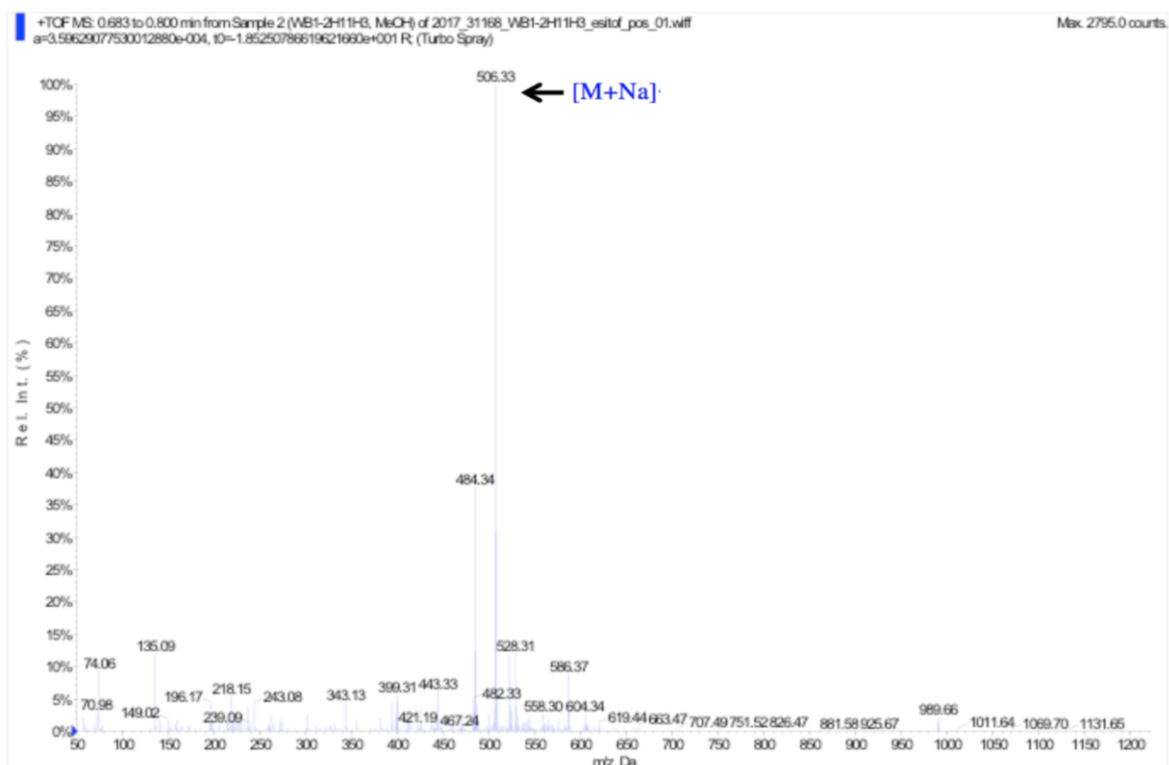


Figure S30. (+)-LRESIMS of ircinalactam L (6).

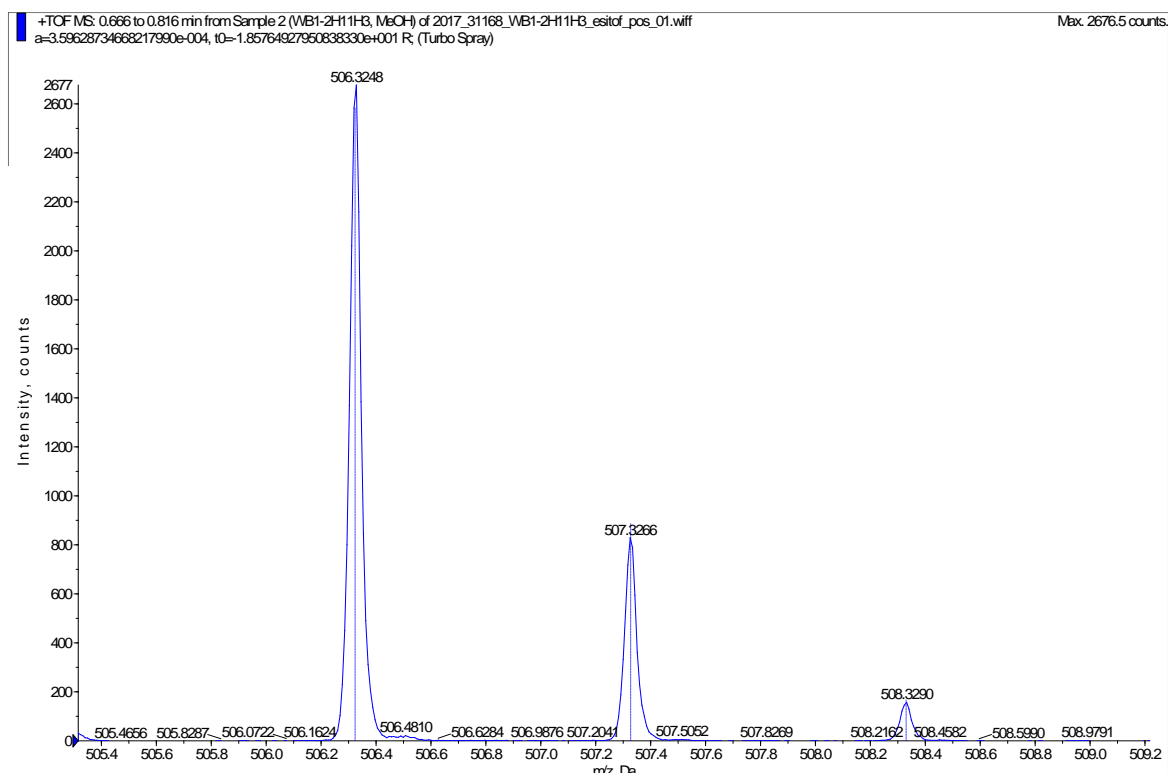


Figure S31. (+)-HRESIMS of ircinalactam L (6).

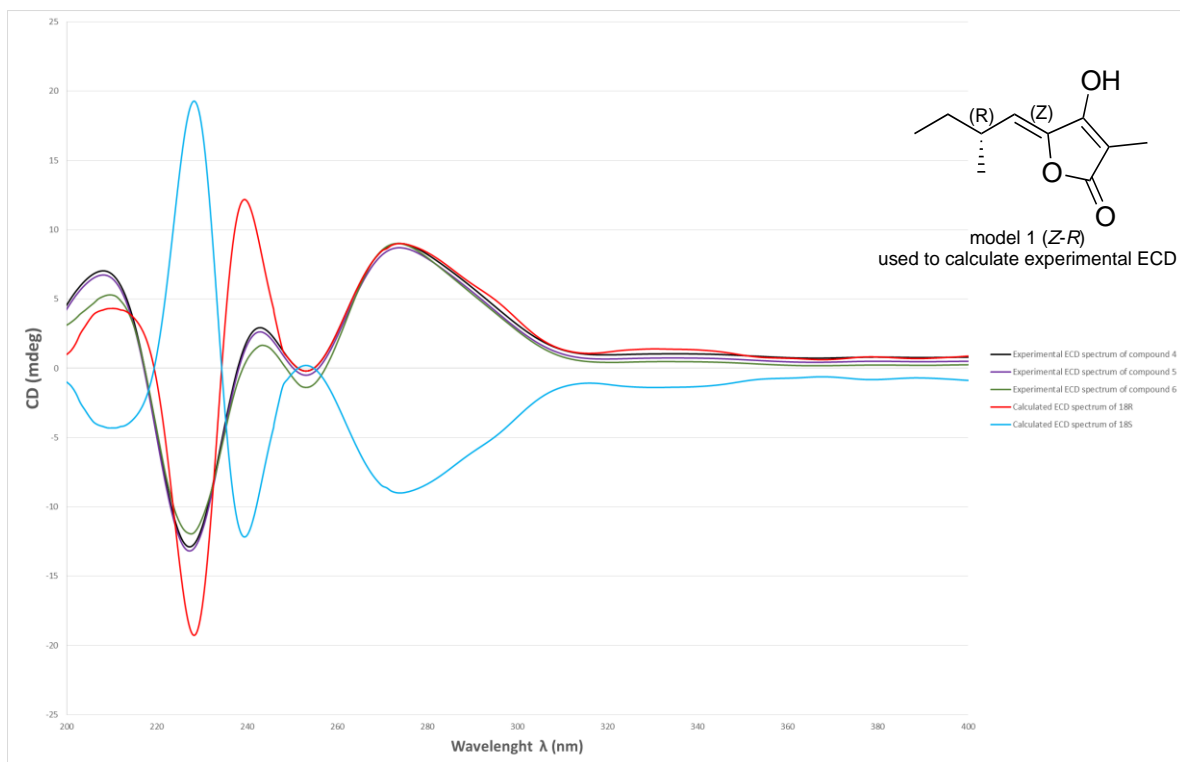


Figure S32. Comparison of ECD spectra of compounds 4, 5 and 6 in CHCl_3 .

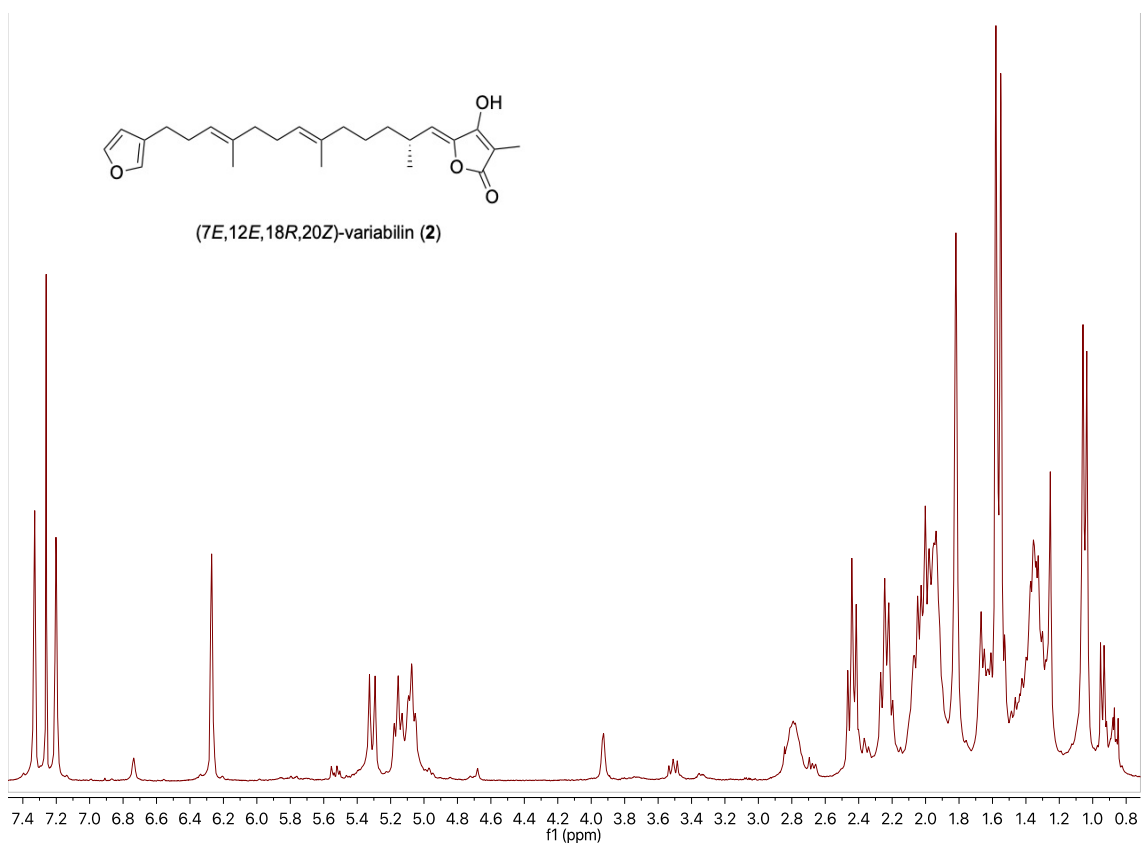


Figure S33. ^1H NMR spectrum of compound 2 (500 MHz, CDCl_3).

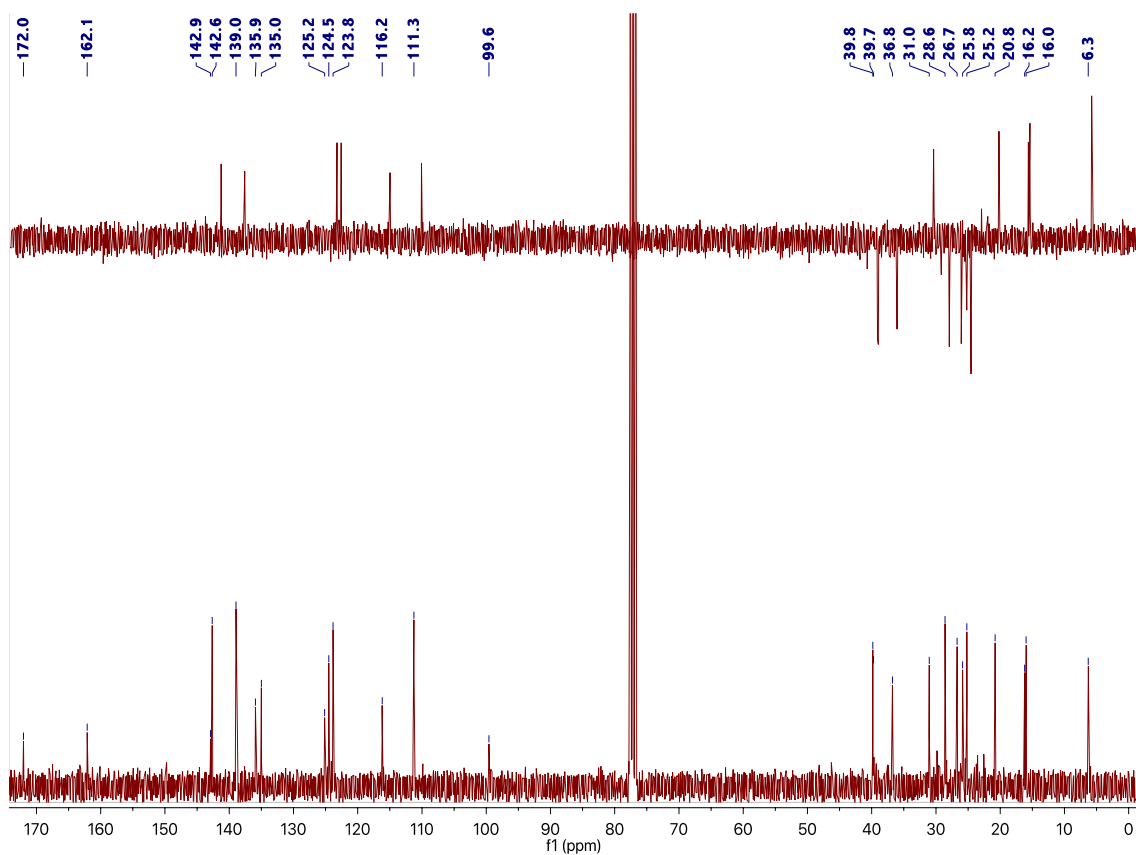


Figure S34. ^{13}C NMR and DEPT-135 spectra of compound **2** (500 MHz, CDCl_3).

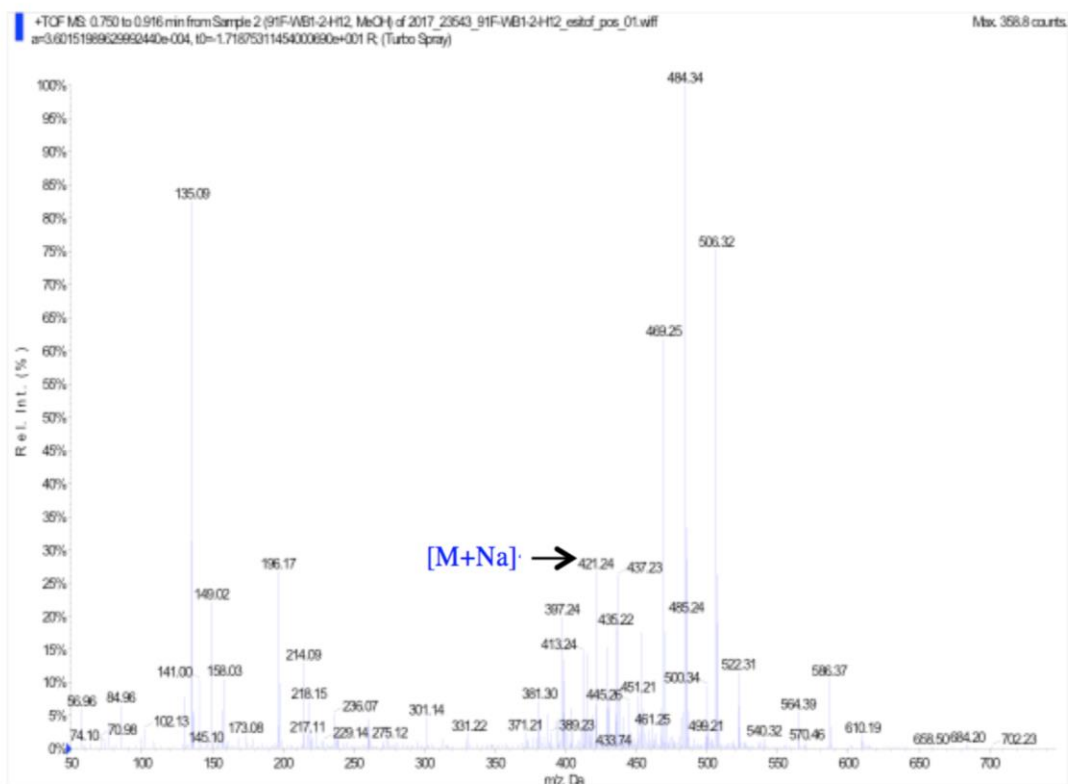


Figure S35. (+)-LRESIMS of compound **2**.

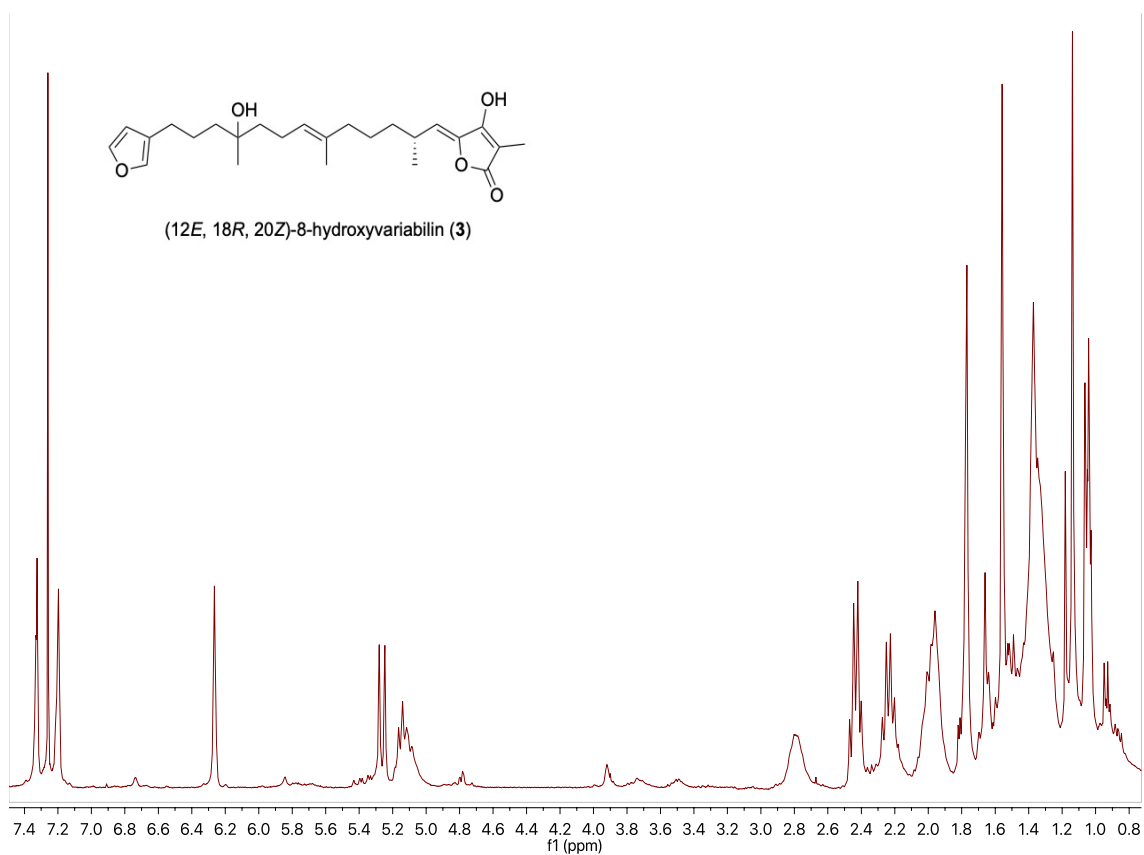


Figure S36. ^1H NMR spectrum of compound **3** (500 MHz, CDCl_3).

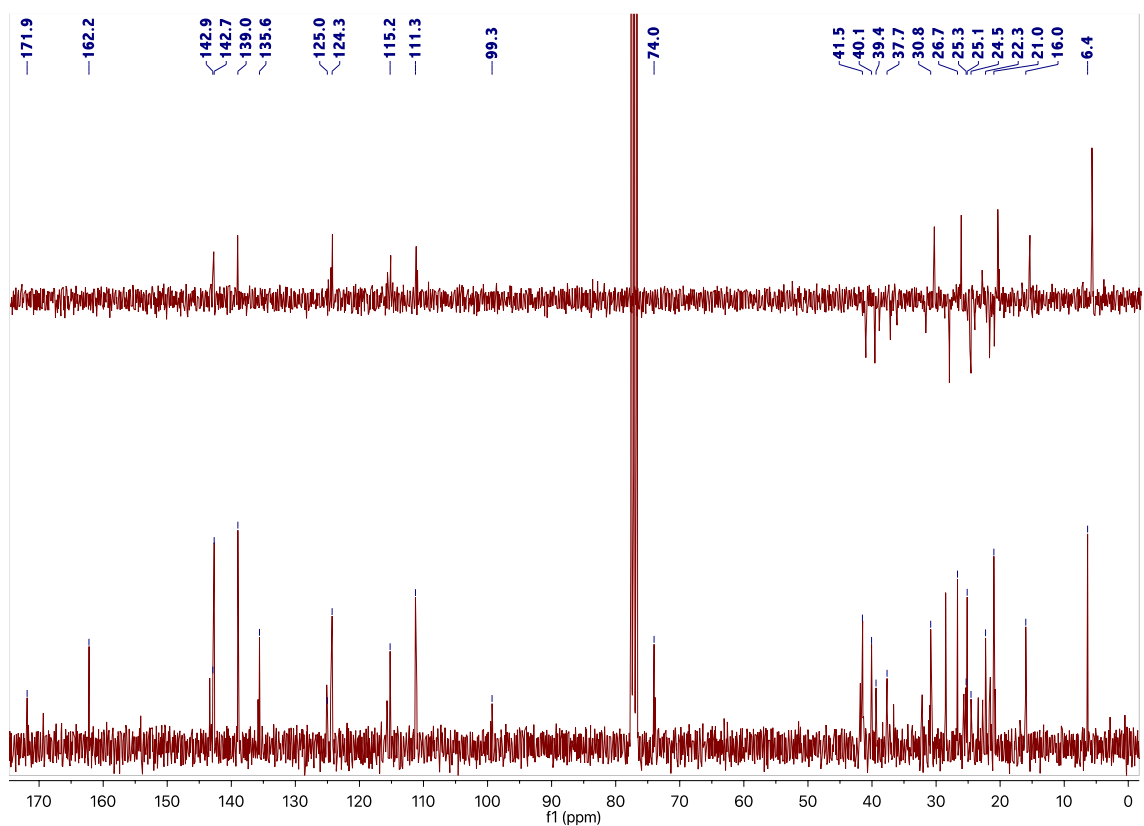


Figure S37. ^{13}C NMR and DEPT-135 spectra of compound **3** (500 MHz, CDCl_3).

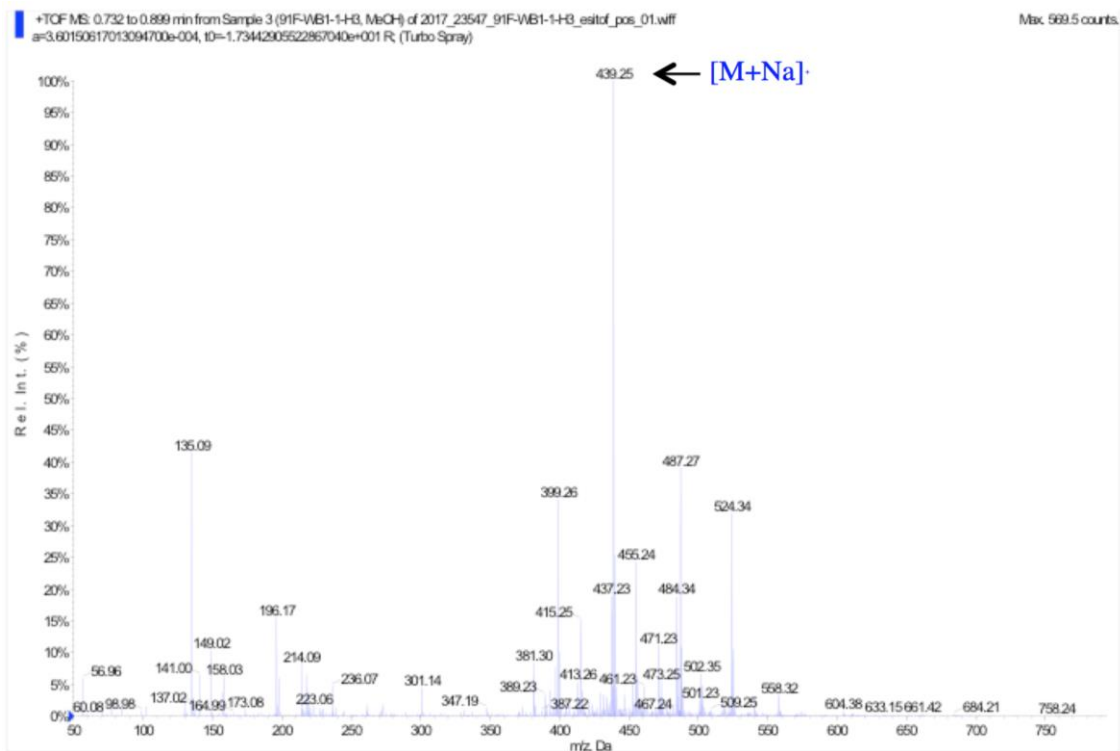
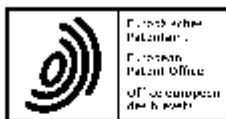


Figure S38. (+)-LRESIMS of compound **3**.

Patent request



Request for grant of a European patent

<i>For official use only</i>	
1 Application number:	<input type="text" value="MIKEY"/>
2 Date of receipt (Rule 36(2) EPC):	<input type="text" value="DREC"/>
3 Date of receipt at EPO (Rule 36(4) EPC):	<input type="text" value="RENA"/>
4 Date of filing:	

6 Grant of European patent, and examination of the application under Article 94, are hereby requested.

Request for examination in an admissible non-EPO language:

Se solicita el examen de la solicitud según el artículo 94.

6.1 The applicant waives his right to be asked whether he wishes to proceed further with the application (Rule 70(2))

Procedural language:

en

Filing Language:

en

6 Applicant's or representative's reference

P5160EP00

Filing Office:

ES

Applicant 1

7-1 Name:

UNIVERSIDADE DA CORUÑA

8-1 Address:

OTRI-Edificio de Servizos Centrais de Investigación
Campus de Elviña
15071 A CORUÑA
Spain

10-1 State of residence or of principal place of business:

Spain

Applicant 2

7-2 Name:

UNIVERSIDAD DE SEVILLA

8-2 Address:

Pabellón de Brasil,
Pº de las Delicias, s/n
41013 SEVILLA
Spain

10-1 State of residence or of principal place of business:

Spain

Applicant 3

7-3	Name:	SERVICIO ANDALUZ DE SALUD
8-3	Address:	Avda. de la Constitución, 18 41071 SEVILLA Spain
10-1	State of residence or of principal place of business:	Spain
14.1	The/Each applicant hereby declares that he is an entity or a natural person under Rule 6(4) EPC.	<input type="checkbox"/>

Representative 1

16-1	Name:	ZBM Patents - Zea, Barlocchi & Markvardsen
	Association No.:	371
16-1	Address of place of business:	Pl. Catalunya, 1 2nd floor 08002 BARCELONA Spain
17-1	Telephone:	+34.93.3426472
17-1	Fax:	+34.93.3427970
17-1	E-mail:	formalities@zbm-patents.eu

Inventor(s)

23	Designation of inventor attached	<input checked="" type="checkbox"/>
24	Title of invention	

Title of invention:	FURAN, THIOPHENE OR GAMMA-LACTAM SESTERTERPENE TETRONIC ACIDS USEFUL AS ANTIVIRAL COMPOUNDS AGAINST INFECTIONS CAUSED BY HUMAN ADENOVIRUS
---------------------	---

Resumen

Ácidos tetrónicos de furano, tiofeno o γ -lactama sesterterpeno útiles como compuestos antivirales contra infecciones causadas por adenovirus humanos.

Ácidos tetrónicos de furano, tiofeno o γ -lactama sesterterpeno, procedimiento para su preparación o para su aislamiento de esponjas marinas, así como composiciones farmacéuticas que los comprenden y su uso en farmacia, en particular como agentes antivirales contra adenovirus humanos (HAdV).

Form 1002 - 1: Public inventor(s)

Designation of inventor

User reference: P5160EP00
 Application No:

Public

<p>Inventor</p> <p>The applicant has acquired the right to the European patent:</p>	<p>Name: PECH PUCH Dawrin Jesús Address: Universidade da Coruña Centro de Investigaciones Científicas Avanzadas As Carballeiras, s/n, Campus de Elviña 15071 A CORUÑA Spain</p>	<p>As employer</p>
<p>Inventor</p> <p>The applicant has acquired the right to the European patent:</p>	<p>Name: JIMÉNEZ GONZÁLEZ Carlos Address: Universidade da Coruña Centro de Investigaciones Científicas Avanzadas As Carballeiras, s/n, Campus de Elviña 15071 A CORUÑA Spain</p>	<p>As employer</p>
<p>Inventor</p> <p>The applicant has acquired the right to the European patent:</p>	<p>Name: RODRÍGUEZ GONZÁLEZ Jaime Address: Universidade da Coruña Centro de Investigaciones Científicas Avanzadas As Carballeiras, s/n, Campus de Elviña 15071 A CORUÑA Spain</p>	<p>As employer</p>
<p>Inventor</p> <p>The applicant has acquired the right to the European patent:</p>	<p>Name: PACHÓN DÍAZ Jerónimo Address: IBIS Campus Hospital Universitario Virgen del Rocío Avda. Manuel Siurot, s/n Laboratorio: 208 41013 SEVILLA Spain</p>	<p>As employer</p>

	Inventor The applicant has acquired the right to the European patent:	Name: BERASTEGUI CABRERA Judith Address: IBIS Campus Hospital Universitario Virgen del Rocío Avda. Manuel Siurot, s/n Laboratorio: 208 41013 SEVILLA Spain As employer
	Inventor The applicant has acquired the right to the European patent:	Name: SANCHEZ CESPEDES Javier Address: SERVICIO ANDALUZ DE SALUD Avda. de la Constitución, 18 41071 SEVILLA Spain As employer

Signature(s)

Place: Barcelona
Date: 07 August 2019
Signed by: Montserrat Jané Bonet 17614
Association: ZBM Patents - Zea, Barlocchi & Markvardsen
Representative name: Montserrat Jané
Capacity: (Representative)



Acknowledgement of receipt

We hereby acknowledge receipt of your request for grant of a European patent as follows:

Submission number	300330402	
Application number	EP19382697.1	
File No. to be used for priority declarations	EP19382697	
Date of receipt	07 August 2019	
Your reference	P5160EP00	
Applicant	UNIVERSIDADE DA CORUÑA	
Country	ES	
Title	FURAN, THIOPHENE OR γ -LACTAM SESTERTERPENE TETRONIC ACIDS USEFUL AS ANTIVIRAL COMPOUNDS AGAINST INFECTIONS CAUSED BY HUMAN ADENOVIRUS	
Documents submitted	package-data.xml application-body.xml SPECEPO-1.pdfP5160EP00_specification_20190805.pdf (43 p.) OLF-ARCHIVE.zip\version final para presentar.zip f1002-1.pdf (2 p.)	ep-request.xml ep-request.pdf (5 p.) SPECTRANONEP.pdfP5160EP00 Resumen castellano.pdf (1 p.) SEQLTXT.txtP5160EP00_ST25.txt
Submitted by	CN=Montserrat Jané Bonet 17614	
Method of submission	Online	
Date and time receipt generated	07 August 2019, 14:34:31 (CEST)	

3.4 Estudio químico de la esponja *Agelas dilatata*

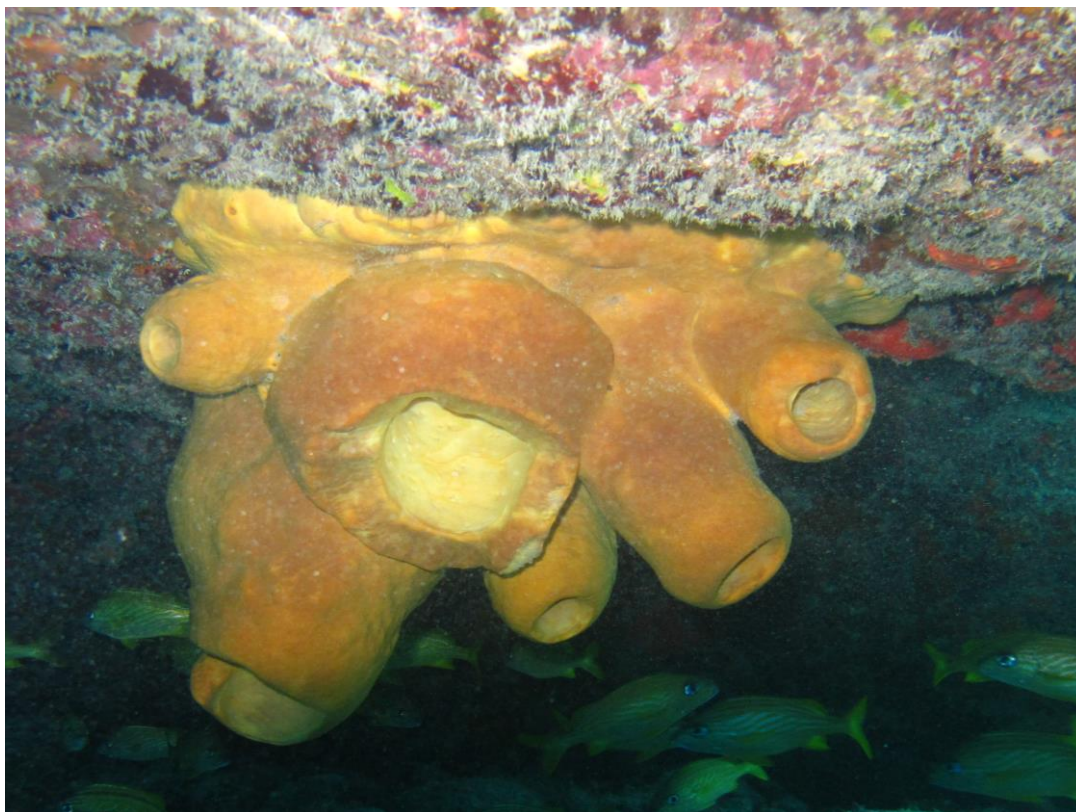


Figura 3.4. Fotografía de la esponja *Agelas dilatata*, Isla de Cozumel-México.

En este apartado se describe el aislamiento y elucidación estructural de ocho alcaloides obtenidos a partir de la esponja *Agelas dilatata* recolectada en la isla de Cozumel, México. Todos los compuestos habían sido reportados previamente; sus estructuras se elucidaron mediante el empleo de RMN 1D y 2D e HRESIMS, y la comparación de los datos espectrales obtenidos, con los que aparecen en la bibliografía reportados para estos compuestos. Dos de ellos mostraron una actividad antibacteriana interesante frente a *Pseudomonas aeruginosa* y *Klebsiella pneumoniae*, y están siendo sometidos a ensayos adicionales con el fin de conocer su mecanismo de acción. Una vez finalicen estos ensayos, los resultados darán origen a una publicación.

Antibacterial activity of alkaloids isolated from the sponge *Agelas dilatata* collected in Yucatan Peninsula

Dawrin Pech-Puch¹, Mar Perez-Povedano¹, Marta Martínez-Guitián², Cristina Lasarte-Monterrubio², Juan Carlos Vázquez-Ucha², Germán Bou², Jaime Rodríguez¹, Alejandro Beceiro² and Carlos Jiménez¹

¹Centro de Investigaciones Científicas Avanzadas (CICA) e Departamento de Química, Facultade de Ciencias, AE CICA-INIBIC, Universidade da Coruña, 15071 A Coruña, Spain

²Servicio de Microbiología. Instituto de Investigación Biomédica, Agrupación Estratégica INIBIC-CICA, Complejo Hospitalario Universitario A Coruña, 15006, A Coruña, Spain

* Correspondence: Centro de Investigaciones Científicas Avanzadas (CICA), AE CICA-INIBIC, Departamento de Química, Facultade de Ciencias, Universidade da Coruña, 15071 A Coruña, Spain. Tel: +34 981 167000. Fax: +34 981 167065. *E-mail address*: jaime.rodriguez@udc.es (Jaime Rodríguez); carlos.jimenez@udc.es, (Carlos Jiménez).

Abstract: Eight known compounds, ageliferin (**1**), bromoageliferin (**2**), dibromoageliferin (**3**), sceptrin (**4**), nakamuric acid (**5**), 4-bromo-1H-pyrrole-2-carboxylic acid (**6**), 4,5-dibromopyrrole-2-carboxylic acid (**7**) and 3,7-dimethylisoguanine (**8**), were isolated from the methanolic extract of the sponge *Agelas dilatata*, collected in the Cozumel Island, Quintana Roo. The planar structures of the new compounds were elucidated by 1D/2D NMR and IR spectroscopic analysis, HRESIMS and comparison of their spectral data with those reported in the literature. The compounds **1** and **2** displayed a high activity against two bacteria species *Klebsiella pneumoniae* and *Pseudomonas aeruginosa*, with a MIC between 64 to 8 mg/mL.

Keywords: Antibacterial; *Agelas dilatata*; Yucatan Peninsula

1. Introduction

More than two million people are infected by multidrug resistant (MDR) bacterial pathogens each year in the United States, resulting in more than 23,000 deaths.¹ There is therefore an urgent need for new therapies to combat these infections. The traditional approach to identify new antibacterial therapies is the search of bacteriostatic or bactericidal compounds from natural sources or by synthetic processes. However, bacteria invariably develop resistance to such compounds, sometimes as early as one year after clinical deployment. This was the case of daptomycin.² In the face of rapid resistance acquisition and the dire state of our antibiotic pipeline (especially with respect to Gram-negative bacteria), the need for new therapeutic options for the treatment of multi-resistant pathogen infections is indisputable.

Sponges belonging to the genus *Agelas* constitutes an important source of marine pyrrole-imidazole alkaloids.^{3,4} Since the structural elucidation of the first alkaloid, almost 50 years ago,⁵ more than 200 pyrrole-imidazoles have been described from a variety of

tropical sponges, displaying a wide range of biological properties including antitumor, antifungal and antibacterial activities.^{6,7}

Continuing with our chemical studies of marine organisms from Yucatan (Mexico),⁸ we focused our attention on the sponge *A. dilatata* collected in Cozumel Island, due to the antibacterial activity found in its organic extracts. There are only two reports on *A. dilatata*: a comparative study of the microbial diversity and the fatty acids composition of specimens collected at Bahamas⁹ and a taxonomic study of specimens belonging to genus *Agelas* from the Caribbean Sea.¹⁰ Here we want to report the isolation and structural characterization of seven known alkaloids from the organic extracts of specimens of this sponge collected at Cozumel Island in the Quintana Roo state of the Yucantan Peninsula.

2. Results and discussion

2.1 Animal material extraction and isolation

Specimens of the sponge *Agelas dilatata* were extracted several times using with a 1:1 mixture of CH₃OH-CH₂Cl₂ to give a crude extract. This organic extract was then partitioned between water and solvents of increasing polarity to give an enriched bromopyrroles *n*-butanol and aqueous methanolic fractions. The *n*-BuOH fraction was submitted to a solid phase extraction (SPE)-C18 (H₂O/MeOH/CH₂Cl₂ gradient system) and the resulting fractions were separated by reversed-phase HPLC to afford compounds **1**, **2**, and **4-8**. On the other hand, the aqueous MeOH fraction was submitted to reversed-phase HPLC to afford compounds **1-3** and **5-7**. (Figure 1).

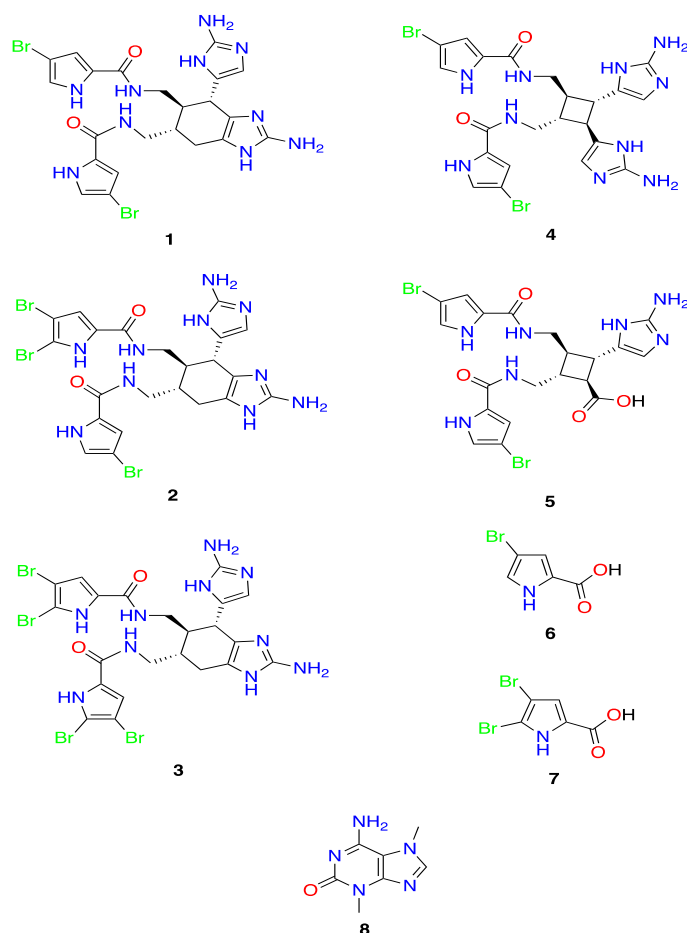


Figure 1. Alkaloids **1-8** isolated from *Agelas dilatata*.

Comparison of the NMR spectral data (1D and 2D NMR) and MS data to those of reported in the literature allowed us to determine the structures of compounds **1-8**. In this way, we could identify the following compounds: ageliferin (**1**),^{11,12} bromoageliferin (**2**),^{9,10} dibromoageliferin (**3**),^{11,12} sceptrin (**4**),¹³ nakamuric acid (**5**),¹⁴ 4-bromo-1H-pyrrole-2-carboxylic acid (**6**),¹⁵ 4,5-dibromopyrrole-2-carboxylic acid (**7**)¹⁶ and 3,7-dimethylisoguanine (**8**)¹⁷. All of them were previously isolated from different sponge species of the genus *Agelas*, but this is the first time that the former compounds were isolated from *Agelas dilatata*.

2.2 Antibacterial activity

All the isolated compounds were submitted to antibacterial evaluation against three Gram-negative pathogens, *Acinetobacter baumannii* (ABRIM and ATCC 17978), *Klebsiella pneumoniae* (ATCC 700603 and ST15) and *Pseudomonas aeruginosa* (ATCC 27853, PA01, 29-200 SV, 30-127 VI, 30-223 SV and 30-230 SV) and the results are displayed in Table 1. In order to classify their antibacterial activity, three categories were established: high active, MIC \leq 8 mg/L; intermediate active, MIC 16-64 mg/L and low or no active, MIC \geq 128 mg/L. Following the former classification, we found that 1 and 2 display an intermediate to high activity against the Gram-negative *Klebsiella pneumoniae* and *Pseudomonas aeruginosa* (Table 1).

Table 1. Antibacterial Activity Data (mg/L) of the compounds **1-8**.

Compound	<i>Acinetobacter baumannii</i>		<i>Klebsiella pneumoniae</i>		<i>Pseudomonas aeruginosa</i>					
	ABRIM	ATCC 17978	ATCC 700603	ST15	ATCC 27853	PA01	29-200 SV	30-127 VI	30-223 SV	30-230 SV
Ageliferin (1)	nt	\geq 128	64	64	64	64	nt	nt	nt	nt
Bromoageliferin (2)	\geq 128	\geq 128	64	64	8	16	32	32	32	32
Dibromoageliferin (3)	nt	nt	nt	nt	nt	nt	nt	nt	nt	nt
Sceptrin (4)	nt	$>$ 128	128	128	128	128	nt	nt	nt	nt
Nakamuric acid (5)	\geq 128	\geq 128	\geq 128	\geq 128	\geq 128	\geq 128	nt	nt	nt	nt
4-bromo-1H-pyrrole-2-carboxylic acid (6)	nt	$>$ 128	$>$ 128	128	$>$ 128	$>$ 128	nt	nt	nt	nt
4,5-dibromopyrrole-2-carboxylic acid (7)	$>$ 64	$>$ 64	128	128	128	128	nt	nt	nt	nt
3,7-dimethylisoguanine (8)	nt	\geq 128	\geq 128	\geq 128	\geq 128	\geq 128	nt	nt	nt	nt
Imipenem (positive control)	0.5	0.5	0.25	0.25	2	2	2	2	2	2

*nt: not tested

Ageliferin (**1**) has been previously reported as antibacterial (*Bacillus subtilis* (168), *Staphylococcus aureus* (ATCC 25923), *Micrococcus luteus* and *Escherichia coli* (ATCC 25922 and HB101)),^{12,14,18} antiviral (*Herpes simplex virus*-type 1 and *Vesicular stomatitis virus*), antifouling (*Balanus amphitrite amphitrite*),¹⁴ potent actomyosin ATPase activator,¹⁹ activity on the somatostatin receptor and vasoactive intestinal peptide (VIP) receptor.^{11,12, 20} However, this is the first time that the antibacterial activity against *Acinetobacter baumannii*, *Klebsiella pneumoniae* and *Pseudomonas aeruginosa* is

reported for ageliferin (**1**). Furthermore, **1** displays the same MIC values (64 mg/L) against all the strains for each bacteria tested.

Additionally, **1** was reported inactive as antifungal (*Penicillium atrovenetum* and *Saccharomyces cerevisiae*), cytotoxic (*Artemia salina* and monkey kidney cells), antifouling (*Barnacle improvisus*)²¹ and as biochemical prophage inducer (BIA) assay¹² and inhibitory activity against protein phosphatase type 2A.¹⁸

Bromoageliferin (**2**) was the most active compound against the *Pseudomonas aeruginosa* ATCC27853 reference strain with a MIC of 8 mg/L, while it displays MIC values of 16-32 mg/mL against the other clinical strains. Previously, **2** has been reported as antibacterial (*Bacillus subtilis*, *Staphylococcus aureus* (MRSA), *Micrococcus luteus*, *Escherichia coli*, *Rhodospirillum salexigens* (SCRC 113) and *Acinetobacter baumannii*),^{18,22,23} antiviral (*Herpes simplex*-type 1 and *Vesicular stomatitis*),¹² potent actomyosin ATPase activator,¹⁹ inhibitor of voltage-operated, but not store-operated calcium entry in PC12 cells²⁴ and potent feeding deterrent (*Thalassoma bifasciatum*).²⁵ Other biological studies of **2** report that it is not active as antifungal (*Penicillium atrovenetum* and *Saccharomyces cerevisiae*), cytotoxic (monkey kidney cells) and biochemical prophage induction (BIA) assay,¹² antitumoral against three human tumor cell lines (A549 lung cancer cells, HT29 colonic cancer cells, and MDA-MB-231 breast cancer cells)²⁶ and as inhibitor against protein phosphatase type 2A.¹⁸ Compounds **4-8** were classified as low or no active against the bacteria strains tested. Compound **3** was not tested. However, a review of the reported biological evaluation for each compound is described.

Dibromoageliferin (**3**) has been reported active as: antibacterial (*Bacillus subtilis*, *Micrococcus luteus* and *Escherichia coli*),^{12,18} antiviral (*Herpes simplex* virus-type 1 and *Vesicular stomatitis* virus),¹² potent actomyosin ATPase activator,¹⁹ inhibit voltage-operated, but not store-operated calcium entry in PC12 cells²⁴ and potent feeding deterrent (*Thalassoma bifasciatum*).²⁵ Compound **3** was reported not active as: antifungal (*Penicillium atrovenetum* and *Saccharomyces cerevisiae*), cytotoxic (monkey kidney cells) and biochemical prophage induction (BIA) assay¹² and antitumoral against three human tumor cell lines (A549 lung cancer cells, HT29 colonic cancer cells and MDA-MB-231 breast cancer cells).²⁶

Sceptrin (**4**) has been reported active as: antibacterial (*A. baumannii* (19606), MRSA (BAA-1685), *K. Pneumoniae*, *Micrococcus luteus*, *Staphylococcus aureus* (ATCC 25923), *Bacillus subtilis* (168), *Pseudomonas aeruginosa* and *Escherichia coli* (ATCC 25922 and HB 101)),^{27,18,28,14,12,13,29} antiviral (*Herpes simplex* virus-type 1 and *Vesicular stomatitis* virus), biochemical prophage induction (BIA) assay, antifouling (*Balanus amphitrite amphitrite*),¹² inhibitory activity against protein phosphatase type 2A,¹⁸ feeding deterrent (*Thalassoma bifasciatum*)²⁵, reduced voltage dependent calcium elevation in PC12 cells,³⁰ antifungal (*C. neoformans*),³¹ fungicidal (*Phytophthora infestans*, *Candida albicans*, *Alternaria* sp. and *Cladosporium cucumerinum*),^{32,13} inhibits cell motility in a variety of cancer cell lines (HeLa cells, metastatic breast cancer cell line (MDA-MB-231), lung cancer cell line (A549) and mouse fibroblasts (3T3)),³³ antiparasitic (*Trypanosoma brucei rhodesiense* and *Plasmodium falciparum*),³⁴ activity on the somatostatin receptor and vasoactive intestinal peptide (VIP) receptor,²⁰ antihistaminic activity (guinea pig ileum),³⁵ anti-muscarinic activity (muscarinic acetylcholine receptors (mAChR))³⁶ and interaction with bacterial MreB protein.³⁷

However, **4** was reported no active as: antimicrobial (*C. albicans*, *S. aureus*, MRS, *P. aeruginosa*, *M. intracellulare*, and *A. fumigatus*), antimalarial activity (*P. falciparum*, D6 and W2 clone), not antiparasitic activity (*Leishmania donovani*), no antiviral (HIV-1 in PBM cells),³¹ antifungal (*Penicillium atrovirens* and *Saccharomyces cerevisiae*),¹² insecticidal (*Diabrotica virgifera virgifera*, *Heliothis virescens* and *Lygus hesperus*), herbicidal (*Agrostis stolonifera* and *Nicotiana tabacum*), fungicidal (*Stagonospora nodorum*, *Fusarium culmorum*, *Pyricularia grisei* and *Puccinia recóndita*),³² cytotoxicity (monkey kidney cells, KB cell line, L6 cells 10MD2162, L929, KB-31, MCF-7, and FS4-LTM),^{12,27,38} Inhibitory activity in *P. falciparum* enzymes (PfFabI, PfFabG and PfFabZ), antiparasitic (*Trypanosoma cruzi* and *Leishmania donovani*)³⁴ and antifouling (*Artemia salina* and *Barnacle improvisus*).²¹

Nakamuric acid (**5**) has been reported active as: antibacterial against *Bacillus subtilis* (168) and inactive against *Staphylococcus aureus* (ATCC 25923) and *Escherichia coli* (ATCC 25922 and HB101).¹⁴

4-bromo-1H-pyrrole-2-carboxylic acid (**6**) has been reported active as: feeding deterrent (*Thalassoma bifasciatum*)²⁵ and no active as reduced voltage dependent calcium elevation in PC12 cells,³⁰ cytotoxic (HL-60, K562, A549, and HCT-116 tumor cell lines) and antimicrobial (*Staphylococcus aureus*, *Escherichia coli*, *Proteus bacillus vulgaris*, and *Candida albicans*).³⁹

4,5-dibromopyrrole-2-carboxylic acid (**7**) has been reported active as: antibacterial (*S. aureus*, *E. coli*, *Serratia marcescens* and *Micrococcus* sp.),⁴⁰ feeding deterrent (*Thalassoma bifasciatum*).^{25,41,15} reduced voltage dependent calcium elevation in PC12 cells,^{30,42} enzyme inhibitory activity (PfFabI), antiprotozoal activities (*Plasmodium falciparum*, *Trypanosoma brucei rhodesiense*, *T. cruzi* and *Leishmania donovani*),⁴³ immunosuppressive activity⁴⁴ and antifouling (*Balanus amphitrite*).⁴⁵ However **7** was reported not active as: antibacterial (*Bacillus megaterium*, *Bacillus subtilis* (168), *S. aureus* (ATCC 25923) *E. coli* (ATCC 25922) and *Mycobacterium smegmatis* (NBRC 3207)),^{46,47,48} enzyme inhibitory activity in analogous FabI enzymes from *M. tuberculosis* (MtFabI, InhA) and *E. coli* (EcFabI), citotoxicity in rat skeletal myoblasts (L6 cells)⁴³, mouse lymphoma (L5178Y), rat brain cancer (PC12) and human cervix cancer cells (HeLa)⁴⁴, fungicidal (*Ustilago violacea*, *Mycotypha microspora*, *Eurotium repens*, *Fusarium oxysporum*, *Saccharomyces cerevisiae*, *Cladosporium cucumerinum*, and *C. herbarum*),^{46,47} algicidal (*Chlorella fusca*),⁴⁷ protein kinase inhibition assays (cyclin-dependent kinase-1, cyclin-dependent kinase-5 and glycogen synthase kinase-3),⁴⁶ inhibitory activities against 2,2-diphenyl-1-picrylhydrazyl (DPPH) radical scavenging, acetylcholinesterase (AChE)⁴⁹ and protein tyrosine phosphatase 1B (PTP1B).⁴⁸

3,7-dimethylisoguanine (**8**) was reported inactive as antifouling, to inhibit biofilm formation of three marine bacterial strains, *Pseudoalteromonas* spp. (D41 and TC8) and *Paracoccus* sp. (4M6).⁵⁰

3. Material and Methods

3.1 General Experimental Procedures

Optical rotations were measured on a JASCO DIP-1000 polarimeter, with a Na (589 nm) lamp and filter. ^1H , ^{13}C , and 2D NMR spectra were recorded on a Bruker Avance 500 spectrometer at 500.13 and 125.0 MHz, respectively, using CD_3OD and D_2O . HRESIMS experiments were performed on the Applied Biosystems QSTAR Elite system. HREIMS Mass Spectrometer Thermo MAT95XP. HPLC separations were performed on the Agilent 1100 liquid chromatography system equipped with a solvent degasser, quaternary pump, and diode array detector (Agilent Technologies, Waldbronn, Germany) using a semipreparative reversed phase column Luna C18, 5μ , 100 Å, 250 x 10 mm. Precoated silica gel plates (Merck, Kieselgel 60 F254, 0.25 mm) were used for TLC analysis and the spots were visualized under a UV light (254 nm) or by heating the plate pretreated with $\text{H}_2\text{SO}_4/\text{H}_2\text{O}/\text{AcOH}$ (1:4:20).

3.2 Animal Material

The sponge *Agelas dilatata* was collected by hand and traditional SCUBA-diving in Cozumel Island, Quintana Roo ($20^\circ 43' 55.03''\text{N}$ / $87^\circ 00' 24.70''\text{W}$) at depths ranging from 10 to 15 meters in October 2016 and frozen immediately after collection. A voucher specimen E25-1 was deposited in the Phylum Porifera Gerardo Green National Collection of the Instituto de Ciencias del Mar y Limnología (ICMyL) at the National Autonomous University of Mexico (UNAM).

3.3 Extraction and Isolation

Sliced bodies of *A. dilatata* (wet weight, 431.2 g; dry weight, 113.0 g) were exhaustively extracted with $\text{CH}_3\text{OH}-\text{CH}_2\text{Cl}_2$ (1:1, 3 x 1.5 L) at room temperature. The combined extracts were concentrated under reduced pressure to give 20.0 g of a crude residue that was first partitioned between $\text{CH}_2\text{Cl}_2/\text{H}_2\text{O}$ (1:1 v/v). The resulting aqueous portion was extracted with *n*-butanol (200 mL) to yield the *n*-butanol fraction (3.25 g). The organic phase was concentrated under reduced pressure and partitioned between 10% aqueous CH_3OH (400 mL) and hexane (2×400 mL) to give, after removing the solvent under reduced pressure, 227.4 mg of the hexane fraction. The H_2O content (% v/v) of the methanolic fraction was adjusted to 50% aqueous CH_3OH , and this mixture was extracted with CH_2Cl_2 (100 mL) to afford, after removing the solvent under reduced pressure, 109.4 mg of the CH_2Cl_2 fraction and 150.4 mg of the remaining aqueous methanolic fraction.

The *n*-butanol fraction was subjected to Solid Phase Extraction (SPE) with RP-18 (Merck KGaA) using a stepped gradient from H_2O to CH_3OH and then CH_2Cl_2 . Separation of the fraction eluted with $\text{H}_2\text{O}/\text{CH}_3\text{OH}$ (2:1, 520 mg) by RP-HPLC with a mobile phase consisting of 3 min of a gradient from 40% to 60% of CH_3OH in H_2O (v/v, each containing 0.04% trifluoroacetic acid) followed by a 13 min isocratic at 60% of CH_3OH and, finally, a 9 min of a gradient from 60% to 100% of CH_3OH in H_2O at a flow rate of 2.0 mL/min afforded 3,7-dimethylisoguanine (**8**) (30.0 mg; t_{R} = 6.1 min), sceptrin (**4**) (5.8 mg; t_{R} = 10.2 min), ageliferin (**1**) (6.5 mg; t_{R} = 15.1 min), 4-bromo-1H-pyrrole-2-carboxylic acid (**6**) (10.0 mg; t_{R} = 16.6 min) and bromoageliferin (**2**) (2.3 mg; t_{R} = 23.8 min).

Separation of the fraction eluted with $\text{H}_2\text{O}/\text{CH}_3\text{OH}$ (1:1, 250.6 mg) by RP-HPLC with a mobile phase consisting in 2 min of a gradient from 40% to 50% of CH_3OH in H_2O (v/v, each containing 0.04% trifluoroacetic acid), followed by a 8 min isocratic at 50% of CH_3OH , followed by a 9 min of a gradient from 50% to 60% of CH_3OH in H_2O ,

followed by a 8 min isocratic at 60% of CH₃OH and, finally, a 13 min of a gradient from 60% to 100% of CH₃OH in H₂O at a flow rate of 2.0 mL/min yielded 4-bromo-1H-pyrrole-2-carboxylic acid (**6**) (7.3 mg; t_R = 24.7 min), nakamuric acid (**5**) (3.0 mg; t_R = 26.5 min), bromoageliferin (**2**) (2.5 mg; t_R = 34.7 min) and 4,5-dibromopyrrole-2-carboxylic acid (**7**) (**6**) (12.2 mg; t_R = 36.5 min).

Separation of the fraction eluted with H₂O/CH₃OH (1:2, 212.7 mg) by RP-HPLC with a mobile phase consisting in 5 min of an isocratic at 50% CH₃OH in H₂O (v/v, each containing 0.04% trifluoroacetic acid), followed by a 10 min of an gradient from 50% to 60% of CH₃OH in H₂O, followed by a 10 min isocratic at 60% of CH₃OH and, finally, a 15 min of a gradient from 60% to 100% of CH₃OH in H₂O at a flow rate of 2.0 mL/min yielded nakamuric acid (**5**) (1.8 mg; t_R = 19.7 min), 4-bromo-1H-pyrrole-2-carboxylic acid (**6**) (2.4 mg; t_R = 20.8 min), bromoageliferin (**2**) (1.7 mg; t_R = 22.8 min) and 4,5-dibromopyrrole-2-carboxylic acid (**7**) (17.7 mg; t_R = 32.6 min).

The aqueous methanolic fraction (150.4 mg) was submitted to RP-HPLC separation using a mobile phase consisting of 5 min of an isocratic at 50% CH₃OH in H₂O (v/v, each containing 0.04% trifluoroacetic acid), followed by a 10 min of an gradient from 50% to 60% of CH₃OH in H₂O, followed by a 15 min of an gradient from 60% to 65% of CH₃OH in H₂O and, finally, a 10 min of a gradient from 65% to 100% of CH₃OH in H₂O at a flow rate of 2.0 mL/min to afford ageliferin (**1**) (2.6 mg; t_R = 17.3 min), 4-bromo-1H-pyrrole-2-carboxylic acid (**6**) (3.3 mg; t_R = 18.2 min), nakamuric acid (**5**) (3.6 mg; t_R = 19.3 min), bromoageliferin (**2**) (3.2 mg; t_R = 23.8 min), 4,5-dibromopyrrole-2-carboxylic acid (**7**) (4.2 mg; t_R = 29.2 min) and dibromoageliferin (**3**) (1.2 mg; t_R = 33.0 min).

3.4 Structural characterization

Ageliferin (1). $[\alpha]_D^{25} +15.1^\circ$ (c 0.2, MeOH); ¹H NMR and ¹³C NMR (125 MHz) see SI; (-)-HRESIMS m/z 617.0380 (M-H)⁻ (calcd. For C₂₂H₂₃⁷⁹Br₂N₁₀O₂, 617.0378).

Bromoageliferin (2). $[\alpha]_D^{25} +9.1^\circ$ (c 0.2, MeOH); ¹H NMR and ¹³C NMR (125 MHz) see SI; (-)-HRESIMS m/z 694.9482 (M-H)⁻ (calcd. For C₂₂H₂₂⁷⁹Br₃N₁₀O₂, 694.9483).

Dibromoageliferin (3). $[\alpha]_D^{25} +4.0^\circ$ (c 0.2, MeOH); ¹H NMR and ¹³C NMR (125 MHz) see SI; (-)-HRESIMS m/z 772.8582 (M-H)⁻ (calcd. For C₂₂H₂₁⁷⁹Br₄N₁₀O₂, 772.8588).

Sceptrin (4). $[\alpha]_D^{25} - 13.8^\circ$ (c 0.2, MeOH); ¹H NMR and ¹³C NMR (125 MHz) see SI; (-)-HRESIMS m/z 619.0531 (M-H)⁻ (calcd. For C₂₂H₂₅⁷⁹Br₂N₁₀O₂, 619.0523).

Nakamuric acid (5). $[\alpha]_D^{25} - 9.5^\circ$ (c 0.2, MeOH); ¹H NMR and ¹³C NMR (125 MHz) see SI; (-)-HRESIMS m/z 579.9945 (M-H)⁻ (calcd. For C₂₀H₂₀⁷⁹Br₂N₇O₄, 579.9949).

4-bromo-1H-pyrrole-2-carboxylic acid (6). ¹H NMR and ¹³C NMR (125 MHz) see SI; (-)-HRESIMS m/z 187.9353 (M-H)⁻ (calcd. For C₅H₃⁷⁹BrNO₂, 187.9353).

4,5-dibromopyrrole-2-carboxylic acid (7). ¹H NMR and ¹³C NMR (125 MHz) see SI; (-)-HRESIMS m/z 265.8455 (M-H)⁻ (calcd. For C₅H₂⁷⁹Br₂NO₂, 265.8458).

3,7-dimethylisoguanine (8). ¹H NMR and ¹³C NMR (125 MHz) see SI; (-)-HRESIMS m/z 180.0881 (M+H)⁺ (calcd. For C₇H₁₀N₅O, 180.0880).

3.5 Antibacterial activity assays

3.5.1. Culture preparation.

The bacterial strains of reference used in this study were four Gram-negative pathogens, *A. baumannii* (strain ATCC 17978), *K. pneumoniae* (strain ATCC 700603) and *P. aeruginosa* (strains ATCC 27853 and PA01) and also we used other six clinical strains that were isolated from samples of our hospital, *A. baumannii* (strain ABRIM), *K.*

pneumoniae (strain ST15) and *P. aeruginosa* (strains 29-200 SV, 30-127 VI, 30-223 SV and 30-230 SV).

Gram-negative strains were routinely grown or maintained in Luria-Bertani (LB) and all strains were grown at 37 °C and stored in 10 % glycerol at -80 °C.

3.5.2. Microdilution method: Minimum inhibitory concentration

The minimum inhibitory concentration (MIC) assays were performed through microdilution method, as described by CLSI (CLSI, 2012). Dimethylsulfoxide (DMSO) was used to dissolve the crude extracts, at a maximum concentration of 2.5% v/v in the well with the highest concentration of the plate (256 mg/L). Briefly, the strains were cultured overnight in Mueller Hinton II agar plates (Becton Dickinson) to 37 °C and then, the turbidities of bacterial suspensions were standardized at 0.5 on the McFarland scale to establish the inocula. Two-fold serial dilutions of extracts were performed in 96-wells microplates using Mueller Hinton II broth medium (Sigma). The range of extracts concentrations for MIC analysis was 0.5-256 mg/L. One well was used in each row as growth positive control, composed of growth media and bacterial suspension, and another well was used as negative control, consisted of medium without bacterial inoculum. Solvent controls of DMSO were performed on the growth medium to determine if the used concentration interfered with bacterial growth. The minimum inhibitory concentration was evaluated after incubation 20-24 h to 37 °C and was established as the lowest concentration of the compound in which the bacterial strains did not grow. All extracts were tested in triplicate.

4. Conclusions

Eight known alkaloids were isolated from sponge *Agelas dilatata* collected in the Cozumel Island. The structure elucidation of the compounds were determined by 1D and 2D NMR and by comparison with the literature data. Compounds **1** and **2** display significant antibacterial activity against two Gram-negative bacteria strains.

This work represents the first chemical study of the secondary metabolites from *A. dilatata* and this is the first time where the activity of all the compounds were evaluated on gram negative bacteria: *Klebsiella pneumoniae* and *Pseudomonas aeruginosa*.

The present report is the first time where the antibacterial activity of the compounds against gram negative bacteria is confirmed using several clinical strains.

Supplementary Materials: Figures S1-S6: NMR spectra in CD₃OD and HRESIMS of the compounds **1-8**.

Author Contributions: Conceptualization, Carlos Jiménez, Dawrin Pech-Puch and Jaime Rodríguez; Extraction process: Dawrin Pech-Puch; Formal analysis, Dawrin Pech-Puch, Jaime Rodríguez and Carlos Jiménez; Investigation, Dawrin Pech-Puch, Funding acquisition and Resources, Jaime Rodríguez and Carlos Jiménez Writing – original draft, Dawrin Pech-Puch; Writing – review & editing, Dawrin Pech-Puch, Carlos Jiménez and Jaime Rodríguez.

Funding: This work was supported by Grants AGL2015-63740-C2-2-R and RTC-2016-4611-1 (AEI/FEDER, EU) from the State Agency for Research (AEI) of Spain, both co-funded by the FEDER Programme from the European Union. DPP received a fellowship from the program National Council of Science and Technology (CONACYT) of Mexico and the Secretariat of Research, Innovation and Higher Education (SIIES) of Yucatan.

Mexico and the Secretariat of Research, Innovation and Higher Education (SIIES) of Yucatan.

Acknowledgments: We gratefully acknowledge the help of colleagues, Daniel Catzim Pech, Carlos González-Salas, Gabriel González Mapen, Jorge Peniche Pérez, Melissa Llanes López and Rodrigo Garcia Uribe for collecting the marine samples. We thank to Patricia Gomez for the taxonomic identification of the sponge.

References

1. Dolgin, E. Sequencing of superbugs seen as key to combating their spread. *Nat. Med.* **2010**, *16*, 1054–1054.
2. Lewis 2nd J.S.; Owens A.; Cadena J.; Sabol K.; Patterson J.E.; Jorgensen J.H. Emergence of daptomycin resistance in *Enterococcus faecium* during daptomycin therapy. *Antimicrob Agents Chemother* **2005**, *49*, 1664–1665. [L]
[SEP]
3. Lindel, T. Chemistry and Biology of the Pyrrole–Imidazole Alkaloids. *Alkaloids Chem. Biol.* **2017**, *77*, 117–219.
4. Zhang, H.; Dong, M.; Chen, J.; Wang, H.; Tenney, K.; Crews, P. Bioactive Secondary Metabolites from the Marine Sponge Genus *Agelas*. *Mar. Drugs* **2017**, *15* (11).
5. Sharma, G.M.; Burkholder, P.R. Structure of Dibromophakellin a New Bromine-Containing Alkaloid from the Marine Sponge *Phakellia flabellata*. *J. Chem. Soc. D* **1971**, No. 3, 151–152.
6. Rane, R.; Sahu, N.; Shah, C.; Karpoormath, R. Marine Bromopyrrole Alkaloids: Synthesis and Diverse Medicinal Applications. *Curr. Top. Med. Chem.* **2014**, *14* (2), 253–273.
7. Forte, B.; Malgesini, B.; Piutti, C.; Quartieri, F.; Scolaro, A.; Papeo, G.A. Submarine Journey: The Pyrrole-Imidazole Alkaloids. *Mar. Drugs* **2009**, *7* (4), 705–753.
8. Pech-Puch, D.; Rodríguez, J.; Cautain, B.; Sandoval-Castro, C.A.; Jiménez, C. Cytotoxic Furanoditerpenes from the Sponge *Spongia tubulifera* Collected in the Mexican Caribbean. *Mar. Drugs* **2019**, *17* (7), 1–10.
9. Hochmuth, T.; Niederkrüger, H.; Gernert, C.; Siegl, A.; Taudien, S.; Platzer, M.; Crews, P.; Hentschel, U.; Piel, J. Linking Chemical and Microbial Diversity in Marine Sponges: Possible Role for Poribacteria as Producers of Methyl-Branched Fatty Acids. *ChemBioChem* **2010**, *11* (18), 2572–2578.
10. Parra-velandia, F. J.; Zea, S.; Soest, R. O. B. W. M. V. A. N. Reef Sponges of the Genus *Agelas* (Porifera: Demospongiae) from the Greater Caribbean. *Zootaxa* **2014**, *3794* (3), 301–343.
11. Rinehart, K. L. Biologically Active Marine Natural Products. *Pure Appl. Chem.* **1989**, *61* (3), 525–528.
12. Keifer, P.A.; Schwartz, R.E.; Koker, M.E.S.; Hughes, R.G.J.; Rittschof, D.; Rinehart, K.L. Bioactive Bromopyrrole Metabolites from the Caribbean Sponge *Agelas conifera*. *J. Org. Chem.* **1991**, *54*, 2965–2975.
13. Walker, R.P.; John Faulkner, D.; Van Engen, D.; Clardy, J. Sceptrin, an Antimicrobial Agent from the Sponge *Agelas sceptrum*. *J. Am. Chem. Soc.* **1981**, *103* (22), 6772–6773.
14. Eder, C.; Proksch, P.; Wray, V.; Van Soest, R.W.M.; Ferdinandus, E.; Pattisina, L.A.; Sudarsono. New Bromopyrrole Alkaloids from the Indopacific Sponge *Agelas nakamura*. *J. Nat. Prod.* **1999**, *62* (9), 1295–1297.

15. Chanas, B.; Pawlik, J. R.; Lindel, T.; Fenical, W. Chemical Defense of the Caribbean Sponge *Agelas clathrodes* (Schmidt). *J. Exp. Mar. Bio. Ecol.* **1996**, *208* (1–2), 185–196.
16. Forenza, S.; Minale, L.; Riccio, R.; Fattorusso, E. New Bromo-Pyrrole Derivatives from the Sponge *Agelas oroides*. *J. Chem. Soc. D Chem. Commun.* **1971**, 285 (18), 1129–1130.
17. Cafieri, F.; Fattorusso, E.; Mangoni, A.; Taglialatela-Scafati, O. Longamide and 3,7-Dimethylisoguanine, Two Novel Alkaloids from the Marine Sponge *Agelas longissima*. *Tetrahedron Lett.* **1995**, *36* (43), 7893–7896.
18. Endo, T.; Tsuda, M.; Okada, T.; Mitsuhashi, S.; Shima, H.; Kikuchi, K.; Mikami, Y.; Fromont, J.; Kobayashi, J. Nagelamides A-H, New Dimeric Bromopyrrole Alkaloids from Marine Sponge *Agelas* Species. *J. Nat. Prod.* **2004**, *67* (8), 1262–1267.
19. Kobayashi, J.; Tsuda, M.; Murayama, T.; Nakamura, H.; Ohizumi, Y.; Ishibashi, M.; Iwamura, M.; Ohta, T.; Nozoe, S. Ageliferins, potent actomyosin ATPase activators from the okinawan marine sponge *Agelas* sp. *Tetrahedron* **1990**, *46* (16), 5579–5586.
20. Vassas, A.; Bourdy, G.; Paillard, J.J.; Lavayre, J.; Païs, M.; Quirion, J.C.; Debitus, C. Naturally Occurring Somatostatin and Vasoactive Intestinal Peptide Inhibitors. Isolation of Alkaloids from Two Marine Sponges. *Planta Med.* **1996**, *62* (1), 28–30.
21. Ortlepp, S.; Sjögren, M.; Dahlström, M.; Weber, H.; Ebel, R.; Edrada, R.A.; Thoms, C.; Schupp, P.; Bohlin, L.; Proksch, P. Antifouling Activity of Bromotyrosine-Derived Sponge Metabolites and Synthetic Analogues. *Mar. Biotechnol.* **2007**, *9* (6), 776–785.
22. Yamada, A.; Kitamura, H.; Yamaguchi, K.; Fukuzawa, S.; Kamijima, C.; Yazawa, K.; Kuramoto, M.; Wang, G.Y.S.; Fujitani, Y.; Uemura, D. Development of Chemical Substances Regulating Biofilm Formation. *Bulletin of the Chemical Society of Japan.* 1997, pp 3061–3069.
23. Melander, R. J.; Liu, H. Bing; Stephens, M.D.; Bewley, C.A.; Melander, C. Marine Sponge Alkaloids as a Source of Anti-Bacterial Adjuvants. *Bioorganic Med. Chem. Lett.* **2016**, *26* (24), 5863–5866.
24. Bickmeyer, U. Bromoageliferin and Dibromoageliferin, Secondary Metabolites from the Marine Sponge *Agelas conifera*, Inhibit Voltage-Operated, but Not Store-Operated Calcium Entry in PC12 Cells. *Toxicon* **2005**, *45* (5), 627–632.
25. Assmann, M.; Lichte, E.; Pawlik, J.R.; Köck, M. Chemical Defenses of the Caribbean Sponges *Agelas Wiedenmayeri* and *Agelas conifera*. *Mar. Ecol. Prog. Ser.* **2000**, *207*, 255–262.
26. Regalado, E.L.; Laguna, A.; Mendiola, J.; Thomas, O.P.; Nogueiras, C. Bromopyrrole Alkaloids from the Caribbean Sponge. *Quim. Nova* **2011**, *34* (2), 289–291.
27. Muñoz, J.; Köck, M. Hybrid Pyrrole-Imidazole Alkaloids from the Sponge *Agelas sceptrum*. *J. Nat. Prod.* **2016**, *79* (2), 434–437.
28. Melander, R.J.; Liu, H. Bing; Stephens, M.D.; Bewley, C.A.; Melander, C. Marine Sponge Alkaloids as a Source of Anti-Bacterial Adjuvants. *Bioorganic Med. Chem. Lett.* **2016**, *26* (24), 5863–5866.
29. Bernan, V.S.; Roll, D.M.; Ireland, C.M.; Greenstein, M.; Maiese, W.M.; Steinberg, D.A. A Study on the Mechanism of Action of Scepttrin, an Antimicrobial Agent Isolated from the South Pacific Sponge *Agelas mauritiana*. *J. Antimicrob. Chemother.* **1993**, *32* (4), 539–550.

30. Bickmeyer, U.; Drechsler, C.; Köck, M.; Assmann, M. Brominated Pyrrole Alkaloids from Marine Agelas Sponges Reduce Depolarization-Induced Cellular Calcium Elevation. *Toxicol* **2004**, *44* (1), 45–51.
31. Mohammed, R.; Peng, J.; Kelly, M.; Hamann, M.T. Cyclic Heptapeptides from the Jamaican Sponge *Stylissa caribica*. *J. Nat. Prod.* **2006**, *69* (12), 1739–1744.
32. Peng, J.; Shen, X.; Sayed, K.A.; Dunbar, D. C.; Perry, T.L.; Wilkins, S.P.; Hamann, M.T. Marine Natural Products as Prototype Agrochemical Agents. *J. Agric. Food Chem.* **2003**, *51*, 2246–2252.
33. Cipres, A.; O'Malley, D.P.; Li, K.; Finlay, D.; Baran, P.S.; Vuori, K. Scepttrin, a Marine Natural Compound, Inhibits Cell Motility in a Variety of Cancer Cell Lines. *ACS Chem. Biol.* **2010**, *5* (2), 195–202.
34. Scala, F.; Fattorusso, E.; Menna, M.; Tagliatalata-Scafati, O.; Tierney, M.; Kaiser, M.; Tasdemir, D. Bromopyrrole Alkaloids as Lead Compounds against Protozoan Parasites. *Mar. Drugs* **2010**, *8* (7), 2162–2174.
35. Cafieri, F.; Carnuccio, R.; Fattorusso, E.; Tagliatalata-Scafati, O.; Vallefucio, T. Anti-Histaminic Activity of Bromopyrrole Alkaloids Isolated from Caribbean *Agelas* Sponges. *Bioorganic Med. Chem. Lett.* **1997**, *7* (17), 2283–2288.
36. Rosa, R.; Silva, W.; de Motta, G.E.; Rodríguez, A.D.; Morales, J.J.; Ortiz, M. Anti-Muscarinic Activity of a Family of C11N5 Compounds Isolated from *Agelas* Sponges. *Experientia* **1992**, *48* (9), 885–887.
37. Rodríguez, A.D.; Lear, M.J.; La Clair, J.J. Identification of the Binding of Scepttrin to MreB via a Bidirectional Affinity Protocol. *J. Am. Chem. Soc.* **2008**, *130* (23), 7256–7258.
38. Tilvi, S.; Moriou, C.; Martin, M.T.; Gallard, J.F.; Sorres, J.; Patel, K.; Petek, S.; Cécile Debitus; Ermolenko, L.; Al-Mourabit, A. Agelastatin E, Agelastatin F, and Benzoscepttrin C from the Marine Sponge *Agelas dendromorpha*. *J. Nat. Prod.* **2010**, *73*, 720–723.
39. Chu, M.J.; Tang, X.L.; Qin, G.F.; Sun, Y.T.; Li, L.; de Voogd, N.J.; Li, P.L.; Li, G.Q. Pyrrole Derivatives and Diterpene Alkaloids from the South China Sea Sponge *Agelas nakamurai*. *Chem. Biodivers.* **2017**, *14* (7).
40. Barrow, R.A.; Capon, R.J. Brominated Pyrrole Carboxylic Acids from an Australian Marine Sponge, *Axinella* sp. *Nat. Prod. Lett.* **1993**, *1* (4), 243–250.
41. Lindel, T.; Hoffmann, H.; Hochgürtel, M.; Pawlik, J.R. Structure-Activity Relationship of Inhibition of Fish Feeding by Sponge-Derived and Synthetic Pyrrole-Imidazole Alkaloids. *J. Chem. Ecol.* **2000**, *26* (6), 1477–1496.
42. Bickmeyer, U.; Assmann, M.; Köck, M.; Schütt, C.A Secondary Metabolite, 4,5-Dibromopyrrole-2-Carboxylic Acid, from Marine Sponges of the Genus *Agelas* Alters Cellular Calcium Signals. *Environ. Toxicol. Pharmacol.* **2005**, *19* (3), 423–427.
43. Tasdemir, D.; Topaloglu, B.; Perozzo, R.; Brun, R.; O'Neill, R.; Carballeira, N. M.; Zhang, X.; Tonge, P.J.; Linden, A.; Rüedi, P. Marine Natural Products from the Turkish Sponge *Agelas oroides* That Inhibit the Enoyl Reductases from *Plasmodium falciparum*, *Mycobacterium tuberculosis* and *Escherichia coli*. *Bioorganic Med. Chem.* **2007**, *15* (21), 6834–6845.
44. Gunasekera, S.P.; Cranick, S.; Longley, R.E. Immunosuppressive Compounds from a Deep Water Marine Sponge, *Agelas flabelliformis*. *J. Nat. Prod.* **1989**, *52* (4), 757–761.
45. Ponasik, J.A.; Conova, S.; Kinghorn, D.; Kinney, W.A.; Rittschof, D.; Ganem, B. Pseudoceratidine, a Marine Natural Product with Antifouling Activity: Synthetic and Biological Studies. *Tetrahedron* **1998**, *54* (25), 6977–6986.

46. Hassana, W.; Elkhayata, E.S.; Edradaa, R.A.; Rainer, E.; Proksch, P. New Bromopyrrole Alkaloids from the Marine Sponges *Axinella damicornis* and *Stylissa flabelliformis*. *Nat. Prod. Commun.* **2007**, *2* (11), 1149–1154.
47. König, G.M.; Wright, A.D.; Linden, A. Antiplasmodial and Cytotoxic Metabolites from the Maltese Sponge *Agelas oroides*. *Planta Med.* **1998**, *64* (5), 443–447.
48. Abdjul, D.B.; Yamazaki, H.; Kanno, S. ichi; Tomizawa, A.; Rotinsulu, H.; Wewengkang, D.S.; Sumilat, D.A.; Ukai, K.; Kapojos, M.M.; Namikoshi, M. An Anti-Mycobacterial Bisfunctionalized Sphingolipid and New Bromopyrrole Alkaloid from the Indonesian Marine Sponge *Agelas* sp. *J. Nat. Med.* **2017**, *71* (3), 531–536.
49. Orhan, I.E.; Ozcelik, B.; Konuklugil, B.; Putz, A.; Kaban, U.G.; Proksch, P. Bioactivity Screening of the Selected Turkish Marine Sponges and Three Compounds from *Agelas oroides*. *Rec. Nat. Prod.* **2012**, *6* (4), 356–367.
50. Pérez, N.; Culioli, G.; Pérez, T.; Briand, J.F.; Thomas, O.P.; Blache, Y. Antifouling Properties of Simple Indole and Purine Alkaloids from the Mediterranean Gorgonian *Paramuricea clavata*. *J. Nat. Prod.* **2011**, *74* (10), 2304–2308.

Supplementary Materials

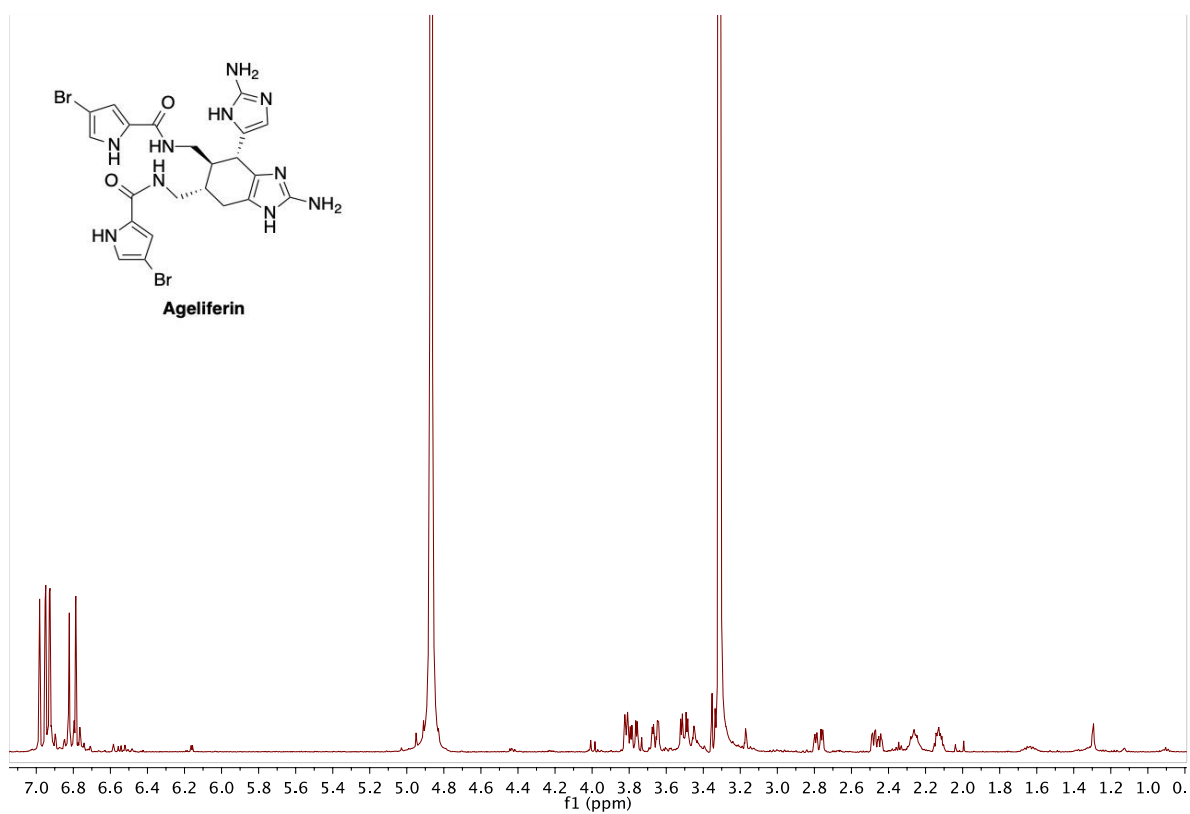


Figure S1. ¹H NMR spectrum of **1** (500 MHz, CD₃OD).

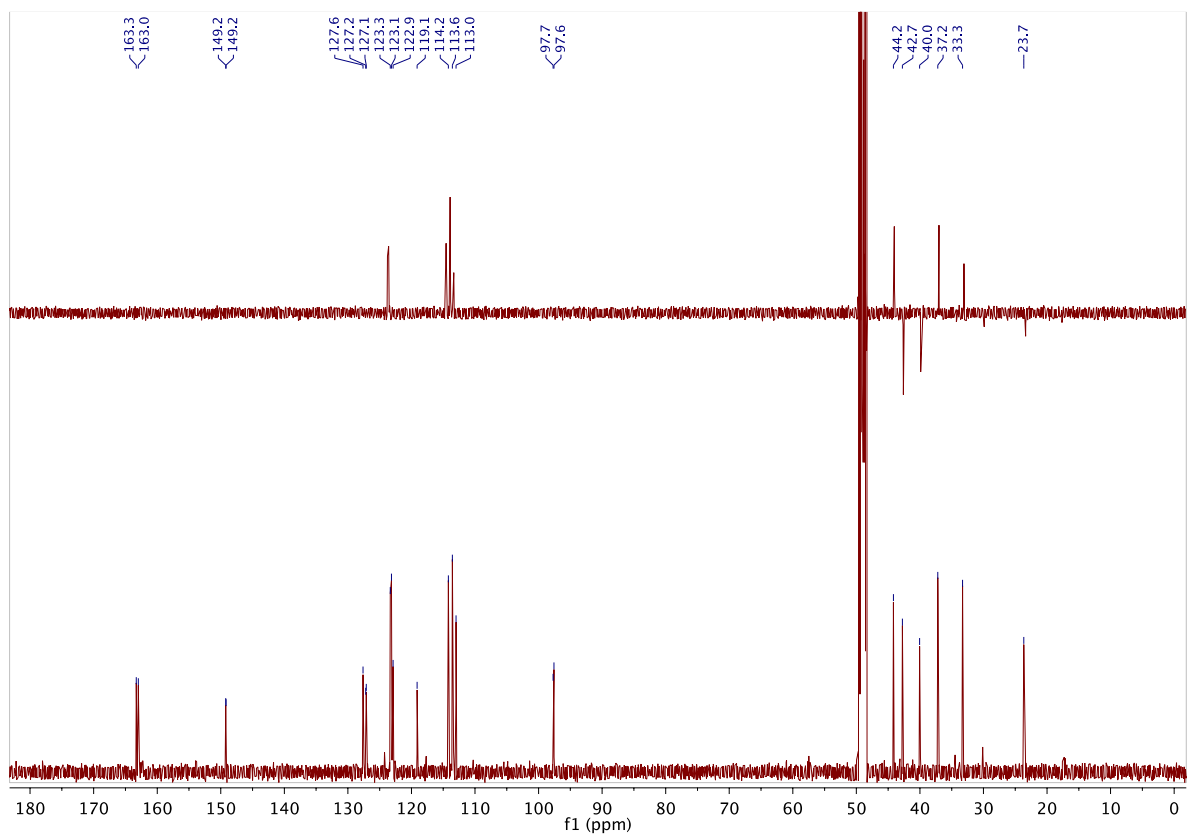


Figure S2. ¹³C NMR and DEPT-135 spectra of **1** (125 MHz, CD₃OD).

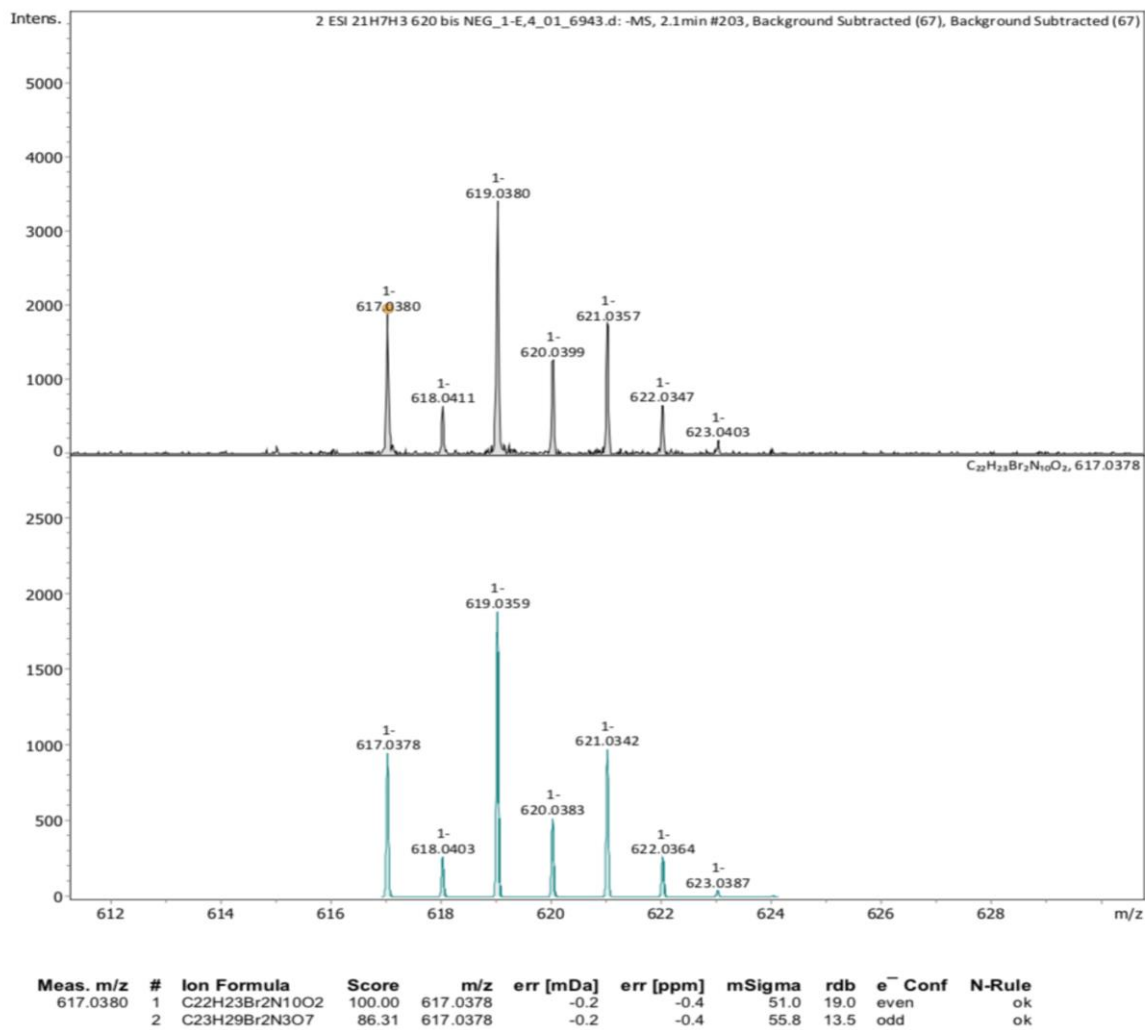
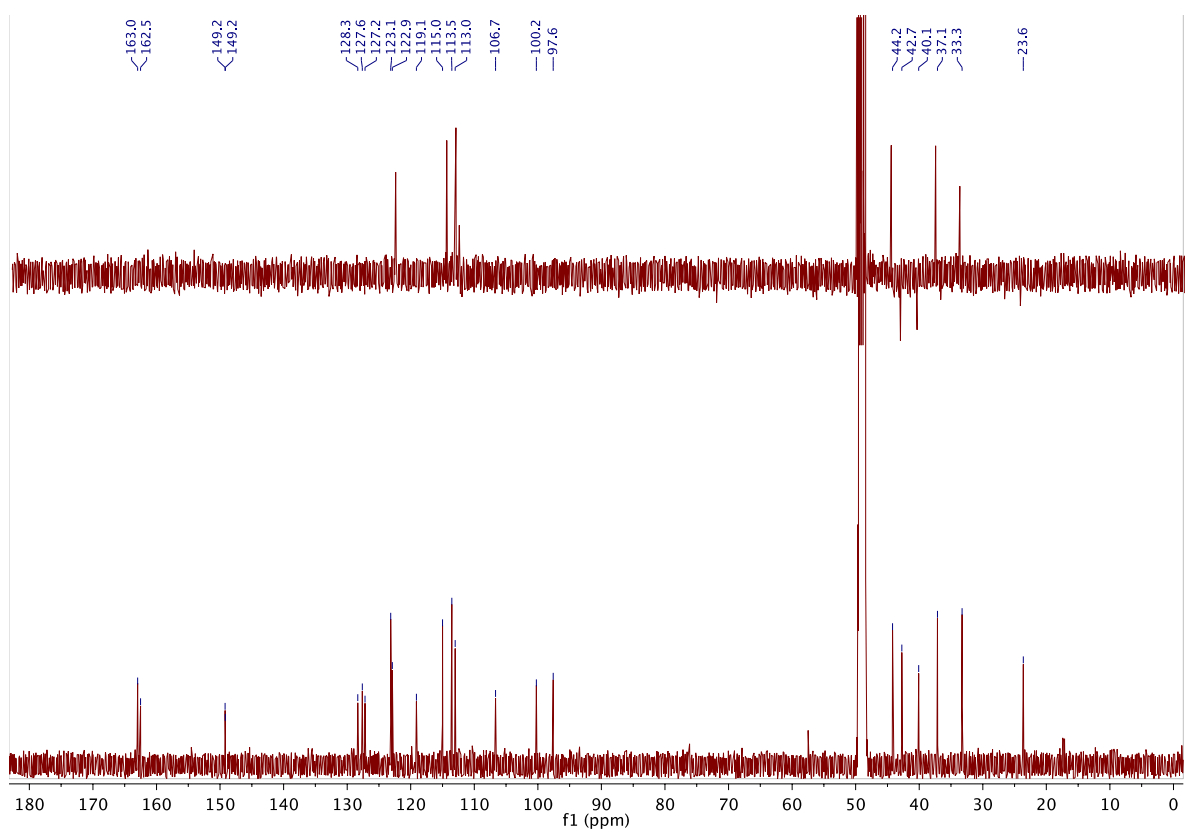
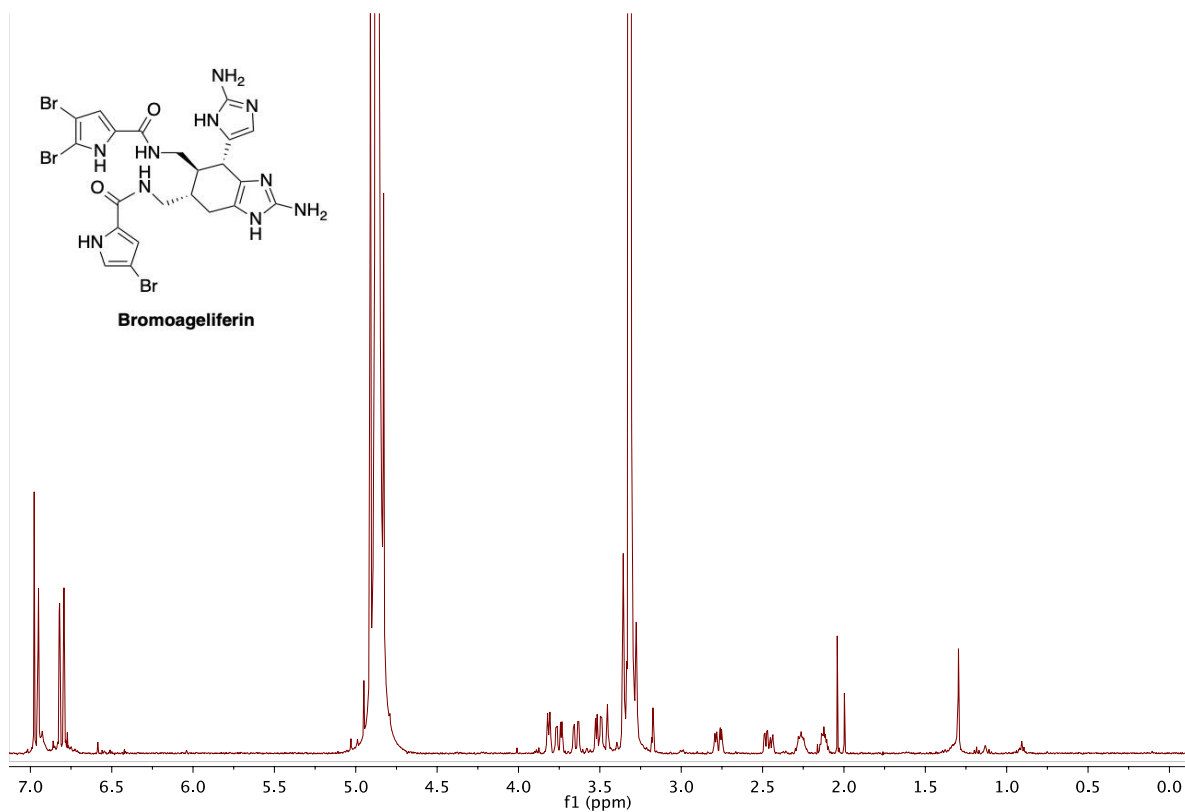
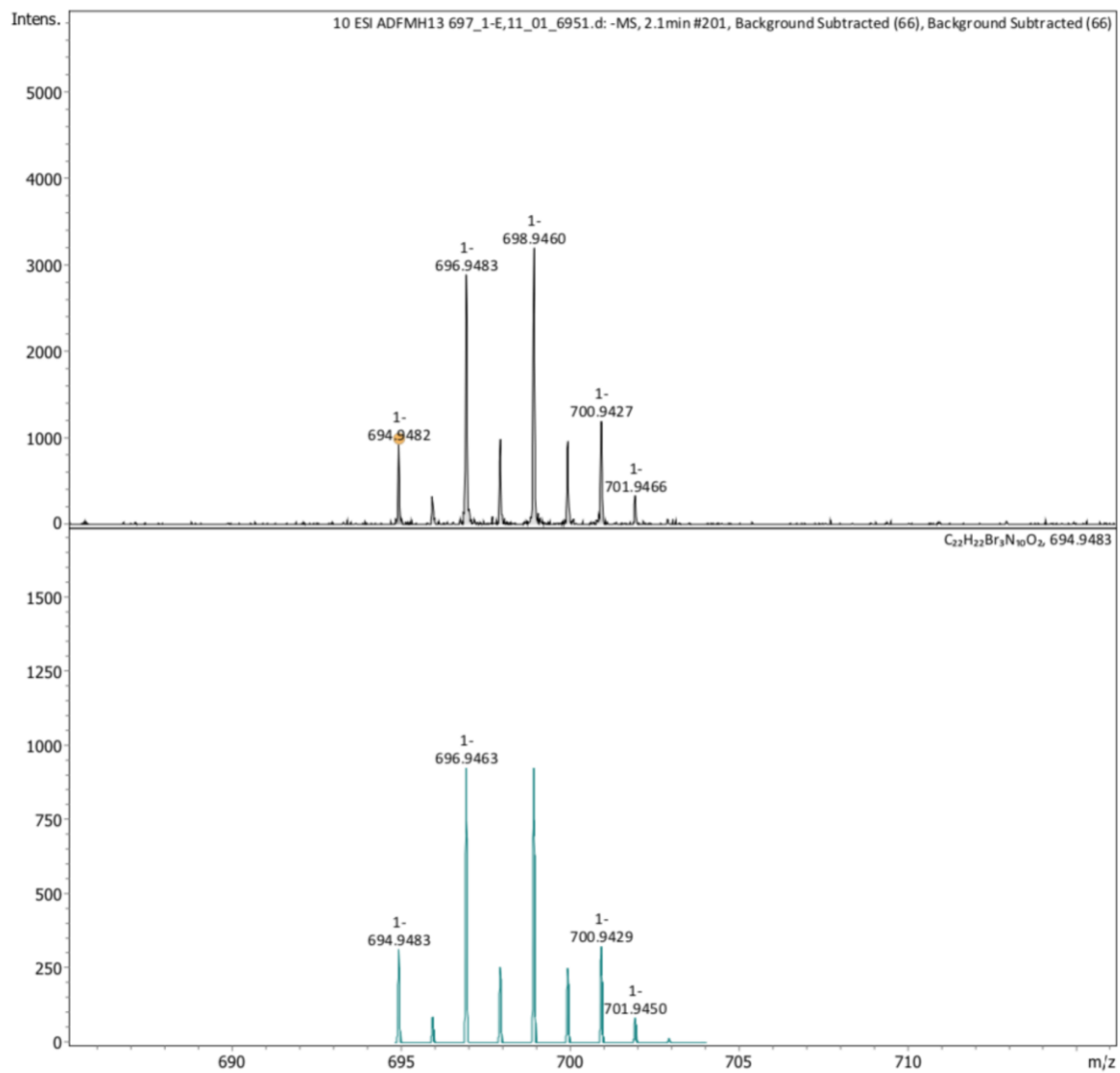


Figure S3. (-)-HRESIMS of 1.





Meas. m/z	#	Ion Formula	Score	m/z	err [mDa]	err [ppm]	mSigma	rdb	e ⁻ Conf	N-Rule
694.9482	1	C ₂₃ H ₂₈ Br ₃ N ₃ O ₇	100.00	694.9483	0.1	0.2	41.7	15.5	odd	ok
	2	C ₂₂ H ₂₂ Br ₃ N ₁₀ O ₂	86.11	694.9483	0.1	0.2	42.9	21.0	even	ok

Figure S6. (-)-HRESIMS of 2.

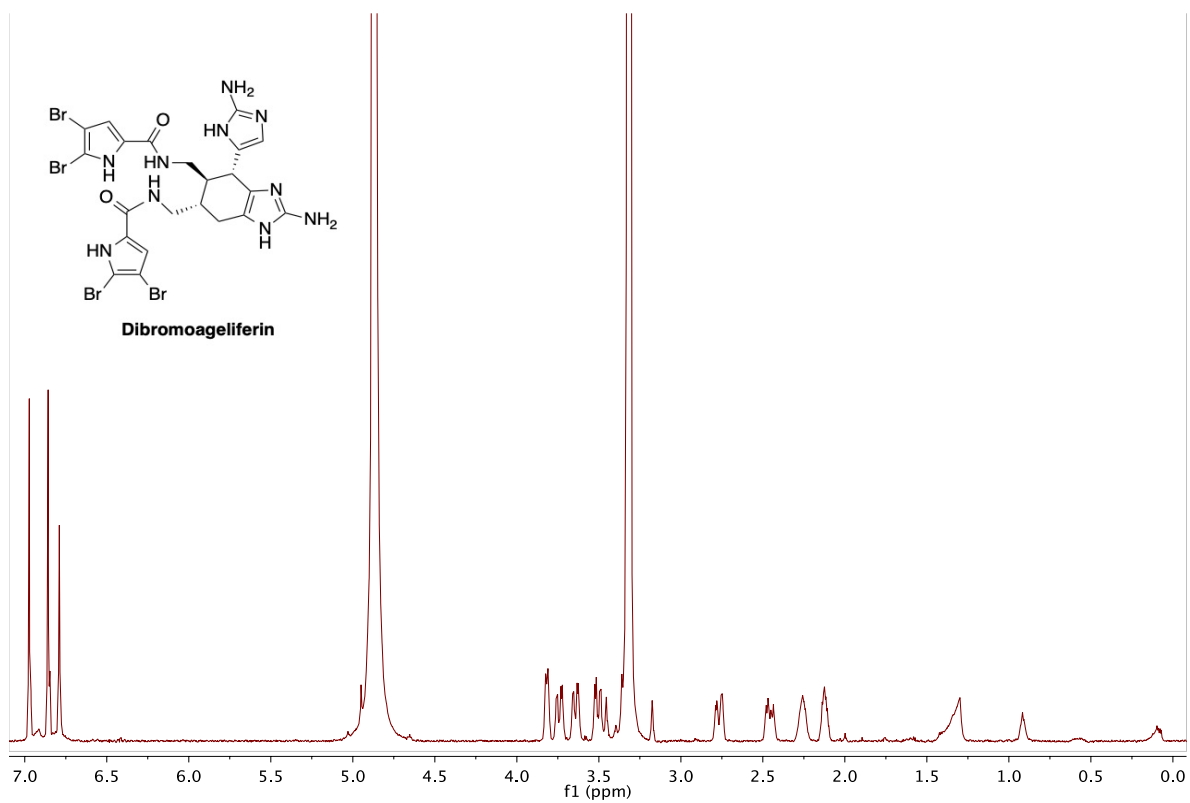


Figure S7. ^1H NMR spectrum of **3** (500 MHz, CD_3OD).

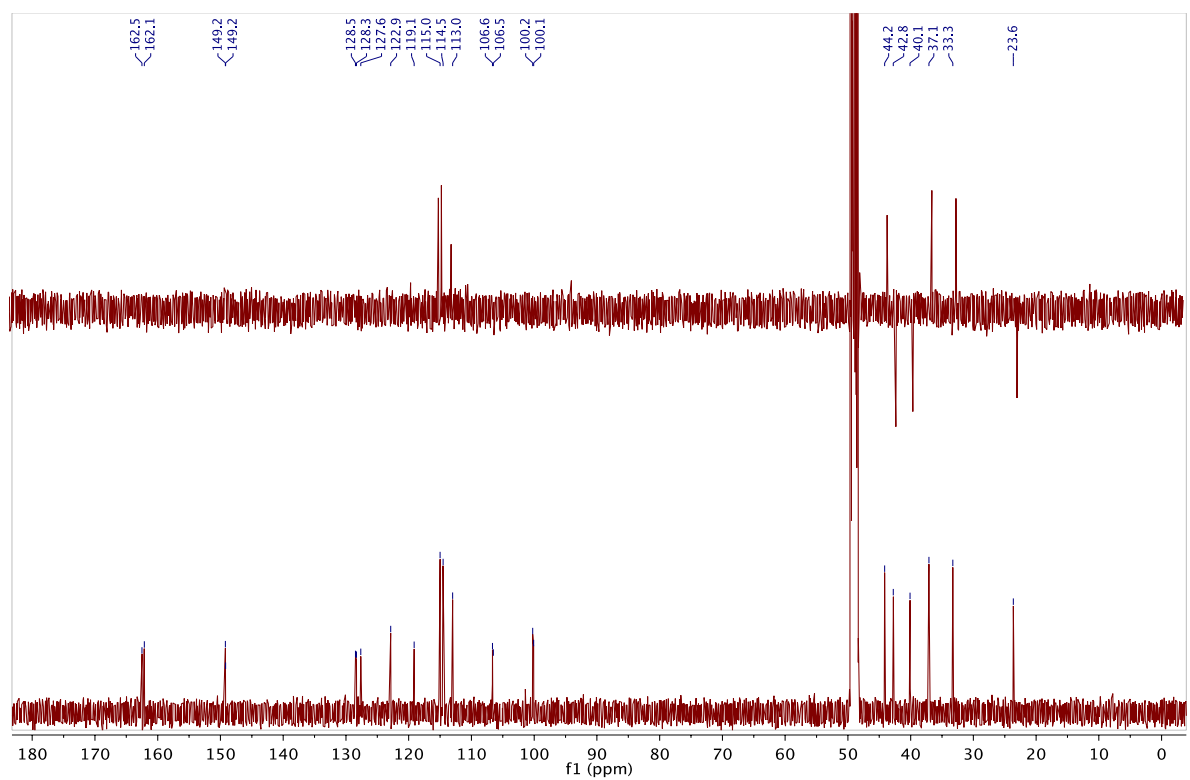
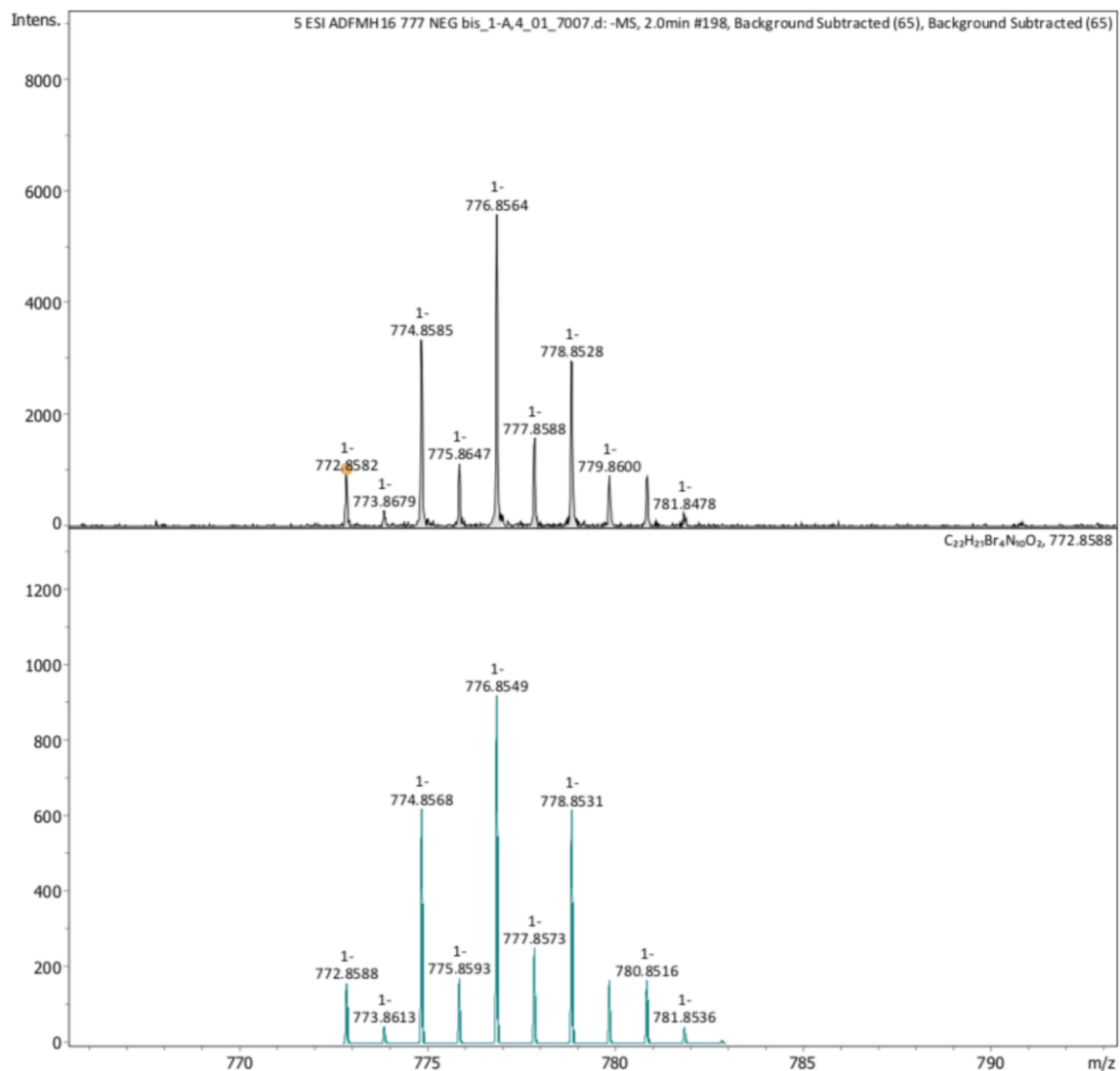


Figure S8. ^{13}C NMR and DEPT-135 spectra of **3** (125 MHz, CD_3OD).



Meas. m/z	#	Ion Formula	Score	m/z	err [mDa]	err [ppm]	mSigma	rdb	e ⁻ Conf	N-Rule
772.8582	1	C20H19Br4N13O	94.77	772.8575	-0.7	-1.0	52.5	23.5	odd	ok
	2	C18H17Br4N16	39.54	772.8561	-2.1	-2.7	52.6	24.0	even	ok
	3	C22H21Br4N10O2	100.00	772.8588	0.6	0.8	52.8	23.0	even	ok
	4	C24H23Br4N7O3	42.17	772.8601	2.0	2.5	53.6	22.5	odd	ok
	5	C23H27Br4N3O7	95.59	772.8588	0.6	0.8	54.2	17.5	odd	ok

Figure S9. (-)-HRESIMS of 3.

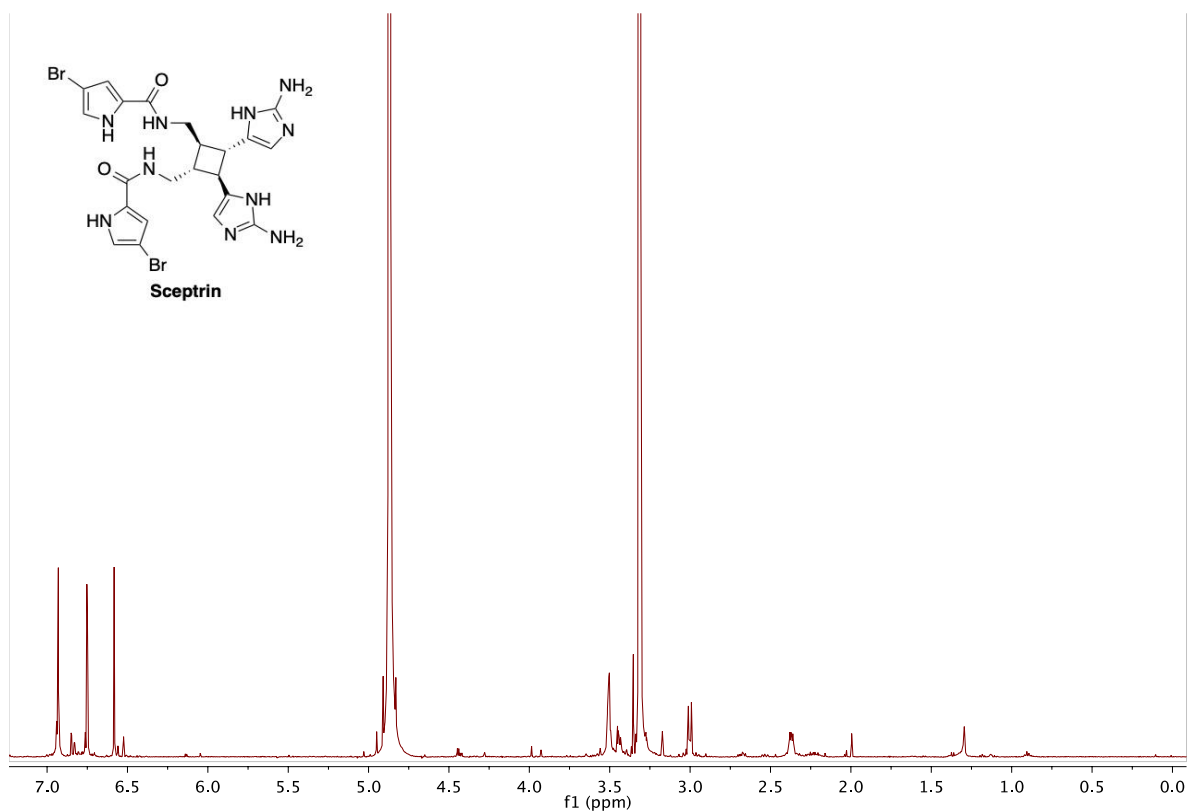


Figure S10. ^1H NMR spectrum of **4** (500 MHz, CD_3OD).

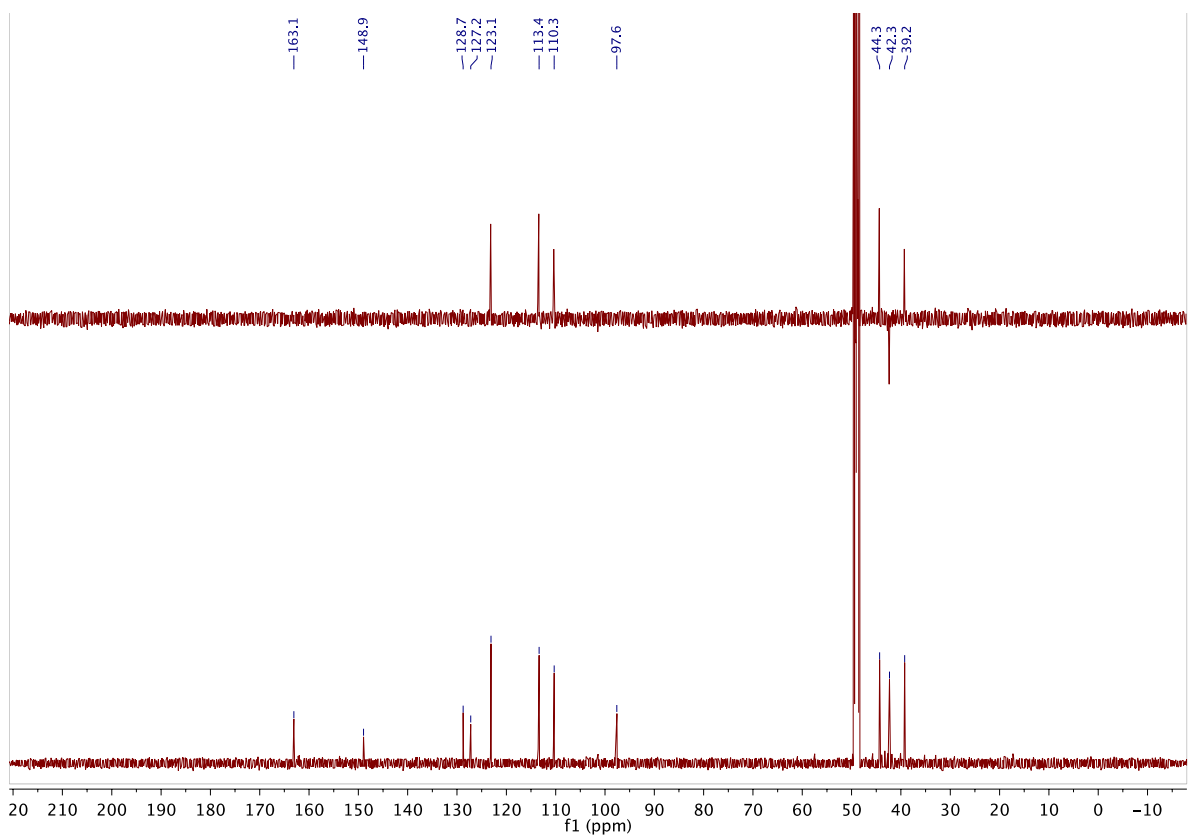
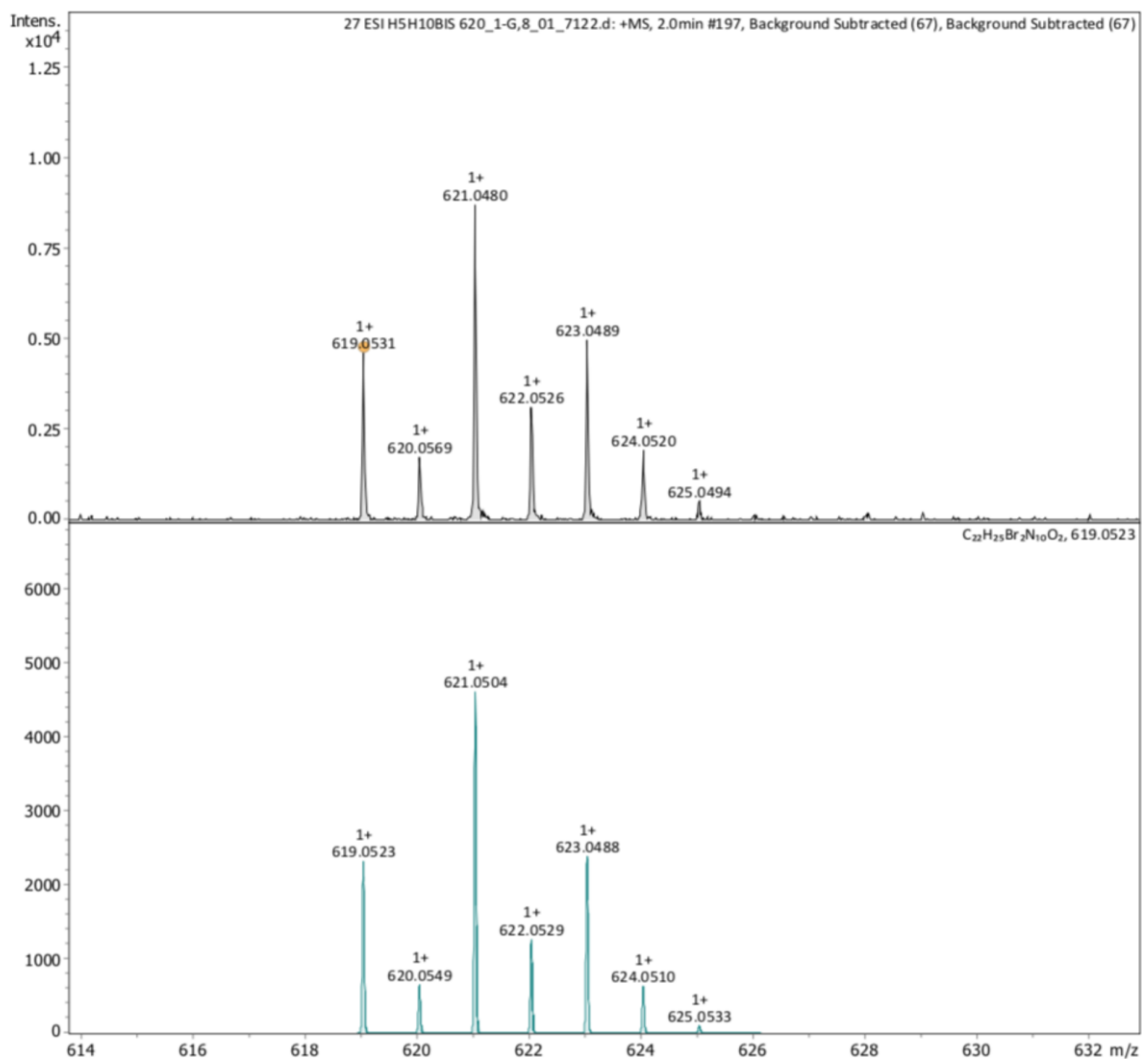
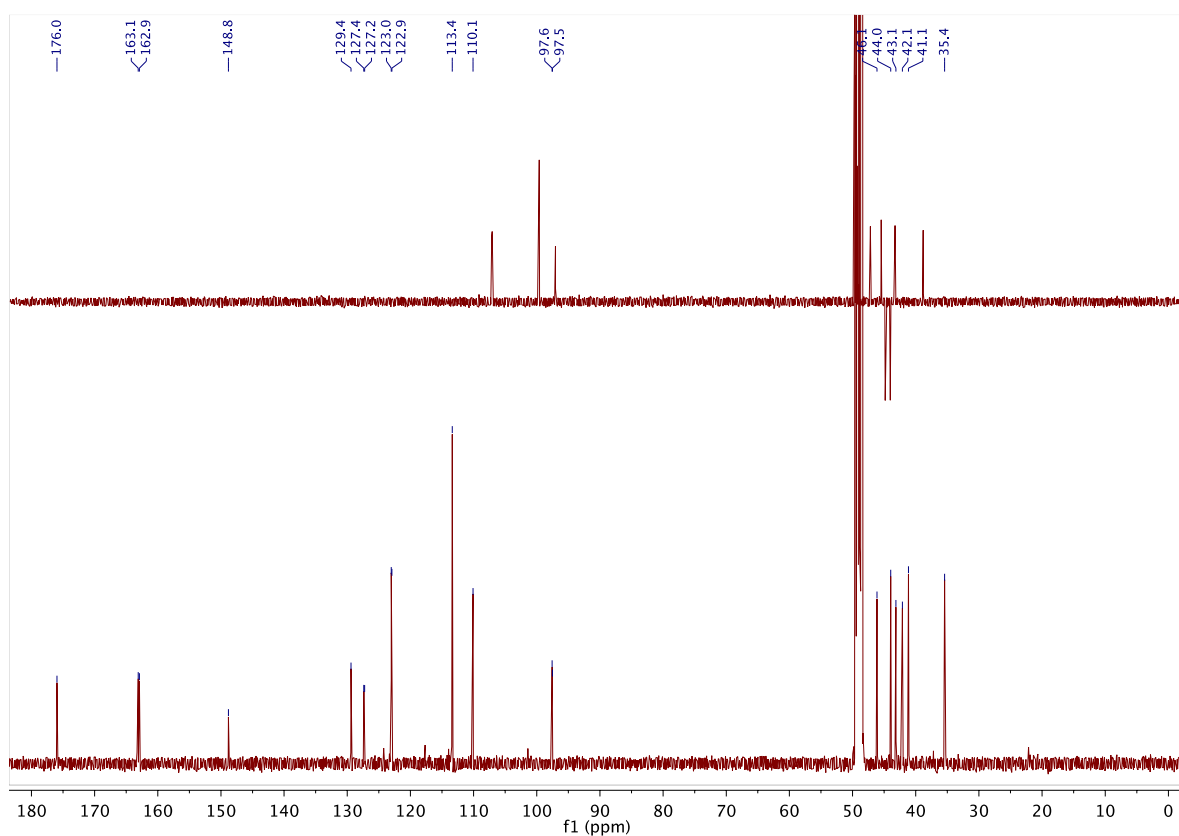
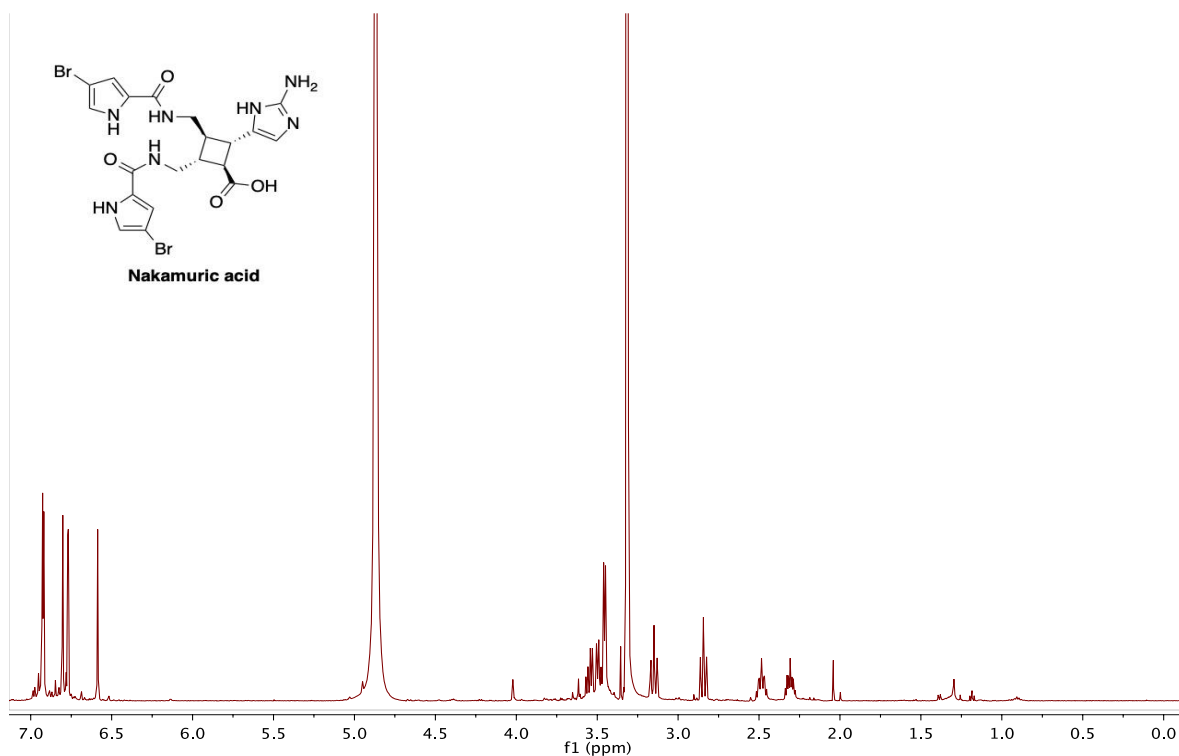


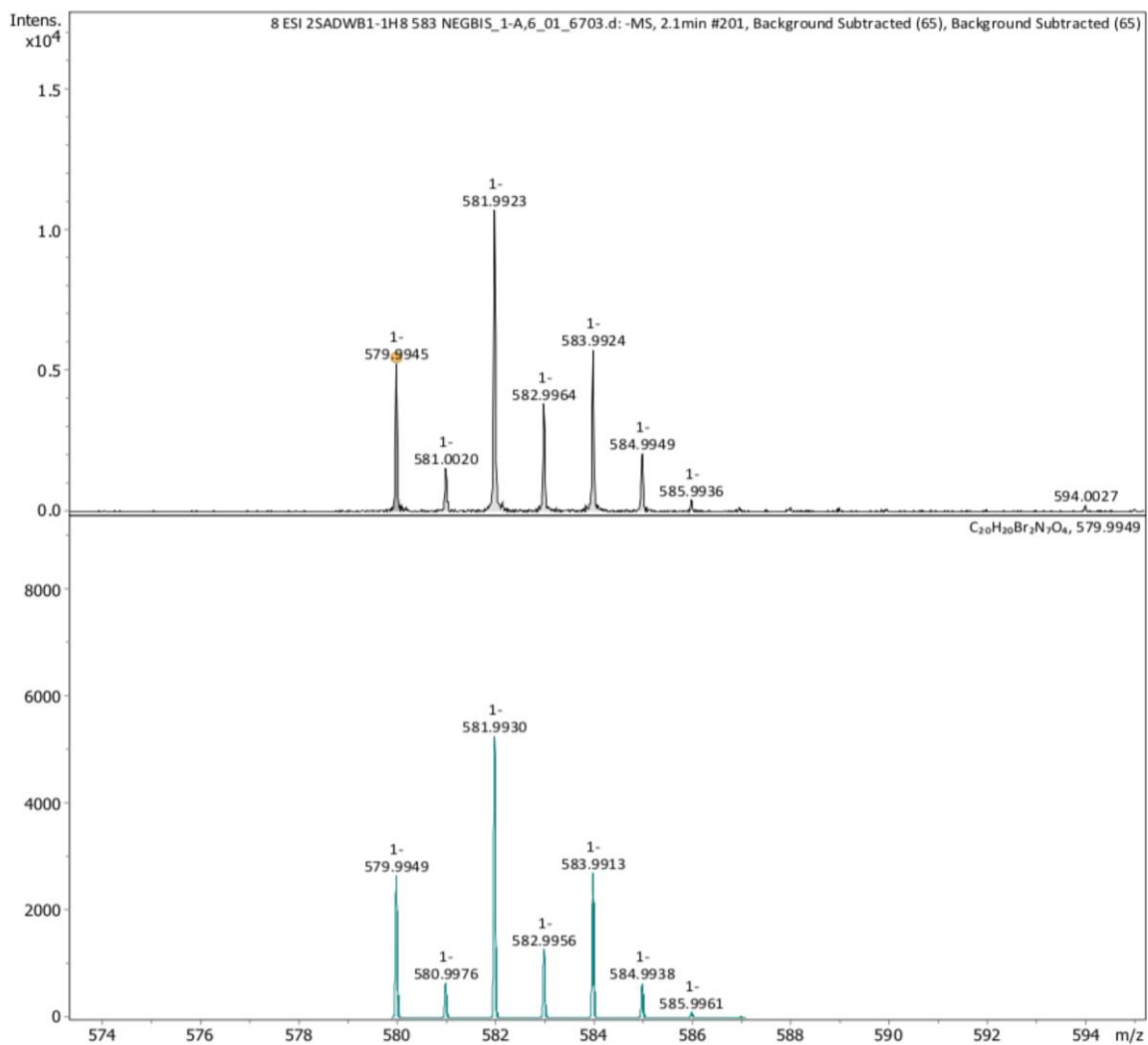
Figure S11. ^{13}C NMR and DEPT-135 spectra of **4** (125 MHz, CD_3OD).



Meas. m/z	#	Ion Formula	Score	m/z	err [mDa]	err [ppm]	mSigma	rdb	e ⁻ Conf	N-Rule
619.0531	1	C ₂₆ H ₂₉ Br ₂ N ₄ O ₄	50.48	619.0550	1.9	3.1	47.1	18.0	even	ok
	2	C ₂₄ H ₂₇ Br ₂ N ₇ O ₃	100.00	619.0537	0.6	0.9	52.0	18.5	odd	ok
	3	C ₂₅ H ₃₃ Br ₂ O ₈	89.48	619.0537	0.6	0.9	55.4	13.0	even	ok
	4	C ₂₂ H ₂₅ Br ₂ N ₁₀ O ₂	77.93	619.0523	-0.8	-1.2	56.9	19.0	even	ok
	5	C ₂₃ H ₃₁ Br ₂ N ₃ O ₇	69.50	619.0523	-0.8	-1.2	60.4	13.5	odd	ok

Figure S12. (-)-HRESIMS of 4.





Meas. m/z	#	Ion Formula	Score	m/z	err [mDa]	err [ppm]	mSigma	rdb	e ⁻ Conf	N-Rule
579.9945	1	C20H20Br2N7O4	100.00	579.9949	0.4	0.6	52.2	17.0	even	ok
	2	C21H26Br2O9	86.64	579.9949	0.4	0.6	56.6	11.5	odd	ok
	3	C18H18Br2N10O3	61.72	579.9936	-1.0	-1.7	57.4	17.5	odd	ok
	4	C19H24Br2N3O8	53.34	579.9936	-1.0	-1.7	61.8	12.0	even	ok

Figure S15. (-)-HRESIMS of 5.

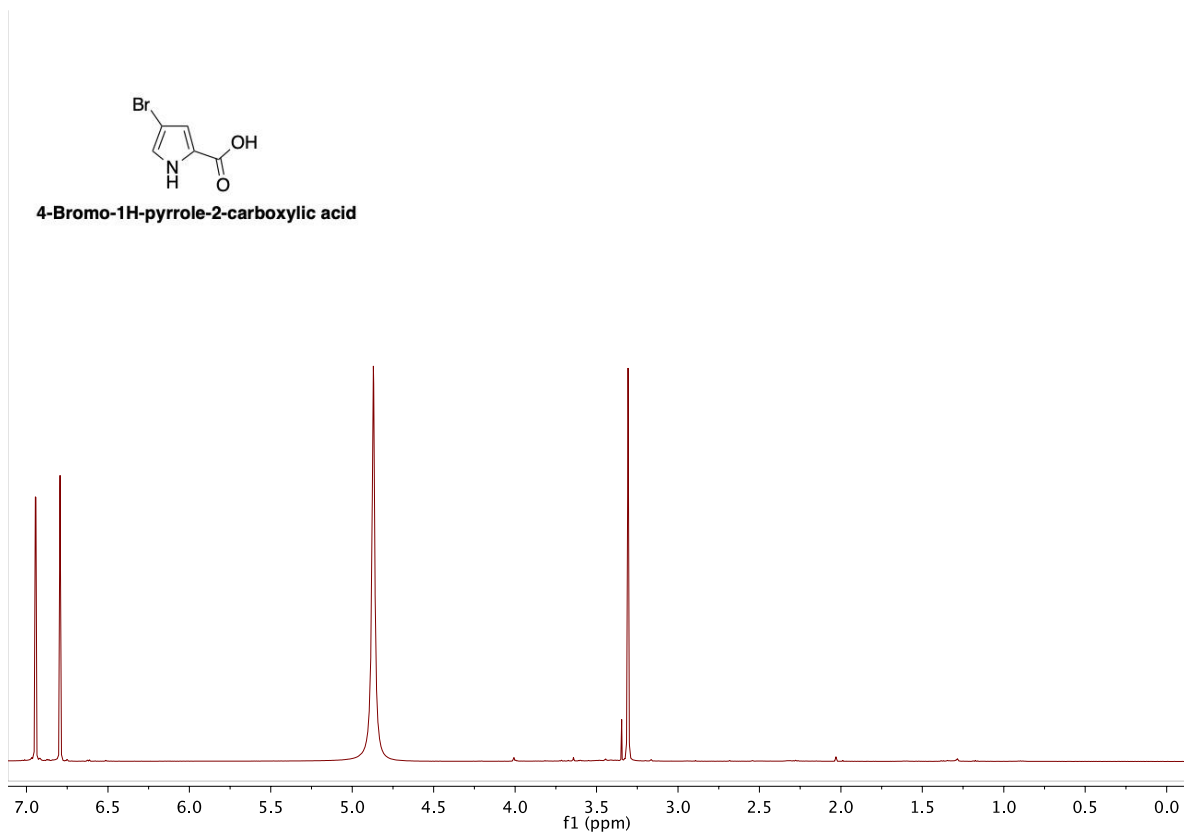


Figure S16. ^1H NMR spectrum of **6** (500 MHz, CD_3OD).

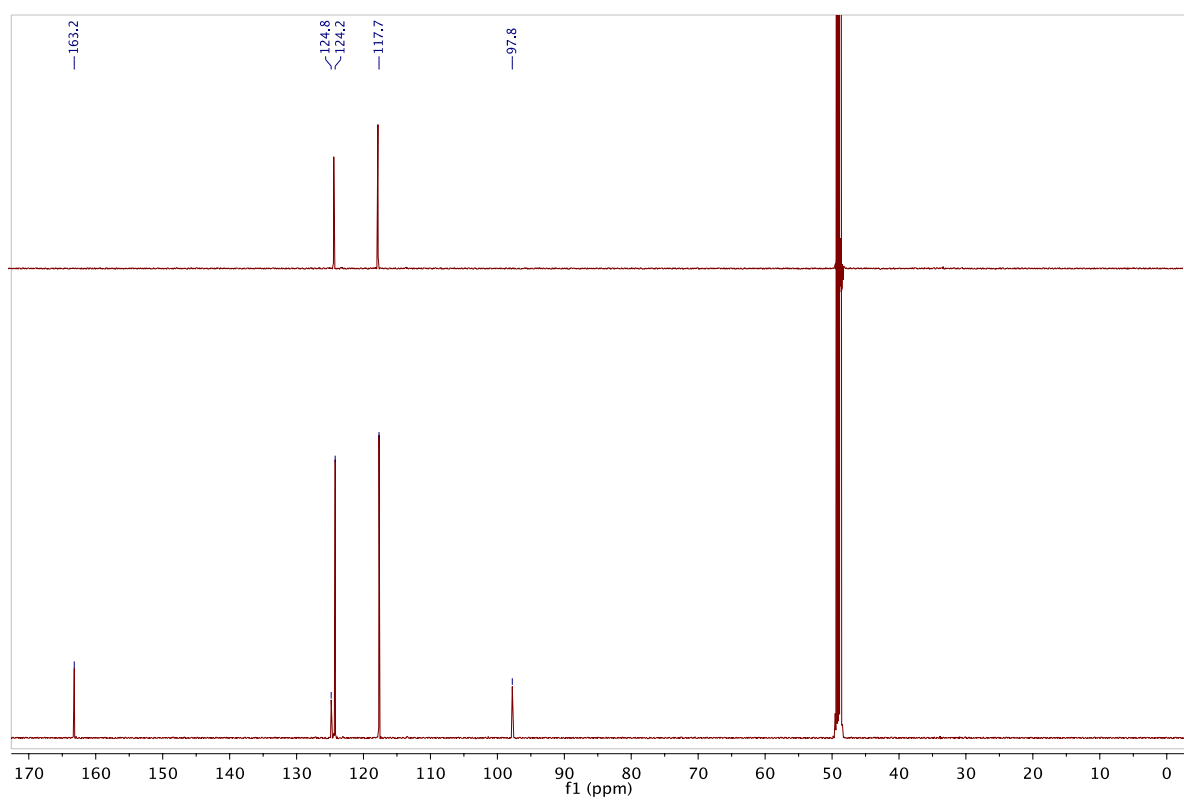
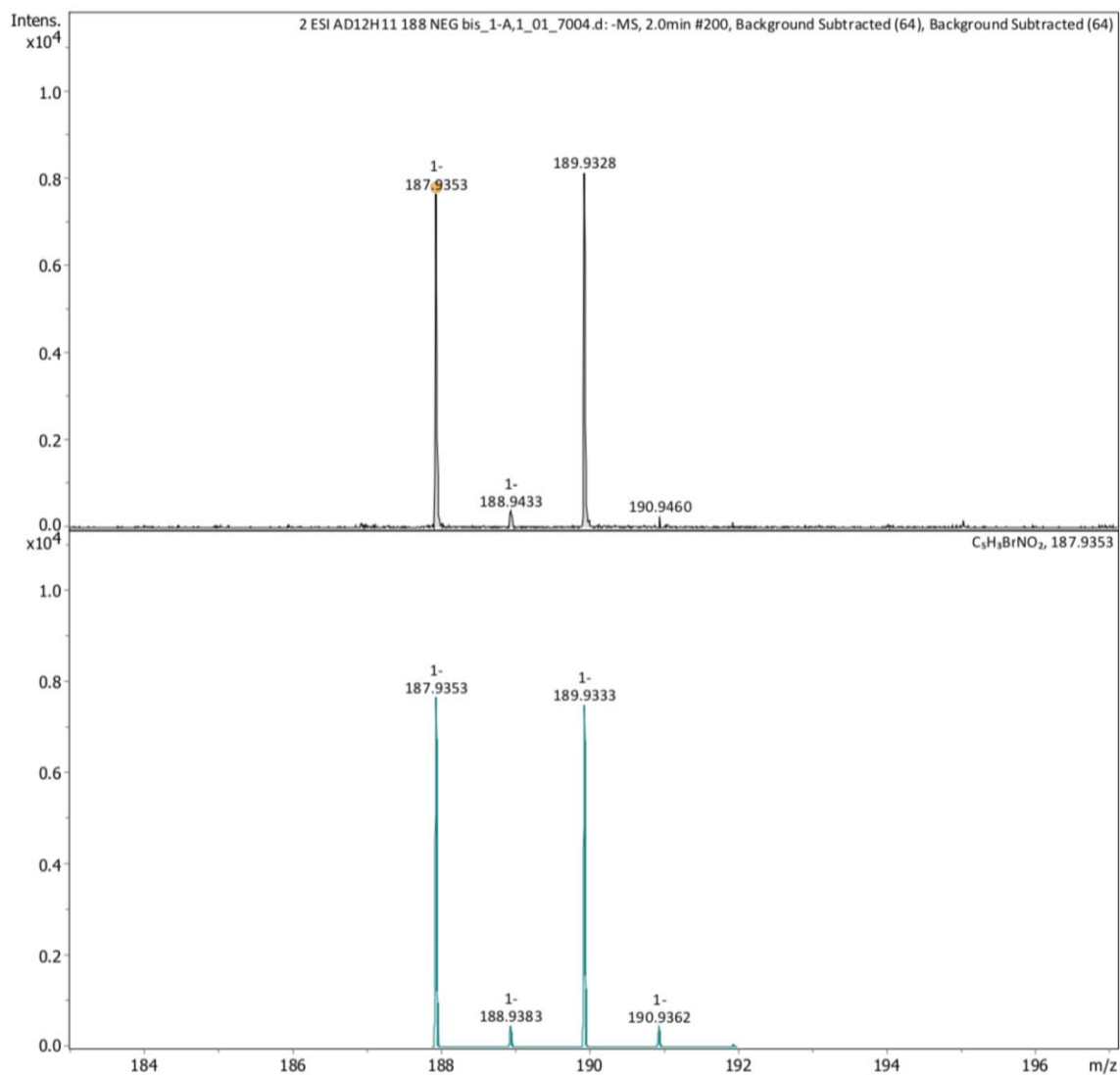


Figure S17. ^{13}C NMR and DEPT-135 spectra of compound **6** (125 MHz, CD_3OD).



Meas. m/z	#	Ion Formula	Score	m/z	err [mDa]	err [ppm]	mSigma	rdb	e ⁻ Conf	N-Rule
187.9353	1	C ₅ H ₃ BrNO ₂	100.00	187.9353	-0.0	-0.3	34.9	6.0	even	ok

Figure S18. (-)-HRESIMS of **6**.

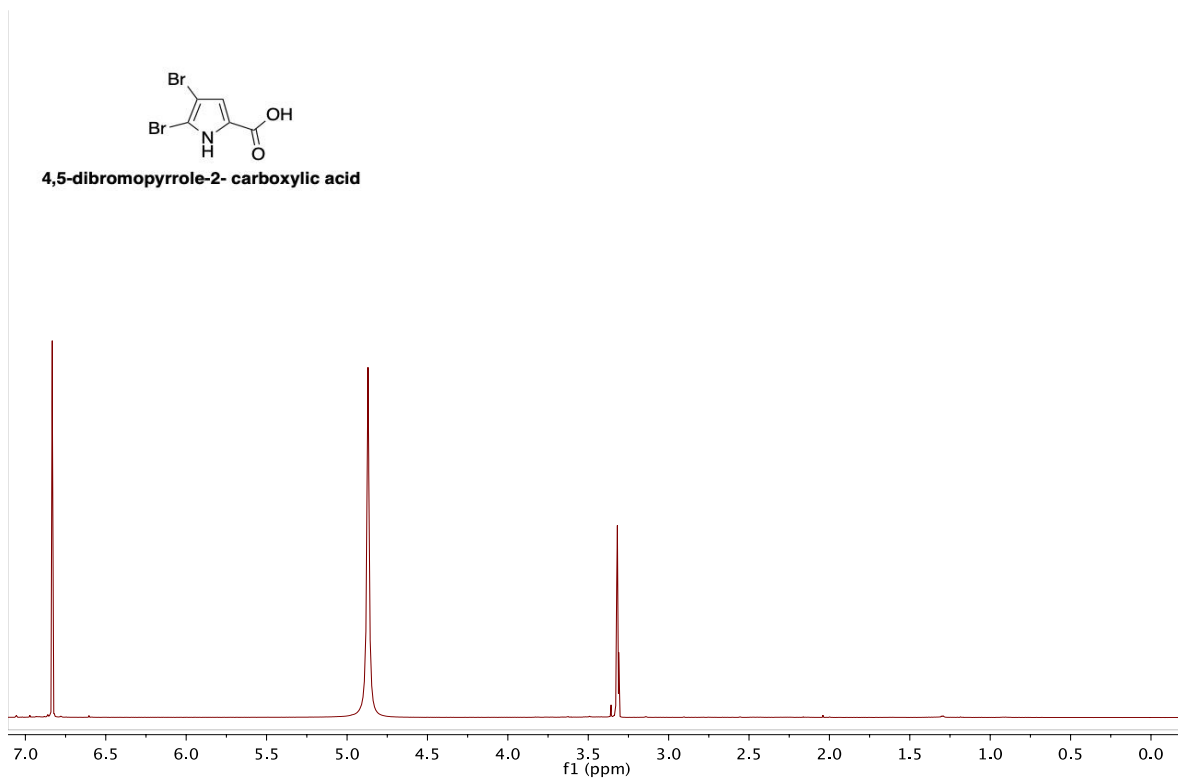


Figure S19. ^1H NMR spectrum of **7** (500 MHz, CD_3OD).

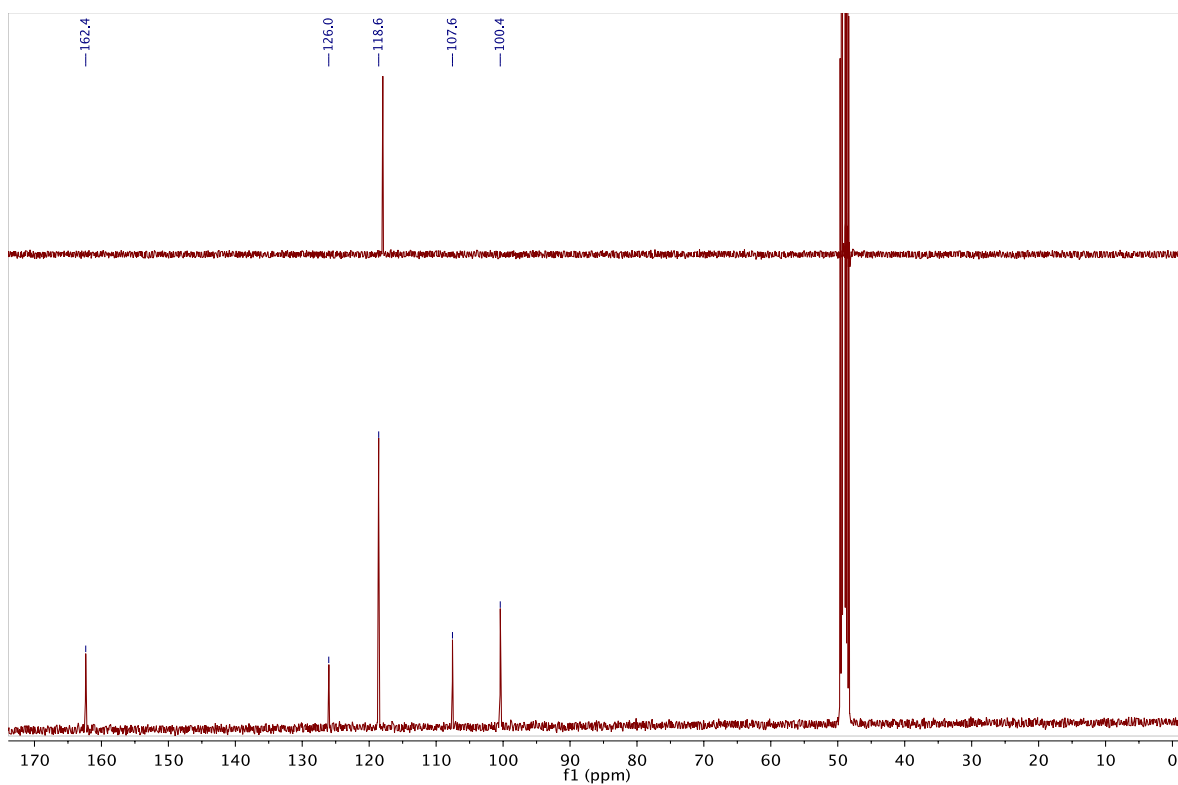
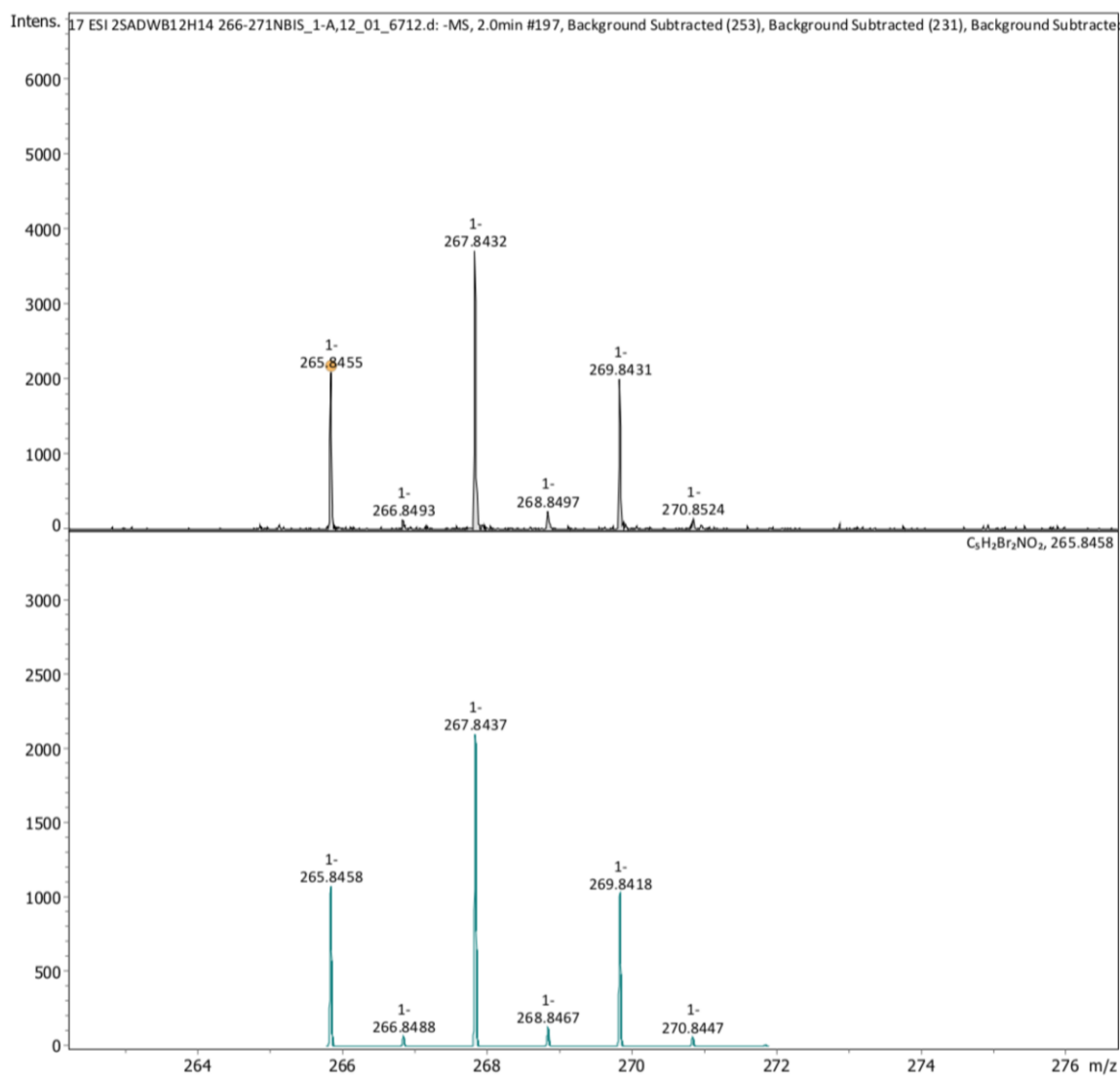


Figure S20. ^{13}C NMR and DEPT-135 spectra of **7** (125 MHz, CD_3OD).



Meas. m/z	#	Ion Formula	Score	m/z	err [mDa]	err [ppm]	mSigma	rdb	e ⁻ Conf	N-Rule
265.8455	1	C5H2Br2NO2	100.00	265.8458	0.2	0.9	28.7	8.0	even	ok

Figure S21. (-)-HRESIMS of 7.

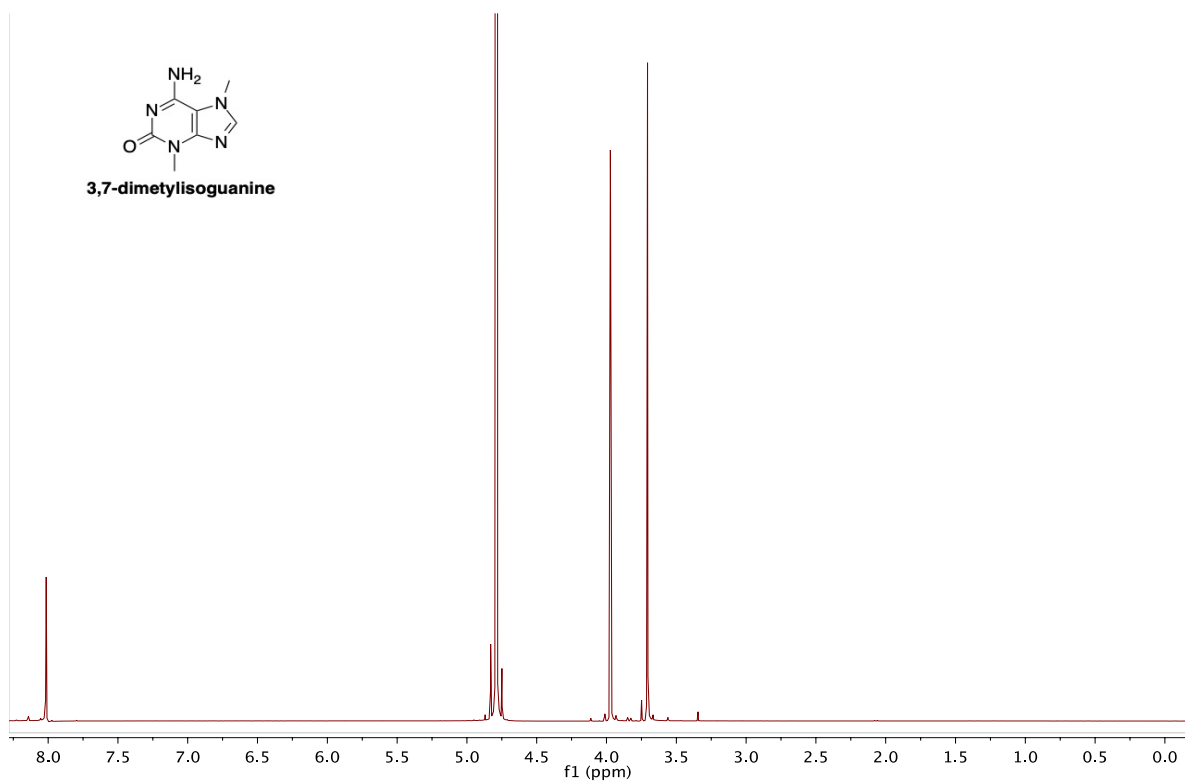


Figure S22. ^1H NMR spectrum of **8** (500 MHz, D_2O).

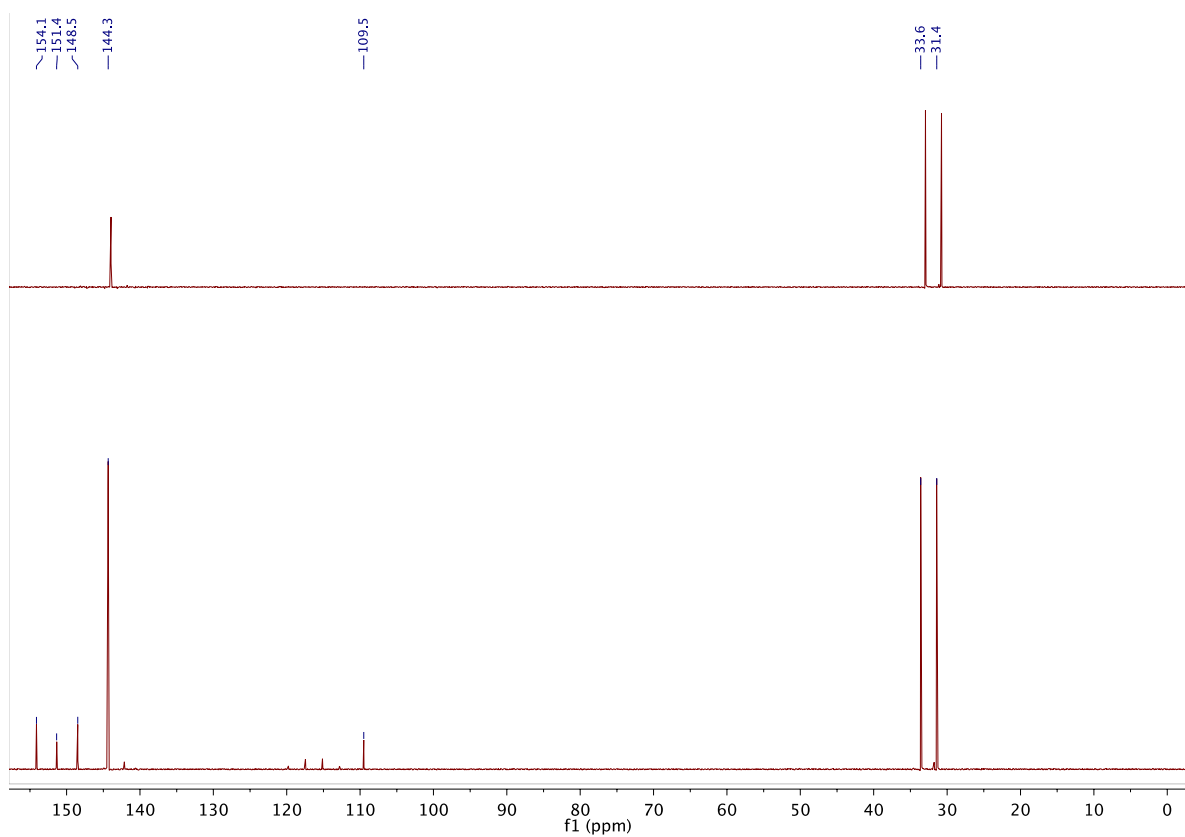
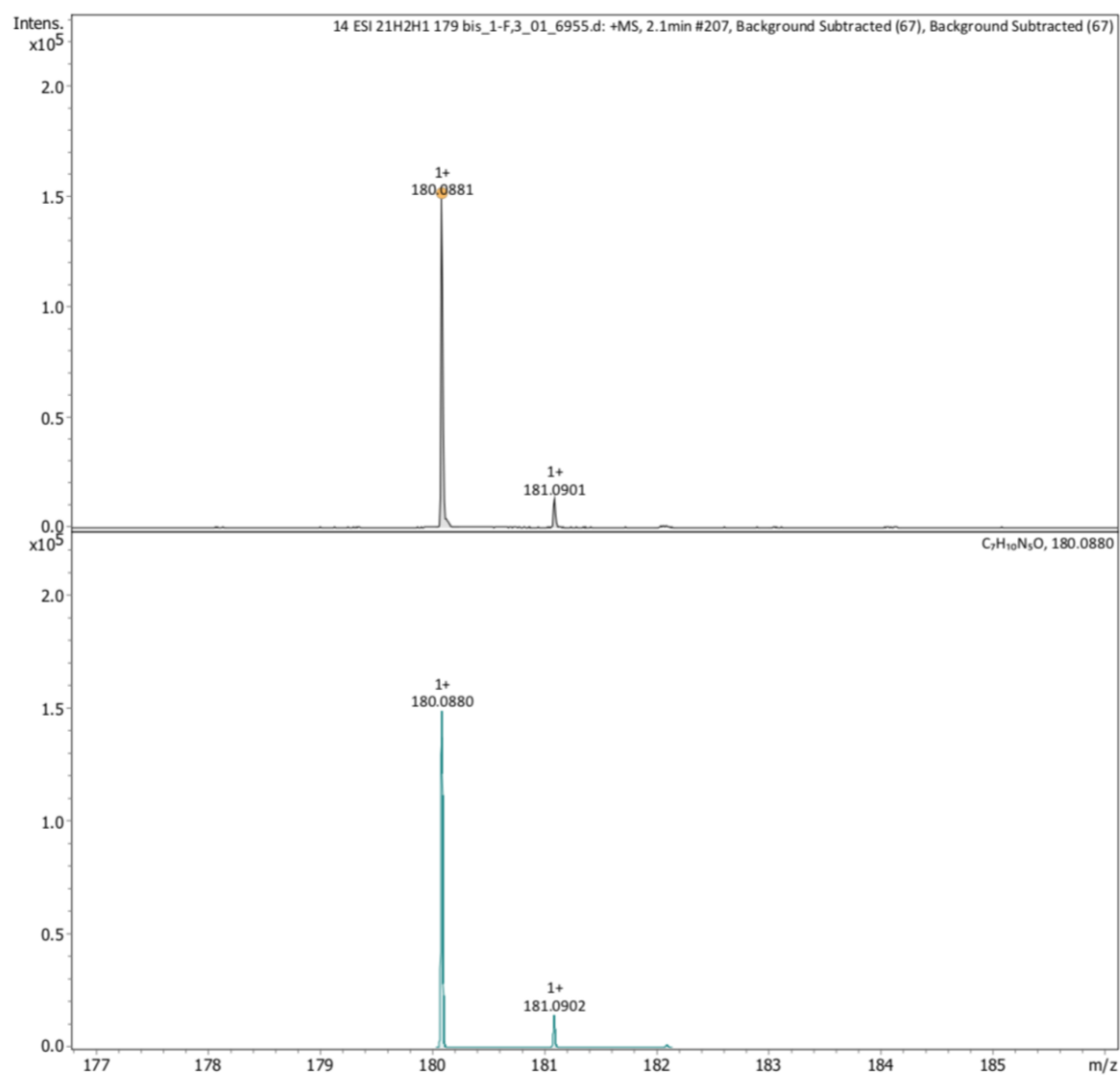


Figure S23. ^{13}C NMR and DEPT-135 spectra of **8** (125 MHz, D_2O).



Meas. m/z	#	Ion Formula	Score	m/z	err [mDa]	err [ppm]	mSigma	rdb	e ⁻ Conf	N-Rule
180.0881	1	C ₇ H ₁₀ N ₅ O	100.00	180.0880	-0.1	-0.7	6.1	6.0	even	ok

Figure S24. (-)-HRESIMS of 8.

3.5 Estudio químico de la gorgonia *Briareum asbestinum*



Figura 3.5. Fotografía de la gorgonia *Briareum asbestinum*, Rio Indio-México.

En este apartado se describe el aislamiento y elucidación estructural de diez compuestos de naturaleza diterpenoide obtenidos a partir de la gorgonia *Briareum asbestinum* recolectada en la costa de Rio Indio, Caribe Mexicano. El análisis de los espectros de RMN 1D y 2D, HRESIMS e IR permitieron establecer que poseían una estructura de tipo briarano, siendo cuatro de ellos nuevos productos naturales y otro con una estructura ya publicada pero sin los correspondientes datos espectroscópicos que permitieran confirmar su estructura. La configuración absoluta de este ultimo compuesto fue determinada por Rayos X.

Estos resultados darán origen a un trabajo que será sometido a una revista científica.

A New Briarane Diterpenoids from the Gorgonian *Briareum Asbestinum* collected in Yucatan Peninsula

Dawrin Pech-Puch¹, Pedro Joseph-Nathan², Carlos Jiménez^{1*}, and Jaime Rodríguez^{1*}

¹ Centro de Investigaciones Científicas Avanzadas (CICA) e Departamento de Química, Facultad de Ciencias, Universidade da Coruña, 15071 A Coruña, Spain.

² Departamento de Química, Centro de Investigación y de Estudios Avanzados del Instituto Politécnico Nacional, Apartado 14-740, México, D. F., 07000 México.

* Correspondence: Centro de Investigaciones Científicas Avanzadas (CICA) e Departamento de Química, Facultad de Ciencias, Universidade da Coruña, 15071 A Coruña, Spain. Tel: +34 981 167000. Fax: +34 981 167065. *E-mail address*: jaime.rodriguez@udc.es (Jaime Rodríguez); carlos.jimenez@udc.es, (Carlos Jiménez).

Abstract: Four new briarane diterpenoids, 2-butyratebriarane B-3 (**2**), 16-chlorobriarane B-3 (**3**), 16-deschlorobriarane B-3 (**4**), and isobriarenolide P (**5**) along six known briaranes (**1**, **6-10**) were isolated from the gorgonian *Briareum asbestinum* collected off the Yucatan Peninsula (Mexico). All structures were elucidated based on detailed 1D and 2D NMR spectroscopy, mass spectrometry and X-Ray for compound **1**. The structure for compound **1**, briarane B-3, was published by Fenical in 1993 without spectroscopic support. All the isolated compounds did not show any cytotoxic, antiviral, antibacterial, and topoisomerase inhibition activity.

Keywords: Briarane Diterpenoids; Gorgonian; Octocoral; *Briareum asbestinum*

1. Introduction

Nature's prodigious creativity is understood in the biosynthesis of diterpenes, the largest class of natural products with more than 80000 knowns, all created from simple linear and achiral precursors.¹ Among them, briarane-type represents one of the more common families isolated from marine sources. Particularly, the gorgonian *Briareum asbestinum* is a prolific source of this type of diterpenes,¹⁻⁴ which molecular architecture shows a trans-fused bicyclo[8.4.0]tetradecane ring system with hydroxyl, esters, epoxides, and chlorine atoms in their skeletons. Very distinctive is a γ -lactone moiety between C7 and C8 atoms, along with a congested unusual four-contiguous stereogenic carbons at C1-C2-C10-C14. Since the first structural elucidation of briarein A isolated from *Briareum asbestinum* in 1977,¹ more than 450 briarane-type diterpenoids have been reported from Octocorallia, including Gorgonacea, Pennatulacea, Alcyonacea and Stolonifera.² Some of these compounds displayed interesting biological activities such as cytotoxic, antiviral, anti-inflammatory, immunomodulatory, antifouling and icototoxicity.²

In the course of our ongoing chemical research on diterpenes from marine sources,¹ we paid attention to the soft coral *Briareum asbestinum* collected off Yucatan peninsula (Mexico), where we were able to isolate four novel briarane-type diterpenoids (**2-5**), along with six known analogues, brianthein X (**6**), Y (**7**) and Z (**8**), asbestinin-10 (**9**) and lactone-14 (**10**) and the briarane B-3 (**1**), which structure was published by Fenical in

1993 without any spectroscopic evidences (Figure 1).² Herein, the isolation, structure elucidation, and the biological activities of the new diterpenes are described along with spectroscopic details to describe the abovementioned compound **1**. Particular consideration was paid to the relative and absolute stereochemistry of the all compounds **1-5**, which were established by using standard 2D NMR spectra (COSY, NOESY, edited HSQC and HMBC) and in the case of briarane B-3 (**1**) J-HMBC, HSQC-HECADE experiments and X-Ray.

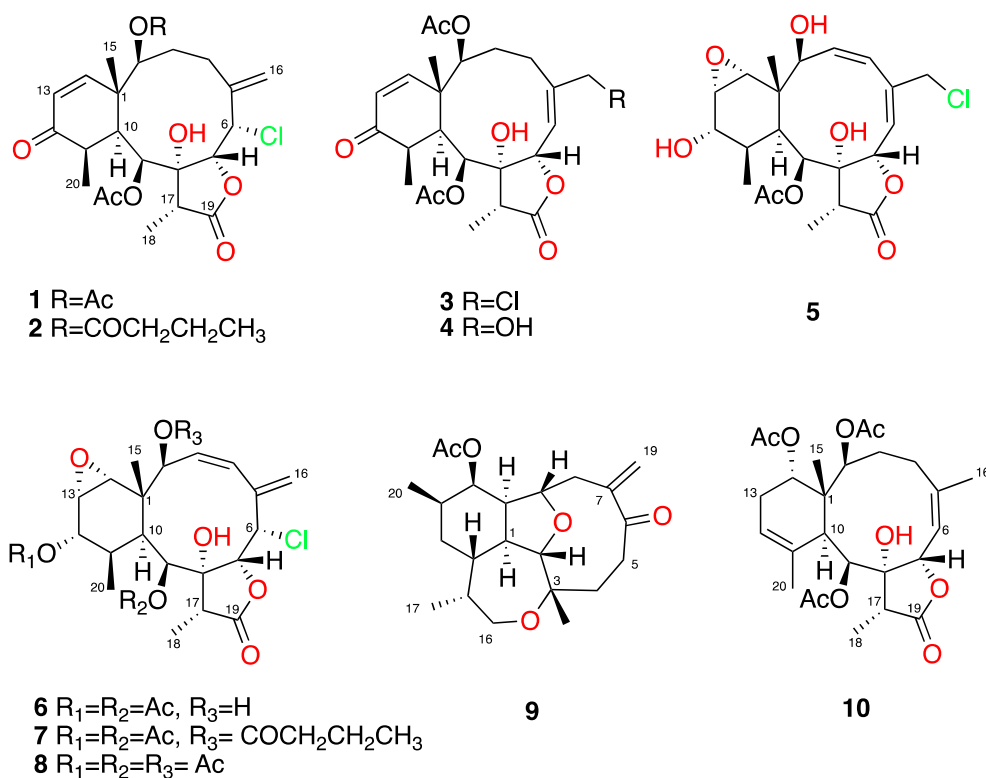


Figure 1. Structures of diterpenes **1-10** isolated from *Briareum asbestinum*.

2. Results and discussion

Briareum asbestinum collected off Yucatan Peninsula was extracted with CH₂Cl₂-MeOH (1:1 v/v) and the crude extract obtained after evaporation of the solvent was partitioned using the Kupchan solvent dependent fractionation, and the dichloromethane soluble portion was subjected firstly to a column chromatography separation and then to a normal phase HPLC purification using isocratic mixtures of hexane-acetone as mobile phases to afford pure compounds **1-10**.

Compound **1** was isolated as a white powder, presenting a (+)-LRESIMS [M+Na]⁺ ion peaks at *m/z* 505 and 507 in a ratio 3:1, indicative of a typical cluster of chlorine-35 and chlorine-37 isotopes. The (+)-HRESIMS measurement at *m/z* 505.1584, matched with a molecular formula C₂₄H₃₁³⁵ClO₈Na⁺ (calculated for C₂₄H₃₁³⁵ClO₈Na⁺, 505.1605), accounting for nine degrees of unsaturation. The IR spectrum of **1** shows absorption frequencies at 3520, 1765 and 1736 cm⁻¹ indicating the presence of hydroxyl, γ -lactone and carbonyl ester functionalities, respectively.

Compound **1** exhibits signals in the NMR spectra (Tables 1 and 2) of two acetate methyl singlets at δ_{H} 2.14 (δ_{C} 21.9) and δ_{H} 2.24 (δ_{C} 21.2), with the corresponding carbonyl signals at δ_{C} 170.3 and 169.6. From the ¹H-¹H COSY, it was possible to establish

a set of separate spin-spin systems that map out the proton sequences from H-2/H-3/H-4, (by allylic coupling), H-6/H-7, and H-9/ H-10 (Figure 2).

Each proton and their attached carbon was deduced by an DEPT-135 edited HSQC experiment, and then HMBC correlations were needed to build the briarane skeleton as follows: cross peaks from H-2 to C-1; H-3 to C-5; H-6 to C-5 and C8; H-9 to C-7 and C-8; H-10 to C-1; H-16 to C-4, C-5 and C-6; and finally the proton at δ_{H} 3.43, assigned to and OH group showed long range correlation to C-9, establishing the connectivity from C-1 to C-10 in the ten-membered ring present in the compound. The fusion of this ring to a methylcyclohexane thru C-1 and C-10, was elucidated also from the ^1H - ^1H COSY correlations between protons H-10/H-11, H-13/H-14, and H-11/H₃-20 and from the HMBC correlations from H-1 to C-14 and C-13; from H-10 to C-11; from H-14 to C-12, and from H₃-20 to C-10, H₃-20 to C-11 and C-12. The methyl group C-15 was positioned at C-1 ring junction from the HMBC correlations between H₃-15 to C-1, H₃-15 to C2, and H-14 to C-15. The carbonyl-acetate signals at δ_{C} 170.3 and 169.6 were correlated in the HMBC experiment (Figure 2) with two methine doublets at δ_{H} 4.81 and 5.11 respectively, revealing the positions of each acetate group at C-2 and C-9. Another carbonyl signal, assigned to a γ -lactone (δ_{C} 176.4), was assembled along with a secondary methyl doublet at δ_{H} 1.30 (δ_{C} 10.1) by the HMBC (H-19/C-18) and COSY (H-18/H-17) correlations. Final connection between C-17 and C-8 (δ_{C} 82.9) was elucidated by the HMBC correlation from H-17 to C-8. These correlations along with the H-6/H-7 COSY correlation, fixed the position of the lactone ring.

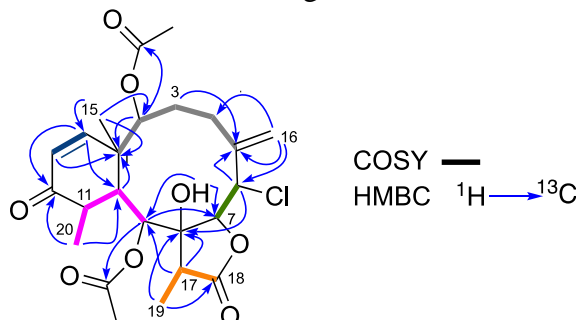


Figure 2. ^1H - ^1H COSY and HMBC correlations found in **1**.

Three dimensional arrangement of **1** was completed by using NOE distance restraints, that allowed us to fix the relative configurations at C-2,C-3,C-4,C-5 and C-16 as *S**,*R**,*R**,*S** and *R**, respectively remaining the relative configurations at C-1, C-9, C-10 and C-14 undetermined. A strong NOE correlation observed between the methyl groups H₃-15 and H₃-20 indicated that these two methyl groups were in a *syn* relationship. The absence of NOE correlations between H-1 and the methyl group at C-10 suggest that these protons are *anti*. The NOE data also supports that H-1 and methyl group at C-14 are also *anti*. These data showed the relative configurations of C-1 and C-10 either *RR* or *SS*, which was further corroborated by the presence of strong HMBC correlations between carbon of the methyl at C-10 and H-1; and C-14 and H-1.

Table 1. $^1\text{H-NMR}$ spectroscopic data (in ppm, J in Hz) of briaranes **1–5**.

N.	1	2	3	4	5
2	4.81 (d, 9.4)	4.82 (d, 9.5)	4.37 (d, 6.0)	4.40 (d, 5.4)	4.27 (d, 9.7)
3	2.41 (dt, 15.6, 9.4, 9.4)	2.40 (m)	2.78 (dt, 15.4, 15.4, 5.5)	2.85 (dt, 15.5, 15.5, 4.9)	5.89 (dd, 11.0, 9.7)
4	1.87 (dd, 15.6, 10.9) 2.61 (dd, 15.0, 10.9) 1.62 (m)	1.86 (m) 2.57 (m) 1.60 (m)	1.77 (m) 2.56 (m) 2.05 (m)	1.74 (m) 2.55 (m) 2.00 (m)	6.21 (ddd, 11.0, 1.2)
6	4.83 (bs)	4.84 (d, 9.3)	5.88 (dd, 10.3, 0.6)	5.72 (d, 10.2)	5.83 (dq, 8.6, 1.2, 1.2, 1.2)
7	5.77 (bs)	5.71 (bs)	5.23 (d, 10.3)	5.28 (d, 10.2)	5.07 (d, 8.6)
9	5.11 (d, 5.1)	5.11 (d, 5.5)	5.28 (d, 4.7)	5.30 (d, 5.2)	5.14 (d, 6.7)
10	2.99 (dd, 4.7, 5.1)	2.99 (dd, 5.0, 5.5)	2.64 (dd, 4.6, 4.7)	2.77 (t, 5.2)	2.12 (d, 6.7)
11	2.61 (dq, 4.7, 7.4)	2.61 (m)	2.53 (m)	2.52 (m)	1.80 (m)
12	-	-	-	-	3.94 (dd, 5.9, 2.3)
13	5.97 (d, 10.4)	5.97 (d, 10.5)	5.84 (d, 10.5)	5.80 (d, 10.5)	3.56 (ddd, 5.9, 3.6, 0.9)
14	6.19 (d, 10.4)	6.20 (d, 10.5)	6.40 (d, 10.5)	6.40 (d, 10.5)	3.41 (d, 3.6)
15	1.16 (s)	1.16 (s)	1.22 (s)	1.16 (s)	1.11 (s)
16	5.69 (bs)	5.69 (q, 2.0)	4.32 (d, 12.0)	4.32 (d, 15.8)	4.24 (d, 12.8)
17	5.37 (s) 2.41 (q, 7.7)	5.37 (bs) 2.45 (q, 7.3)	4.18 (d, 12.0) 2.45 (q, 7.2)	4.07 (d, 15.8) 2.41 (q, 7.1)	4.18 (d, 12.8) 2.31 (d, 7.1)
18	1.30 (d, 7.7)	1.30 (d, 7.3)	1.19 (d, 7.2)	1.23 (d, 7.1)	1.17 (d, 7.1)
20	1.30 (d, 7.4)	1.33 (d, 7.4)	1.30 (d, 7.4)	1.29 (d, 7.4)	1.01 (d, 7.5)
21	2.14 (s)	2.15 (s)	2.25 (s)	2.24 (s)	2.18 (s)
22	2.24 (s)		2.14 (s)	2.14 (s)	
1'		2.45 (q, 7.4)			
2'		1.77 (m)			
3'		1.02 (t, 7.4)			
O	3.43 (bs)	3.42 (bs)			
H					

Recorded in CDCl_3 at 500 MHz**Table 2.** $^{13}\text{C-NMR}$ spectroscopic data (δ in ppm) of briaranes **1–5**.

No.	1	2	3	4	5
1	44.9	44.8	44.2	44.2	40.4
2	79.3	79.2	79.6	80.6	76.5
3	28.5	28.6	31.7	31.7	137.2
4	28.5	31.7	26.2	25.5	125.0
5	142.6	142.6	144.2	147.8	141.2
6	67.3	67.3	123.3	118.3	126.7
7	78.2	78.3	77.4	77.5	79.2
8	82.98	83.0	82.6	82.4	82.5
9	74.4	73.5	71.1	71.2	70.0
10	38.5	38.5	38.3	37.9	31.3
11	46.8	46.9	48.6	48.1	41.7
12	202.7	202.8	203.1	203.9	66.7
13	126.1	126.0	124.3	124.2	55.2
14	154.7	154.9	154.8	155.4	64.4
15	19.0	19.0	15.4	6.8	14.7
16	119.9	120.0	51.2	67.5	46.6
17	42.3	42.3	42.6	42.8	43.2
18	10.1	14.0	6.8	15.4	6.5
19	176.4	175.9	175.7	176.7	175.7
20	15.1	15.2	15.2	15.3	13.3
21Ac	170.3	170.4	169.0	169.1	169.9
22Ac	169.6	172.6	170.7	171.1	
CH ₃ 21	21.9	21.9	21.3	21.2	21.9
CH ₃ 22	21.2		21.9	21.9	
OH					
1'CH ₂		36.3			
2'CH ₂		18.5			
3'CH ₃		14.3			

Recorded in CDCl_3 at 500 MHz

The abovementioned presumptions of the relative configurations of C-1, C-10 and C-11 were confirmed by a *J*-based configurational analysis that showed two large values of 6.7 and 6.5 Hz for $^3J(\text{C}_{20}\text{-H}_{10})$ and $^3J(\text{C}_{15}\text{-H}_{10})$, respectively measured in a *J*-HMBC experiment.¹ Since C1 and C10 must be either $1R^*,10R^*$ or $1S^*,10S^*$, the four possible relative configurations for those stereogenic centers can be either $(1S^*,2R^*,10S^*,11R^*)$ or $(1S^*,2S^*,10S^*,11R^*)$. In all naturally-occurring briaranes, H-10 is *trans* to the C-15 methyl group, and these two groups are assigned as α - and β -oriented in most briarane derivatives.^{2,3} The relative configuration of **1** was elucidated from the interactions observed in the NOESY experiment and was found to be compatible with that of **1** deduced by a computer model deduced by a conformational search performed in the Macromodel module implemented in Maestro Quantum mechanical software (Figure 2a).² The NOESY correlations between H-2 and Me-15, H-9 and H-17, Me-15 and Me-20, H-17 and H-7 and H-7 and H-6 required that all of these groups were in β -face, and correlations of H-10 and H-21, H-10 and H-OH, and H-10 and H-16 indicated α -disposition for these groups (see Figure 3a).

In order to dereplicate possible candidates for the structure of diterpene **1**, searches in SciFinder and MarinLit databases gave across the structure of briarane B-3, which its three-dimensional skeleton was proposed in 1993 by Harvell et al.,¹⁰ however no spectroscopic evidence was published to support such structure.

A final confirmation of the 3D structure of **1** was achieved by the examination of single-crystal X-ray diffraction (Figure 3b). The X-ray structure validates the proposed stereochemistry showed recently by us thru ^1H RCSA's measurements (next chapter).

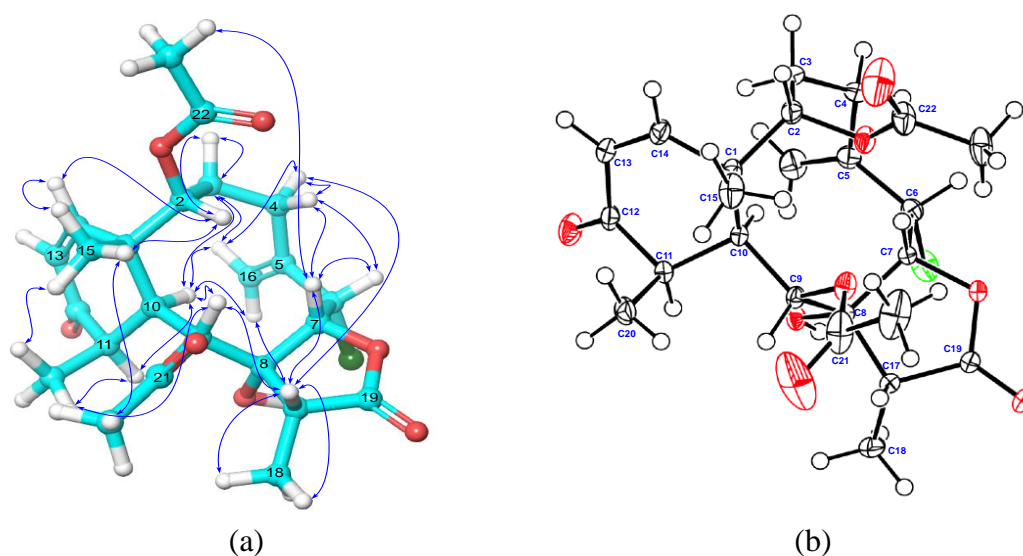


Figure 3. (a) NOESY correlations observed in compound **1**. b) ORTEP X-Ray representation of compound **1**.

2-butiratebriarane B-3 (**2**) was also isolated as a white powder, presenting a molecular formula of $\text{C}_{26}\text{H}_{35}\text{ClO}_8$ as deduced from its high-resolution (+)-ESIMS. Similarly to those of **1**, compound **2** showed IR bands at 3520, 1750 and 1675 cm^{-1} , indicating an hydroxyl, a γ -lactone and an ester carbonyl functionalities, respectively. Comparisons of its ^1H - and ^{13}C -NMR data (Tables 1 and 2) with those of **1** revealed a strong resemblance in all signals, differing just in the high-field region of their respective spectra. While two ester-type carbonyls persisted in the ^{13}C -NMR, only one

acetate methyl signal was observed at δ_{H} 2.0 in the ^1H -NMR spectrum of **2**. Instead, a methyl triplet at δ_{H} 1.03 showed a ^1H - ^1H COSY cross peak to a multiplet at 1.77 (m), and this to another multiplet centered at 2.45 (m), which strongly suggest the presence of a butyrate ester. Two additional sp^3 methylenes were observed in the ^{13}C -NMR of **2** and the increased molecular weight from 482 to 510 Da substantiated this the substitution of an acetate for a butyrate group. The structure of **2** was further supported by more COSY correlations, edited-HSQC and HMBC experiments. Also the NOESY cross-peaks of **2** and **1** were very similar (see figure 4), suggesting that they have the same relative configuration. A similar optical rotation was also found for **2** in comparison with that of **1**, which strongly support that **2** is a 2-butirate derivative of **1**.

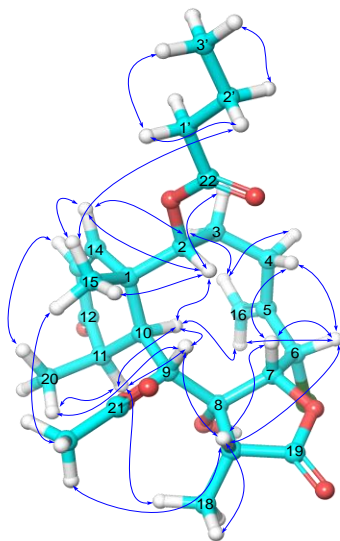


Figure 4. NOESY correlations observed in 2-butiratebriarane B-3 (**2**)

The HRESIMS and ^{13}C -NMR data (Table 2) of compound **3**, implied a molecular formula of $\text{C}_{24}\text{H}_{31}\text{ClO}_8$. Spectral comparison of ^1H , ^{13}C -NMR and IR data of **3** with that of **1**, suggested a similar briarane skeleton. The absence of the exocyclic carbon-carbon double bond at C-5/C-16 present in **1** and **2**, and the chloride atom at C-6 were evident by the presence of a chloromethyl group and a carbon-carbon double bond between C-5/C-6 in **3**. The structure of **3** was further supported by COSY, HSQC and HMBC experiments.

To confirm the position of the chlorine atom attached to C16, we measured the vicinal proton-proton coupling constant of vicinal $^2J(\text{H-16}/\text{H-16}')$ and the heteronuclear $^1J(\text{C16-H-16})$ couplings, by inspection of the ^1H NMR spectrum and by a coupled ^1H - ^{13}C HSQC experiment, respectively. The comparison of these two coupling constants with those obtained from a theoretical DFT calculation of chloromethylcyclohexene as a model, were in perfect agreement when the combination of B3LYP as functional and C-PVTZ basis set was used. The NOESY cross-peaks of **3** and **1** were rather similar, suggesting that they have the same relative configurations.

16-deschlorobriarane B-3 (**4**) was also isolated as a white powder with a molecular formula $\text{C}_{24}\text{H}_{32}\text{O}_9$, determined by its HRESIMS. The IR, ^1H , and ^{13}C NMR spectra of **4** were almost similar to those obtained for 16-chlorobriarane B-3 (**3**). Just a small difference was observed in the ^{13}C NMR of **4** for C-16, which resonated at δ_{c} 67.5 instead of δ_{c} 51.2 in the compound **3** (Table 2), revealing that the chlorine of the compound **3** had been replaced by a hydroxyl group. To confirm this observation, we compared the coupling constants $^2J(\text{H-16}/\text{H-16}')$ and $^1J(\text{C-16}/\text{H-16})$ found in **4** with those DFT

computational theoretical coupling constants observed for hydroxymethylcyclohexene. The data were also in perfect agreement for the presence of hydroxyl group at this position.

The relative configuration of this compound at positions C-1, C-2, C-8, C9, C-10 and C-11, was determined to be identical to that of **1** on the basis of the NOE correlations observed in the NOESY experiment (see Figure 5), and therefore we assigned to this compound a structure of 16-deschlorobriarane B-3.

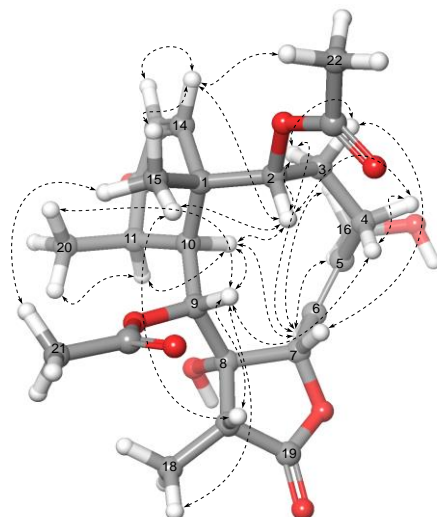


Figure 5. NOESY correlations observed in 16-deschlorobriarane B-3 (**4**).

Finally, another briarane analog (**5**) was isolated as a white powder. Its (+)-LRESIMS revealed two isotopic $[M+Na]^+$ and $[M-H+2Na]^+$ cluster of peaks for molecular ions at m/z 479/481 (3:1) and 499/501 (3:1), which along with the (+)-HRESIMS at m/z 479.1437, clearly indicated a molecular formula $C_{22}H_{29}ClO_8$. Basic spectroscopic data (IR, 1H , and ^{13}C NMR) of **5** were very similar to those briarenolide P, a briarane diterpenenoid isolated in 2016 from the octocoral *Briareum sp.*² However, by comparison of the NMR data, we found that the 1H and ^{13}C NMR data for the six membered ring present in the briarane skeleton were quite different, particularly, the ^{13}C chemical shifts of the carbons C-10, C-12, C-13, and remarkably the methyl C-15. The data for this carbon showed a lack of the compression effect expected for a 1,3-dimethyl axial-axial interaction,² shifting the resonance from δ_C 9.1 in briarenolide P to 15.3 in **5** (see Figure 6). This change in chemical shift indicates a different conformation of the cyclohexane ring due to the axial disposition of the hydroxyl group at position 12.

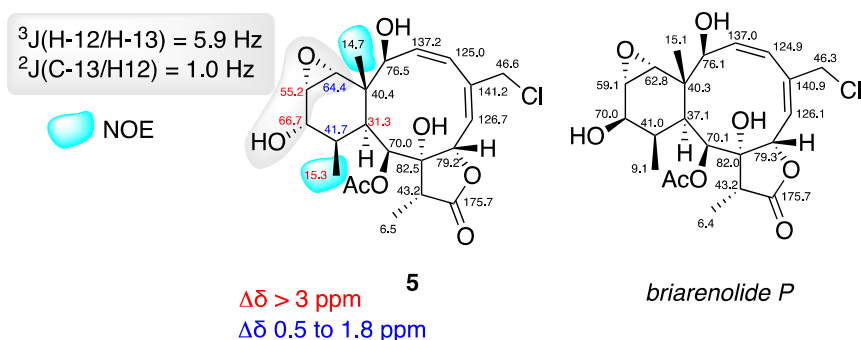


Figure 6. ^{13}C NMR data comparison with briarenolide P (data taken from Reference 17), key coupling constants (see Reference 19) and NOE found in compound **5**.

To confirm the disposition of methyl, hydroxyl, and the epoxy groups at C-11, C-12, and C-13/C-14 respectively, reexamination of ^1H - ^1H NMR coupling constants, measurement of long range ^1H - ^{13}C coupling constants from a HSQC-HECADE experiment and NOESY connections were required. The coupling the constant $^3\text{J}(\text{H-12}/\text{H-13})$ of 5.9 Hz along the small coupling $^2\text{J}(\text{C-13}/\text{H-12})$ of 1 Hz implies and *cis* disposition of hydroxyl and epoxy groups.² Besides, strong NOESY cross peak between Me-20 and H-12 clearly places both protons to the same side of the ring, completing in this way the relative configuration of this fragment. With of the data in hand, along with the NOESY data support a proposed structure for **5** as an epimer at C-12 of briarenolide P, therefore we have named this compound as isobriarenolide P.

All the isolated compounds were submitted to several biological evaluations but did not show any significant cytotoxic activity against the human tumor cell lines (MDA-MB-231 (breast), HT-29 (colon), NSLC A549 (lung) and PSN1 (pancreas)), antibacterial activity against *Acinetobacter baumannii*, *Pseudomonas aeruginosa*, *Klebsiella pneumoniae*, *Staphylococcus aureus* or antiviral activity against Human adenoviruses (HAdV5 y HAdV5-GFP).

3. Materials and Methods

3.1 General experimental procedures

The melting point was measured on a BÜCHI Melting Point B-540 apparatus (Buchi, Flawil, Switzerland) and uncorrected. Optical rotations were measured on a JASCO DIP-1000 polarimeter, with a Na (589 nm) lamp and filter. IR spectra were measured on a FTIR Bruker Vector 22 spectrometer. ^1H , ^{13}C , and 2D NMR spectra were recorded on a Bruker Avance 500 spectrometer at 500 and 125 MHz, respectively, using CDCl_3 . Low resolution electrospray mass spectrometry (LRESIMS) and high resolution electrospray mass spectrometry (HRESIMS) experiments were performed on the Applied Biosystems QSTAR Elite system. The chemical shifts were given in δ (ppm) and coupling constants in Hz. HPLC separations were performed on the Agilent 1100 liquid chromatography system equipped with a solvent degasser, quaternary pump, and diode array detector (Agilent Technologies, Waldbronn, Germany) using a semipreparative normal phase column Nova-pak[®], silica 6 μm 60 Å, 300 \times 7.8 mm (Waters). Precoated silica gel plates (Merck, Kieselgel 60 F254, 0.25 mm) were used for TLC analysis, and the spots were visualized under a UV light (254 nm) or by heating the plate pretreated with $\text{H}_2\text{SO}_4/\text{H}_2\text{O}/\text{AcOH}$ (1:4:20).

3.2. Animal Material

The gorgonian, *Briareum asbestinum*, was collected in the coast of Mexican Caribbean (18° 84' 75.61''N / 87° 65' 04.55''W) by scuba diving at a depth of 10 m, in march 2017. The fresh gorgonian was immediately frozen after collection and kept at -20 °C until being processed. A voucher specimen 17YUBA1 was deposited in the collection of Marine Biology of Autonomous University of Yucatan, Yucatan, Mexico.

3.3. Extraction and isolation

Sliced bodies of *Briareum asbestinum* (wet weight, 1.37 kg; dry weight, 513.70 g) were exhaustively extracted with a mixture of $\text{CH}_3\text{OH}-\text{CH}_2\text{Cl}_2$ (1:1, 3 X 1.5L) at 25 °C for 24 h each extraction, and the extracts were combined and concentrated under vacuum. The dark green crude residue (20.0g) was partitioned using the Kupchan methodology;

the first partition was between CH₂Cl₂/H₂O (1:1 v/v). The organic phase was concentrated under reduced pressure and partitioned between 10% aqueous MeOH (400 mL) and hexane (2 × 400 mL). The H₂O content (% v/v) of the methanolic fraction was adjusted to 50% aqueous MeOH and this mixture was extracted with CH₂Cl₂ (100 mL). The CH₂Cl₂-soluble portion was subjected to column chromatography using silica gel and a gradient of n-hexane/EtOAc (0-100%) to obtain 14 fractions (C1-C14).

Fraction C9-C11 was separated by NP-HPLC using isocratic mixture of 80:20 hexane-acetone as the mobile phase, to obtain compounds asbestinin-10 (**9**) (10 mg), **2** (1 mg) lactone-14 (**10**) (4 mg), **3** (2mg), **1** (25 mg) and brianthein Z (**8**) (10 mg). Crystallization of fracción C10H8 (n-hexane/EtOAc, 4:1) furnished brianthein Y (**7**) (8 mg). Fraction C12 and C13 was purified by NP-HPLC using isocratic mixture of 60:40 hexane-acetone as the mobile phase, to obtain compounds brianthein X (**6**) (11 mg), **4** (2 mg) and **5** (2 mg).

3.4 Metabolite characterization

Briarane B-3 (1). Colorless white powder; $[\alpha]_{\text{D}}^{25} +36.50$ (c 0.1, MeOH); IR ν_{max} 3520, 2980 1750, 1736, 1475, 1225, 1050, 900, 725 cm⁻¹; ¹H-NMR data (500 MHz, CDCl₃), see Table 1; ¹³C-NMR data (125 MHz, CDCl₃), see Table 2; HRESIMS m/z 505.1584 [M + Na]⁺ (calcd. For C₂₄H₃₁ClO₈Na, 505.1605).

X-ray crystallographic analysis of 1. A suitable colorless crystal (0.53 × 0.312 × 0.178 mm³) of **1** for diffraction was obtained by simple evaporation from methanol solution. Crystal data: C₂₄H₃₁ClO₈, orthorhombic, a=12.6098(4) Å, b=14.09741(5) Å, c=27.0326(10) Å, V= 4805.5(3) Å³, space group P212121, Z = 4, D_{calcd} = 1.359 g/cm³, λ= 0.71073 (MoKα), 0.208 μ/mm⁻¹, F(000) = 2084, T = 100 K. A total of 668,812 reflections were collected, of which 25,782 unique reflections (R_{int} = 0.0453) with I > 2σ(I) were used for the analysis. The data was solved using the direct method, and the structure was refined by a full-matrix least-squares procedure on F² values. All non-hydrogen atoms were refined with anisotropic thermal parameters. The hydrogen atom positions were geometrically idealized and allowed to ride on their parent atoms. The final indices were R₁ 0.0354, wR₂ 0.0961 with goodness-of-fit = 1.093. The final X-ray molecular model is shown in Figure 3b with a Flack parameter= 0.017.

2-butiratebriarane B-3 (2). Colorless white powder; $[\alpha]_{\text{D}}^{25} +33.20$ (c 0.1, MeOH); IR ν_{max} 3520, 2925, 1750, 1675, 1350, 1210, 1025, 950, 725 cm⁻¹; ¹H-NMR data (500 MHz, CDCl₃), see Table 1; ¹³C-NMR data (125 MHz, CDCl₃), see Table 2; HRESIMS m/z 533.1910 [M + Na]⁺ (calcd. For C₂₆H₃₅ClO₈Na, 533.1918).

16-chlorobriarane B-3 (3). Colorless white powder; $[\alpha]_{\text{D}}^{25} -35.10$ (c 0.1, MeOH); IR ν_{max} 3520, 2925, 1800, 1750, 1675, 1350, 1210, 1025, 950, 725 cm⁻¹; ¹H-NMR data (500 MHz, CDCl₃), see Table 1; ¹³C-NMR data (125 MHz, CDCl₃), see Table 2; HRESIMS m/z 505.1596 [M + Na]⁺ (calcd. For C₂₄H₃₁ClO₈Na, 505.1605).

16-deschlorobriarane B-3 (4). Colorless white powder; $[\alpha]_{\text{D}}^{25} -34.40$ (c 0.1, MeOH); IR ν_{max} 3500, 2925, 1750, 1675, 1350, 1220, 1025, 950, 725 cm⁻¹; ¹H-NMR data (500 MHz, CDCl₃), see Table 1; ¹³C-NMR data (125 MHz, CDCl₃), see Table 2; HRESIMS m/z 487.1953 [M + Na]⁺ (calcd. For C₂₄H₃₂O₉Na, 487.1944).

Isobriarenolide P (5). Colorless white powder; $[\alpha]_{\text{D}}^{25} -20.00$ (c 0.1, MeOH); IR ν_{max} 3520, 2925, 1775, 1750, 1675, 1350, 1220, 1025, 950, 750 cm⁻¹; ¹H-NMR data (500 MHz, CDCl₃), see Table 1; ¹³C-NMR data (125 MHz, CDCl₃), see Table 2 and 2; HRESIMS m/z 479.1437 [M + Na]⁺ (calcd. For C₂₂H₂₉ClO₈Na, 479.1449).

Brianthein X (6). Colorless white powder; $[\alpha]_{\text{D}}^{25} -49.61$ (c 0.3, MeOH); IR ν_{max} 3566, 2963, 1788, 1739, 1363, 1220, 1025, 950, 750 cm⁻¹; HRESIMS m/z 521.1543 [M + Na]⁺

(calcd. For C₂₄H₃₁ClO₉Na, 521.1554).

Brianthein Y (7). Colorless white powder; [α]_D²⁵ +35.46 (c 0.3, MeOH); IR ν_{max} 3575, 2964, 1788, 1739, 1364, 1220, 1025, 925, 750 cm⁻¹; HRESIMS m/z 591.1966 [M + Na]⁺ (calcd. For C₂₈H₃₇ClO₁₀Na, 591.1973).

Brianthein Z (8). Colorless white powder; [α]_D²⁵ +28.90 (c 0.3, MeOH); IR ν_{max} 3550, 2930, 1790, 1739, 1365, 1220, 1025, 950, 750 cm⁻¹; HRESIMS m/z 563.1663 [M + Na]⁺ (calcd. For C₂₆H₃₃ClO₁₀Na, 563.1660).

Asbestinin-10 (9). Colorless white powder; [α]_D²⁵ -17.63 (c 0.2, MeOH); IR ν_{max} 3550, 2968, 2926, 2872, 1731, 1726, 1687, 1638, 1440, 1385, 1235, 1126, 918, 758 cm⁻¹; HRESIMS m/z 399.2165 [M + Na]⁺ (calcd. For C₂₂H₃₂O₅Na, 399.2147).

Lactone 14 (10). Colorless white powder; [α]_D²⁵ +42.65 (c 0.1, MeOH); IR ν_{max} 3550, 2968, 2926, 2872, 1731, 1726, 1687, 1638, 1440, 1385, 1340, 1220, 1126, 1025, 900, 775 cm⁻¹; HRESIMS m/z 515.2240 [M + Na]⁺ (calcd. For C₂₆H₃₆O₉Na, 515.2257).

4. Conclusions

In summary, four new diterpenoids, **2-5**, together with six known diterpenes, one Briarane **1**, three Briantheins **6-8**, one asbestinin **9** and one diterpene **10**, were isolated from gorgonian *Briareum asbestinum* collected in the Mexican Caribbean as its metabolic components. The absolute configurations of the new compounds **2-5** were determined by comparison of experimental NMR and X-Ray.

Supplementary Materials: Figures S1-S47: NMR spectra in CDCl₃ and HRESIMS of the compounds 1-5 and 10., Table S1. NMR data of 1 in CDCl₃, Table S2. NMR data of 2 in CDCl₃, Table S3. NMR data of 3 in CDCl₃, Table S4. NMR data of 4 in CDCl₃, Table S5. NMR data of 5 in CDCl₃, Table S6. NMR data of 10 in CDCl₃. Figures S48-S60: NMR spectra and MS of compounds 6-9, and ORTEP X-Ray of 7.

Acknowledgments. We thank to Xunta de Galicia for the support of the CICA-INIBIC strategic group (ED431E 2018/03). JR, CJ, and DPP acknowledge CESGA for the use of the computational facilities. DPP received a fellowship from the program National Council of Science and Technology (CONACYT) of Mexico and the Secretariat of Research, Innovation and Higher Education (SIIES) of Yucatan (Mexico). We gratefully acknowledge the help of colleagues, Daniel Catzim Pech, Gabriel González Mapen, Jorge Peniche Pérez, Melissa Llanes López, and Rodrigo Garcia Uribe for collecting the marine samples.

References

1. Dickschat, J. S. *Angew. Chem. Int. Ed.* **2019**, *58*, 2 – 15.
2. Su, Y.-D.; Su, J.-H.; Hwang, T.-L.; Wen, Z.-H.; Sheu, J.-H.; Wu, Y.-C.; Sung, P.-J. *Mar. Drugs* **2017**, *15*, 44-56.
3. Gómez-Reyes, J. F.; Salazar, A.; Guzmán, H. M.; González, Y.; Fernández, P. L.; Ariza-Castolo, A.; Gutierrez, M. *Mar. Drugs* **2012**, *10*, 2608-2617.
4. Gupta, P.; Sharma, U.; Schulz, T. C.; Sherrer, E. S.; McLean, A. B.; Robins, A. J.; West, L. M. *Org. Lett.* **2011**, *13*, 3920-3923.
5. Meginley, R. J.; Gupta, P.; Schulz, T. C.; McLean, A. B.; Robins, A. J.; West, Lyndon M. *Mar. Drugs* **2012**, *10*, 1662-1670.
6. Burks, J. E.; der Helm, D. van; Chang, C. Y.; Ciereszko, L. S. *Acta Cryst.* **1977**, *B33*, 704.

7. (a) Sung, P.-J.; Sheu, J.-H.; Xu, J.-P. *Heterocycles* **2002**, *57*, 535–579. (b) Sung, P.-J.; Chang, P.-C.; Fang, L.-S.; Sheu, J.-H.; Chen, W.-C.; Chen, Y.-P.; Lin, M.-R. *Heterocycles* **2005**, *65*, 195–204. (c) Sung, P.-J.; Sheu, J.-H.; Wang, W.-H.; Fang, L.-S.; Chung, H.-M.; Pai, C.-H.; Su, Y.-D.; Tsai, W.-T.; Chen, B.-Y.; Lin, M.-R. *Heterocycles* **2008**, *75*, 2627–2648. (d) Sung, P.-J.; Su, J.-H.; Wang, W.-H.; Sheu, J.-H.; Fang, L.-S.; Wu, Y.-C.; Chen, Y.-H.; Chung, H.-M.; Su, Y.-D.; Chang, Y.-C. *Heterocycles* **2011**, *83*, 1241–1258. (e) Sheu, J.-H.; Chen, Y.-H.; Chen, Y.-H.; Su, Y.-D.; Chang, Y.-C.; Su, J.-H.; Weng, C.-F.; Lee, C.-H.; Fang, L.-S.; Wang, W.-H.; Wen, Z.-H.; Wu, Y.-C.; Sung, P.-J. *Mar. Drugs* **2014**, *12*, 2164–2181.
8. Liaw, C.C.; Cheng, Y.B.; Lin, Y.S.; Kuo, Y.H.; Hwang, T.L.; Shen, Y.C. *Mar. Drugs*, **2014**, *12*, 4677-4692.
9. (a) Rodríguez, J.; Nieto, R.M.; Hunter, L. M.; Cristina-Diaz, C.; Crews, P.; Lobkovsky, E.; Clardy, J. *Tetrahedron*, **1994**, *50*, 11079-11090. (b) Rodríguez, J.; Nieto, R.M.; Jiménez, C. *J. Nat. Prod.* **1998**, *61*, 313-317. (c) García, M.; Rodríguez, J.; Jiménez, C. *J. Nat. Prod.* **1999**, *62*, 257-260. (d) Anta C.; González, N.; Santafé, G.; Rodríguez, J.; Jiménez, C. *J. Nat. Prod.* **2002**, *65*, 766-768. (e) Pardo-Vargas, A.; De Oliveira Barcelos, I.; Soares Stephens, P. R.; Cirne-Santos, C.; Nunes De Palmer Paixão, I. C.; Ramos, F. A.; Jiménez, C.; Rodríguez, J.; Teixeira, V.; Castellanos, L. *Marine Drugs* **2014**, *12*, 4247-4259.
10. Meissner, A.; Sorensen, O.W. *Magn. Reson. Chem.* **2001**, *39*, 49-52.
11. Stierle, D.B.; Carté, B.; Faulkner, D. J.; Tagle, B.; Clardy, J. *J. Am. Chem. Soc.* **1980**, *102*, 5088-5092.
12. Su, Y.; Cheng, C.; Chen, W.; Chang, Y.; Chen, Y.; Hwang, T.; Wen, Z.; Wang, W.; Fang, L.; Chen, J.; Wu, Y.; Sheu, J.; Sung, P. *Tet. Lett.* **2014**, *55*, 6065-6067.
13. Schrödinger suite, V. 2016-4. Schrödinger, LCC.
14. Harvell, C. D.; Fenical, W.; Roussis V., Ruesink, J.L., Griggs; C.C.; Greenel, C.H. *Mar. Ecol. Prog. Ser.*, **1993**, *93*, 165-173.
15. Nath, N.; Fuentes-Monteverde, J. C.; Pech-Puch, D.; Rodríguez, J.; Jiménez, C.; Noll, M.; Kreiter, A.; Reggelin, M.; Navarro-Vázquez, A.; Griesinger, C. *Nature Chem.* 2019, in revision.
16. Pesticelli, G; Bruhn, T. *Chirality* **2016**, *28*, 466-474
17. Su, Y.-D.; Wen, Z.-H.; Wu, Y.-C.; Fang, L.-S.; Chen, Y.-H.; Chang, Y.-C.; Sheu, J.-H.; Sung, P.-J. *Tetrahedron*, **2016**, *72*, 944-951.
18. Crews, P.; Rodríguez, J.; Jaspars; M. *Organic Structure Analysis*, Chapter 3, page 85. 2nd Ed. **2010**. Oxford University Press. New York.
19. Poza, J. J.; Jiménez, C.; Rodríguez, J. *Eur. J. Org. Chem.* **2008**, 3960–3969.

Supplementary Materials

Table S1. NMR data of **1** in CDCl₃ (125 MHz for ¹³C and 500 MHz for ¹H).

no.	δ_c type	δ_H , mult. (<i>J</i> in Hz)	COSY	HMBC	NOESY
1	44.9, qC			2, 10,13, 14, 15	
2	79.3, CH	4.81, d (9.4)	3	14, 15, 22	3, 10, 14, 15
3	28.5, CH ₂	2.41, dt (15.6, 9.4, 9.4)-1.87, dd (15.6, 10.9)	2, 4		2, 3, 10, 16
4	28.5, CH ₂	2.61, dd (15.0, 10.9)-1.62, m	3	16	4, 6, 7, 9, 16
5	142.6, qC			3, 6, 16	
6	67.3, CH	4.83, bs	7	16	4, 7
7	78.2, CH	5.77, bs	6	6, 9, OH	4, 6, 10, 17, 22
8	82.9, qC			6, 9, 10, 17, 18, OH	
9	74.4, CH	5.11, d (5.1)	10	10, 17, 21, OH	4, 10, 17, 20
10	38.5, CH	2.99, dd (4.7, 5.1)	9, 11	2, 14, 20	2, 3, 7, 9, 11, 16, OH
11	46.8, CH	2.61, dq (4.7, 7.4)	10, 20	9, 20	10, 20
12	202.7, qC			14, 20	
13	126.1, CH	5.97, d (10.4)	14	14	
14	154.7, CH	6.19, d (10.4)	13	2, 13, 15	2, 15
15	19.0, CH	1.16, s		14	2, 14, 20, 21
16	119.9, CH ₂	5.69, bs-5.37, s		6	3, 4, 10, 16, OH
17	42.3, CH	2.41, q (7.7)	18	9	7, 9, 18,
18	10.1, CH	1.30, d (7.7)	17	17	17
19	176.4, qC			17, 18	
20	15.1, CH	1.30, d (7.4)	11	10	9, 11, 15
21 Ac	170.3, qC			9	
22 Ac	169.6, qC			2	
CH ₃ 21	21.9, CH ₃	2.14, s		21	15
CH ₃ 22	21.2, CH ₃	2.24, s		22	7
OH		3.43, bs			10, 16

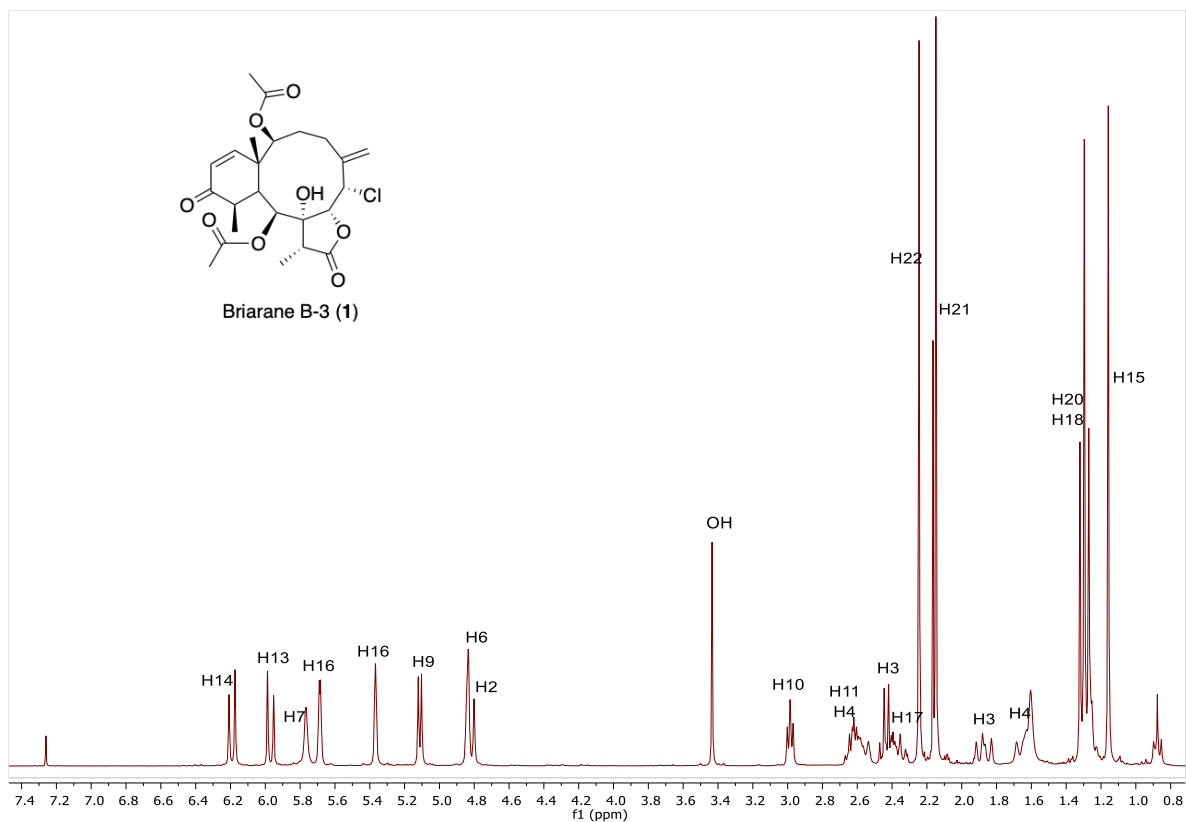


Figure S1. ¹H NMR spectrum of **1** (500 MHz, CDCl₃).

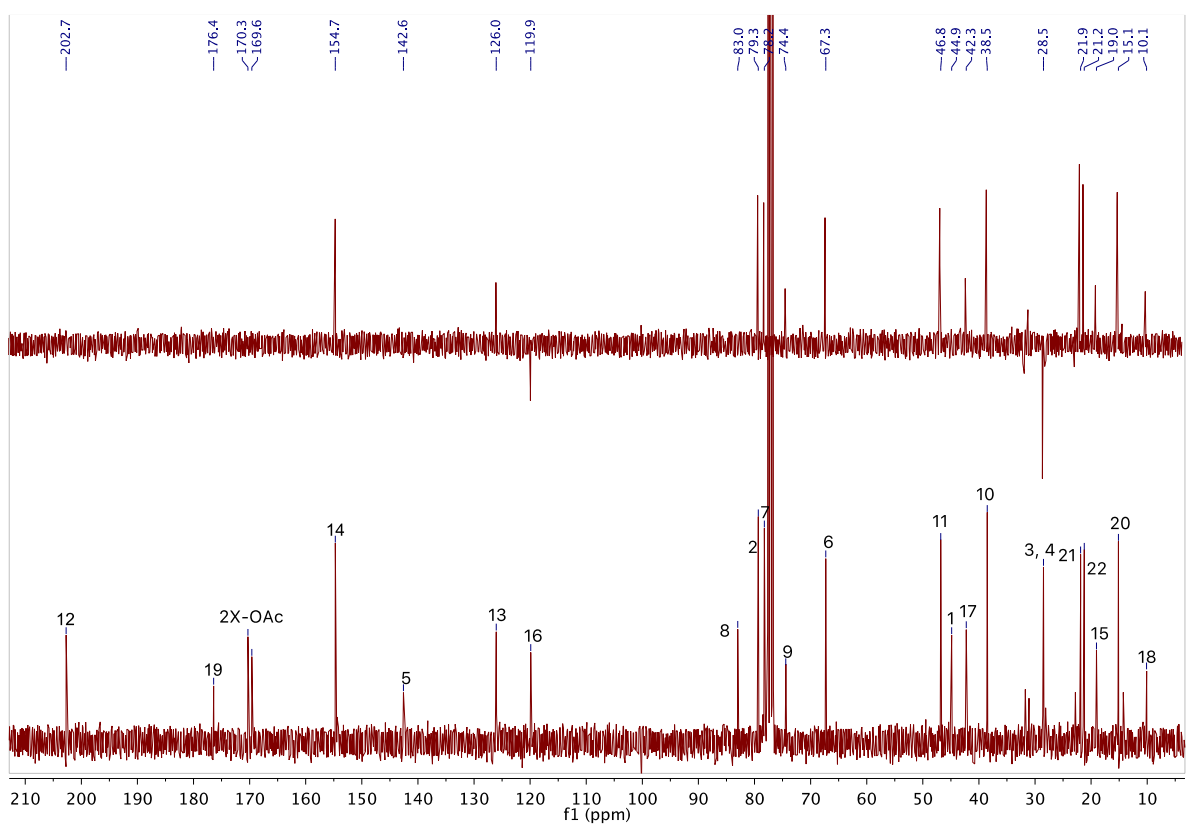


Figure S2. ¹³C NMR and DEPT-135 spectra of **1** (125 MHz, CDCl₃).

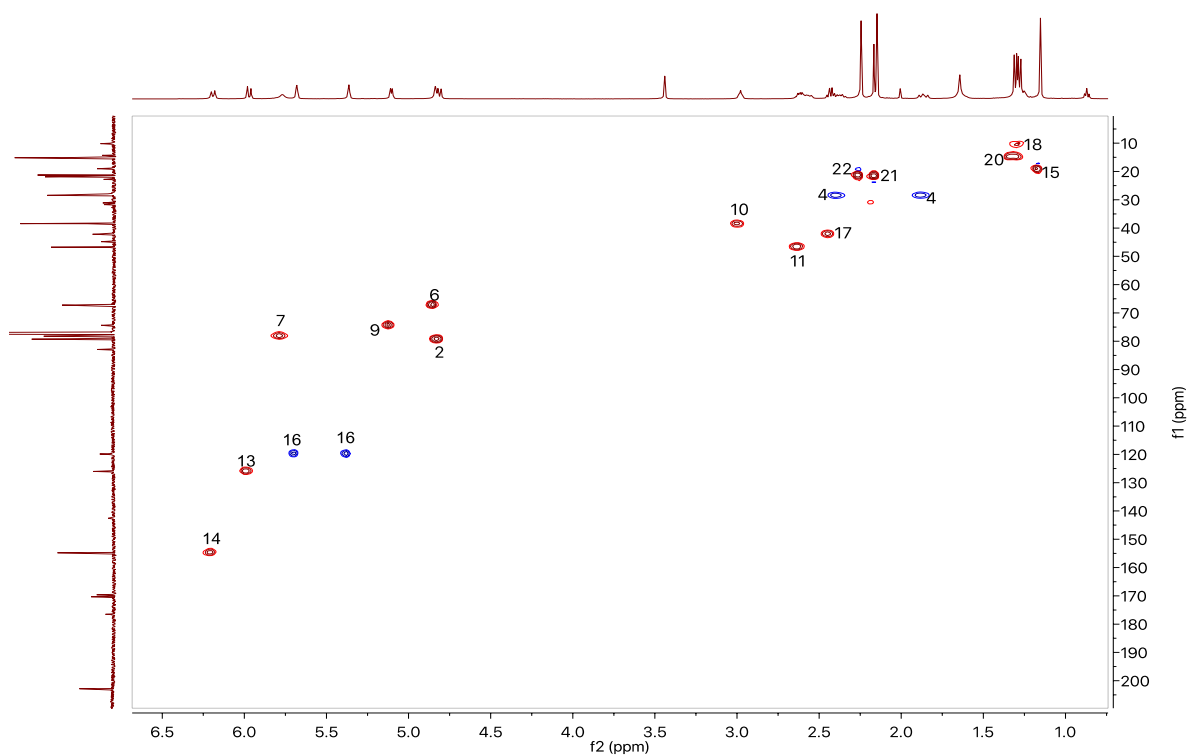


Figure S3. HSQC spectrum of **1** (500 MHz, CDCl₃). CH₂: blue cross-peaks and CH or CH₃: red cross-peaks.

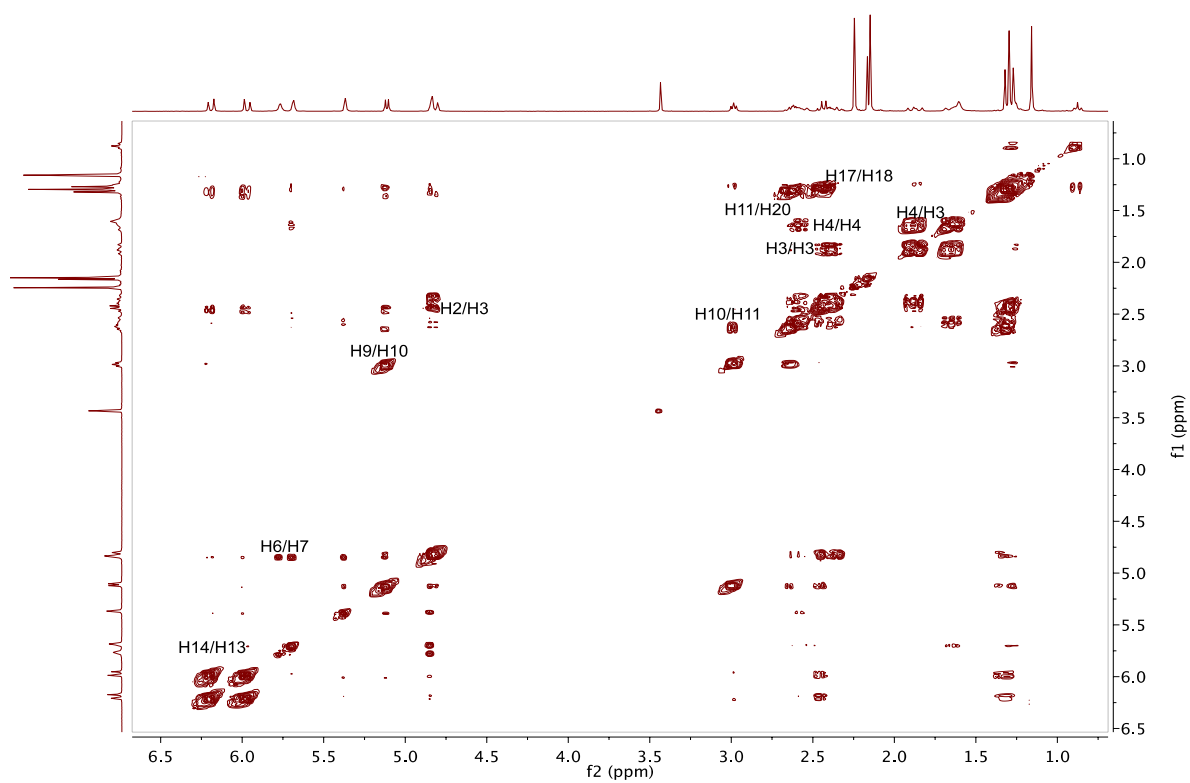


Figure S4. COSY spectrum of **1** (500 MHz, CDCl₃).

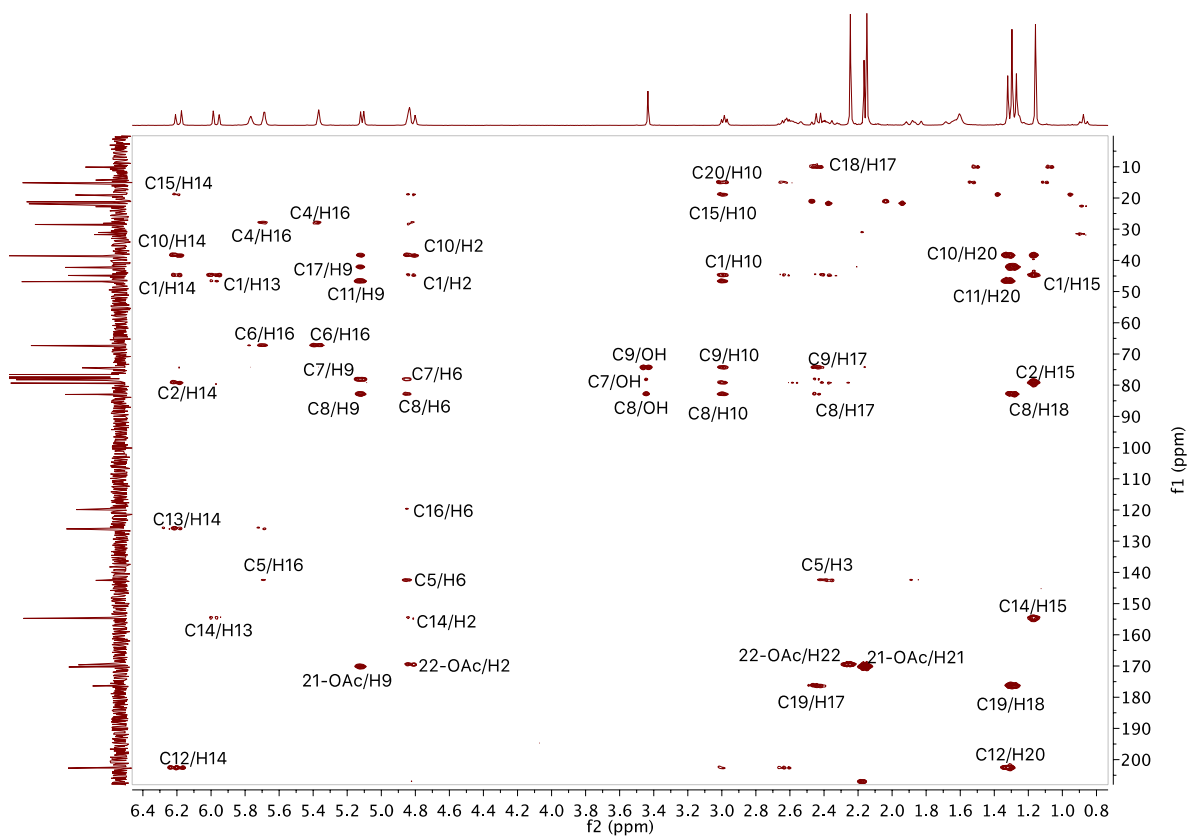


Figure S5. HMBC spectrum of **1** (500 MHz, CDCl₃).

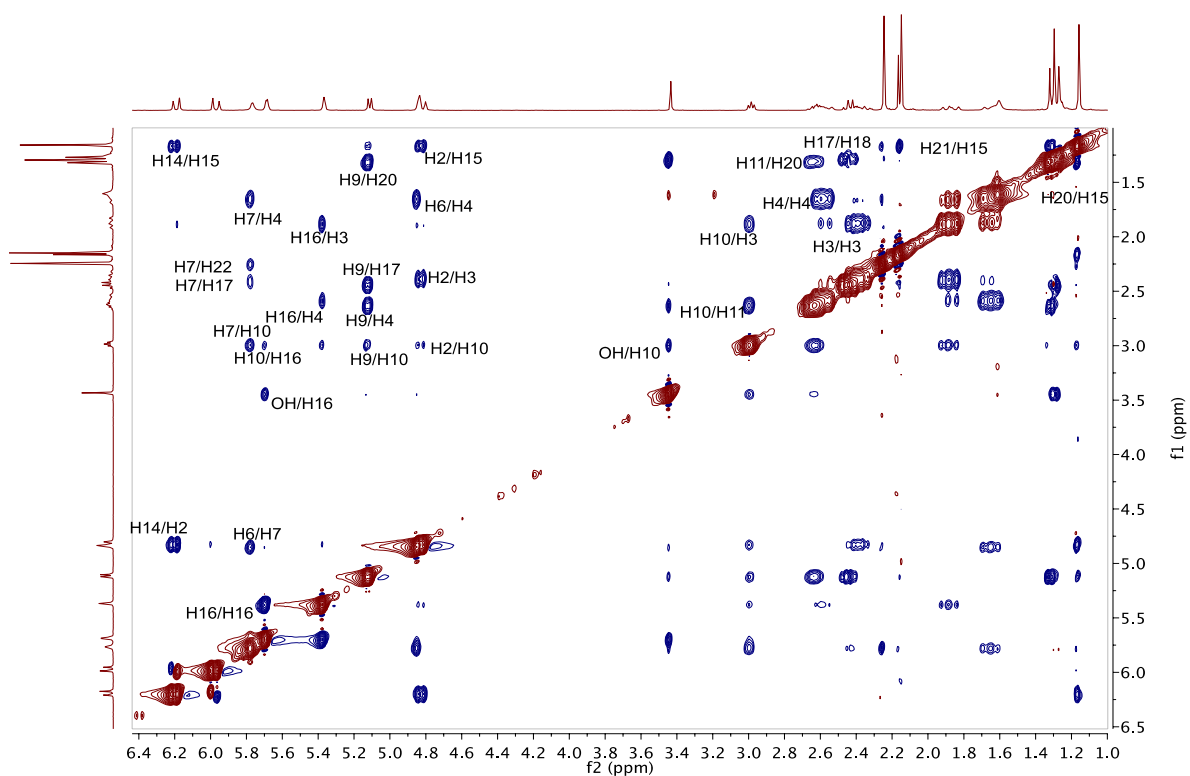


Figure S6. NOESY spectrum of **1** (500 MHz, CDCl₃).

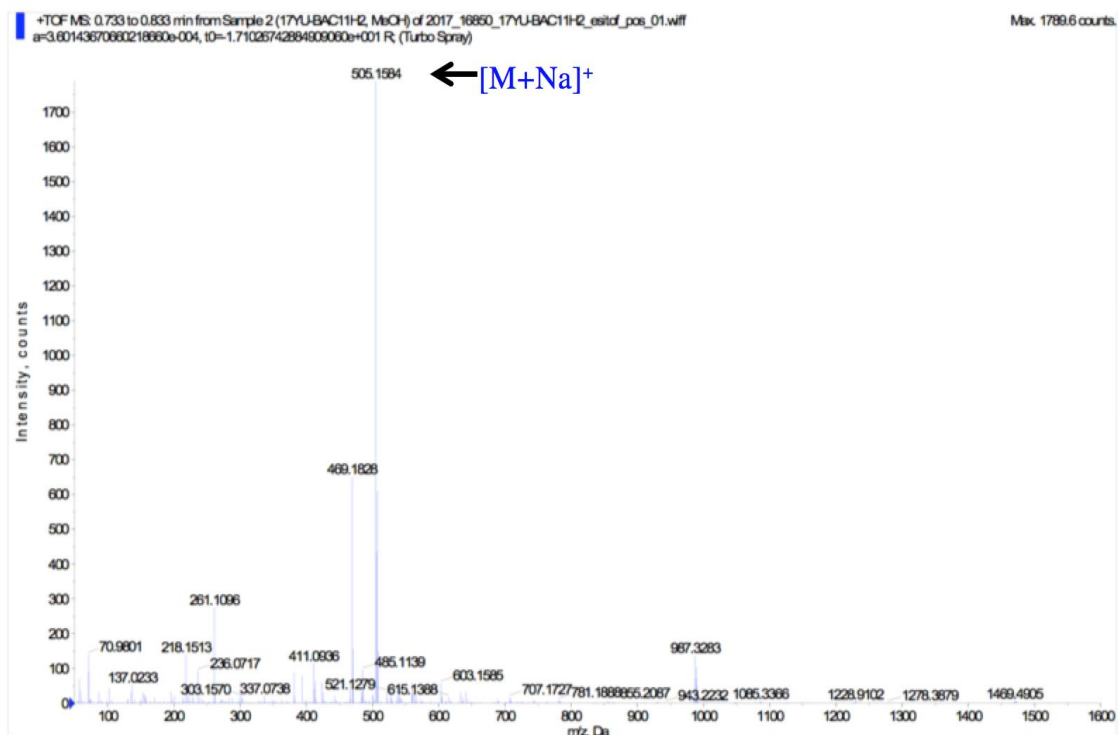


Figure S7. (+)-LRESIMS of 1.

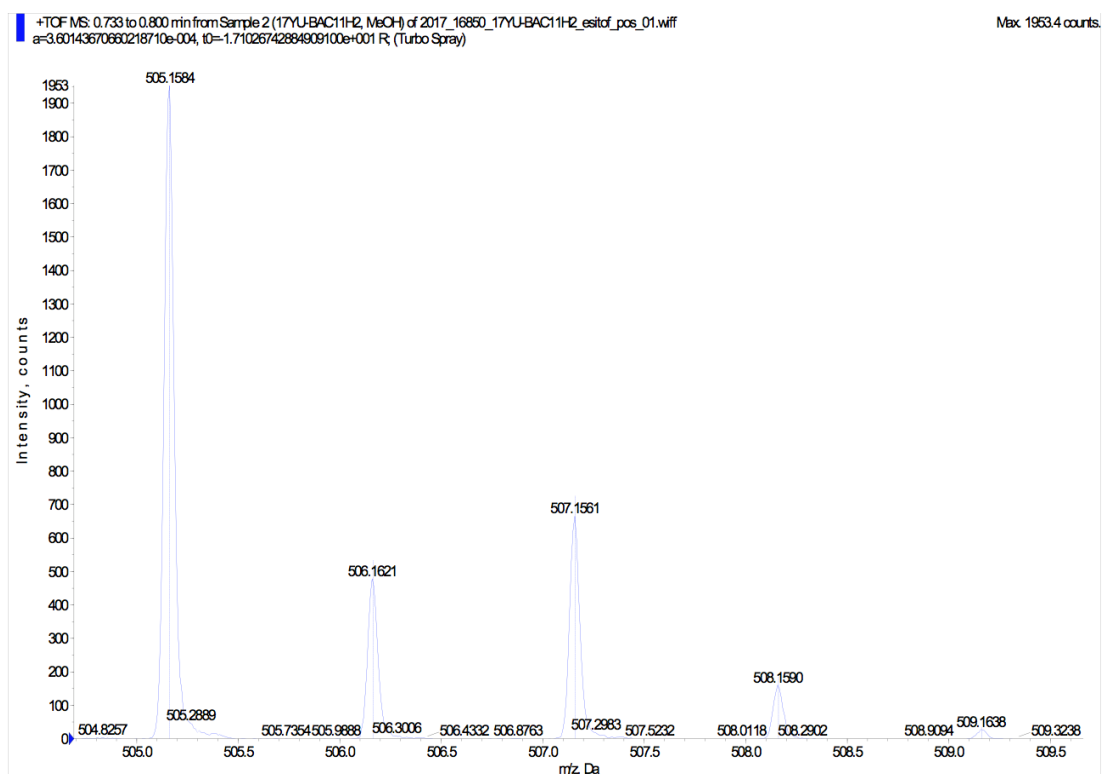
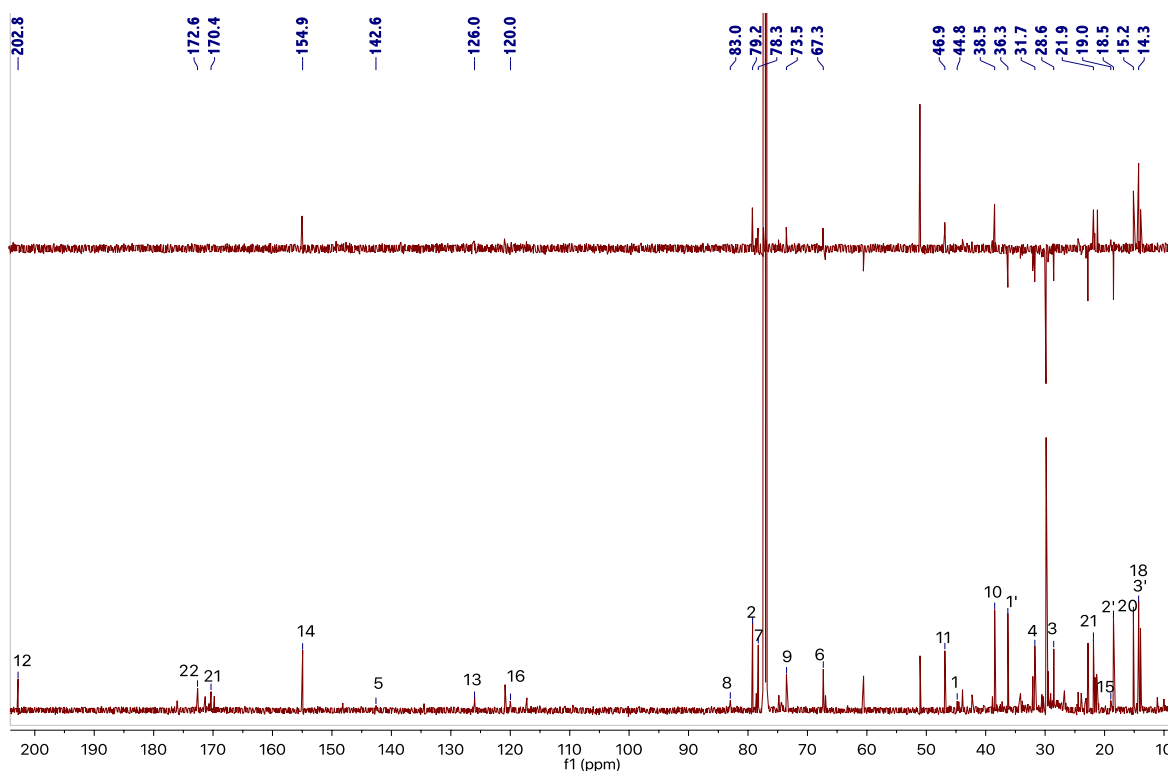
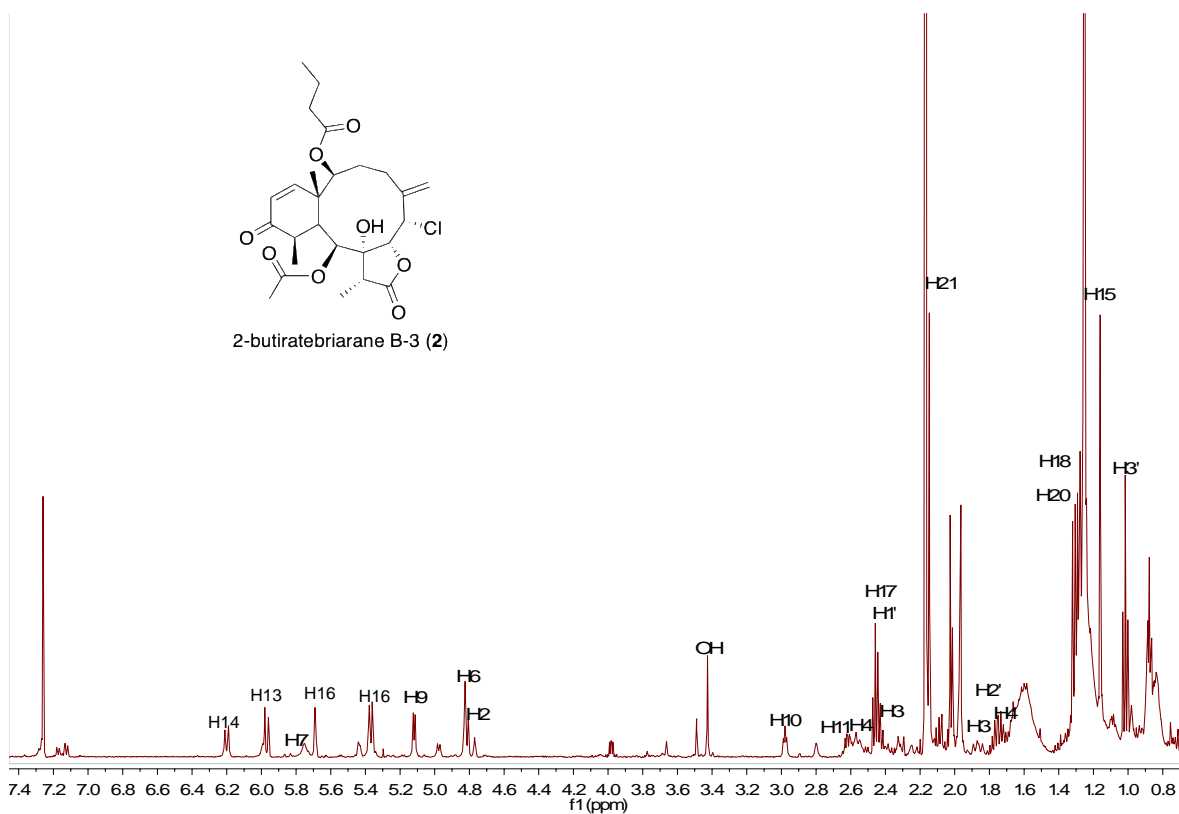


Figure S8. (+)-HRESIMS of 1.

Table S2. NMR data of **2** in CDCl₃ (125 MHz for ¹³C and 500 MHz for ¹H).

no.	δ_c type	δ_H , mult. (<i>J</i> in Hz)	COSY	HMBC	NOESY
1	44.8, qC			13, 15	
2	79.2 CH	4.82, d (9.5)	3	15	3, 10, 14, 15
3	28.6, CH ₂	2.40, m	2, 4		2, 3, 10, 16
4	31.7, CH ₂	2.57, m-1.60, m	3		4, 6, 7, 16
5	142.6, qC			3, 6, 16	
6	67.3, CH	4.84, d (9.3)	7	16	4, 7, 17
7	78.3, CH	5.71, bs	6	6, 9	4, 6, 10, 17
8	83.0, qC			6, 18	
9	73.5, CH	5.11, d (5.5)	10	17, OH	10, 17, 20
10	38.5, CH	2.99, dd (5.0, 5.5)	9, 11	2, 14, 15, 20	2, 3, 7, 9, 11, 16, OH
11	46.9, CH	2.61, m	10, 20	9, 20	10, 20
12	202.8, qC			14, 20	
13	126.0, CH	5.97, d (10.5)	14	14	20
14	154.9, CH	6.20, d (10.5)	13	2, 15	2, 15
15	19.0, CH	1.16, s			2, 2', 14, 21
16	120.0, CH ₂	5.69, q (2.0)-5.37 (bs)		6	3, 4, 10, 16, OH
17	42.3, CH	2.45, q (7.3)	18	9, 18	6, 7, 9, 18, 21
18	14.0, CH	1.30, d (7.3)	17	17	17
19	175.9, qC			17, 18	
20	15.2, CH	1.33, d (7.4)	11		9, 11, 13
21 Ac	170.4, qC			9	
22 Ac	172.6, qC			2	
CH ₃ 21	21.9, CH ₃	2.15, s		21	15, 17
1'CH ₂	36.3, CH ₂	2.45, q (7.4)	2'	22	2', 3'
2'CH ₂	18.5, CH ₂	1.77, m	1', 3'		1', 3'15
3'CH ₃	14.3 CH ₃	1.02, t (7.4)	2'		1', 2'
OH		3.42, bs			10, 16



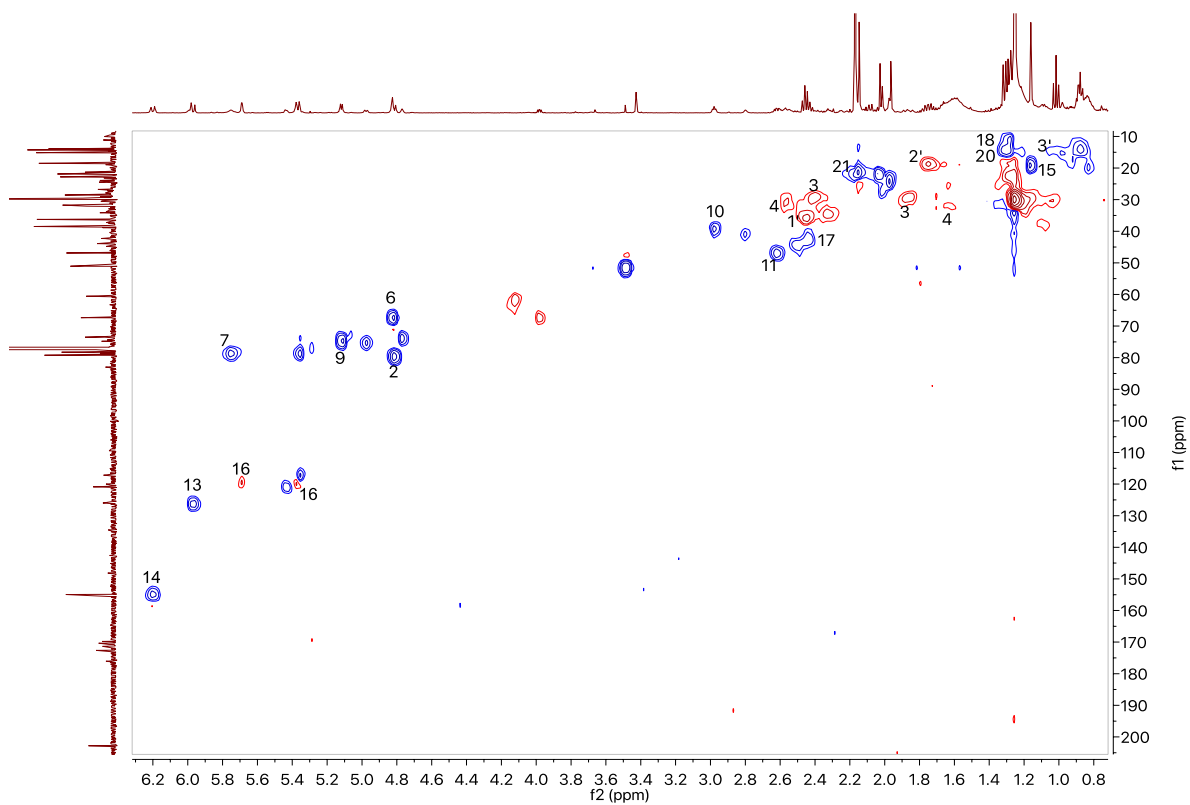


Figure S11. HSQC spectrum of **2** (500 MHz, CDCl₃). CH₂: blue cross-peaks and CH or CH₃: red cross-peaks.

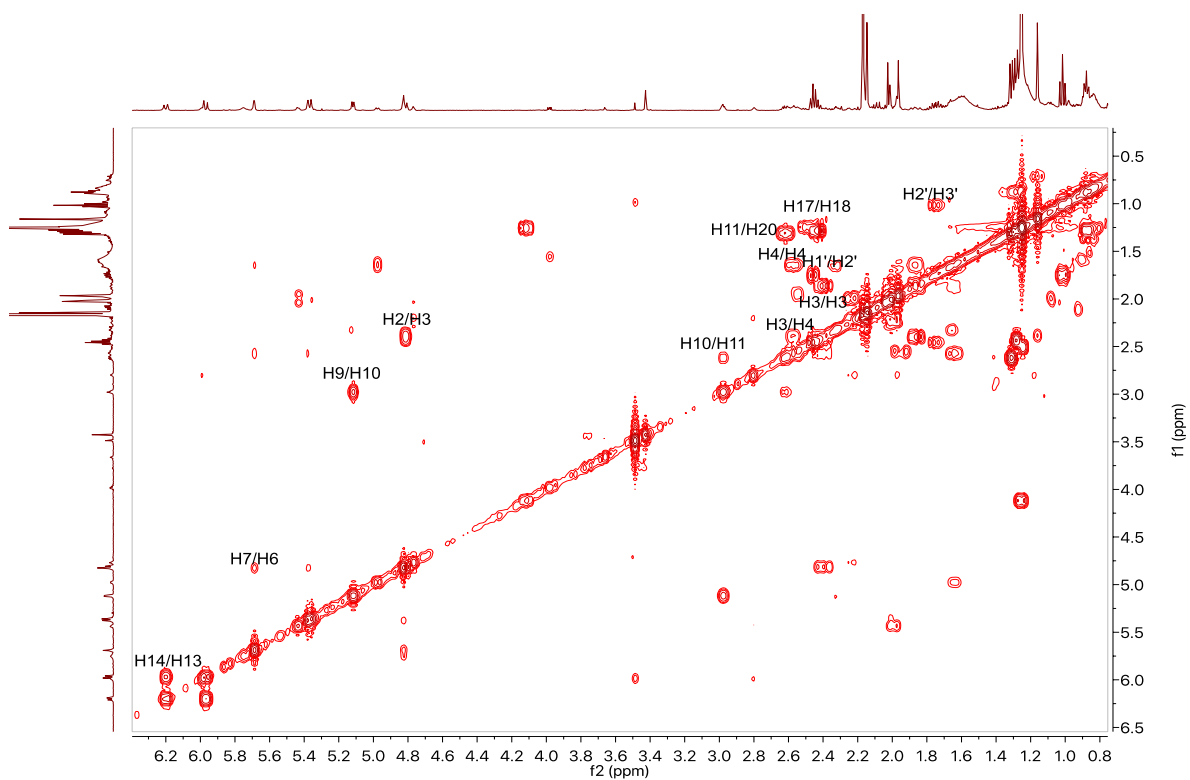


Figure S12. COSY spectrum of **2** (500 MHz, CDCl₃).

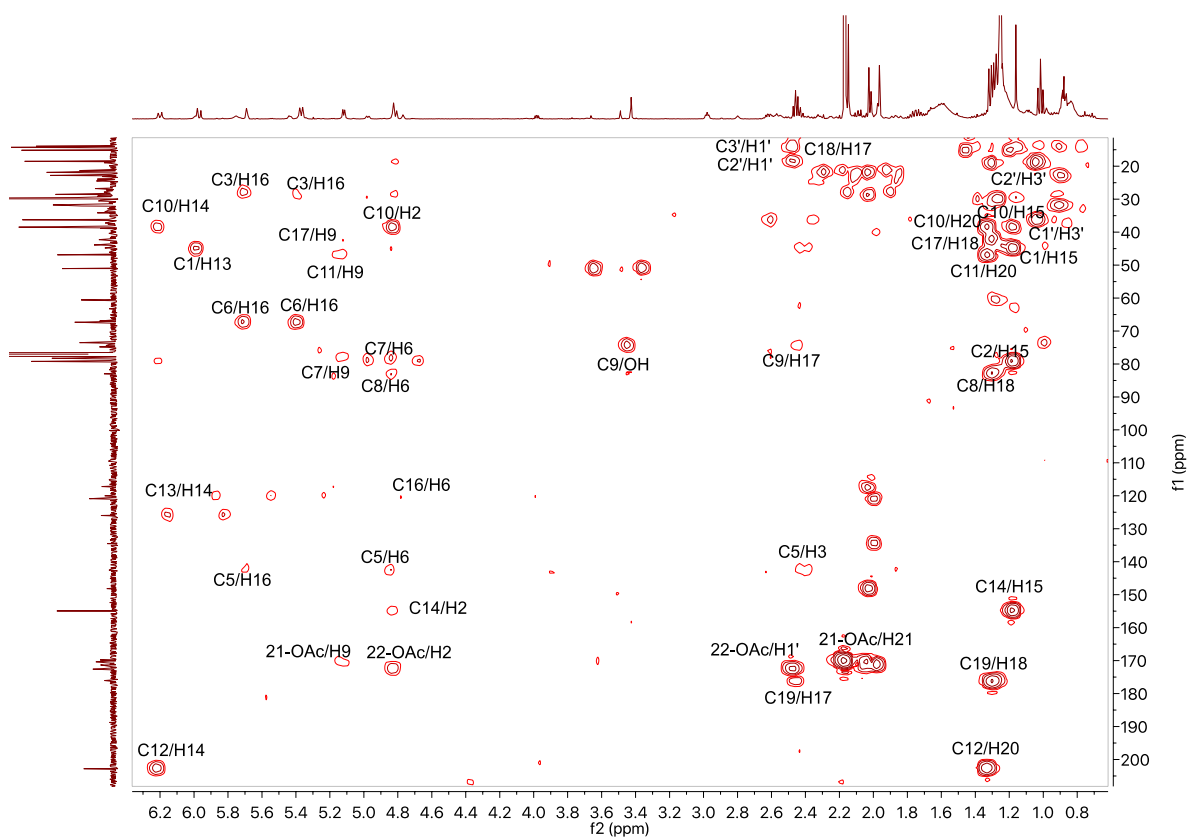


Figure S13. HMBC spectrum of **2** (500 MHz, CDCl₃).

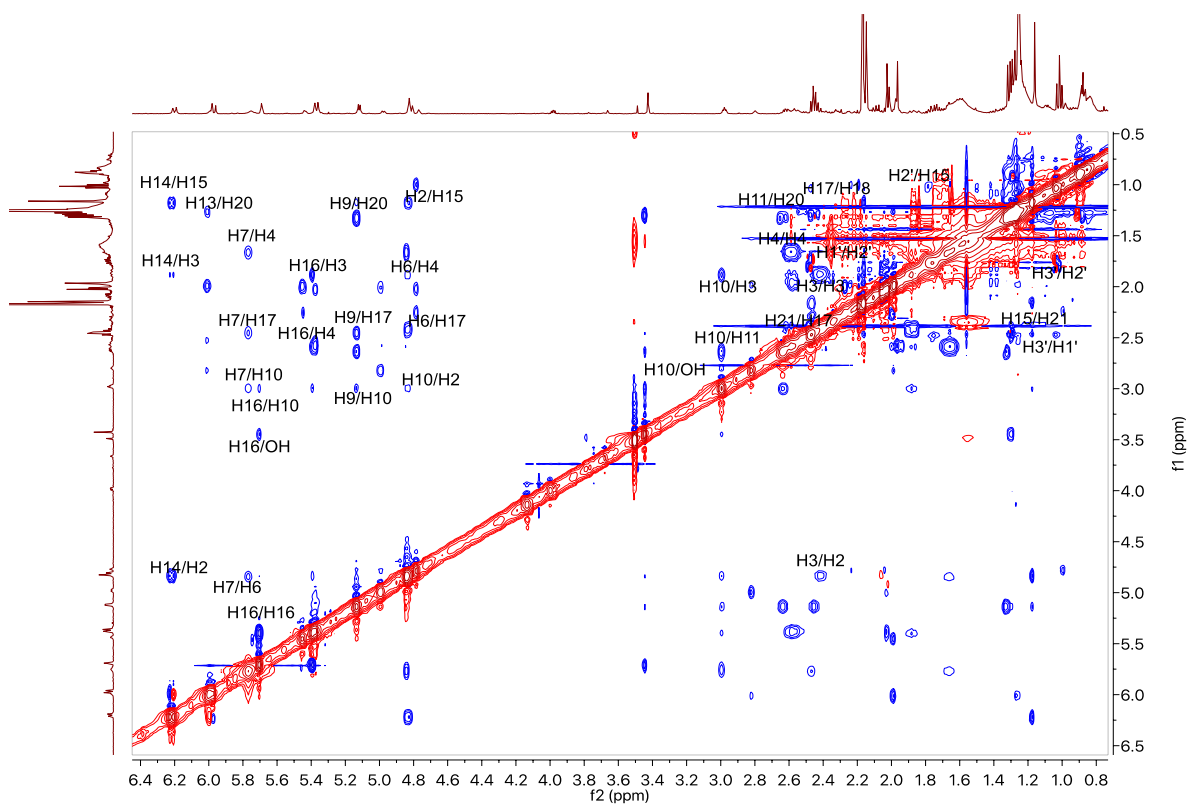


Figure S14. NOESY spectrum of **2** (500 MHz, CDCl₃).

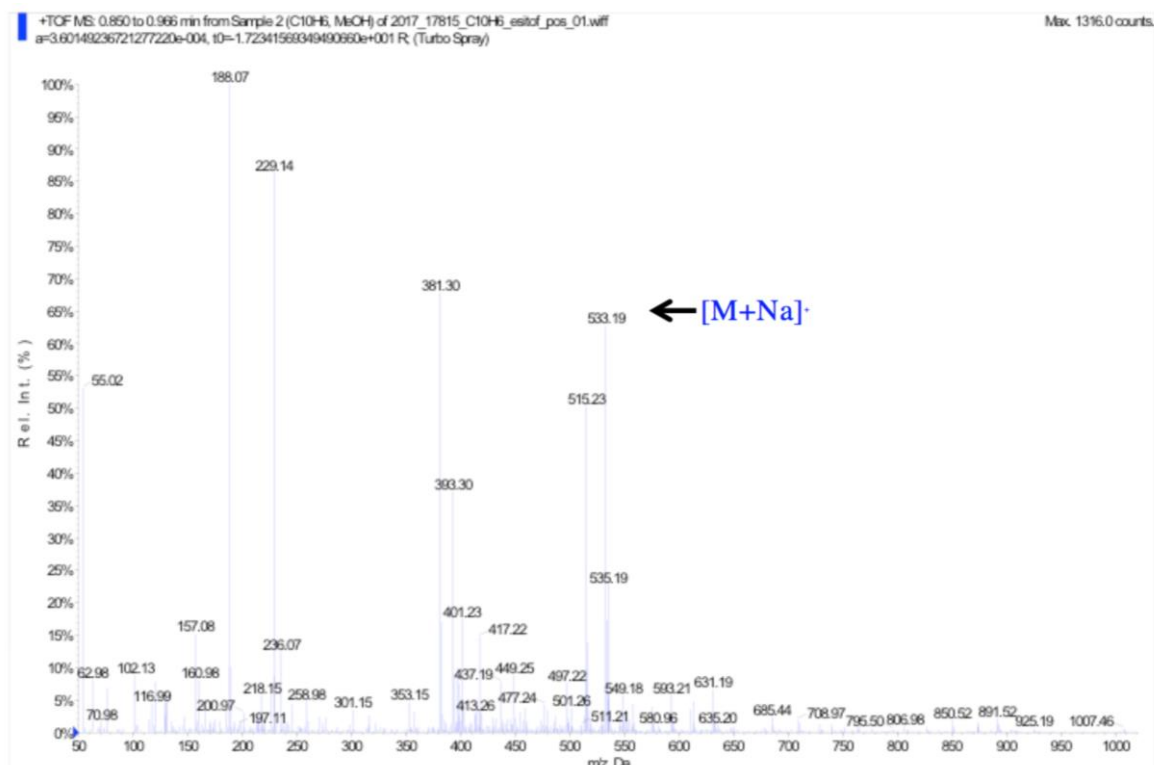


Figure S15. (+)-LRESIMS of 2.

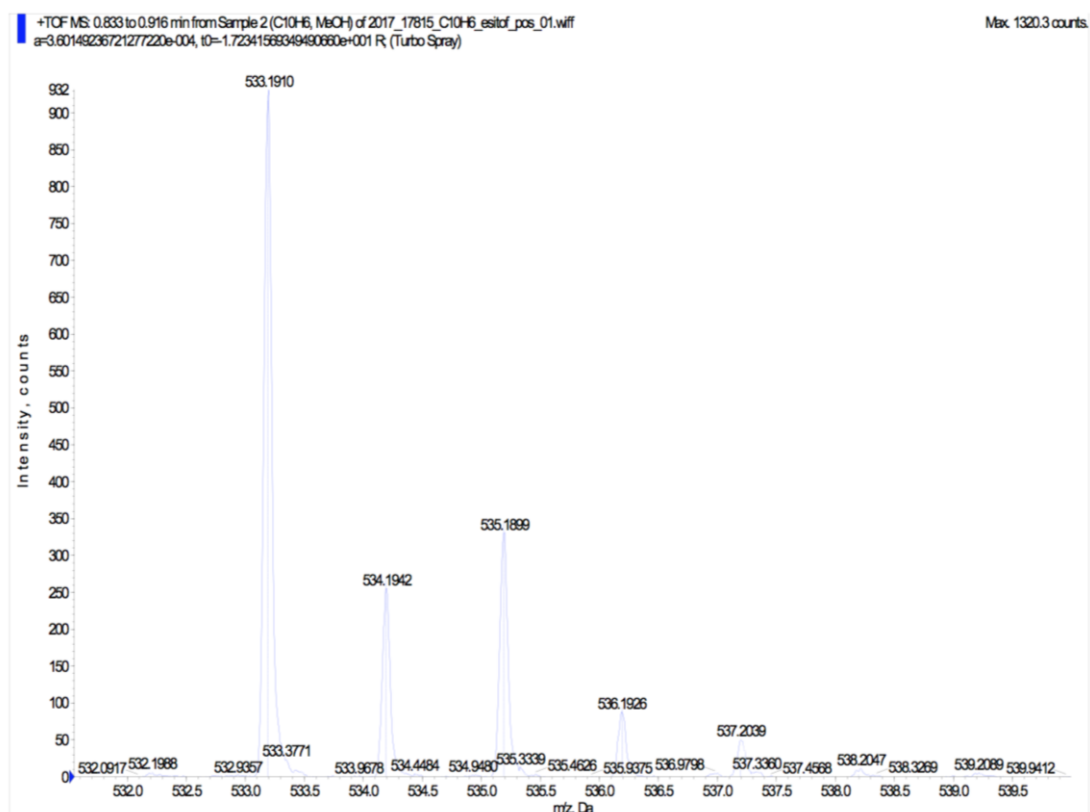


Figure S16. (+)-HRESIMS of 2.

Table S3. NMR data of **3** in CDCl₃ (125 MHz for ¹³C and 500 MHz for ¹H).

no.	δ_c type	δ_H , mult. (<i>J</i> in Hz)	COSY	HMBC	NOESY
1	44.2, qC			13, 14, 15	
2	79.6 CH	4.37, d (6.0)	3	15	3, 4, 10, 15
3	31.7, CH ₂	2.78, dt (15.4, 15.4, 5.5)-1.77, m	2, 4		2, 3, 7
4	26.2, CH ₂	2.56, m-2.05, m	3	2, 6, 16	2, 4, 7, 16
5	144.2, qC			7, 16	
6	123.3, CH	5.88, dd (10.3, 0.6)	7	16	7
7	77.4, CH	5.23, d (10.3)	6		3, 4, 6, 17
8	82.6, qC			18	
9	71.1, CH	5.28, d (4.7)	10	17	10, 17, 15, 20
10	38.3, CH	2.64, dd (4.6, 4.7)	9, 11	14, 15, 20	2, 9, 16,
11	48.6, CH	2.53, m	10, 20	9, 20	15, 21
12	203.1, qC			14, 20	
13	124.3, CH	5.84, d (10.5)	14		14
14	154.8, CH	6.40, d (10.5)	13	15	13, 15
15	15.4, CH	1.22, s			2, 9, 11, 14, 17,
16	51.2, CH ₂	4.32, d (12.0)- 4.18, d (12.0)		6	4, 10,
17	42.6, CH	2.45, q (7.2)	18		7, 9, 15, 18, 20, 22
18	6.8, CH	1.19, d (7.2)	17	17	9, 17
19	175.7, qC			17, 18	
20	15.2, CH	1.30, d (7.4)	11		9, 17, 18
21 Ac	169.0, qC			9	
22 Ac	170.7, qC			2	
CH ₃ 21	21.3, CH ₃	2.25, s		21	11
CH ₃ 22	21.9, CH ₃	2.14, s		22	4, 17
OH					

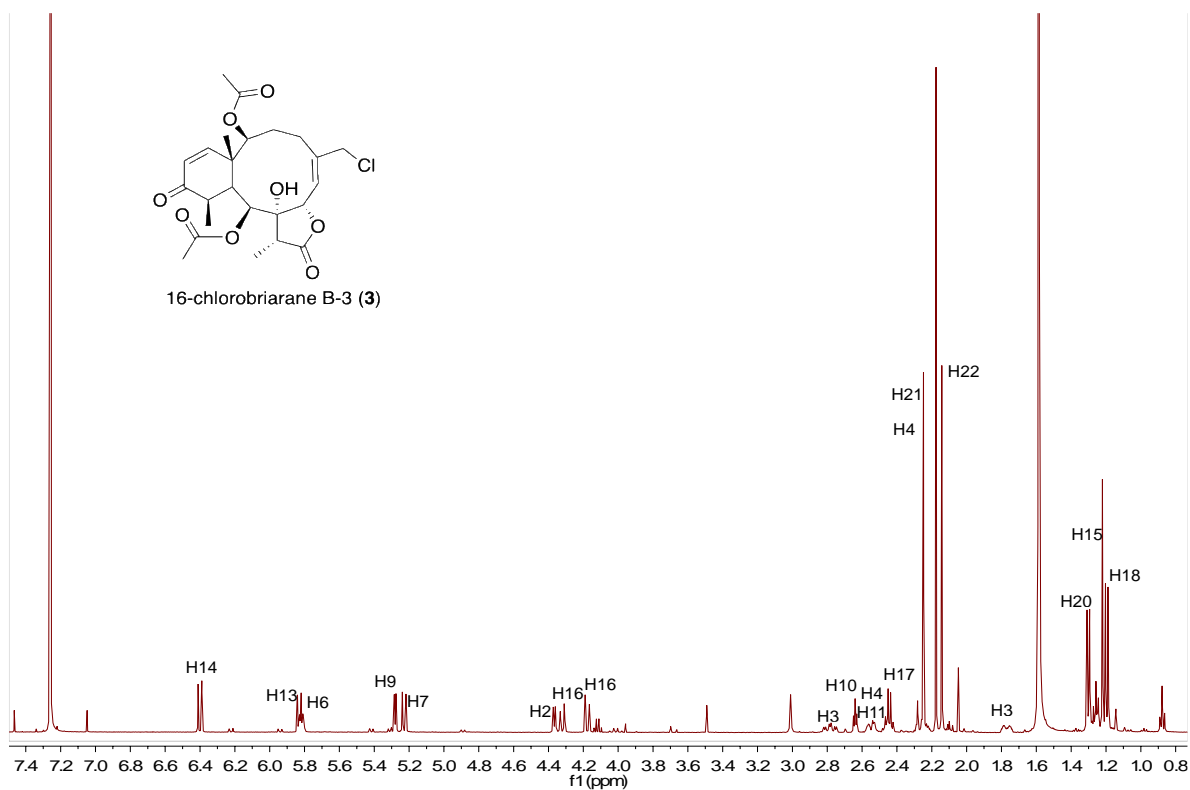


Figure S17. ^1H NMR spectrum of **3** (500 MHz, CDCl_3).

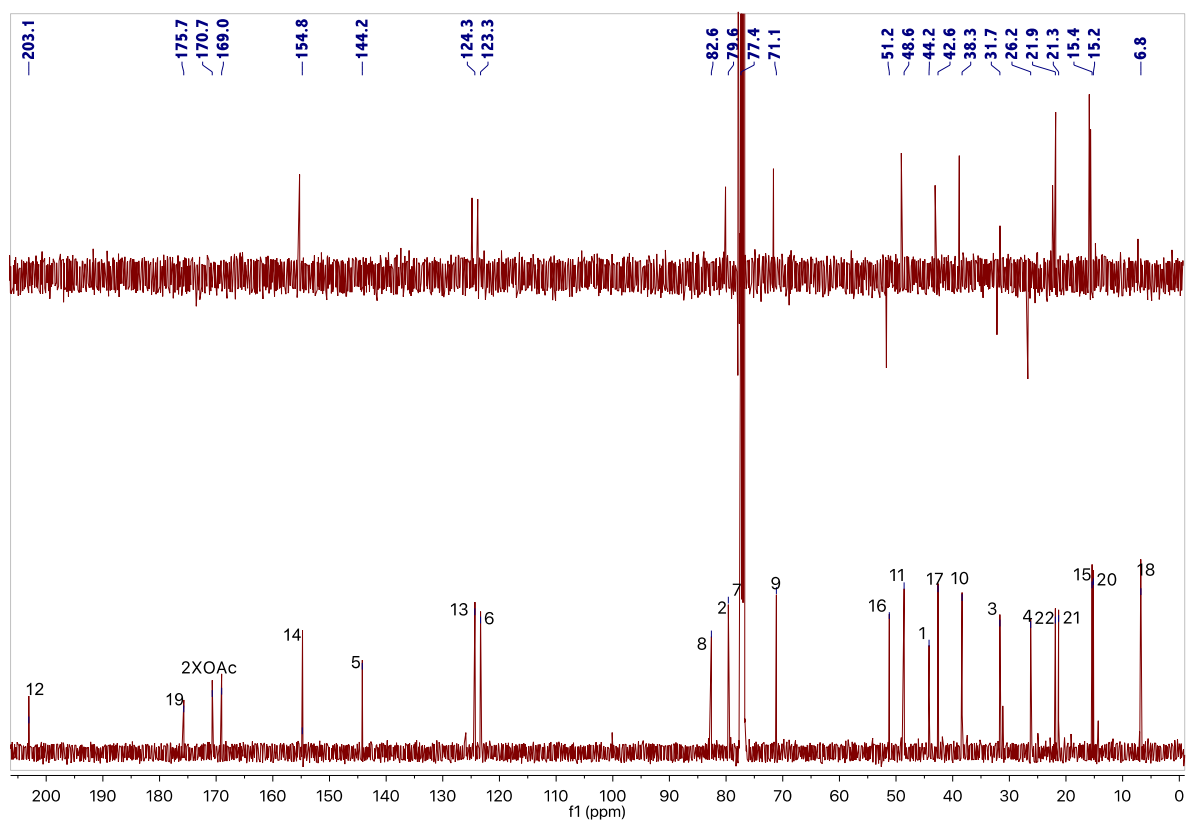


Figure S18. ^{13}C NMR and DEPT-135 spectra of **3** (125 MHz, CDCl_3).

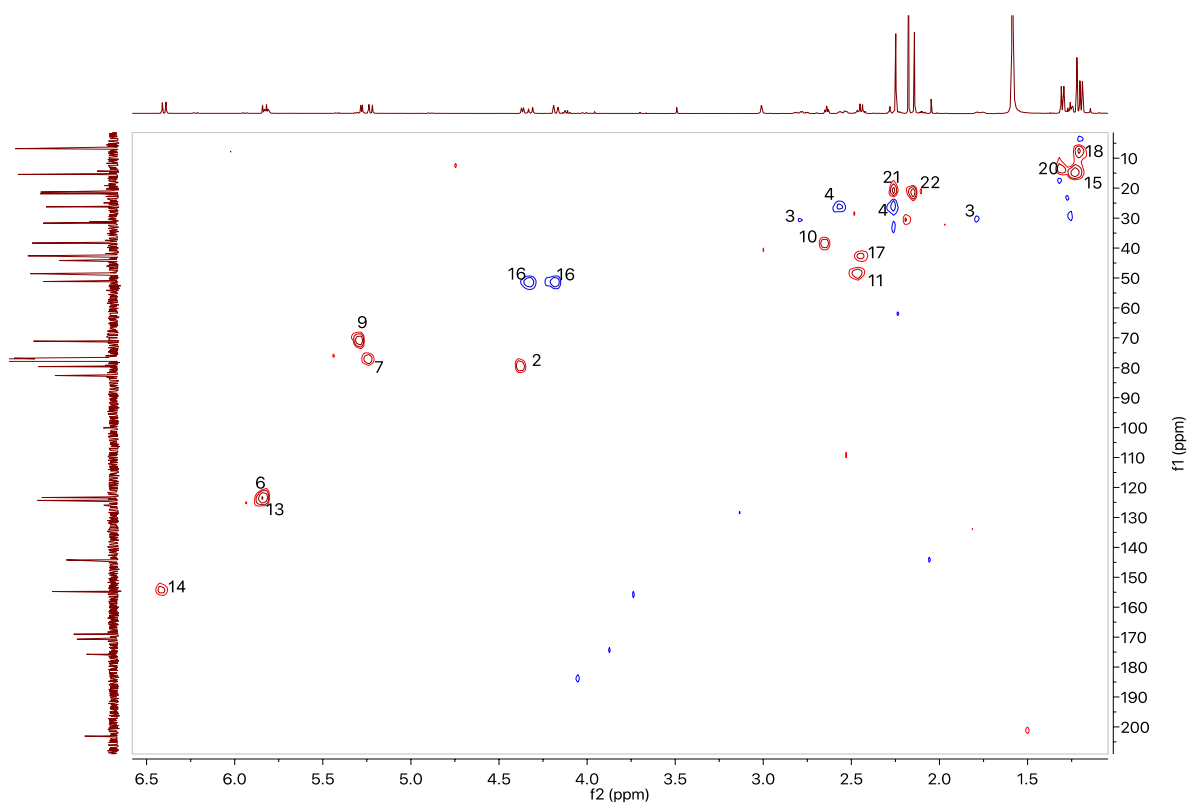


Figure S19. HSQC spectrum of **3** (500 MHz, CDCl_3). CH_2 : blue cross-peaks and CH or CH_3 : red cross-peaks.

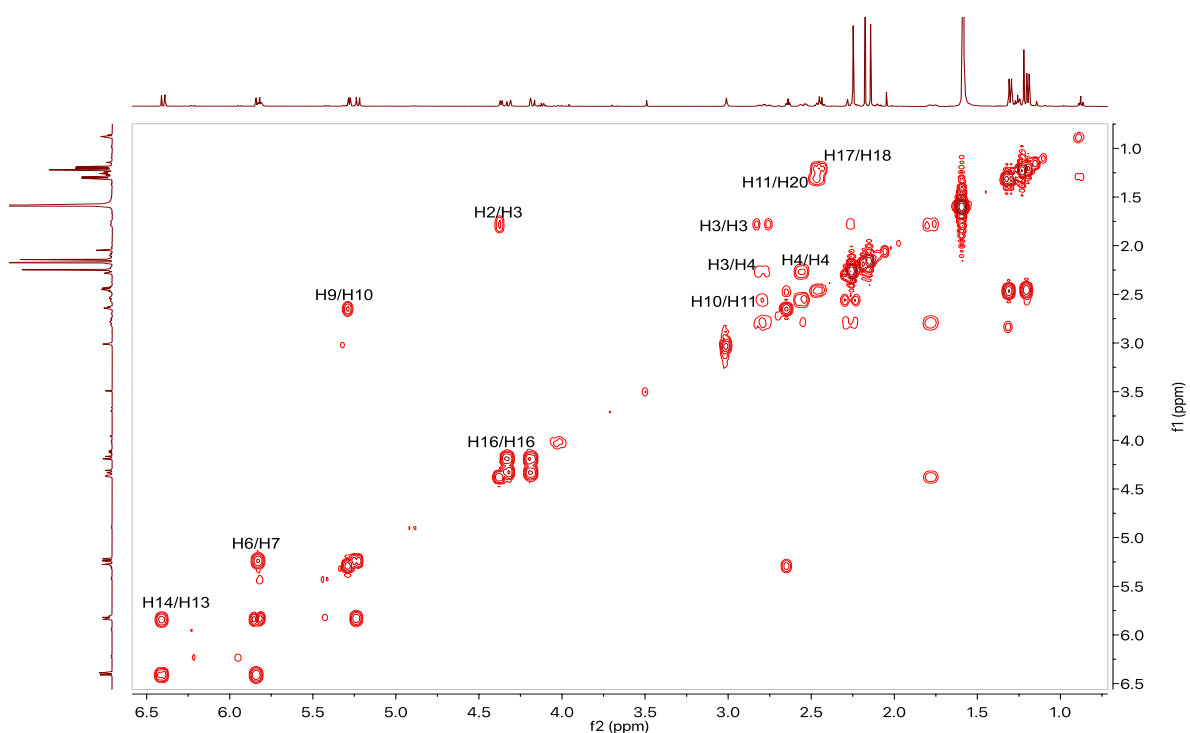


Figure S20. COSY spectrum of **3** (500 MHz, CDCl_3).

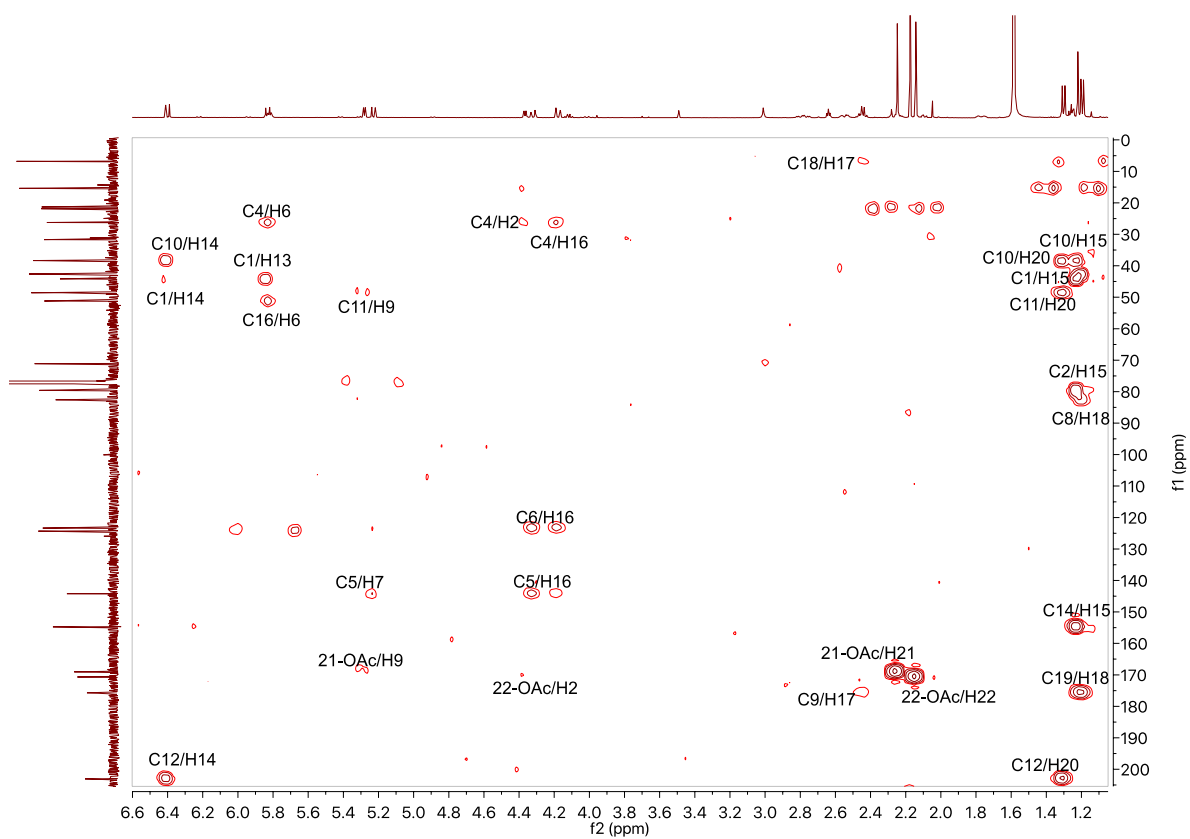


Figure S21. HMBC spectrum of **3** (500 MHz, CDCl₃).

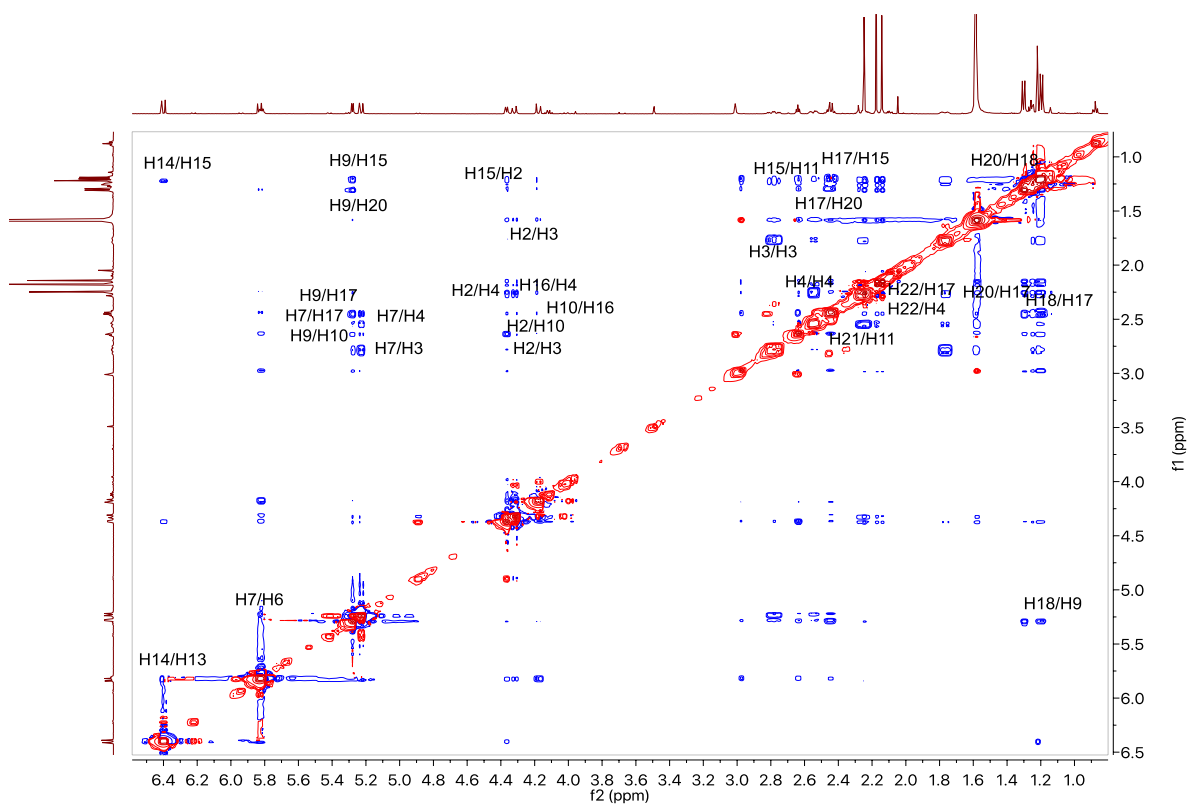


Figure S22. NOESY spectrum of **3** (500 MHz, CDCl₃).

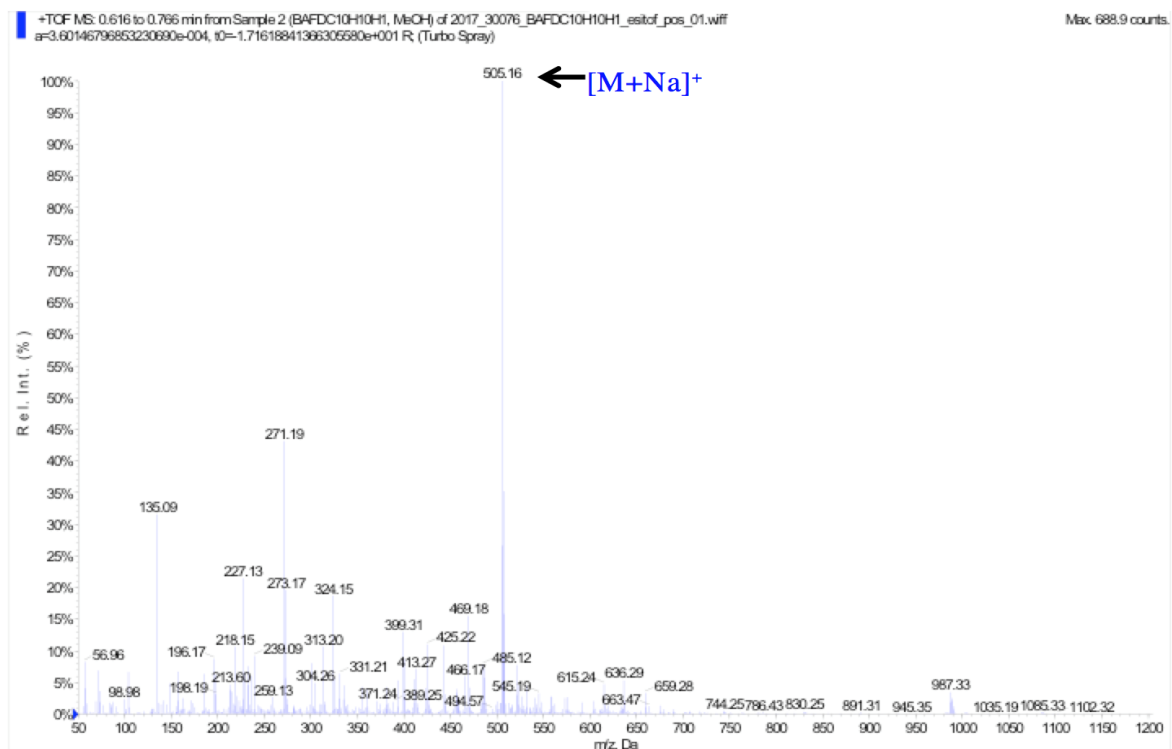


Figure S23. (+)-LRESIMS of 3.

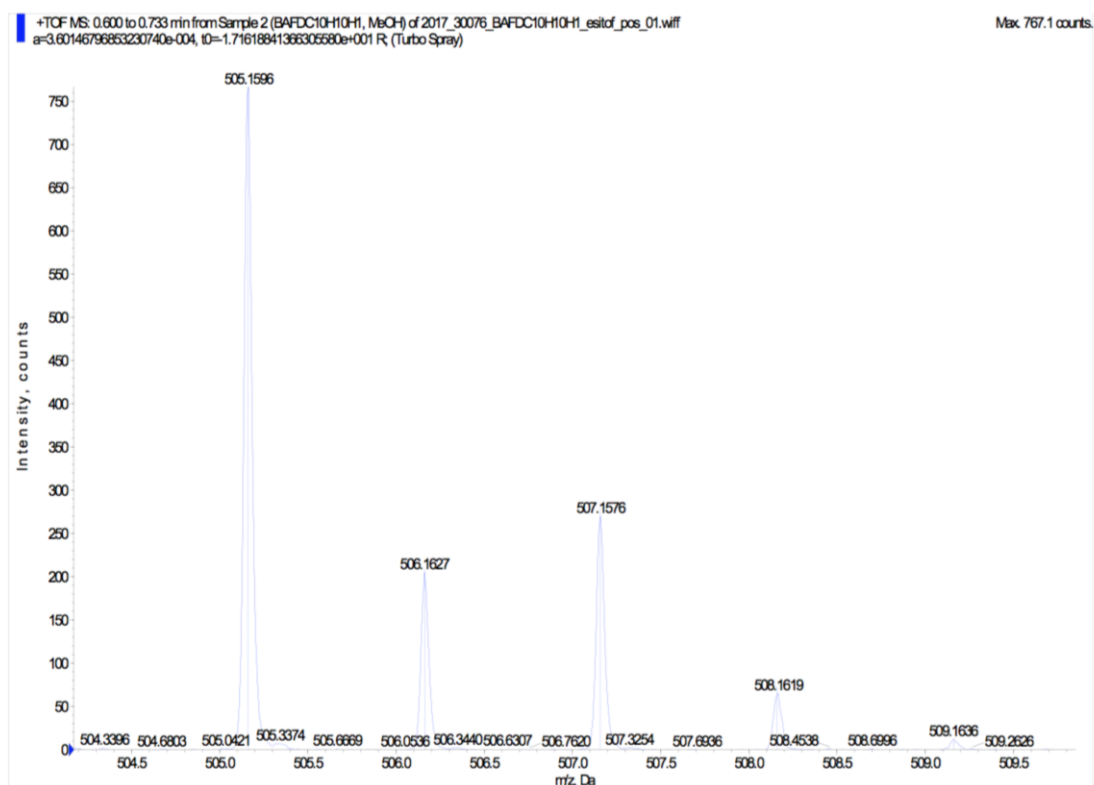
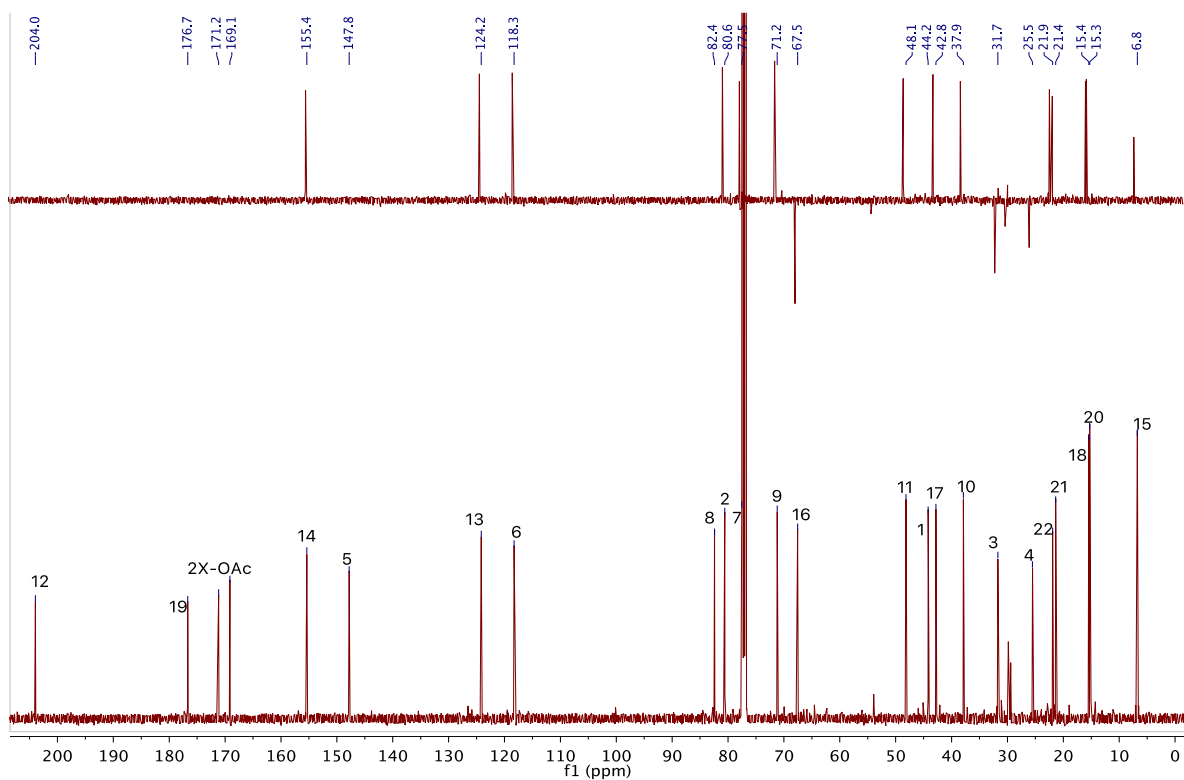
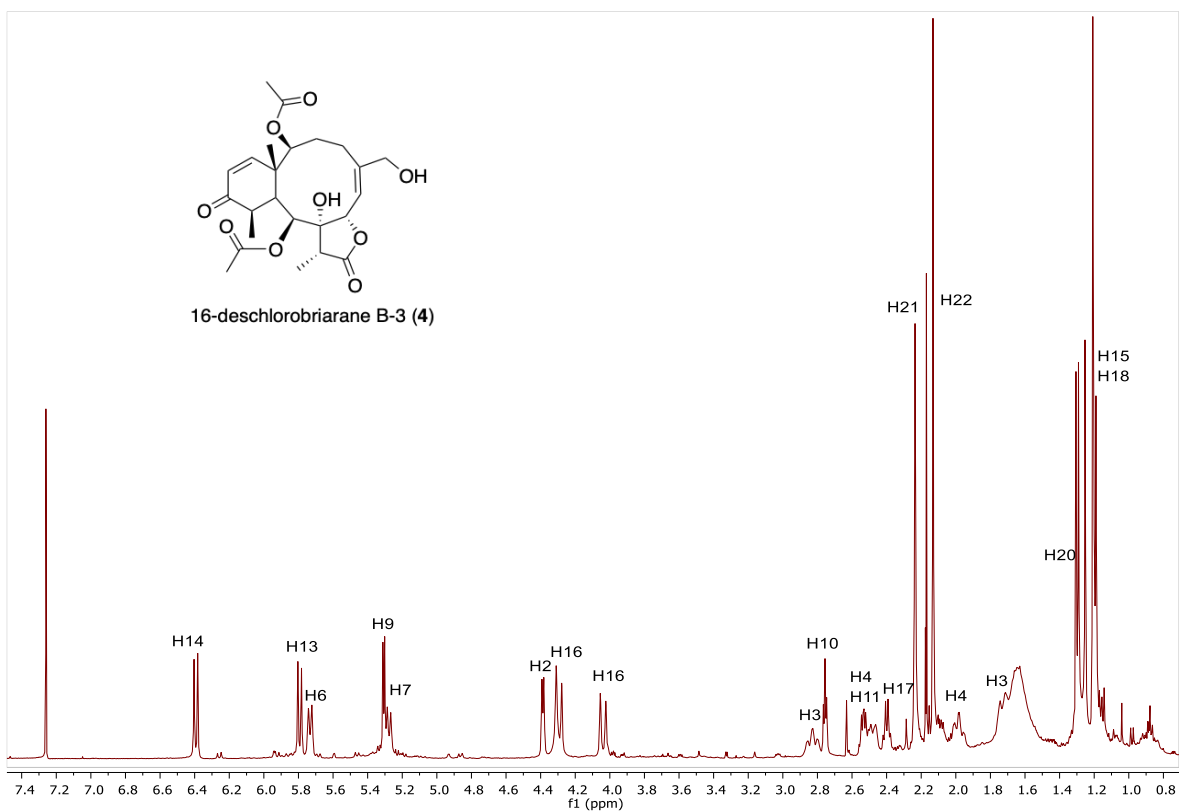


Figure S24. (+)-HRESIMS of 3.

Table S4. NMR data of **4** in CDCl₃ (125 MHz for ¹³C and 500 MHz for ¹H).

no.	δ_c type	δ_H , mult. (<i>J</i> in Hz)	COSY	HMBC	NOESY
1	44.2, qC			13, 14, 15	
2	80.6 CH	4.40, d (5.4)	3	14, 15	3, 4, 10, 14, 15
3	31.7, CH ₂	2.85, dt (15.5, 15.5, 4.9)-1.74, m	2, 4		2, 3, 6, 7
4	25.5, CH ₂	2.55, m-2.00, m	3	2, 6, 16	2, 4, 9
5	147.8, qC			7, 16	
6	118.3, CH	5.72, d (10.2)	7	16	3, 7, 16
7	77.5, CH	5.28, d (10.2)	6		3, 6, 17
8	82.4, qC			9, 18	
9	71.2, CH	5.30, d (5.2)	10		10, 17, 18, 20
10	37.9, CH	2.77, t (5.2)	9, 11	14, 15, 20	2, 9, 11, 17
11	48.1, CH	2.52, m	10, 20	9, 13, 20	10, 20
12	203.9, qC			14, 20	
13	124.2, CH	5.80, d (10.5)	14		14
14	155.4, CH	6.40, d (10.5)	13	20	2, 13, 15, 22
15	6.8, CH	1.16, s			2, 14, 17, 21
16	67.5, CH ₂	4.32, d (15.8)-4.07, d (15.8)		6	6
17	42.8, CH	2.41, q (7.1)	18		7, 9, 15, 18
18	15.4, CH	1.23, d (7.1)	17		9
19	176.7, qC			17, 18	
20	15.3, CH	1.29, d (7.4)	11		9, 11
21 Ac	169.1, qC			9	
22 Ac	171.1, qC			2	
CH ₃ 21	21.2, CH ₃	2.24, s		21	
CH ₃ 22	21.9, CH ₃	2.14, s		22	14
OH					



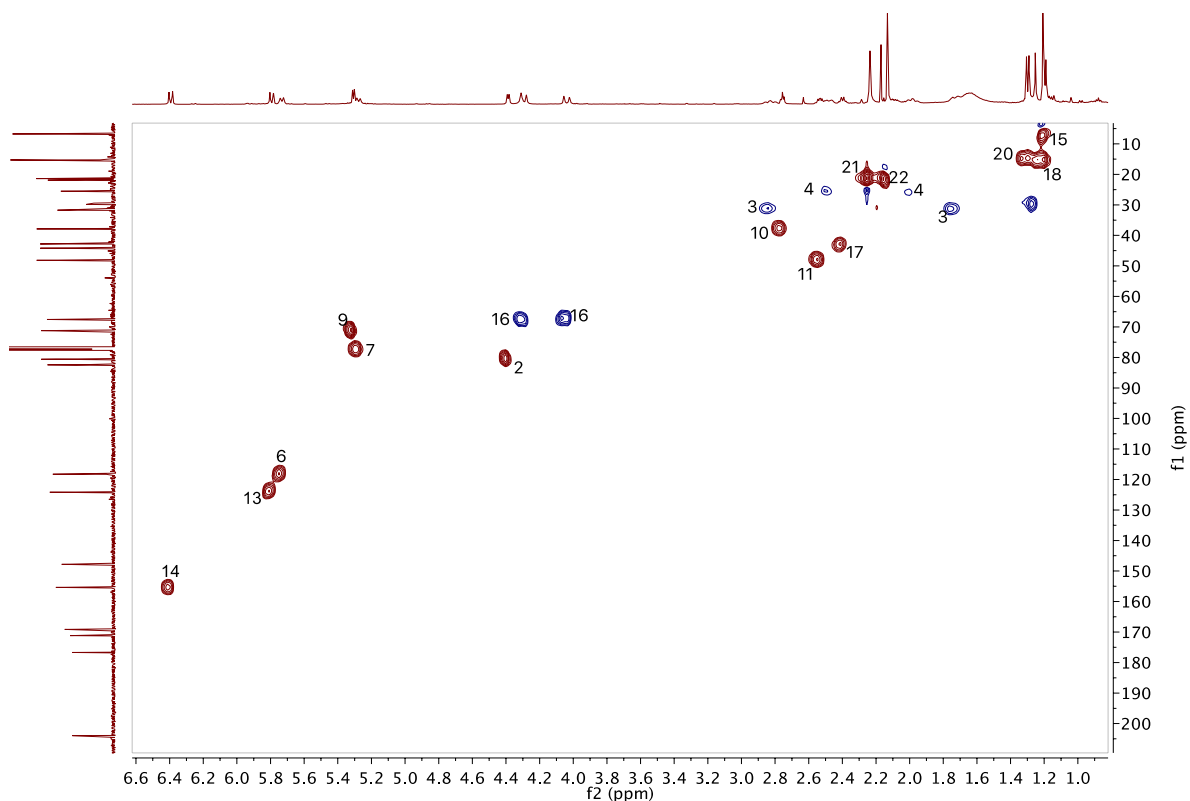


Figure S27. HSQC spectrum of **4** (500 MHz, CDCl_3). CH_2 : blue cross-peaks and CH or CH_3 : red cross-peaks.

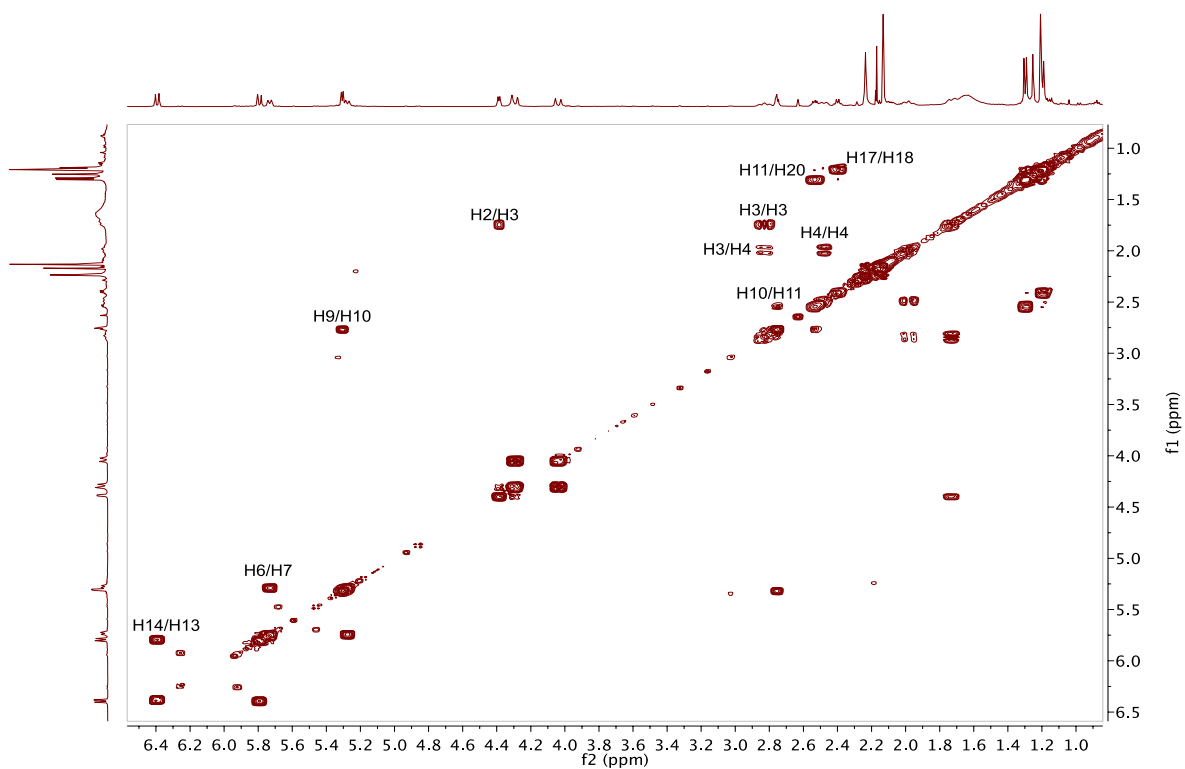


Figure S28. COSY spectrum of **4** (500 MHz, CDCl_3).

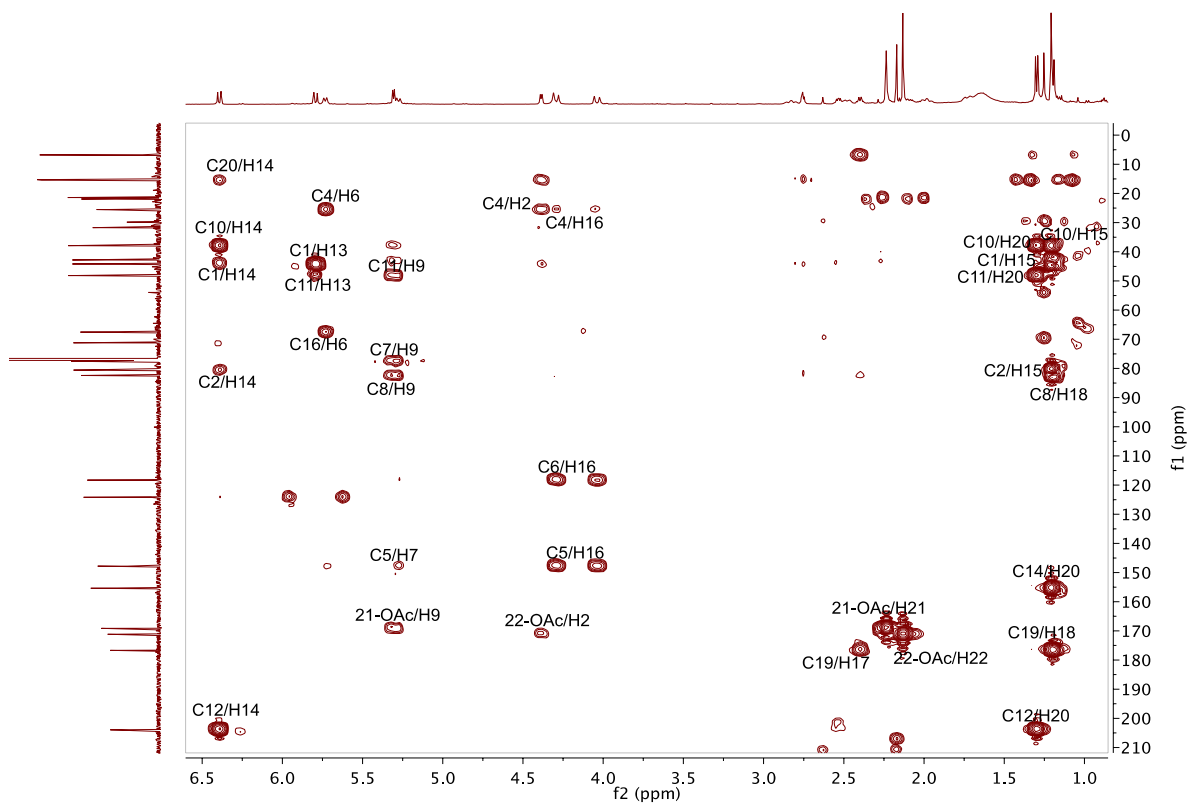


Figure S29. HMBC spectrum of **4** (500 MHz, CDCl_3).

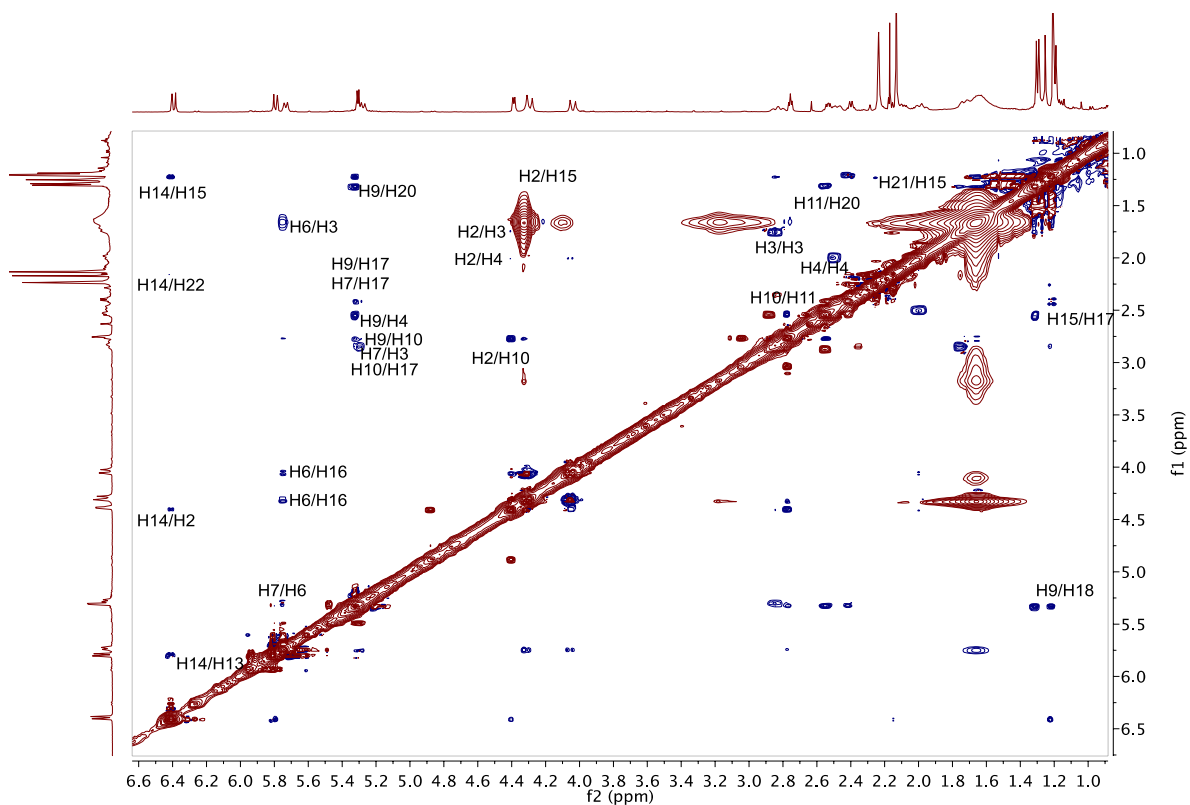


Figure S30. NOESY spectrum of **4** (500 MHz, CDCl_3).

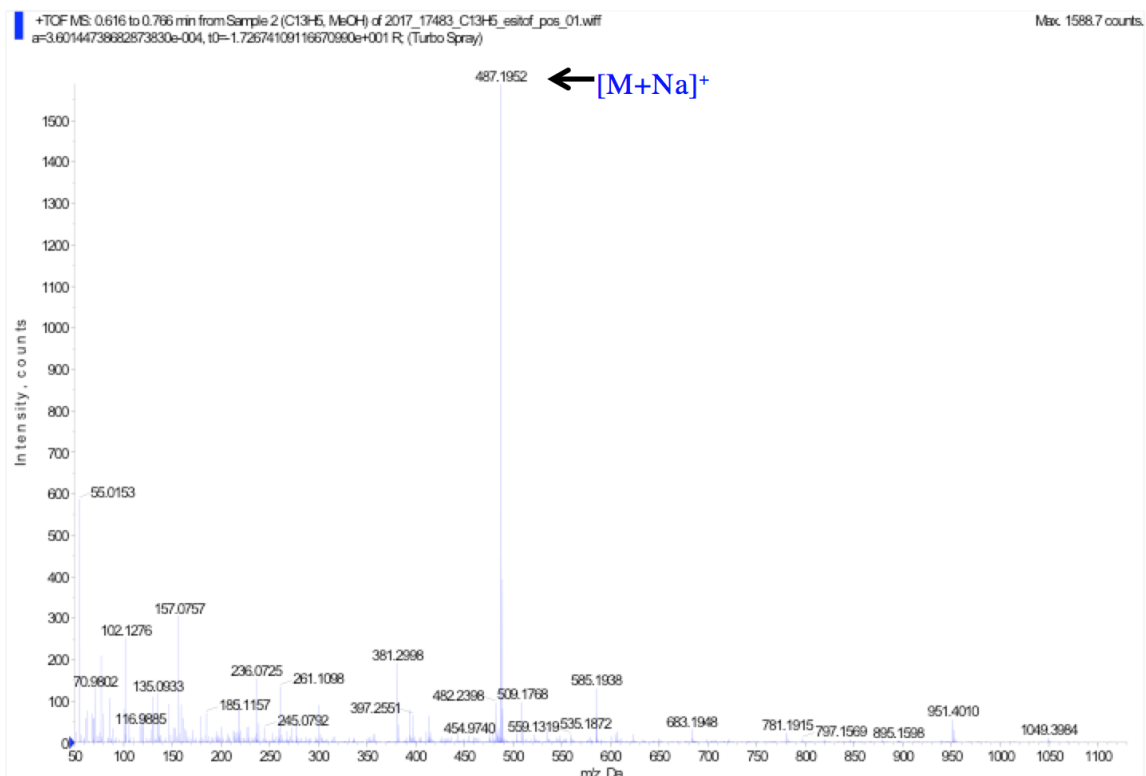


Figure S31. (+)-LRESIMS of 4.

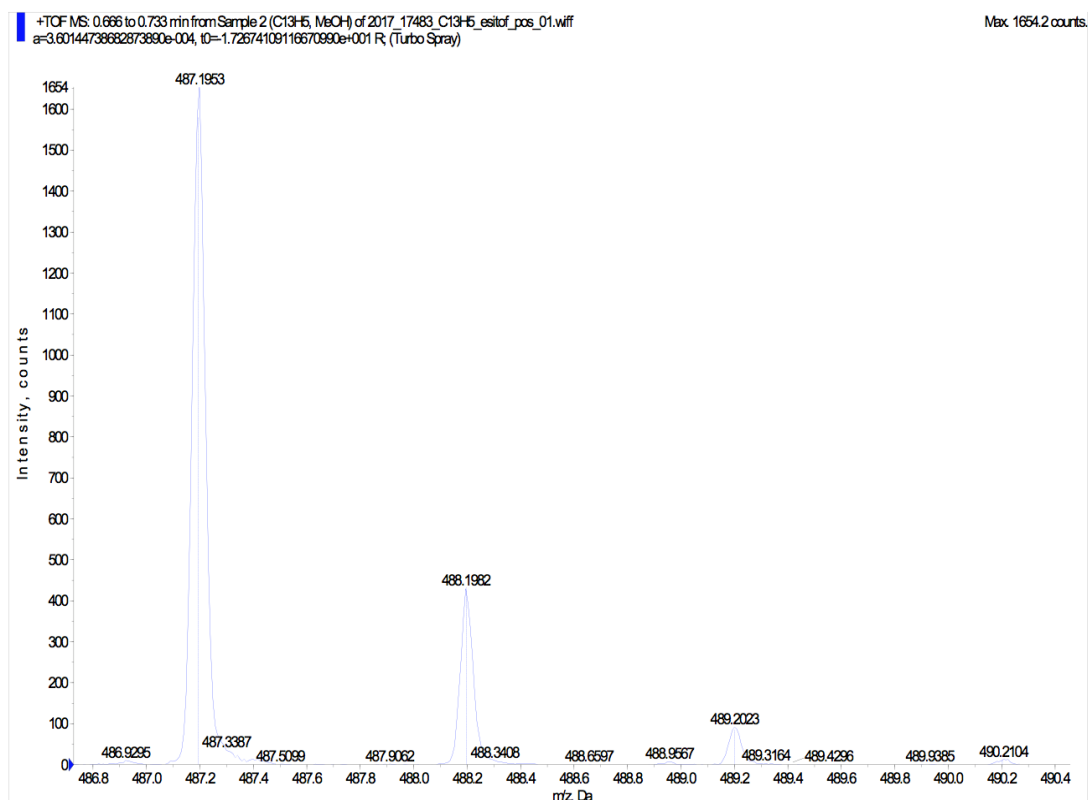


Figure S32. (+)-HRESIMS of 4.

Table S5. NMR data of **5** in CDCl₃ (125 MHz for ¹³C and 500 MHz for ¹H).

no.	δ_c type	δ_H , mult. (<i>J</i> in Hz)	COSY	HMBC	NOESY
1	40.4, qC			14, 15	
2	76.5 CH	4.27, d (9.7)	3	4, 10, 15	3, 10
3	137.2, CH ₂	5.80, dd (11.0, 9.7)	2, 4		2, 15, 21
4	125.0, CH ₂	6.21, dd (11.0, 1.2)	3	6, 16	3, 7
5	141.2, qC			3, 7, 16	
6	126.7, CH	5.83, dq (8.6, 1.2, 1.2, 1.2)	7	4	16
7	79.2, CH	5.07, d (8.6)	6	9	4, 9, 17
8	82.5, qC			9, 10, 18	
9	70.0, CH	5.14, d (6.7)	10	10	10, 11, 15, 17, 18, 20
10	31.3, CH	2.12, d (6.7)	9, 11	12, 20	2, 9, 11, 16
11	41.7, CH	1.80, m	10, 12, 20	9, 20	9, 10, 12, 20
12	66.7, qC	3.94, dd (5.9, 2.3)	11, 13	20	11, 13, 20
13	55.2, CH	3.56, ddd (5.9, 3.6, 0.9)	12, 14		12, 20
14	64.4, CH	3.41, d (3.6)	13	15	2, 13, 15
15	14.7, CH	1.11, s		2, 10	3, 9, 14, 21
16	46.6, CH ₂	4.24, bd (12.8)- 4.18, bd (12.8)		6	6, 10
17	43.2, CH	2.31, d (7.1)	18		7, 9, 18
18	6.5, CH	1.17, d (7.1)	17		9, 17
19	175.7, qC			17, 18	
20	13.3, CH	1.01, d (7.5)	11		9, 11
21 Ac	169.9, qC			9	15
CH ₃ 21	21.9, CH ₃	2.18, s		21	

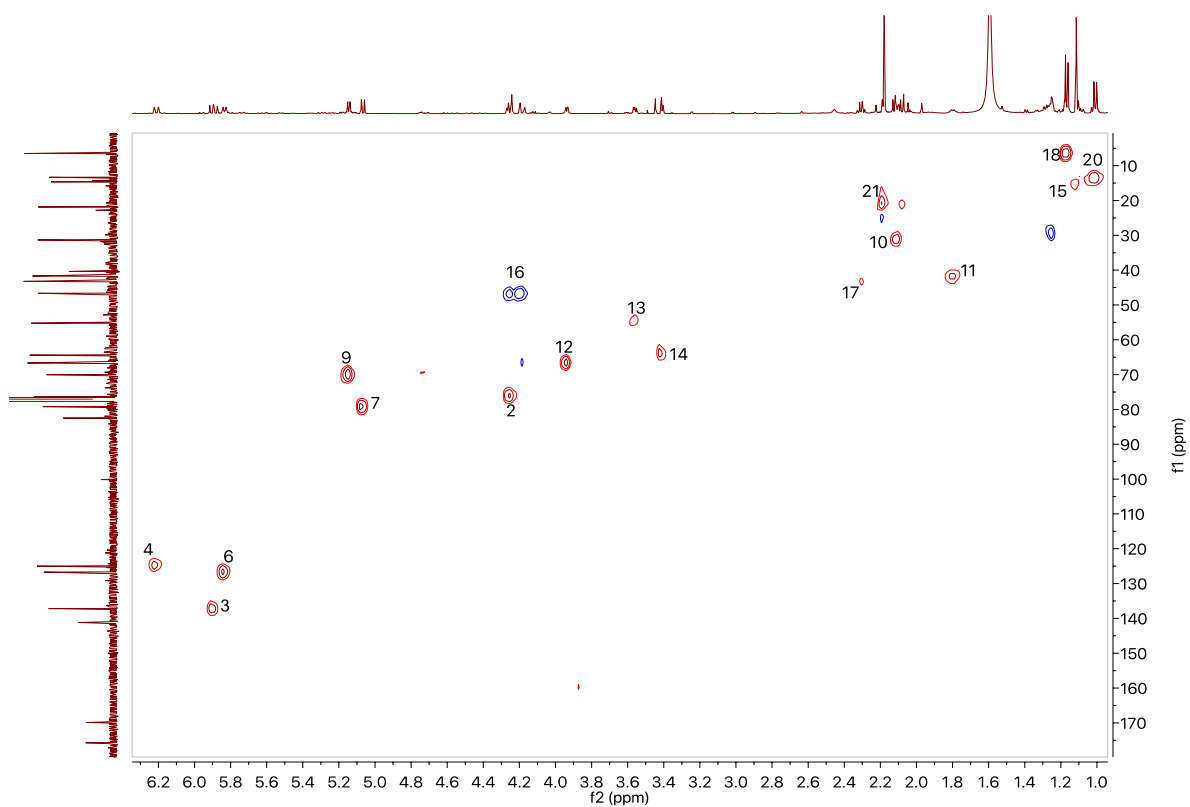


Figure S35. HSQC spectrum of **5** (500 MHz, CDCl_3). CH_2 : blue cross-peaks and CH or CH_3 : red cross-peaks.

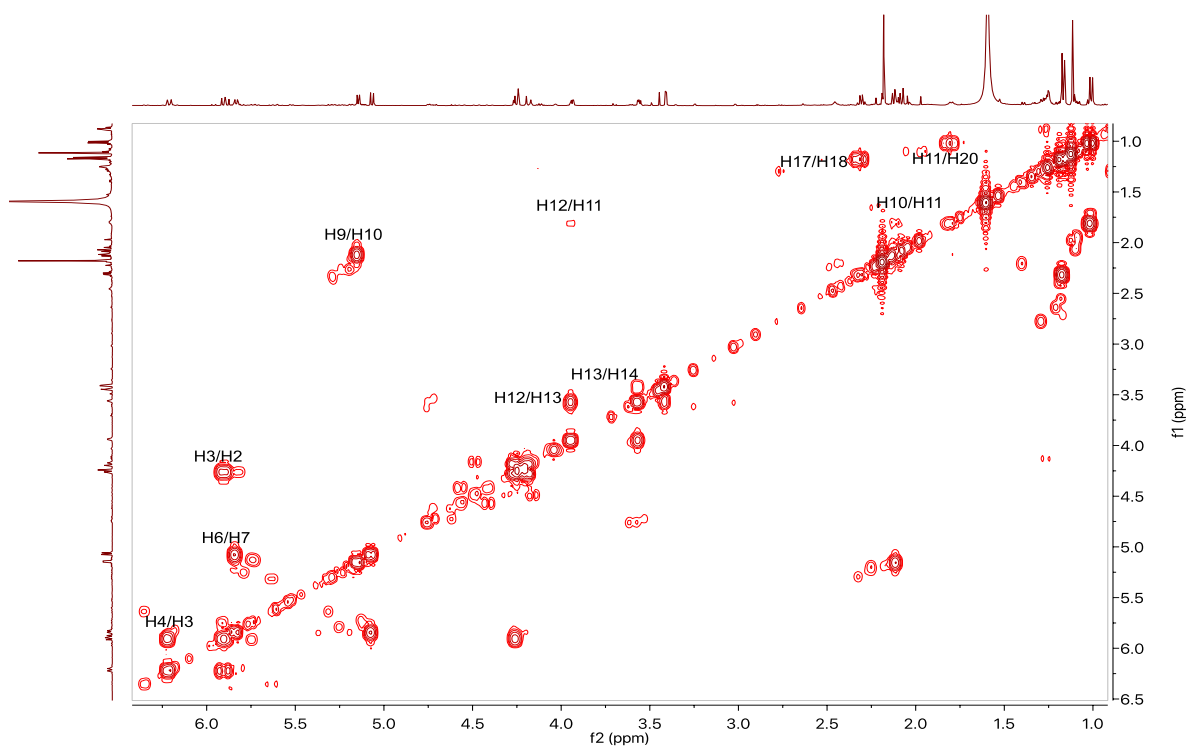


Figure S36. COSY spectrum of **5** (500 MHz, CDCl_3).

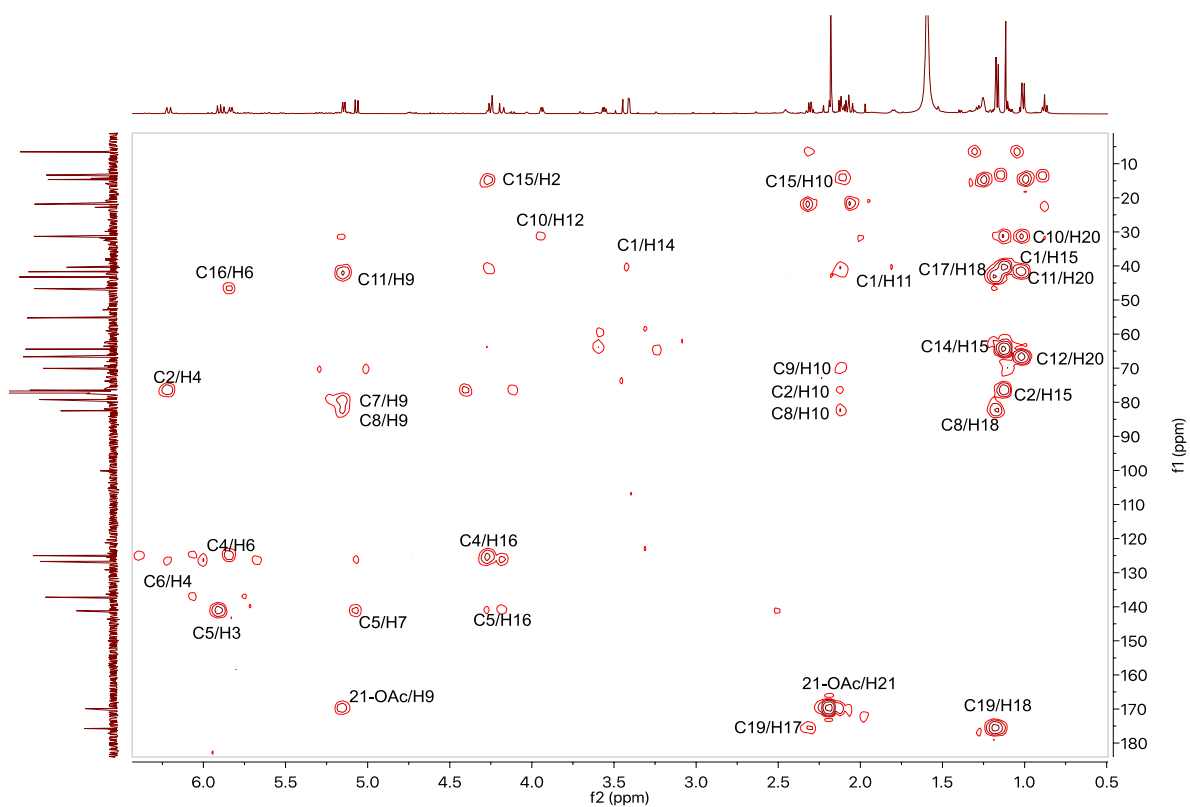


Figure S37. HMBC spectrum of **5** (500 MHz, CDCl_3).

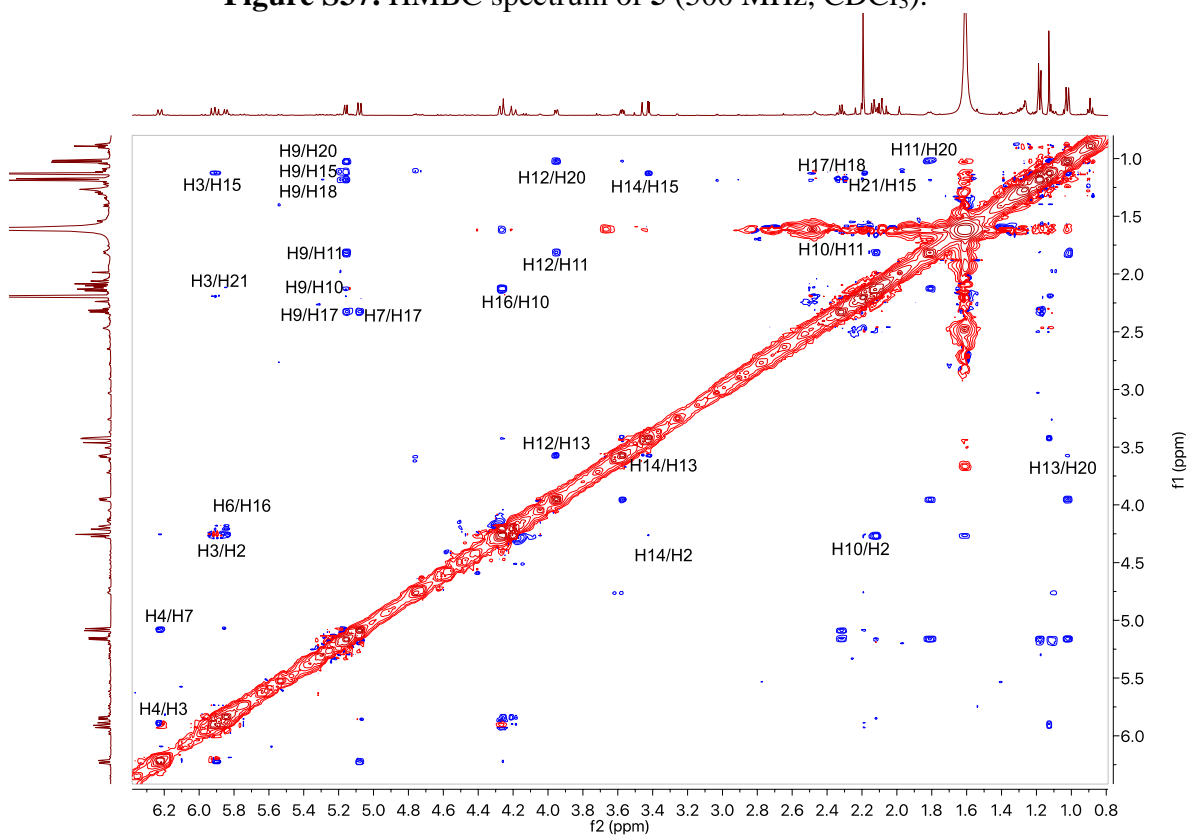


Figure S38. NOESY spectrum of **5** (500 MHz, CDCl_3).

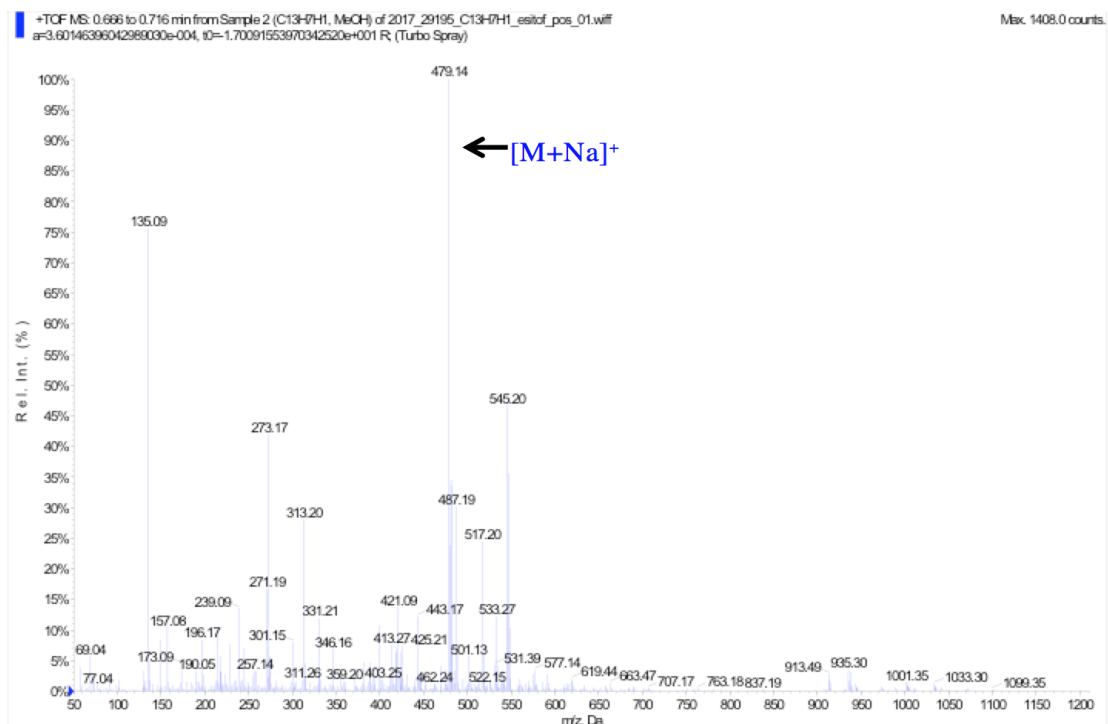


Figure S39. (+)-LRESIMS of 5.

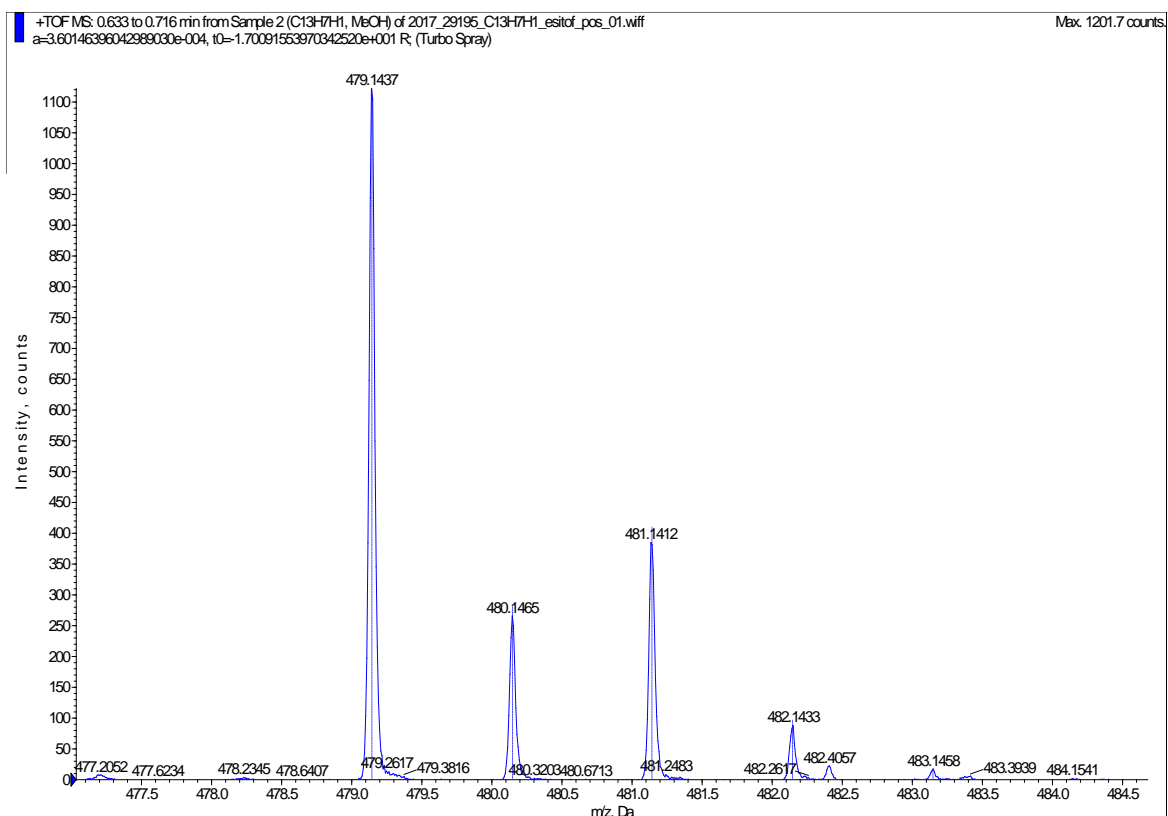


Figure S40. (+)-HRESIMS of 5.

Table S6. NMR data of **10** in CDCl₃ (125 MHz for ¹³C and 500 MHz for ¹H).

no.	δ_C type	δ_H , mult. (<i>J</i> in Hz)	COSY	HMBC
1	44.5, qC			4, 14, 15
2	73.5, CH	4.77, d (3.4)	3	15, 23
3	28.8, CH ₂	1.96, m-2.20, m	2, 4	14
4	29.9, CH ₂	2.55, m-1.25, m	3	
5	148.3, qC			3, 16
6	120.9, CH	5.41, bs	7	2, 3
7	78.6, CH	5.35, bs	6	9
8	81.8, qC			9, 18
9	70.3, CH	5.99, bs	10	10, 21
10	40.4, CH	2.80, bs	9	20
11	134.5, qC			9, 10, 20
12	117.1, CH	5.36, bs	13	20
13	32.0, CH ₂	2.56, t (3.8)-1.65 (bs)	12, 14	
14	74.8, CH	4.98, d (7.4)	13	13, 22
15	14.6, CH ₃	0.98, s		10, 14
16	27.8, CH ₃	2.02, s		3, 7
17	43.9, CH ₃	2.51, d (7.2)	18	18
18	7.2, CH ₃	1.21, d (6.6)	17	17
19	176.0, qC			17, 18
20	26.8, CH ₃	1.97, s		12
21 Ac	169.8, qC			9
22 Ac	170.7, qC			14
23 Ac	171.3, qC			2
CH ₃ 21	21.3, CH ₃	2.17, s		21
CH ₃ 22	21.6, CH ₃	2.02, s		22
CH ₃ 23	21.7, CH ₃	2.02, s		24
OH				

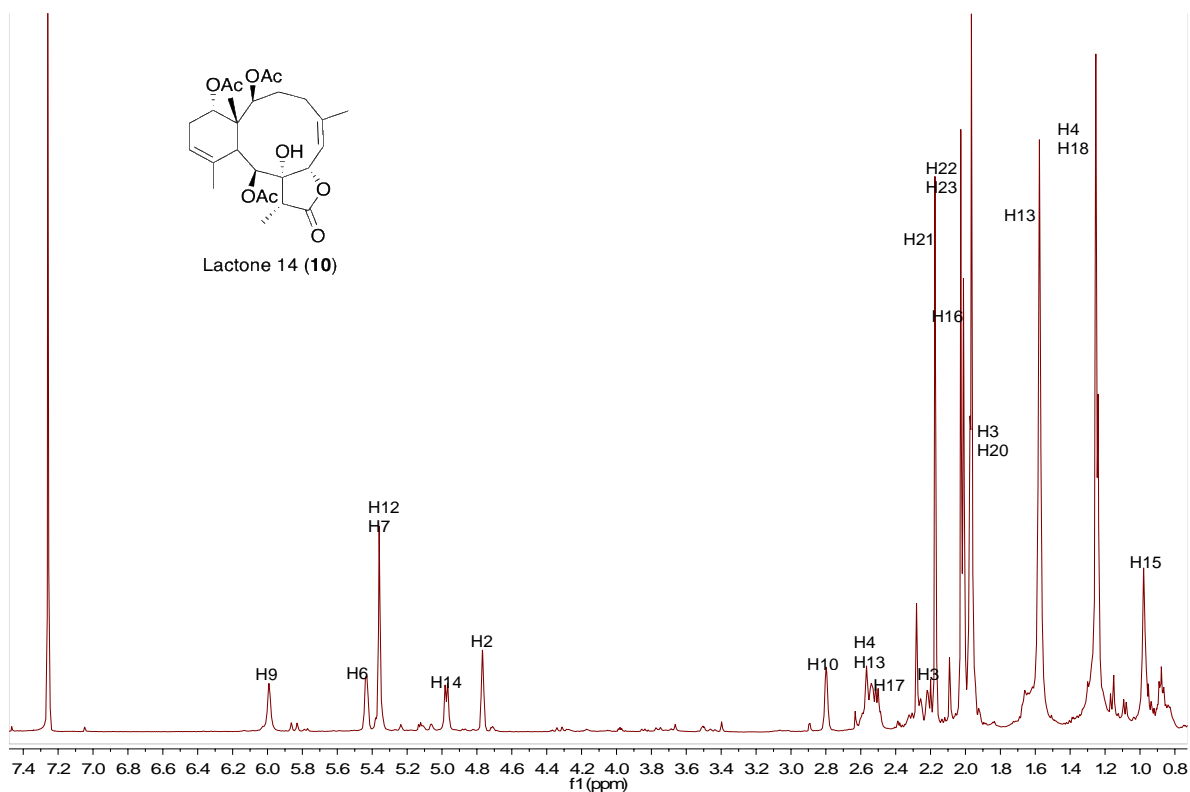


Figure S41. ¹H NMR spectrum of **10** (500 MHz, CDCl₃).

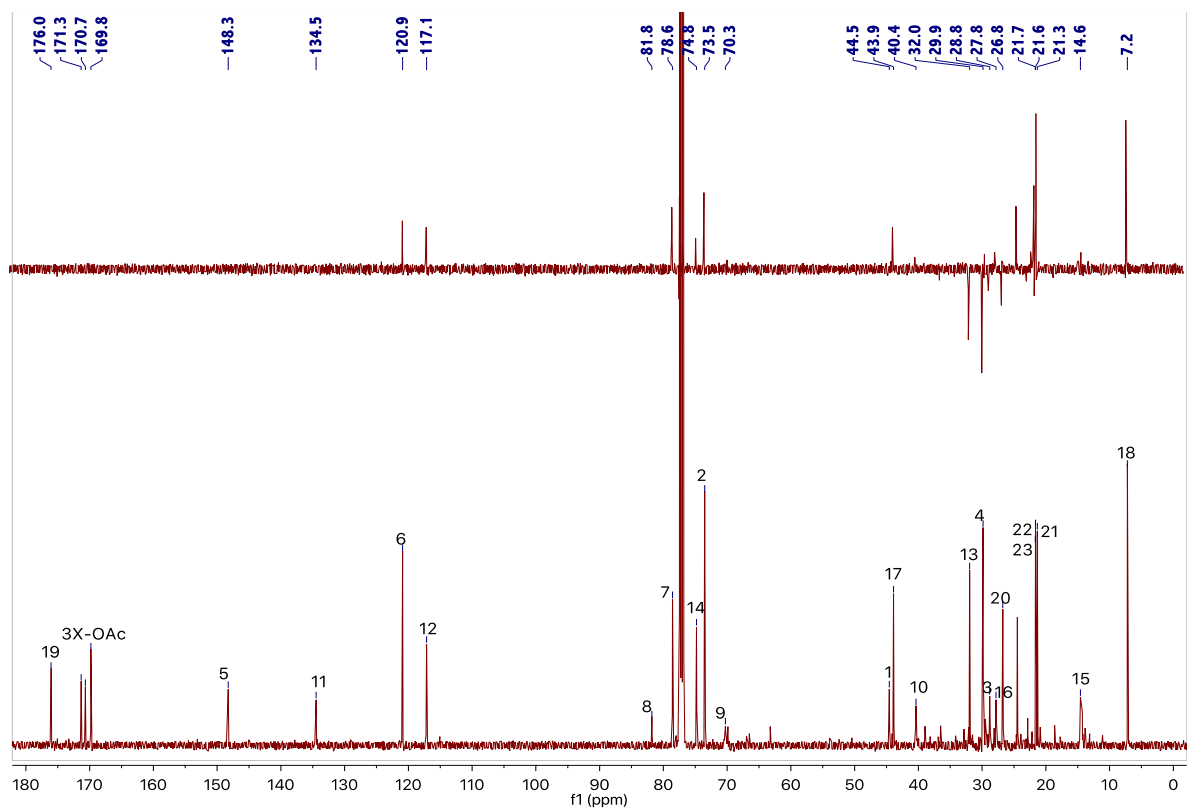


Figure S42. ¹³C NMR and DEPT-135 spectra of **10** (125 MHz, CDCl₃).

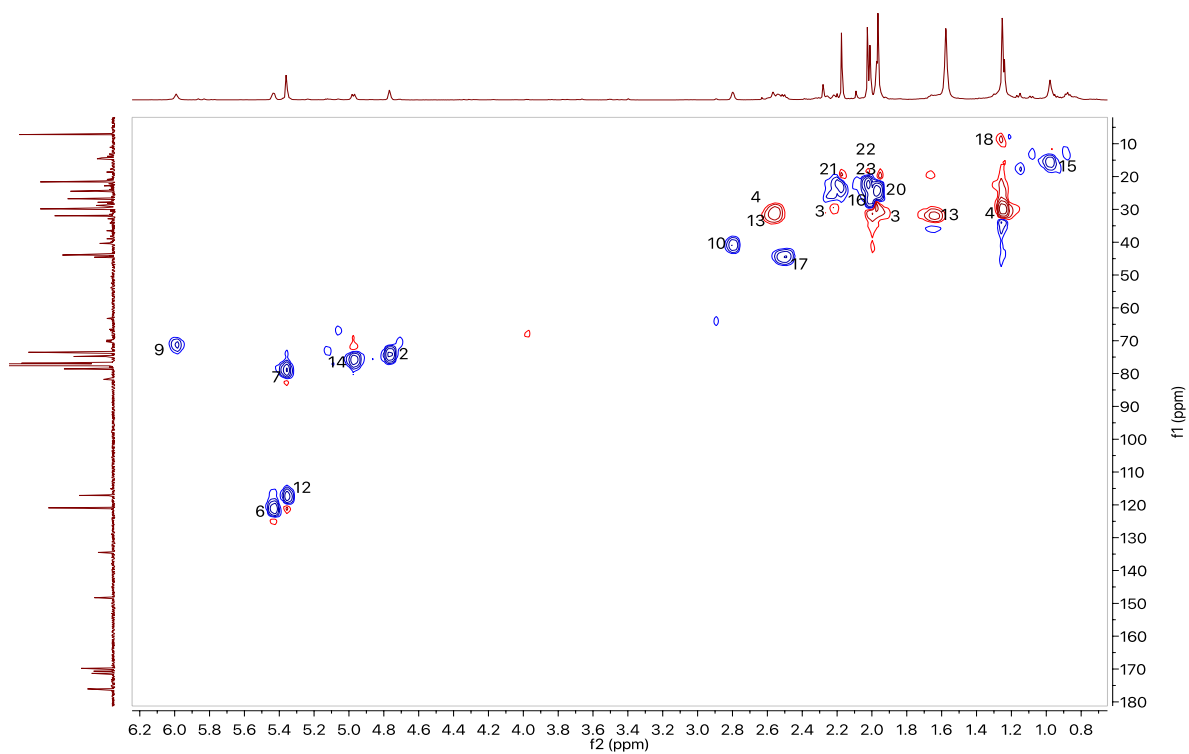


Figure S43. HSQC spectrum of **10** (500 MHz, CDCl_3). CH_2 : red cross-peaks and CH or CH_3 : blue cross-peaks.

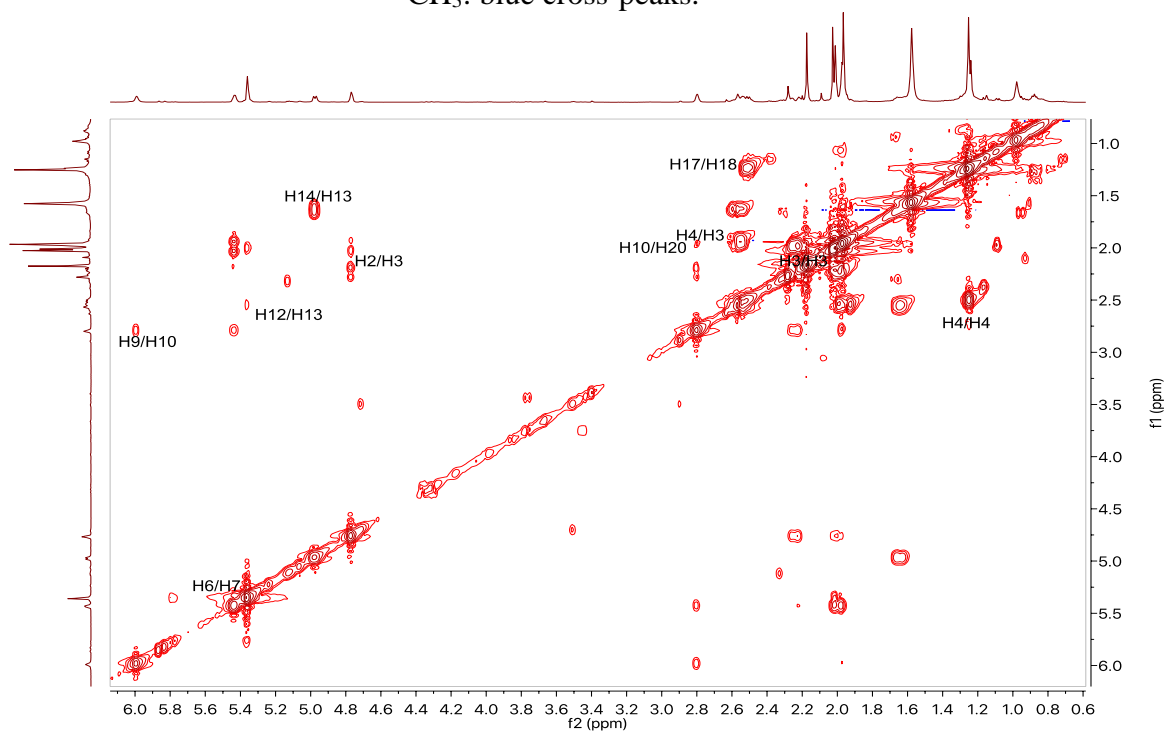


Figure S44. COSY spectrum of **10** (500 MHz, CDCl_3).

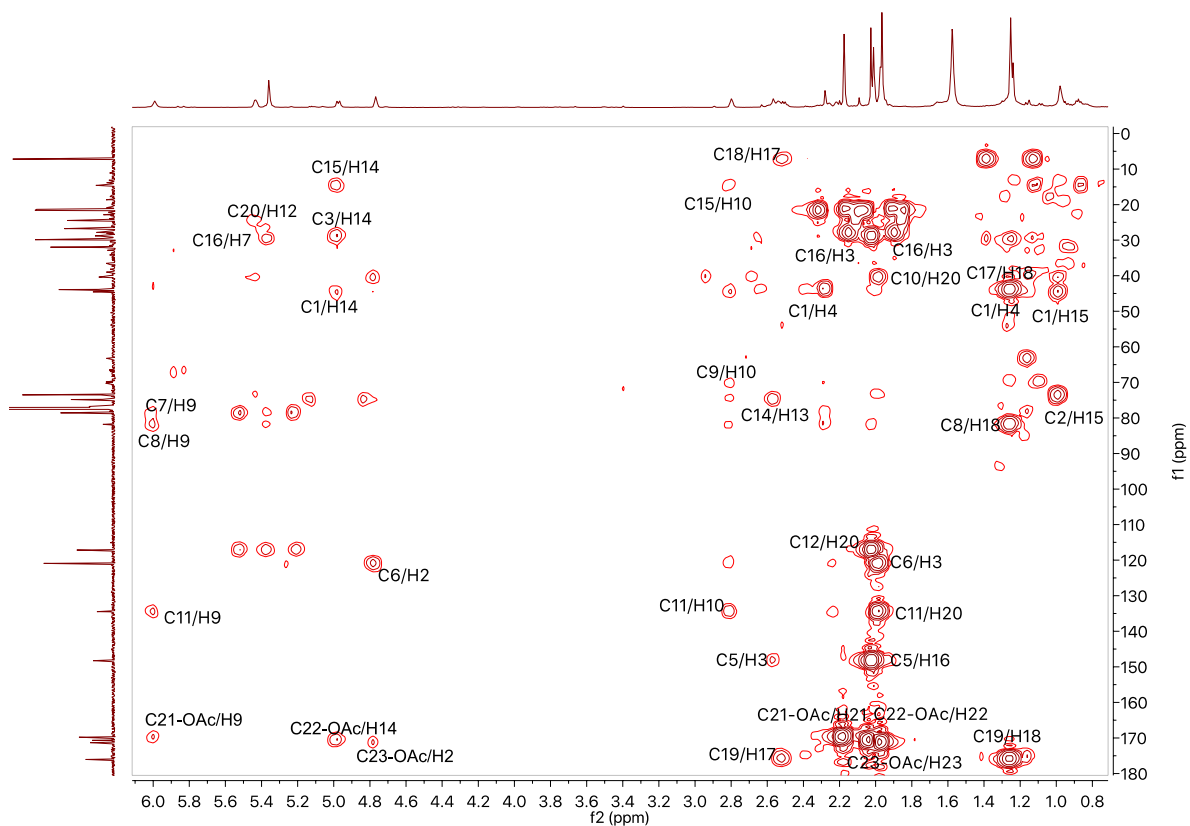


Figure S45. HMBC spectrum of **10** (500 MHz, CDCl₃).

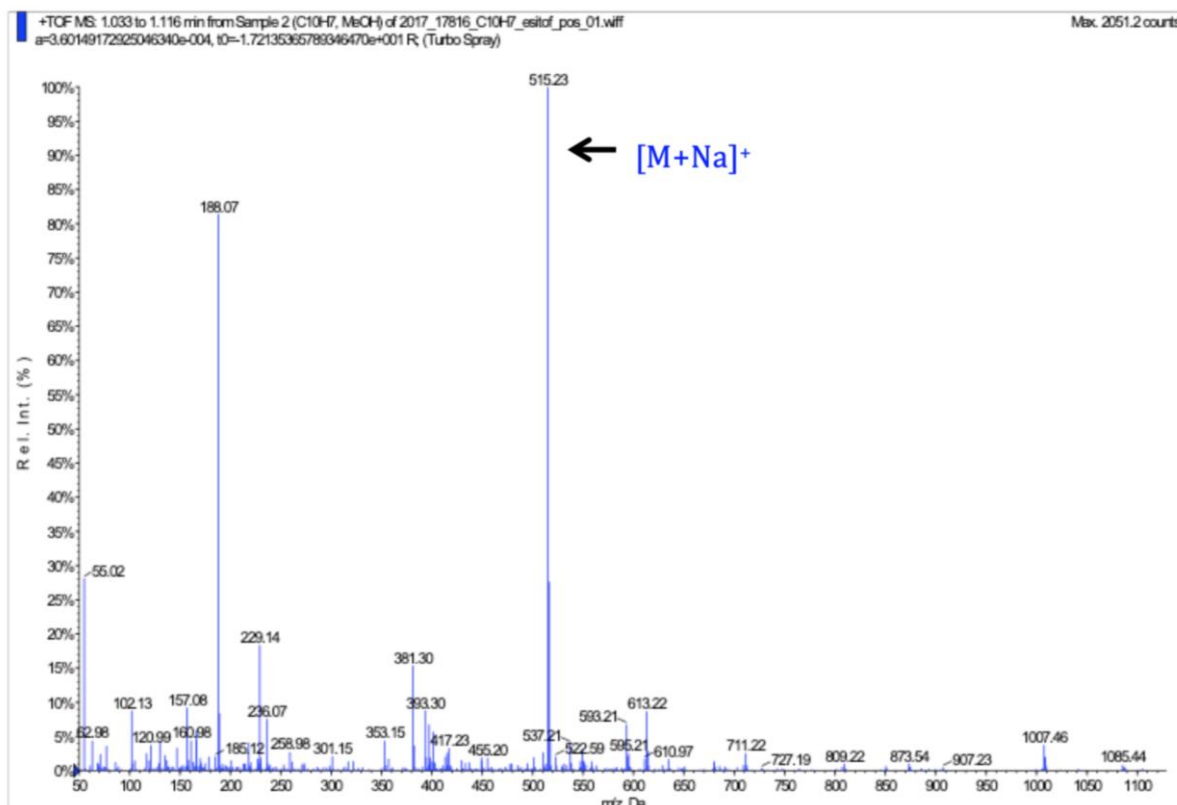


Figure S46. (+)-LRESIMS of **10**.

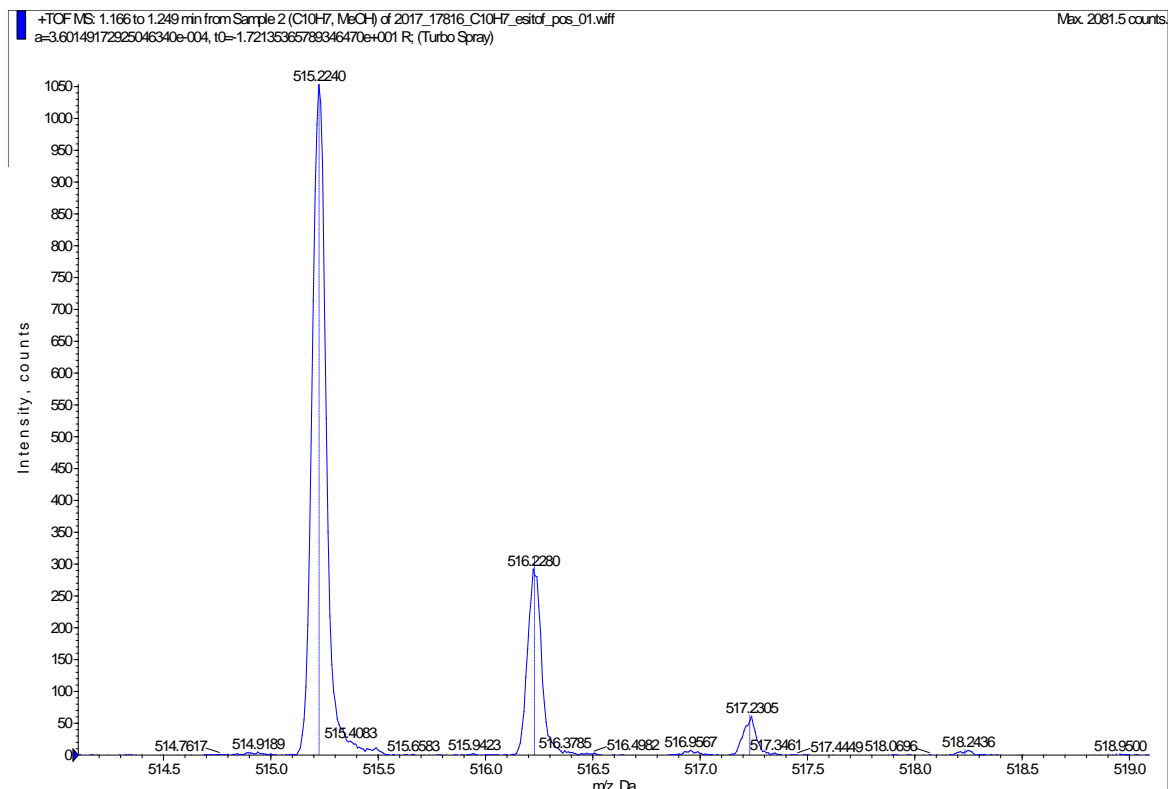


Figure S47. (+)-HRESIMS of **10**.

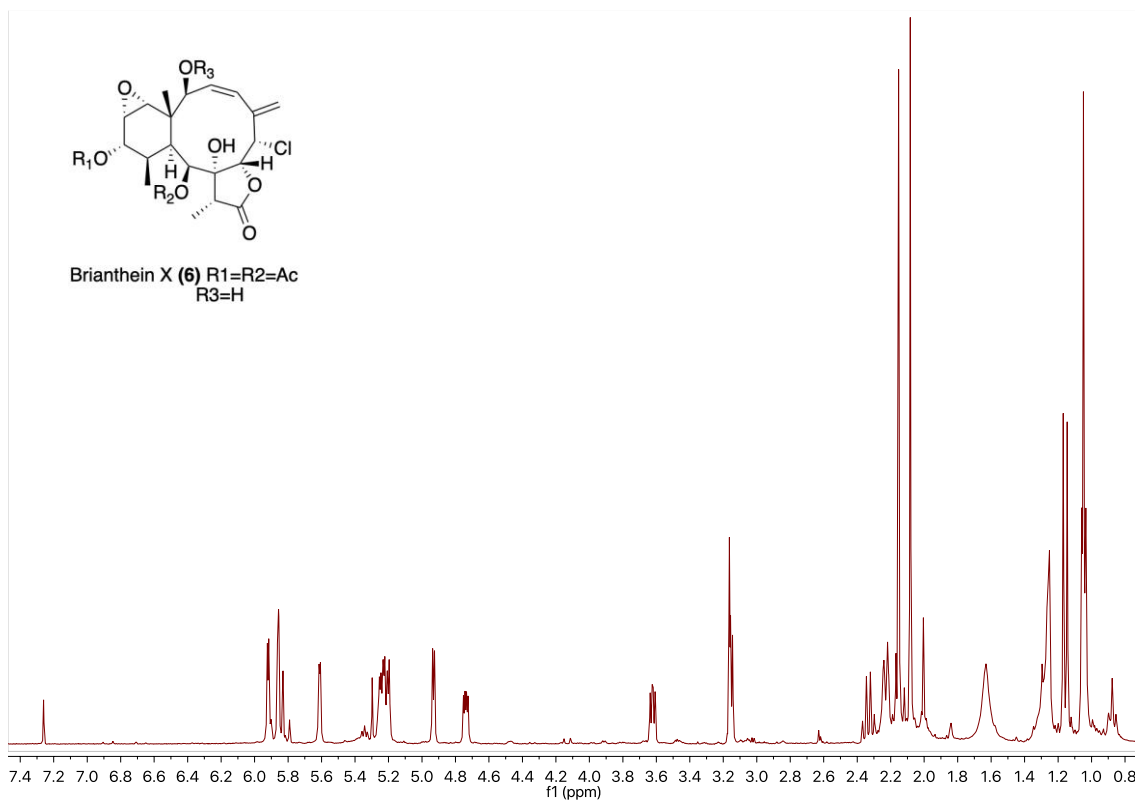


Figure S48. ^1H NMR spectrum of **6** (500 MHz, CDCl_3).

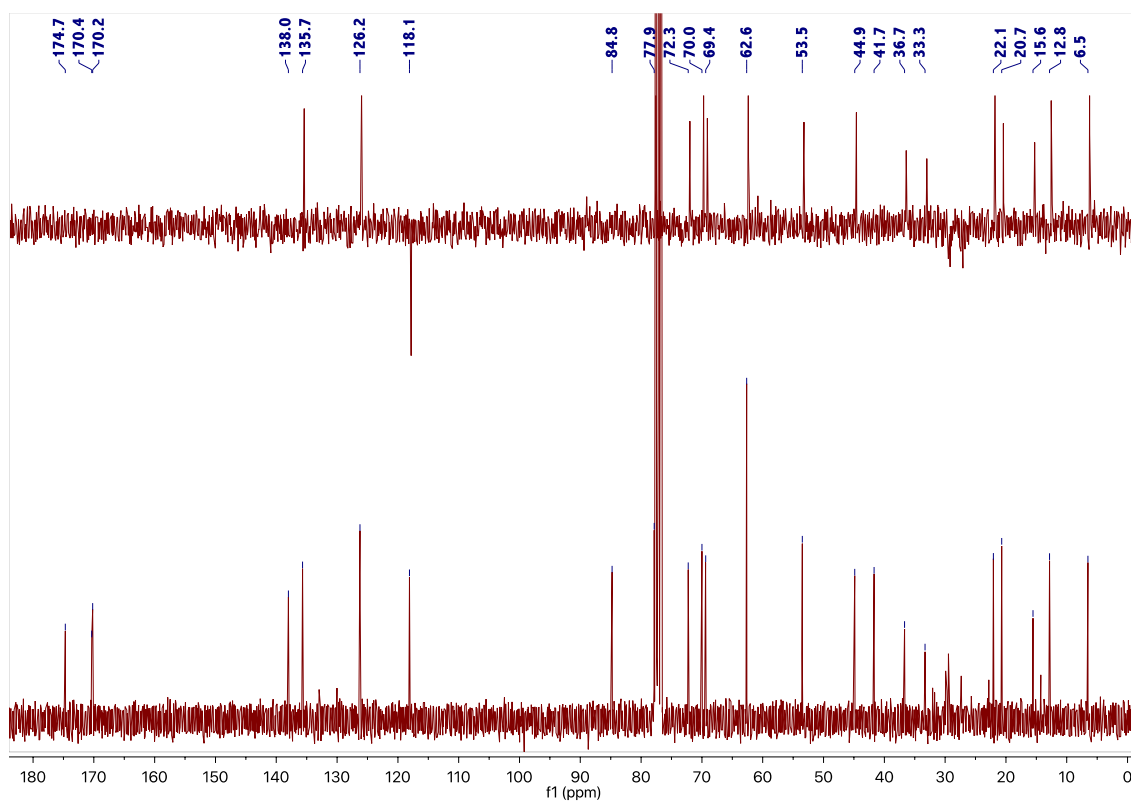


Figure S49. ^{13}C NMR and DEPT-135 spectra of **6** (125 MHz, CDCl_3).

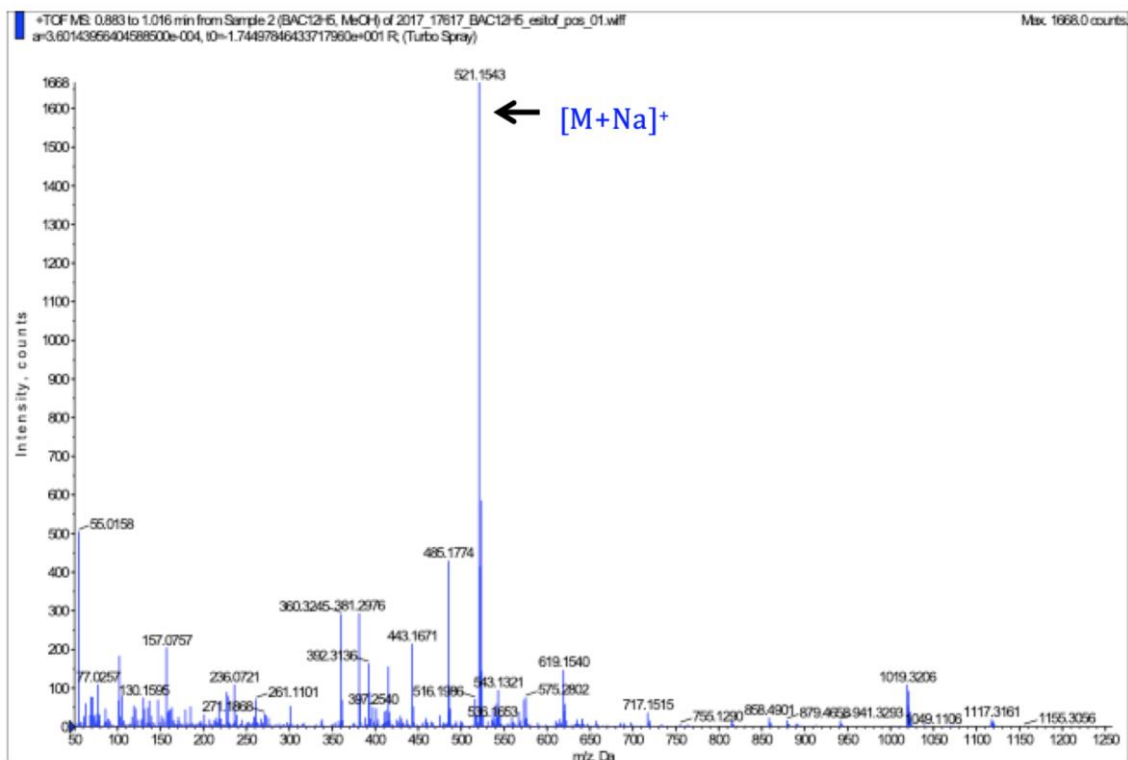
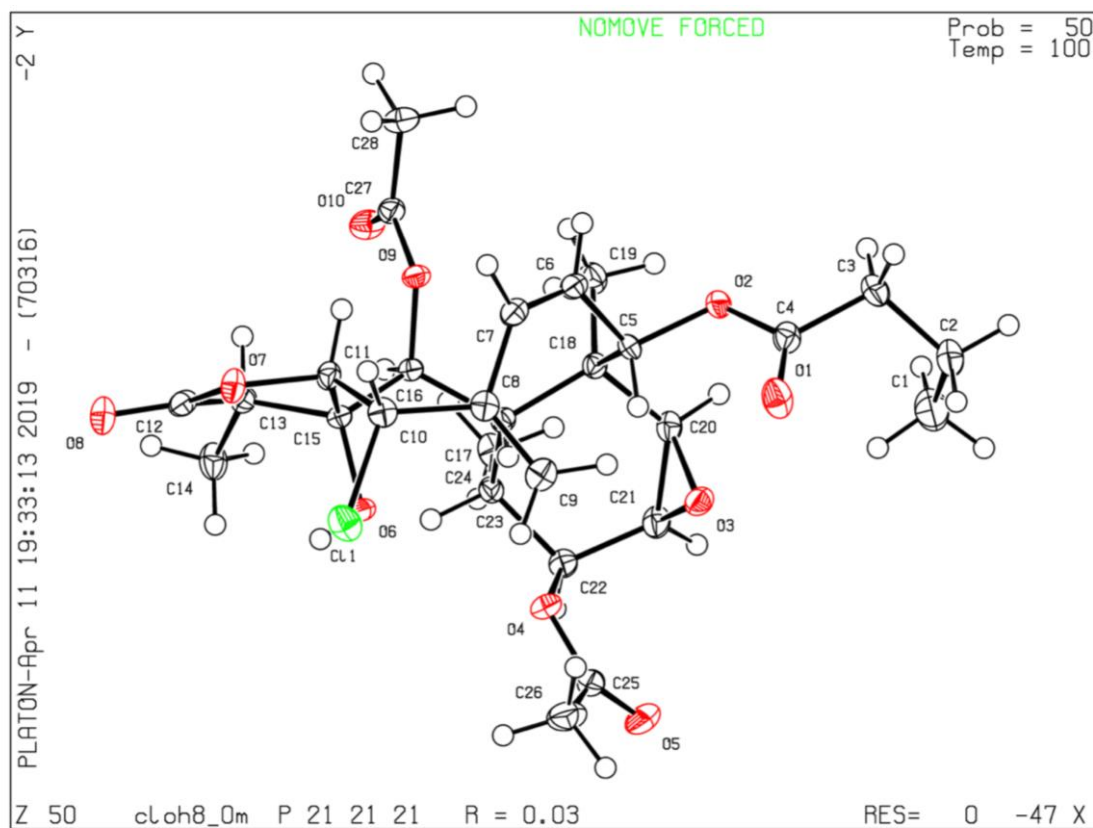
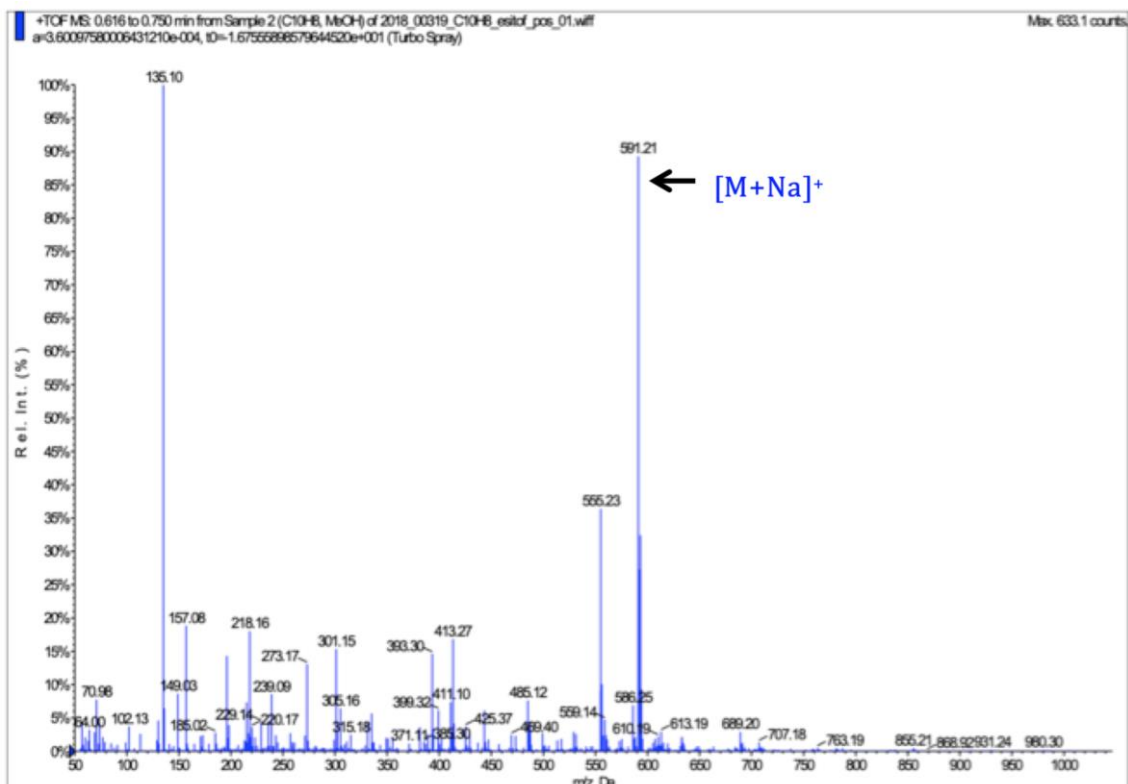


Figure S50. (+)-LRESIMS of **6**.



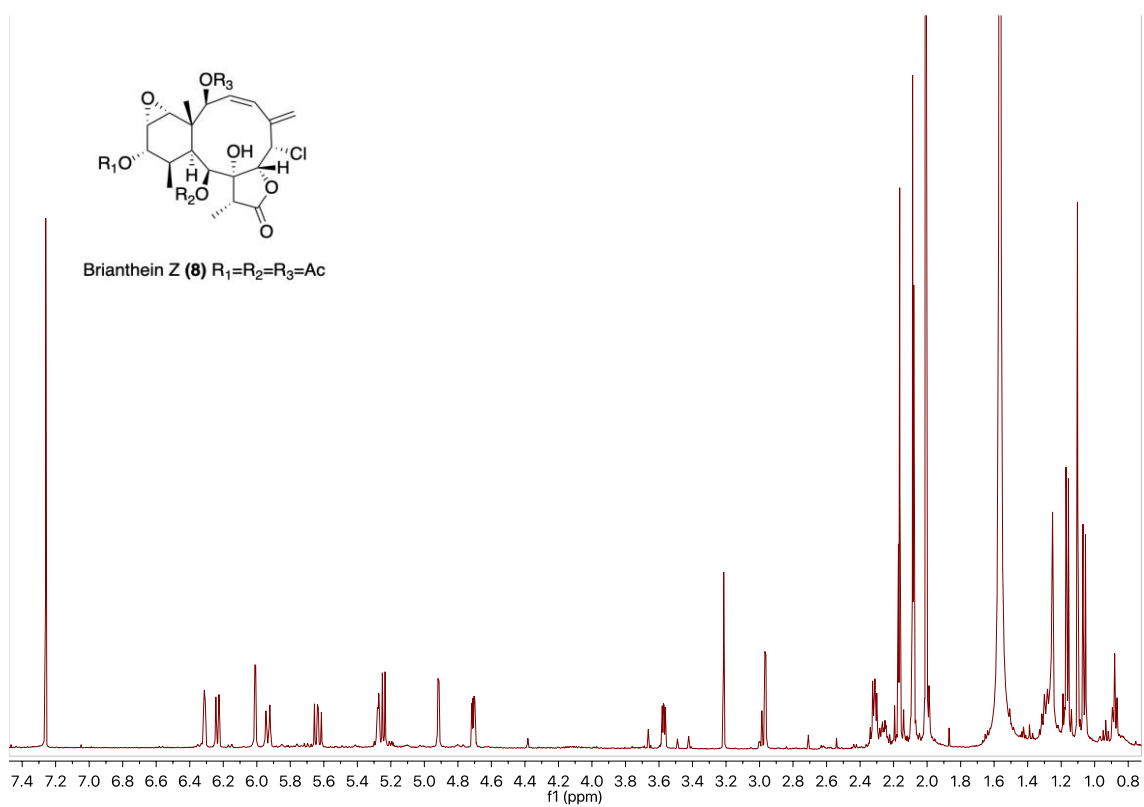


Figure S55. ¹H NMR spectrum of **8** (500 MHz, CDCl₃).

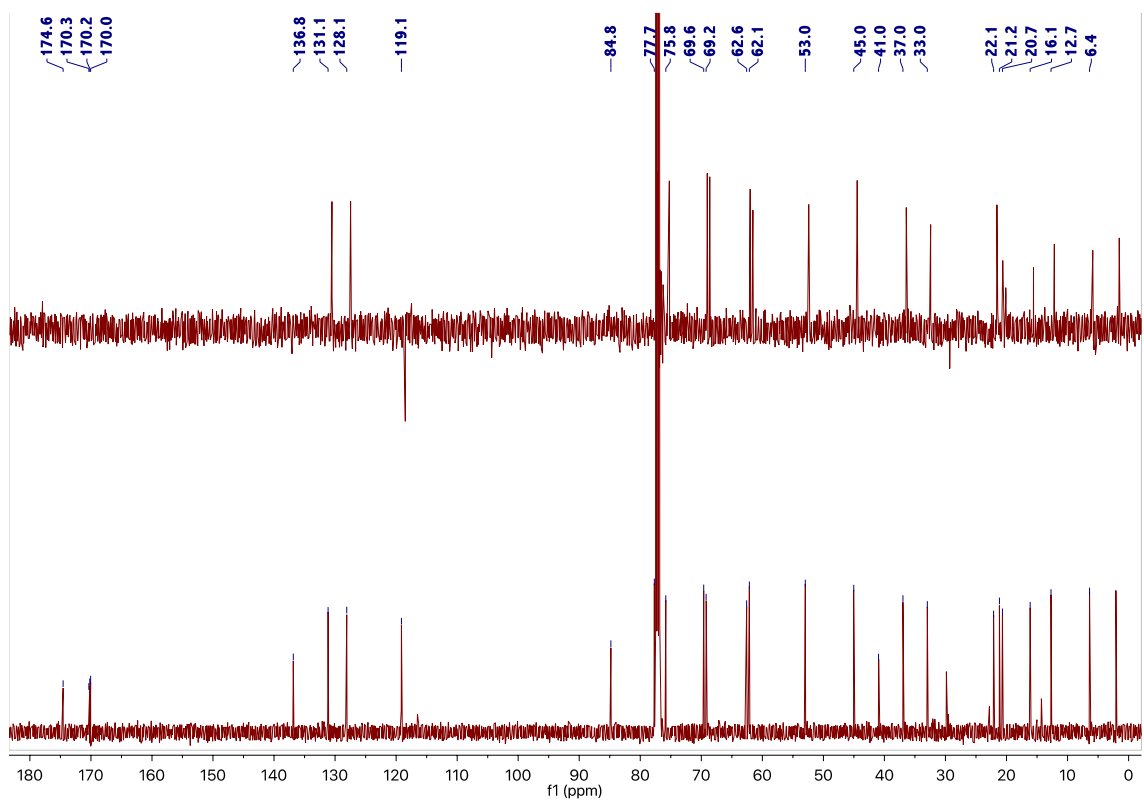


Figure S56. ¹³C NMR and DEPT-135 spectra of **8** (125 MHz, CDCl₃).

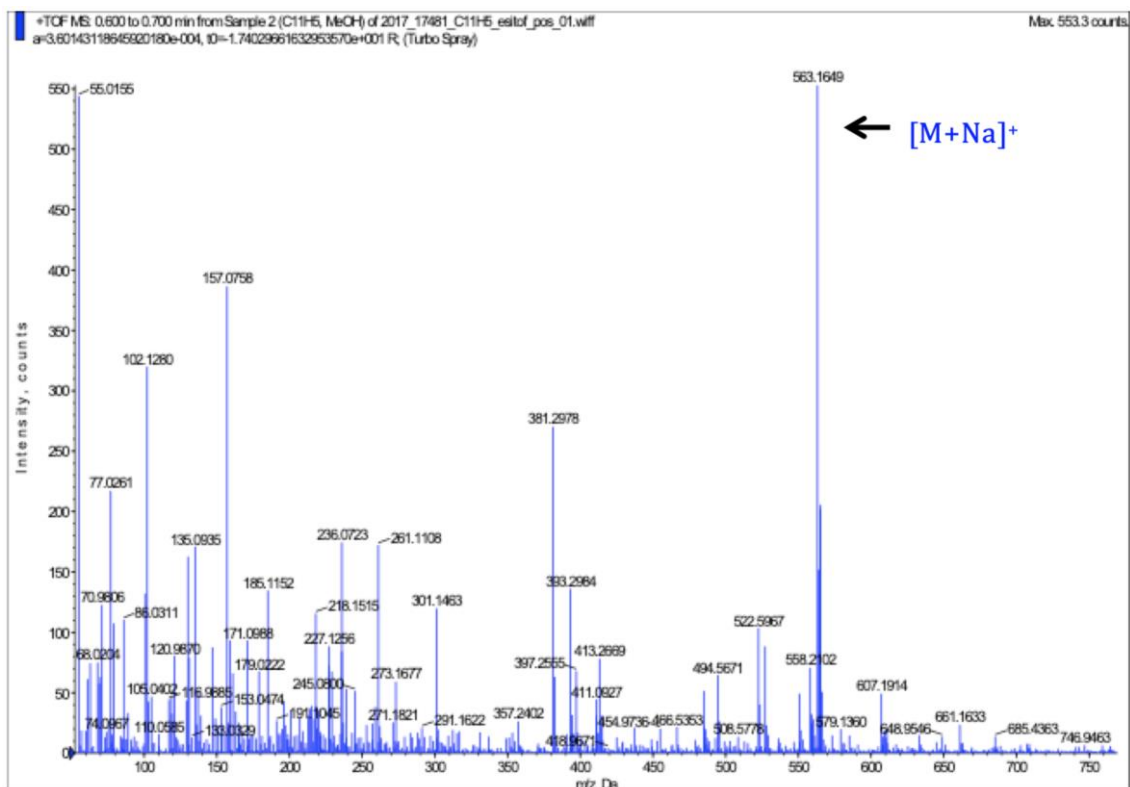


Figure S57. (+)-LRESIMS of **8**.

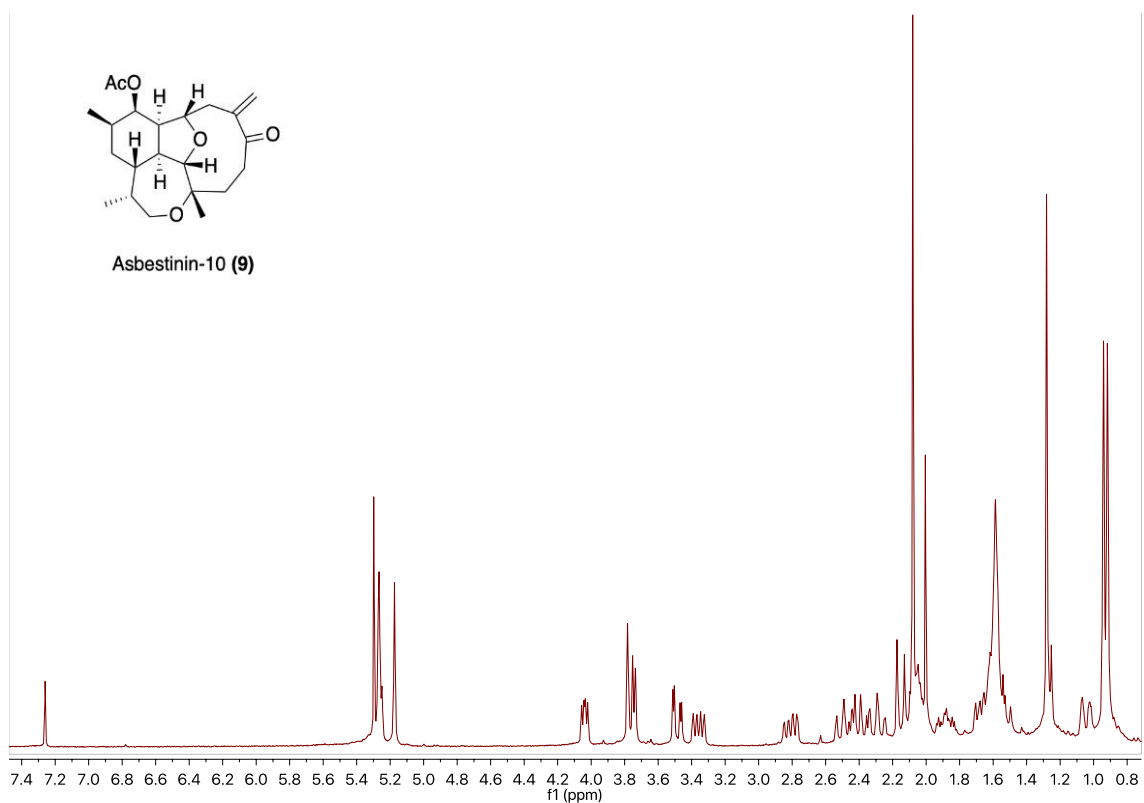


Figure 58. ¹H NMR spectrum of **9** (500 MHz, CDCl₃).

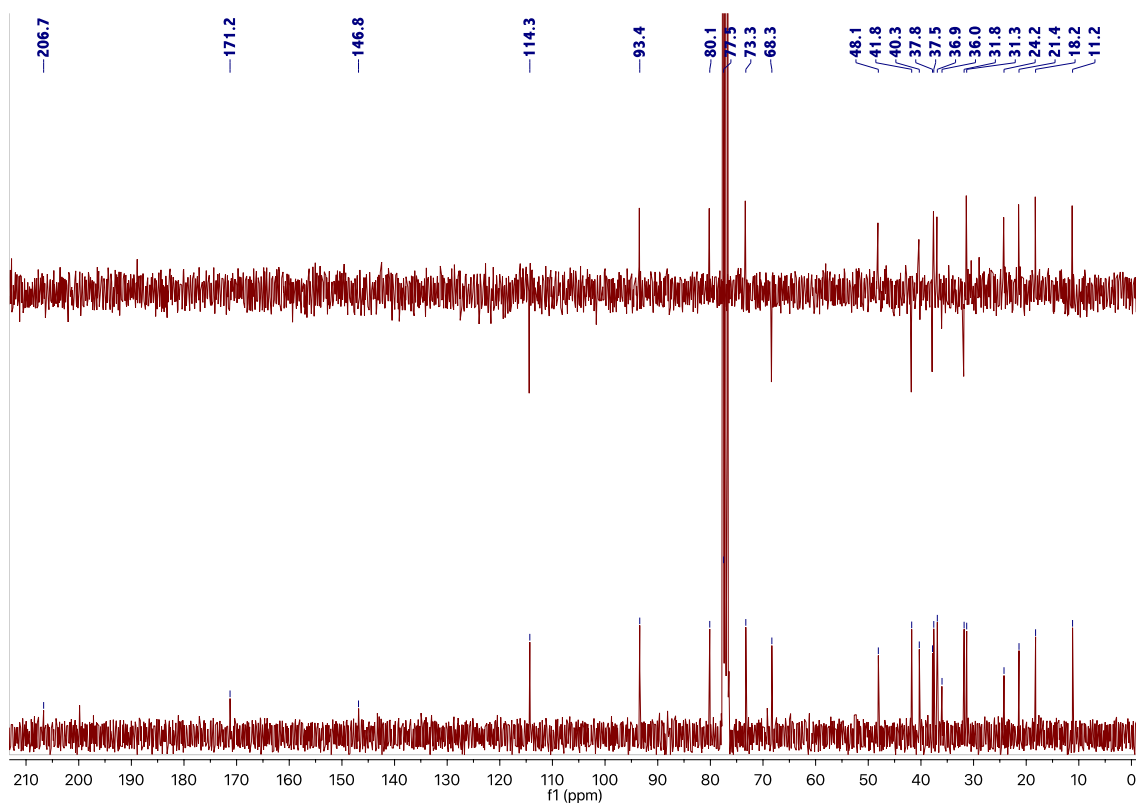


Figure S59. ^{13}C NMR and DEPT-135 spectra of **9** (125 MHz, CDCl_3).

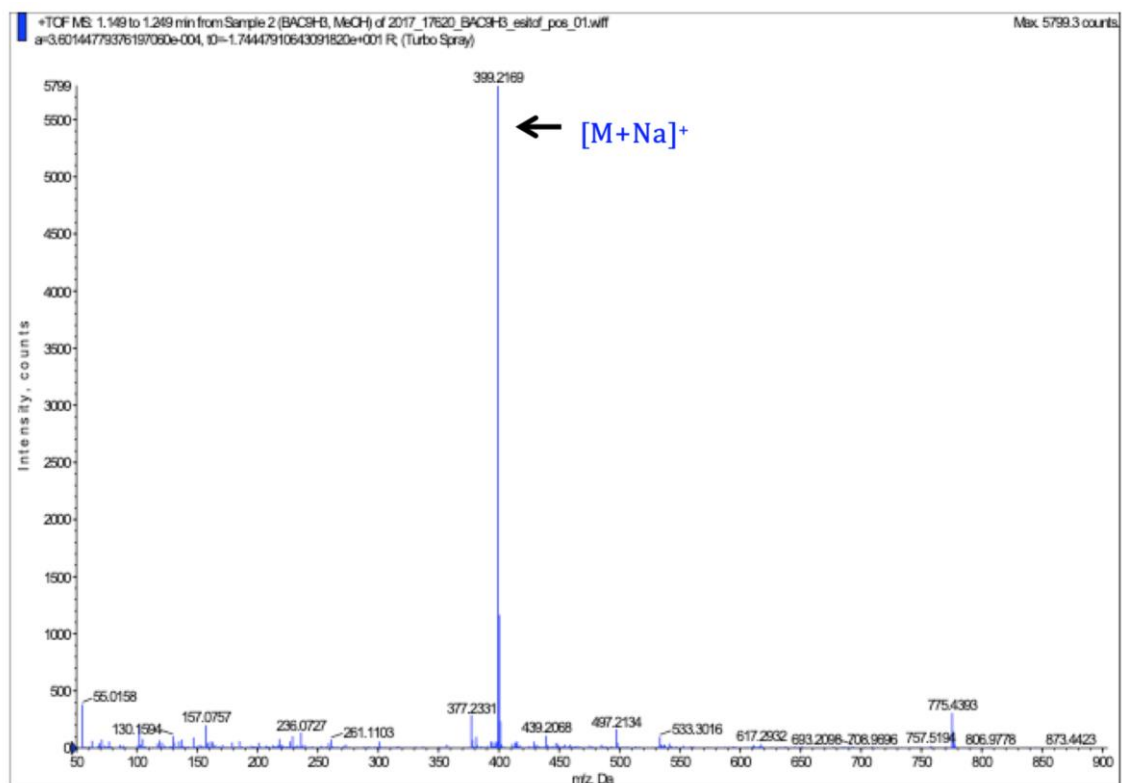


Figure S60. (+)-LRESIMS of **9**.

CAPÍTULO 4

Aplicación de nuevas metodologías de RMN en la determinación de la configuración relativa de productos naturales

4.1 Metodologías utilizadas para la determinación de la estructura tridimensional de un compuesto orgánico

En el proceso de elucidación estructural de un nuevo compuesto orgánico, la determinación de la estereoquímica es un paso crítico y muchas veces complejo. Mientras que en un compuesto con estructura plana no tenemos la necesidad de determinar su configuración tridimensional, en una estructura que posee centros estereogénicos, es necesario discernir entre los 2^n (n = número de carbonos quirales) posibles diastereoisómeros que puede tener el compuesto a elucidar.

La resolución tanto de la configuración relativa como absoluta en compuestos naturales puede convertirse en la tarea más difícil, especialmente en el caso de aquellos centros estereogénicos que se encuentran en cadenas acíclicas con gran libertad conformacional. El uso de técnicas espectroscópicas, como la resonancia magnética nuclear, y en especial la utilización de experimentos homonucleares basados en ROE o NOE, junto con el estudio de las constantes de acoplamiento homo (J_{HH}) y heteronucleares ($^2J_{CH}$), supone una gran ayuda a la hora de abordar la estereoquímica relativa de un compuesto. Otras estrategias muy empleadas son la derivatización química de determinados grupos funcionales, la observación de otras propiedades físicas como el poder rotatorio o el dicroísmo circular, que nos permiten determinar en algunos casos la estereoquímica absoluta.

En los últimos años, el uso de cálculos computacionales basados en la teoría de funcionales de densidad (DFT) ha supuesto una gran ayuda a la hora de determinar las disposiciones espaciales de muchos centros estereogénicos. Algunas de estas técnicas que se utilizan en la actualidad para la determinación de la estereoquímica relativa y absoluta de compuestos orgánicos, se introducen de forma básica a continuación.

4.1.1 Ejemplos de metodologías en la determinación de la configuración relativa

4.1.1.1 Espectroscopia de resonancia magnética nuclear

La espectroscopia de RMN nos permite afrontar, en ciertos casos, la resolución de la estereoquímica relativa de dos o más centros estereogénicos de una molécula. Estas técnicas no destructivas permiten acotar, en ocasiones, el número de estereoisómeros posibles y facilitar la determinación de la configuración absoluta mediante el uso de derivatizaciones químicas. En el caso de sistemas rígidos, el uso de constantes de acoplamiento o correlaciones espaciales obtenidas mediante experimentos ROE/NOE nos permite relacionar la disposición espacial de dos o más centros estereogénicos entre sí.

4.1.1.2 Asignación directa de la configuración relativa en sistemas 1,3- dimetilo

Con el fin de determinar la estereoquímica relativa de los centros estereogénicos en sistemas 1,3-dimetilo, Schmidt y Breit^{4.1} estudiaron los desplazamientos químicos de los protones del grupo metileno intercalado entre ambos carbonos metilados sin necesidad de recurrir a derivatizaciones u otras técnicas más complejas. A partir del estudio de las conformaciones de las dos posibles configuraciones relativas *sin* o *anti* (Figura 4.1), propusieron que los entornos de los protones diastereotópicos entre los dos centros quirales en sistemas con configuración *sin* serían muy distintos, originando que la diferencia entre los desplazamientos químicos sea grande, mientras que en sistemas *anti*, donde los protones metilénicos tienen entornos similares, dicha diferencia sería mucho menor.

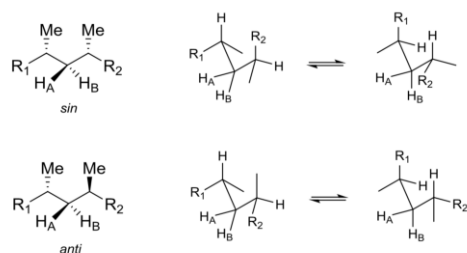


Figura 4.1. Conformación de las configuraciones *sin* y *anti* en sistemas 1,3-dimetilo.

Dicho estudio se realizó en mas de 80 productos naturales, así como en productos sintéticos ya conocidos, observándose que la mayoría de compuestos con configuración *anti* mostraban una diferencia de desplazamiento químico entre los dos protones metilénicos de 0.0-0.2 ppm, mientras que la mayor parte de los compuestos con configuración *sin* exhibieron una diferencia mayor, entre 0.2 y 0.5 ppm. Un punto importante a destacar, es que dependiendo de los sustituyentes de las cadenas laterales, es posible encontrar compuestos con configuración *anti* o *sin* con valores de $\Delta\delta$ de 0.1-0.4, por lo que este método solo es aplicable cuando se trabaja con valores extremos (Figura 4.2).

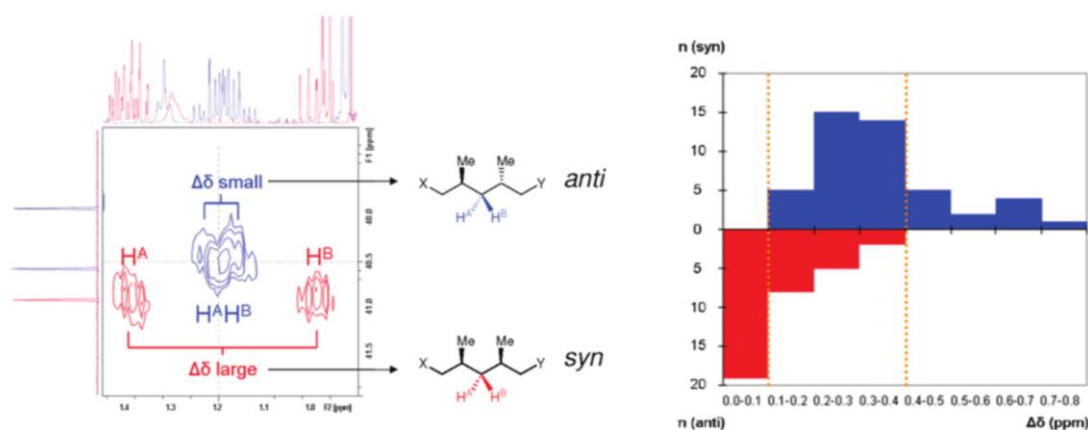


Figura 4.2. Valores de $\Delta\delta$ para los compuestos conocidos estudiados (extraído de la referencia 4.1).

4.1.1.3 El método de análisis configuracional basado en las constantes de acoplamiento (JBCA)

La elucidación de la configuración relativa de sistemas acíclicos fue desarrollada por Murata y col.^{4.2} y publicada en 1999, y consiste en el análisis de las constantes homo (H-H) y heteronucleares (C-H) a dos y tres enlaces. Esta metodología permite la determinación de la configuración relativa de sistemas carbonados dimetínicos con centros quirales en posiciones relativas 1,2- o 1,3-, disustituidos donde al menos uno de los sustituyentes es un heteroátomo.

Este método se basa en el estudio de los tres rotámeros alternados mayoritarios en torno a los dos centros estereogénicos adyacentes, a partir de la comparación de los valores experimentales de las $^{2,3}J_{C,H}$ y $^3J_{H,H}$. Las constantes homonucleares se obtienen a través de experimentos de RMN de 1H y las heteronucleares mediante experimentos bidimensionales J -HMBC, PIP-HSQMBC, HSQC-HECADE o HETLOC.^{4.2}

Para los acoplamientos vecinales homo y heteronucleares a tres enlaces de distancia ($^3J_{CH}$ y $^3J_{HH}$), en función del ángulo diedro que forman los átomos de hidrógeno,

se puede determinar el valor teórico de su constante de acoplamiento homonuclear protón-protón. Tal como fue deducido por Karplus,^{4,3} cuando el ángulo diedral es 0 ó 180°, la curva (Figura 4.3) alcanza un valor máximo, mientras que cuando el ángulo formado entre los dos protones es de 90°, la curva adopta su valor mínimo. De este modo, para los diferentes modelos estudiados se clasifican las constantes de acoplamiento próximas al valor máximo como constantes grandes, mientras que las que se encuentran próximas al valor mínimo como pequeñas.

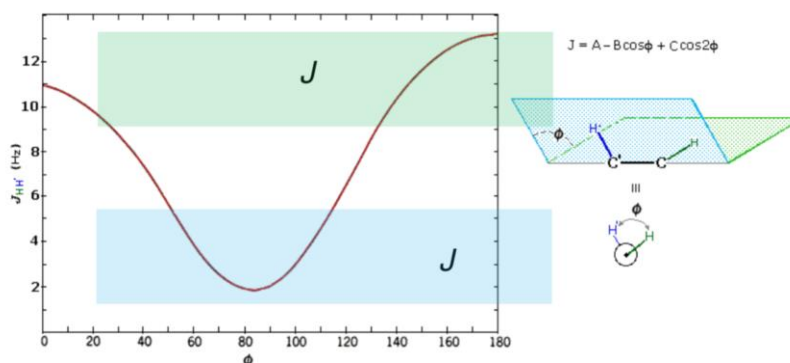


Figura 4.3. Curva definida por la ecuación de Karplus que relaciona $^3J(H,H)$ (Hz) con el ángulo diedro.

En el caso de las constantes de acoplamiento geminales heteronucleares a dos enlaces de distancia ($^2J_{CH}$), estas no mantienen una relación directa con un único parámetro molecular, sino que intervienen un cúmulo de factores que las hace ser más imprecisas a cambios estructurales. En función del sistema pueden adquirir valores muy diferentes, desde -4.5 Hz para el etano, hasta de 49.6 Hz para un sistema acetilénico, aunque en general, suelen presentar para derivados saturados valores negativos (de -10 Hz a +1 Hz). Teóricamente su valor debería ser la cuarta parte del valor de la constante $^2J_{HH}$, aunque el real es de un 60-70%.

La metodología consiste en el estudio de cada sistema, sus dos posibles configuraciones relativas *anti* y *sin*, y para cada una de ellas, los tres posibles rotámeros alternados mayoritarios: antiperiplanar, *gauche* (+) y *gauche* (-). En la Figura 4.4, se muestran los 6 posibles rotámeros mayoritarios con sus correspondientes valores de constantes de acoplamiento entre los átomos pertenecientes al sistema que se está estudiando.

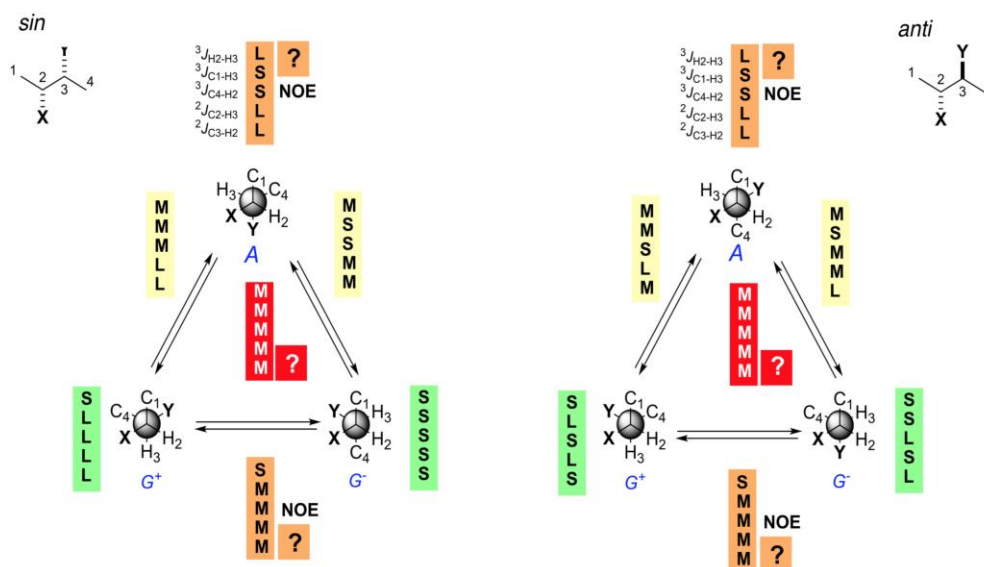


Figura 4.4. Patrón de las constantes de acoplamiento para cada uno de los seis rotámeros alternados mayoritarios. (Adaptado de la referencia 4.1). S: pequeña, L: grande, M: mediana.

Las constantes de acoplamiento ${}^3J_{CH}$ y ${}^3J_{HH}$ entre dos átomos en posición antiperiplanar son grandes, por lo que reciben la etiqueta L (large/grande), mientras que cuando dos átomos se disponen en posición gauche, dichas constantes de acoplamiento son pequeñas y reciben la etiqueta S (small/pequeña). Cuando uno de los átomos implicados está sobre uno de los carbonos asimétricos que se están estudiando, se mide el ángulo que tiene el heteroátomo unido al carbono asimétrico con el protón correspondiente a tres enlaces de distancia. En las constantes ${}^2J_{CH}$, para medir la constante de acoplamiento entre C_2 y H_3 en el conformero antiperiplanar (A) del isómero con configuración *anti*, se mide el ángulo diedral entre el enlace C_2 -heteroátomo X y el enlace C_3 - H_3 . Como X y H_3 están en posición gauche, la constante entre C_2 y H_3 tendría un valor grande. Con todo esto, se consigue un conjunto de etiquetas (las constantes de acoplamiento características para cada sistema) para cada uno de los rotámeros correspondientes. Estos valores teóricos mostrados en la tabla 4.1, se comparan con los valores experimentales para obtener las coincidencias necesarias para clasificar el sistema como *sin* o *anti*.^{4.2}

Tabla 4.1. Intervalos de valores de las ${}^3J_{HH}$ y ${}^{2,3}J_{CH}$ en Hz para los rotámeros antiperiplanar y gauche.

oxigenación	${}^3J_{HH}$		${}^2J_{C-H}$		${}^3J_{C-H}$	
	<i>antiperiplanar</i>	<i>gauche</i>	<i>antiperiplanar</i>	<i>gauche</i>	<i>antiperiplanar</i>	<i>gauche</i>
	grande	pequeña	grande	pequeña	grande	pequeña
ninguna	9-12	2-4	-	-	6-8	1-3
mono	8-11	1-4	-5 a -7	0 a -2	6-8	1-3
di	7-10	0-3	-4 a -6	2-0	5-7	1-3

Uno de los problemas al estudiar sistemas acíclicos es la gran flexibilidad de rotación en torno al enlace entre los dos carbonos asimétricos, por lo que nos podemos encontrar mezclas de 2 ó 3 rotámeros en proporciones similares que originan que se obtengan valores intermedios de J . En el caso de que tengamos dos rotámeros mayoritarios, si las constantes de acoplamiento de esos dos rotámeros son similares, ya

sean grandes o pequeñas, el valor medio resultante se mantiene como grande o pequeño, pero si uno de los rotámeros tiene una J grande y el otro pequeña, se obtiene un valor resultante intermedio.

Así se determinan el conjunto de valores (etiquetas) resultantes de las medias de los dos rotámeros. En el caso de que tengamos mezclas de los tres rotámeros en similar proporción, todos tendrán valores intermedios de J y por tanto el conjunto de etiquetas del isómero de configuración *sin* como la del isómero de configuración *anti* serían idénticas, y no se podrían distinguir mediante esta metodología. Lo mismo ocurre con la etiqueta intermedia entre los rotámeros gauche (+) y gauche (-).

Para solucionar el problema en estos casos, una de las alternativas planteadas y posteriormente publicada por nuestro grupo de investigación fue realizar las medidas experimentales a baja temperatura, con el fin de desplazar el equilibrio rotacional a un sistema donde predomine uno de los rotámeros.^{4.4} La comparación de las medidas de las constantes de acoplamiento homo/heteronucleares a baja temperatura con las obtenidas a temperatura ambiente permite saber las tendencias de variación de las mismas y a partir de estas tendencias se puede deducir la configuración relativa de los centros estereogénicos implicados.^{4.4} Por último, si se observan las etiquetas de los dos rotámeros antiperiplanar en los isómeros *sin* y *anti*, los valores de las J serán idénticas. Una posible solución para discernirlos es recurrir a experimentos de RMN de disposición espacial tipo 1D-ROE, 1D-NOE, ROESY o NOESY.

Cuando se estudian sistemas 1,3 disustituídos como el mostrado en la figura 4.5, el procedimiento requiere que los protones diastereotópicos Ha y Hb del metileno intercalado entre ambos centros estereogénicos tengan desplazamientos químicos diferentes en el espectro de RMN de protón. En estos casos, se aplica la metodología JBCA a la disposición espacial entre los átomos de cada uno de los dos centros estereogénicos y cada uno de los protones metilénicos diastereotópicos, para finalmente relacionarlos entre sí.

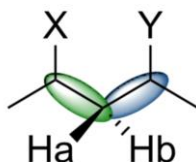


Figura 4.5. Estructura general de los sistemas 1,3-disustituídos.

4.1.1.4 Cálculos computacionales

De todas las técnicas espectroscópicas aplicables a la determinación de la estructura de nuevos compuestos orgánicos, la resonancia magnética nuclear es una de las más potentes. Dentro de los tres tipos de datos importantes que nos ofrece esta técnica, desplazamientos químicos, constantes de acoplamiento e integración relativa de las señales en caso de la RMN de protón, son los valores de los desplazamientos químicos los que nos dan mayor información acerca del entorno magnético en el que se encuentra cada átomo. La química computacional desarrollada durante los últimos años, nos permiten calcular propiedades espectroscópicas teóricas de RMN (desplazamientos químicos y constantes de acoplamiento) para compararlas con los datos experimentales. Mediante el uso de cálculos computacionales también se pueden predecir otras propiedades físicas como el perfil de UV e IR, incluso el de dicroísmo circular.

Las técnicas más utilizada para la realización de cálculos computacionales en la simulación de espectros de RMN, emplean la teoría de funcionales de densidad (DFT).

La metodología es muy similar al de los cálculos *ab initio*, pero el funcional de energía electrónica se minimiza con respecto a la densidad electrónica. La importancia de esta metodología se vio reconocida en 1998 cuando el premio Nobel de Química se otorgó a quién la desarrolló, Walter Kohn.

El uso de esta técnica está cada vez más extendido en el mundo de la química orgánica debido al desarrollo de software y la existencia de ordenadores personales potentes cada vez más accesibles. A continuación, se explica brevemente los diferentes pasos a seguir a la hora de calcular el espectro teórico de RMN de ^1H o ^{13}C mediante cálculos DFT siguiendo el protocolo de Willoughby y col.^{4,5} Es importante recordar, que los espectros de RMN de dos enantiómeros son idénticos, por lo que esta metodología nos permite resolver las configuraciones relativas pero no las absolutas.

a) El primer paso consiste en realizar una búsqueda conformacional (Figura 4.6) para cada uno de los posibles diastereoisómeros. El número de diastereoisómeros dependerá del número de centros estereogénicos que queden sin relacionar entre sí. Este proceso se lleva a cabo en un software del tipo PCModel o MacroModel. Se utilizan campos de fuerza moleculares donde la ventana de energía que se utiliza suele estar entre 3-5 kcal/mol.

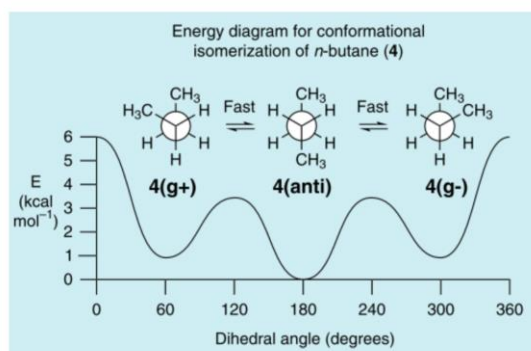


Figura 4.6. Diagrama de energía del equilibrio conformacional del n-butano. Adaptada de la referencia 4.5.

b) Todos los conformeros obtenidos para cada diastereoisomero se minimizan utilizando cálculos DFT, con el fin de conocer su energía libre y su aportación a la propiedad física que se va a calcular mediante la distribución de Boltzmann. El funcional más utilizado es el de Becke, three-parameter, Lee-Yang-Parr (B3LYP) con uno de los conjuntos base que incluyen funciones de polarización para átomos de hidrógeno, el 6-31G (d,p) o el 6-31+G(2d,p), siendo este último el que origina mejores resultados cuando se quieren obtener cálculos teóricos de espectros de RMN.

c) Mediante el método Gauge-Independent Atomic Orbitals (GIAO) se calcula el tensor de apantallamiento de RMN. El uso de este tensor de apantallamiento permite obtener los desplazamientos químicos de RMN de ^1H y ^{13}C para cada conformero en función del desplazamiento del TMS. Es importante añadir en los cálculos los efectos de solvatación del disolvente usando, por ejemplo, el método de polarización continua (PCM),^{4,5} por lo que se indicará el disolvente en el que se llevan a cabo las medidas experimentales.

d) Obtenidos los valores de energía DFT de cada uno de los conformeros, el siguiente paso es calcular su aportación al espectro de RMN, con lo que se obtiene un

espectro de RMN teórico con la media ponderada de todos ellos.

e) Finalmente se comparan los desplazamientos químicos teóricos obtenidos para cada diastereoisómero con los desplazamientos experimentales con el fin de conocer el candidato que más se aproxima a los valores reales. Existen diferentes alternativas para realizar dicha comparación como son la regresión lineal o el uso de MAE. En la actualidad, el uso del método de probabilidad DP4^{4.6} está cada vez más extendido, especialmente mediante la aplicación desarrollada por el grupo del Godmann.^{4.7} En los últimos años, Sarotti y col han desarrollado una versión mejorada de dicho método de probabilidad al que denominaron DP4⁺ y el recientemente publicado J-DP4.^{4.8}

4.1.1.5 Resonancia Magnética Nuclear anisotrópica

La anisotropía de RMN ha encontrado recientemente una amplia gama de aplicaciones en RMN de alta resolución de productos naturales. Aunque los componentes anisotrópicos de los parámetros de RMN promedian a cero en la solución isotrópica, esto no ocurre en un medio anisotrópico, lo que permite la observación controlada de los parámetros residuales de RMN anisotrópicos, es decir, acoplamiento dipolares residuales (RDC) y acoplamiento cuadrupolares residuales (RQC).^{4.9} Todos estos datos proporcionan una información valiosa sobre la orientación de los vectores entre espines y la contribución anisotrópica del entorno local a los cambios químicos de los núcleos, respectivamente.^{4.10}

La interpretación estructural de estos datos observables requiere parametrización de su dependencia angular en términos de un tensor de alineamiento. Esta información puede usarse para refinar una estructura local y puede hacer una contribución única para determinar la orientación relativa de partes remotas de las moléculas, que están localmente bien estructuradas pero mal conectadas según los datos de NOE. El análisis de los acoplamiento dipolares en términos de matrices de orden, proporciona una descripción concisa de las propiedades de orientación y movimiento de los fragmentos estructurados localmente en estos casos.^{4.11} Ambas metodologías anisotrópicas son altamente complementarias. Mientras que los RDC ofrecen información sobre los ángulos entre los vectores internucleares, los desplazamientos químicos residuales anisotrópicos (RCSA) proporcionan evidencias sobre las orientaciones relativas de los tensores de desplazamiento químico y, por lo tanto, pueden dar cuenta de la información sobre los carbonos protonados y no protonados en cualquier estructura orgánica.

Tanto los RDC como los RCSA proporcionan restricciones tridimensionales en relación con un marco de referencia global y, por lo tanto, son complementarios a las mediciones convencionales de RMN con restricción de distancia de NOE (o ROE) o acoplamiento en *J*. En comparación con los RDC, los ¹³C RCSA tienen la ventaja adicional de proporcionar información sobre la ubicación de los carbonos cuaternarios, que de otro modo solo se puede alcanzar a través de mediciones de RDC de largo alcance menos sensibles.^{4.12} Esta ventaja puede ser aprovechada para la determinación de la orientación de los carbonos cuaternarios en aquellas moléculas deficientes de protones, donde los datos de NOE, acoplamiento (*J*) y RDC de un enlace pueden ser insuficientes. Las estructuras moleculares de la hipericina y los gimocromos son buenos ejemplos de compuestos cuya determinación estructural puede facilitarse con el uso de ¹³C RCSA^{4.13,4.14} (Figura 4.7).

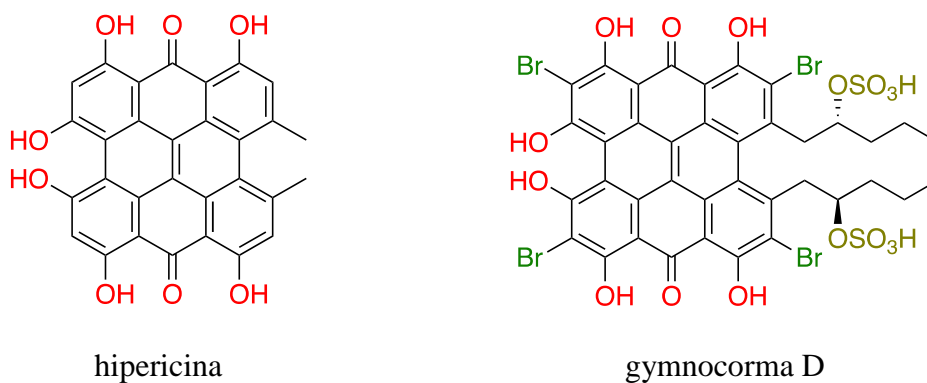


Figura 4.7. Estructuras de productos naturales ricos en carbonos cuaternarios: hipericina y gymnocorma D.

4.1.1.5.1 Metodología integrada para determinar la estructura de productos naturales por anisotropía de RMN

El enfoque general, representado en la Figura 4.8, se puede dividir en:

(a) Búsqueda conformacional usando restricciones. Para describir la molécula en equilibrio, es indispensable una búsqueda conformacional asistida por ordenador. Estos conformeros deben satisfacer las restricciones de las distancias NOE y los ángulos diédricos deducidos a partir de las constantes de acoplamiento (J).

(b) Mediciones anisotrópicas experimentales (RDC y RCSA). Los datos se obtienen principalmente mediante el uso de dos tipos de dispositivos, ambos disponibles en New Era Company:^{4.15,4.16}

- Un dispositivo de estrechamiento utilizado originalmente para medir RCSA en proteínas, que produce datos RCSA libres de interferencia de desplazamiento isotrópico.
- Un dispositivo de compresión que sufre interferencia de desplazamiento químico isotrópico. En este caso, los datos de RCSA deben corregirse antes del ajuste.

Un factor crucial para un buen análisis anisotrópico es la elección del disolvente y el medio de alineación correctos. El disolvente deuterado debe disolver completamente la muestra evitando la formación de agregados. Por otro lado, el medio de alineación debe proporcionar un grado de orden que permita la discriminación entre las posibles configuraciones.

(c) Cálculo de los valores teóricos de las RDC/RCSAs y del tensor de desplazamiento químico anisotrópico (CSA) por DFT. Los cálculos de DFT brindan un grado de precisión suficiente cuando se utiliza el método Orbital atómico independiente del indicador (GIAO). Nath y colaboradores^{4.16} recientemente han demostrado que la aproximación del Conjunto Continuo de Transformaciones de Indicadores (CSGT) también puede usarse sin perjudicar los resultados.

(d) Cálculo del tensor de alineamiento (\hat{A}). En este paso se ajustan todos los RDC/RCSAs a la estructura computada por DFT junto con el tensor CSA calculado y los valores experimentales de RDC/RCSAs obtenidos, a través del método de descomposición de valor singular (SVD, Single Value Decomposition).^{4.17}

(e) *Las comparaciones del factor de calidad del ajuste.* El factor se expresa ya sea por el factor de Cornilescu's (Q) o por el factor de calidad Q (CSA).^{4,18} Este último se calcula mediante el escalado de los valores anisotropicos de desplazamiento químico, tanto de RCSAs experimentales como calculados de cada átomo correspondiente. En el caso de las RDCs, los valores de desplazamiento químico son sustituidos por los valores de constantes de acoplamiento (J).

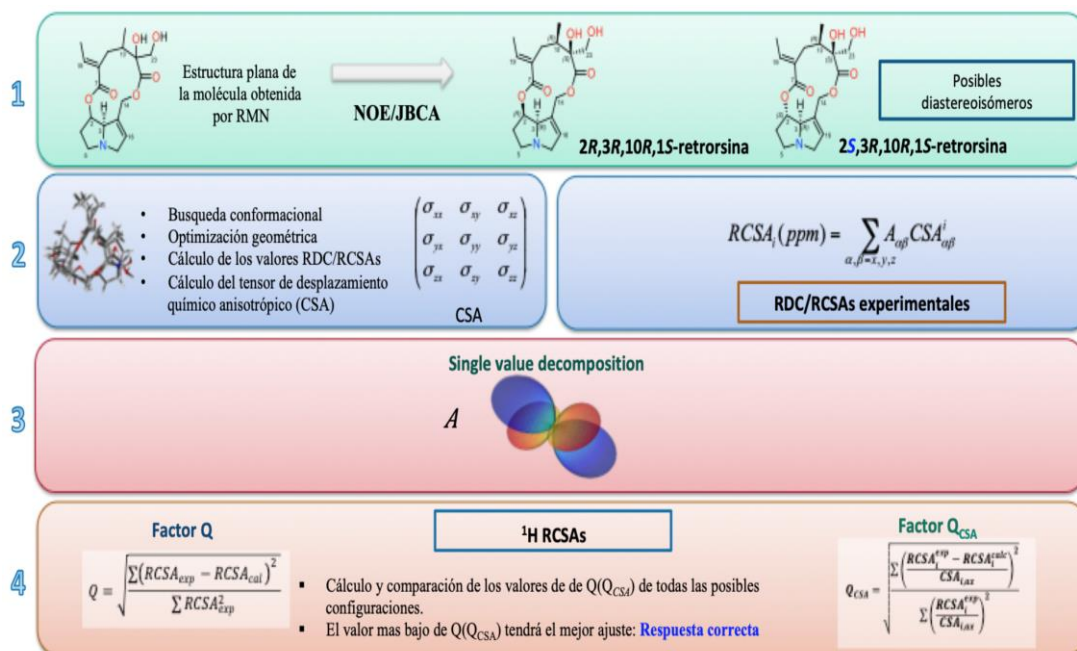


Figura 4.8. Estrategia general utilizada en el análisis de RDC y ^{13}C y ^1H RCSA para resolver la configuración relativa de moléculas pequeñas flexibles.

4.1.2 Ejemplos de metodologías en la determinación de la configuración absoluta

4.1.2.1 Rotación óptica, dicroísmo circular y difracción de RX

A partir de los valores de la rotación óptica específica $[\alpha]^D$ y los espectros de dicroísmo circular (CD), se puede resolver la configuración absoluta de un compuesto. Dos enantiómeros tendrán valores idénticos de rotación óptica específica, pero de signo contrario (Figura 4.9a) y además tendrán curvas idénticas de dicroísmo circular (CD) pero de diferente signo (Figura 4.9b).

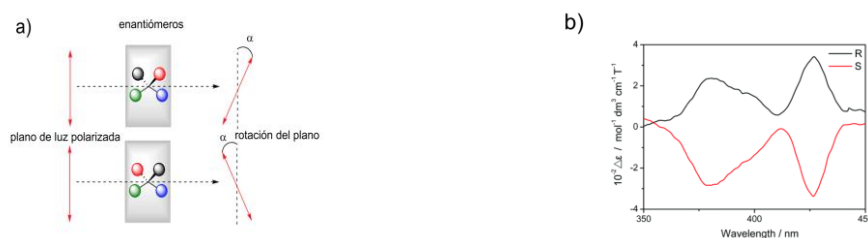


Figura 4.9. Rotación óptica específica $[\alpha]^D$ y curva de dicroísmo circular (CD) de dos enantiómeros.

La técnica de difracción de rayos X de monocristal permite conocer la configuración absoluta de todos los centros estereogénicos de la molécula, siempre que se consiga obtener unos cristales adecuados y en la mayoría de las ocasiones debe de contener un átomo pesado. Este proceso está muy limitado por la necesidad de obtener sólidos cristalinos, que es difícil en el caso de los productos naturales dado las escasas cantidades de los compuestos aislados. La determinación de la configuración relativa o absoluta mediante esta técnica se hace en función de la distancia entre los diferentes átomos de la molécula y de mapas de densidad electrónica. En el caso de cristales de buena calidad de compuestos ópticamente activos que tengan en la molécula un átomo pesado de $Z > 14$, se podría determinar la configuración absoluta de los mismos. De no ser así, sólo podría determinarse la configuración relativa de sus centros.

4.1.2.2 Derivatización quiral de alcoholes secundarios

Cuando los espectros de resonancia magnética nuclear de dos enantiómeros son idénticos, una de las alternativas más usadas consiste en introducir alguna modificación que logre diferenciarlos estereoquímicamente para obtener espectros diferentes. Esto se puede conseguir mediante la introducción de un reactivo quiral que interaccione con nuestros compuestos y obtener así diferentes espectros de RMN. Para ello, se puede utilizar un disolvente quiral o reactivos quirales que se unan con nuestra molécula mediante un enlace covalente.^{4.19} Esta reacción fue propuesta por H.R. Mosher^{4.20} y col. en 1973, modificada por Ohtani^{4.21} y col. en 1991 y desarrollada por Riguera y col.^{4.19}

Esta metodología permite determinar la configuración absoluta de algunos centros estereogénicos de una molécula que contenga o tenga próximos determinados grupos funcionales como alcoholes, aminas, ácidos o amidas. Para ello, se derivatiza el compuesto de forma separada con cada uno de los dos enantiómeros del reactivo quiral, para obtener dos derivados diastereoisómeros. La comparación de los dos espectros de RMN ^1H obtenidos permite localizar ambos ligandos en el espacio alrededor del carbono estereogénico y conocer así la configuración absoluta (Figura 4.10). El estudio de los desplazamientos de protón en los espectros de resonancia determinará la disposición que adopten los sustituyentes alrededor del carbono estereogénico y esta permitirá, a su vez, determinar la configuración absoluta.

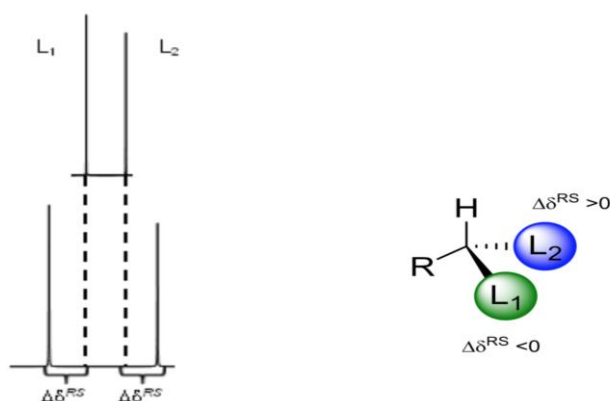


Figura 4.10. Representación esquemática del uso de reactivos quirales.

A pesar de ello, no todos los reactivos quirales son adecuados para la determinación de la configuración de un centro estereogénico, ya que debe existir una correlación entre los desplazamientos químicos de los sustituyentes y la disposición espacial de estos. Los derivados de ácidos arilmetoxiacéticos (AMAAs) son los más empleados (Figura 4.11), ya que la aplicación a un gran número de sustratos ha permitido validar los resultados obtenidos y determinar en profundidad su mecanismo de acción.^{4,19} Estos reactivos se caracterizan por la presencia de un grupo polar, un grupo funcional que permita su unión al sustrato (ácido carboxílico, hidroxilo, amino, etc.) y un grupo con anisotropía magnética (anillo aromático, carbonilo, etc.).

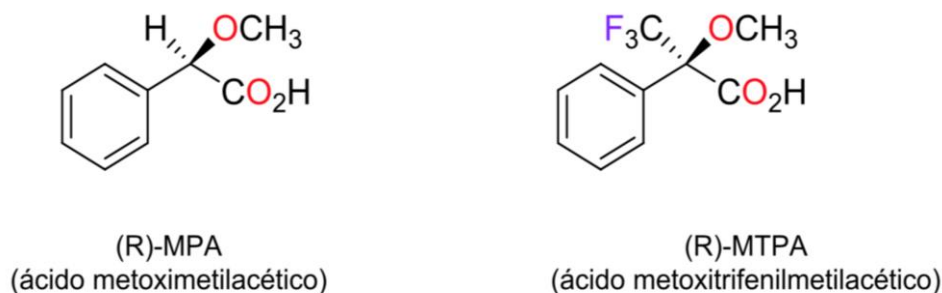


Figura 4.11. Reactivos quirales más utilizados en el estudio de alcoholes secundarios.

Uno de los principales usos de estos agentes es la determinación de la configuración absoluta de carbonos estereogénicos en alcoholes secundarios. La unión del grupo hidroxilo unido al carbono asimétrico con el agente quiral a través del ácido carboxílico, resulta en la formación de un éster donde el protón del centro quiral y el protón en la posición α o el grupo trifluorometilo del agente quiral (dependiendo del uso de MPA o MTPA) se sitúan en el mismo plano.

Es entonces, cuando el efecto anisotrópico producido por el anillo aromático del reactivo quiral ejerce su influencia sobre el ligando más próximo afectando a su desplazamiento a valores más bajos, (Figura 4.12) permitiendo la translación de la información estereoquímica del grupo auxiliar, cuya estereoquímica absoluta es conocida, al sustrato, el alcohol de configuración desconocida.

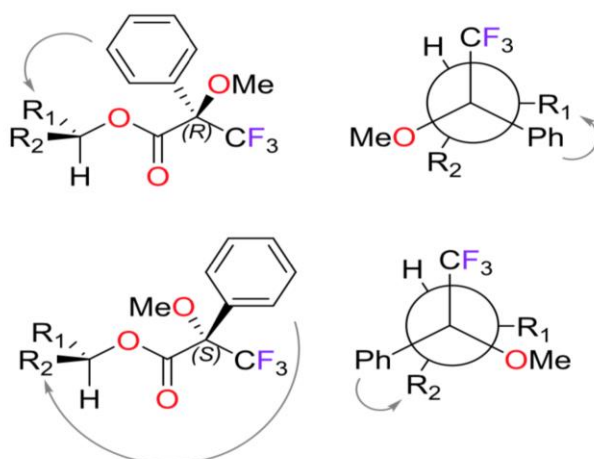


Figura 4.12. Esquema del efecto anisotrópico del grupo fenilo sobre el sustrato con MTPA en alcoholes secundarios.

De esta forma, al hacer reaccionar el alcohol con los dos enantiómeros del agente quiral se obtienen los dos ésteres diastereoisoméricos. Si se restan los desplazamientos químicos de los protones cercanos al carbono asimétrico del éster *S* menos los del *R*, se obtienen valores positivos para aquellos protones que han sufrido el apantallamiento del anillo aromático en el éster *R* y valores negativos para aquellos que lo han sufrido en el éster *S*.^{4.22} Si se sitúa el éster y el protón del sustrato en el mismo plano y el grupo de señales con valores de $\Delta\delta_{RS}$ positivos por delante del plano, y las negativas hacia detrás, se determina la configuración absoluta del carbono estereogénico estudiado (Figura 4.13).

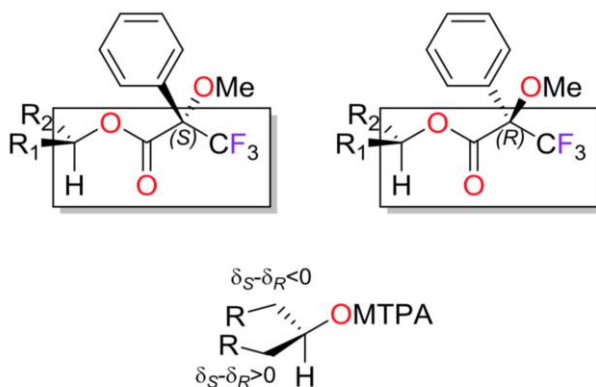


Figura 4.13. Determinación de la configuración absoluta del carbono asimétrico en alcoholes secundarios usando MTPA como agente quiral.

La asignación de la configuración absoluta mediante el uso de reactivos quirales suele realizarse mediante el experimento de RMN de ^1H . La metodología implica la utilización de una pequeña cantidad de muestra, ya que los experimentos son más rápidos que usando otros núcleos. Actualmente, los avances tecnológicos en la espectroscopia de RMN permiten el uso de esta metodología con experimentos de RMN de ^{13}C ,^{4.23} observándose que usando únicamente los desplazamientos de carbono o en combinación con los de protón se obtienen excelentes resultados.^{4.24}

4.1.2.3 Determinación de la configuración absoluta de aminoácidos en derivados peptídicos

Los aminoácidos forman parte de manera habitual en muchos metabolitos secundarios encontrados en organismos marinos, por lo que la determinación de su estereoquímica supone un desafío a la hora de determinar su configuración absoluta. El uso de la *N*^α-(5-fluoro-2,4-dinitrofenil)-L-alaninamida (Figura 4.14) como reactivo quiral para la determinación de la estereoquímica de aminoácidos fue propuesto por P. Marfey en 1984.^{4,25} Al hacer reaccionar el reactivo de Marfey con la pareja de aminoácidos enantioméricos se forman sus respectivos diastereoisómeros, que son fácilmente separables mediante HPLC sin necesidad del uso de columnas quirales. El diastereoisómero más retenido suele ser casi siempre el D debido a su interacción con la fase reversa de la columna. Los aminoácidos derivatizados se pueden detectar fácilmente en HPLC mediante el máximo de UV a 340 nm del anillo aromático presente en el reactivo de Marfey, o mediante extracción iónica en un detector de masas acoplado al HPLC, lo que permite llevar a cabo el experimento con cantidades muy pequeñas de sustrato.

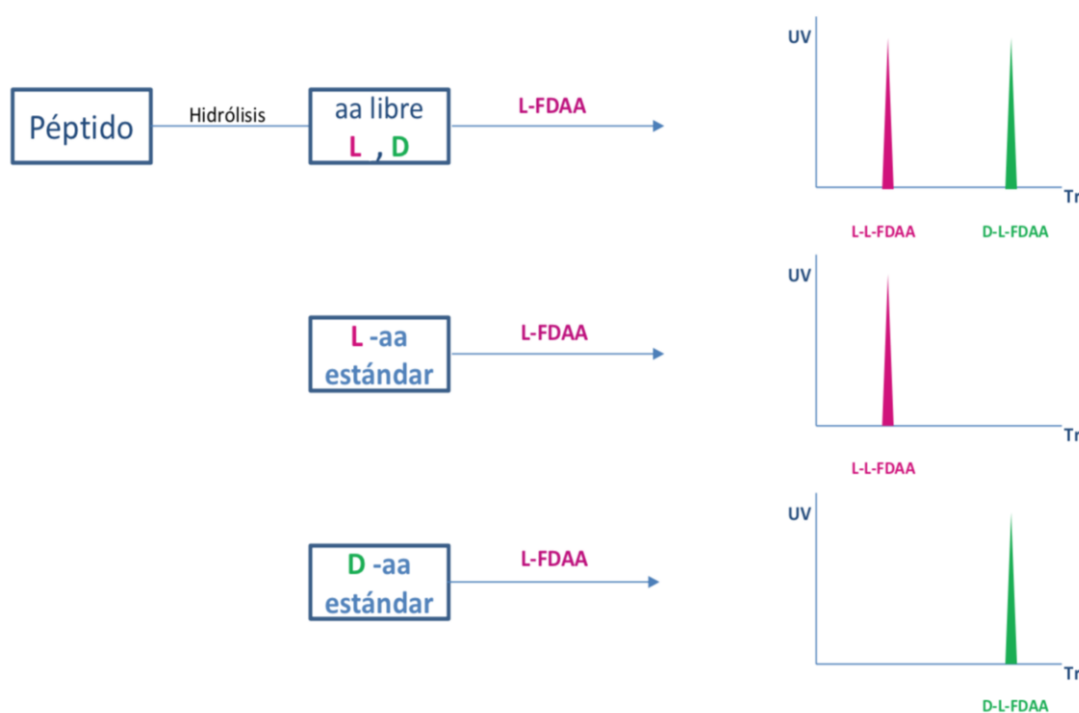


Figura 4.14. Estrategia de determinación de la configuración absoluta de aminoácidos empleando el método de Marfey.

El procedimiento consiste, en primer lugar, en la obtención de los aminoácidos libres del péptido a estudiar, lo cual se consigue en la mayoría de los casos rompiendo el enlace peptídico con una hidrólisis ácida, a continuación los aminoácidos libres se hacen reaccionar con el reactivo L-FDAA.^{4,26} A su vez se obtienen los derivados de L-FDAA de los patrones (comerciales u obtenidos de forma sintética) de los aminoácidos a estudiar (Figura 4.15). Que son analizados mediante HPLC acoplado a un detector de fotodiodos (DAD) y/o masas, con el fin de determinar los tiempos de retención de los diferentes enantiómeros de los aminoácidos del péptido a estudiar.

Finalmente, la comparación del tiempo de retención de los patrones derivatizados con el de los aminoácidos derivatizados obtenidos de la hidrólisis del péptido permite

establecer la configuración absoluta de cada uno de ellos.

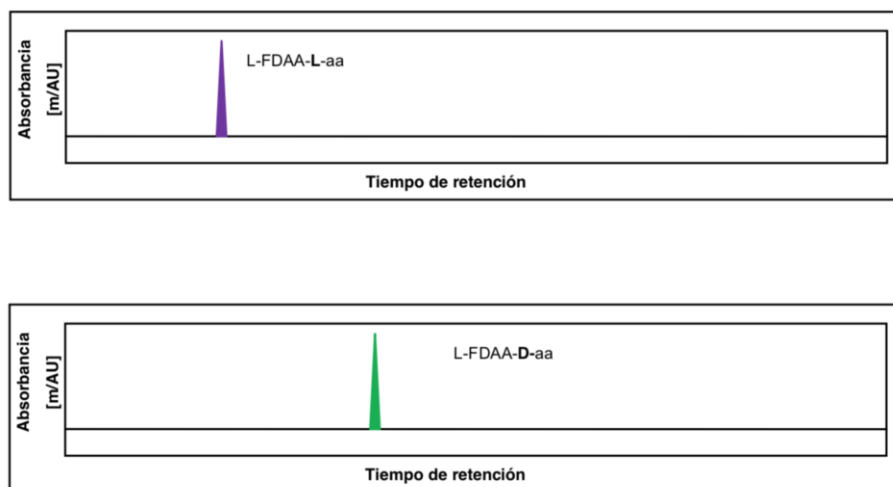


Figura 4.15. Cromatograma de los dos diastereoisómeros formados con la unión del reactivo L-FDAA a cada uno de los dos enantiómeros del aminoácido analizado.

Debido a la dificultad de conseguir en algunas ocasiones todos los patrones, Fujii y col.^{4,27} desarrollaron el método avanzado de Marfey. Este método consiste en la separación de los aminoácidos derivatizados con el reactivo de Marfey, pero utilizando los reactivos L-FDAA y D-FDAA con el fin de sustituir los patrones no disponibles por sus enantiómeros. Si mediante la derivatización con L-FDAA es necesario tener todos los diastereoisómeros de un mismo aminoácido para poder comparar sus tiempos de retención con el del aminoácido derivatizado del sustrato a estudiar, con el método avanzado de Marfey se realiza una derivatización con los dos enantiómeros D y L del FDAA, por lo que solo es necesario disponer de uno de los enantiómeros del aminoácido. Por ejemplo, al derivatizar solo el L-aa, se obtendrán los diastereoisómeros L-FDAA-L-aa y el D-FDAA-L-aa. Debido a que los enantiómeros presentan el mismo tiempo de retención, el aminoácido derivatizado D-FDAA-L-aa será equivalente al L-FDAA-D-aa, por lo que partiendo de un único enantiómero, podremos conocer el tiempo de retención de la pareja de los enantiómeros derivatizados (Figura 4.16).

En caso de no conocer cuál de los dos aminoácidos derivatizados tiene mayor tiempo de retención, se realiza por separado una derivatización L-FDAA para conocer el tiempo de retención del aminoácido L-aa derivatizado.

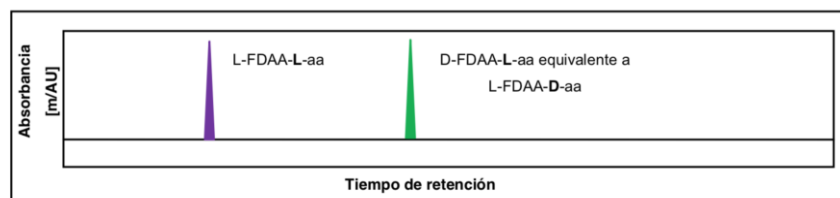


Figura 4.16. Cromatograma de los diastereoisómeros obtenidos mediante la derivatización con los reactivos D y L-FDAA empleando el método avanzado de Marfey.

Para la determinación de la configuración absoluta de aminoácidos con más de un centro asimétrico, sería necesario disponer de todos los isómeros posibles para la resolución mediante el método de Marfey, pero sólo uno de cada pareja de enantiómeros si se recurre al método avanzado de Marfey.

Referencias

- 4.1 Schmidt Y.; Breit B. *Org. Lett.* **2010**, *12*, 2218–2221. [SEP]
- 4.2 a) Parella T.; Espinosa J. F., *Prog. Nucl. Magn. Reson. Spectrosc.* **2013**, *73*, 17–55. b) Kurz M.; Schmieder Peter; Kessler H. *Angew. Chem. Int. Ed. Engl.* **1991**, *30*, 1329–1331. c) Wollborn U.; Leibfritz D. *J. Magn. Reson.* **1992**, *98*, 142–146. d) Matsumori N.; Kaneno D.; Murata M.; Nakamura H.; Tachibana K.J. *Org. Chem.* **1999**, *64*, 866–876. e) Matsumori N.; Murata M.; Tachibana K.; *Tetrahedron* **1995**, *51*, 12229–12238. f) Nonomura T.; Sasaki M.; Nobuaki M.; Murata M.; Tachibana K.; Yasumoto T. *Angew. Chem. Int. Ed. Engl.* **1996**, *35*, 1675–1678. g) Sasaki M.; Matsumori N.; Maruyama T.; Nonomura T.; Murata M.; Tachibana K.; Yasumoto T. *Angew. Chemie (International Ed. English)* **1996**, *35*, 1672–1675. h) Sakai R.; Kamiya H.; Murata M.; Shimamoto K. *J. Am. Chem. Soc.* **1997**, *119*, 4112–4116.
- 4.3 Karpus M. *J. Am. Chem. Soc.* **1963**, *85*, 2870–2871. [SEP]
- 4.4 Ardá A.; Nieto, M.I.; Blanco, M.; Jiménez, C.; Rodríguez, J. *J. Org. Chem.* **2010**, *75*, 7227–7232.
- 4.5 a) Willoughby P.H.; Jansma M.J.; Hoye T.R. *Nat. Protoc.* **2014**, *9*, 643–660. b) Mennucci E.; Cances J.; Tomasi J. *Chem. Phys.* **1997**, *101*, 10506–10517.
- 4.6 Smith S.G.; Goodman J.M. *J. Am. Chem. Soc.* **2010**, *132*, 12946–12959.
- 4.7 <http://www-jmg.ch.cam.ac.uk/tools/nmr/DP4/>. Última entrada 9 enero de **2020**.
- 4.8 a) Grimblat N.; Zanardi M.M.; Sarotti A.M. *J. Org. Chem.* **2015**, *80*, 12526–12534. b) Grimblat N.; Gavín J.A; Hernández Daranas A.; Sarotti A.M. *Org. Lett.* **2019**, *21*, 4003–4007.
- 4.9 a) Kummerlöwe G.; Luy B. in G.A.B.T.-A.R. on N.M R.S. (ed. Webb)232 Academic Press, **2009**. b) Thiele C.M.; Maliniak A.; Stevensson B.; *J. Am. Chem. Soc.* **2009**, *131*, 12878–12879. c) Schuetz A.; Junker J.; Leonov A.; Lange O.F.; Molinski T.F.; Griesinger C. *J. Am. Chem. Soc.* **2007**, *129*, 15114–15115. d) Schmid M.B.; Fleischmann M.; D’Elia V.; Reiser O.; Gronwald W.; Gschwind R.M. *ChemBioChem.* **2009**, *10*, 440–444. e) Gayathri C.; Tsarevsky N.V.; Gil R.R. *Chem. - A Eur. J.* **2010**, DOI 10.1002/chem.200903378. f) Trigo-Mouriño P.; Navarro-Vázquez A.; Ying J.; Gil R.R.; Bax A. *Angew. Chemie - Int. Ed.* **2011**, *50*, 7576–7580. g) Li G.W.; Liu H.; Qiu F.; Wang X.J.; Lei X.X.; *Nat. Products Bioprospect.* **2018**, *8*, 279–295. h) Kummerlöwe G.; Grage S.L.; Thiele C.M.; Kuprov I.; Ulrich A. S.; Luy B. *J. Magn. Reson.* **2011**, *209*, 19–30. i) Liu Y.; Prestegard J. H. *J. Biomol. NMR* **2010**, *47*, 249–258. j) Hallwass F.; Teles R.R.; Hellemann E.; Griesinger C.; Gil R.R.; Navarro-Vázquez A. *Magn. Reson. Chem.* **2018**, *56*, 321–328. k) Nath N.; Schmidt M.; Gil R.R.; Williamson R.T.; Martin G.E.; Navarro-Vázquez A.; Griesinger C.; Liu Y.; *J. Am. Chem. Soc.* **2016**, *138*, 9548–9556. l) Liu Y.; Navarro-Vázquez A.; Gil R.R.; Griesinger C.; Martin G.E.; Williamson R.T. *Nat. Protoc.* **2019**, *14*, 217–247.
- 4.10 N Wirz L.; R Allison J. *Prog. Biophys. Mol. Biol.* **2017**, *128*, 117–129.
- 4.11 Saupe A.; Englert, G. *Phys. Rev. Lett.* **1963**, *11*, 462–464.
- 4.12 Nath N. *et al. J. Am. Chem. Soc.* **2016**, *138*, 9548–9556.
- 4.13 Falk H. *Angew. Chemie Int. Ed.* **1999**, *38*, 3116–3136.
- 4.14 De Riccardis F. *et al. J. Org. Chem.* **1991**, *56*, 6781–6787.
- 4.15 Liu Y.; Prestegard J. H. *J. Biomol. NMR.* **2010**, *47*, 249–258.
- 4.16 Nath N.; Schmidt M.; Navarro-Vázquez A.; Gil R. G. C. Determination of Configuration of Small Molecules from Residual Chemical Shift Anisotropy (RCSAs) at Microgram Levels. In

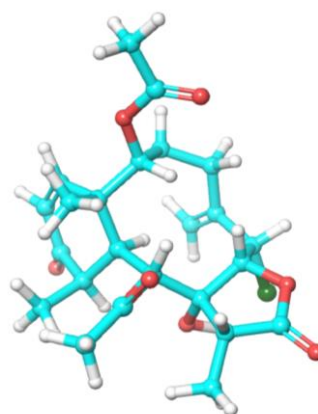
(http://209.237.166.70/media/smash/2016/posters/abstract-poster-Nath_1.pdf)
2016.

- 4.17 Losonczi J.A.; Andrec M.; Fischer M.W.F.; Prestegard J.H. *J. Magn. Reson.* **1999**, *138*, 334–342.
- 4.18 Cornilescu G.; Marquardt J.L.; Ottiger M.; Bax A. *J. Am. Chem. Soc.* **1998**, *120*, 6836–6837.
- 4.19 Seco, J.M.; Quiñoá, E.; Riguera, R. The Assignment of the Absolute Configuration by NMR Using Chiral Derivatizing Agents, **2015** Oxford University Press.
- 4.20 Dale, J.A.; Mosher, H.S.J. *Am. Chem. Soc.* **1973**, *95*, 512–519. [SEP]28.
- 4.21 Ohtani, I.; Kusumi, T.; Kashman, Y.; Kakisawa, H. *J. Am. Chem. Soc.* **1991**, *113*, 4092–4096.
- 4.22 Hoye, T. R.; Jeffrey, C. S.; Shao, F. *Nat. Protoc.* **2007**, *2*, 2451–2458.
- 4.23 a) Louzao, I.; Seco, J. M.; Quiñoá, E.; Riguera, R. *Chem. Commun.* **2010**, *46*, 7903–7905. b) Yabuuchi, T.; Kusumi, T. *J. Org. Chem.* **2000**, *65*, 397–404.
- 4.24 Jimenez C. Establecimiento de la configuración absoluta de productos naturales por RMN. En *Manual de Determinación Estructural de Compuestos Naturales*, **2008** Programa Iberoamericano de Ciencia y Tecnología, CYTED.
- 4.25 Marfey P. *Carlsberg Res. Commun.* **1984**, *49*, 591–596. [SEP]34.
- 4.26 Bhushan R.; Brückner H.J. *Chromatogr. B Anal. Technol. Biomed. Life Sci.* **2011**, *879*, 3148–3161.
- 4.27 Fujii K.; Shimoya T.; Ikai Y.; Oka H.; Harada K.I. *Tetrahedron Lett.* **1998**, *39*, 2579–2582.

4.2 Determinación de la configuración relativa del briarano B-3 usando ^1H RCSA



Briareum asbestinum



Briarane B-3

En esta sección se describe brevemente la aplicación de una técnica de anisotropía de RMN conocida como ^1H RCSA que fue utilizada por primera vez para determinar la configuración relativa del briarano B-3 utilizando tan solo 35 microgramos de muestra. Este nuevo producto natural marino fue aislado de la gorgonia *Briareum asbestinum* colectada en la Península de Yucatán, México y aunque ya se ha descrito su determinación estructural en la sección 3.5, esta metodología fue la primera que se utilizó para obtener la configuración relativa del briarano B-3.

Es importante mencionar que los resultados que se presentan, forman parte un proyecto en colaboración con el Instituto Max Planck de Química Biofísica (Göttingen-Alemania), la Universidad de Gauhati (Guwahati-India), la Universidad Técnica de Darmstadt (Darmstadt, Alemania) y la Universidad de Pernambuco (Recife-Brasil) cuyo objetivo principal es el desarrollo de nuevas metodologías para la determinación estructural de moléculas orgánicas. En esta memoria de tesis doctoral se describe el caso particular del briarano B-3, como uno de los ejemplos empleados para el desarrollo de la metodología.

Mi aportación en particular dentro de este proyecto, además del aislamiento de la molécula y su determinación estructural por RMN y MS, fue realizar el estudio de búsqueda conformacional de los posibles diastereoisómeros, aplicar las restricciones NOE para elegir los conformeros posibles y hacer los cálculos computacionales DFT de cada uno de los conformeros de todos los diastereoisómeros probados. La obtención de las medidas anisotrópicas ya fue presentada como parte de la Tesis del Dr. Juan Carlos Fuentes Monteverde en el año 2019.

Estos resultados se han enviado a publicación, y en la actualidad está en proceso de revisión.

Using proton residual chemical shift anisotropy at microgram level for the determination of the relative configuration of briarane B-3

Abstract: Determination of the 3D molecular structure remains challenging for natural products or organic compounds available in minute amounts. While the constitution can be derived from proton/proton and proton/carbon correlations, J couplings and NOEs are used to determine the relative configuration oftentimes supported by one-bond ^1H , ^{13}C RDCs or by ^{13}C RCSAs. However, these RDCs or carbon RCSAs rely on 1% natural abundance of ^{13}C preventing their use for compounds available only in quantities of a few 10 μg . By contrast, ^1H RCSAs provide spatial orientation of structural moieties within a molecule, and use the abundant ^1H . Robust measurement of ^1H RCSAs is shown using constrained aligning gels or liquid crystals. The 3D molecular structures of molecules with varying complexity are determined. Deuterated alignment media allow the elucidation of the relative configuration of around 35 μg of a briarane isolated from *Briareum asbestinum* for observation of its RCSAs.

Results and Discussion:

We used ^1H RCSA data for the configuration analysis of a new briarane diterpenoid, which was isolated from the gorgonian *Briareum asbestinum* collected in Yucatan Peninsula (Mexico). The structure of the new briarane, deduced by standard NMR and MS analysis, resulted to be the same as that of briarane B-3, which was reported by Fenical in 1993 without spectroscopic support (Figure 1).

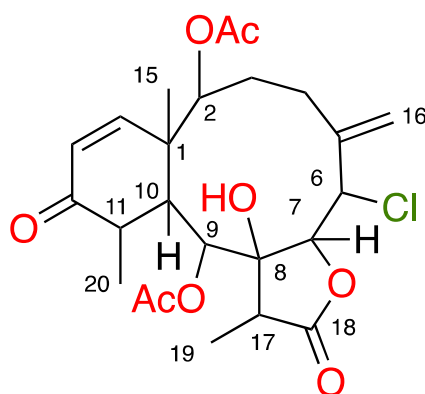


Figure 1: Planar structure of diterpene briarane B-3.

Taking into account the large number of stereogenic centers present in B-3, its conformational flexibility and the lack of reported data supporting its structure, lead us to consider this compound as a good model to establish its relative configuration using the ^1H NMR RCSA methodology. The determination of the stereochemistry is a key step in its structural elucidation, since the biological activity is closely related to the configuration. Briaranes have a wide range of biological activities such as anti-inflammatory, antibacterial, cytotoxic, etc. For instance, solenolide E, structurally related to B-3, exhibits a very pronounced antiviral activity against Rhinovirus, Herpes and Ann Arbor viruses, displays anti-inflammatory activity and is an inhibitor of a cyclooxygenase enzyme.

The stereochemical analysis of B-3 started with conventional NMR, the NOE distance restraints fixes relative configurations at C6, C7, C8, C9 and C17 as *S*, *R*, *R*, *S* and *R*, respectively and leaves the relative configurations at C1, C2, C10 and C11 undetermined. This provides a total of 16 absolute and 8 relative configurations. However, there is a strong NOE correlation between the methyl group at C1 and C11 indicating that they are located on the same side of the cyclohexanone. The absence of NOE correlations a between H10 and the methyl groups at C1 and C11 seems to indicate an *anti*-dispositions between H10/Me15 and H10/Me20. This was confirmed by a *J*-based configurational analysis that showed two large values of 6.7 and 6.5 Hz for $^3J(C_{20}-H_{10})$ and $^3J(C_{15}-H_{10})$, respectively. Since C1 and C10 must be either *RR* or *SS*, the four possible relative configurations for those stereogenic centers are: *SRSR*, *SSSR*, *RRRS* and *RSRS* (C1, C2, C10, C11). The *RR* or *SS* configurations of C1 and C10 can also be further corroborated by the presence of medium sized HMBC correlations between carbon of the methyl at C15 and H10; carbon of the methyl at C20 and H10.

The four possible configurations at C1, C2, C10 and C11, *SRSR*, *SSSR*, *RRRS* and *RSRS*, amount to 4 possible pairs of enantiomers: (keeping the order C6,C7,C8,C9,C17,C1,C2,C10,C11): *SRRSRRSR*/enantiomer (**2a**), *SRRSRRRS*/enantiomer (**2b**), *SRRSRSSSR*/enantiomer (**2c**), and finally *SRRSRRRS*/enantiomer (**2d**) showed in Figure 2.

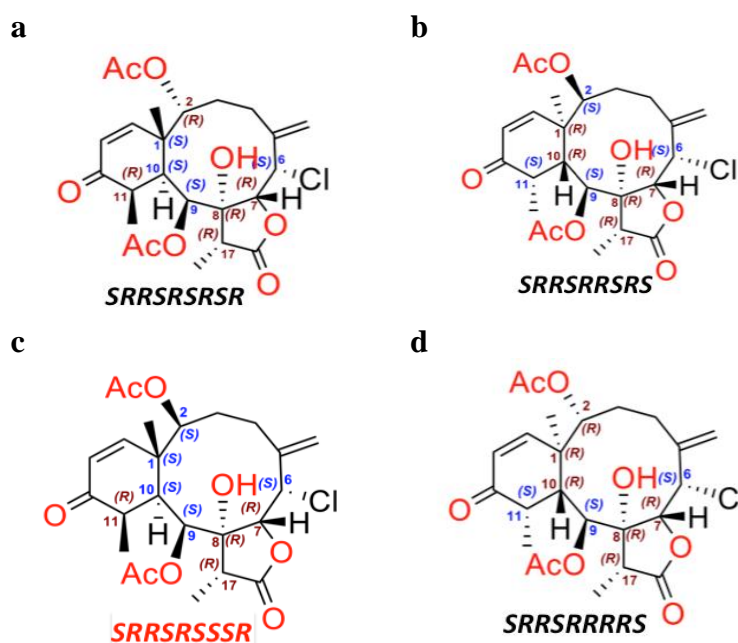


Figure 2. The four diastereomers possible for the structure of B-3 of which the *SRRSRSSSR* (**2c**) (red) is found to be the correct one.

To determine the relative configuration of these stereogenic centers, 1H RCSA of B-3 were measured in $PMMA-d_8$ gel using the Hilgenberg's micro stretching device with 2.2 and 1.8 mm inner diameters. The sample amount was only 35 μ g and experimental RCSAs range from 1.8 to 3.2 Hz at a 1H frequency of 800 MHz. Compound B-3 is a flexible molecule, therefore we fitted the 1H RCSA data to multiple conformers using a single tensor for the four relative configurations. The *SRRSRSSSR* configuration (**2c**) furnished the lowest $Q(Q_{CSA})$ factor of $0.176(0.219) \pm 0.036(0.047)$, while the other configurations had $Q(Q_{CSA})$ factor of $0.284(0.308) \pm 0.027(0.031)$, $0.315(0.376) \pm 0.032(0.042)$ and $0.315(0.375) \pm 0.033(0.042)$ for *SRRSRRRS* (**2d**), *SRRSRRRS* (**2b**),

and *SRRSRRSR* (**2a**), respectively. The $Q(Q_{CSA})$ factor difference of 0.108(0.089) between *SRRSRSSSR* (**2c**) and other three diastereomers shown in Figure 2c established unequivocally the former as the correct relative configuration (Figure 3). This result is in agreement with the DP4+ analysis where we used the conformations derived from ^1H RCSA analysis.

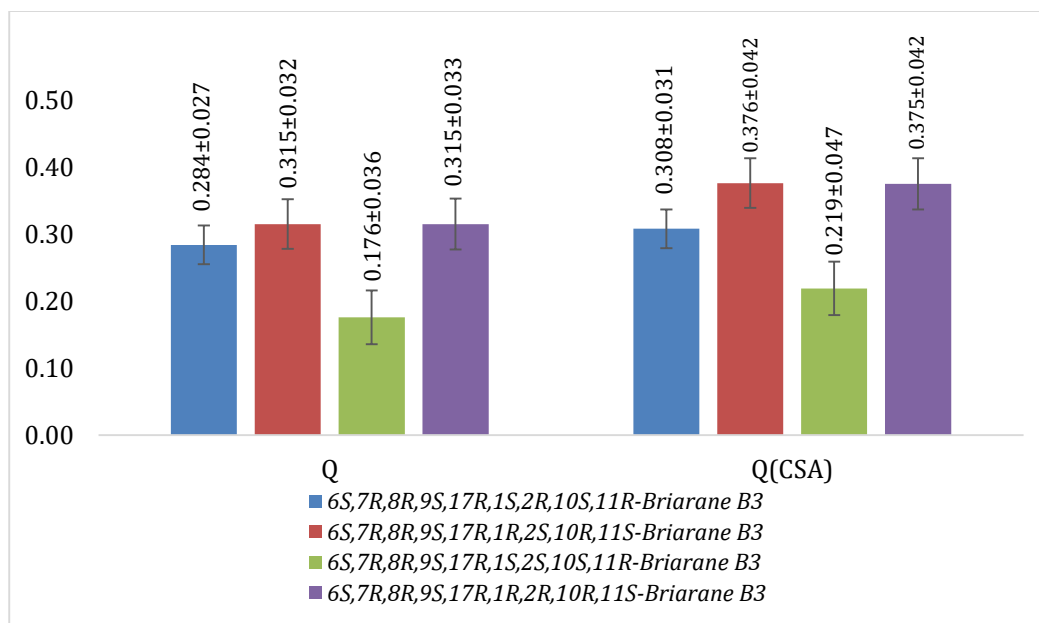


Figure 3. Bar plot for the briarane B-3 ^1H RCSA fitting, error are expressed as the standard deviation (StdDev).

With the relative configuration already established, we further computed the ECD spectrum of the enantiomers *SRRSRSSSR* and *RSSRSRRRS* in order to establish the absolute stereochemistry of the Briarane B-3 (Figure 4). We used the time-dependent DFT approach at the CAM-B3LYP/6-311g++(2d,p) and PBE1PBE/DEF2TZVP optimized geometries in acetonitrile applying the IEFPCM solvent model after a conformational search. ECD calculated for each conformer of both configurations were individually compared with the experimental ECD. The calculated data showed a negative and two positive Cotton Effect which fitted very well within the experimental data (see Figure 4b); where the intensity of the first (198 nm) and third band (338 nm) matches remarkably. The conformer-populated averaged ECD spectrum for the *SRRSRSSSR* stereoisomer and experimental data were in good agreement, indicating it as the absolute configuration of briarane B-3 as *SRRSRSSSR*.

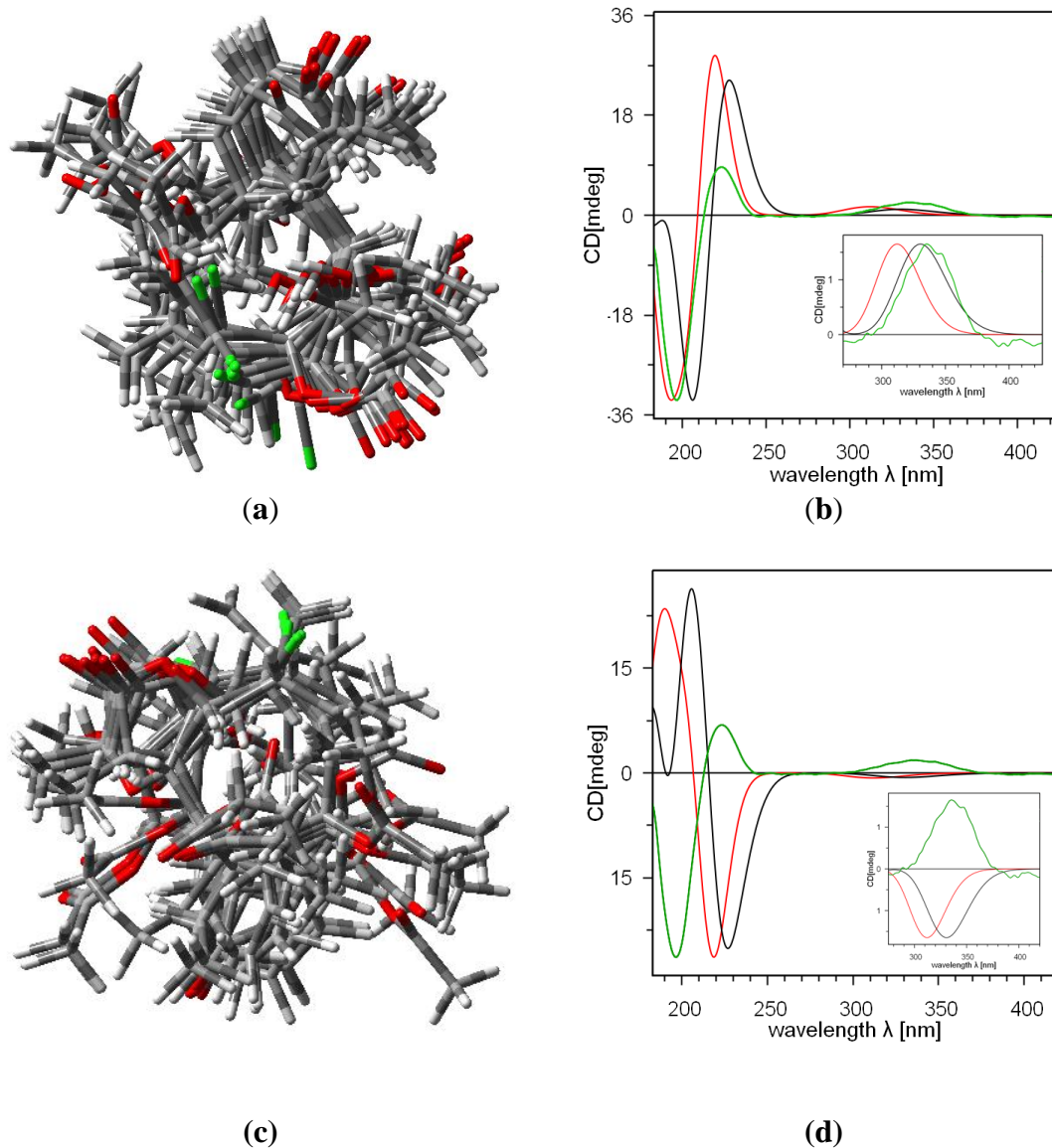


Figure 4. (a) Superimposition of 11 minimum energy conformers of *SRRSRSSSR* briarane B-3 that are consistent with the experimental NMR data. (b) Comparison between experimental (green) and TD-SCF DFT calculated (Boltzmann-weighted) ECD of briarane-B-3. Red and black solid lines are the calculated ECD of *SRRSRSSSR* briarane B-3 at CAM-B3LYP/6-311g++(2d,p) and PBE1PBE/DEF2TZVP level of theory, respectively. (c) Superimposition of 10 minimum energy conformers of *RSSRSRRRS* briarane B-3 (*ent*-briarane B-3) that are consistent with the experimental NMR data. (d) Comparison between experimental (green solid line) and TD-SCF DFT calculated (Boltzmann-weighted) ECD of *ent*-briarane B-3. Red and black solid lines are the calculated ECD of at CAM-B3LYP/6-311G++(2d,p) and PBE1PBE/DEF2TZVP level of theory, respectively.

Based on the above findings, the structure, including the absolute stereochemistry of briarane B-3, was elucidated and confirmed unambiguously as *SRRSRSSSR*.

Conclusions:

¹H-RCSAs are powerful parameters as they complement conventional *J*-couplings, and NOEs, without the necessity to resort to one bond and long range ¹H-¹³C RDCs or ¹³C RCSAs. We demonstrated that ¹H RCSAs can be successfully utilized to determine the correct relative configuration using *Q* or *Q*_{CSA} values. In addition, chemists not well trained in NMR will find it more appealing to use RCSAs than RDCs since RCSAs can be easily read from the 1D ¹H or ¹³C spectra while RDC measurements require some training with 2D spectroscopy. The analysis tools are available in MagNes-RDC software and the CSA tensor calculations can be done with the Gaussian program package. Therefore, measurement of ¹H RCSA will open up new avenues for the structural analysis of synthetic and natural products that are hitherto not solvable due to their limited amount down to 1 digit microgram quantities.

4.3 Determinación de la configuración relativa de la Nocardiomicina usando el análisis configuracional de RMN basado en J dependiente de la temperatura y en cambios de disolvente.



Theonella swinhoei



Nocardioopsis halotolerans

En esta sección se describe la utilización de una nueva metodología de análisis configuracional basado en constantes de acoplamiento, puesta a punto por varios investigadores del equipo PRONAMAR y que se pueden aplicar a sistemas acíclicos con gran libertad conformacional. Esta metodología está basada en la variación que se observa en las constantes de acoplamiento, tanto homonucleares como heteronucleares, debido al cambio de la temperatura o al disolvente deuterado en el que se registran los espectros de RMN. Esta aproximación ya observada por otros miembros del grupo en sistemas-modelo sintéticos, se aplica por primera vez a un compuesto natural, la nocardiomicina, un ciclopéptido aislado por investigadores de la empresa PharmaMar, a partir de la actinobacteria *Nocardioopsis halotolerans* aislada de la esponja marina *Theonella swinhoei* recolectada cerca de las islas Gloriosas en el Océano Indico.

La parte realizada por mi consistió en la determinación estructural de nocardiomicina mediante el estudio de sus espectros de RMN monodimensionales de protón y carbono-13, la descripción de los sistemas de espín del compuesto mediante los experimentos ^1H - ^1H COSY y HSQC editado y la conexión final de los sistemas de espín mediante el experimento HMBC.

También realicé la determinación de la estructura tridimensional junto con el Dr. Fuentes-Monteverde, concretamente hice la búsqueda conformacional de los posibles diastereoisómeros, he aplicado las restricciones NOE para elegir los conformeros posibles e hice los cálculos computacionales DFT de cada uno de los conformeros de todos los diastereoisómeros probados. He obtenido finalmente los parámetros DP4+ para la determinación de la configuración absoluta del compuesto final.

Estos resultados darán origen a un trabajo que será sometido para publicación a una revista científica.

Variable Temperature and Solvent Dependent NMR *J*-Based Configurational Analysis for Stereochemical Determination of Flexible Acyclic Systems

Yuri Segade,^[a] María Blanco,^[a] Miriam Rega,^[a] Ramón E. Millán, Dawrin Pech-Puch, Juan Carlos Fuentes-Monteverde,^[b] Christian Griesinger,^[b] Rogelio Fernandez,^[c] Marta Pérez,^[c] Carmen Cuevas,^[c] Carlos Jiménez*,^[a] Jaime Rodríguez*^[a]

[a] Departamento de Química, Facultade de Ciencias e Centro de Investigacións Científicas Avanzadas (CICA), Universidade da Coruña. A Coruña E-15071, Spain.

[b] NMR based Structural Biology, MPI for Biophysical Chemistry, Am Fassberg 11, 37077, Göttingen, Germany.

[c] Natural Products Department, PharmaMar S.A., Pol. Ind. La Mina Norte, Avda. de los Reyes 1, 28770 Colmenar Viejo, Madrid, Spain

Email: jaime.rodriguez@udc.es; carlos.jimenez@udc.es

Keywords: NMR, conformational analysis, coupling constants, cyclopeptide

Abstract: Two different general approaches based on the change of temperature or deuterated solvents is applied to NMR coupling measurements in chiral acyclic systems. These changes cause alterations in the population of the staggered rotamers in each carbon-carbon dimethine stereogenic centers and, consequently, the set of carbon-proton and proton-proton coupling constants. The two approaches enhance the *J*-based configurational analysis (JBCA) when some rotamers of both *syn* or *anti* configurations are undistinguishable because the absence NOE/ROE. This application has been applied firstly to synthetic models and to a new marine natural product the cyclopeptide, nocardiomycin.

Introduction

Coupling constants and chemical shifts are the most widely NMR parameters used to deduce organic skeleton frameworks and three-dimensional arrangements in a molecule with an unknown stereochemistry. Several research areas account on such important experimental

data, therefore, the precise assessment of the three-dimensional features is critical because all chemical or biological properties are entirely dependent on the chirality of the substance. Usually, awareness of the stereochemistry is appreciably more puzzling than that of synthetic organic compounds due to the reduced amounts of sample available, sometimes having been isolated from unusual sources or from species challenging to collect. Besides the correct assignment of stereochemistry is indispensable for a whole characterization of new drug candidates and it is key for a correct synthesis and the development and further regulatory documentation to prove the structure of the compound.

This intricate task becomes a challenge, and sometimes is the bottleneck in the full characterization, when a compound contains flexible moieties, such as polysubstituted open acyclic chains. Along with the anisotropic Residual Chemical Shift Anisotropy (RCSA)^[1-5] and Residual Dipolar Couplings (RDC)^[6-11] approximations, or the use Universal NMR databases,^[12] some isotropic approaches

have becoming very popular in the last years to study the relative stereochemistry in these acyclic compounds. A key paper published in 1999 by Murata and Yasumoto formalized^[13] a new robust and logical methodology known as *J*-based configurational analysis (JBCA)^[14–17] which, since then, has been commonly incorporated in the “spectroscopic toolbox” of all research groups involved in the organic structure elucidation field.

The methodology is based on the general use of the proton-proton ($^3J_{HH}$) and carbon-proton coupling constants ($^3J_{CH}$ and $^2J_{CH}$) and it has been applied with great success in dimethine systems that contain 1,2 and 1,3 hydroxyl,^[18–22] hydroxymethyl, amino^[23–28] or chlorine^[20,29] substituents attached to stereogenic carbons. To obtain $^3J_{CH}$ and $^2J_{CH}$ data, NMR experiments such as *J*-HMBC, HSQC-TOCSY type or HSQMBC^[30–32] and the development of new NMR pulse sequences has greatly improved the way in having reliable data. A quantitative improvement of the JBCA was developed by Bifulco, Gomez-Paloma and co-workers including the use of *ab initio* DFT methods to calculate *J*-coupling values of all possible stereoarrangements and, subsequently, being compared to the experimental set of coupling constants.^[33,34] There are many examples in the literature where the relative stereochemistry of molecules were easy solved because the dimethine stereogenic carbon-carbon frameworks fully satisfy the original Murata’s methodology. For the purpose of this paper we will classify them as *Murata-models*. When this type of equilibrium subsists between two rotamers with large and small couplings, an averaged value (medium) is observed. As is depicted in Figure 1 only the positive gauche (G^+) and the anti (*A*) rotamers, or negative gauche (G^-) and *anti* conformer equilibria of both *syn* and *anti* configurations will be distinguishable (sets of yellow tags in Figure 1). Yet again, out six possible pairs of equilibrated rotamers, the G^+/G^- equilibrium in both

configurations will not be distinguished as is noted in the brown tags in Figure 1. Furthermore, there are some situations where the analysis becomes very complex because four different factors come in consideration:

a) The three staggered rotamers are present in some extent in the equilibrium, making all the coupling constants be an average (red tags in Figure 1) and therefore medium values are measured.

b) A G^+/G^- equilibrium is displayed in the C-C dimethine framework, along with the absence of either NOE or ROE that could discriminate *syn* or *anti* dispositions (brown tags in Figure 1).

c) The anti (*A*) conformers of both *syn* or *anti* configurations cannot be distinguish because the absence of NOE/ROE (pink tags in Figure 1).

d) The medium values of the coupling constants are on the edge of the small/medium or medium/large Karplus-type curves (see yellow bands of approximately 1 Hz between large and small values in Figure 2), and therefore the coupling constants cannot be unequivocally classified.

When at least one of these cases are present in the configurational analysis of a dimethine carbon-carbon framework, the relative configuration cannot be established by the Murata’s strategy and consequently, an alternative approach is necessary.

This type of systems will be classified in our methodology as Non Murata, and those are where our proof of concept needs to be affirmed. In this paper we want to introduce this new strategy based on the variable temperature NMR coupling constant measurements with the purpose in solving these drawbacks. The approach is quite simple: having in consideration that the rotamers population *will change with the temperature*, the coupling constants will undergo also a modification that can be rationalized with the appearance/disappearance of distinguished staggered conformations from the

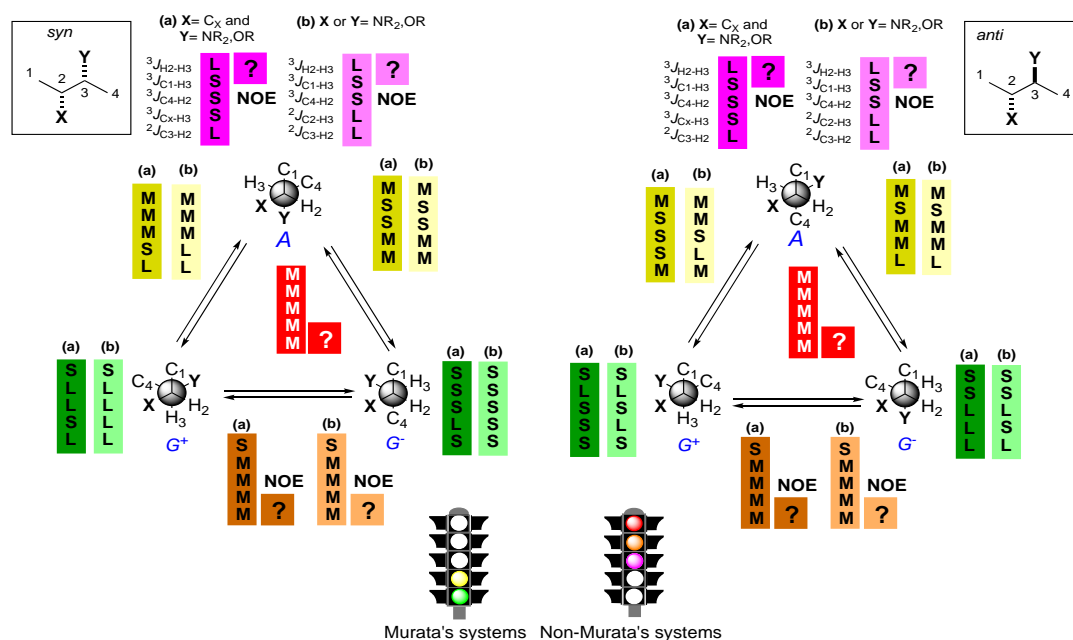


Figure 1. Fundamentals of the Murata's Methodology or *J* Configurational Based Analysis (JBCA): conformers within green (one major populated) or yellow (equilibrium of two rotamers) labels will discriminate a *syn* or *anti* configuration. Brown or pink labels cannot distinguish either *syn* or *anti* configurations, if NOE is not observed between C1, C4 or H2 and H3 no configuration can be called. Red labels give no evidences of *syn* or *anti* configuration. Values of the coupling constants: L: Large, M: medium, S (small) taken from Figure 2. Darker colours are used for (a) entries and lighter colours are used for entries (b).

anti or *syn* configurations predicted in the original Murata methodology.

This modification in the coupling constants can be also produced by changing the NMR deuterated solvent polarity, always when a clear conformation in the molecule is observed by a distinct change in the proton-proton coupling constant involved in the carbon-carbon framework.

Results and Discussion

In the structure elucidation literature, the use of the JBCA did not follow any systematized protocol, and therefore we would like to propose a nomenclature to novice users and make easier their use.

Numbering and classifying methine-methine or methine-methylene frameworks with stereogenic centers.

As starting point, we suggest building sets of label-tags of each methine-methine or

methylene-methine arrangements following the next criteria: within the carbon-carbon skeleton already numbered (e.g, C1-C4, methine protons located at positions 2 and 3), we will organize the tag beginning with the homonuclear proton-proton coupling ($^3J_{H2-H3}$), followed by the alphabetically list of three bonds carbon-proton couplings ($^3J_{C1-H3}$, $^3J_{C4-H2}$, and $^3J_{CX-H2}$), concluding by the two bond couplings ($^2J_{C3-H2}$ see entries (a) in Figure 1). The tag when two heteroatoms (nitrogen or oxygen) are attached to C2 and C3 will be constructed with one $^3J_{HH}$, three $^3J_{CH}$ and two $^2J_{CH}$ couplings. Consequently, the tag will be arranged as follows: $^3J_{H2-H3}$, $^3J_{C1-H3}$, $^3J_{C4-H2}$, $^2J_{C2-H3}$, $^2J_{C3-H2}$ (see entries (b) in Figure 1).

Also, a terminology based on colors may well be very informative: when green or yellow tags are used, we will be in the presence of a carbon-carbon dimethine dichiral centers that follows simple Murata's rules (standard JBCA analysis).

When brown, pink or red tags are employed, no easy guidelines can be followed and therefore the J -based configurational analysis cannot be easily applied. In summary, it is easy to recognize that brown, pink or red tags mean *Non-Murata's* systems, and yellow or green *Murata's* systems. At the present is very important to distinguish those carbon-carbon bonds within just a heteroatom in the framework (either oxygen or nitrogen (a), entries depicted in darker colors in Figure 1,) and those with two heteroatoms in positions 2 and 3 ((b), entries showed in lighter-colored tags in Figure 1).

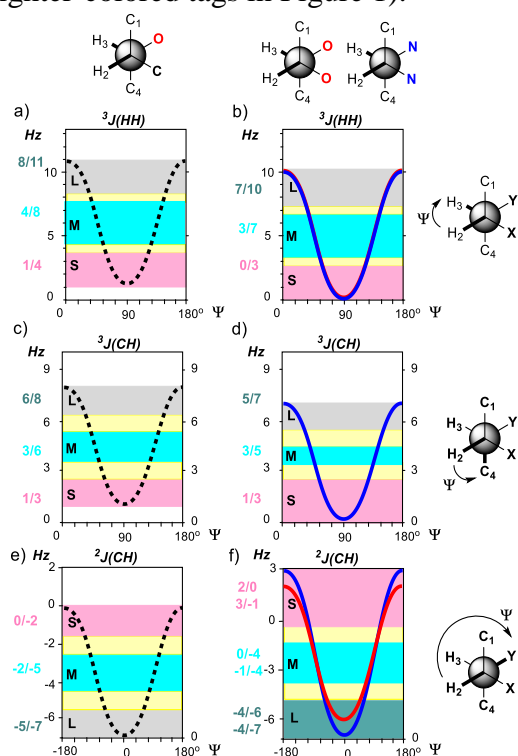


Figure 2. Large (L), medium (M) and small (S) J values as function of dihedral angles (Ψ) in 1,2-dimethine systems. The two curves in each a)-f) representations report the maximum and minimum expected values. (Ref [35]). Yellow bands are 1 Hz wide and states uncertainty between small/medium or medium/large values. In d) blue curve represents the expected values for a 1,2-dimethine diaminated system.

Proton-proton and carbon-proton coupling constant measurements, using different 2D-NMR methods based either on HMBC

or HSQC-TOCSY pulse sequences, need to be measured at room temperature. Then the values of the coupling constants have to quantitatively classify as small (S), medium (M) or large (L) by use of Karplus type equations (see Figure 2). This step will complete the tag for each carbon-carbon framework. At this point is easy to diagnose each system as one conformer, a mixture of two conformers or a complex mixture of three. Just with the yellow or green tags used in Figure 1, the relative stereochemistry can clearly identified as *anti* or *syn*. The problem arises when brown or pink tags are describing the rotamers, hence the relative stereochemistry cannot be addressed.

How to alter the conformational equilibrium? The new variable temperature coupling constants measurements approximation (VT-JBCA).

The new methodology is based in the modifications that we can introduce in the system, by changing the temperature, therefore also in both proton-proton and carbon-proton coupling constants. This general strategy would complete our previous work that involved the aptitude of the NMR J values in becoming larger or smaller at lower temperatures, when a complex equilibrium between staggered conformers (red tags) and being simplified. The alteration in the relative population towards to a most stable staggered conformer is showed in each coupling constant becoming larger or smaller in absolute value.^[36] In this way, an expected trend for a labeled tag can be found for the coupling constant values of a particular rotamer, with changes from medium values in complex equilibrium becoming smaller or larger depending of the coupling constant.

In other hand when just one undistinguishable *anti* staggered conformer (A) either of the *syn* or *anti* configuration (no NOE/ROE is observed) is present in

the equilibrium, making the measurements at higher temperature will cause a change in the coupling constants, because the increase of the population on the G^+ or G^- conformers. The small changes observed it will make possible the discrimination between *anti* or *syn* configurations.

Looking for a CNMS: Synthesis of distereoisomeric models with three stereogenic centers.

There are not too many compounds with a *Non-Murata* system in their skeletons. Consequently, our first goal was to search for those compounds containing a *Non-Murata* carbon-carbon framework, namely as *Chemical Non-Murata Space* (CNMS), where some of the dimethine or a methine-methylene structure did not follow a straightforward *J*-Based Analysis.

One main characteristic is needed in this search: to reduce difficulties that can be created by hydrogen bonding between adjacent hydroxyl and/or amino groups, we have selected a series of compounds with oxygen or amino protected groups. This strategy precludes us in having possible non-staggered rotamers due to the mentioned hydrogen bonding interactions.

Three different sets of synthetic models were used for our goals. a) 1,2,3-trimethine stereogenic systems (models **1-6**, **19**, and **20** in Figure 3) in all possible *anti-anti*, *syn-syn*, *anti-syn* and *syn-anti* configurations, b) 1,2,4-trimethine dispositions where a methylene moiety was placed in the middle of two stereogenic centers (see models **7-10**), c) 1,2,3 dimethine stereogenic centers with two oxygenated and a carbon-carbon framework (models **11-18** in Figure 3), and d) models within two nitrogenated stereogenic centers separated by an methylene (models **19** and **20**).

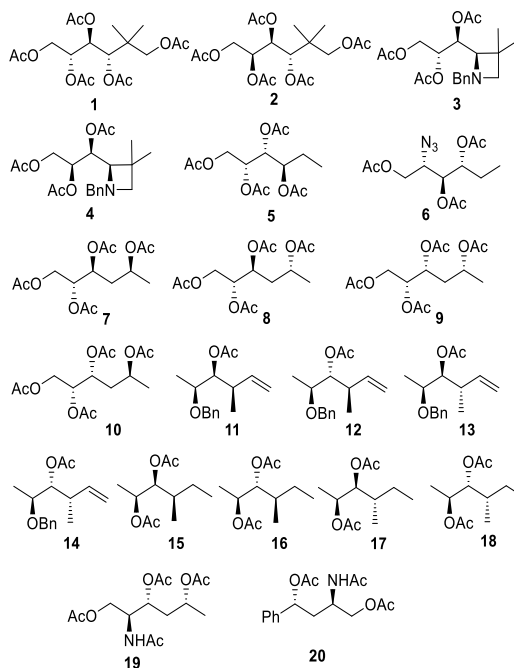


Figure 3. Looking for a *Chemical Non-Murata Space* (CNMS): 1,2,3 and 1,2,4-trimethine models used.

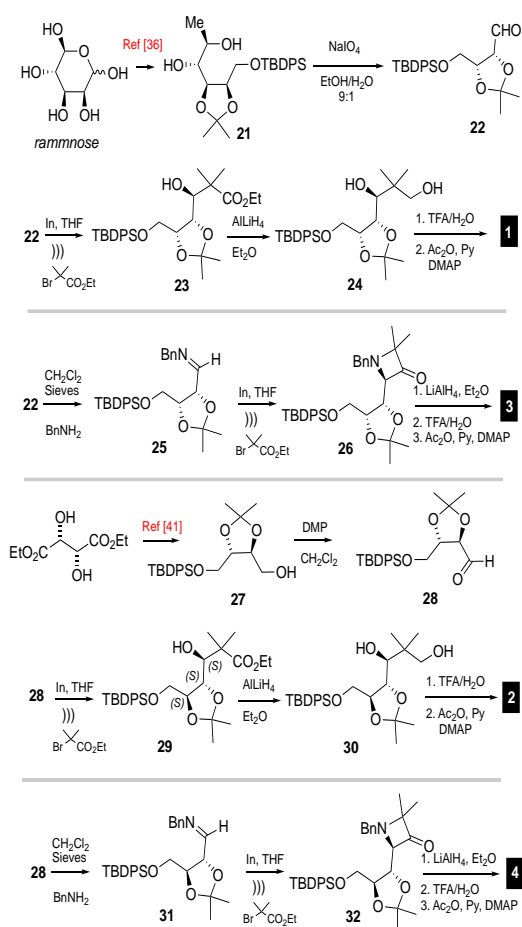
a. Synthesis of 1,2,3-trimethine systems with C-O or C-N stereogenic centers.

Following our synthetic studies of indium in carbohydrate chemistry,^[37–40] we wanted to make use the presence of several centers in such carbohydrate framework to create stereochemical diversity. We found a highly diastereoselectivity when the ethyl α -bromoisobutyrate reacted with the aldehyde **22**^[41] with in powder, to create three stereocenters in a controlled manner (compound **23**) which were easily converted in our model **1** with all the hydroxy groups protected as acetates. Same distereoselectivity was observed in the imine **25** to easily access to three-stereogenic-centers model with an 1,2,3-trimethine aminodihydroxy framework in a 1,2-*anti*, 2,3-*syn* disposition (see Scheme 1, compound **3**).^[38]

Compounds **2** and **4** were also synthesized via aldehyde **28** using a similar set of reacciones, but coming from aldehyde **28** and iminodioxolane **31**, respectively.^[42]

A practical synthesis for models **5** and **6** (see Scheme 2) was planned based on the alkylation of the epoxide **33** following a

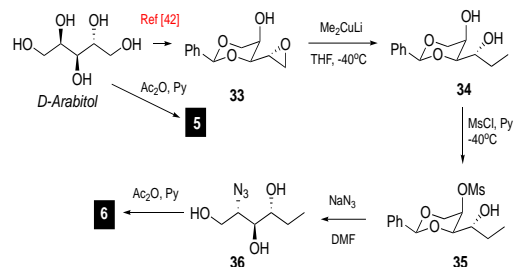
similar procedure used by the synthesis of the immunosuppressive glycolipid OCH. [43].



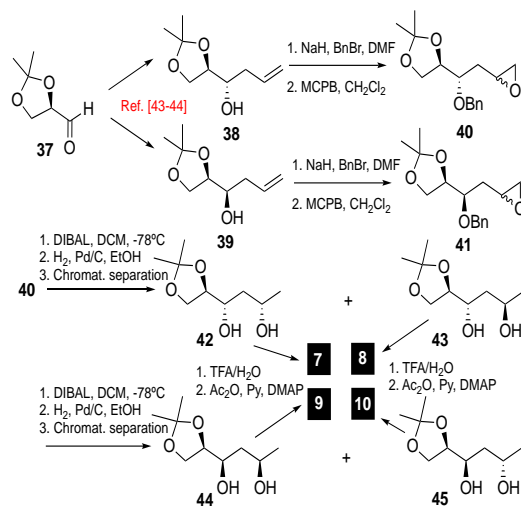
Scheme 1. Synthesis of 1,2,3-trimethime models **1-4** with C-O bonds.

b. Synthesis of 1,2,4-trimethime systems with C-O stereogenic centers.

Looking for more chemostereodiversity, all possible *syn-syn*, *anti-syn* and *anti-anti* 1,2,4 triols **7-10** were obtained from the homoallylic alcohols **38** and **39** in a similar way developed by Kishi in the synthesis of the mycolactones (see Scheme 3). [44-46] In our case the mixture 2:1 of epoxides **40** and **41**, facilitated us in having stereochemical diversity with the stereoisomers **42-45** which were converted after chromatographic separations in the desired models **7-10** once dioxolane was deprotected and the subsequent alcohols converted in acetates.



Scheme 2. Synthesis of 1,2,3-trimethime systems with C-O (**5**) and C-N (**6**) bonds.



Scheme 3. Synthesis of 1,2,4-trimethime models **7-10** with C-O bonds.

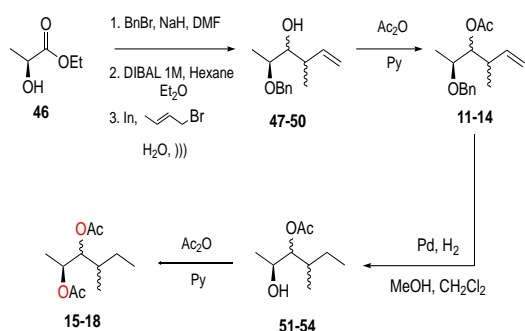
c. Synthesis of 1,2,3-trimethime systems with C-O and C-C stereogenic centers.

We wanted to complete our models with the presence of one stereogenic center without nitrogen or oxygen on it. For this purpose we fixed our attention in simple models such as **11-14**, which their syntheses were easily approached using the *anti*-selective addition of crotyl organometallic reagents to α -alkoxy aldehydes (see Scheme 4). [47,48] Consequent hydrogenation and acetylation of each diastereoisomer gave model compounds **15-18**.

d. Synthesis of models 19 and 20 with C-O and C-N stereogenic centers.

Finally we accessed to compounds **19** from L-serine following the stereoselective synthesis of 2-amino-1,4,5-hexane triols

using a L-proline catalyzed aldol reaction published by Rode et al.^[49] **20** was prepared from D-arabitol following the procedure by Tamura.^[50]



Scheme 4. Synthesis of 1,2,3-trimethine models **11-18** with C-O and C-C bonds.

Classifying Murata and Non-Murata systems.

With all the 20 compounds in hand, every carbon-carbon dimethine 1,2- or 1-3 systems were studied in order to classify them whether or not present set of coupling constants that follows Murata methodology. For this purpose all heteronuclear coupling constants were extracted by either HSQC-HECADE-spectrum (*heteronuclear couplings from ASSCI-domain experiments with E.COSY-type cross-peaks*), HETLOC or *J*-HMBC experiments.^{23,24}

Each carbon-carbon framework was then classified following the abovementioned nomenclature based on colors: green, yellow, brown, pink, and red tags. Specifically, *A* conformers are tagged with pink colors, meaning they are undistinguishable in both *syn* or *anti* configurations. We found also a different situation when the equilibrium between both *G*⁺ and *G*⁻ conformations are present. Then a set of values SMMMM does not discriminate the anti or syn configuration (in absence of NOE or ROE). This carbon-carbon framework will be tagged with brown colors in our system. Finally, red tags will be representative of all medium coupling constants values and therefore a

very complex mixture in the equilibria of conformers.

Out of 45 carbon-carbon dimethine or methine-methylene frameworks analyzed, we found 12 situations within the presence of just one rotamer (green tags), 18 equilibria between anti-gauche (+) or anti-gauche (-) rotamers, 3 with three rotamers in the equilibrium, and 11 frameworks were *syn* or *anti* configurations that cannot be concluded because the indistinguishable conditions of *A* conformers or an equilibrium between both frameworks analyzed, we found 12 situations within the presence of just one rotamer (green tags), 18 equilibria between *A/G*⁺ or *A/G*⁻ rotamers, 3 with three rotamers in the equilibrium, and 11 frameworks were *syn* or *anti* configurations that cannot be concluded because the indistinguishable conditions of *A* conformers or an equilibrium between both *G*⁺/*G*⁻ dispositions. Therefore, we have conquered a good *Chemical Non-Murata Space*, where, somehow in those situations, red, pink, brown tags, need to be distinguished in order to be solved.

In our previous paper,^[36] we have solved the case of the red tags running the measurements of the carbon-proton coupling constants at low temperature. This situation can be deciphered by observing the variation in the coupling constant values from *rt* to lower temperatures because of the alteration in the relative population towards the most stable staggered conformers.

In this way, the coupling constant values were modified by the appearance of a particular rotamer at lower temperature, which turn the medium values observed to larger or smaller. Consequently, observing the tendencies of the coupling constants the rotamers can be discriminated.

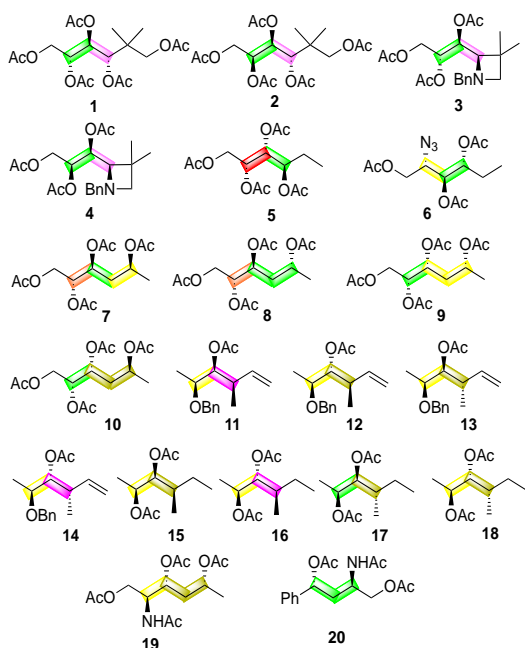


Figure 4. Tagging C-C dimethine systems: Green and yellow tags are single or two isomers as in Figure 1. Red tags are complex rotamer equilibrium, brown or pink tags are indistinguishable situations. Darker colours are used for (a) entries in Figure 1 and lighter colors are used for entries (b) in Figure 1.

A different approach is needed when pink tags describe the carbon-carbon framework. With an anti conformer (*A*) in place, with absence of additional NOE data, the configurational analysis cannot be addressed because the two indistinguishable conformers. Raising the temperature, this unique conformer will be in equilibrium with the distinguishable G^+ or G^- conformers (from *anti* or *syn* configuration), therefore we will notice a change in the coupling constants values. This is the proof of concept we want to demonstrate in our Variable-Temperature J-Based Configurational Analysis (VT-JBCA, see Figure 5).

From the 45 carbon-carbon framework we analyzed, we came across with two different cases of indistinguishable labels (Non-Murata models).

a) Non-Murata Models with an equilibrium between Gauche Conformers (G^+/G^-) (Brown tags).

A first case found was the C2—C3 bonds of compounds **7** and **8**, in which an equilibrium between G^+ and G^- was observed. In those cases, to deduce the relative stereochemistry, we have to trigger a shift in such equilibrium in order to know the principal gauche conformer, which has a unique label. For this purpose, lowering the temperature should result in a variation in the values of the coupling constants due to the relative population change of the equilibrium rotamers towards the more stable. This modification of the coupling constants would allow us to deduce which conformer would be the predominant in the equilibrium, leading us the assignment of the relative stereochemistry of the fragment C—C of study. The key strategy of this method implies to those constants that at ambient temperature have medium values (M), at lower temperatures we will observe a tendency in changing into larger or smaller values (in absolute value). As a model, its application is explained in compound **8**, which around the C2-C3 bond presents the same label for the configuration *syn* or *anti*: SMMMM.

The ^1H , HSQC-HECADE and J-HMBC experiments were conducted at low-temperature (207K) to observe the trend of the medium values of the coupling constants and therefore to resolve their relative stereochemistry. Toluene- d_8 was used as a deuterated solvent, because its low melting point of -95°C , allowed us a wide margin to low the temperature. The ^1H NMR spectra showed $^3J_{\text{H2-H3}}$ became smaller (from 3.5 Hz at *rt* to 2.9 at 207K), while $^3J_{\text{C4-H2}}$ measured from a HSQC-HECADE and J-HMBC experiments is shifting from 2.8 Hz at *rt* to 1.3 Hz at 207K and $^2J_{\text{C2-H3}}$ from -2.8 Hz at *rt* to -4.2 Hz at 207K) clearly indicates the apparition of the conformer G^+ of the *anti* (as expected) configuration (see Figure 6).

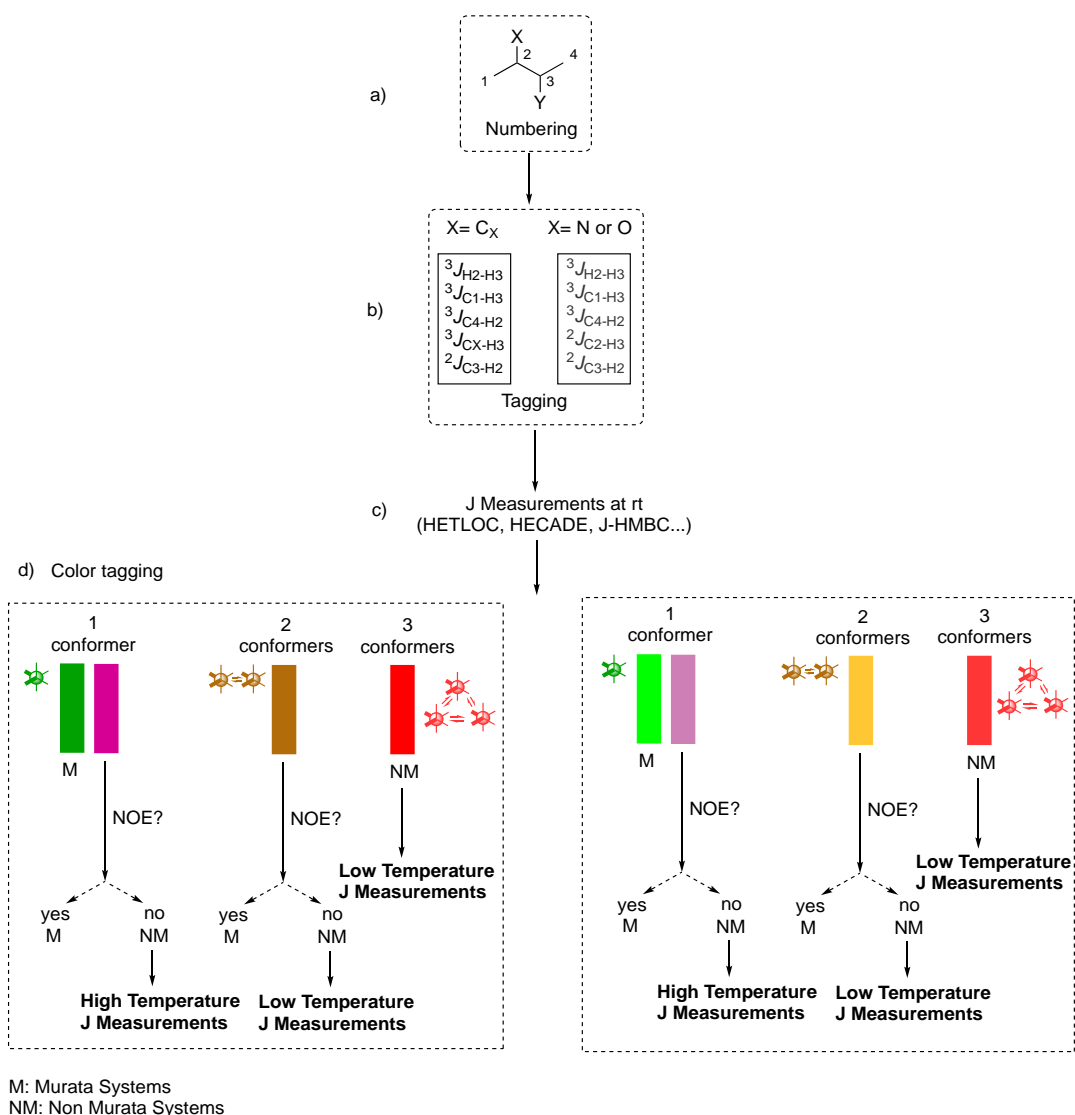


Figure 5. Summary of the VT-JBCA methodology.

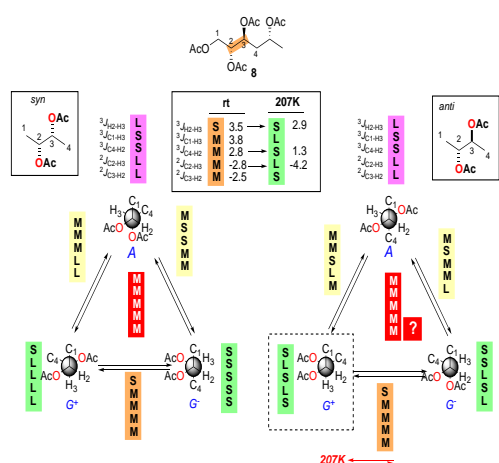


Figure 6. Resolution of a Non-Murata Model (bond C2-C3 in **8**) with an equilibrium between Gauche Conformers (G^+/G^- , brown tags). Measurements of the coupling constants in Hz were made at 207K in C₇D₈.

b) Non-Murata Models with the presence of an anti conformer (A) with absence of NOE/ROE (pink tags).

A second case found around the C3-C4 bond of compounds **1**, **2**, **3** and **4**, in which the presence of a major conformer is observed, the anti-periplanar arrangement between H-3 and H-4, but with indistinguishable labels for relative configuration (conformers **A** in Figure 1). In these cases, the measurements of the low-temperature constants would not be useful, because there is already a single conformer. However, when the temperature increases a second conformer in the equilibrium should appear which

would produce a variation in the values of the coupling constants. The key to this method, as in the case of low temperature, lays in how the trend of the coupling constants values shift to larger or smaller. Following is the procedure to resolve a Non-Murata system existing in the C3-C4 bond of the synthetic model **1**, in which the large value observed for ${}^3J_{\text{H3H4}}$ (6.5 Hz) indicates that both protons are in anti-periplanar arrangement, therefore only conformers A in both *syn* or *anti* configuration can be account for. As for heteronuclear carbon-proton constants, their small values indicate a synclinal arrangement of C-2 with respect to H-4 and C-5 with respect to H-3. Finally, the large values of ${}^2J_{\text{CH}}$ heteronuclear constants show that the electronegative atom (O) is also in synclinal disposition to H-3 and H-4. All these relationships are met for conformers A (pink tags in Figure 1) and since they cannot be differentiated, the C3—C4 bond corresponds to a Non-Murata system.

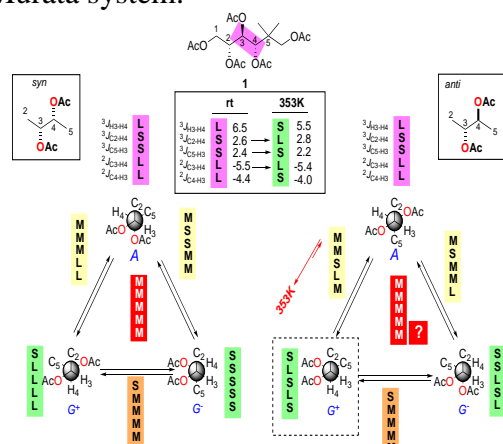


Figure 7. Resolution of a Non-Murata Model (bond C3-C4 in **1**) with the presence of one conformer (A, pink tags). Measurements of the coupling constants in Hz were made at 353K in DMSO- d_6 .

DMSO- d_6 measurements of the coupling constants of the C3-C4 bond at 353K shows a clearer shifting from the A conformer to the G^+ of the anti configuration (see Figure 6). All the coupling constants were trending to smaller, larger, smaller, larger, smaller tag

represented for the green tag of the G^+ conformer. Just a value gets out of the expected trend, ${}^2J_{\text{C3-H4}}$, becoming almost the same value from -5.5 to -5.4 Hz. In this case both values are similar but seems reasonable, that even though both are large (in absolute value) the coupling constant for the G^+ conformer is smaller in relation to that of the A conformer. In order to confirm this assumption, we made theoretical DFT calculations of the coupling constants for ${}^2J_{\text{C3-H4}}$ for both A and G^+ conformers following Serianni recommendations.^[51] We observed smaller values for the case of the G^+ conformer, which explains the diminishing of the coupling constant.

Changing the polarity of the NMR solvent. The Solvent Dependent approximation.

The same conformer “equilibrium-shifting” monitored with the change of temperature, can be observed when coupling constant measurements are made in a different NMR deuterated solvent. This change of solvent polarity modifies the conformation of the molecule and therefore dihedral angles responsible for the coupling constants. In this case the rule of thumb is observing a evident change in the ${}^3J_{\text{HH}}$ implicated in the C-C dimethine bond.

As a proof of concept we have applied the methodology to synthetic model **2** again for C3-C4 bond, which as it was discussed before for compound **1**, exhibits a Non-Murata behavior in absence of NOE or ROE. A pink tag was assigned for this bond and therefore rising the temperature the relative stereochemistry of both stereogenic centers can be elucidated. However, when we change the deuterated solvent from DMSO- d_6 to CDCl_3 a small change from 8.0 to 7.5 Hz was observed in the ${}^1\text{H}$ NMR spectrum for ${}^3J_{\text{H3-H4}}$. Surprisingly, the initial pink tag LSSLL evolved to the green label SLSLS, the gauche(-) conformer of the anti

configuration that resolves the relative stereochemistry of C3-C4.

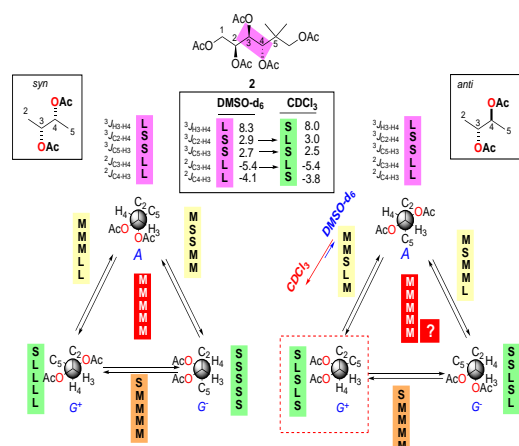


Figure 8. Resolution of a Non-Murata Model (bond C3-C4 in **2**) by changing deuterated solvent from DMSO-d₆ to CDCl₃ at 600 MHz and *rt*.

Applying the method to solve the absolute configuration of a natural compound. The case of the marine cyclopeptide nocardimycin.

We want to apply the new approximation to a natural compound with a problematic of a C-C dimethine stereocluster. This is the case of the cyclopeptide nocardimycin produced by the marine actinobacteria *Nocardioopsis halotolerans* 99.69 % PH-05-TS1-041, isolated from the sponge *T. swinhoei*, collected near Gloriosos Islands in the Indian Ocean. The fermentation broth was extracted and after successive bioassay-guided chromatographic purifications and the pure compound finally isolated by semi-preparative HPLC chromatography. Nocardimycin (**55**) was obtained as a white amorphous solid with a molecular formula C₂₄H₃₉N₃O₆ determined by the [M+Na]⁺ ion peak at *m/z* 488.2727 detected in its (+)-HRESIM spectrum (calculated for C₂₄H₃₉N₃O₆Na, 488.2737, 7 degrees of unsaturation). The peptide nature of this natural compound was suggested by the three nitrogen atoms present in its molecular formula, along with the four *sp*² carbon signals between δ_C 166.9 and 169.1 observed in its ¹³C NMR

spectrum (Table S1 suppl. material). The presence of only three amide NH signals at δ_H 9.20, 8.22, and 7.67 observed in the ¹H NMR spectrum run in DMSO-d₆ of **55**, suggested the existence of four cyclically modified amino acids.

Extensive analysis of the 2D NMR experiments of **55** including COSY, TOCSY and HSQC, revealed the presence of four spin systems corresponding to two standard amino acid Gly (glycine), Val (valine), one unusual amino acid [APDAc (4-aminopenta-2,4-dienoic acid)] and two hydroxyl acids [HMDMNAa (3-hydroxy-2-methoxy-4,6-dimethylnonanoic acid), these fragments were correlated using HMBC experiments to get a new structure of cyclopeptic nature with five stereogenic centers, H2(Val), H2 (HMDMNAa), H3 (HMDMNAa), H12 (HMDMNAa) and H14(HMDMNAa) (Figure 9).

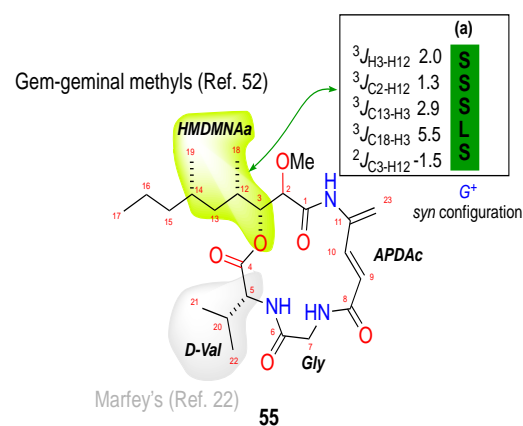


Figure 9. Planar structure of nocardimycin (**55**). The absolute stereochemistry of the D-Val was decided by Marfey's method. The relative configuration for the C3-C12 bond was deduced by the presence of the green tag belonging to the G⁺ of the syn configuration (see entries (a) in Figure 1)

The NOESY correlations from H5 (Val) at δ_{H} 4.31 to H3 (HMDMNAa) at δ_{H} 5.16 and H12 (HMDMNAa) at δ_{H} 2.19 to H14 (HMDMNAa) at δ_{H} 1.56 indicated that these protons were in the same face of the molecule. The relative configuration from H12(HMDMNAa) and H14 (HMDMNAa) was established in *syn* position using the methodology of direct assignment in 1,3-dimethyl systems (Figure 2).^[52] The absolute configuration of D-Valine was determined by comparing the hydrolysis products of **55** (6 N HCl, 110 °C, 18h), after derivatization with Marfey's reagent ((N-(3-fluoro-4,6-dinitrophenyl)-L-alaninamide, L-FDAA), with appropriate amino acid standard using HPLC-MS chromatography.^[22]

The relative configuration of the C3-C12 bond was easily deduced because the presence of an unique G^+ conformer of the *syn* disposition (Murata system). At this point just the C2-C3 bond remains to be known, and as we have proceeded in all the compounds, this C2-C3 was tagged-classified on basis of the coupling constants measured in DMSO-d₆. Surprisingly, we came across to an A conformer, which we were not able to discriminate either its *syn* or *anti* configuration because the complete absence of NOE data between protons present in the C2-C3 framework. This is the case we are looking for to apply either the VT-JBCA approximation or the solvent dependent JBCA analysis. After HSQC-HECADE and *J*-HMBC experiments were performed at 358K, we observed the change on coupling constants that clearly pointed out the apparition of the G^+ conformer belonging to the *anti* configuration (see Figure 10).

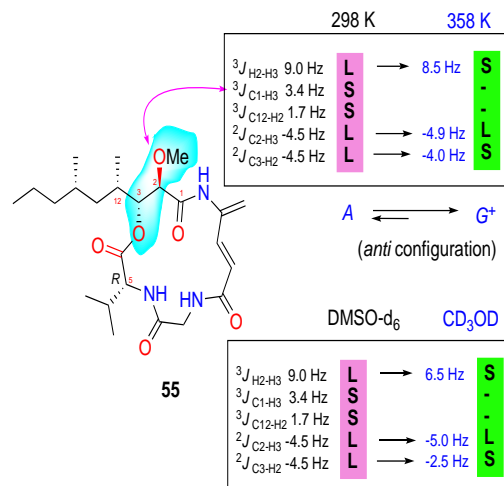


Figure 10. VT-JBCA applied to the C2-C3 bond of nocardimycin (**55**). The high temperature measurements were made at 500 MHz in DMSO-d₆. The change of solvent approximation was run in CD₃OD.

Very interestingly, when we run the NMR experiments at CD₃OD we observed a huge change in the coupling constant for $^3J_{\text{H2-H3}}$ (9.0 Hz in DMSO-d₆ and 6.5 Hz in CD₃OD, which is the rule of thumb we are looking for good resolution. The changes were observed also in the $^2J_{\text{C2-H3}}$ and $^2J_{\text{C3-H2}}$ becoming larger and smaller as the G^+ conformer of the *anti* configuration comes to be a part of the equilibrium of both conformers.

Finally, we were able to connect H5 to H3 and H12 thru NOESY correlations, which completes the absolute configuration of this new compound as 2*R*, 3*R*, 5*R*, 12*S*, 14*S*.

DP4+ calculations of four diastereoisomers **55a** (2*R*,3*R*,5*R*,12*S*,14*S*), **55b** (2*R*,3*R*,5*R*,12*S*,14*S*), **55c** (2*R*,3*R*,5*R*,12*S*,14*S*), **55d** (2*R*,3*R*,5*R*,12*S*,14*S*) submitted to a restricted conformational search using NOE and ROE distance and dihedral angles were classified by energy and frequencies using the B3LYP27/6-31+G(d,p) functional. Finally, the combination MPW1PW9128/6-311+G(2d,p)-polarizable continuum model was used for proton and carbon chemical shift calculations. The sets of ¹H and ¹³C

chemical shifts were compared by mean absolute error (MAE), R_2 of $\delta_{\text{calcd}}/\delta_{\text{expt}}$, by the linear regression of calculated (δ_{scaled}) and by the statistical DP4+ parameter developed by Sarotti and co-workers.^[53] A 100 % probability DP4+ value for both carbon and proton chemical shifts for **55** was in perfect agreement with the already elucidated thru our VT-JBCA and solvent dependent JBCA method as *2R,3R,12S,14S* (**55d**).

Norcardiomyacin (**55**) showed strong cytotoxic effect against antitumor cell lines with LC50 values of 1.4, 2.0 and 2.6 mM respectively against HT-29 (colon), MDA-MB-231 (breast), and A-549 (lung) cell lines.

Conclusions

We have shown how some unsolvable cases in the configurational analyses based on coupling constants (JBCA) can be accomplished using two different approaches. a) Lowering temperature and observing the trend of tendencies of the coupling constants, the equilibrium of gauche conformations can be discriminated, and therefore the *anti* or *syn* configuration in a 1,2 or 1,3 dimethine acyclic system. b) Increasing the temperature in the NMR measurements causes the appearance of an extra conformer in equilibrium with antiperiplanar conformers (*A*) which allowed us to discriminate the configuration in absence of NOE. This approximation called VT-JBCA (variable temperature -JBCA) can resolve

A similar effect can be reached, by changing the conformer populations by using two different deuterated solvents that should produce changes in the conformation of each carbon-carbon framework. These approaches complete the *J*-based configurational analysis (JBCA) when some rotamers of both *syn* or *anti* configurations are undistinguishable because the absence NOE/ROE.

Experimental Section

General Experimental Procedures.

Optical rotations were determined using a Jasco P-1020 polarimeter. UV spectra were performed using an Agilent 8453 UV-vis spectrometer. IR spectra were obtained with a Perkin-Elmer Spectrum 100 FT-IR spectrometer with ATR sampling. NMR spectra were recorded on a Varian "Unity 500" spectrometer at 500/125 MHz ($^1\text{H}/^{13}\text{C}$). Chemical shifts were reported in ppm using residual CD_3OH (δ 3.30 ppm for ^1H and 49.0 ppm for ^{13}C) and DMSO-d_6 (δ 2.50 ppm for ^1H and 39.5 ppm for ^{13}C) as an internal reference. HRESITOFMS was performed on an Agilent 6230 TOF LC/MS chromatograph spectrometer. (+)-ESIMS were recorded using an Agilent 1100 Series LC/MSD spectrometer. HRESITOFMS was performed on an Agilent 6230 TOF LC/MS chromatograph spectrometer.

Acknowledgements

This work was supported by grants RTC-2016-4611-1 from the State Agency for Research (AEI) of Spain, co-funded by the FEDER Programme from the European Union, and GRC2018/039 and ED431E 2018/03 of CICA-INIBIC strategic group from Xunta de Galicia. D.P.P. received a fellowship from the program National Council of Science and Technology (CONACYT) of Mexico and the Secretariat of Research, Innovation and Higher Education (SIIES) of Yucatan (Mexico).

Supplementary Materials: Figures S1-S10 and Table S1-S2: NMR spectra, NMR data, NMR correlations, ESIMS and DP4+ analysis.

References

- [1] G. Kummerlöwe, S. L. Grage, C. M. Thiele, I. Kuprov, A. S. Ulrich, B. Luy, *J. Magn. Reson.* **2011**, *209*, 19–

- 30.
- [2] Y. Liu, J. H. Prestegard, *J. Biomol. NMR* **2010**, *47*, 249–258.
- [3] F. Hallwass, R. R. Teles, E. Hellemann, C. Griesinger, R. R. Gil, A. Navarro-Vázquez, *Magn. Reson. Chem.* **2018**, *56*, 321–328.
- [4] N. Nath, M. Schmidt, R. R. Gil, R. T. Williamson, G. E. Martin, A. Navarro-Vázquez, C. Griesinger, Y. Liu, *J. Am. Chem. Soc.* **2016**, *138*, 9548–9556.
- [5] Y. Liu, A. Navarro-Vázquez, R. R. Gil, C. Griesinger, G. E. Martin, R. T. Williamson, *Nat. Protoc.* **2019**, *14*, 217–247.
- [6] C. M. Thiele, A. Maliniak, B. Stevansson, *J. Am. Chem. Soc.* **2009**, *131*, 12878–12879.
- [7] A. Schuetz, J. Junker, A. Leonov, O. F. Lange, T. F. Molinski, C. Griesinger, *J. Am. Chem. Soc.* **2007**, *129*, 15114–15115.
- [8] M. B. Schmid, M. Fleischmann, V. D’Elia, O. Reiser, W. Gronwald, R. M. Gschwind, *ChemBioChem* **2009**, *10*, 440–444.
- [9] C. Gayathri, N. V. Tsarevsky, R. R. Gil, *Chem. - A Eur. J.* **2010**, DOI 10.1002/chem.200903378.
- [10] P. Trigo-Mouriño, A. Navarro-Vázquez, J. Ying, R. R. Gil, A. Bax, *Angew. Chemie - Int. Ed.* **2011**, *50*, 7576–7580.
- [11] G. W. Li, H. Liu, F. Qiu, X. J. Wang, X. X. Lei, *Nat. Products Bioprospect.* **2018**, *8*, 279–295.
- [12] Y. Kobayashi, J. Lee, K. Tezuka, Y. Kishi, *Org. Lett.* **1999**, *1*, 2177–2180.
- [13] N. Matsumori, D. Kaneno, M. Murata, H. Nakamura, K. Tachibana, *J. Org. Chem.* **1999**, *64*, 866–876.
- [14] N. Matsumori, M. Murata, K. Tachibana, *Tetrahedron* **1995**, *51*, 12229–12238.
- [15] T. Nonomura, Taro; Sasaki, Makoto; Nobuaki Matsumori; Murata, Michio; Tachibana, Kazuo; Yasumoto, *Angew. Chem. Int. Ed. Engl.* **1996**, *35*, 1675–1678.
- [16] M. Sasaki, N. Matsumori, T. Maruyama, T. Nonomura, M. Murata, K. Tachibana, T. Yasumoto, *Angew. Chemie (International Ed. English)* **1996**, *35*, 1672–1675.
- [17] R. Sakai, H. Kamiya, M. Murata, K. Shimamoto, *J. Am. Chem. Soc.* **1997**, *119*, 4112–4116.
- [18] B. Göricke, M. F. Bieber, K. E. Mohr, D. Menche, *Angew. Chemie - Int. Ed.* **2019**, *58*, 13019–13023.
- [19] K. Li, Z. Liang, W. Chen, X. Luo, W. Fang, S. Liao, X. Lin, B. Yang, J. Wang, L. Tang, et al., *J. Org. Chem.* **2019**, *84*, 12626–12631.
- [20] P. Sondermann, E. M. Carreira, *J. Am. Chem. Soc.* **2019**, *141*, 10510–10519.
- [21] M. C. Kim, H. Machado, K. H. Jang, L. Trzoss, P. R. Jensen, W. Fenical, *J. Am. Chem. Soc.* **2018**, *140*, 10775–10784.
- [22] G. Tarazona, R. Fernández, P. G. Cruz, M. Pérez, J. Rodríguez, C. Jiménez, C. Cuevas, *Org. Chem. Front.* **2019**, *6*, 15–21.
- [23] Y. Tokairin, K. Maita, S. Takeda, H. Konno, *Synth.* **2014**, *46*, 351–358.
- [24] A. Ardá, J. Rodríguez, R. M. Nieto, C. Bassarello, L. Gomez-Paloma, G. Bifulco, C. Jiménez, *Tetrahedron* **2005**, *61*, 10093–10098.
- [25] A. Ardá, C. Jiménez, J. Rodríguez, *European J. Org. Chem.* **2006**, 3645–3651.
- [26] Y. Segade, M. A. Montaos, J. Rodríguez, C. Jiménez, *Org. Lett.* **2014**, *16*, 5820–5823.
- [27] A. Preciado, P. G. Williams, *J. Org. Chem.* **2008**, *73*, 9228–9234.
- [28] A. Randazzo, G. Bifulco, C. Giannini, M. Bucci, C. Debitus, G. Cirino, L. Gomez-Paloma, *J. Am. Chem. Soc.* **2001**, *123*, 10870–10876.
- [29] C. Nilewski, R. W. Geisser, M. O. Ebert, E. M. Carreira, *J. Am. Chem.*

- Soc.* **2009**, *131*, 15866–15876.
- [30] T. Parella, J. F. Espinosa, *Prog. Nucl. Magn. Reson. Spectrosc.* **2013**, *73*, 17–55.
- [31] H. Kurz Michael; Schmieder, Peter; Kessler, *Angew. Chem. Int. Ed. Engl.* **1991**, *30*, 1329–1331.
- [32] U. Wollborn, D. Leibfritz, *J. Magn. Reson.* **1992**, *98*, 142–146.
- [33] G. Bifulco, C. Bassarello, R. Riccio, L. Gomez-Paloma, *Org. Lett.* **2004**, *6*, 1025–1028.
- [34] A. E. Aliev, Z. A. Mia, H. S. Khaneja, F. D. King, *J. Phys. Chem. A* **2012**, *116*, 1093–1109.
- [35] G. Palermo, R. Riccio, G. Bifulco, *J. Org. Chem.* **2010**, *75*, 1982–1991.
- [36] A. Ardá, M. I. Nieto, M. Blanco, C. Jiménez, J. Rodríguez, *J. Org. Chem.* **2010**, *75*, 7227–7232.
- [37] L. O. H.Han, Chung; Sillerud, *Carbohydr. Res.* **1986**, *147*, 247–264.
- [38] R. G. Soengas, Y. Segade, C. Jiménez, J. Rodríguez, *Tetrahedron* **2011**, *67*, 2617–2622.
- [39] R. G. Soengas, *Tetrahedron Lett.* **2010**, *51*, 105–108.
- [40] R. G. Soengas, *Tetrahedron Asymmetry* **2010**, *21*, 2249–2253.
- [41] W. Van Brabandt, M. Vanwalleghem, M. D’Hooghe, N. De Kimpe, *J. Org. Chem.* **2006**, *71*, 7083–7086.
- [42] M. D. Smith, D. Gong, C. G. Sudhahar, J. C. Reno, R. V. Stahelin, M. D. Best, *Bioconjug. Chem.* **2008**, *19*, 1855–1863.
- [43] K. Murata, T. Toba, K. Nakanishi, B. Takahashi, T. Yamamura, S. Miyake, H. Annoura, *J. Org. Chem.* **2005**, *70*, 2398–2401.
- [44] W. R. Roush, L. K. Hoong, M. A. J. Palmer, J. C. Park, *J. Org. Chem.* **1990**, *55*, 4109–4117.
- [45] W. R. Roush, A. E. Walts, L. K. Hoong, *J. Am. Chem. Soc.* **1985**, *107*, 8186–8190.
- [46] A. B. Benowitz, S. Fidanze, P. L. C. Small, Y. Kishi, *J. Am. Chem. Soc.* **2001**, *123*, 5128–5129.
- [47] S. F. Martin, W. Li, *J. Org. Chem.* **1989**, *54*, 6129–6133.
- [48] L. A. Paquette, T. M. Mitzel, *J. Org. Chem.* **1996**, *61*, 8799–8804.
- [49] I. Kumar, C. V. Rode, *Tetrahedron Asymmetry* **2006**, *17*, 763–766.
- [50] N. Morita, K. Fukui, J. Irikuchi, H. Sato, Y. Takano, I. Okamoto, H. Ishibashi, O. Tamura, *J. Org. Chem.* **2008**, *73*, 7164–7174.
- [51] R. Stenutz, I. Carmichael, G. Widmalm, A. S. Serianni, *J. Org. Chem.* **2002**, *67*, 949–958.
- [52] Y. Schmidt, B. Breit, *Org. Lett.* **2010**, *12*, 2218–2221.
- [53] N. Grimblat, M. M. Zanardi, A. M. Sarotti, *J. Org. Chem.* **2015**, *80*, 12526–12534.

Supplementary materials

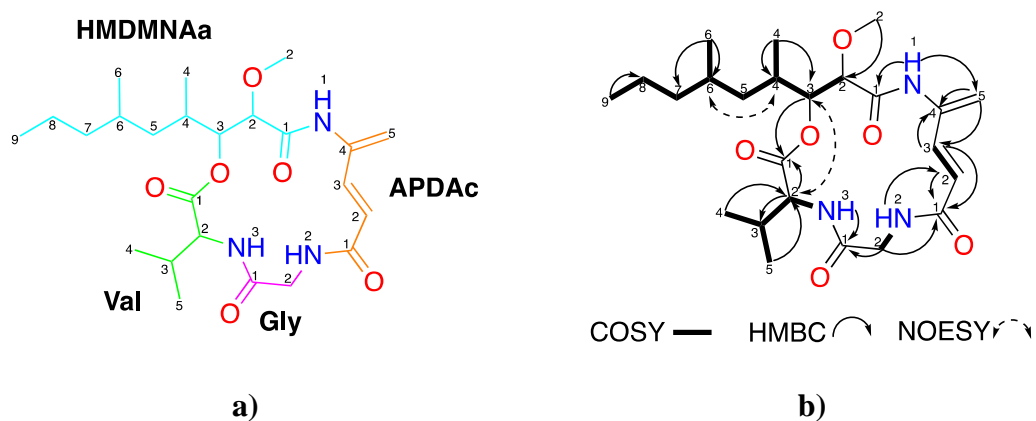


Figure S1. Structure of nocardiomycin. **a)** fragments corresponding to four cyclically-modified amino acids; **b)** key ^1H - ^1H COSY, NOESY and HMBC correlations of **55**.

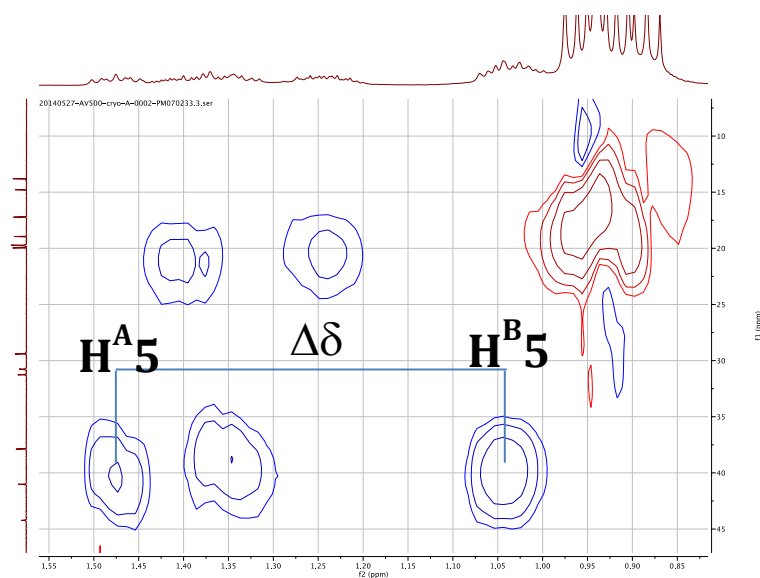


Figure S2. HSQC spectrum large coupling constant of proton $\text{H}5$ (HMDMNAa).

Table S1. NMR Data of **55** in DMSO and CD₃OD (500 MHz for ¹H and 125 MHz for ¹³C).

residue	position	DMSO		CD ₃ OD	
		δ_C , type	δ_H , mult. (J in Hz)	δ_C , type	δ_H , mult. (J in Hz)
Gly	1	168.9, C		171.4, C	
	2	44.3, CH ₂	4.02, dd (17.4); 3.59, dd (17.4)	45.5, CH ₂	4.10, d (17.4); 3.83, d (17.4)
Val	1	169.1, C		171.1, C	
	2	57.5, CH	4.31, dd (9.8)	59.2, CH	4.61, d (6.2)
	3	31.3, CH	1.98, h (6.7)	32.7, CH	2.23, m
	4-CH ₃	19.2, CH ₃	0.88, d (6.8)	19.9, CH ₃	0.97, d (6.9)
	5-CH ₃	18.2, CH ₃	0.86, d (6.8)	18.4, CH ₃	0.94, d (6.8)
HMDMNAa	1	168.0, C		171.2, C	
	2	78.9, CH	3.99, d (8.9)	81.7, CH	4.02, d (6.9)
	3	73.8, CH	5.16, dd (8.9)	76.9, CH	5.35, dd (6.9, 4.9)
	4	30.0, CH	2.10, m	32.0, CH	2.30, m
	5	40.5, CH ₂	1.26, m; 0.95, m	42.4, CH ₂	1.45, m 1.03, m
	6	28.8, CH	1.56, m	30.7, CH	1.66, m
	7	38.5, CH ₂	1.22, m; 1.02, m	39.7, CH ₂	1.32, m 1.04, m
	8	19.7, CH ₂	1.33, m; 1.22, m	21.0, CH ₂	1.41, m; 1.25, m
	9	14.2, CH ₃	0.84, t (7.3)	14.7, CH ₃	0.90, t (7.2)
	2-OCH ₃	56.9, CH ₃	3.31, s	58.1, CH ₃	3.44, s
	4-CH ₃	14.3, CH ₃	0.95, d (6.9)	15.5, CH ₃	0.98, d (6.9)
	6-CH ₃	19.4, CH ₃	0.84, d (6.6)	20.6, CH ₃	0.91, d (6.6)
APDAc	1	166.9, C		170.1, C	
	2	118.9, CH	6.10, d (15.2)	119.5, CH	6.07, d (15.1)
	3	138.1, CH	6.88, d (15.2)	141.0, CH	7.12, d (15.1)
	4	137.0, C		139.2, C	
	5	116.3, CH ₂	5.59, s 5.46, s	119.5, CH ₂	5.62, s 5.55, s
NH-1			7.67, d (7.7, 5.3)		
NH-2			8.22, d (9.8)		
NH-3			9.20, s		

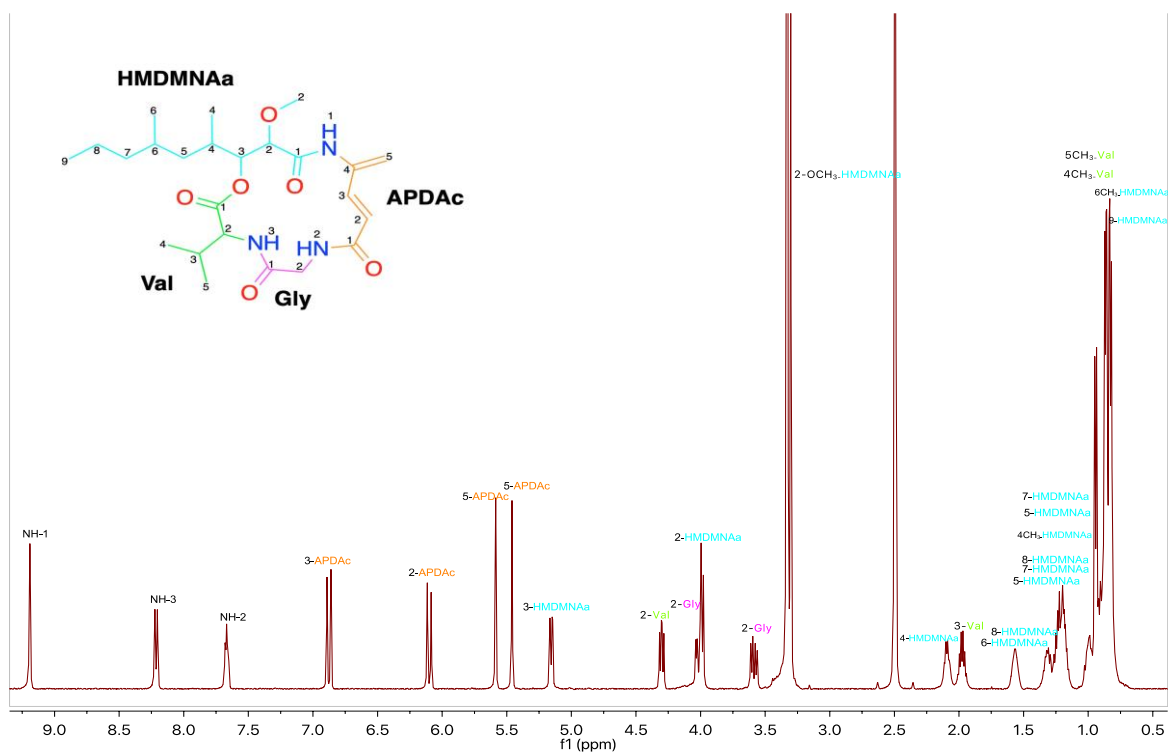


Figure S3. ^1H NMR spectrum of **55** (500 MHz, DMSO).

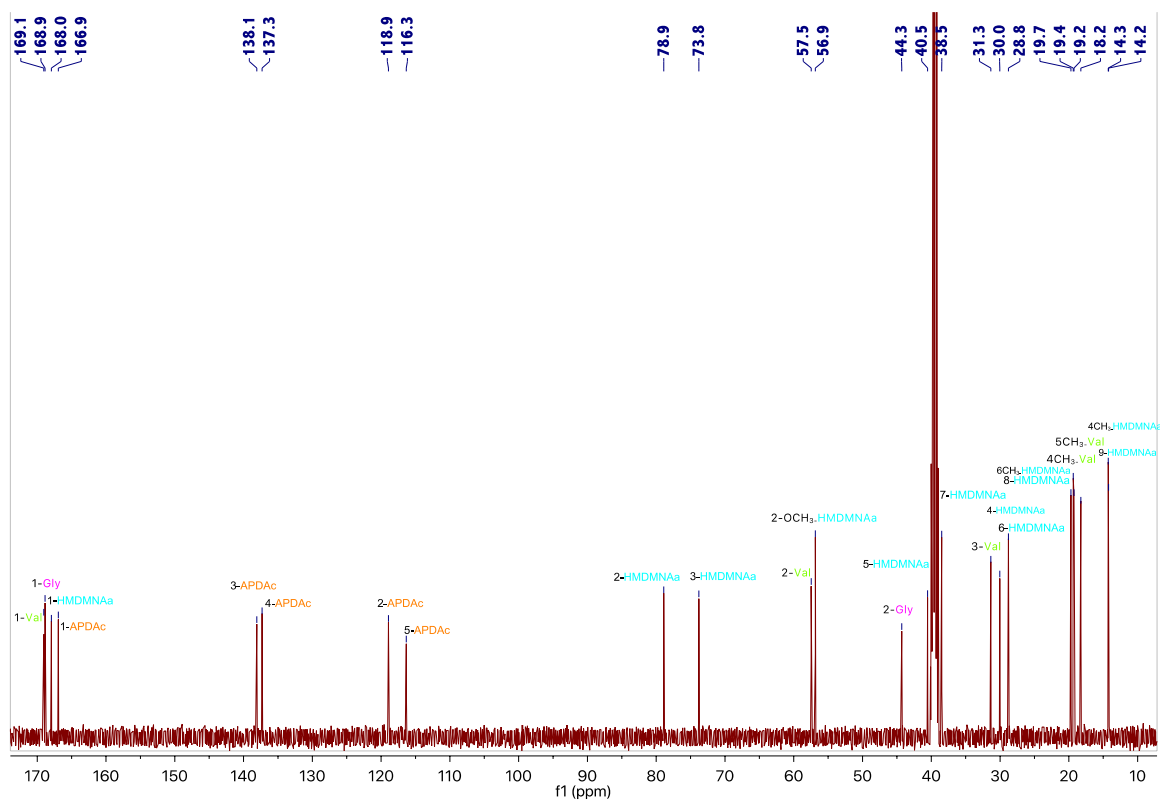


Figure S4. ^{13}C NMR spectrum of **55** (125 MHz, DMSO).

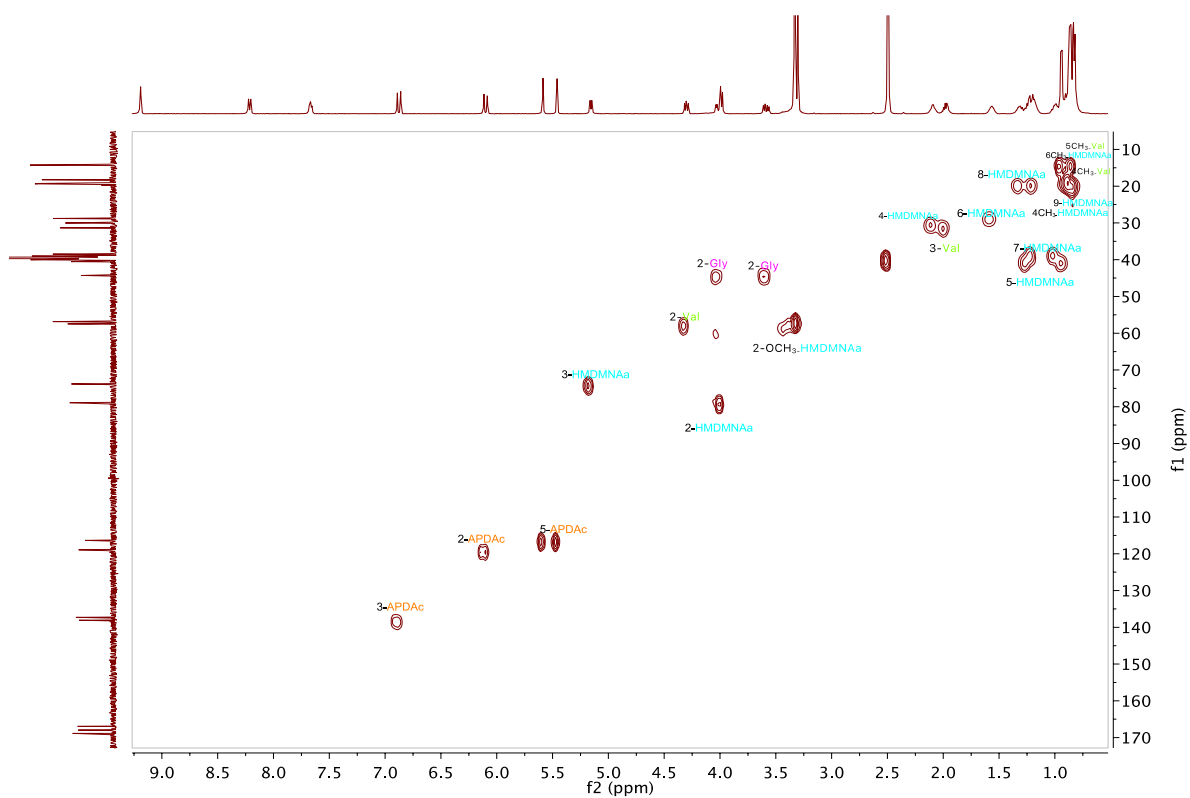


Figure S5. HSQC spectrum of **55** (500 MHz, DMSO).

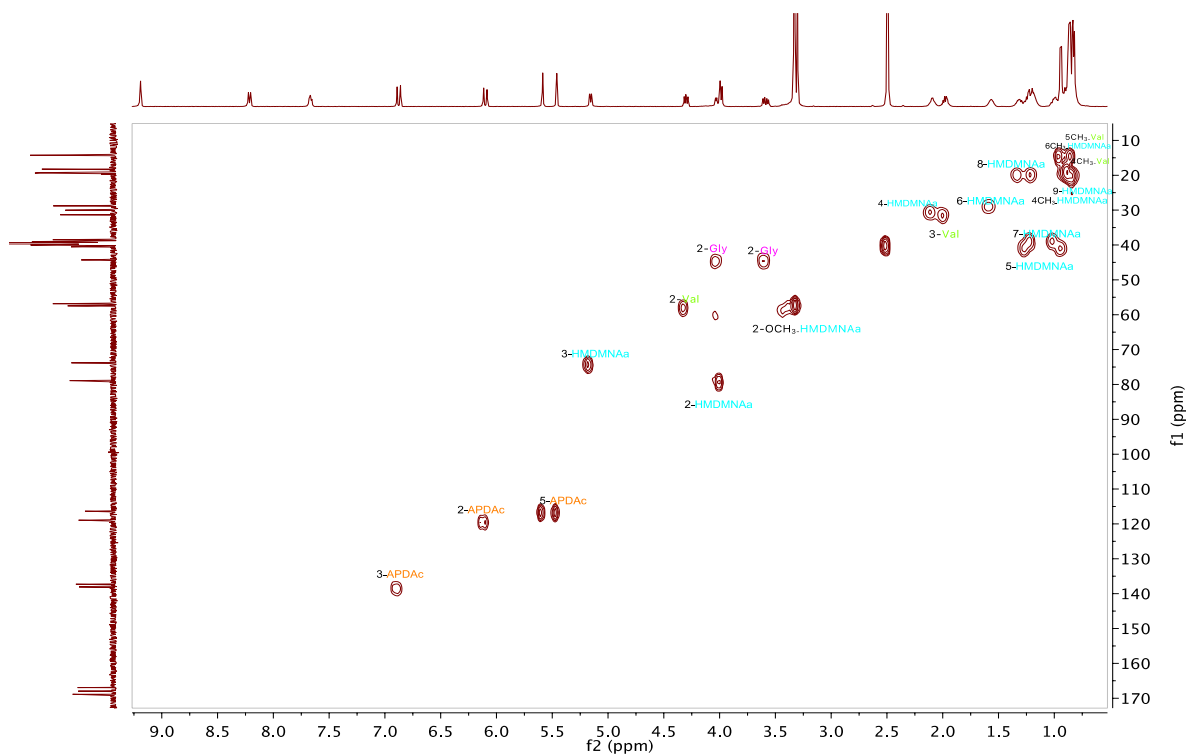


Figure S6. COSY spectrum of **55** (500 MHz, DMSO).

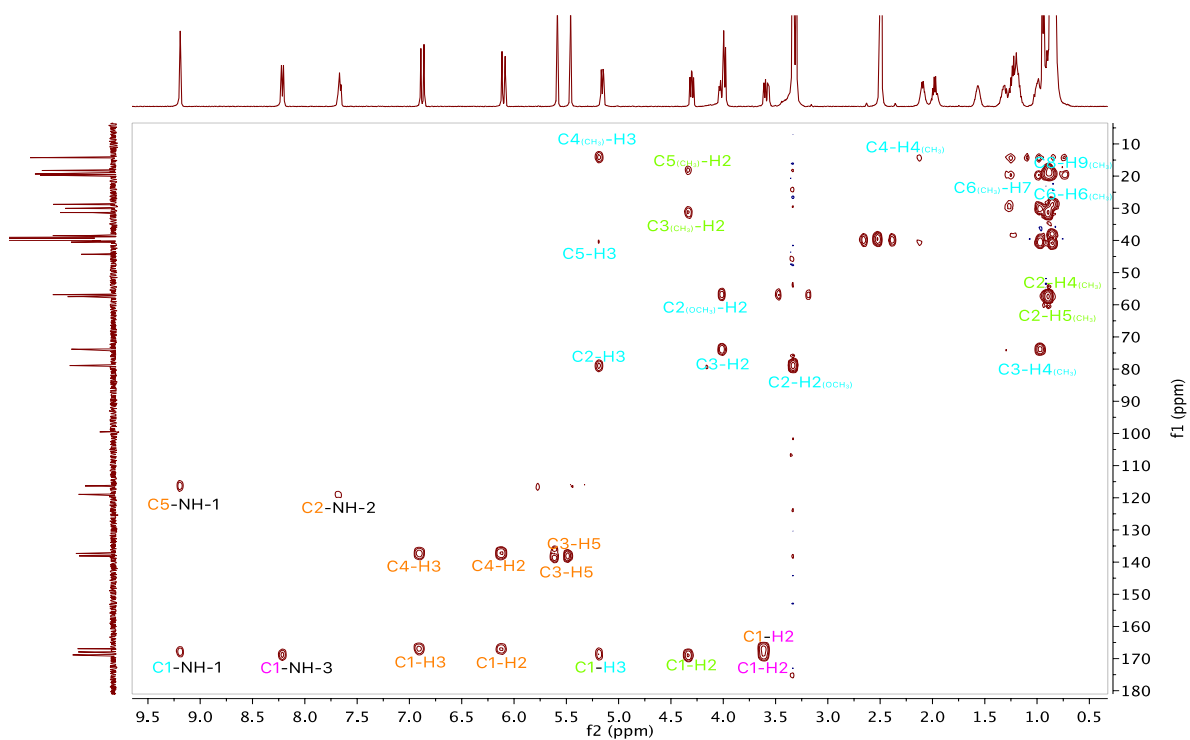


Figure S7. HMBC spectrum of **55** (500 MHz, DMSO).

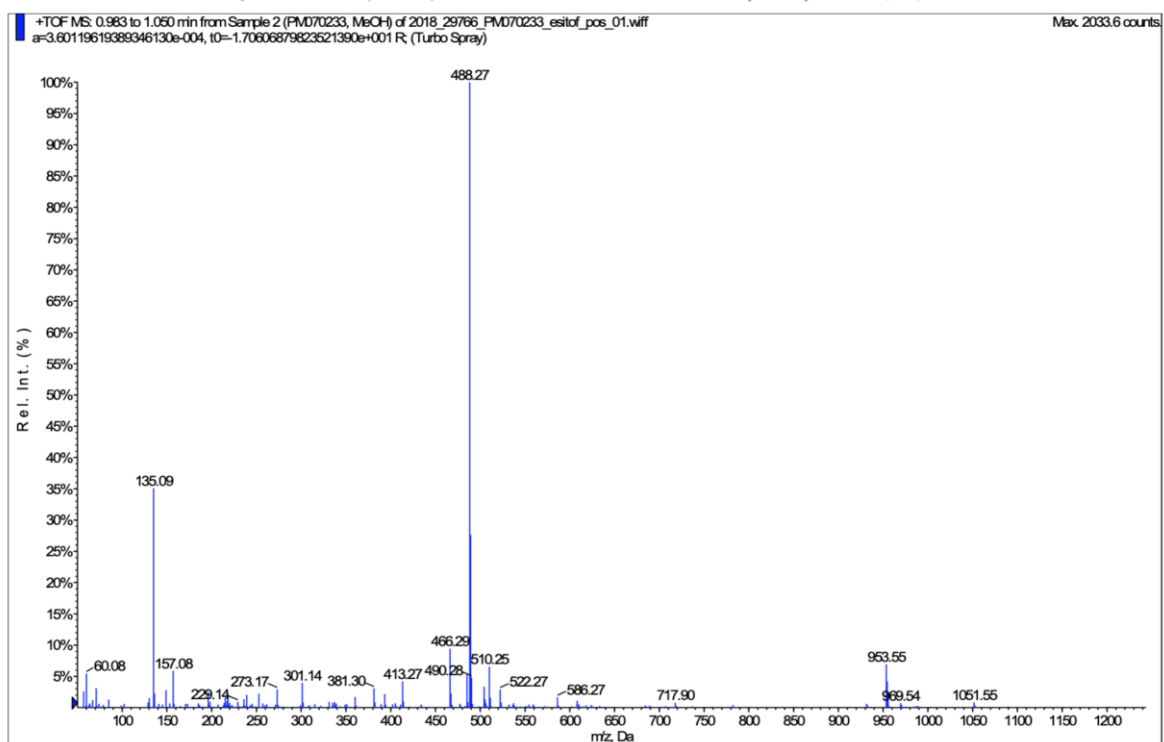


Figure S8. (+)-LRESIMS of **55**.

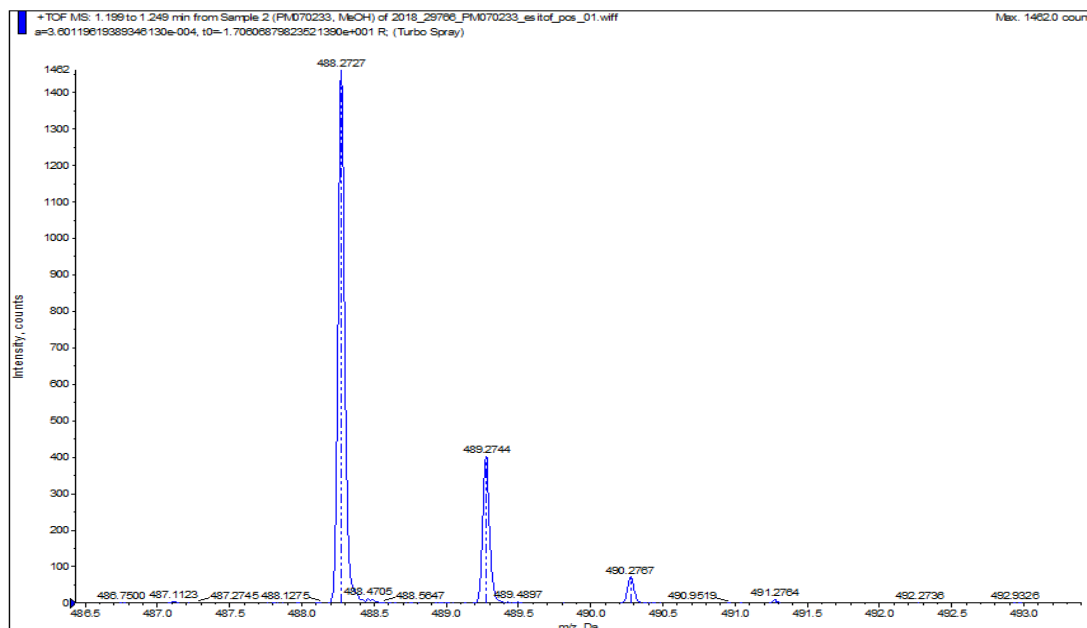


Figure S9. (+)-HRESIMS of **55**.

DP4+ analysis

Considering that the relative stereochemistry relation between the stereogenic centers C2 and C3 was defined as *anti* through VT-JBCA configurational analysis. It was obtained four possible nocardiomycin diastereoisomers (**55a-d**) to compute.

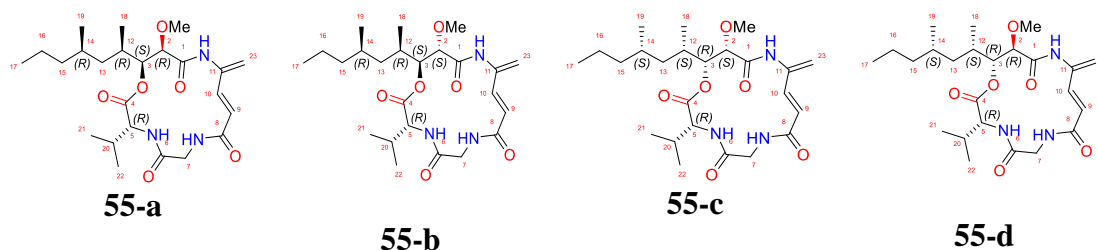


Figure S10. Diastereoisomers of nocardiomycin.

The diastereoisomers were initially submitted to a restricted conformational search using NOE and ROE distance and angle with Maestro Software. Thus, 76 conformers for **55a.**, 129 for **55-b**, 118 for **55-d** were found within a 3.0 kcal/mol window. The restriction used discarded the diastereoisomer **55-c**.

All conformers were classified by energy and frequencies using the B3LYP27/6-31+G(d,p) functional. Finally, the combination MPW1PW9128/6311+G (2d,p)-polarizable continuum model was used for proton and carbon chemical shift calculations. The sets of ^1H and ^{13}C chemical shifts were compared by mean absolute error (MAE), R^2 of $\delta_{\text{calcd}}/\delta_{\text{expt}}$, by the linear regression of calculated (δ_{scaled}) and by the statistical DP4+ parameter developed by sarroti and co-workers.

A 100 % probability DP4+ value for both carbon and proton chemical shifts in favor to **55** was in agreement with the 2R, 3R, 12S, 14S configuration (**55-d**).




























	Isomer 1	Isomer 2	Isomer 3
sDP4+ (H data)	 99.46%	 0.05%	 0.49%
sDP4+ (C data)	 99.99%	 0.00%	 0.01%
sDP4+ (all data)	 100.00%	 0.00%	 0.00%
uDP4+ (H data)	 99.59%	 0.00%	 0.41%
uDP4+ (C data)	 99.10%	 0.00%	 0.90%
uDP4+ (all data)	 100.00%	 0.00%	 0.00%
DP4+ (H data)	 100.00%	 0.00%	 0.00%
DP4+ (C data)	 100.00%	 0.00%	 0.00%
DP4+ (all data)	 100.00%	 0.00%	 0.00%

Table S2. DP4+ Statistical correlations of diastereoisomers **55** (**a** (isomer 3), **b** (isomer 2) and **d** (isomer 1)) of nocardimycin.

General conclusions

- The results of the literature review showed the potential of the Yucatan Peninsula as an interesting source of new marine natural products, not only because of its unique and rich diversity of marine organisms, but also due to the small number of works published so far, which indicates that this area of research has been poorly investigated.
- 51 sponges corresponding to 41 species (Porifera), 13 ascidians corresponding to 12 species (Chordata) and 1 gorgonian (Cnidaria), were collected by snorkelling and SCUBA diving in different coastal zones of the Yucatan Peninsula, Mexico, during three different periods: September-December 2016, January-March 2017 and September 2018. The selected species were collected from two different regions: Mexican Caribbean (Cozumel Island, Rio Indio, Mahahual and Bermejo, Quintana Roo) and Campeche Bank (Alacranes Reef and Progreso, Yucatan) in areas with high biological diversity such as coral reefs, islands and mangrove forests.
- Sixty-five organic extracts from marine organisms, corresponding to 51 sponges (Porifera), 13 to ascidians (Chordata) and 1 gorgonian (Cnidaria), were submitted to an *in vitro* antibacterial, antiviral and antiproliferative screening against four species of multidrug-resistant (MDR) bacterial pathogens, two types of virus and five cancer cell lines.
- MICs indicated antibacterial activity of nine extracts from 8 sponges *Agelas citrina*, *Agelas dilatata*, *Agelas sceptrum*, *Aiolochoiria crassa* (collected from two different locations, Mahahual, Quintana Roo and Alacranes Reef), *Amphimedon compressa*, *Dysidea* sp., *Monanchora arbuscula* and *Haliclona (Rhizoniera) curacaoensis*. The extracts of the sponges *Agelas citrina* and *Dysidea* sp. showed the best antibacterial activity. The bioguided fractionation of one of the active extracts, from the sponge *Amphimedon compressa*, produced a mixture of halitoxins and amphitoxins which displayed notable antibacterial *in vitro* activity against four pathogenic bacteria. This is the first report of the antimicrobial activity of halitoxins and amphitoxins against major multidrug-resistant human pathogens.
- Evaluation through microdilution assays displayed an important antiviral activity of nine extracts corresponding to 8 sponges (*Agelas citrina*, *Myrmekioderma gyroderma*, *Ectyoplasia* sp., *Chondrilla* sp., *Dysidea* sp., *Monanchora arbuscula*, *Aaptos* sp., and *Cinachyrella kuekenthali*) and one ascidian (*Clavelina* sp.). The extracts of the sponges *Dysidea* sp., *Agelas citrina* and *Chondrilla* sp. showed the best antiviral activity.
- Twenty-four extracts showed antiproliferative activity and corresponding to 20 sponges (*Agelas citrina*, *Myrmekioderma gyroderma*, *Chondrilla caribensis* f. *hermatypica*, *Leucetta floridana*, *Cliona varians*, *Dysidea* sp., *Spongia tubulifera*, *Haliclona (rhizoniera) curacaoensis*, *Amphimedon compressa*, *Plakinastrella onkodes*, *Monanchora arbuscula*, *Clathria gomezae*, *Mycale laevis*, *Scopalina ruetzleri* (collected in Progreso, Yucatan and Rio Indio, Quintana Roo), *Aaptos* sp., *Tethya* sp., *Cinachyrella kuekenthali* and *Aiolochoiria crassa* (collected in

Alacranes Reef, Yucatan and Mahahual, Quintana Roo) and 4 ascidians (*Clavelina* sp., *Trididemnum solidum*, *Polysyncrator* sp. and *Eudistoma amanitum*). The best antiproliferative activity was showed by two organism, ascidian *Eudistoma amanitum* and the sponge *Haliclona (rhizoniera) curacoensis*, and more than 50 % of the extracts tested showed antiproliferative activity against the hepatocyte carcinoma cell line (HepG2).

- Seven compounds were isolated for the sponge *Spongia tubulifera* collected in Rio Indio, Mexican Caribbean, two new spongian furanoditerpenes together with five known terpenes (four furanoditerpenes and one sesterterpene). Three compounds (one new, the 3 β -hydroxyspongia-13(16),14-dien-2-one and two known, 3 β ,19 dihydroxyspongia-13(16),14-dien-2-one (epispongiadiol) and the furanoditerpene ambliol C) displayed weak cytotoxic activity against a panel of five human tumor cell lines. This work represents the first chemical study of the secondary metabolites from *S. tubulifera*.
- Three new sesterterpene lactams together with three known sesterterpene furans were isolated for the sponge *Ircinia felix*, collected in Rio Indio, Mexican Caribbean. Two sesterpenes exhibited significant anti-HAdV activity (one new, ircinialactam J and one know, (7Z,12Z,18R,20Z)-variabilin). The mechanism by which these compounds block HAdV infections seems to be related with the entrance of the virus into the cell, but further studies will be necessary to verify their mechanisms of action. These two molecules may be used as prototypes for the optimization of a new set of antiviral molecules that could lead to the clinical development of a new anti-HAdV drug with high efficacy and low toxicity to be used for treatment of infections by this pathogen.
- Four new diterpenoids, together with six known diterpenes (one briarane, three briantheins, one asbestinin and one diterpene) were isolated for the gorgonian *Briareum asbestinum* collected in Rio Indio, Mexican Caribbean. All the isolated compounds were submitted to several biological evaluations but did not show any significant cytotoxic activity against the human tumor cell lines (MDA-MB-231 (breast), HT-29 (colon), NSLC A549 (lung) and PSN1 (pancreas)), antibacterial activity against *Acinetobacter baumannii*, *Pseudomonas aeruginosa*, *Klebsiella pneumoniae*, *Staphylococcus aureus* or antiviral activity against Human adenoviruses (HAdV5 y HAdV5-GFP).
- Eight known alkaloids were isolated from sponge *Agelas dilatata* collected in the Cozumel Island, Mexican Caribbean. Two of them, ageliferin and bromogeliferin, displayed significant antibacterial activity against two Gram- negative bacteria strains. This work represents the first chemical study of the secondary metabolites from *A. dilatata* and this is the first time where the activity of all the compounds were evaluated on gram negative bacteria: *Klebsiella pneumoniae* and *Pseudomonas aeuroginosa*.
- We demonstrated that ¹H RCSAs can be successfully utilized to determine the correct relative configuration using *Q* or *Q*_{CSA} values. This is the first time that this methodology is applied to a natural product.

- We have shown how some unsolvable cases in the configurational analyses based on coupling constants (JBCA) can be accomplished using two different approaches: changing the temperature or the deuterated solvent in the NMR measurements.

Difusion de la investigación

Congresos:

a) Internacionales

Dawrin Pech-Puch, Jaime Rodríguez and Carlos Jiménez. “Four new briarane diterpenoids from caribbean gorgonian *Briareum asbestinum*”. I Euroindoamerican Natural Products Meeting (I EIAMNP), Oral Presentation, from 29 May to 1 June, Madrid, España, 2018.

Juan Carlos Fuentes, Nilamoni Nath, **Dawrin Pech-Puch**, Jaime Rodríguez, Carlos Jiménez, Michael Reggelin and Christian Griesinger. “Using proton residual chemical shift anisotropy at microgram level for the determination of the relative configuration in small molecules: the case of briarane-B3”. Conference on Magnetic Resonance in Medicine and 25th National Magnetic Resonance Society Meeting, Oral presentation, from 13 to 16 February, New Delhi, India, 2018.

Juan Carlos Fuentes-Monteverde, Nilamoni Nath, **Dawrin Pech-Puch**, Armando Navarro-Vázquez, Elena Balboa, Jaime Rodríguez, Carlos Jiménez, and Christian Griesinger. “Using Proton Residual Chemical Shift Anisotropy at Microgram Level for the Determination of the Relative Configuration in Marine Natural Products”. SMASH-Small Molecule NMR Conference 2019, Oral presentation, from 22 to 25 September, Porto, Portugal, 2019.

b) Nacionales

Dawrin Pech-Puch, Jaime Rodríguez, Carlos Jiménez and Mar Anabel Pérez-Povedano. “New diterpenes from the sponge *Spongia tubulifera*, collected in the Mexican Caribbean”. XXXVII Reunion Bienal de la RSEQ, Poster, from 26 to 30 May, San Sebastian, España, 2019.

Juan Carlos Fuentes, Nilamoni Nath, **Dawrin Pech-Puch**, Jaime Rodríguez, Carlos Jiménez and Christian Griesinger. “New devices for the measurement of anisotropic parameters in small molecules”. XXXVII Reunion Bienal de la RSEQ, Poster, from 26 to 30 May, San Sebastian, España, 2019.

Juan Carlos Fuentes, Nilamoni Nath, **Dawrin Pech-Puch**, Jaime Rodríguez, Carlos Jiménez, Herminia Dominguez, Elena M. Balboa, Christian Griesinger. “Relative configuration of natural compounds using proton residual chemical shift anisotropy”. XXXVII Reunion Bienal de la RSEQ, Oral presentation, From 26 to 30 May, San Sebastian, España, 2019.

Dawrin Pech-Puch, Mar Anabel Pérez-Povedano, Marta Martínez-Gutián, María L. Novoa, German Bou, Jaime Rodríguez, Alejandro Beceiro and Carlos Jiménez. Antibacterial activity of compounds isolated from the sponge *Agelas dilatata* collected in Yucatan, Peninsula. IV QuimBioQuim Meeting, Poster, from 23 to 25 October, Santiago de Compostela, España, 2019.

Cristina Lasarte-Monterrubio, Marta Martínez-Gutián, **Dawrin Pech-Puch**, Mar Pérez-Povedano, Juan Carlos Vázquez-Ucha, German Bou, Jaime Rodríguez, Carlos Jiménez, Alejandro Beceiro. “Marine organisms from Yucatán Peninsula (México) as a potential

natural source of new antimicrobial compounds against multidrug-resistant pathogens". 30th European Congress of Clinical Microbiology and Infectious Diseases (ECCMID), Poster, from 18-21 April, 2020.

Publicaciones:

a) Publicaciones aceptadas

Pech-Puch, D.; Rodríguez, J.; Cautain, B.; Sandoval-Castro, C. A.; Jiménez, C. Cytotoxic Furanoditerpenes from the Sponge *Spongia tubulifera* Collected in the Mexican Caribbean. *Mar. Drugs* **2019**, *17*, 416.

Pech-Puch D.; Pérez-Povedano M.; Lenis-Rojas O.A.; Rodríguez J.; Jiménez C. Marine Natural Products from the Yucatan Peninsula. *Mar. Drugs* **2020**, *18*, 59.

b) Publicaciones en preparación

Marine organisms from Yucatan Peninsula (Mexico) as potential natural source of new antibacterial compounds.

Antiviral and antiproliferative potential of marine organisms from the Yucatan Peninsula, Mexico.

Two antiviral Sesterterpenoids from the Marine Sponge *Ircinia felix*, Collected in Yucatan (Mexico).

Antibacterial activity of alkaloids isolated from the sponge *Agelas dilatata* collected in Yucatan Peninsula.

A new Briarane Diterpenoids from the Gorgonian *Briareum Asbestinum* collected in Yucatan Peninsula.

Relative configuration of micrograms of natural compounds using proton residual chemical shift anisotropy.

Variable Temperature and Solvent Dependent NMR J-Based Configurational Analysis for Stereochemical Determination of Flexible Acyclic Systems.

Patente internacional:

Pech-Puch D.; Berastegui-Cabrera J.; Pachón J.; Rodríguez J.; Jiménez C.; Sánchez-Céspedes J. Furan, thiophene or γ -lactam sesterpene tetronic acids useful as antiviral compounds against infections caused by human adenovirus. En trámite.